

Enantioselective Hydroalkylation and Natural Product Modification Mediated by Radical Reactions

Inaugural dissertation
of the Faculty of Science,
University of Bern

presented by

Elena Hofstetter

from Moldova

Supervisor of the doctoral thesis:
Prof. Dr. Philippe Renaud

Department of Chemistry, Biochemistry and Pharmaceutical Sciences

Original document saved on the web server of the University Library of Bern



This work is licensed under the Creative Commons Attribution-NonCommercial-NoDerivatives 2.5 Switzerland License. To view a copy of this license, visit [Creative Commons Attribution-NonCommercial-NoDerivatives 2.5 Switzerland License](https://creativecommons.org/licenses/by-nc-nd/2.5/ch/) or send a letter to Creative Commons, PO Box 1866, Mountain View, CA 94042, USA.

Copyright notice

This document is licensed under the Creative Commons Attribution-Non-Commercial-No derivative 2.5 Switzerland Licence. <http://creativecommons.org/licenses/by-nc-nd/2.5/ch/>

You are free:



to copy, distribute, display, and perform the work

Under the following conditions:



Attribution. You must give the original author credit.



Non-Commercial. You may not use this work for commercial purposes.



No derivative works. You may not alter, transform, or build upon this work.

For any reuse or distribution, you must take clear to others the license terms of this work.

Any of these conditions can be waived if you get permission from the copyright holder.

Nothing in this license impairs or restricts the author's moral rights according to Swiss law.

The detailed license agreement can be found at:

[Creative Commons Attribution-NonCommercial-NoDerivatives 2.5 Switzerland License](http://creativecommons.org/licenses/by-nc-nd/2.5/ch/)

**Enantioselective Hydroalkylation and Natural Product Modification
Mediated by Radical Reactions**

Inaugural dissertation
of the Faculty of Science,
University of Bern

presented by

Elena Hofstetter

from Moldova

Supervisor of the doctoral thesis:

Prof. Dr. Philippe Renaud

Department of Chemistry, Biochemistry and Pharmaceutical Sciences

Accepted by the Faculty of Science.

Bern, 21.10.2022

The Dean
Prof. Dr. Marco Herwegh

"It is possible to fly without motors,
but not without knowledge and skill."
- Wilbur Wright -

Acknowledgements

First, I would like to express my thankfulness to Prof. Philippe Renaud for given opportunity to perform my PhD studies in his group at the University of Bern. I am grateful for his supervision and patience, for his teaching and knowledge, for the freedom to work in the lab and develop myself during these four years. It was a challenge to come to Switzerland, but an interesting and fruitful experience to work together and explore the chemistry of radicals in organic synthesis and natural product modification.

I am thankful to Prof. Eoin Scanlan and PD Dr. Martin Lochner for accepting examining my thesis.

I am thankful as well to Dr. Fabrice Dénès for interesting discussions and provided support. His animated talks will not be forgetable.

Many thanks I would like to give to the "Legendary" Lab S375. I am happy that I could share the lab with the best colleagues ever - Manü, Lars, Gaetano and Remo. Their experience and guidance help me to do this possible. I learned a lot not just about chemistry, but life in general. Not to forget about our apprentices: Robin, Alex, Levi and Leo - *Danke vielmal* for funny and amazing time in the lab.

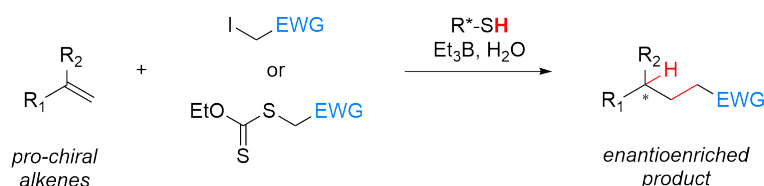
Cheers to all other group members: Semra, Elöise, Yanis, Ravi, Lise, Gulsana, Lukas, for all the good time and atmosphere in the group. Thanks to former members: Dace, Camilo, Valentine, Anja, Julien, Luca, Qi, Joy, Emy, Mariam, Eleonore, for their support and discussions. Special thanks as well to other coleagues from DCBP (Reymond, Häner and Paradisi group). Many connections were formed and moments to remember.

Thanks to all the people in the department who helped me, the Ausgabe, the NMR, MS and X-ray team; as well as for the administrative job carried out by Franziska, Sandra and Beatrice.

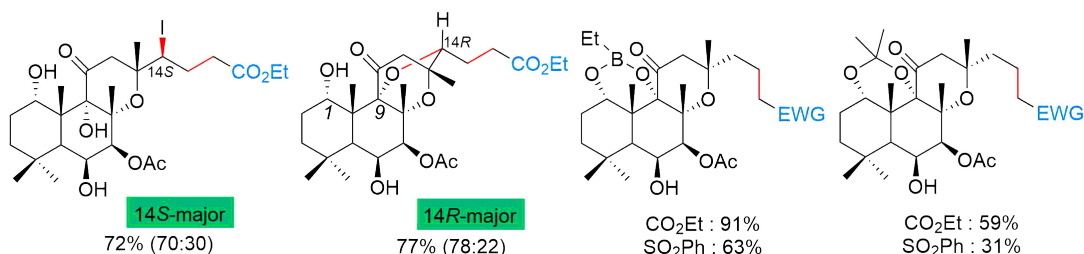
Last, but most important, a Big Thank you I would like to say to my parents, my brothers, and my Swiss family - Mike, Matthias and Sandra, Anja and Koni, for all the support and love offered all this years. Without them nothing of this would be possible!

Abstract

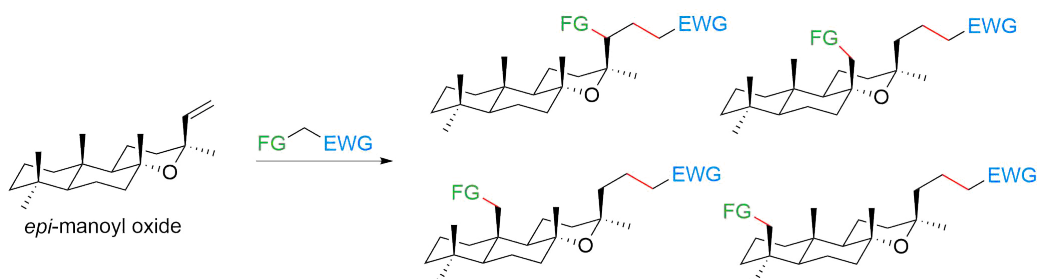
The enantioselective hydroalkylation of prochiral alkenes employing catalytic amount of chiral thiols was investigated. The transition metal-free process, using Et_3B and air as radical initiator and H_2O for catalyst regeneration, is an easy, cheap and eco-friendly way to perform this transformation under mild conditions. Cysteine-based peptides showed high enantioselectivity ratios for the hydroalkylation of 1,3-oxazolidin-2-one derivatives delivering the desired products in high yields. The investigation of a chiral system compatible with the linear pro-chiral alkenes is still on-going.



Additionally, we performed the modification of highly oxygenated forskolin via intermolecular carbon-centered radical addition to the vinyl moiety. Two less functionalized model substrates sharing the same polycyclic skeleton - manoyl oxide and its 13-*epimer* - were as well investigated. Highly regio- and reasonably stereoselective iodine atom transfer radical addition (ATRA) reactions were developed. The formation of tetracyclic ether derivative and in situ protection of the forskolin 1,3-diol moiety as a cyclic boronic ester were reported.



Furthermore, we took advantage of manoyl oxide and *epi*-manoyl oxide structure conformation and investigated the remote long range 1,5-hydrogen atom transfer. This concept is known as "billiard reaction" or "travelling radical". Remote C-H functionalization of labdane diterpenoids via iodine atom transfer radical addition and further functionalization was reported.



List of Abbreviations and Symbols

α_D	optical rotation
δ	chemical shift (ppm)
3,5-DNBZCl	3,5-dinitrobenzoyl chloride
4DPAIPN	1,3-Dicyano-2,4,5,6-tetrakis(diphenylamino)-benzene
Alox	aluminium oxide
aq.	aqueous
ATRA	Atom Transfer Radical Addition
BDE	Bond Dissociation Energy
<i>c</i>	concentration
cat.	catalytic
calcd.	calculated
conc.	concentrated
COSY	Correlated Spectroscopy (2D NMR experiment)
Cys	Cysteine
DCE	dichloroethane
DCM	dichloromethane
DEPT	Distortionless Enhancement by Polarization Transfer (1D NMR experiment)
DLP	dilauroyl peroxide
DMAP	4-dimethylaminopyridine
DMF	dimethylformamide
DMSO	dimethylsulfoxide
DTBHN	di- <i>tert</i> -butylhyponitrite
<i>dr</i>	diastereomeric ratio
<i>ee</i>	enantiomeric excess
equiv.	equivalents
<i>er</i>	enantiomeric ratio
ER	'ene' reductase
ESI	Electron spray ionization
EWG	Electron Withdrawing Group
FC	Flash Chromatography
FID	Free Induction Decay
GSH	L-gluthathione reduced
GSSH	gluthathione hydropersulfide
$h\nu$	light irradiation
HAT	Hydrogen Atom Transfer
HMBC	Heteronuclear Multiple Bond Correlation (2D NMR experiment)
HPLC	High Performance Liquid Chromatography
HRMS	High Performance Mass Spectroscopy
HSQC	Heteronuclear Single Quantum Coherence (2D NMR experiment)
IR	Infrared spectroscopy
<i>J</i>	coupling constant (in Hz)
<i>k</i>	rate constant
LSF	Late Stage Functionalization
<i>m/z</i>	mass to charge ratio
Mp	melting point
NMR	Nuclear Magnetic Resonance

NOESY	Nuclear Overhauser Enhancement Spectroscopy (2D NMR experiment)
PC	photocatalyst
ppm	parts per million
Pro	Proline
pyr	pyridine
R	rest (or substituent)
rt	room temperature
RP-HPLC	Reversed Phase - High Performance Liquid Chromatography
qunt.	quantitative
TEA	triethylamine
TBC	4- <i>tert</i> -butylcatechol
TBME	<i>tert</i> -butylmethyl ether
THF	tetrahydrofuran
TLC	Thin Layer Chromatography
sat.	saturated
sat.	saturated
sol.	solution
SET	Single Electron Transfer
UV	ultra-violet

Contents

I	Enantioselective Hydroalkylation by Radical Reactions	1
1	Enantioselective Hydroalkylation in Organic Synthesis	3
1.1	Introduction	4
1.2	Enantioselective Hydroalkylation	6
1.2.1	Radical hydroalkylation catalysed by chiral thiols	6
1.2.2	Photoenzymatic mediated hydroalkylation	11
1.2.3	Metal catalysed hydroalkylation	13
1.3	Conclusion	18
	References	19
2	Chiral Thiols in Asymmetric Synthesis	23
2.1	Introduction	24
2.2	Chiral Thiols in Asymmetric Synthesis	27
2.2.1	Chiral thiols derived from available commercial alcohols	27
2.2.2	Chiral thiols derived from the chiral pool	28
2.2.3	Terpenes derived thiols	29
2.2.4	Chiral thiols derived from amino acids	31
2.2.5	Others reported chiral thiols	32
2.3	Hydropersulfides or "Superthiols" Concept	36
2.4	Conclusion	39
	References	40
3	Thiol Catalysed Enantioselective Hydroalkylation	45
3.1	Introduction	46
3.2	Results and Discussion	48
3.2.1	Optimization	48
3.2.2	Scope and limitation	50
3.2.3	Screening of chiral thiols	51
3.2.4	Proposed mechanism	55
3.3	Conclusion	57
3.4	Additional Results and Outlook	58
	References	59
3.5	Experimental Section	61

II	Natural Product Modification by Radical Reactions	105
4	Late Stage Functionalization in Drug Discovery	107
4.1	Introduction	108
4.2	Photocatalytic Promoted 1,5-HAT	110
4.2.1	Alkylation	111
4.2.2	Hydroxyalkylation	111
4.2.3	Allylation	112
4.2.4	Heteroarylation	113
4.2.5	Pyridylation	115
4.2.6	Remote functionalization	116
4.3	Conclusion	120
	References	121
5	Forskolin Editing via Radical Iodo- and Hydroalkylation	125
	Abstract	126
	Key words	126
5.1	Introduction	126
5.2	Results and Discussion	129
5.2.1	Iodoalkylation (ATRA reaction) of manoyl and <i>epi</i> -manoyl oxide	129
5.2.2	Iodoalkylation and alkoxyalkylation of (–)-forskolin	130
5.2.3	Stereoselectivity of the iodoalkylation	133
5.2.4	Hydroalkylation of manoyl and <i>epi</i> -manoyl oxide	135
5.2.5	Hydroalkylation of (–)-forskolin	138
5.3	Conclusion	139
	References	140
5.4	Experimental Section	144
6	C–H Functionalization of Manoyl Oxide Derivatives via Selective 1,5-HAT	177
6.1	Introduction	178
6.2	Literature Precedents	181
6.2.1	Steroid and related natural scaffolds modifications	181
6.2.2	Manoyl oxide derivatives functionalization	187
6.3	Results and Discussion	189
6.3.1	Manoyl oxide modifications	189
6.3.2	<i>epi</i> -Manoyl oxide modifications	195
6.4	Conclusion	204
	References	205
6.5	Experimental Section	208
7	Appendix	223
7.1	NMR and X-ray Chapter 3	225

7.2 NMR and X-ray Chapter 5	281
7.3 NMR and X-ray Chapter 6	359

Part I

Enantioselective Hydroalkylation by Radical Reactions

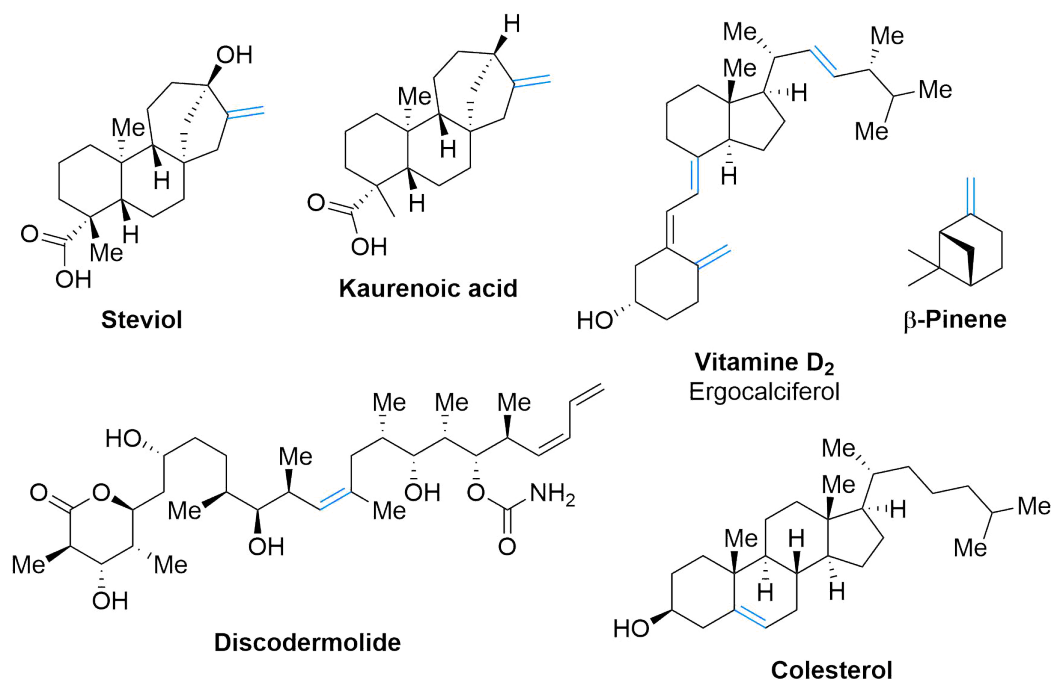
1 Enantioselective Hydroalkylation in Organic Synthesis

This chapter is dedicated to the reported in literature methods in performing the enantioselective hydroalkylation of alkenes.

1.1 Introduction

The prevalent occurrence of C(sp³)-C(sp³) structures fascinates chemists and generates interest in improving the construction of these common bonds.¹⁻³ Evolution in pharmaceutical chemistry especially requires new synthetic methods that eases and accelerates alkyl carbon centres formation.^{4,5} High regioselectivity can be realized in alkene hydroalkylation, resulting in the facile formation of C(sp³)-C(sp³) bonds.

Alkenes are both important large-scale products of the petrochemical industry and abundant sources of basic raw materials for the chemical industry.⁶⁻⁸ Moreover, a number of natural products and drugs with complex structures also contain alkenyl groups,^{9,10} such as steviol and vitamin D₂ (Scheme 1.1). In recent studies, alkene hydrofunctionalization reactions have been extensively developed as efficient and prevailing methods to convert abundant alkene feedstock to high-value chemicals.¹¹



Scheme 1.1: Natural products containing double bonds.

Roberts¹²⁻¹⁵ is the main contributor to the classical enantioselective hydroalkylation reaction. The thiol-catalysed radical-chain additions of silanes to a number of cyclic prochiral terminal alkenes carried out in the presence of different radical initiators, were reported. By using homo-chiral thiols to promote a chiral H-atom transfer,¹⁶ enantioenriched products were obtained. The concept of Roberts was later used by other groups in order to find a better system.

Recently, biocatalysis has emerged as a promising method of developing mechanistically novel and synthetically attractive transformations.^{17,18} Reactivity of an 'ene' reductase (ER) using visible-light excitation to accomplish the intermolecular radical hydroalkylation of terminal alkenes

was explored by the group of Zhao^{19,20} and Hyster.²¹

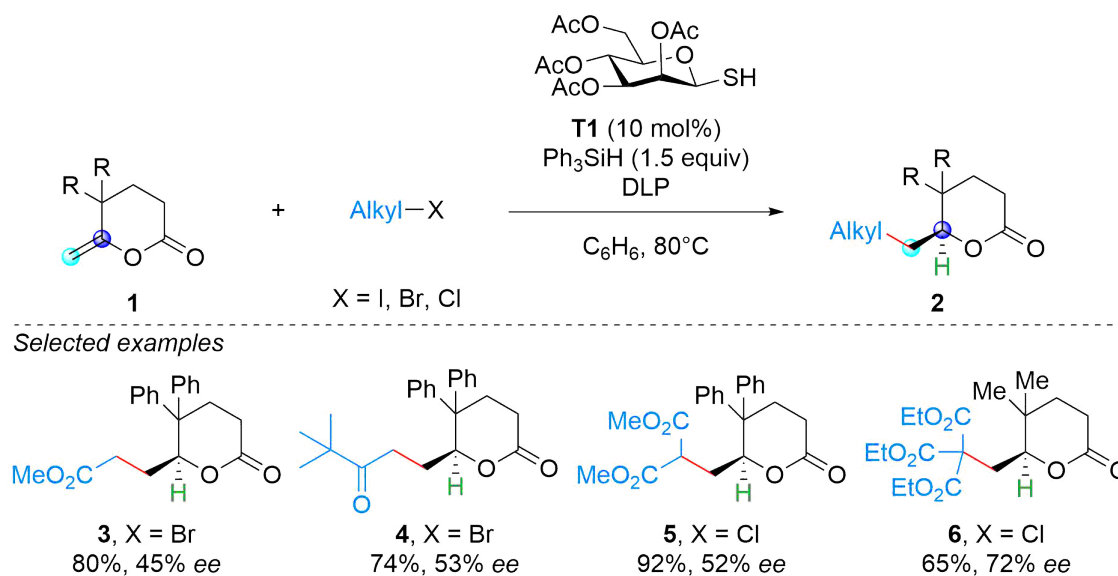
Over the past decade, extensive progress has been made in transition metal-catalyzed C–C bond formation. In particular, nickel-catalyzed reductive hydrofunctionalization of olefins has become a powerful strategy for the synthesis of complex molecules because of nickel's characteristic nature. Nickel catalysts predominantly promote the activation of alkyl electrophiles via radical catalytic cycles and effectively inhibit and/or manipulate β -H elimination reactions. Nickel catalysts also have a number of changeable valence states to flexibly participate in tandem catalytic reactions and reductive cross-coupling reactions.²²

Electrochemistry has been explored as well in the past several years as an efficient, versatile, and sustainable approach for the difunctionalization and hydrofunctionalization of alkenes.^{23,24} Zhand et al.²⁵ reported the use of electrochemistry to the reductive functionalization of alkenes, especially anti-Markovnikov hydroalkylation, by means of the electroreductive generation of alkyl radical and carbanion intermediates. These reactions employ readily available starting materials, transition-metal-free conditions and display broad substrate scope and good tolerance of functional groups.²⁵

1.2 Enantioselective Hydroalkylation

1.2.1 Radical hydroalkylation catalysed by chiral thiols

As pioneer in this field, Roberts and co-workers developed the enantioselective reductive alkylation of the prochiral alkenes (e.g. **1**), mediated by triphenylsilane in the presence of homochiral thiol catalysts^{14,15} (Scheme 1.2).

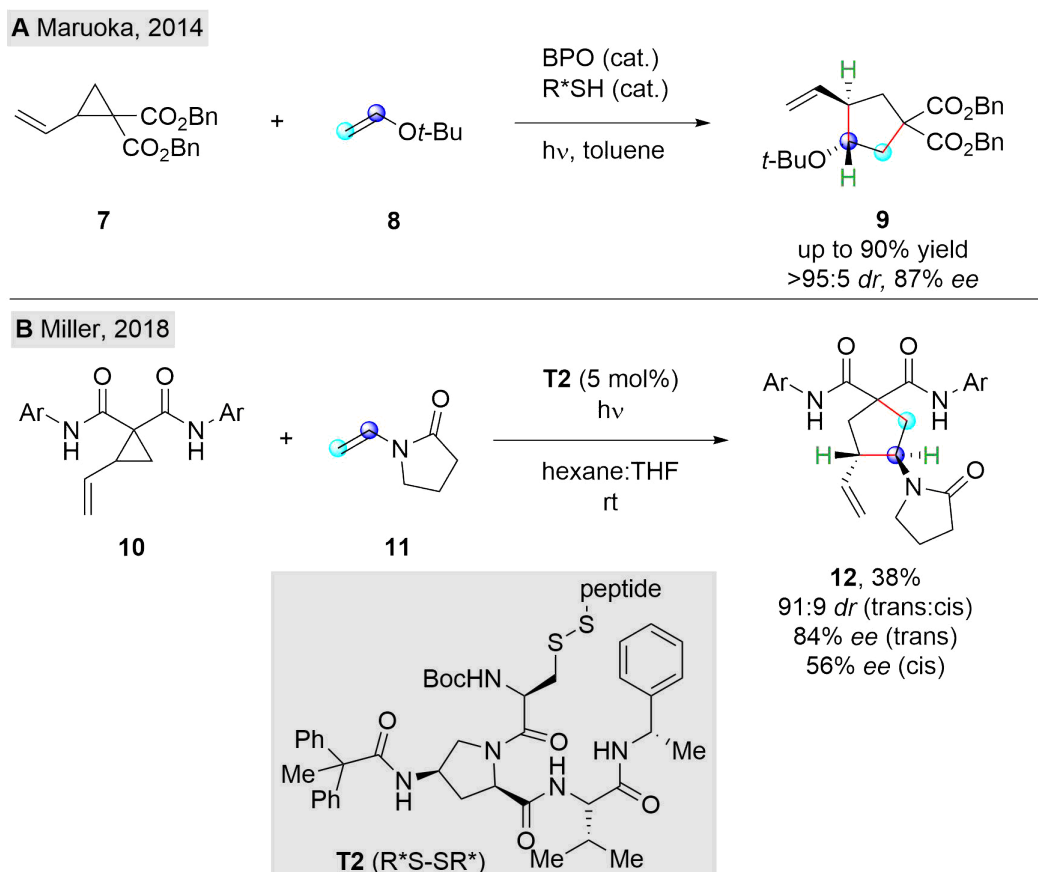


Scheme 1.2: Hydroalkylation catalysed by chiral thiols.¹⁵

Moderate enantiomeric excesses (up to 72% ee) were obtained by replacing the achiral thiol with the carbohydrate derived homochiral thiol **T1** (Scheme 1.2, **3-6**). The triphenylsilane–thiol couple is an effective mediator of the reductive alkylation of electron-rich alkenes by halides that yield electrophilic carbon radicals. By using dilauroyl peroxide (DLP, at 80 °C) as radical initiator - chlorides, bromides and iodides can act as alkylating agents. The authors concluded that both steric and dipole–dipole interactions between the prochiral carbon-centred radical and the thiol are important in determining enantioselectivity and that these interactions can act in opposition as well as co-operatively.²⁶

Later, Maimone reported the total synthesis of the polycyclic terpene - (-)-6-ophiobolin N,²⁷ where as for the key step a final selective reduction of the intermediate was performed. The reaction was closely related to the work of Roberts, however Et₃B was used as radical initiator. Initiation with air and triethylborane generates an ethyl radical, which is reduced by the thiol to form ethane and a thiyl radical (the active species that induces selectivity).²⁷

In 2014, Maruoka and his team reported the first enantioselective vinyl cyclopropane ring opening/cyclization addition cascade reaction catalyzed by thiyl radicals, delivering enantioenriched five membered rings²⁸ (Scheme 1.3, **A, 7-9**). This method was compatible with silyl vinyl ethers,



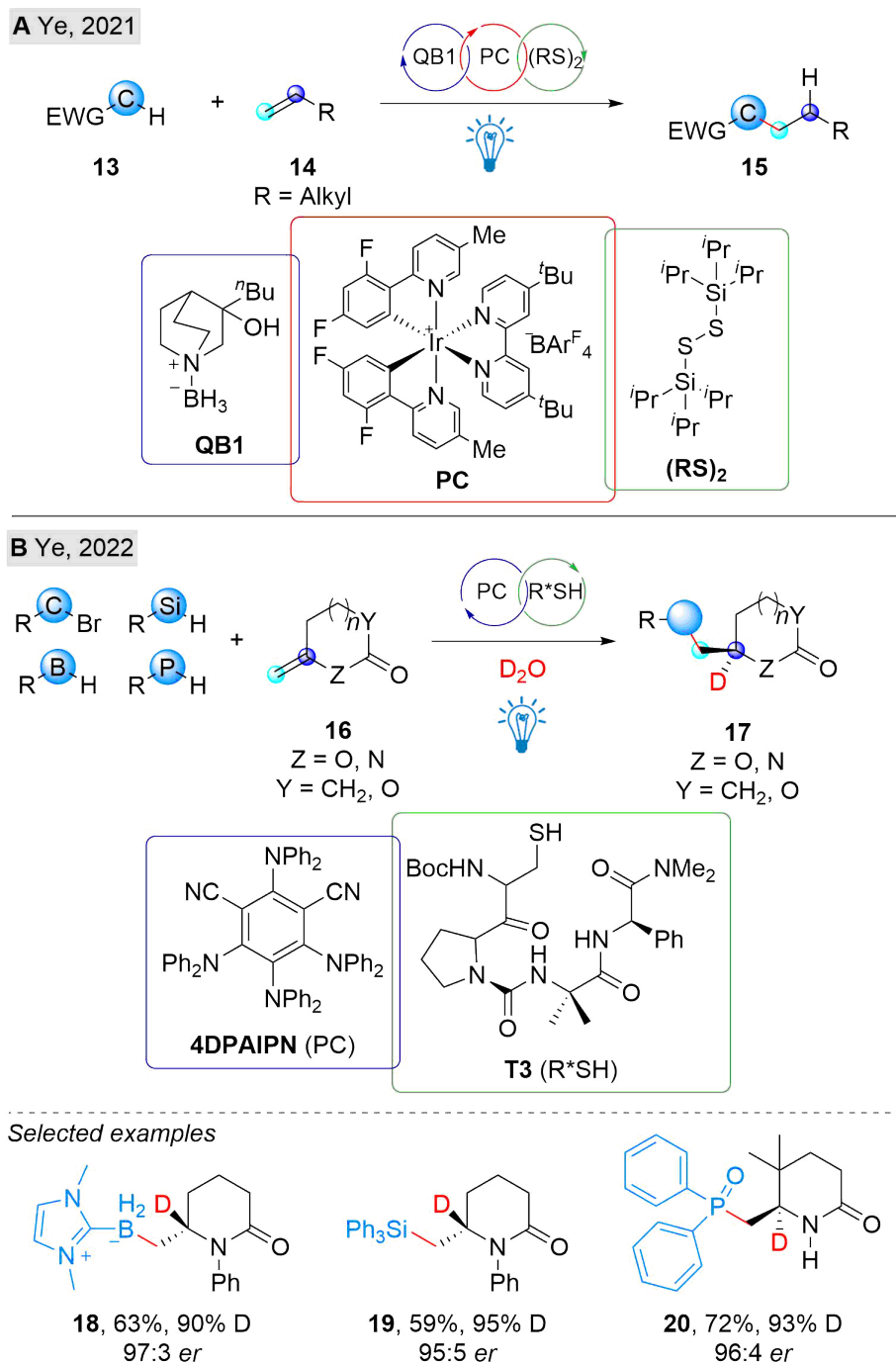
Scheme 1.3: Enantioselective vinylcyclopropane ring-opening/cycloaddition cascade.

enecarbamates, gem-diesters or gem-diketones, however simple alkenes, such as 1-hexene and styrene, gave low conversions and selectivities.²⁸

Inspired by the work of Maruoka, Miller group reported a similar enantioselective vinylcyclopropane ring-opening/cycloaddition cascade employing cysteine derivatives as chiral source²⁹ (Scheme 1.3, **B**, **10-12**). The active thiyl radical catalyst is generated *in situ* via UV light-promoted homolysis of cysteine-based dimer **T2**. The authors speculated that H-bonding from the peptide scaffold to the substrate would control the geometry of the intermediate and thus affording a high selectivity. Moreover, the enantioselectivity was depended of the steric bulkiness of the peptide derivatives, so when steric hindrance was pushed to excess, the selectivity was decreasing.²⁹

In 2021, Lei et al. reported the use of visible-light-driven dual HAT catalysis in hydroalkylation of alkenes³⁰ (Scheme 1.4, **A**, **13-15**). Catalytic amounts of an amine-borane and an *in situ* generated thiol were utilized as the hydrogen atom abstractor and donor, respectively. As photocatalyst, $[\text{Ir}(\text{dF}(\text{CH}_3)\text{ppy})_2(\text{dtbbpy})]\text{BAR}_4^{\text{F}}$ (**PC**) was used. Initially, the 2,4,6-triisopropylbenzenethiol (TRIPSH) was used as a H-atom donor. However, replacing the TRIPSH thiol with 5 mol% of it's easy-to-handle and odorless bis(2,4,6-triisopropylphenyl) disulfide $[(\text{TRIPS})_2]$ derivative, a

better yield was noted. The borane **QB1** was identified as the optimal hydric HAT catalyst, delivering the product up to 92% yield. The utility of the present method was examined on a diverse range of structurally complex olefins derived from drug molecules, natural products, and material precursors.³⁰

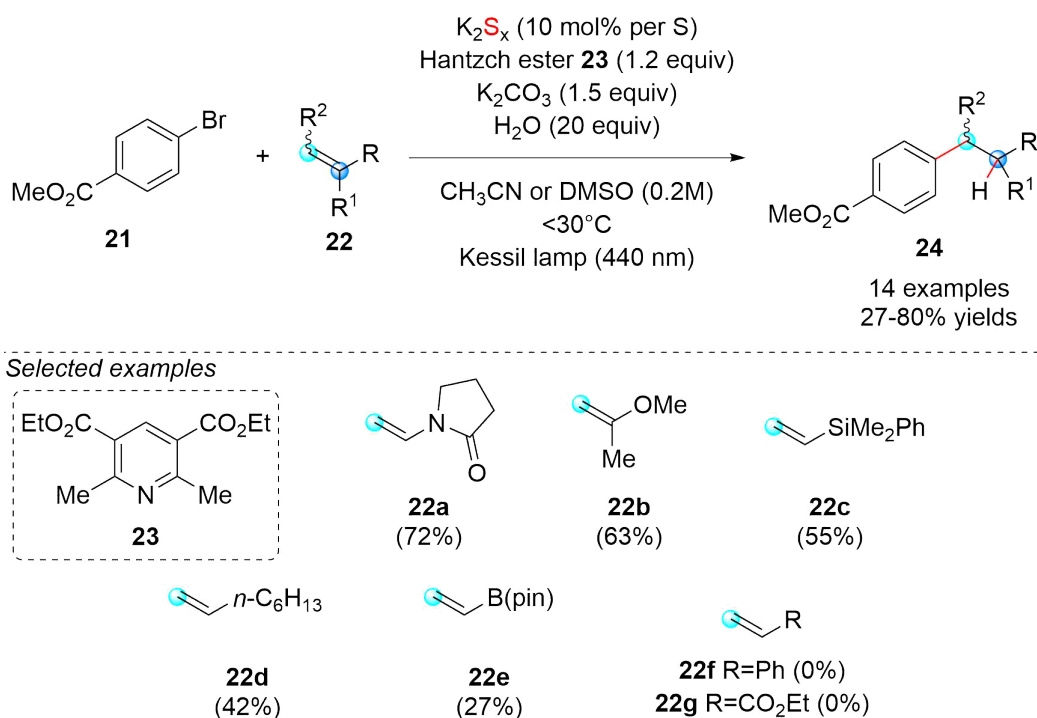


Scheme 1.4: Visible-light driven hydroalkylation of olefins.

Motivated by the initial result, the same group reported in 2022, a photochemical approach for asymmetric radical deuteration by utilizing readily available peptide- or sugar-derived thiols

as the catalyst (e.g. **T1** and **T3**) and inexpensive deuterium oxide as the deuterium source³¹ (Scheme 1.4, **B**, **16-17**). This metal-free approach enables four types of deuterofunctionalization (deuteroboration, deuteriosilylation, deuterophosphinylation, and deuterodifluoroalkylation) reactions of exocyclic olefins and allows deuteration at nonbenzylic positions with high levels of enantioselectivity and deuterium incorporation (Scheme 1.4, **B**, **18-20**).³¹ One could imagine, that the use of water instead of D₂O would deliver in the same fashion the enantio-enriched hydroalkylated product.

Based on the reports of Pratt,^{32,33} Li and co-workers hypothesized that polysulfide anions may function as a polarity reversal catalyst^{12,13,26} via hydrogen polysulfides to efficiently deliver a H-atom to the alkyl radical intermediates.³⁴ They reported this concept on the hydroarylation of alkenes via polysulfide anion photocatalysis (Scheme 1.5).

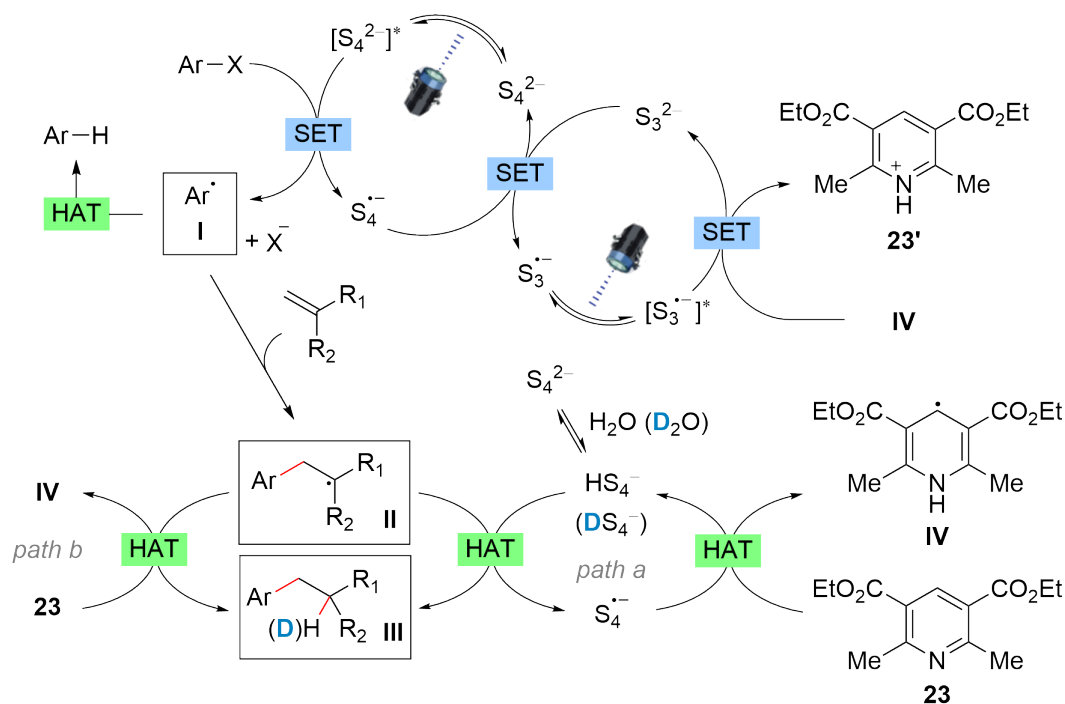


Scheme 1.5: Hydroarylation reported by Li.³⁴

A range of alkenes having various functional groups were engaged in the hydroarylation under the optimized catalytic photoredox-HAT conditions (Scheme 1.5, **22a-22e**). The protocol is applicable to aliphatic alkenes in good to moderate efficiency, whereas the hydroarylation of alkenyl boronate **22e** resulted in a poor yield. The method was incompatible with the use of styrene **22f** and ethyl acrylate **22g** under this conditions.³⁴

The authors³⁴ performed as well mechanistic studies, and the proposed catalytic cycle is represented in the Scheme 1.6. Based on the observations and on the outcomes of the deuterium labelling experiments, two complementary HAT paths could be designed to reduce alkyl radical

II and liberate the final product **III**. First path would be the HAT to alkyl radical **II** from hydrogen tetrasulfide (HS_4^-) that is formed via protonation of S_4^{2-} with H_2O and another HAT to S_4^- from the Hantzsch ester **23** (BDE at C4-H of **23** is 69.4 kcal/mol). The second path would be represented by the HAT to the alkyl radical **II** from the Hantzsch ester **23**, converting the later one to the radical intermediate **IV** involved in the regeneration of S_3^{2-} (Scheme 1.6).



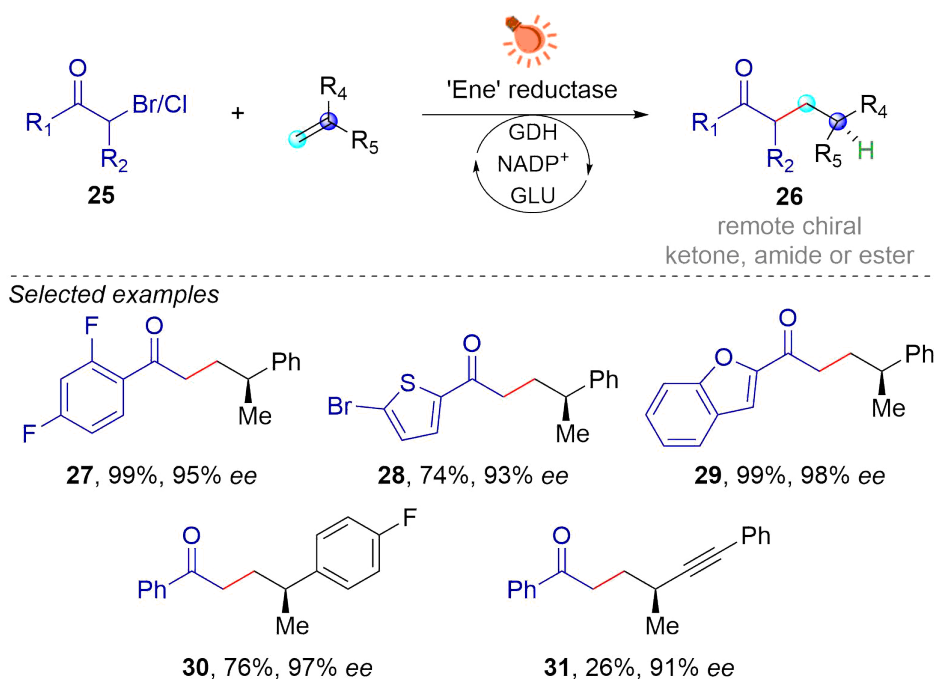
Scheme 1.6: Proposed catalytic cycle for hydroarylation mediated by hydropersulfides.³⁴

The developed hydroarylation protocol by Li³⁴ is the first one describing the use of hydropersulfides in hydrofunctionalization. It offers the opportunity of studying this derivatives as efficient hydrogen-atom carrier in enantioselective hydroalkylation/hydrofunctionalization of alkenes (see *Chapter 2 for more details*).

1.2.2 Photoenzymatic mediated hydroalkylation

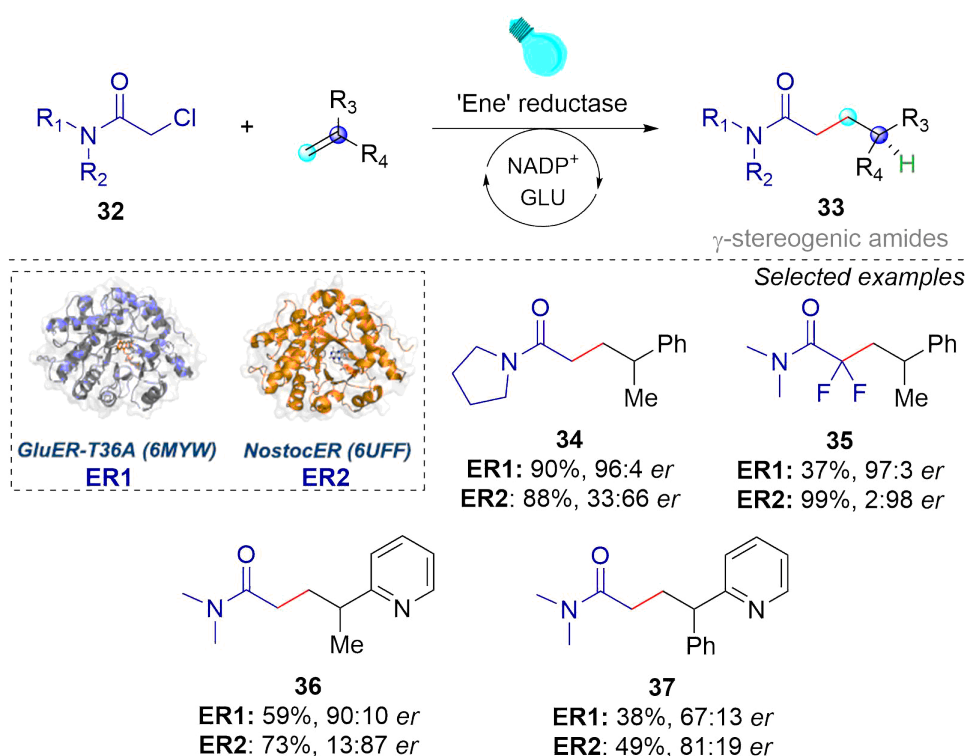
Recently, biocatalysis has emerged as a promising method of developing mechanistically novel and synthetically attractive transformations.¹⁷ Biocatalysis is typically performed at low catalyst loading under environmentally friendly conditions, providing attractive advantages in terms of sustainability, selectivity, promiscuity and evolvability. Additionally, enzymes have been shown to be able to control remote stereocentres and have been increasingly used to synthesize chiral molecules.^{35–37} Reactivity of an 'ene' reductase (ER) using visible-light excitation to accomplish the intermolecular radical hydroalkylation of terminal alkenes was as well explored. In nature, an ER catalyses the 2-electron reduction of carbonyl-substituted alkenes, where histidine and asparagine are the two key amino acid residues for carbonyl binding, the anionic flavin mononucleotide hydroquinone provides the hydride and the tyrosine acts as the proton donor.³⁸

In 2020, Zhao group reported a visible-light-induced intermolecular radical hydroalkylation of terminal alkenes, that does not occur naturally, catalysed by an 'ene' reductase using readily available α -halo carbonyl compounds (**25**) as reactants (Scheme 1.7).¹⁹ The reported method provided an efficient approach to the synthesis of various carbonyl compounds (**26**) bearing a γ -stereocentre with excellent yields and enantioselectivities (up to 99% yield with 99% enantiomeric excess), which otherwise are difficult to access using chemocatalysis (Scheme 1.7, **27–31**). Based on the mechanistic studies, the formation of the complex of the substrates (α -halo carbonyl compounds) and the 'ene' reductase, triggers the enantioselective photoinduced radical reaction.¹⁹



Scheme 1.7: Visible-light-induced enantioselective hydroalkylation catalysed by 'ene' reductases.

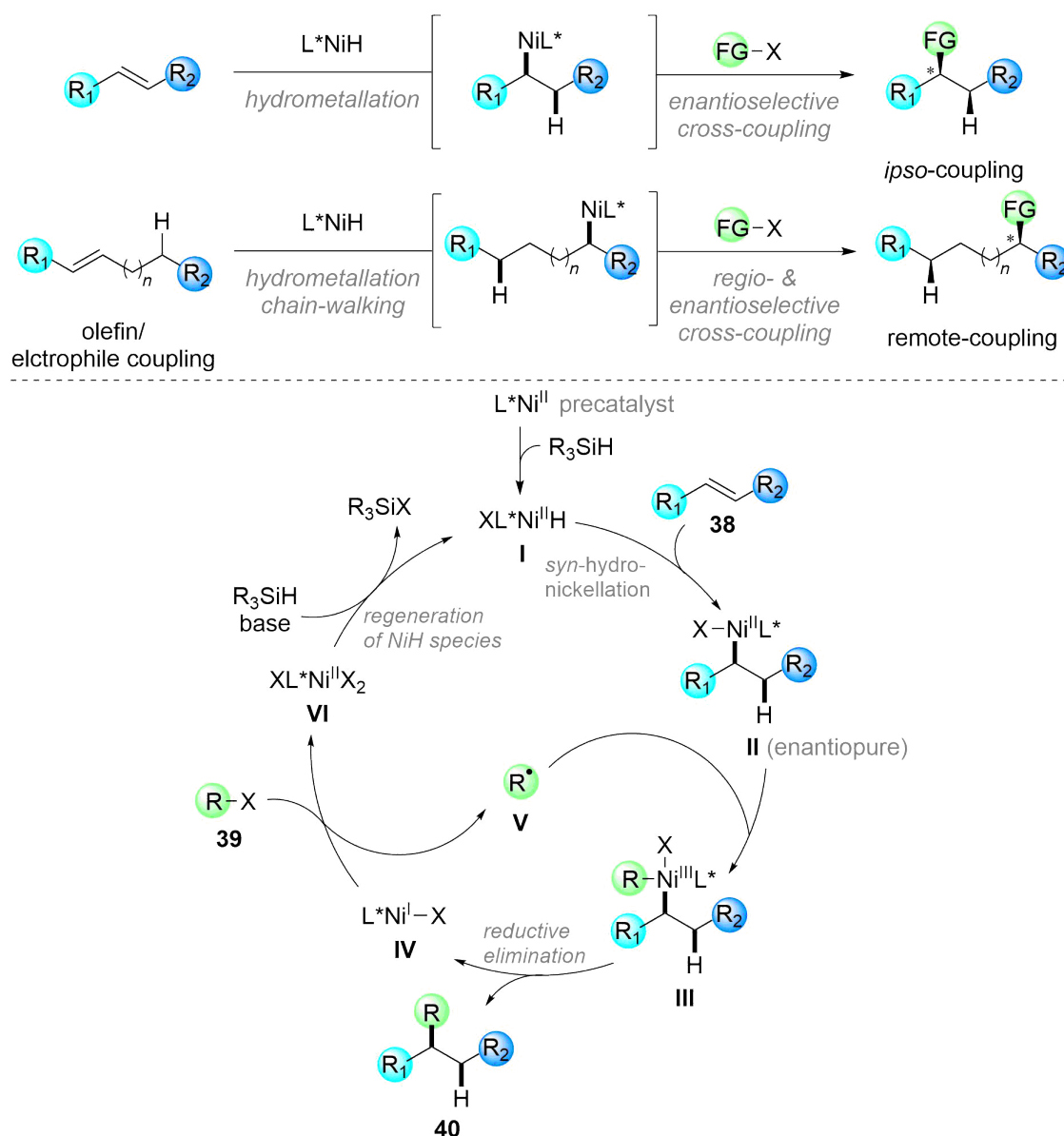
In 2021, Hyster and co-workers reported a photoenzymatic intermolecular hydroalkylation of olefins catalyzed by flavin-dependent 'ene'-reductases (Scheme 1.8).²¹ Based on the mechanism, the radical initiation occurs *via* photoexcitation of the rare high-order enzyme-templated charge-transfer complex that forms between an alkene, α -chloroamide (**32**), and flavin hydroquinone (**ER1** or **ER2**). The radical formation occurs only when both substrates are present within the protein active site, which is responsible for the radical terminating hydrogen atom transfer. The process enables the synthesis of enantioenriched γ -stereogenic amides **33**. This reaction represents a non-natural mechanism of intermolecular C-C bond formation that can be useful for the preparation of various synthetically valuable motifs (Scheme 1.8, **34-37**).²¹



Scheme 1.8: Photoenzymatic intermolecular hydroalkylation of olefins.

1.2.3 Metal catalysed hydroalkylation

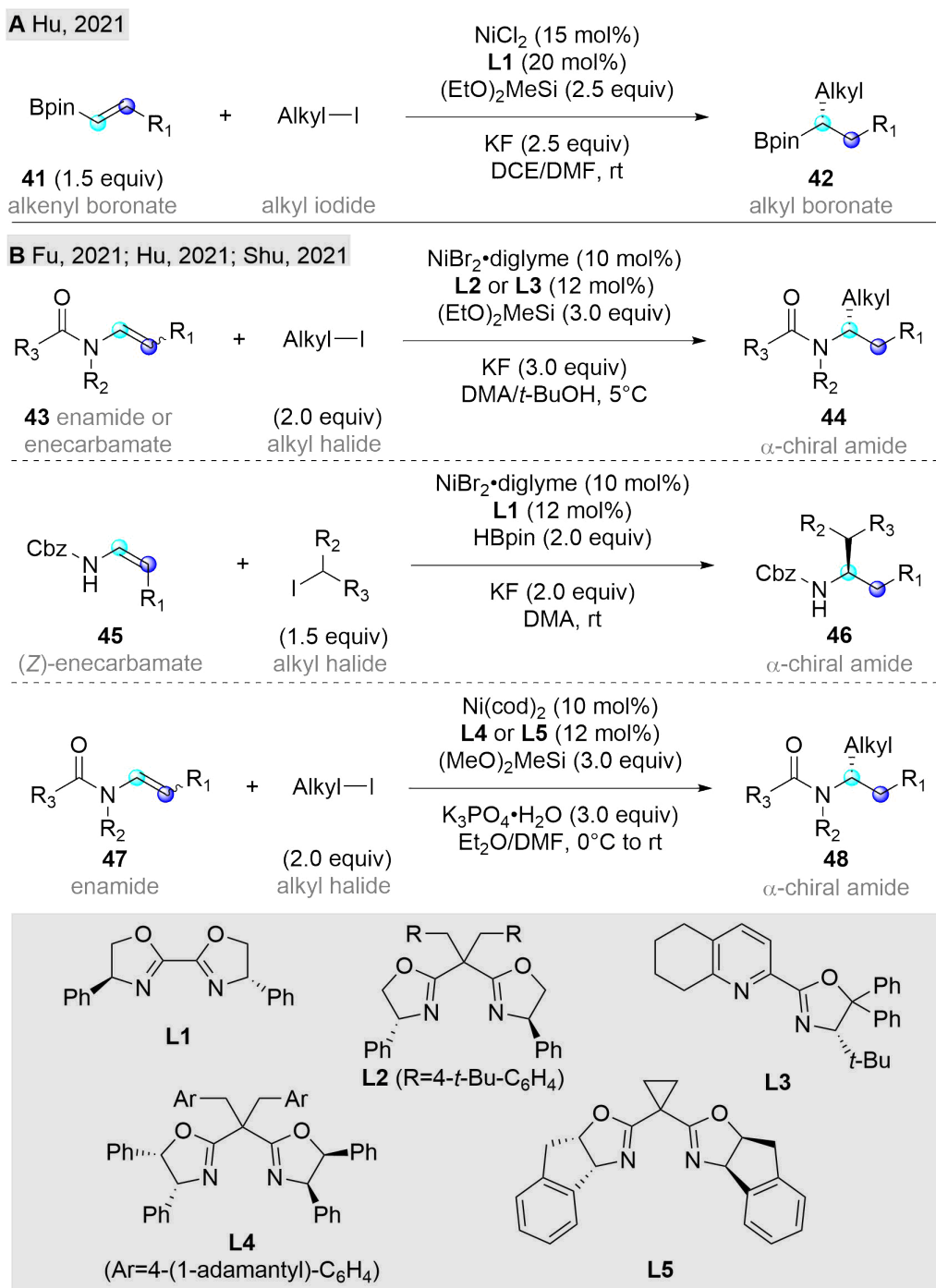
Reductive hydrofunctionalization of alkenes by metal-hydrides of first-row transition metals (Mn, Fe, Co, Ni, and Cu) has recently emerged as one of the most efficient approaches to build structurally complex functionalized compounds.^{39–41} Facilitated by the diverse oxidation states and well-explored cross-coupling chemistry of nickel,^{42–44} NiH-catalyzed enantioselective reductive hydrofunctionalization of alkenes has experienced an impressive growth in the past three years.^{11,22,45,46}



Scheme 1.9: NiH-catalyzed reductive asymmetric (migratory) olefin hydrofunctionalization.

A wide range of olefins and electrophilic coupling partners have been found to react under these mild conditions, allowing access to diverse functionalized products (Scheme 1.9). With a suitable chiral ligand, both enantioselective reductive hydrofunctionalization and remote hy-

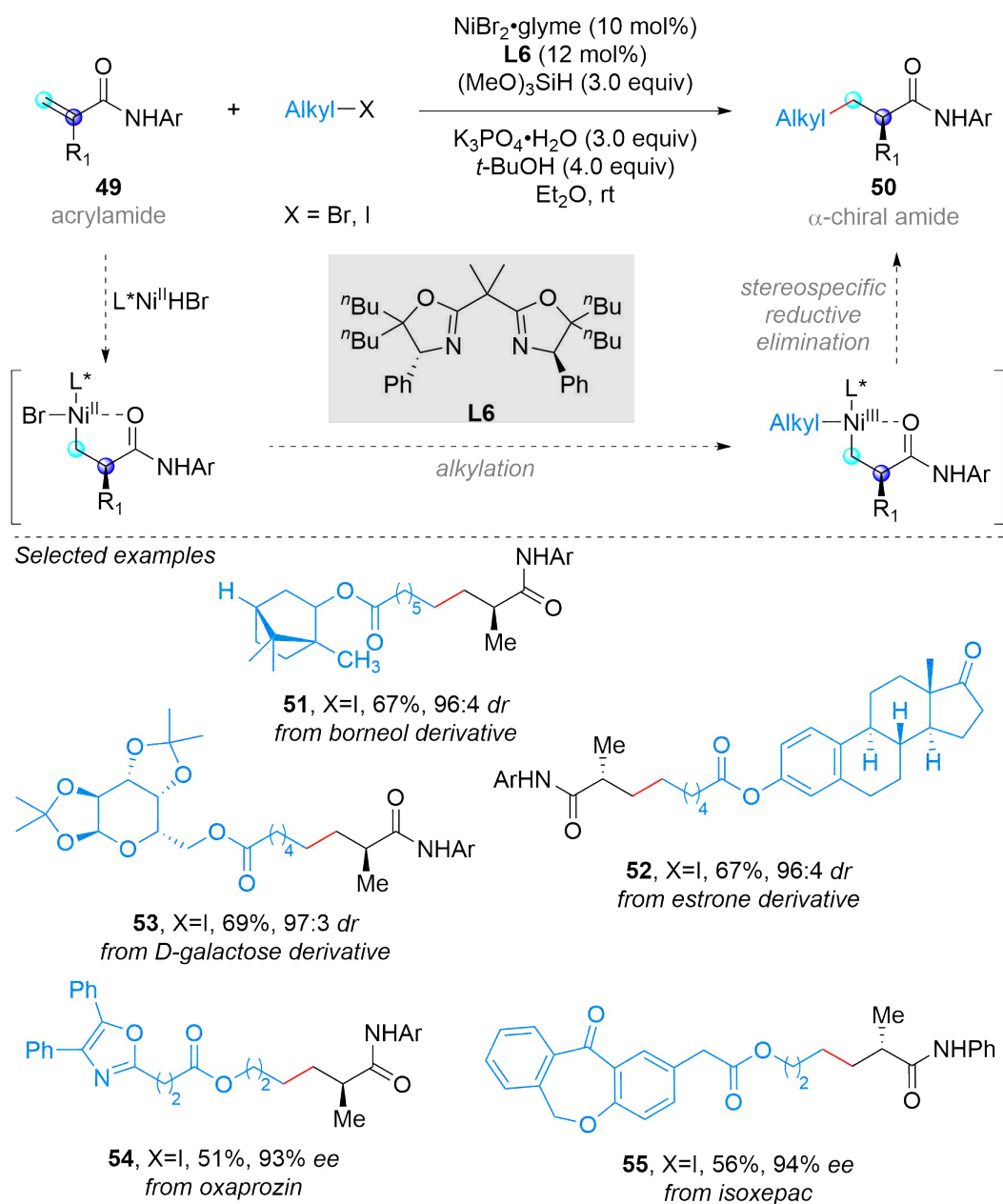
drofunctionalization can be achieved in a regio- and enantioselective fashion. Based on the proposed mechanism, the *syn*-hydronickellation of functionalized alkene **38** with NiH species **I** is the enantio-determining step, delivering the enantioenriched secondary alkylnickel(II) intermediate **II**. A subsequent stereospecific alkylation with a primary or secondary alkyl halide **39**, generates the desired enantioenriched alkylation product **40** (Scheme 1.9).²²



Scheme 1.10: NiH-catalyzed hydroalkylation of alkenyl boronates⁴⁷ and enecarbamates.^{48–50}

Several research group reported the asymmetric hydroalkylation of functionalized alkenes employing Ni catalysis (Scheme 1.10). In 2021, Hu reported an enantioselective hydroalkylation of alkenyl boronates (**41**) in the presence of bis(oxazoline) **L1**-ligated NiH species (Scheme 1.10, **A**)⁴⁷ to form derivatives **42**. In the same year, three other research groups^{48–50} reported independently the NiH-catalyzed hydroalkylation of enecarbamates **43**, **45**, **47** to deliver α -chiral aliphatic amides **44**, **46**, **48** (Scheme 1.10, **B**).

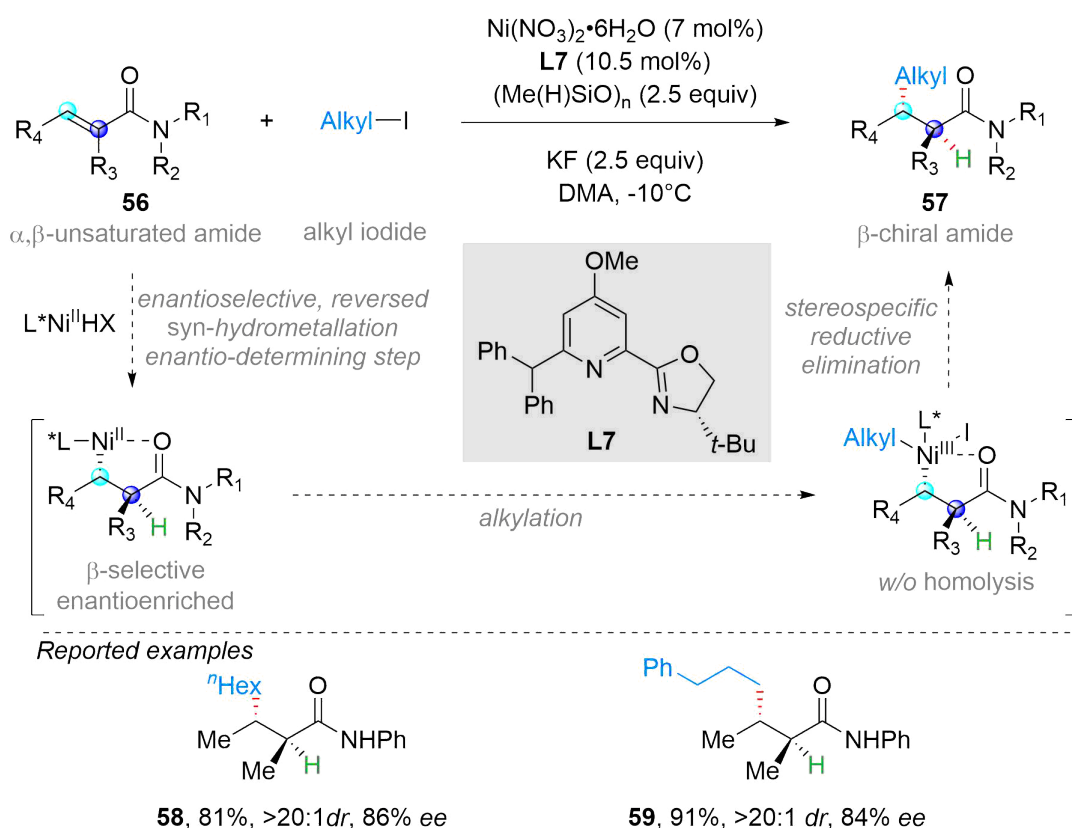
In 2020, Shu group reported the first NiH-catalysed intermolecular regio- and enantioselective anti-Markovnikov hydroalkylation of α -substituted acrylamides **49** (Scheme 1.11).⁵¹



Scheme 1.11: Ni-catalyzed enantioselective hydroalkylation of acrylamides.⁵¹

The use of a newly developed chiral ligand **L6** enables the electronically-reversed formal hydroalkylation, offering an efficient way to access diverse enantioenriched amides **50** with a tertiary α -stereogenic carbon center which is facile to racemize. The operationally simple protocol allows for anti-Markovnikov selectivity, under mild conditions, and with excellent functional group compatibility. *N*-Aryl acrylamides with electron-withdrawing or electron-donating groups are well tolerated under the reaction conditions, affording corresponding hydroalkylated chiral amides in good yields and excellent enantioselectivity (up to 95% ee). Free hydroxy group, ester and ether group, were also tolerated under the reaction conditions. The usefulness of this protocol was applied to late-stage functionalization of complex molecules, like borneol, estrone and D-galactose derivatives delivering the compounds **51-53** in good yields. Drug molecules oxaprozin and isoxepac were transformed into corresponding chiral amide **54** and **55** in 51% and 56% yields with 93% and 94% ee, respectively (Scheme 1.11).⁴⁵

Zhou and Zhu reported in 2021, the enantioselective nickel-hydride catalyzed hydroalkylation of readily accessible α,β -unsaturated amides **56** to form structurally diverse β -chiral amides **57** (Scheme 1.12).⁴⁶



Scheme 1.12: Ni-catalyzed enantioselective hydroalkylation of α,β -unsaturated amides.⁴⁶

Primary and secondary alkyl iodides were examined as reaction partner, delivering the desired product in good yields (65-93% yields). Under mild reaction conditions, nitrile, ester, acetal and *N*-Boc carbamate functional groups were well tolerated. Moreover, α,β -unsaturated

amides with aryl or alkyl substituents on the nitrogen atom, with electron-donating or electron-withdrawing substituents on the *N*-aryl ring, were well-tolerated. Notably, α,β -disubstituted acrylamides could also undergo reversed hydroalkylation to afford the enantioenriched amides **58-59** as a single diastereoisomer with two stereocenters, although a marginal erosion in the *ee* was observed (Scheme 1.12). The reaction was proposed to proceed through an amide directed regio-reversed enantioselective hydrometallation and a subsequent alkylation.⁴⁶

1.3 Conclusion

Alkene hydrofunctionalization reactions have been extensively developed as efficient method and synthetic tool to convert abundant alkene feedstock to high-value chemicals. It facilitates the formation of C(sp³)-C(sp³) bonds formation, that are over present in natural motifs.

Metal-catalysis, photochemistry, biocatalysis, and even electrochemistry, have been explored an efficient and versatile approach for the difunctionalization and hydrofunctionalization of alkenes.

The hydroalkylation catalysed by chiral thiols still remains attractive due to the low toxicity of the reagents and its possibility to functionalize efficiently alkenes. However, the selectivities obtained for small chiral thiols, remain unsatisfactory at the moment to apply this reaction in preparative synthesis. Cysteine-based derivatives offer an interesting alternative for enantioselective hydroalkylation of prochiral alkenes.

An effort into the design of new small catalysts must be carried out. It would be important to develop and understand which motif would be the most efficient not only for cyclic alkenes, but linear ones as well.

References

- (1) Geist, E.; Kirschning, A.; Schmidt, T. *Natural Product Reports* **2014**, *31*, 441.
- (2) Choi, J.; Fu, G. C. *Science* **2017**, *356*, eaaf7230.
- (3) Huo, H.; Gorsline, B. J.; Fu, G. C. *Science* **2020**, *367*, 559–564.
- (4) Boström, J.; Brown, D. G.; Young, R. J.; Keserü, G. M. *Nature Reviews Drug Discovery* **2018**, *17*, 709–727.
- (5) Guillemard, L.; Kaplaneris, N.; Ackermann, L.; Johansson, M. J. *Nature Reviews Chemistry* **2021**, *5*, 522–545.
- (6) Yang, K. S.; Gurak, J. A.; Liu, Z.; Engle, K. M. *Journal of the American Chemical Society* **2016**, *138*, 14705–14712.
- (7) Beller, M.; Seayad, J.; Tillack, A.; Jiao, H. *Angewandte Chemie International Edition* **2004**, *43*, 3368–3398.
- (8) Wang, Z.-X.; Bai, X.-Y.; Li, B.-J. *Chinese Journal of Chemistry* **2019**, *37*, 1174–1180.
- (9) Singh, M.; Ravichandiran, V.; Bharitkar, Y. P.; Hazra, A. *Current Organic Chemistry* **2020**, *24*, 709–745.
- (10) Mak, J. Y. W.; Pouwer, R. H.; Williams, C. M. *Angewandte Chemie International Edition* **2014**, *53*, 13664–13688.
- (11) Wang, X.-X.; Lu, X.; Li, Y.; Wang, J.-W.; Fu, Y. *Science China Chemistry* **2020**, *63*, 1586–1600.
- (12) Haque, M. B.; Roberts, B. P. *Tetrahedron Letters* **1996**, *37*, 9123–9126.
- (13) Haque, M. B.; Roberts, B. P.; Tocher, D. A. *Journal of the Chemical Society, Perkin Transactions 1* **1998**, 2881–2890.
- (14) Dang, H.-S.; Kim, K.-M.; Roberts, B. P. *Chemical Communications* **1998**, 1413–1414.
- (15) Dang, H.-S.; Elsegood, M. R. J.; Kim, K.-M.; Roberts, B. P. *Journal of the Chemical Society, Perkin Transactions 1* **1999**, 2061–2068.
- (16) Reid, D. L.; Shustov, G. V.; Armstrong, D. A.; Rauk, A.; Schuchmann, M. N.; Akhlaq, M. S.; von Sonntag, C. *Physical Chemistry Chemical Physics* **2002**, *4*, 2965–2974.
- (17) Devine, P. N.; Howard, R. M.; Kumar, R.; Thompson, M. P.; Truppo, M. D.; Turner, N. J. *Nature Reviews Chemistry* **2018**, *2*, 409–421.
- (18) *Visible light photocatalysis in organic chemistry*, First edition; Stephenson, C. R. J., Yoon, T. P., MacMillan, D. W. C., Eds.; Wiley-VCH: Weinheim, Germany, 2018, 444 pp.
- (19) Huang, X.; Wang, B.; Wang, Y.; Jiang, G.; Feng, J.; Zhao, H. *Nature* **2020**, *584*, 69–74.
- (20) Huang, X.; Feng, J.; Cui, J.; Jiang, G.; Harrison, W.; Zang, X.; Zhou, J.; Wang, B.; Zhao, H. *Nature Catalysis* **2022**, *5*, 586–593.

- (21) Page, C. G.; Cooper, S. J.; DeHovitz, J. S.; Oblinsky, D. G.; Biegasiewicz, K. F.; Antropow, A. H.; Armbrust, K. W.; Ellis, J. M.; Hamann, L. G.; Horn, E. J.; Oberg, K. M.; Scholes, G. D.; Hyster, T. K. *Journal of the American Chemical Society* **2021**, *143*, 97–102.
- (22) He, Y.; Chen, J.; Jiang, X.; Zhu, S. *Chinese Journal of Chemistry* **2022**, *40*, 651–661.
- (23) Sauer, G. S.; Lin, S. *ACS Catalysis* **2018**, *8*, 5175–5187.
- (24) Mei, H.; Yin, Z.; Liu, J.; Sun, H.; Han, J. *Chinese Journal of Chemistry* **2019**, cjoc.201800529.
- (25) Zhang, W.; Lin, S. *Journal of the American Chemical Society* **2020**, *142*, 20661–20670.
- (26) Cai, Y.; Roberts, B. P.; Tocher, D. A. *J. Chem. Soc., Perkin Trans. 1* **2002**, 1376–1386.
- (27) Brill, Z. G.; Grover, H. K.; Maimone, T. J. *Science* **2016**, *352*, 1078–1082.
- (28) Hashimoto, T.; Kawamata, Y.; Maruoka, K. *Nature Chemistry* **2014**, *6*, 702–705.
- (29) Ryss, J. M.; Turek, A. K.; Miller, S. J. *Organic Letters* **2018**, *20*, 1621–1625.
- (30) Lei, G.; Xu, M.; Chang, R.; Funes-Ardoiz, I.; Ye, J. *Journal of the American Chemical Society* **2021**, *143*, 11251–11261.
- (31) Shi, Q.; Xu, M.; Chang, R.; Ramanathan, D.; Peñin, B.; Funes-Ardoiz, I.; Ye, J. *Nature Communications* **2022**, *13*, 4453.
- (32) Chauvin, J.-P. R.; Griesser, M.; Pratt, D. A. *Journal of the American Chemical Society* **2017**, *139*, 6484–6493.
- (33) Poon, J.-F.; Pratt, D. A. *Accounts of Chemical Research* **2018**, *51*, 1996–2005.
- (34) Li, H.; Liu, Y.; Chiba, S. *Chemical Communications* **2021**, *57*, 6264–6267.
- (35) Alfaro Blasco, M.; Gröger, H. *Bioorganic & Medicinal Chemistry* **2014**, *22*, 5539–5546.
- (36) Gagnon, C.; Godin, É.; Minozzi, C.; Sosoe, J.; Pochet, C.; Collins, S. K. *Science* **2020**, *367*, 917–921.
- (37) Huffman, M. A. et al. *Science* **2019**, *366*, 1255–1259.
- (38) Toogood, H. S.; Scrutton, N. S. *ACS Catalysis* **2018**, *8*, 3532–3549.
- (39) Crossley, S. W. M.; Obradors, C.; Martinez, R. M.; Shenvi, R. A. *Chemical Reviews* **2016**, *116*, 8912–9000.
- (40) Chen, J.; Guo, J.; Lu, Z. *Chinese Journal of Chemistry* **2018**, *36*, 1075–1109.
- (41) Ning, Y.; Ohwada, T.; Chen, F.-E. *Green Synthesis and Catalysis* **2021**, *2*, 247–266.
- (42) Tasker, S. Z.; Standley, E. A.; Jamison, T. F. *Nature* **2014**, *509*, 299–309.
- (43) *Nickel Catalysis in Organic Synthesis: Methods and Reactions*, 1st ed.; Ogoshi, S., Ed.; Wiley: 2020.
- (44) Poremba, K. E.; Dibrell, S. E.; Reisman, S. E. *ACS Catalysis* **2020**, *10*, 8237–8246.
- (45) Shi, L.; Shu, W. *Synlett* **2021**, *32*, 1479–1483.
- (46) Zhou, F.; Zhu, S. *ACS Catalysis* **2021**, *11*, 8766–8773.

- (47) Bera, S.; Mao, R.; Hu, X. *Nature Chemistry* **2021**, *13*, 270–277.
- (48) Wang, J.-W.; Li, Y.; Nie, W.; Chang, Z.; Yu, Z.-A.; Zhao, Y.-F.; Lu, X.; Fu, Y. *Nature Communications* **2021**, *12*, 1313.
- (49) Qian, D.; Bera, S.; Hu, X. *Journal of the American Chemical Society* **2021**, *143*, 1959–1967.
- (50) Wang, S.; Zhang, J.-X.; Zhang, T.-Y.; Meng, H.; Chen, B.-H.; Shu, W. *Nature Communications* **2021**, *12*, 2771.
- (51) Shi, L.; Xing, L.-L.; Hu, W.-B.; Shu, W. *Angewandte Chemie* **2021**, *133*, 1623–1628.

2 Chiral Thiols in Asymmetric Synthesis

This chapter is dedicated to the study of chiral thiols as small molecules that can induce stereoselectivity in the enantioselective processes in organic synthesis. Herein are reported the chiral thiols previously synthesized and, if mentioned, with the application in asymmetric synthesis. Additionally, the concept of "superthiol" is presented and discussed.

2.1 Introduction

Organosulfur compounds play an important role in many biological functions and structures.¹ **Cysteine** and **methionine** (Figure 2.1) may be considered to be the principal sulfur-containing amino acids because they are 2 of the canonical 20 amino acids that are incorporated into proteins.² Cysteine plays a critical role in protein structure by virtue of its ability to form inter- and intrachain disulfide bonds with other cysteine residues. Methionine is among the most hydrophobic of the amino acids and is the initiating amino acid in the synthesis of eukaryotic proteins.

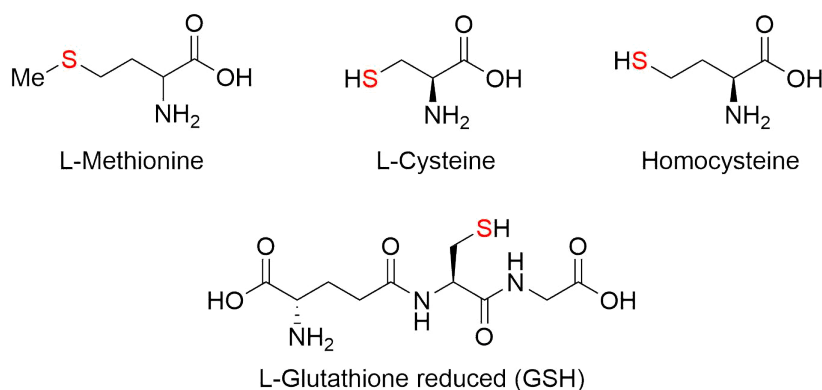


Figure 2.1: Biological active organo-sulfur compounds.

Homocysteine and **glutathione** also play important physiological roles (Figure 2.1).¹ Homocysteine may be converted to cysteine by the transsulfuration pathway or remethylated to methionine, being part of the sulfur-containing amino acid metabolism. Glutathione is a product of conversion of cysteine. It is a tripeptide (consisting of cysteine, glycine, and glutamic acid) found in most of the tissues, and is involved in tissue building and repair, making chemicals and proteins needed in the body, and in immune system function. It plays a crucial role in shielding cellular macromolecules from endogenous and exogenous reactive oxygen and nitrogen species.

The thiol functional group is found as well in a number of drug compounds (Figure 2.2) and confers a unique combination of useful properties.³ Thiol-containing drugs can reduce radicals and other toxic electrophiles, restore cellular thiol pools, and form stable complexes with heavy metals such as lead, arsenic, and copper. **N-acetylcysteine** treats APAP-induced hepatotoxicity (*N*-acetyl-*p*-aminophenol overdose) by acting as a GSH prodrug. **N-acetylcysteine amide** owns an amide group that, unlike carboxylate, is uncharged at a physiological *pH*.

Thus, *N*-acetylcysteine amide exhibits increased lipophilicity, may be more bioavailable than *N*-acetylcysteine and exhibits a greater capacity to restore hepatic GSH and increase survival compared to *N*-acetylcysteine. **D-Penicillamine** is a medication used as a chelating agent

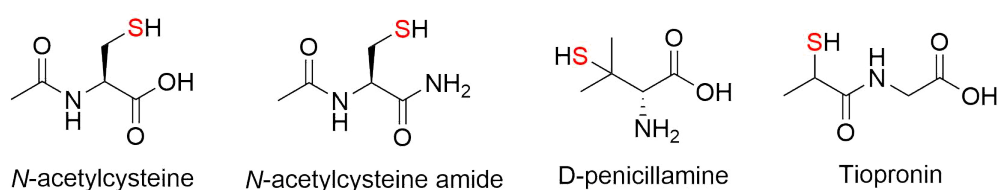


Figure 2.2: Representatives of medicinal important thiols.

primarily in Wilson's disease (a rare genetic disorder of copper metabolism), or treatment for arsenic poisoning. **Tiopronin** is best known as a treatment for cystinuria, where it prevents the formation of cystine kidney stones by forming soluble cysteine-tiopronin disulfides.³

Why does nature engage sulfur in her stock of amino acids?

Replacing oxygen by sulfur in a functional group does not just correspond to a small step in the periodic table, but may lead to another world of chemistry.⁴ Both, sulfur and oxygen, belong to the *Group 6A* of the Periodic Table and are able of making related covalent linkages. However, the differences in chemical reactivity and stability is explained by the change in atomic radii, in electronegativity, and in polarizability between oxygen and sulfur.

One of the critical differences is their electronegativity. Cysteine readily forms disulfide linkages because of the ease with which it dissociates to form a thiolate anion. Sulfur has a lower electronegativity, and replacement of oxygen would result in a much more hydrophobic amino acid.¹ Whatever the direction of the polarization of a C–S bond may be, the polarization is not pronounced and the ionic character of organosulfur compounds is lessened as compared to their oxygen congeners. Therefore, hydrogen bonding is much less important for sulfur compounds, for example the sulfur in thiols is poor at hydrogen bonding. On the other hand, this makes thiocarboxylic acids and thiols stronger acids than their oxygen analogues, so that the alcohol group does not dissociate at physiological pH.¹

An organosulfur compound will have a weaker σ bond and also overlap of p_z orbitals in a π bond will be less efficient in a thiocarbonyl as compared to a carbonyl group. In fact, the dissociation energy of the single bond of carbon with oxygen (355–380 kJ/mol) and of the C–S single bond (255 kJ/mol) quantitatively reflects the change in bonding efficiency.⁴

Use in asymmetric synthesis

The search for new chiral auxiliaries which can induce high stereoselectivities has been the major target for most researchers in the field of asymmetric synthesis. Among many successful cases, chiral thiols have certainly attracted great attention of organic chemists.^{5–7} Moreover, sulfur-containing compounds are easily available, and they are also highly stable, allowing easy storage and handling. This field of asymmetric organosulfur chemistry is particularly well developed in connection with sulfur(IV) and sulfur(VI) species with chirality at sulfur – namely sulfoxides, sulfinates, sulfines and sulfilimines.⁸ Chiral sulfoxides and sulfonium ylids have

themselves been extensively used as tools for asymmetric synthesis.⁹ With regard to chiral sulfur(II) compounds – namely thiols and thioethers (sulfides) with chirality at carbon – methods available for their asymmetric preparation are abundant, and usually rely on stereospecific substitution reactions.^{8,10,11} These reactions are well suited to the construction of secondary thiol derivatives. By contrast, few methods are suitable for the asymmetric preparation of simple tertiary thiols.^{12–16} Asymmetric Michael addition of chiral thiols to unsaturated ketones, followed by base-catalysed elimination was intensively studied for the synthesis of optically active α -mercapto carbonyl compounds.^{17–19}

2.2 Chiral Thiols in Asymmetric Synthesis

2.2.1 Chiral thiols derived from available commercial alcohols

In 1974, Berretta¹⁰ described a mild synthesis of optically active small thiols, such as (-) and (+)-2-octylthiol **1**, (-)-1-phenylpropane-2-thiol **2**, *cis*-4-*tert*-butyl-cyclohexanylthiol **3** and (+)-neomenthylthiol **4**, by use of the xanthogenic ester intermediate (Figure 2.3).

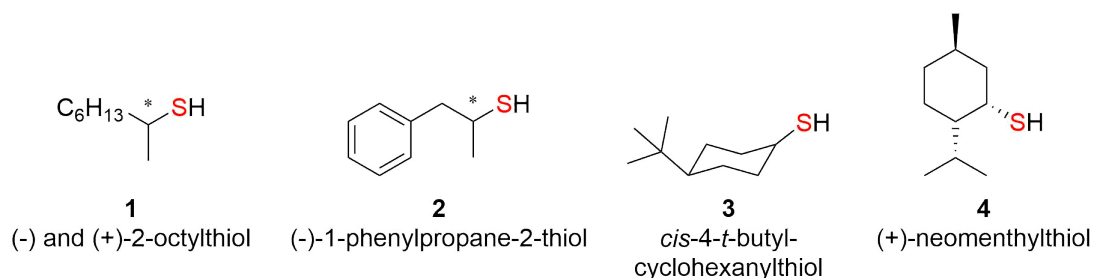


Figure 2.3: Chiral thiols reported by Beretta.¹⁰

In early '80s, Koga and co-workers²⁰ reported the use of novel chiral crown ethers bearing thiol-chiral units in enantioselective thiolysis of α -amino acid *p*-nitrophenyl ester salts or dipeptide *p*-nitrophenyl ester salts (Figure 2.4). The library was later expanded to other 11 derivatives containing various additional substituents²¹ and the importance of the complexation between the crown ether and the α -amino ester salts was demonstrated via kinetic measurements.

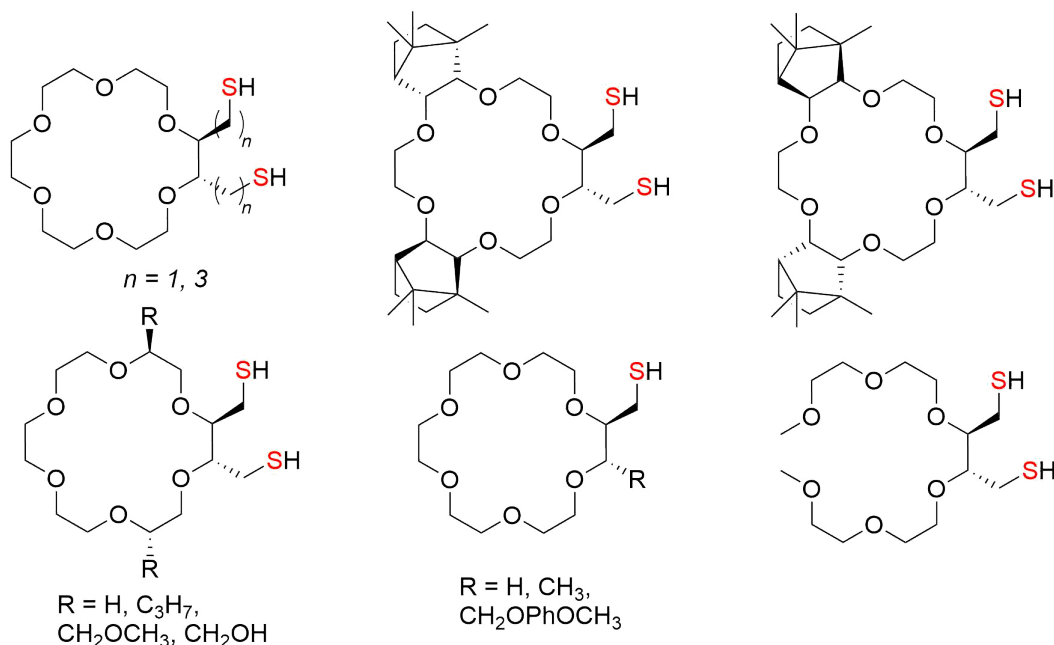


Figure 2.4: Thiol-bearing chiral crown ethers.

Younai²² targeted a set of chiral thiols that could be easily derived from commercially available alcohols (Figure 2.5). Via a two-step sequence 1-indanol, 1,2,3,4-tetrahydro-1-naphthol and

1-(1-naphthyl)ethanol, the thiols **5-7** and corresponding disulfides were prepared. Moreover, the synthesis of thiol **8** was reported. The product was achieved in 4 steps by introducing sulfur to the cyclohexyl scaffold via conjugate addition of benzyl mercaptan to the cyclohexenone.

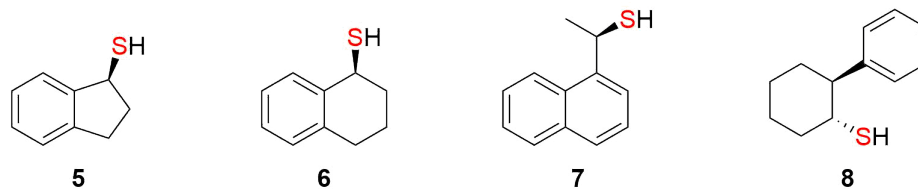


Figure 2.5: Non functionalized secondary thiols.

2.2.2 Chiral thiols derived from the chiral pool

Seebach and co-workers²³ described in 1984 the principle of using chiral building blocks available from the chiral pool, like lactic and malic acid, in order to prepare α -mercapto-carboxylic acids **9** and **10** (Figure 2.6, **A**).

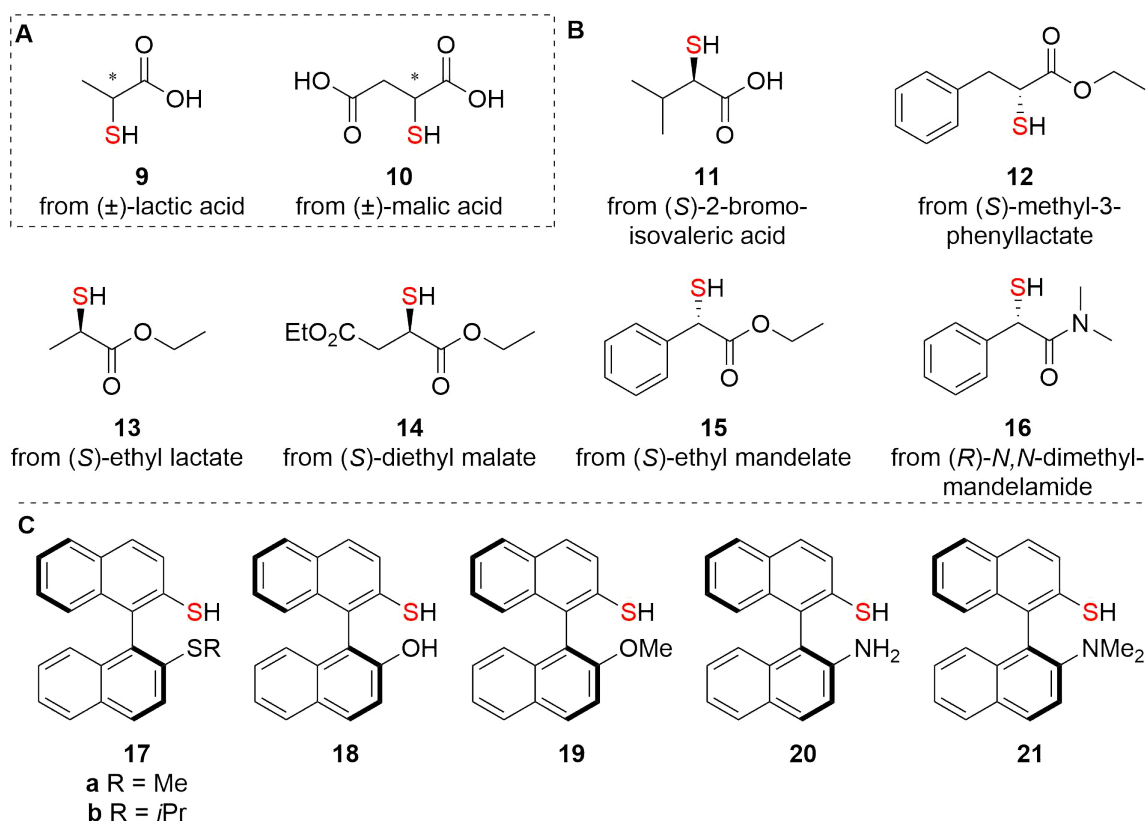


Figure 2.6: Chiral thiols available from the chiral pool.

Strijtveen and Kellogg²⁴ described later a method for preparation of several optically active thiols, especially ones sensitive to racemization. Mercapto-bearing carbons adjacent to an electron-withdrawing group like an ester, carboxylic acid or amide - are prone to partial or

complete racemization. Derivatives of (*S*)-ethyl lactate, (*R*)-ethyl mandelate, (*R*)-*N,N*-dimethyl-mandelamide or (*S*)-2-bromoisovaleric acid²⁵ were reported (Figure 2.6, **B**, 11-16). 2,2'-Substituted 1,1'-binaphthyls are particularly good examples of chiral derivatives due to their stable configuration and are good candidates as chiral ligands for asymmetric catalysis. Their conformational flexibility about the binaphthyl C(1)-C(1') pivot allows a range of bite angles to accommodate a wide variety of transition metals.²⁶ In early '96, Fabbri et al²⁷ reported the synthesis of heterotopic *S*-donor ligands of disubstituted 1,1'-binaphthalene derivatives (Figure 2.6, **C**, 17-19). One year later, Smrcina²⁸ reported the amine derivatives **20** and **21** (Figure 2.6, **C**).

2.2.3 Terpenes derived thiols

Camphor derived chiral auxiliaries attracted quite fast the great attention of organic chemists. Hung²⁹ and Lee³⁰ reported the preparation of optically active mercapto chiral auxiliaries derived

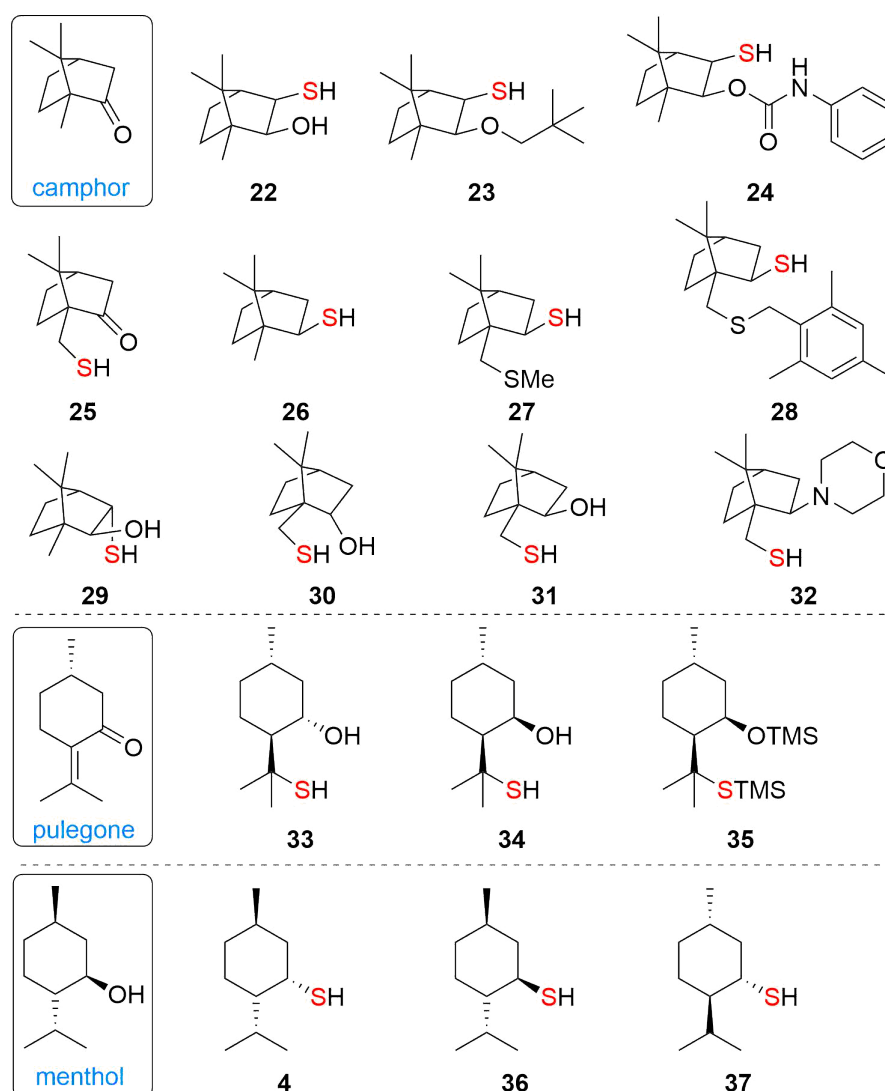


Figure 2.7: Terpene derived thiols.

from camphor (Figure 2.7, **22-24**). Later they were used as chiral auxiliaries by Yang³¹ for the synthesis of optically active primary amines, with subsequent high yield recovery. The group of Riera^{32,33} added few more examples to the library and applied the chiral moieties for the preparation of chiral acetylene dithioesters (Figure 2.7, **25-28**). Fiaud and co-workers³⁴ reported several chiral 1,2- and 1,3-hydroxythiols derived from (*R*)-camphor (Figure 2.7, **22, 29-31**) for enantioselective borane ketone reductions. More recently, Wu³⁵ reported the γ -amino thiol **32** derived from camphor and studied it in the catalytic organozinc addition reaction.

Pulegone derived hydroxy-thiols (Figure 2.7, **33-35**), found their application in asymmetric acetalization-deacetalization for the preparation of chiral α -monosubstituted cyclopentanones from racemic ketones.³⁶ Another monoterpene used for the synthesis of chiral thiols is menthol. Nakano³⁷ reported (+)- and (-)-neomenthanethiol and (-)-menthanethiol (Figure 2.7, **4, 36, 37**) as a chain transfer reagent selective free radical polymerization.

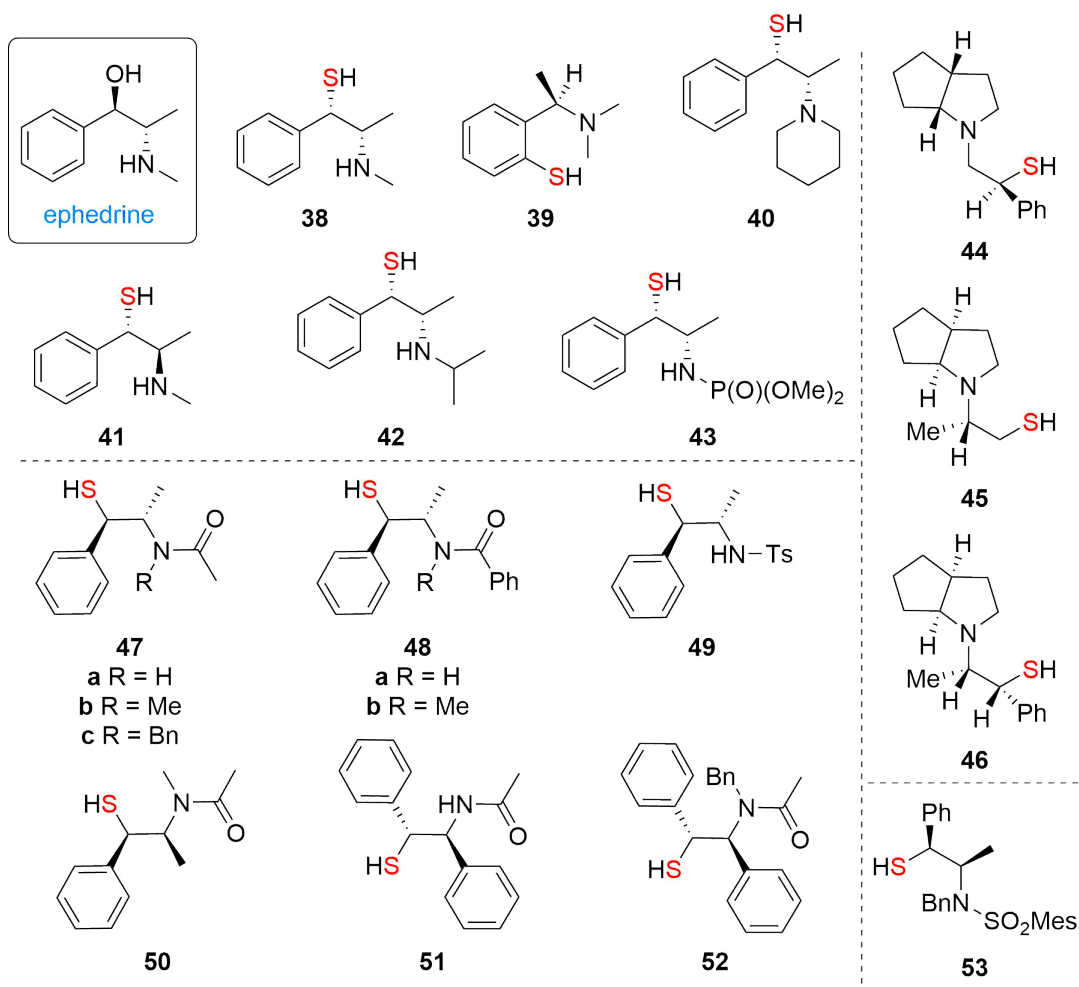


Figure 2.8: Ephedrine derived thiols.

Ephedrine is an alkaloid with a phenethylamine skeleton found in various plants in the genus *Ephedra*. Due to its chiral information and chemical properties, it is used in bulk quantities as

a chiral auxiliary group in chemical synthesis. In the first reports, ephedrine derivatives were applied for catalytic enantioselective alkylation of benzaldehyde with diethylzinc^{38,39} or asymmetric borane reduction of prochiral ketones.⁴⁰ Examples of thioephedrines are represented in the Figure 2.8, **38-43**.

In 1999, Kossenjans⁴¹ reported analogues of ephedrine derivatives, used as chiral ligands, as well in the enantioselective addition of diethylzinc to benzaldehyde. The β -amino thiols **44-46** and their disulfides showed from 60 up to 90% ee selectivity (Figure 2.8). Hsu and Fang⁴² reported the use of ephedrine derived chiral thiols for stereoselective synthesis of δ -lactones (Figure 2.8, **47-52**). The lactonization by cooperative catalysis between samarium ion and mercaptan showed the feature of remote control, which is applicable to the asymmetric synthesis. Fanjul et al⁴³ reported the synthesis of new thiol auxiliary **53** in six-step sequence from (1*S*,2*R*)-(+)-norephedrine. It showed high diastereoselectivity in boron-mediated *anti*-aldol reactions with a range of aldehydes.

2.2.4 Chiral thiols derived from amino acids

Another class of compounds which contain chiral information are the amino acids. Cran et al⁴⁴ reported the synthesis of oxygen sensitive β -amino thiol **54** in a 6 step sequence starting from L-Proline. The authors investigated the use of chiral β -amino sulfides and thiols as ligands and catalysts in transition metal mediated asymmetric carbon-carbon bond forming processes.

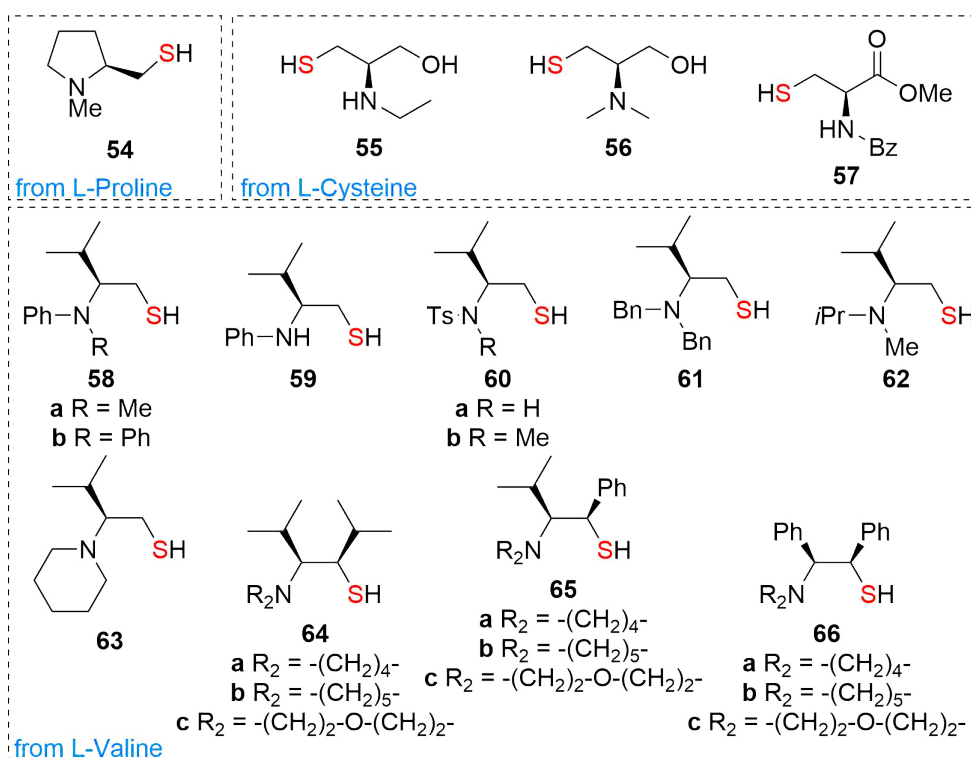


Figure 2.9: Amino acid derived thiols.

Cysteine and Cystine derivatives were reported by Fiaud³⁴ (Figure 2.9). The chiral derivatives **55** and **56** were used as chiral ligands for borane reduction of acetophenone, and showed to be a promising class of sulfur-containing auxiliaries. More recently, Younai²² reported the synthesis of *N*-Benzoyl-L-cysteine methyl ester **57** in a two-step synthesis starting from L-Cystine dimethyl ester dihydrochloride.

A series of chiral sulfur-nitrogen chelate ligands derived from L-Valine (Figure 2.9) were used in the catalytic asymmetric addition of diethylzinc to aromatic or non aromatic aldehydes. Anderson⁴⁵ reported in 1998, the first generation including primary thiols derived from valine - **58-63** - which delivered up to 82% ee selectivity. Later, Tseng^{46,47} published, in 2004, the second generation represented by secondary thiols - **64-66** - which showed excellent enantioselectivities as high as 99% ee for the same process. Wipf⁴⁸ used the same valine derivatives for his alkenylzirconium/zinc addition process where the thiol **64a** showed promising selectivity.

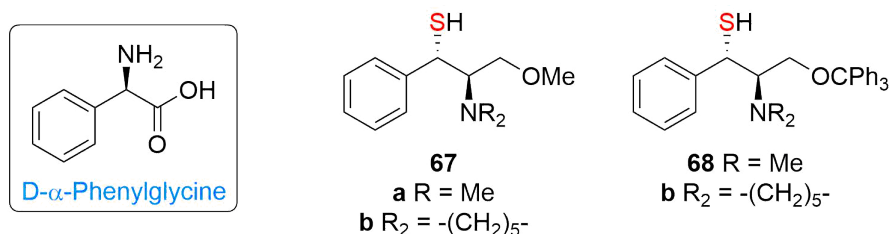


Figure 2.10: Amino acid derived thiols.

Pericas and co-workers⁴⁹ reported the preparation of enantiomerically pure amino thiols **67** and **68** (Figure 2.10) of synthetic origin through the regioselective and stereospecific ring opening sequence of epoxides arising from the Sharpless epoxidation developed in his group.⁵⁰ One could imagine the synthesis of such derivatives starting from D-Phenylglycine - a non-proteinogenic α -amino acid related to Alanine, but with a phenyl group in place of the methyl group.

2.2.5 Others reported chiral thiols

Sulfides form a good perspective for development of new ligands, since sulfur offers a soft complexation site. Koning⁵¹ reported a method for a easy preparation of pyridine thiols and dithiols by base-induced addition of 2,6-lutidine to thioketone (Figure 2.11, **69-71**).

Application of these compounds in palladium-catalyzed allylic substitution on 1,3-diphenylprop-2-enyl acetate gave nearly absolute enantiomeric excess (98%) and high chemical yield (96%). Commercial chiral amines found as well there application in the synthesis of chiral amino thiols. Wipf⁵² reported chiral amino thiol-catalyzed alkenylzirconium/zinc addition process of alkynes to aldehydes providing (*E*)-allylic alcohols. Knotter's thiol amine⁵³ **72** and it's ethyl derivative **73** (with increased steric bulk at the benzylic position) showed excellent enantioselectivities of

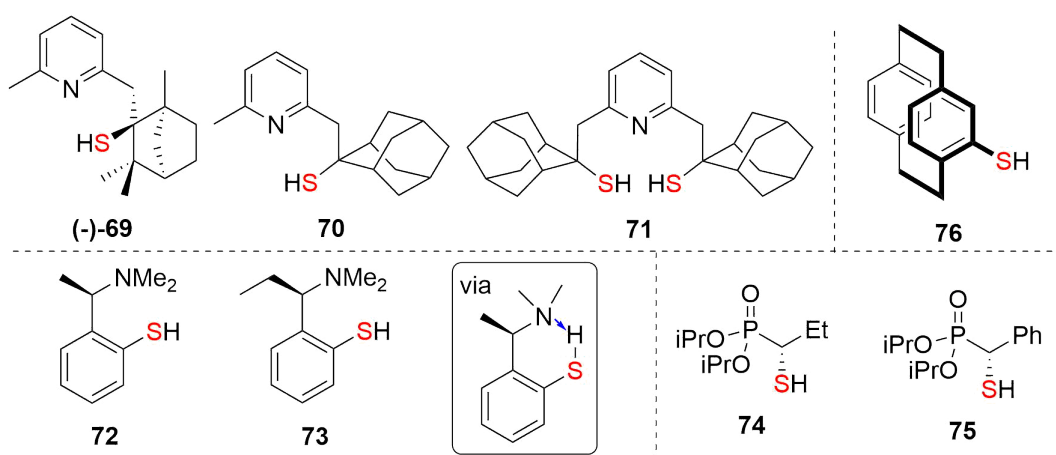


Figure 2.11: Other reported thiols.

89 and 95% ee, respectively (Figure 2.11). One could imagine the hydrogen bonding between the amine and free thiol via a six-member transition state.

Gulea et al⁵⁴ were interested in synthesis and reactivity of organocompounds substituted by both phosphorus and sulfur functional groups. They were able to perform the stereoselective transformation of chiral α -hydroxyphosphonates easily obtained with high enantiomeric excess (ee 93–97%) by hydrolase-catalysed resolutions into α -sulfanylphosphonates **74**, **75** and the corresponding methyl sulfides (Figure 2.11).

Rowlands and Seacome⁵⁵ reported the enantiospecific synthesis of [2.2]paracyclophane-4-thiol **76** and its derivatives. [2.2]Paracyclophane is a fascinating molecule with unique structure and properties. The strong repulsion between the two decks results in distortion of the aryl rings to give a shallow ‘boat’-like conformation. It also engenders a strong π interaction between the rings that leads to a unique extended π -system. Both, its distinct electronic structure and the distortion of the rings increases the basicity/nucleophilicity of [2.2]paracyclophane; it undergoes electrophilic substitution more rapidly than simple aryl systems and has an enhanced ability to form π -complexes.⁵⁶

Monaco et al⁵⁷ described a novel organocascade that is catalyzed by a confined chiral phosphoric acid and furnishes *O*-protected β -hydroxythiols with excellent enantioselectivities (Figure 2.12, **77-84**). The method relies on an asymmetric thiocarboxylation of meso-epoxides, followed by an intramolecular trans-esterification reaction. By varying the reaction conditions, the intermediate thioesters can also be obtained chemoselectively and enantioselectively.

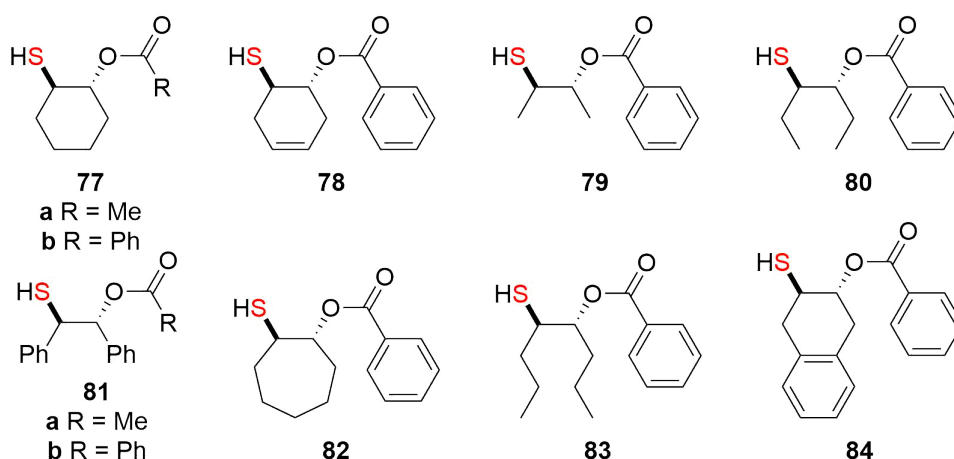


Figure 2.12: Chiral thiols reported by Monaco.⁵⁷

An interesting class of compounds containing chiral information is represented by the carbohydrates. A number of homochiral thiols (**85-92**) were investigated in thiol-catalysed radical-chain additions of triphenylsilane and of tris(trimethylsilyl)silane to a number of cyclic prochiral terminal alkenes.⁵⁸ High enantiomeric excesses were achieved using the tetra-*O*-acetyl derivatives of 1-thio- α -D-glucopyranose and 1-thio- α -D-mannopyranose (Figure 2.13, **85** and **90**). The potential of the method was clearly proven and future development were focused on the design of new thiol catalysts which are capable of reacting with higher enantioselectivity.⁵⁸

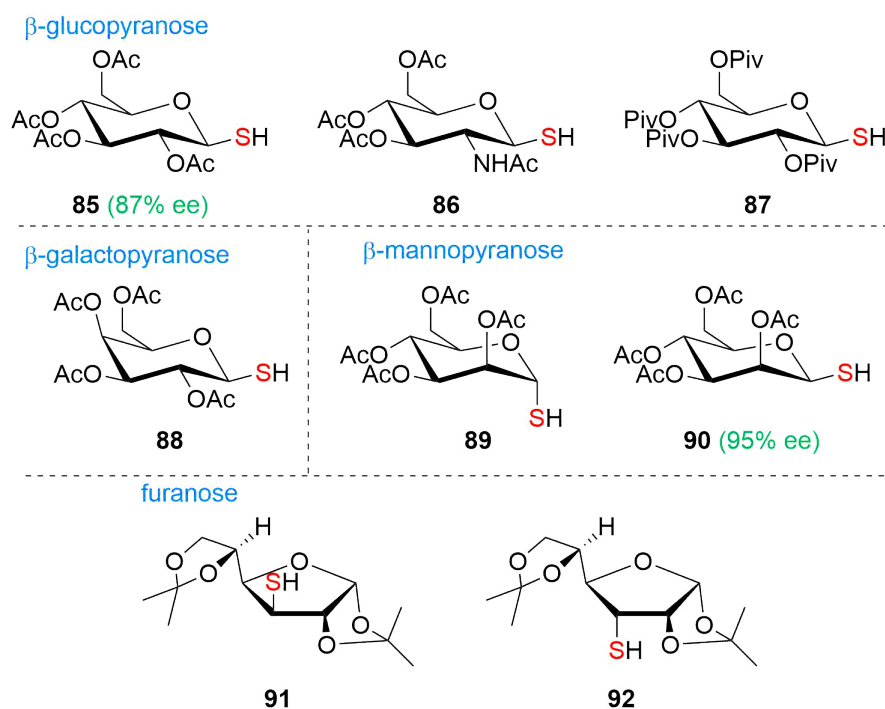


Figure 2.13: 1st Generation of carbohydrate-derived thiols.⁵⁸

Later the same group reported the second generation of carbohydrate-derived thiols.⁵⁹ A variety of novel homochiral carbohydrate-derived thiols, in which the SH group is attached to the anomeric carbon atom, have been prepared and characterised (Figure 2.14, **93-97**). These thiols have been evaluated as protic polarity-reversal catalysts, however no significant improvement in enantioselectivity could be achieved over that obtainable using simple tetra-*O*-acetyl- β -glucopyranose **85** and - β -mannopyranose **90** thiols as catalysts. More than that, it was found that the α -anomers (Figure 2.14, **94c** and **94i**) of the pyranose thiols were ineffective at mediating enantioselective hydrogen-atom transfer. The authors concluded that both steric and dipole-dipole interactions between the prochiral carbon-centered radical and the thiol are important in determining enantioselectivity and that these interactions can act in opposition as well as co-operatively. Solvent effects also showed to be important.⁵⁹

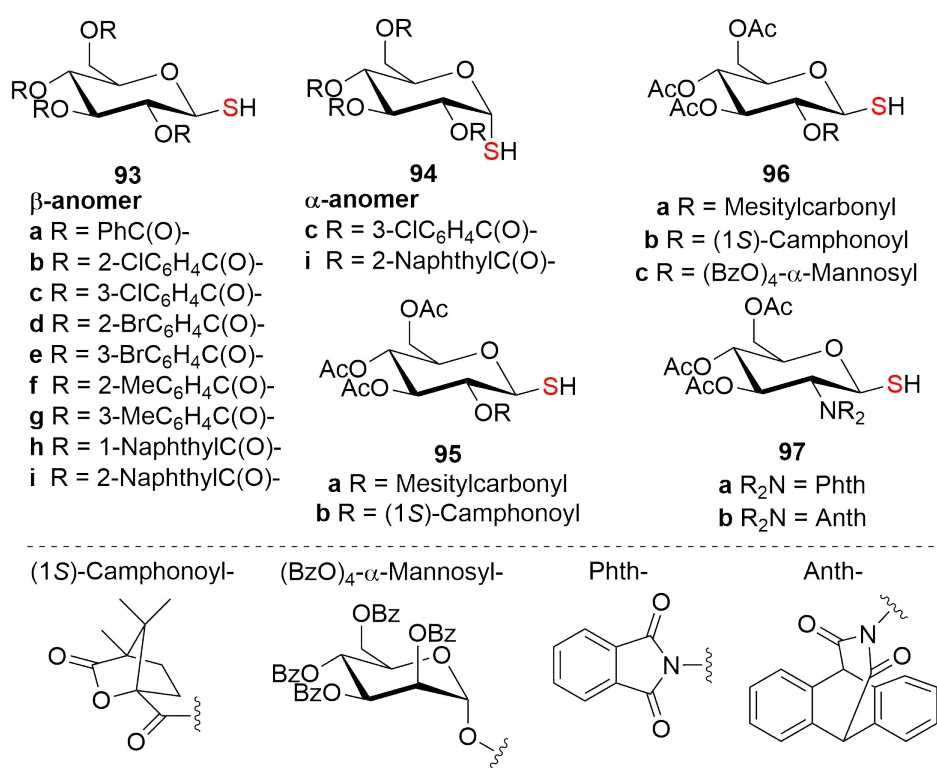


Figure 2.14: 2nd Generation of carbohydrate-derived thiols.⁵⁹

2.3 Hydropersulfides or "Superthiols" Concept

Persulfides, also called hydropersulfides and hydrodisulfides, are compounds with the formula RSSH that are in fast equilibrium with the corresponding ions, RSS⁻, in aqueous solution.⁶⁰ They contain *sulfane sulfur*: sulfur covalently bonded to two sulfur atoms or to a sulfur atom and an ionizable hydrogen. Although the idea that RSSH species can be important biochemical effectors and mediators seems relatively new, it must be emphasized that previous literature published over 50 years ago, reported the existence, activity, and importance of the -SSH functional group along with related polysulfur species in eukaryotic systems.⁶¹

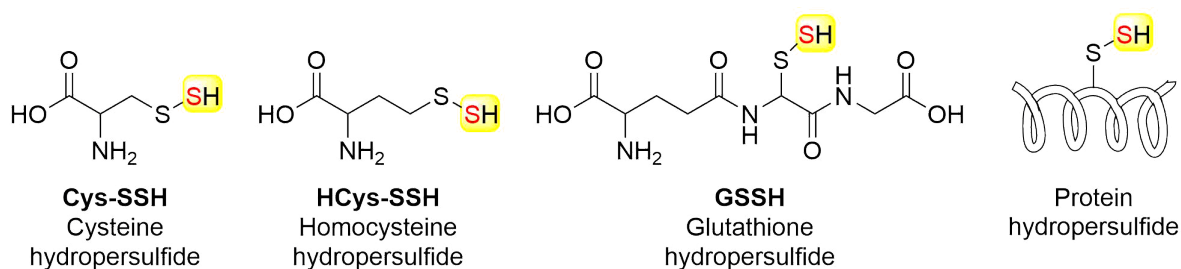


Figure 2.15: Structures of biologically prevalent hydropersulfides.

Considerable interest in hydropersulfides (RSSH) has emerged in recent years owing to their identification at significant levels in mammalian cells, tissues, and plasma.^{61–63} For instance, Cys-SSH and Cys-SSH derived hydropersulfides have been identified in a variety of cell types, including human lung adenocarcinoma A549 cells, neuroblastoma SH-SY5Y cells, cervical cancer HeLa cells, embryonic kidney HEK293 cells, bronchial epithelial cells, and others.⁶⁴ Glutathione hydropersulfide (GSSH) and homocysteine hydropersulfide (HCys-SSH) are observed in mice organs.⁶⁵ The above mentioned hydropersulfides - Cys-SSH, GSSH, HCys-SSH - are found to be superior nucleophiles, playing an important role in regulating electrophilic cell signaling and in redox modulatory effects.⁶⁶

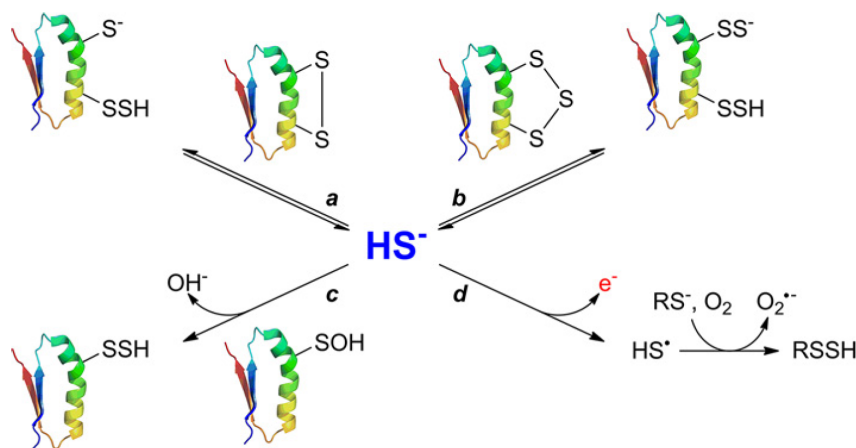


Figure 2.16: Pathways of persulfide formation in biological context that are dependent on H₂S.

The formation of persulfides can occur in biological contexts through several pathways. Some use H₂S and others use different sulfur-containing compounds as source of sulfane sulfur. The main H₂S-dependent pathways are: (I) the reaction of H₂S with disulfides (RSSR) and sulfenic acids (RSOH), which are oxidation products of thiols (RSH) (Figure 2.16, path *a,c*); and (II) the reaction of thiols with products of H₂S oxidation, such as polysulfides, or mediated by free radicals (Figure 2.16, path *b,d*). Importantly, thiols do not react with H₂S.⁶⁰

Persulfides have a very rich chemistry that is still under investigation.⁶⁰ Hydropersulfides are superior to thiols as nucleophiles, more potent reductants, and more acidic (Figure 2.17). It has been proposed that RSSH is equivalent to a chemically hyperactivated RSH which led to the idea that:

“anything a thiol can do, a hydropersulfide can do better”.⁶⁷

One important distinction between thiols and hydropersulfides is the fact that thiols can be nucleophilic while hydropersulfides can be either nucleophilic or electrophilic depending on the protonation state. A persulfide anion (RSS⁻) is extremely nucleophilic while the protonated RSSH species is electrophilic. Thus, hydropersulfides have the properties of both thiols and disulfides.

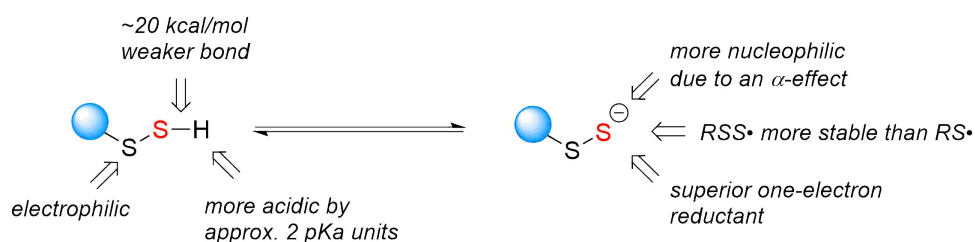


Figure 2.17: Comparative properties of RSSH vs. RSH.

Thiyl radicals (RS•) are used biologically as potent oxidants capable of, for example, breaking a C-H bond via hydrogen atom abstraction^{68,69} and thus initiating radical chemistry. The fact that RS• is a potent one-electron oxidant, indicates its relatively poor ability to serve as a reductant. On the other hand, perthiyl radicals (RSS•) are relatively weak oxidants and are easily formed from one-electron oxidation of RSSH/RSS⁻ (due to the stability of the oxidized RSS• species) (Figure 2.17). The stability of RSS• is similar to the stabilization of analogous nitroxide systems (R₂NO•). In both cases, the stability of the unpaired electron is presumable due to an overlap of the orbital containing the unpaired electron with the adjacent orbital containing a lone pair of electrons.⁷⁰⁻⁷²

The HAT chemistry of hydropersulfides and the stability of the perthiyl radical (RSS•) was intensely investigated by the group of Pratt.^{71,73} Computational studies suggested that the RSS-H bond dissociation energy (BDE) is similar to the RSO-H BDEs in sulfenic acids (~70 kcal/mol) (Figure 2.18). Bond dissociation energy for RS-H is ~89 kcal/mol.^{60,73} Consistent with their weak S-H bond, hydropersulfides were also found to undergo very rapid HAT reactions with

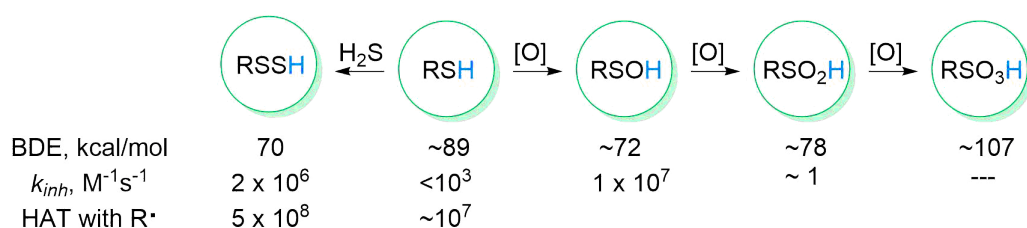


Figure 2.18: Relevant data for some interrelated organosulfur compounds.

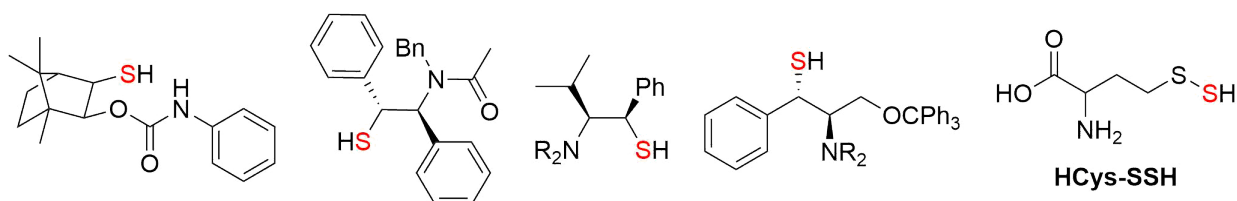
alkyl ($\sim 5 \times 10^8 M^{-1} s^{-1}$), alkoxy ($\sim 1 \times 10^9 M^{-1} s^{-1}$), and thiyl ($> 1 \times 10^{10} M^{-1} s^{-1}$) radicals, acting as “*superthiols*” of sorts.⁷¹ Predicted once again to be enabled by secondary orbital interactions, hydroperulfides react quickly with peroxy radicals with inhibition rate constant $k_{inh} = 2 \times 10^6 M^{-1} s^{-1}$ (Figure 2.18). Most importantly, because hydroperulfides (like thiols) are very weak H-bond donors, their HAT kinetics are not significantly diminished in strong H-bond accepting solvents/media.⁷³ The very weak H-bond donating character of the hydroperulfides make them excellent H-atom donors in good H-bonding media, such as water and its interfacial region with lipid bilayers. The radical-trapping antioxidant (RTA) reactivity of hydroperulfides translates well from organic solutions to aqueous media, and is pH dependent (k_{inh} reaching a maximum of $\sim 5 \times 10^6 M^{-1} s^{-1}$ above pH ~ 8).⁷³ However, due to their instability, the efficacy of the hydroperulfides as RTAs in aqueous solution is limited. A self-reaction between hydroperulfides and water can occur, delivering a mixture of polysulfides and thiols. The stoichiometry of the radical-trapping reaction is significantly less than 1 and decreases with increasing pH owing to competing decomposition of the hydroperulfide to non-RTA products. Transient formation of hydroperulfides where they are stable - in the lipid bilayer - may minimize their decomposition and maximize their efficacy.^{71,73}

Li and co-workers⁷⁴ reported the use of “hydroperulfides” concept on the hydroarylation of alkenes *via* polysulfide anion photocatalysis. This is the single application of hydroperulfides in functionalization of alkenes (*discussed in Chapter 1*).

2.4 Conclusion

Organosulfur compounds play an important role in many biological functions and structures, as well as in organic synthesis. They showed a wide range of applicability in asymmetric synthesis as ligands, chiral auxiliaries or co-catalysts, despite their specific smell. They are stable compounds (except those prone to dimerization), easy to handle and relatively easy to prepare from commercially available nonracemic compounds, like amino acids or terpenes.

Chiral thiols containing hetero atoms in the structure would be of interest in the asymmetric synthesis due to the ability of making hydrogen bonding with the substrate.



Hydropersulfides are as well of interest in the hydroalkylation reaction due to their higher potential in the Hydrogen Atom Transfer to an alkyl radical, comparable to the thiols. Studies in this direction could be performed.

References

- (1) Brosnan, J. T.; Brosnan, M. E. *The Journal of Nutrition* **2006**, *136*, 1636S–1640S.
- (2) Moe, L. A. *American Journal of Botany* **2013**, *100*, 1692–1705.
- (3) Pfaff, A. R.; Beltz, J.; King, E.; Ercal, N. *Mini-Reviews in Medicinal Chemistry* **2020**, *20*, 513–529.
- (4) Schaumann, E. In *Sulfur-Mediated Rearrangements I*, Schaumann, E., Ed., Series Title: Topics in Current Chemistry; Springer Berlin Heidelberg: Berlin, Heidelberg, 2007; Vol. 274, pp 1–34.
- (5) Mikolajczyk, M.; Drabowicz, J. In *Topics in Stereochemistry*, 1982; Vol. 13, pp 333–470.
- (6) Nishide, K.; Ohsugi, S.-i.; Miyamoto, T.; Kumar, K.; Node, M. *Monatshefte für Chemie / Chemical Monthly* **2004**, *135*, 189–200.
- (7) Mellah, M.; Voituriez, A.; Schulz, E. *Chemical Reviews* **2007**, *107*, 5133–5209.
- (8) Procter, D. J. *Journal of the Chemical Society, Perkin Transactions 1* **2001**, 335–354.
- (9) Toru, T.; Carsten, B., *Organosulfur chemistry in asymmetric synthesis*; John Wiley & Sons: 2008.
- (10) Beretta, E.; Cinquini, M.; Colonna, S.; Fornasier, R. *Synthesis* **1974**, 425–426.
- (11) Nam, J.; Lee, S.-k.; Kim, K. Y.; Park, Y. S. *Tetrahedron Letters* **2002**, 3.
- (12) Palomo, C.; Oiarbide, M.; Dias, F.; López, R.; Linden, A. *Angewandte Chemie International Edition* **2004**, *43*, 3307–3310.
- (13) Ikegai, K.; Pluempunapat, W.; Mukaiyama, T. *Chemistry Letters* **2005**, *34*, 638–639.
- (14) Clayden, J.; MacLellan, P. *Beilstein Journal of Organic Chemistry* **2011**, *7*, 582–595.
- (15) MacLellan, P.; Clayden, J. *Chemical Communications* **2011**, 47, 3395.
- (16) Pulis, A. P.; Varela, A.; Citti, C.; Songara, P.; Leonori, D.; Aggarwal, V. K. *Angewandte Chemie International Edition* **2017**, *56*, 10835–10839.
- (17) Node, M.; Nishide, K.; Shigeta, Y.; Shiraki, H.; Obata, K. *Journal of the American Chemical Society* **2000**, 1927–1936.
- (18) Shiraki, H.; Nishide, K.; Node, M. *Tetrahedron Letters* **2000**, *41*, 3437–3441.
- (19) Nishide, K.; Ohsugi, S.-i.; Shiraki, H.; Tamakita, H.; Node, M. *Organic Letters* **2001**, *3*, 3121–3124.
- (20) Koga, K.; Sasaki, S. *HETEROCYCLES* **1979**, *12*, 1305.
- (21) Sasaki, S.; Kawasaki, M.; Koga, K. *Chemical & Pharmaceutical Bulletin* **1985**, *33*, 4247–4266.
- (22) Younai, A.; Fettingner, J. C.; Shaw, J. T. *Tetrahedron* **2012**, *68*, 4320–4327.
- (23) Seebach, D.; Naef, R.; Calderari, G. *Tetrahedron* **1984**, *40*, 1313–1324.

- (24) Strijtveen, B.; Kellogg, R. M. *The Journal of Organic Chemistry* **1986**, *51*, 3664–3671.
- (25) Végh, D.; Uher, M.; Rajniaková, O.; Dandárová, M.; Kováč, M. *Collection of Czechoslovak Chemical Communications* **1993**, *58*, 404–408.
- (26) McCarthy, M.; Guiry, P. J. *Tetrahedron* **2001**, *57*, 3809–3844.
- (27) Fabbri, D.; Pulacchini, S.; Gladiali, S. *Synlett* **1996**, 1054–1056.
- (28) Smrčina, M.; Vyskočil, Š.; Polívková, J.; Poláková, J.; Sejbal, J.; Hanus, V.; Polášek, M.; Verrier, H.; Kočovský, P. *Tetrahedron: Asymmetry* **1997**, *8*, 537–546.
- (29) Hung, S.-M.; Lee, D.-S.; Yang, T.-K. *Tetrahedron: Asymmetry* **1990**, *1*, 873–876.
- (30) Lee, D.-S.; Hung, S.-M.; Lai, M.-C.; Chu, H.-Y.; Yang, T.-K. *Organic Preparations and Procedures International* **1993**, *25*, 673–679.
- (31) Yang, T.-K.; Chen, R.-Y.; Lee, D.-S.; Peng, W.-S.; Jiang, Y.-Z.; Mi, A.-Q.; Jong, T.-T. *The Journal of Organic Chemistry* **1994**, *59*, 914–921.
- (32) Montenegro, E.; Echarri, R.; Claver, C.; Castillon, S.; Pericas, M. A.; Riera, A. *Tetrahedron: Asymmetry* **1996**, *7*, 3553–3558.
- (33) Balsells, J.; Moyano, A.; Pericàs, M. A.; Riera, A. *Tetrahedron: Asymmetry* **1997**, *8*, 1575–1580.
- (34) Fiaud, J.-C.; Mazé, F.; Kagan, H. B. *Tetrahedron: Asymmetry* **1998**, *9*, 3647–3655.
- (35) Wu, H.-L.; Wu, P.-Y.; Cheng, Y.-N.; Uang, B.-J. *Tetrahedron* **2016**, *72*, 2656–2665.
- (36) Nishida, M.; Nakaoka, K.; Ono, S.; Yonemitsu, O.; Nishida, A.; Kawahara, N.; Takayanagi, H. *The Journal of Organic Chemistry* **1993**, *58*, 5870–5872.
- (37) Nakano, T.; Shikisai, Y.; Okamoto, Y. *Polymer Journal* **1996**, *28*, 51–60.
- (38) Hulst, R.; Heres, H.; Fitzpatrick, K.; Peper, N. C.; Kellogg, R. M. *Tetrahedron: Asymmetry* **1996**, *7*, 2755–2760.
- (39) Kellogg, R. M.; Hof, R. P. *Journal of the Chemical Society, Perkin Transactions 1* **1996**, 1651–1657.
- (40) Hulst, R.; Heres, H.; Peper, N. C.; Kellogg, R. M. *Tetrahedron: Asymmetry* **1996**, *7*, 1373–1384.
- (41) Kossenjans, M.; Soeberdt, M.; Wallbaum, S.; Harms, K.; Martens, J.; Aurich, H. G. *Journal of the Chemical Society, Perkin Transactions 1* **1999**, 2353–2365.
- (42) Hsu, J.-L.; Fang, J.-M. *The Journal of Organic Chemistry* **2001**, *66*, 8573–8584.
- (43) Fanjul, S.; Hulme, A. N.; White, J. W. *Organic Letters* **2006**, *8*, 4219–4222.
- (44) Crana, G. A.; Gibson, C. L. *Tetrahedron: Asymmetry* **1995**, *6*, 1553–1556.
- (45) Anderson, J. C.; Cubbon, R.; Harding, M.; James, D. S. *Tetrahedron: Asymmetry* **1998**, *9*, 3461–3490.
- (46) Tseng, S.-L.; Yang, T.-K. *Tetrahedron: Asymmetry* **2004**, *15*, 3375–3380.

- (47) Tseng, S.-L.; Yang, T.-K. *Tetrahedron: Asymmetry* **2005**, *16*, 773–782.
- (48) Wipf, P.; Jayasuriya, N. *Chirality* **2008**, *20*, 425–430.
- (49) Subirats, S.; Jimeno, C.; Pericàs, M. A. *Tetrahedron: Asymmetry* **2009**, *20*, 1413–1418.
- (50) Jimeno, C.; Pastó, M.; Riera, A.; Pericàs, M. A. *The Journal of Organic Chemistry* **2003**, *68*, 3130–3138.
- (51) Koning, B.; Meetsma, A.; Kellogg, R. M. *The Journal of Organic Chemistry* **1998**, *63*, 5533–5540.
- (52) Wipf, P.; Ribe, S. *The Journal of Organic Chemistry* **1998**, *63*, 6454–6455.
- (53) Knotter, D. M.; Van Maanen, H. L.; Grove, D. M.; Spek, A. L.; Van Koten, G. *Inorganic Chemistry* **1991**, *30*, 3309–3317.
- (54) Gulea, M.; Masson, S. In *New Aspects in Phosphorus Chemistry III*, Series Title: Topics in Current Chemistry; Springer Berlin Heidelberg: Berlin, Heidelberg, 2003; Vol. 229, pp 161–198.
- (55) Rowlands, G. J.; Seacome, R. J. *Beilstein Journal of Organic Chemistry* **2009**, *5*, DOI: 10.3762/bjoc.5.9.
- (56) Rowlands, G. J. *Organic & Biomolecular Chemistry* **2008**, *6*, 1527.
- (57) Monaco, M. R.; Prévost, S.; List, B. *Journal of the American Chemical Society* **2014**, *136*, 16982–16985.
- (58) Haque, M. B.; Roberts, B. P.; Tocher, D. A. *Journal of the Chemical Society, Perkin Transactions 1* **1998**, 2881–2890.
- (59) Cai, Y.; Roberts, B. P.; Tocher, D. A. *J. Chem. Soc., Perkin Trans. 1* **2002**, 1376–1386.
- (60) Benchoam, D.; Cuevasanta, E.; Möller, M. N.; Alvarez, B. *Essays in Biochemistry* **2020**, *64*, 155–168.
- (61) Fukuto, J. M. *Antioxidants & Redox Signaling* **2022**, *36*, 244–255.
- (62) Dóka, É.; Pader, I.; Bíró, A.; Johansson, K.; Cheng, Q.; Ballagó, K.; Prigge, J. R.; Pastor-Flores, D.; Dick, T. P.; Schmidt, E. E.; Arnér, E. S. J.; Nagy, P. *Science Advances* **2016**, *2*, e1500968.
- (63) Longen, S.; Richter, F.; Köhler, Y.; Wittig, I.; Beck, K.-F.; Pfeilschifter, J. *Scientific Reports* **2016**, *6*, 29808.
- (64) Khodade, V. S.; Aggarwal, S. C.; Eremiev, A.; Bao, E.; Porche, S.; Toscano, J. P. *Antioxidants & Redox Signaling* **2022**, *36*, 309–326.
- (65) Ida, T. et al. *Proceedings of the National Academy of Sciences* **2014**, *111*, 7606–7611.
- (66) Anglada, J. M.; Crehuet, R.; Adhikari, S.; Francisco, J. S.; Xia, Y. *Physical Chemistry Chemical Physics* **2018**, *20*, 4793–4804.
- (67) Ono, K.; Akaike, T.; Sawa, T.; Kumagai, Y.; Wink, D. A.; Tantillo, D. J.; Hobbs, A. J.; Nagy, P.; Xian, M.; Lin, J.; Fukuto, J. M. *Free Radical Biology and Medicine* **2014**, *77*, 82–94.

- (68) Dénès, F.; Pichowicz, M.; Povie, G.; Renaud, P. *Chemical Reviews* **2014**, *114*, 2587–2693.
- (69) Soulard, V.; Villa, G.; Vollmar, D. P.; Renaud, P. *Journal of the American Chemical Society* **2018**, *140*, 155–158.
- (70) Bianco, C. L.; Chavez, T. A.; Sosa, V.; Saund S., S.; Nguyen, Q. N. N.; Tantillo, D. J.; Ichimura, A. S.; Toscano, J. P.; Fukuto, J. M. *Free Radical Biology and Medicine* **2016**, *101*, 20–31.
- (71) Chauvin, J.-P. R.; Griesser, M.; Pratt, D. A. *Journal of the American Chemical Society* **2017**, *139*, 6484–6493.
- (72) Fukuto, J. M.; Ignarro, L. J.; Nagy, P.; Wink, D. A.; Kevil, C. G.; Feelisch, M.; Cortese-Krott, M. M.; Bianco, C. L.; Kumagai, Y.; Hobbs, A. J.; Lin, J.; Ida, T.; Akaike, T. *FEBS Letters* **2018**, *592*, 2140–2152.
- (73) Poon, J.-F.; Pratt, D. A. *Accounts of Chemical Research* **2018**, *51*, 1996–2005.
- (74) Li, H.; Liu, Y.; Chiba, S. *Chemical Communications* **2021**, *57*, 6264–6267.

3 Thiol Catalysed Enantioselective Hydroalkylation

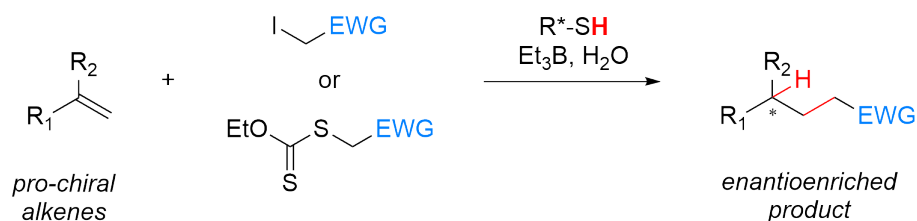
*This chapter includes the **Draft manuscript** on "Thiol catalyzed hydroalkylation of alkenes". This project was started by Dr. V. Soulard, together with the help of Dr. M. Meyer Mojzes. The synthesis of prochiral alkenes and the first attempts to extend the reaction of hydroalkylation through an enantioselective manner were performed. M. Hofstetter and D. Capeder put also an effort for the synthesis of chiral thiols (sugar and TADDOL derivatives) during their bachelor thesis under the supervision of Dr. V. Soulard. J. Heinrich (under the supervision of Dr. Q. Huang) expanded the scope during his master thesis, by using peptide thiols as chiral source and oxazolidinone derivatives as prochiral alkenes. Their contribution is gratefully acknowledged and some of their results are included in this draft.*

The Cysteine-derived peptides were received through the collaboration with Prof. Scott Miller. J. Ryss and S. Mason were involved in preparation and delivery of peptides (as disulfides or in protected form).

Personal contribution includes: the comparison between xanthates and iodides as alkylating agents, expansion of the substrate scope (racemic and enantioselective), screening of chiral thiol, derivatization and preparation of the single crystal for X-ray structure confirmation on the dimethyl-oxazolidinone derivative, update and completion of the draft, as well as combining and preparing the experimental part.

Abstract

The enantioselective hydroalkylation of prochiral alkenes catalyzed by chiral thiols was investigated. This transition metal-free process is a cheap, easy and an eco-friendly way to achieve this transformation under mild conditions. The scope of the reaction is compatible with cyclic alkenes. Iodides and xanthates were used as alkylating agents. Highly enantioselective results (up to 92:8 *er*) were obtained by using cysteine-derived tetrapeptides as catalysts.



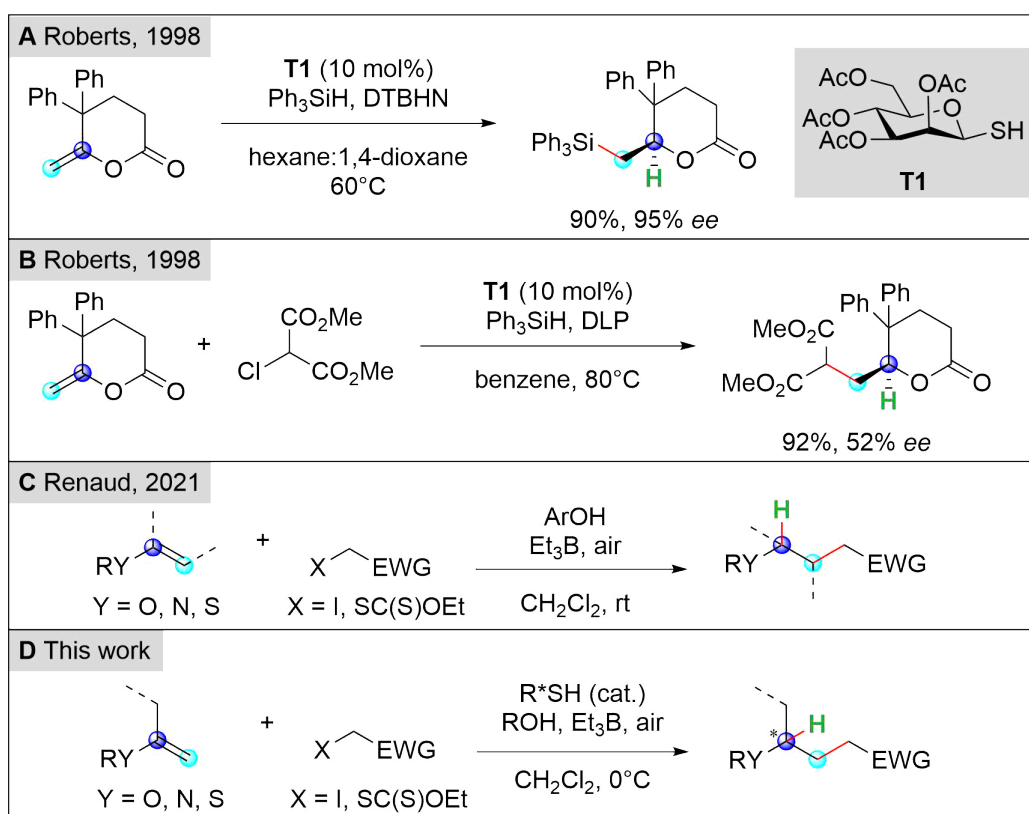
Key words

enantioselective hydroalkylation, chiral thiol, cysteine-tetrapeptide, triethylborane

3.1 Introduction

Synthetic building blocks, natural products and drug candidates^{1,2} that contain electron rich olefinic moieties are very common. Their hydroalkylation represent a very attractive process than can lead to target-oriented synthesis and late stage modification of biologically relevant compounds.³⁻⁵ This reaction has attracted the interest of synthetic chemists for a long time. Transition metal catalyzed processes such as the hydroformylation reaction^{6,7} have been developed with great success leading to powerful industrial applications. Recently, highly efficient radical mediated processes have been developed leading hydroalkylation with Markovnikov^{8,9} and anti-Markovnikov^{10,11} type of regioselectivity.

Electron rich alkenes are known to react efficiently with radicals possessing an electrophilic, such as malonyl and perfluoroalkyl radicals, or at least an ambiphilic, such as α -ester radicals, character. This reactivity has been used by Giese to develop their tin-mediated hydroalkylation with Markovnikov regioselectivity.¹² However, this approach is very limited due to the efficient competitive hydrogen atom transfer process taking place between tin hydride and the electrophilic radicals. Roberts¹³⁻¹⁵ has pioneered the thiol mediated hydroalkylation of alkenes. Initial attempts performed on the intermolecular hydrosilylation catalysed by thiol, high yields and selectivities were obtained (Scheme 3.1, **A**).



Scheme 3.1: Radical mediated hydroalkylation of electron rich alkenes.

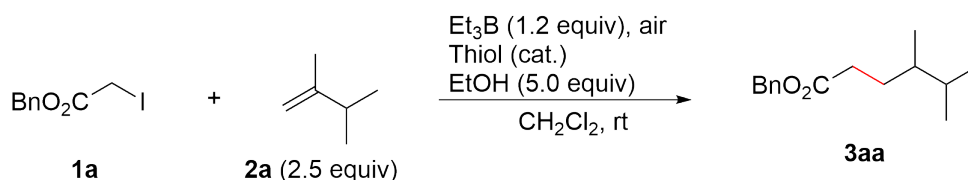
By performing the hydroalkylation of terminal alkene, using the same carbohydrate-derived chiral thiol, high yields were obtained, however moderate enantiomeric excess (Scheme 3.1, **B**).

More recently, this chemistry was revisited and several thiol mediated processes have been developed using mainly photoredox catalyzed reactions.^{16–24} Other processes using diverse C–H hydrogen atom donors^{25,26} such as THF and other solvents^{27–30} have also been reported. Recently, we developed a highly efficient radical chain process mediated by triethylborane/catechol for the hydroalkylation of alkenes, enol esters, enol (thio)ethers, silyl enol ethers, enamides and enecarbamates (Scheme 3.1, **C**).³¹ We have also shown that thiols can be involved as catalysts for triethylborane mediated deiodination reaction.³² In these reactions, best results were obtained with low catalyst loading (1 mol%). In this manuscript, a thiol catalyzed hydroalkylation of electron rich alkenes is described including a promising highly enantioselective version using cystein-containing tetrapeptide catalysts.

3.2 Results and Discussion

3.2.1 Optimization

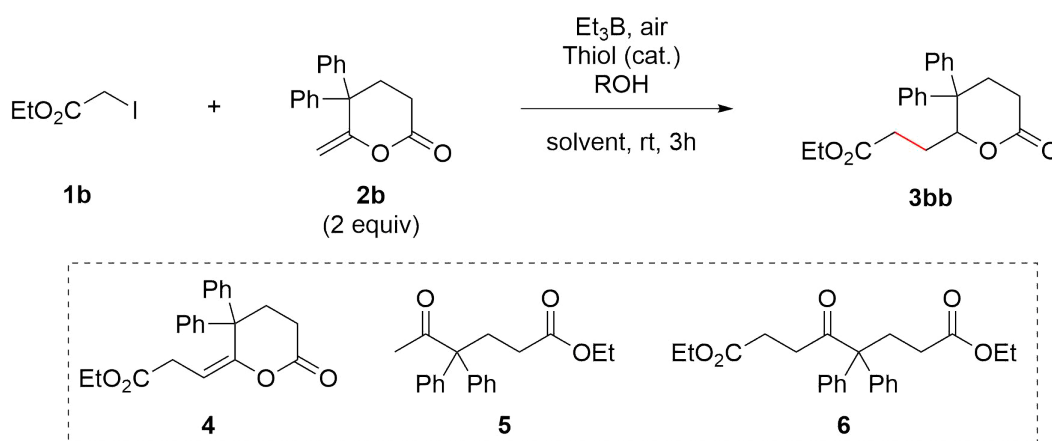
The initial hydroalkylation experiments were run with benzyl iodoacetate **1a** and 2,3-dimethylbut-1-ene **2a** (2.5 equiv) in dichloromethane using variable amount of dodecanethiol as a catalyst and ethanol (5 equiv) as a source of hydrogen atoms (Table 3.1, *entries 1–5*). Within experimental error, no change in yield was observed when lowering the catalyst load from 20% to 2% (Table 3.1, *entries 1–4*). In the absence of catalyst however, the reaction became inefficient, and the product formation (45%) was quantified by gas chromatography, but could not be isolated in pure form (Table 3.1, *entry 5*). Interestingly, thiophenol, 1-butanethiol, isopropanethiol and *tert*-butanethiol (Table 3.1, *entry 6–10*) gave similarly good results. This demonstrates the generality of this approach for a broad range of thiols and therefore opens opportunities to develop an enantioselective reaction based on more complex chiral thiols. Finally, the reaction was also tested using a slight excess of the iodide **1a** (1.2 equiv) and the desired product **3aa** was formed in 79% yield demonstrating that the process can be conducted indifferently with an excess of alkene or iodide (Table 3.1, *entry 11*). Even if 1-dodecanethiol was not the very best catalyst examined during this preliminary optimization process, it was used for most non-enantioselective reactions to limit the inconvenience due to the smell of more volatile thiols. The reaction conditions described in *entry 11* have been used for the scope and limitation study (see below) and is referred as "**conditions A**".



Entry	RSH	Cat. loading	Yield
1	1-dodecanethiol	20 mol%	78%
2	1-dodecanethiol	10 mol%	87%
3	1-dodecanethiol	5 mol%	83%
4	1-dodecanethiol	2 mol%	85%
5	-	-	45% ^a
6	thiophenol	5 mol%	81%
7	thiophenol	2 mol%	92%
8	1-butanethiol	2 mol%	97%
9	2-propanethiol	2 mol%	94%
10	1,1-dimethylethanethiol	2 mol%	76%
11	1-dodecanethiol	2 mol%	79% ^b

Table 3.1: Optimization of the thiol-catalyzed hydroalkylation of alkenes with EtOH as a source of H-atoms. ^a Yield determined by GC. ^b Using 1.2 equiv **1a** and 1.3 equiv Et₃B.

Before examining the substrate scope, the reaction was then tested with the 4,4-diphenyl-5-methylenepentan-2-one lactone **2b** and ethyl iodoacetate **1b**. Under the optimized conditions described below (Table 3.2, *entry 1*), the desired product **3bb** was obtained in low yield ($\leq 10\%$) together with the unsaturated product **4** and the ring-opened ethan-1-olysis products **5** and **6**. Upon previously specified Conditions A, the product was obtained in 47% yield (Table 3.2, *entry 2*). Increasing the amount of iodoester **1b** and of Et₃B, led to an increase of the yield (Table 3.2, *entry 3*). By slightly decreasing the amount of EtOH, the ethan-1-olysis product **5** could be minimized and the desired hydroalkylation product was obtained in 61% yield (*entry 4*). Replacing the EtOH by H₂O allowed to further optimize the reaction by fully suppressing the formation of lactone-opening products (*entry 5*). Finally, replacing CH₂Cl₂ by benzene and using a larger excess of Et₃B had only a marginal effect on the reaction outcome (*entries 6 and 7*). The conditions of *entry 5* were selected and will be referred as "**conditions B**". Finally, the reaction was also repeated using these optimized conditions, but using thiophenol instead of 1-dodecanethiol (*entry 8*) affording the product in 82% yield. These conditions were found to work particularly well and will be referred as "**conditions C**".

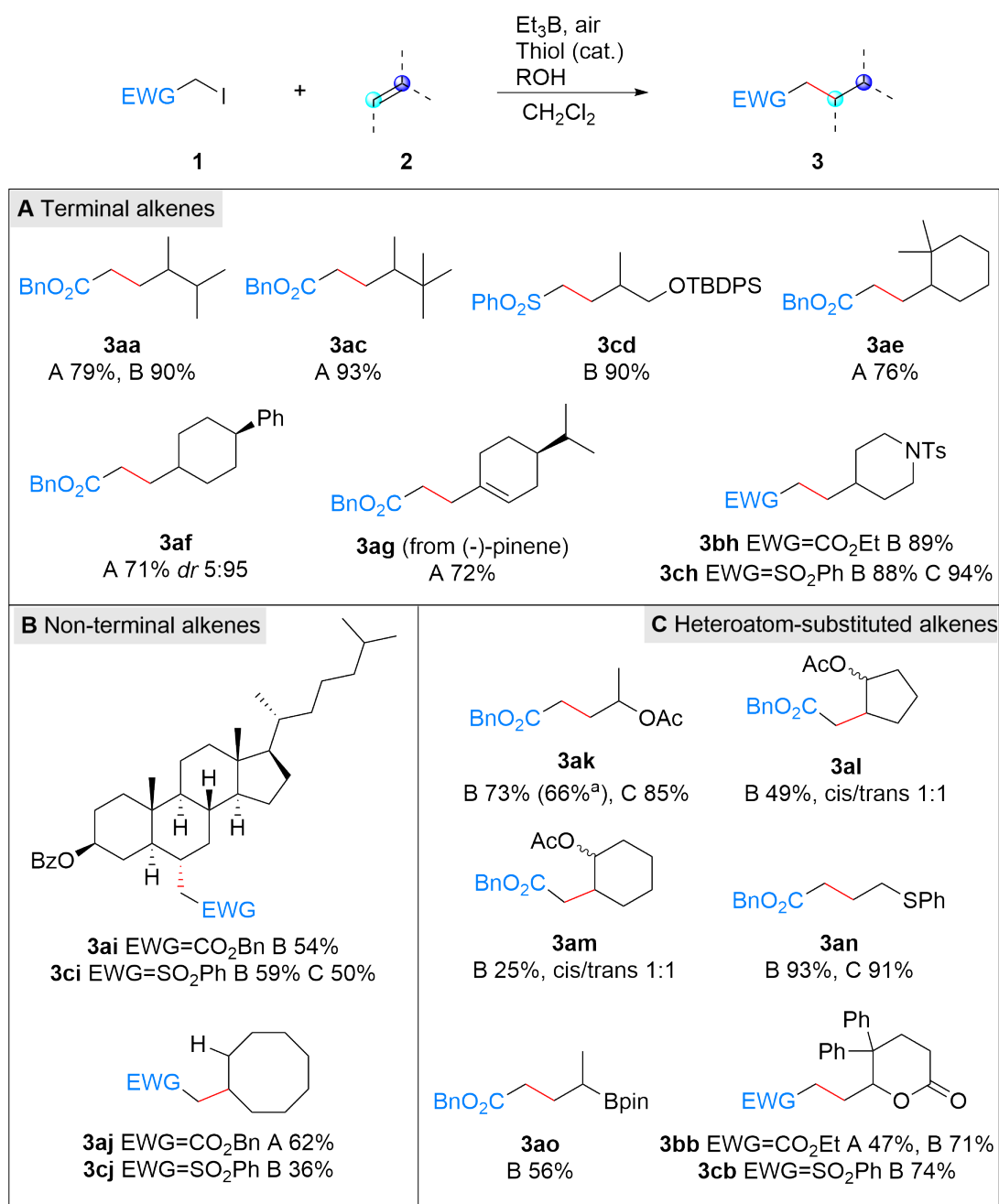


Entry	Equiv 1b	Equiv 2b	Equiv Et ₃ B	Solvent	ROH (equiv)	Yield
1	1	2	1.3	CH ₂ Cl ₂	EtOH (5)	<10%
2	1.2	1	1.3	CH ₂ Cl ₂	EtOH (5)	47%
3	2	1	2.5	CH ₂ Cl ₂	EtOH (5)	54%
4	2	1	2.5	CH ₂ Cl ₂	EtOH (3)	61%
5	2	1	2.5	CH ₂ Cl ₂	H ₂ O (4)	71%
6	2	1	2.5	benzene	H ₂ O (4)	73%
7	2	1	3	benzene	H ₂ O (4)	75%
8	2	1	2.5	CH ₂ Cl ₂	H ₂ O (4)	82% ^a

Table 3.2: Optimization of the hydroalkylation of the 5-methylenepentan-2-one lactone **2b**. ^a Using thiophenol as catalyst.

3.2.2 Scope and limitation

The scope of the thiol catalyzed reaction was then examined with a series of different alkenes under reaction *conditions A–C*. Results are summarized in Scheme 3.2.



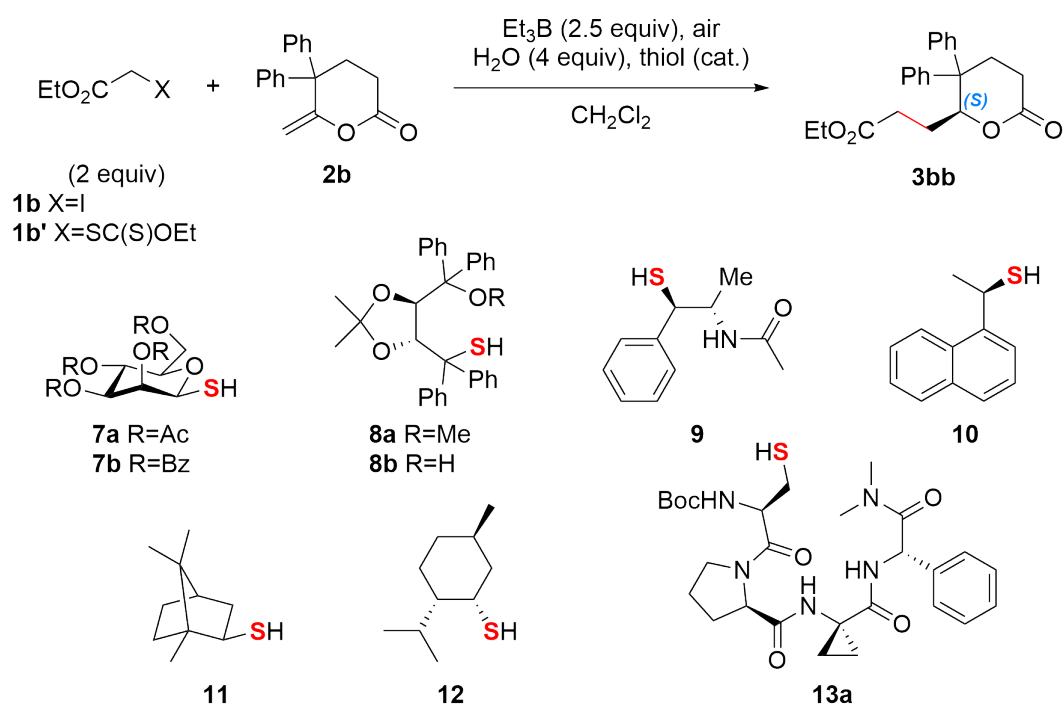
Scheme 3.2: Scope and limitation of thiol catalyzed hydroalkylation process.

Terminal alkenes **2a, c–h** reacted efficiently with the iodoesters **1a/1b** and with the iodosulfone **1c** under all reaction conditions and afforded the expected hydroalkylated products in good yields (Scheme 3.2, **A**). Non-terminal alkenes such as cholesteryl benzoate and cyclooctene were also reacting under these conditions (Scheme 3.2, **B**) although yields are moderate com-

pared to terminal alkenes. Heteroatom-substituted terminal alkenes such as enol esters **1k-m**, enol lactone **1b** and enol thioester **1n** are all reacting efficiently even though the non terminal systems **1l, m** proved again to react less efficiently. Interestingly, all three methods A–C gave good results with most substrates, however the water based methods *B* and *C* are recommended with substrate sensitive to solvolysis. The hydroalkylation leading to **3ak** was scaled up to 10 mmol scale with similar yield despite the fact that only 1.2 equivalents of the iodide was used.

3.2.3 Screening of chiral thiols

Based on these promising results with diverse thiols and the literature precedent by Roberts,¹⁵ Maruoka³³ and Knowles,³⁴ we decided to investigate if this hydroalkylation process could be performed in an enantioselective manner. For this purpose, electron rich alkenes leading to prochiral radical intermediates were tested. Preliminary experiments were made with Robert's lactone **2b** using the iodide **1b** (Scheme 3.3).



Scheme 3.3: Screening of chiral thiols.

The results of chiral thiol screening are summarized in the table below (Table 3.3). With the previously reported chiral thiols **7a** and **7b** good enantioselectivities were obtained (Table 3.3, entry 1-2). With TADDOL derivatives **8a** and **8b** (Table 3.3, entry 7-8), low yields and almost no enantioselectivity were observed. The amide derivative **9** delivered the product in high yield with a moderate selectivity, although modification of such thiol can be performed to reach a

Entry	X	Thiol	T	Yield	E.r.
1	I	7a (5 mol%)	rt	74%	73:27
2	SC(S)OEt	7a (5 mol%)	rt	87%	73:27
3	I	7a (10 mol%)	rt	82%	75:25
4	I	7a (10 mol%)	0 °C	88%	77:23
5	I	7a (10 mol%)	-78 °C	62%	85:15
6	I	7b (10 mol%)	rt	79%	72:28
7	I	8a (5 mol%)	rt	29%	51:49
8	I	8b (5 mol%)	rt	32%	52:48
9	I	9 (5 mol%)	0 °C	79%	70:30
10	I	10 (5 mol%)	0 °C	78%	50:50
11	I	11 (5 mol%)	0 °C	79%	57:43
12	I	12 (5 mol%)	rt	61%	53:47
13	SC(S)OEt	12 (5 mol%)	rt	75%	53:47
14	I	13a (2 mol%)	rt	63%	35:65
15	SC(S)OEt	13a (5 mol%)	rt	81%	35:65
16	SC(S)OEt	13a (2 mol%)	rt	82%	35:65

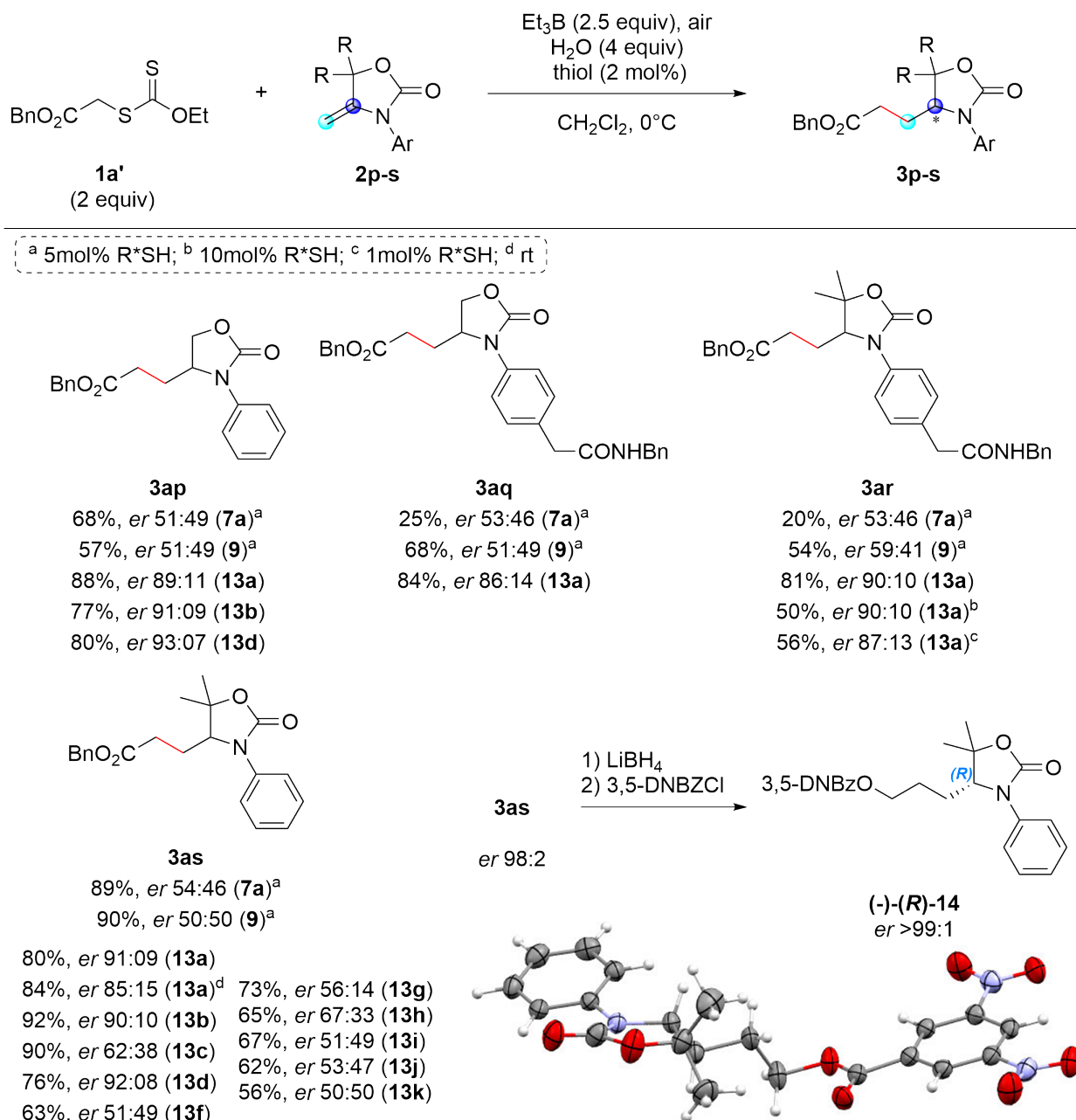
Table 3.3: Screening of chiral thiols.

higher selectivity. Additionally, the alkyl thiols **10-12** (Table 3.3, entry 10-13) afforded the product in good yield but with a poor enantioselectivity. Surprisingly, the cysteine-based peptide **13a** delivered the desired product with an excellent yield (up to 89%) and a moderate er ratio of 35:65 (Table 3.3, entry 14-16). Additionally, comparison between iodinated alkylating agent and the xanthate derivative showed no impact on the enantioselectivity, but a slight improve of yield due to SET disruptive side reactions that might take place between the electron-rich radical from the substrate and the radical precursor (Table 3.3, entry 1, 2, 14, 16).

Later on we applied the reaction conditions on the oxazolidinone derivatives (Scheme 3.3). The 1,3-oxazolidin-2-one scaffold provides an interesting electron density to the cyclic system and gives access to a wide range of chemical modifications making them a desirable substrate with great synthetic purpose. Moreover, this scaffolds were reported to be biologically active, so that they have become key building blocks for drug and antibiotic substances like Tedizolid and Linezolid.³⁵⁻³⁷

Hydroalkylation of oxazolidinone derivatives **2p-s** was performed with xanthate derivative **1a'**. By using Roberts' optimal thiol **7a** under indicated conditions, the desired products was obtained in moderate yield (from 20 to 89%) and low enantioselectivity (*er* up to 54:46) (Scheme 3.4). No improvement was observed by employing the ephedrine derived thiol **9** (*er* up to 59:41). Interestingly, the cysteine derivative **13a** delivered the desired products in high yields (up to

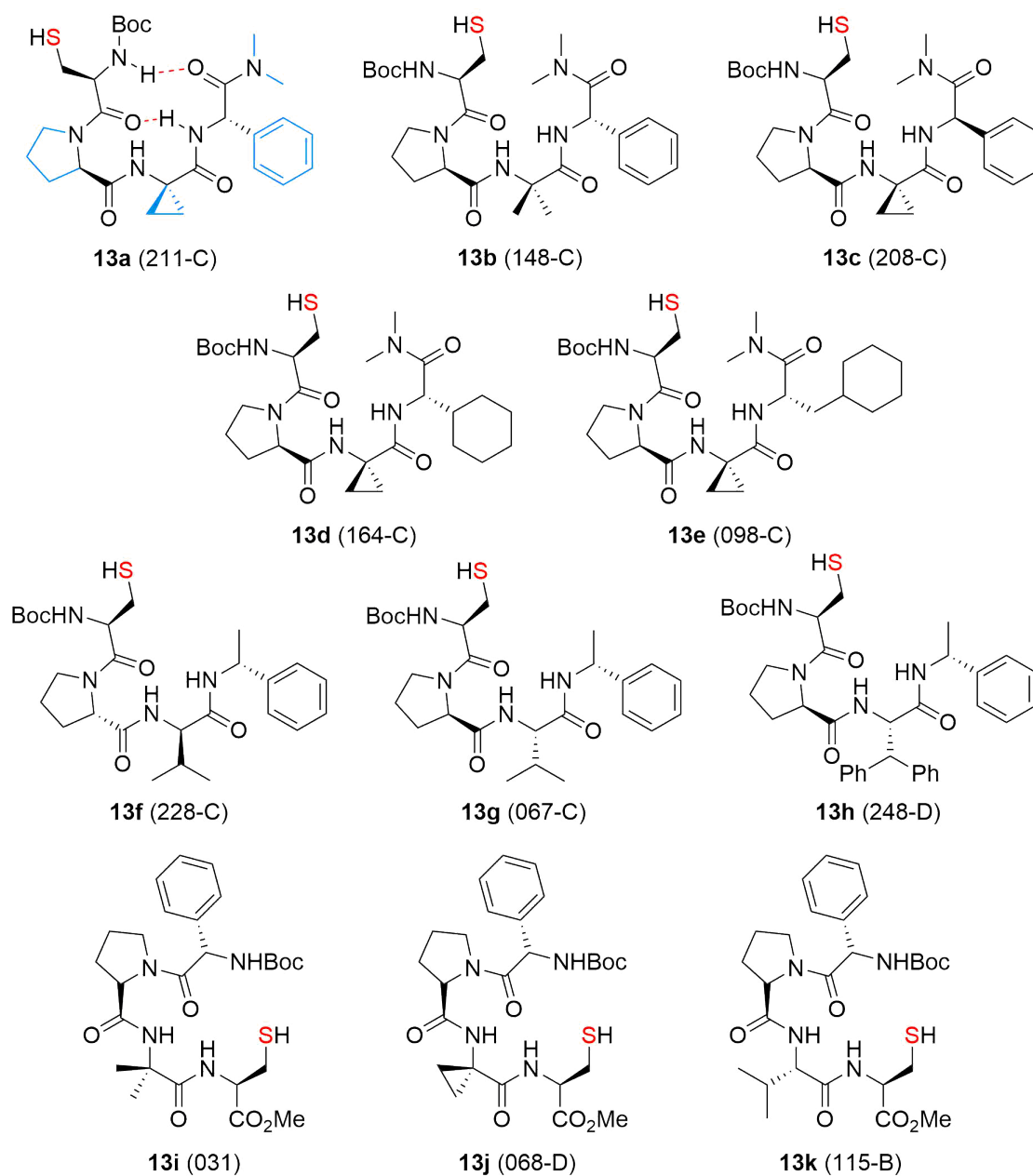
88%) and high selectivity - up to 91:09 (Scheme 3.4). This promising results motivated us to explore the system further.



Scheme 3.4: Hydroalkylation of 1,3-oxazolidin-2-one derivatives.

In a serie of experiments changing the amount of catalyst loading, 2 mol% was identified as optimum. Higher amount of catalyst up to 10 mol% resulted in lowering the yield (from 81% to 50%, for **3ar**), while for 1 mol% of catalyst the maximal enantioselectivity can not be sustained. Performing the reaction at room temperature, decreases slightly the enantiomeric excess (from 91:09 to 85:15, for **3as**) however the reaction yield is not affected.

Next, we turned our attention to explore the tetrapeptide derivatives and the influence on the enantioselectivity of the reaction. Ten other cysteine-derived peptides were prepared in collaboration with S. Miller and tested on the oxazolidinone derivative **2s** (Scheme 3.5). The results are summarized in the Scheme 3.4. High enantioselectivity were observed for analogues of **13a**: **13b** - 92%, *er* 90:10 and **13d** - 76%, *er* 92:08. The enantioenriched sample of **3as** was derivatized to the 3,5-dinitrobenzoic ester **14**. The single crystal X-ray diffraction data analysis showed that the major isomer possesses the (*R*)-conformation. The conformation of **3ap** product needs to be confirmed.

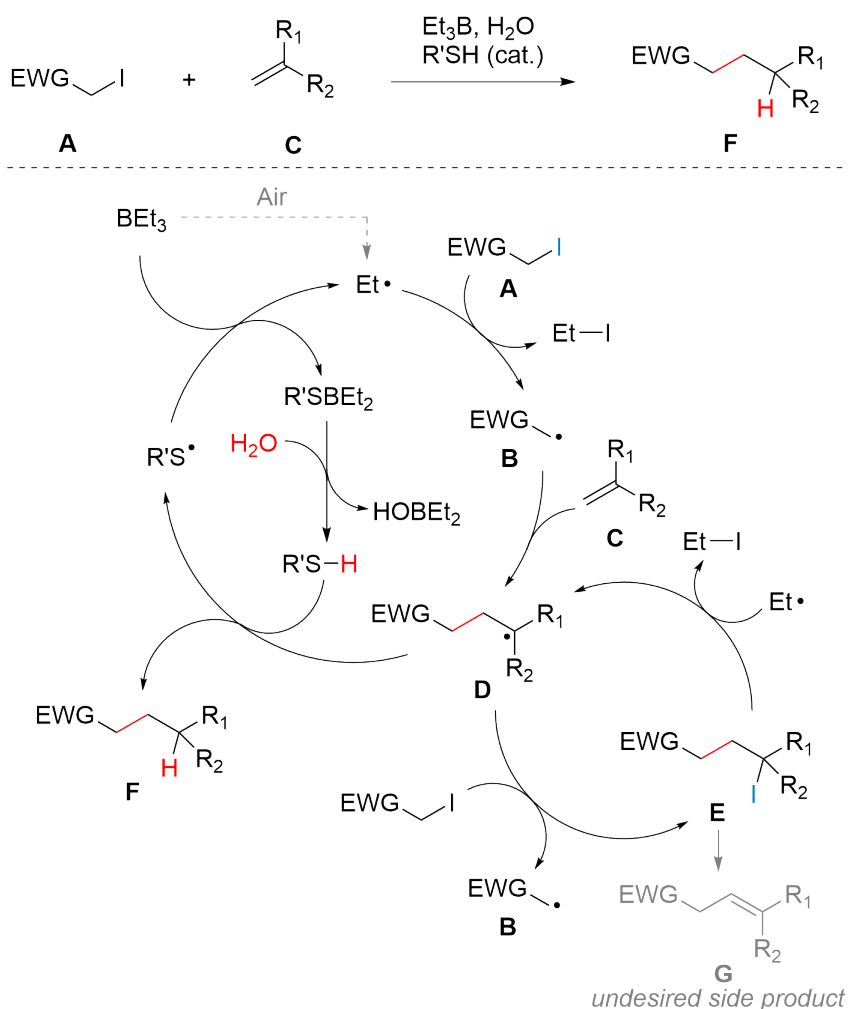


Scheme 3.5: Cysteine-derived peptides.

The tetrapeptide **13a** consists of the sequence Boc-Cys-DPro-Acpc-Phg-NMe₂. This sequence makes the tetrapeptide relatively non-polar and therefore soluble in many solvents, at the same time the aliphatic residues lowers the risk of interfering in the radical process. Proline and Acpc induce a rigid determined conformation. When dissolved in a non-protic solvent of moderate polarity like CH₂Cl₂, the backbone of the tetrapeptide is stabilized through H-bonding in the inside and hydrophobic residues pointing to the outside, forming a loop-like structure, similar to the conformation depicted in Scheme 3.5.³⁸ A prediction model that would explain the selectivity of the reaction is under investigation.

3.2.4 Proposed mechanism

Based on our previous results on deuteration³² and hydroalkylation mediated by triethylborane,³¹ the following mechanism was proposed (Scheme 3.6).



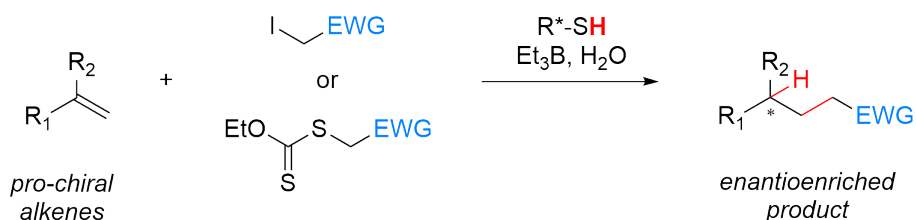
Scheme 3.6: Proposed mechanism for the hydroalkylation catalyzed by thiol.

The radical process is initiated by reaction of the triethylborane and oxygen (air), generating an ethyl radical. Then, the latter one abstracts an iodine atom from the alkyl iodide **A**, leading to the formation of the ethyl iodide as by product and the electron poor radical intermediate **B**. The primary radical **B** adds on the alkene **C**, forming the C-C bond and generating tertiary radical intermediate **D**. In the absence of a reducing agent, the radical intermediate **D** undergoes I-atom transfer with another molecule of the starting iodide **A** to give the corresponding tertiary alkyl iodide **E**. When most of the iodide **A** is consumed, the equilibrium is displaced. The iodide **E** is a precursor in the formation of the unsaturated side product **G**, due to its high unstability. Radical **D** can be regenerated from **E** (by I-atom abstraction by another active ethyl radical) and further be reduced by the thiol to give hydroalkylated product **F** and a thiyl radical. The latter reacts with another molecule of triethylborane to produce an ethyl radical which propagates the chain reaction and the thioborinic ester. Hydrolyzed by water, the thioborinic ester generates the borinic acid and regenerates the thiol.

3.3 Conclusion

The enantioselective hydroalkylation catalysed by cysteine derived peptides is reported. The process can be applied on electron rich prochiral alkenes using iodoalkylating agent or xanthate derivative. This procedure is very attractive being a metal-free and low toxicity process, using water as hydrogen source, offering mild conditions, low energy consumption and minimal waste.

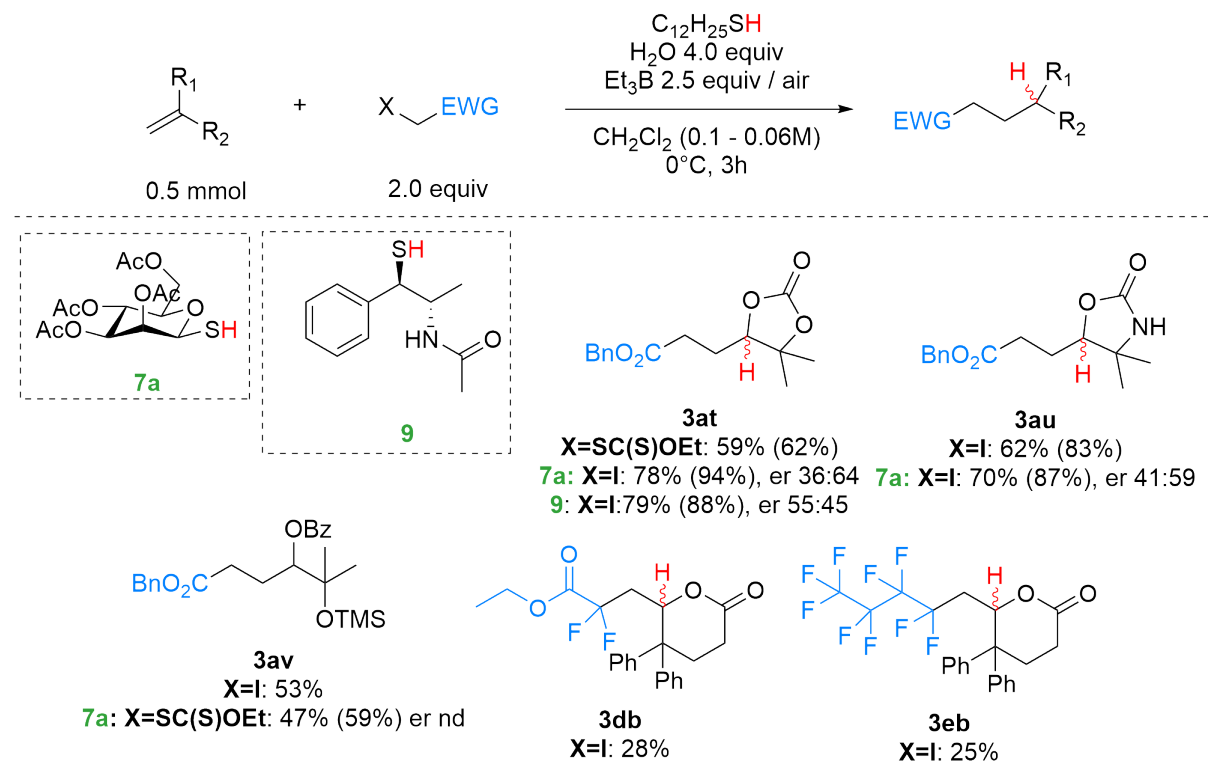
Due to its possibility to functionalize efficiently alkenes, it could be an interesting tool in the late stage functionalization of natural products or drug candidates.



Cysteine derivative tetrapeptides afforded the formation of the desired products in high yields (up to 92%) and high enantioselectivity (up to 92:08). A prediction model that would explain the selectivity of the reaction is under investigation.

3.4 Additional Results and Outlook

An expanded version of the substrate scope is under investigation. Different 5-member ring scaffolds and acyclic alkenes were synthesized and are currently tried for enantioselective hydroalkylation.



Scheme 3.7: Proposed mechanism for the hydroalkylation catalyzed by thiol.

Moreover, fluorinated alkylating agents were tried on the Roberts lactone and dodecanthiol as thiol source. Preliminary results with a modest yield, give as further opportunities to investigate this process.

References

- (1) *Natural Products: Drug Discovery and Therapeutic Medicine*; Zhang, L., Demain, A. L., Eds.; Humana Press: Totowa, NJ, 2005.
- (2) Sorokina, M.; Steinbeck, C. *Journal of Cheminformatics* **2020**, *12*, 20.
- (3) Cannalire, R.; Pelliccia, S.; Sancineto, L.; Novellino, E.; Tron, G. C.; Giustiniano, M. *Chemical Society Reviews* **2021**, *50*, 766–897.
- (4) Mandal, D.; Roychowdhury, S.; Biswas, J. P.; Maiti, S.; Maiti, D. *Chemical Society Reviews* **2022**, 10.1039.D1CS00923K.
- (5) Huang, X.; Wang, B.; Wang, Y.; Jiang, G.; Feng, J.; Zhao, H. *Nature* **2020**, *584*, 69–74.
- (6) *Applied Homogeneous Catalysis with Organometallic Compounds: A Comprehensive Handbook in Four Volumes*, 1st ed.; Cornils, B., Herrmann, W. A., Beller, M., Paciello, R., Eds.; Wiley: 2017.
- (7) Ning, Y.; Ohwada, T.; Chen, F.-E. *Green Synthesis and Catalysis* **2021**, *2*, 247–266.
- (8) Green, S. A.; Huffman, T. R.; McCourt, R. O.; van der Puyl, V.; Shenvi, R. A. *Journal of the American Chemical Society* **2019**, *141*, 7709–7714.
- (9) Yang, P.-F.; Zhu, L.; Liang, J.-X.; Zhao, H.-T.; Zhang, J.-X.; Zeng, X.-W.; Ouyang, Q.; Shu, W. *ACS Catalysis* **2022**, 5795–5805.
- (10) Zhang, Y.; Mao, L.-L.; Hu, S.; Luan, Y.; Cong, H. *Chinese Chemical Letters* **2021**, *32*, 681–684.
- (11) Zhu, C.; Zhang, H.; Liu, Q.; Chen, K.; Liu, Z.-Y.; Feng, C. *ACS Catalysis* **2022**, *12*, 9410–9417.
- (12) Giese, B.; Horler, H.; Leising, M. *Chemische Berichte* **1986**, *119*, 444–452.
- (13) Haque, M. B.; Roberts, B. P. *Tetrahedron Letters* **1996**, *37*, 9123–9126.
- (14) Haque, M. B.; Roberts, B. P.; Tocher, D. A. *Journal of the Chemical Society, Perkin Transactions 1* **1998**, 2881–2890.
- (15) Dang, H.-S.; Elsegood, M. R. J.; Kim, K.-M.; Roberts, B. P. *Journal of the Chemical Society, Perkin Transactions 1* **1999**, 2061–2068.
- (16) Wilger, D. J.; Gesmundo, N. J.; Nicewicz, D. A. *Chemical Science* **2013**, *4*, 3160.
- (17) Huang, W.; Chen, W.; Wang, G.; Li, J.; Cheng, X.; Li, G. *ACS Catalysis* **2016**, *6*, 7471–7474.
- (18) Miura, T.; Funakoshi, Y.; Nakahashi, J.; Moriyama, D.; Murakami, M. *Angewandte Chemie* **2018**, *130*, 15681–15685.
- (19) Wang, H.; Jui, N. T. *Journal of the American Chemical Society* **2018**, *140*, 163–166.
- (20) Vogt, D. B.; Seath, C. P.; Wang, H.; Jui, N. T. *Journal of the American Chemical Society* **2019**, *141*, 13203–13211.

- (21) Su, Y.-L.; Liu, G.-X.; Liu, J.-W.; Tram, L.; Qiu, H.; Doyle, M. P. *Journal of the American Chemical Society* **2020**, *142*, 13846–13855.
- (22) Lei, G.; Xu, M.; Chang, R.; Funes-Ardoiz, I.; Ye, J. *Journal of the American Chemical Society* **2021**, *143*, 11251–11261.
- (23) Yu, Y.-J.; Zhang, F.-L.; Peng, T.-Y.; Wang, C.-L.; Cheng, J.; Chen, C.; Houk, K. N.; Wang, Y.-F. *Science* **2021**, *371*, 1232–1240.
- (24) Liu, C.; Li, K.; Shang, R. *ACS Catalysis* **2022**, *12*, 4103–4109.
- (25) Yu, P.; Lin, J.-S.; Li, L.; Zheng, S.-C.; Xiong, Y.-P.; Zhao, L.-J.; Tan, B.; Liu, X.-Y. *Angewandte Chemie* **2014**, *126*, 12084–12088.
- (26) Li, Z.; Xiao, Y.; Liu, Z.-Q. *Chemical Communications* **2015**, *51*, 9969–9971.
- (27) Lin, Q.-Y.; Xu, X.-H.; Zhang, K.; Qing, F.-L. *Angewandte Chemie* **2016**, *128*, 1501–1505.
- (28) Meyer, C. F.; Hell, S. M.; Misale, A.; Trabanco, A. A.; Gouverneur, V. *Angewandte Chemie International Edition* **2019**, *58*, 8829–8833.
- (29) Yang, J.; Zhu, S.; Wang, F.; Qing, F.-L.; Chu, L. *Angewandte Chemie* **2021**, *133*, 4346–4352.
- (30) Shi, Q.; Xu, M.; Chang, R.; Ramanathan, D.; Peñin, B.; Funes-Ardoiz, I.; Ye, J. *Nature Communications* **2022**, *13*, 4453.
- (31) Huang, Q.; Suravarapu, S. R.; Renaud, P. *Chemical Science* **2021**, *12*, 2225–2230.
- (32) Soulard, V.; Villa, G.; Vollmar, D. P.; Renaud, P. *Journal of the American Chemical Society* **2018**, *140*, 155–158.
- (33) Hashimoto, T.; Kawamata, Y.; Maruoka, K. *Nature Chemistry* **2014**, *6*, 702–705.
- (34) Shin, N. Y.; Ryss, J. M.; Zhang, X.; Miller, S. J.; Knowles, R. R. *Science* **2019**, *366*, 364–369.
- (35) Moellering, R. C. *Annals of Internal Medicine* **2003**, *138*, 135.
- (36) Leach, K. L.; Swaney, S. M.; Colca, J. R.; McDonald, W. G.; Blinn, J. R.; Thomasco, L. M.; Gadwood, R. C.; Shinabarger, D.; Xiong, L.; Mankin, A. S. *Molecular Cell* **2007**, *26*, 393–402.
- (37) Burdette, S. D.; Trotman, R. *Clinical Infectious Diseases* **2015**, *61*, ed. by Saravolatz, L. D., 1315–1321.
- (38) Komarov, I. V.; Grigorenko, A. O.; Turov, A. V.; Khilya, V. P. *Russian Chemical Reviews* **2004**, *73*, 785–810.

3.5 Experimental Section

General Information

Techniques

All reactions requiring anhydrous conditions were performed in flame dried glassware under an argon atmosphere. Silica gel 60Å(40–63 μm) from *Silicycle* was used for flash column chromatography (FCC). Thin layer chromatography (TLC) was performed on *Silicycle* or *Macherey* silica gel 60 F254 plates, visualization under UV light (254 nm) and by dipping in a solution of cerium ammonium molybdate - $(\text{NH}_4)_2\text{MoO}_4$ (15.0 g), $\text{Ce}(\text{SO}_4)_2$ (0.5 g), H_2O (90 mL), conc. H_2SO_4 (10 mL) - and subsequent heating. Silver nitrate impregnated silica gel was prepared according to ratio: SiO_2 (50 g), AgNO_3 (5.5 g) and H_2O (30 mL) for flash column chromatography and AgNO_3 (1 g), H_2O (2.5 mL) and acetone (10 mL) for TLC, followed by activation at 105–110 °C (light sensitive, to be covered with aluminium foil and/or stored in the dark). Anhydrous sodium sulfate was used as drying reagent.

Materials

Commercial reagents were used without further purification unless otherwise stated. Dry solvents for reactions were filtered over columns of dried alumina under a positive pressure of argon and/or stored over 3Å molecular sieves. Solvents for extractions (Et_2O , *n*-pentane, CH_2Cl_2 , AcOEt) and flash column chromatography were of technical grade and distilled prior to use.

Instrumentation

^1H and ^{13}C NMR spectra were recorded on a *Bruker Avance IIIHD-300* spectrometer operating at 300 MHz for ^1H and 75 MHz for ^{13}C at rt (24–25°C) unless otherwise stated. Some ^1H and ^{13}C NMR spectra were recorded on a *Bruker Avance IIIHD-400* or a *Bruker Avance II-400* spectrometer (^1H : 400 MHz; ^{13}C : 100 MHz). Chemical shifts (δ) are reported in parts per million (ppm) downfield from tetramethylsilane $\text{Si}(\text{CH}_3)_4$ ($\delta = 0.00$ for ^1H NMR spectra) using residual solvent signal as an internal standard: δ singlet 7.26 (^1H), triplet 77.0 (^{13}C) for CDCl_3 or δ singlet 7.16 (^1H), triplet 128.0 (^{13}C) for C_6D_6 . Multiplicities are given as s (singlet), d (doublet), t (triplet), q (quadruplet), m (multiplet), and br (broad). Coupling constants (J) are reported in Hz. In ^{13}C -NMR spectra, the peak positions are reported on one decimal unless the difference in chemical shift between two signals is small and required two decimals. Due to coupling to the quadrupolar ^{11}B and ^{10}B nuclei, the carbons linked to boron atoms generally give a broad signal in ^{13}C NMR, sometimes not detected.

Diastereomeric ratio were determined by NMR on crude reaction mixtures.

Infrared spectra were recorded on a *Jasco FT-IR-460* plus spectrometer equipped with a *Specac MKII Golden Gate Single Reflection Diamond ATR* system and are reported in wave

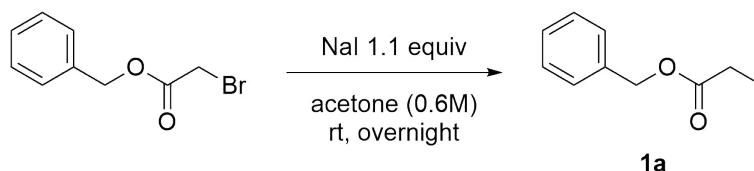
numbers (cm^{-1}). At maximum, the ten most prominent peaks are reported. **HRMS** analyses and accurate mass determinations were performed on a *Thermo Scientific LTQ Orbitrap XL* mass spectrometer using ESI mode (positive ion mode). Melting points were measured on a *Büchi B545* apparatus.

Specific rotation $[\alpha]_D^{20}$ are expressed in $\text{deg}\cdot\text{mL}\cdot\text{g}^{-1}\cdot\text{dm}^{-1}$. The concentration c is in $\text{g}/100\text{ mL}$ and the path length l is in decimeters. The units of the specific rotation, $\text{deg}\cdot\text{mL}\cdot\text{g}^{-1}\cdot\text{dm}^{-1}$, are implicit and are not included with the reported value.

Synthesis

Preparation of the reagents

benzyl 2-iodoacetate (**1a**)



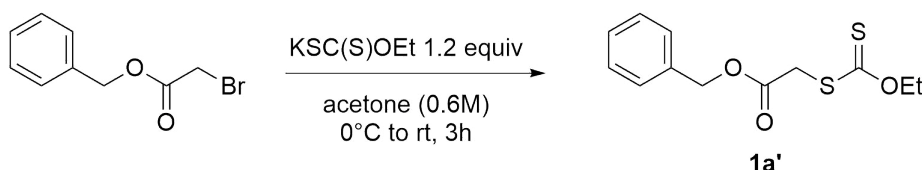
To a solution of NaI (16.5 g, 110 mmol, 1.1 equiv) in acetone (150 mL, 0.6M) was added benzyl 2-bromoacetate (22.9 g, 100 mmol). The mixture was stirred at room temperature overnight in the dark room or covered with Alu foil. The suspension was filtered and washed with pentane. The liquid was transferred to a separating funnel, diluted with water (120 mL) and extracted with pentane (240 / 120 mL). The combined organic phases were washed with 5% Na₂S₂O₃ solution (120 mL), water and brine. The organic layers were dried over Na₂SO₄, filtered, and concentrated under reduced pressure (<40° water bath, covered from light). Rotation under high vacuum for 1h at rt, afforded the iodide **1a** (25.37 g, 91.9 mmol, 92%) as a colorless oil. Used as such without additional purification.

Colorless oil. ¹H NMR (300 MHz, CD₂Cl₂) δ 7.38 (s, 5H), 5.16 (s, 2H), 3.75 (s, 2H). ¹³C NMR (75 MHz, CD₂Cl₂) δ 168.9, 135.8, 129.0 (2C), 128.8, 128.6 (2C), 68.1, -4.8.

The physical and spectral data are in accordance with literature data:

Lebedeva, M. A.; Chamberlain, T. W.; Davies, E. S.; Thomas, B. E.; Schröder, M.; Khlobystov, A. N. Beilstein J. Org. Chem. 2014, 10, 332.

benzyl 2-((ethoxycarbonothioyl)thio)acetate (**1a'**)

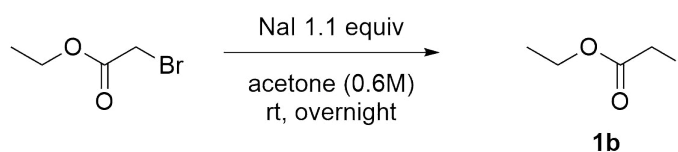


To a solution of benzyl 2-bromoacetate (12.0 g, 50 mmol) in acetone (83 mL, 0.6M) cooled at 0°C, was added potassium ethylxanthogenate (10.0 g, 60 mmol). The mixture was stirred from 0°C to room temperature over 3h covered with Alu foil. The reaction mixture was diluted with water (40 mL) and extracted with Et₂O (3 x 40 mL). The combined organic phases were washed with water and brine, then dried over Na₂SO₄, filtered, and concentrated under reduced pressure to deliver the xanthate **1a'** (13.5 g, 49.9 mmol, quant.) as a yellowish oil. Used as such without additional purification.

Yellowish oil. $^1\text{H NMR}$ (300 MHz, CDCl_3) δ 7.44 – 7.29 (m, 5H), 5.20 (s, 2H), 4.60 (q, $J = 7.1$ Hz, 2H), 3.95 (s, 2H), 1.37 (t, $J = 7.1$ Hz, 3H). $^{13}\text{C NMR}$ (75 MHz, CDCl_3) δ 212.3, 167.7, 135.3, 128.6 (2C), 128.4, 128.3 (2C), 70.6, 67.5, 37.8, 13.6.

The physical and spectral data are in accordance with literature data:
Huang, Z.; Xu, J. *RSC Adv.*, 2013, 3, 15114-15120.

ethyl 2-iodoacetate (**1b**)

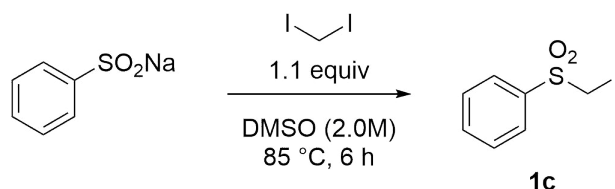


To a solution of NaI (16.5 g, 110 mmol, 1.1 equiv) in acetone (150 mL, 0.6M) was added ethyl 2-bromoacetate (17.0 g, 100 mmol). The mixture was stirred at room temperature overnight in the dark room or covered with Alu foil. The suspension was filtrated and washed with pentane. The liquid was transferred to a separating funnel, diluted with water (120 mL) and extracted with pentane (240 / 120 mL). The combined organic phases were washed with 5% $\text{Na}_2\text{S}_2\text{O}_3$ solution (120 mL), water and brine. The organic layers were dried over Na_2SO_4 , filtered, and concentrated under reduced pressure ($<40^\circ$ water bath, covered from light). Rotation under high vacuum for 1h at rt, afforded the iodide **1b** (19.54 g, 91.3 mmol, 91%) as a yellowish oil. Used as such without additional purification.

Colorless oil. $^1\text{H NMR}$ (300 MHz, C_6D_6) δ 3.82 (p, $J = 6.5, 5.1$ Hz, 2H), 3.31 – 3.04 (m, 2H), 0.98 – 0.77 (m, 3H). $^{13}\text{C NMR}$ (75 MHz, C_6D_6) δ 168.4, 61.8, 13.8, -5.1.

The physical and spectral data are in accordance with literature data:
Meyer, D.; Renaud, P. *Angewandte Chemie International Edition*, 2017, 56(36), 10858-10861.

iodomethylsulfonylbenzene (**1c**)



To a solution of sodium benzenesulfinate (8.2 g, 50 mmol) in DMSO (20 mL, 2.0M) at room temperature under Ar was added diiodomethane (4.4 mL, 55 mmol, 1.1 equiv). The mixture was then stirred for 6 h at 85 °C protected from light. It was then diluted with CH_2Cl_2 and water. The organic layer was then washed with brine, dried over Na_2SO_4 , filtered, and concentrated under reduced pressure. Purification by FC (4:6 EtOAc/heptanes) delivered the iodide **1c** as

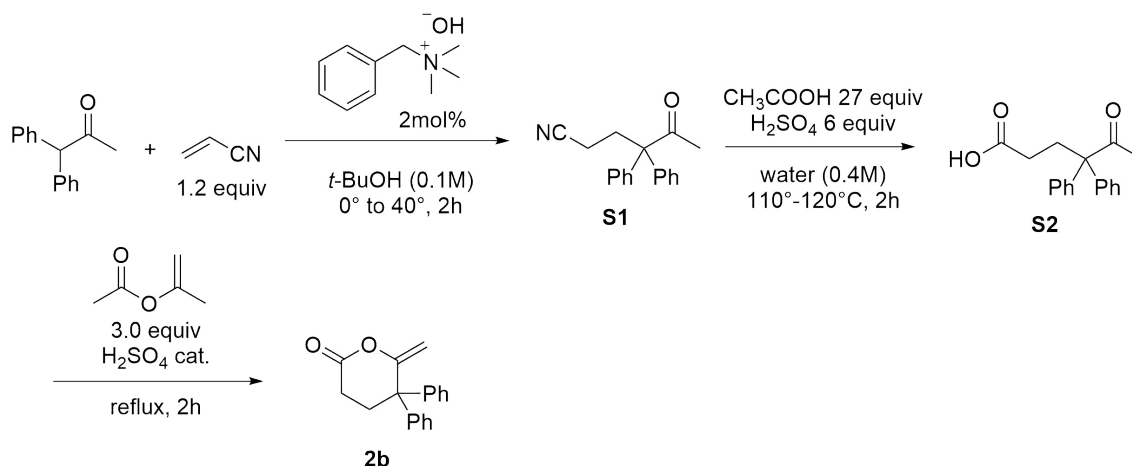
white solid (11.5 g, 40.8 mmol, 82% yield).

White solid. R_f 0.63 (3:7 heptanes/EtOAc). $^1\text{H NMR}$ (300 MHz, CDCl_3) δ 8.05 – 7.92 (m, 2H), 7.76 – 7.66 (m, 1H), 7.65 – 7.54 (m, 2H), 4.47 (s, 2H). $^{13}\text{C NMR}$ (75 MHz, CDCl_3) δ 136.1, 134.7, 129.5 (2C), 129.1 (2C), 16.9.

The physical and spectral data are in accordance with the following reference:
Pospíšil, J.; Robiette, R.; Sato, H.; Debrus, K. *Org. Biomol. Chem.* 2012, 10, 1225.

Synthesis of alkenes

Preparation of Roberts lactone 2b



5-oxo-4,4-diphenyl-hexanenitrile (**S1**)

To a solution of 1,1-diphenylacetone (11.5g, 54.7 mmol) in *t*-BuOH (50 mL, 0.1 M) was added Triton B (0.44 mL, 1.09 mmol, 2 mol%, 40% in MeOH) at rt. Acrylonitrile (4.4 mL, 65.6 mmol, 1.2 equiv.) was then added dropwise to the reaction mixture at 0°C. After the addition, the solution was allowed to warm up to 40 °C and stirred during 2 h. Upon completion, the solution was then neutralized with few drops of conc H_2SO_4 . The solid formed was isolated by filtration and rinsed with water, then solubilized with CH_2Cl_2 and transferred to the separating funnel. The organic phase was treated with water and extracted 2 times more with CH_2Cl_2 . The combined organic phases were washed with water, then sat NaHCO_3 solution, water, and brine. The final organic phase was dried over Na_2SO_4 , filtered, and concentrated under reduced pressure to give a brownish solid. Purification by recrystallization from CH_2Cl_2 /pentane 1:1, cooling at -78°C, afforded **S1** as white solid (8.307 g, 31.5 mmol, 58%).

White solid. R_f 0.44 (2:8 EtOAc/heptanes). **Mp** 114.4-115.1 °C, from CH_2Cl_2 (lit. 117-118 °C from $\text{Et}_2\text{O}/\text{MeOH}$). $^1\text{H NMR}$ (300 MHz, CDCl_3) δ 7.45 – 7.32 (m, 6H), 7.27 – 7.23 (m, 4H), 2.70 – 2.61 (m, 2H), 2.06 – 1.97 (m, 5H). $^{13}\text{C NMR}$ (75 MHz, CDCl_3) δ 207.5, 139.7 (2C), 129.1

(4C), 129.0 (4C), 128.0 (2C), 119.9, 65.6, 34.2, 27.8, 13.8.

Physical and spectral data are in accordance with literature data:

Walker, G.N.; Alkalay, D. *Journal of Organic Chemistry*, 1967, 32, 2213 - 2225.

5-oxo-4,4-diphenyl-hexanoic acid (S2)

To a solution of **S1** (8.2 g, 31 mmol) in acetic acid (48 mL, 841 mmol, 27.0 equiv) and water (15 mL, 0.4 total molarity) was added at room temperature conc. H₂SO₄ (10 mL, 187 mmol, 6.0 equiv). The reaction mixture was stirred at reflux for 2h. The reaction mixture was poured into cold water and stirred vigorously. Then the organic phase was extracted with CH₂Cl₂ (3 x 100 mL). The combined organic layers were washed with water (100 mL) and brine, dried over Na₂SO₄, filtered and concentrated under reduced pressure. Purification by recrystallization from EtOAc/heptanes 3:7, afforded **S2** as white solid (6.699 g, 23.7 mmol, 76%).

White solid. $R_f = 0.28$ (6:4 EtOAc/heptanes). **Mp** 137.7-138.8 °C, from EtOAc/heptanes (lit. 138 – 140 °C). ¹H NMR (300 MHz, CDCl₃) δ 7.38 – 7.23 (m, 10H), 2.64 – 2.57 (m, 2H), 2.08 – 2.00 (m, 5H). ¹³C NMR (75 MHz, CDCl₃) δ 207.9, 179.6, 140.6 (2C), 129.3 (4C), 128.7 (4C), 127.5 (2C), 65.8, 32.5, 30.3, 27.7.

Physical and spectral data are in accordance with literature data:

Cragoe Jr, E.J.; Pietruszkiewicz, A.M.; Robb, C.M. *J. Org. Chem.* 1958, 23(7), 971-980.

Walker, G.N.; Alkalay, D. *Journal of Organic Chemistry*, 1967, 32, 2213 - 2225.

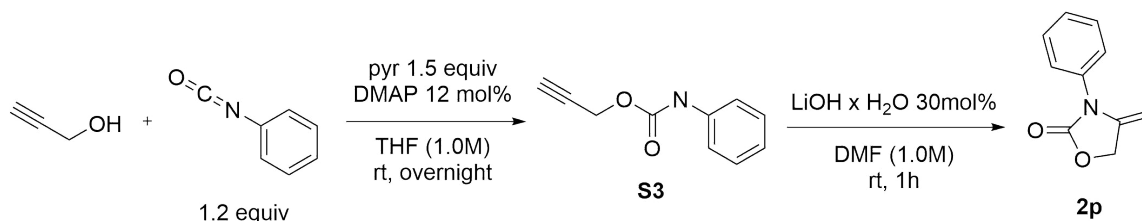
6-methylene-5,5-diphenyl-tetrahydropyran-2-one (2b)

To a solution of the **S2** (6.7 g, 23.7 mmol) with isopropenyl acetate (7.84 mL, 3.0 eq) under Ar at rt was added conc H₂SO₄ (3 drops) in a flask equipped with a distillation apparatus. The mixture was heated so that a slow reflux occurred (around 2 hours) and the mixture became dark brown. Upon completion, the mixture was diluted with cold water and extracted with Et₂O (3 x 100 mL). Combined organic phases were washed with water (150 mL) and brine, dried over Na₂SO₄, filtered, and concentrated under reduced pressure. Purification by FC (2:8 EtOAc/heptanes) afforded the **2b** as white solid (3.377 g, 12.8 mmol, 54%).

Physical and spectral data are in accordance with literature data:

Cragoe Jr, E.J.; Pietruszkiewicz, A.M.; Robb, C.M. *J. Org. Chem.* 1958, 23(7), 971-980.

Preparation of 4-methylene-3-phenyl-oxazolidin-2-one (**2p**)



prop-2-ynyl N-phenylcarbamate (**S3**)

To a solution of propargyl alcohol (2.24 g, 40.0 mmol) in dry THF (30 mL, 1.0 M) under Argon, was added pyridine (4.9 mL, 60.0 mmol, 1.5 equiv) and DMAP (0.58 g, 4.8 mmol, 12 mol%). Then phenyl isocyanate (5.3 mL, 48.0 mmol, 1.2 equiv) was added at room temperature. The reaction mixture was stirred at rt and monitored by TLC. Upon completion, the reaction mixture was treated with 2M HCl (50 mL) and extracted with EtOAc (3 \times 50 mL). The combined organic phases were washed with water (100 mL) and brine (100 mL), then dried over Na₂SO₄, filtered, and concentrated under reduced pressure to give the crude product as dark yellow oil. The crude intermediate **S3** was used as such in the next step.

Dark yellow oil. ¹H NMR (300 MHz, CD₂Cl₂) δ 7.43 – 7.26 (m, 4H), 7.16 – 7.04 (m, 1H), 6.89 (s, 1H), 4.78 (d, J = 2.4 Hz, 2H), 2.57 (t, J = 2.5 Hz, 1H). ¹³C NMR (75 MHz, CD₂Cl₂) δ 152.8, 138.1, 129.4 (2C), 124.1, 119.1 (2C), 78.4, 75.1, 53.0.

4-methylene-3-phenyl-oxazolidin-2-one (**2p**)

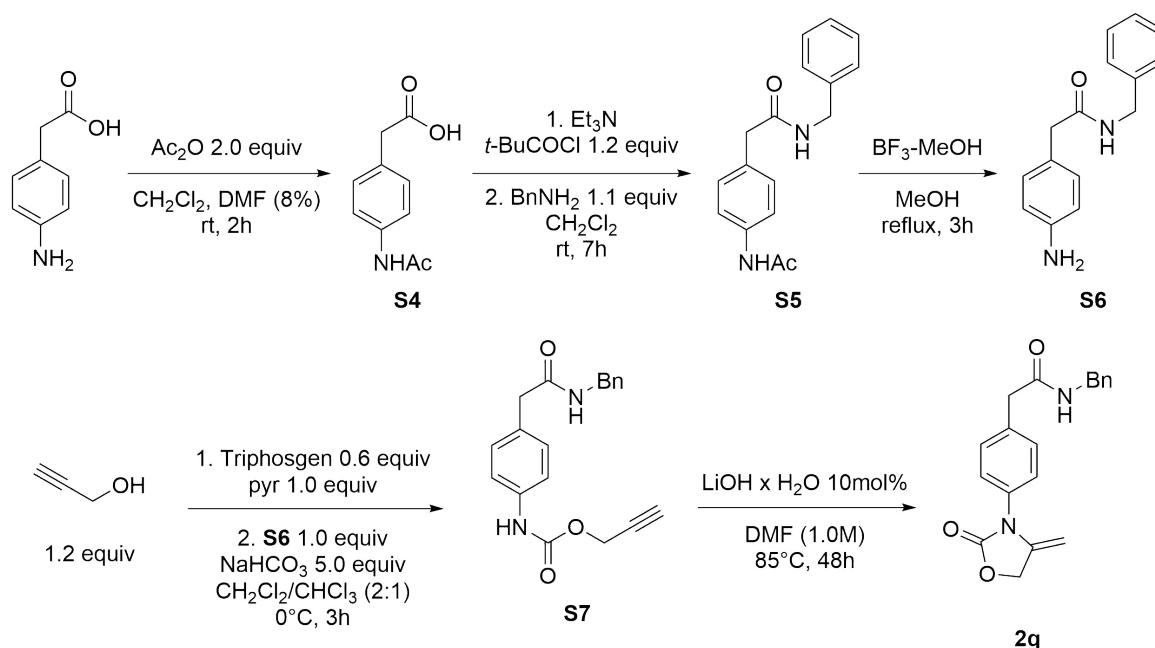
Lithium hydroxide monohydrate (514 mg, 4.0 mmol, 30 mol%) was added under Argon to a solution of **S3** (40.0 mmol) in DMF (40 mL, 1.0 M) at room temperature. The reaction was stirred at room temperature and monitored by TLC. Upon completion, the reaction mixture was diluted with water (50 mL) and extracted with diethyl ether (3 \times 50 mL). The combined organic phases were then washed with water (100 mL) and brine, dried over Na₂SO₄, filtered, and concentrated under reduced pressure to return the crude as yellowish solid. Purification by FC (1:1 pentane/[8:1.5:0.5 DCM/pentane/Et₂O]) afforded the **2p** as white solid (5.32 g, 30.3 mmol, 76%). Product is acid labile and needs to be stored under a positive Argon atm, in the freezer.

White solid. *R_f* 0.50 (1:1 Et₂O/pentane). *Mp* 90.3-91.8 °C, from CH₂Cl₂. ¹H NMR (300 MHz, CD₂Cl₂) δ 7.56 – 7.31 (m, 5H), 5.04 (t, J = 2.3 Hz, 2H), 4.23 – 4.13 (m, 2H). ¹³C NMR (75 MHz, CD₂Cl₂) δ 156.3, 142.5, 134.3, 130.0 (2C), 128.7, 127.5 (2C), 81.9, 67.7.

Physical and spectral data are in accordance with literature data:

Newton, R.; Savage, G. P. Australian journal of chemistry, 2008, 61(6), 432-437.

Preparation of 4-methylene-3-phenyl-oxazolidin-2-one (2q)



2-(4-acetamidophenyl)acetic acid (S4)

In a 500 mL flask 2-(4-aminophenyl)acetic acid (98.0%, 15.43 g, 100 mmol) was partly dissolved in chloroform (300 mL) together with acetic anhydride (18.9 mL, 200 mmol). The mixture was stirred 3 h at room temperature. Acetic acid (5 mL) was added to mixture before washing it with water (5 x 30 mL) and sat. Na₂CO₃ (50 mL). The organic layer was dried over Na₂SO₄, filtered and concentrated under reduced pressure. The residue was dissolved in acetone (25 mL), precipitated by adding Et₂O (300 mL), filtered and triturated with water. A second crop was recrystallized from the Et₂O mixture, by adding heptane to it and removing the ether by evaporation. The acetamido acid **S4** was obtained as a white solid (7.87 g, 41%).

White solid. ¹H NMR (300 MHz, CD₂Cl₂) δ 7.43 – 7.26 (m, 4H), 7.16 – 7.04 (m, 1H), 6.89 (s, 1H), 4.78 (d, J = 2.4 Hz, 2H), 2.57 (t, J = 2.5 Hz, 1H). ¹³C NMR (75 MHz, CD₂Cl₂) δ 152.8, 138.1, 129.4 (2C), 124.1, 119.1 (2C), 78.4, 75.1, 53.0.

The physical and spectral data are in accordance with the following reference:

Urgin, K.; Jida, M.; Ehrhardt, K.; Müller, T.; Lanzer, M.; Maes, L.; Elhabiri, M.; Davioud-Charvet, Molecules 2017, 22 (1).

2-(4-acetamidophenyl)-N-benzylacetamide (S5)

2-(4-acetamidophenyl)acetic acid **S4** (5.60 g, 29.0 mmol) and TEA (4.04 mL, 29.0 mmol) were stirred in chloroform (20 mL) until complete dissolution, followed by addition of pivaloyl chloride (3.57 mL 29.0 mmol) at 0 °C. After 30 min, benzylamine (3.16 mL, 29.0 mmol) was added and the reaction mixture was stirred for 7h at room temperature till TLC revealed full consumption of the amine. Volatilities were removed by evaporation under reduced pressure and the crude

was triturated with water. Recrystallization in aqueous methanol afforded the diamide **S5** as a white solid (7.89 g, 96%).

White solid. $^1\text{H NMR}$ (300 MHz, DMSO- d_6): δ 9.88 (s, 1H), 8.49 (t, $J = 7$ Hz, 1H), 7.48 (d, $J = 9$ Hz), 7.33 – 7.15 (m, 7H), 4.25 (d, $J = 7$ Hz, 2H), 3.40 (s, 2), 2.02 (s, 3H). $^{13}\text{C NMR}$ (75 MHz, DMSO- d_6) δ 170.3, 168.1, 139.5, 137.7, 130.9, 129.2 (2C), 128.3 (2C), 127.2 (2C), 126.8, 118.9 (2C), 42.2, 41.8, 23.9.

The physical and spectral data are in accordance with the following reference:

Miltsov, S.; Karavan, V.; Misharev, A.; Alonso-Chamarro, J.; Puyol, M. *Tetrahedron Lett.* 2016, 57 (6), 641–644.

2-(4-aminophenyl)-N-benzylacetamide (S6)

The acetamide **S5** (4.24 g, 15.0 mmol) was dissolved in 75 mL dry methanol under inert atmosphere. The solution was treated with BF_3 (10.1 mL, 90 mmol) as boron trifluoride–methanol complex (50% BF_3 , Aldrich®) and the reaction solution was stirred 3 h at reflux. The reaction mixture was cooled down to 0°C and neutralized with aqueous ammonia (5 M, 100 mL). The solution was extracted with chloroform (1 x 100 mL, 3 x 30 mL) and the combined organic layers were then washed with brine, dried over Na_2SO_4 and evaporated under reduced pressure. The residue was recrystallized in chloroform/heptane to afford the amine **S6** as a white solid (2.64 g, 73%).

White solid. $^1\text{H NMR}$ (DMSO- d_6) δ 8.34 (br. s, 1H), 7.33–7.18 (m, 5H), 6.92 (d, $J = 6$ Hz, 2H), 6.48 (d, $J = 6$ Hz, 2H), 4.89 (br. s, 2H), 4.24 (d, $J = 7$ Hz, 2H), 3.26 (s, 2H). $^{13}\text{C NMR}$ (75 MHz, DMSO- d_6) δ 171.0, 147.0, 139.6, 129.4 (2C), 128.2 (2C), 127.1 (2C), 126.7, 123.2, 113.8 (2C), 42.1, 41.7.

The physical and spectral data are in accordance with the following reference:

Miltsov, S.; Karavan, V.; Misharev, A.; Alonso-Chamarro, J.; Puyol, M. *Tetrahedron Lett.* 2016, 57 (6), 641–644.

prop-2-yn-1-yl (4-(2-(benzylamino)-2-oxoethyl)phenyl)carbamate (S7)

To a stirred solution of triphosgene (3.03 g, 10.0 mmol) in dry ether (40 mL), activated charcoal (0.07 g) was added and the mixture was stirred 1 h at room temperature. The solution was cooled to 0°C and propargyl alcohol (1.18 mL, 20.0 mmol) diluted in dry ether (10 mL) was added dropwise. The reaction was stirred 12 h allowing it to reach room temperature. The reaction mixture was filtered and solvents were gently evaporated under reduced pressure to yield the chloroformate as a greenish liquid that was directly used for further reactions without purification.

The amine **S6** (2.40 g, 10.0 mmol) and NaHCO_3 (2.44 g, 29.0 mmol) were stirred in chloro-

form (40 mL) for 30 min at room temperature. Then, the chloroformate previously prepared (2.37 g, 20.0 mmol) was added dropwise and the reaction mixture was stirred for 4h at room temperature till the full consumption of the amine. Dilution with heptane (100 mL) afforded the precipitation of the product which was filtered from the solution and purified by FC (TBME) to give the propargyl intermediate **S7** as a white solid (2.45 g, 76%).

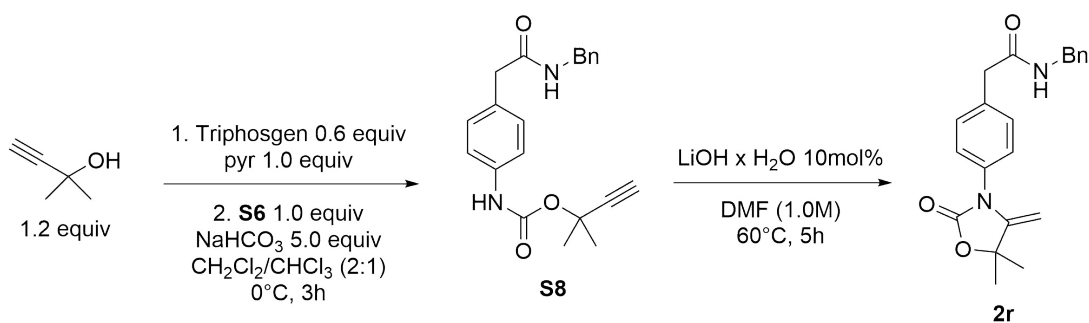
White solid. **Mp**: 144 °C. **¹H NMR** (300 MHz, CD₃CN) δ 7.91 (br s, 1H), 7.40 – 7.21 (m, 9H), 6.90 (br s, 1H), 4.73 (d, *J* = 2.7 Hz), 4.30 (d, *J* = 6.2 Hz), 3.46 (s, 2H), 2.79 – 2.99 (m, 1H). **¹³C NMR** (75 MHz, CD₃CN) δ 153.9, 130.8 (2C), 129.5 (2C), 128.3 (2C), 128.0, 120.0, 76.1, 53.2, 43.7, 43.2. **HRMS** (ESI): calc. for C₁₉H₁₉N₂O₃: 323.1390, found: 323.1391. **IR** (cm⁻¹): 2161 (w), 2023 (s), 1722 (s), 1495 (m), 1387 (m), 1354 (m), 1219 (m), 1183 (s), 1162 (s), 1083 (s), 1048 (s), 955 (m), 782 (m), 743 (s), 694 (s), 423 (s).

N-Benzyl-2-(4-(4-methylene-2-oxooxazolidin-3-yl)phenyl)acetamide (**2q**)

To a solution of the propargyl intermediate **S7** (860 mg, 2.67 mmol) in dry DMF (5 mL), was added LiOH (22 mg, 0.27 mmol). The reaction mixture was stirred for 48h at 85°C, let to cool to room temperature and diluted with Et₂O (50 mL). The product was fully precipitated by adding heptane (20 mL). In order to remove traces of DMF, the residue was dissolved in EtOAc (100 mL), washed with brine (15 mL), water (5 x 15 mL), brine (15 mL), dried over Na₂SO₄ and concentrated under reduced pressure to yield the oxazolidinone **2q** as a white solid (690 mg, 80% yield).

White solid. **Mp**: 145.8-147.3 °C, recryst. from CH₂Cl₂. **¹H NMR** (300 MHz, CD₂Cl₂) δ 7.47 – 7.37 (m, 2H), 7.37 – 7.17 (m, 7H), 6.12 (s, 1H), 5.03 (t, *J* = 2.3 Hz, 2H), 4.39 (d, *J* = 5.9 Hz, 2H), 4.19 (dq, *J* = 16.3, 2.5 Hz, 2H), 3.59 (s, 2H). **¹³C NMR** (75 MHz, CD₂Cl₂) δ 170.4, 156.3, 142.3, 139.0, 136.1, 133.2, 130.9 (2C), 128.9 (2C), 127.8 (2C), 127.7, 127.6 (2C), 82.1, 67.7, 43.9, 43.4. **HRMS** (ESI): calc. for C₁₉H₁₉N₂O₃: 323.1390, found: 323.1400. **IR** (cm⁻¹): 3737 (s), 2986 (s), 2899 (s), 2358 (w), 2147 (w), 1971 (w), 1758 (s), 1685 (s), 1637 (s), 1559 (s), 1407 (s).

Preparation of 4-methylene-3-phenyl-oxazolidin-2-one (**2r**)



2-methylbut-3-yn-2-yl (4-(2-(benzylamino)-2-oxoethyl)phenyl)carbamate (**S8**)

To a stirred solution of triphosgene (1.05 g, 3.5 mmol) in dry CH₂Cl₂ (5 mL) was added the

mixture of 2-methylbut-3-yn-2-ol (0.68 mL, 7.0 mmol) and pyridine (0.56 mL, 7 mmol) dissolved in dry CH₂Cl₂ (5 mL) via constant voltage funnel at 0 °C. The reaction was stirred for 2.5 h at 0 °C and the mixture was used directly for the next step.

To a solution of the amine **S6** (1.44 g, 6 mmol) and NaHCO₃ (2.52 g, 30 mmol) in chloroform (20 mL) at 0 °C, the previous prepared mixture was added dropwise via syringe and let to stir for 3 hours. The reaction mixture was allowed to reach room temperature. All volatiles were evaporated under reduced pressure and the residue was dissolved in chloroform/methanol mixture (10:1) and filtered over a thin layer of Alox. Solvents were evaporated and the crude was purified by FC (3:97 MeOH/CH₂Cl₂) to obtain the alkyne carbamate **S8** as a pale yellow solid (1.20 g, 57%).

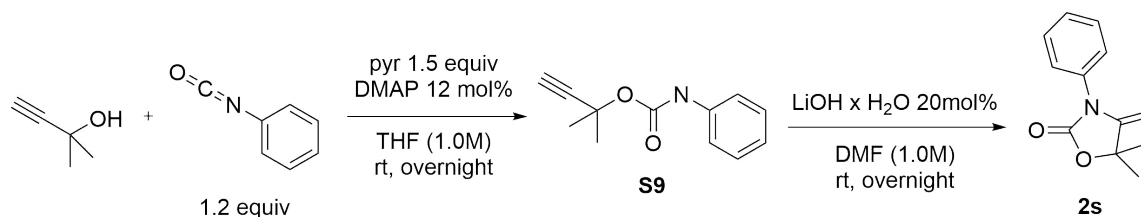
Pale yellow solid. **Mp**: 116 °C – 120 °C. **¹H NMR** (DMSO-d₆) δ 9.50 (s, 1H), 8.47 (t, J = 5.4 Hz, 1H), 7.39 – 7.26 (m, 4H), 7.25 – 7.14 (m, 5H), 4.25 (d, J = 5.9 Hz, 2H), 3.51 (s, 1H), 3.40 (s, 2H), 1.67 (s, 6H). **¹³C NMR** (75 MHz, DMSO-d₆) δ 170.2, 151.6, 139.5, 137.4, 130.3, 129.2 (2C), 128.2 (2C), 127.2 (2C), 126.7 (2C), 118.1, 74.8, 71.0, 42.1, 41.7, 29.0 (2C). **HRMS** (ESI): calc. for C₂₁H₂₃N₂O₃: 351.1703, found: 351.1697. **IR** (cm⁻¹): 3035 (w), 2152 (w), 1994 (w), 1971 (w), 1634 (s), 1513 (s), 1431 (m), 1257 (m), 1029 (m).

N-benzyl-2-(4-(5,5-dimethyl-4-methylene-2-oxooxazolidin-3-yl)phenyl)acetamide (2r)

LiOH·H₂O (9 mg, 0.22 mmol) was added to a stirred solution of the alkyne **S8** (739 mg, 2.1 mmol) in DMF (4.2 mL). The reaction mixture was stirred 5 h at 60 °C till complete conversion of the starting material. Solvents were partly removed by evaporation under reduced pressure (30 mbar, 65 °C) and the residue was dissolved in EtOAc (200 mL), washed with brine (30 mL), water (5 x 50 mL), brine (30 mL), dried over Na₂SO₄, filtered and concentrated under reduced pressure. The product was purified by FC (7:93 MeOH/CH₂Cl₂) to obtain the oxazolidinone alkene **2r** as a pale orange solid (680 mg, 92%).

Pale orange solid. **Mp**: 108 °C. **¹H NMR** (CD₃OD) δ 7.47 (d, J=8.6Hz, 2H), 7.32 – 7.22 (m, 7H), 4.37 (s, 2H), 4.20 (d, J = 2.9 Hz, 1H), 4.08 (d, J = 2.9 Hz), 3.62 (s, 2H), 1.64 (s, 6H). **¹³C NMR** (75 MHz, CD₃OD) δ 173.5, 156.6, 153.5, 140.0, 137.9, 134.3, 131.6 (2C), 130.6, 129.7 (2C), 128.7 (2C), 128.4, 128.3, 84.5, 82.4, 44.4, 43.5, 28.3 (2C). **HRMS** (ESI): calc. for C₂₁H₂₃N₂O₃: 351.1703, found: 351.1696. **IR** (cm⁻¹): 2987 (m), 2966 (m), 2897 (m), 2348 (m), 1961 (w), 1743 (s), 1675 (s), 1649 (s), 1520 (m), 1402 (m).

Preparation of 5,5-dimethyl-4-methylene-3-phenyl-oxazolidin-2-one (**2s**)



1,1-dimethylprop-2-ynyl N-phenylcarbamate (**S9**)

To a solution of 2-methylbut-3-yn-2-ol (3.36 g, 40.0 mmol) in dry THF (30 mL, 1.0 M) under Argon was added pyridine (4.9 mL, 60.0 mmol, 1.5 equiv) and DMAP (0.58 g, 4.8 mmol, 12 mol%). Then phenyl isocyanate (5.3 mL, 48.0 mmol, 1.2 equiv) was added at room temperature. The reaction mixture was let to stir at rt overnight. Upon completion, the reaction mixture was treated with 2M HCl (50 mL) and extracted with EtOAc (3×50 mL). The combined organic phases were washed with water (100 mL) and brine (100 mL), then dried over Na₂SO₄, filtered, and concentrated under reduced pressure to give the crude product as whitish solid. The crude intermediate was used as such in the next step.

¹H NMR (300 MHz, CDCl₃) δ 7.43 – 7.22 (m, 4H), 7.09 – 6.99 (m, 1H), 6.55 (s, 1H), 2.57 (s, 1H), 1.75 (s, 6H). ¹³C NMR (75 MHz, CDCl₃) δ 151.8, 137.9, 129.2 (2C), 123.5, 118.7 (2C), 85.0, 72.5, 72.4, 29.4 (2C).

5,5-dimethyl-4-methylene-3-phenyl-oxazolidin-2-one (**2s**)

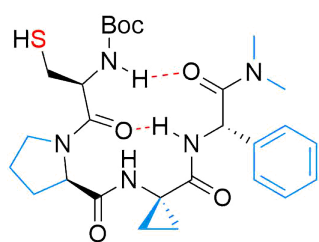
To a solution of **S9** (40.0 mmol) in DMF (40.0 mL, 1.0M) under Argon was added lithium hydroxide monohydrate (342 mg, 8.0 mmol, 0.2 equiv) and the reaction mixture was let to stir at rt overnight. Upon completion, the reaction mixture was diluted with water (50 mL) and extracted with EtOAc (3 × 60 mL). The combined organic phases were then washed with water (100 mL) and brine (100 mL), dried over Na₂SO₄, filtered, and concentrated under reduced pressure to return the crude as white solid. Purification by FC (4:6 pentane/(8:1.5:0.5 CH₂Cl₂/pentane/Et₂O)) afforded the **2s** as white solid (6.76 g, 33.3 mmol, 84%).

White solid. *R*_f = 0.37 (2:8 EtOAc/heptane). *Mp* 131.1-131.6°C, from EtOH (lit: 119.3-122.6°C, from EtOH). ¹H NMR (300 MHz, CD₂Cl₂) δ 7.54 – 7.46 (m, 2H), 7.45 – 7.31 (m, 3H), 4.11 (d, *J* = 2.8 Hz, 1H), 4.06 (d, *J* = 2.8 Hz, 1H), 1.63 (s, 6H). ¹³C NMR (75 MHz, CD₂Cl₂) δ 154.7, 152.4, 134.8, 129.9 (2C), 128.6, 127.5 (2C), 82.9, 81.1, 28.2 (2C).

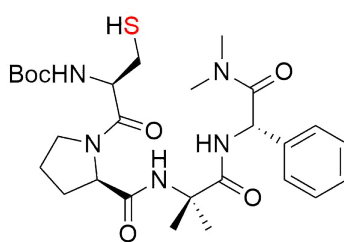
Physical and spectral data are in accordance with literature data:

Newton, R.; Savage, G. P. Australian journal of chemistry, 2008, 61(6), 432-437.

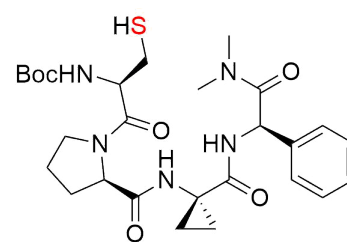
Preparation of cysteine derived peptides



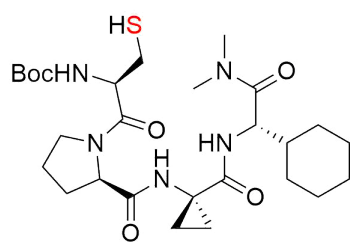
13a (211-C)



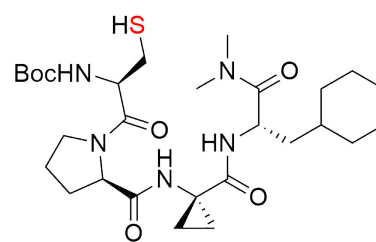
13b (148-C)



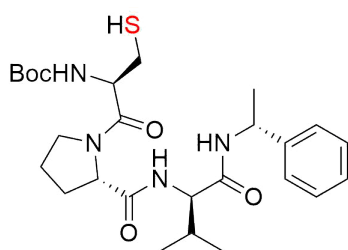
13c (208-C)



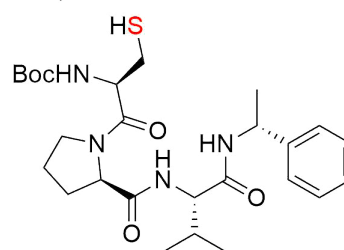
13d (164-C)



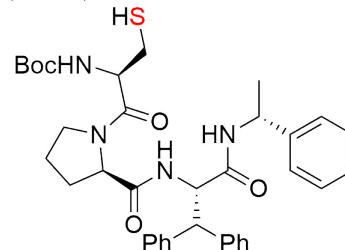
13e (098-C)



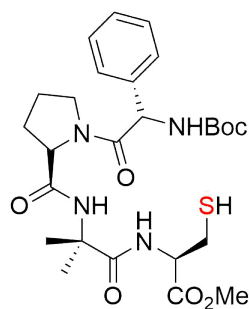
13f (228-C)



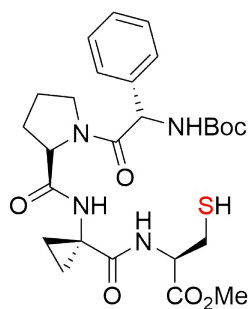
13g (067-C)



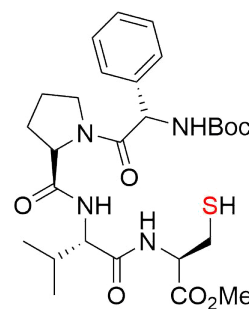
13h (248-D)



13i (031)



13j (068-D)



13k (115-B)

General Method of Reduction of Disulfide Dimers:

(Boc-Cys-Dpro-Acpc-Phg-NMe₂)₂ (75 mg, 0.067 mmol) and tris(2-carboxyethyl)phosphine hydrochloride (TCEP·HCl, 37 mg, 0.13 mmol, 2.0 eq.) were dissolved in MeOH/H₂O 4:1 (2 mL). The reaction mixture was stirred at room temperature for 3h. The volume of the mixture was adjusted to 8 mL resulting in a 1:1:1 MeCN/H₂O/MeOH solvent ratio. In order to isolate the product, preparative RP-HPLC from waters® was performed by A/D = 100/ to 70/30 in 10 min followed by 70/30 to 0/100 in 40 min, 8 ml injection, DAD: λ = 214 nm. Product containing fractions analyzed by HPLC-MS were pooled and concentrated by lyophilization to provide Boc-Cys-DPro-Acpc-Phg-NMe₂ (**JMR-VII-211-C**, **13a**) as a foamy white solid (65 mg, 86% yield).

HRMS (ESI): calc. for $C_{27}H_{40}N_5O_6S^+$: 562.2694, found: 562.2681.

JMR-VII-208-C, 13c

Following the general procedure with (Boc-Cys-DPro-Acpc-DPhg-NMe₂)₂ (52 mg, 0.046 mmol) and TCEP·HCl (27 mg, 0.094 mmol) to result in Boc-Cys-DPro-Acpc-DPhg-NMe₂ (46 mg, 82%).

HRMS (ESI): calc. for $C_{27}H_{40}N_5O_6S^+$: 562.2694, found: 561.2688.

JMR-VII-228-C, 13f

Following the general procedure with (Boc-Cys-Pro-DVal-(*R*)-Mba)₂ (93 mg, 0.089 mmol) and TCEP·HCl (52 mg, 0.181 mmol) to result in Boc-Cys-Pro-DVal-(*R*)-Mba (73 mg, 78%).

HRMS (ESI): calc. for $C_{26}H_{41}N_4O_5S^+$: 521.2792, found: 561.2784.

JMR-III-067-C, 13g

Following the general procedure with (Boc-Cys-DPro-Val-(*R*)-Mba)₂ (94 mg, 0.090 mmol) and TCEP·HCl (52 mg, 0.181 mmol) to result in Boc-Cys-DPro-Val-(*R*)-Mba (79 mg, 88%).

HRMS (ESI): calc. for $C_{26}H_{41}N_4O_5S^+$: 521.2792, found: 561.2787.

JMR-VII-248-D, 13h

Following the general procedure with (Boc-Cys-(4*S*-NH(CHPh₂)Ac)Pro-DVal-(*R*)-Mba)₂ (115 mg, 0.078 mmol) and TCEP·HCl (45 mg, 0.157 mmol) to result in Boc-Cys-(4*S*-NH(CHPh₂)Ac)Pro-DVal-(*R*)-Mba (70 mg, 83%).

HRMS (ESI): calc. for $C_{41}H_{54}N_5O_6S^+$: 744.3789, found: 744.3798.

JMR-I-031, 13i

Following the general procedure with (Boc-Phe-DPro-Aib-Cys-OMe)₂ (80 mg, 0.071 mmol) and TCEP·HCl (41 mg, 0.143 mmol) to result in Boc-Phe-DPro-Aib-Cys-OMe (70 mg, 87%).

HRMS (ESI): calc. for $C_{27}H_{41}N_4O_7S^+$: 565.2690, found: 565.2679.

JMR-II-068-D, 13j

Following the general procedure with (Boc-Phe-DPro-Acpc-Cys-OMe)₂ (93 mg, 0.83 mmol) and TCEP·HCl (48 mg, 0.167 mmol) to result in Boc-Phe-DAcpc-Val-Cys-OMe (84 mg, 71%).

HRMS (ESI): calc. for C₂₇H₃₉N₄O₇S⁺: 563.2534, found: 563.2541.

JMR-II-115-B, 13k

Following the general procedure with (Boc-Phe-DPro-Val-Cys-OMe)₂ (119 mg, 0.114 mmol) and TCEP·HCl (66 mg, 0.230 mmol) to result in Boc-Phe-DPro-Val-Cys-OMe (84 mg, 71%).

HRMS (ESI): calc. for C₂₈H₄₃N₄O₇S⁺: 579.2847, found: 579.2839.

General Method of Deprotection of Cys(*St*-Bu):

Boc-Cys(*St*-Bu)-DPro-Aib-Phg-NMe₂ (115 mg, 0.176 mmol) and tris(2-carboxyethyl)phosphine hydrochloride (TCEP·HCl, 252 mg, 0.88 mmol, 5.0 eq.) were dissolved in MeOH/H₂O 4:1 (2 mL). The reaction mixture was stirred at room temperature for 48h. The volume of the mixture was adjusted to 8 mL resulting in a 1:1:1 MeCN/H₂O/MeOH solvent ratio. In order to isolate the product, preparative RP-HPLC from waters® was performed by A/D = 100/ to 70/30 in 10 min followed by 70/30 to 0/100 in 40 min, 8 ml injection, DAD: λ = 214 nm. Product containing fractions analyzed by HPLC-MS were pooled and concentrated by lyophilization to provide Boc-Cys-DPro-Aib-Phg-NMe₂ (**JMR-VII-148-C, 13b**) as a foamy white solid (63 mg, 64% yield).

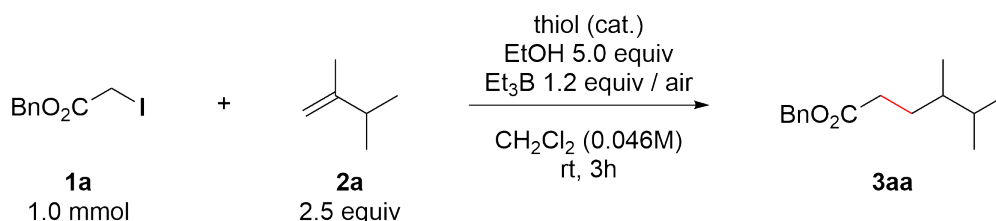
HRMS (ESI): calc. for C₂₇H₄₂N₅O₆S: 564.2850, found: 564.2844

JMR-VII-164-C, 13d

Following the general procedure with Boc-Cys(*St*Bu)-DPro-Acpc-Chg-NMe₂ (96 mg, 0.146 mmol) and TCEP·HCl (126 mg, 0.440 mmol) to result in Boc-Cys-DPro-Acpc-Chg-NMe₂ (26 mg, 32%).

HRMS (ESI): calc. for C₂₇H₄₆N₅O₆S⁺: 568.3163, found: 568.3171.

Optimization of the thiol-catalyzed hydroalkylation of alkenes with EtOH as a source of H-atoms



Entry	RSH	Cat. loading	Yield
1	1-dodecanethiol	20 mol%	78%
2	1-dodecanethiol	10 mol%	87%
3	1-dodecanethiol	5 mol%	83%
4	1-dodecanethiol	2 mol%	85%
5	-	-	45% ^a
6	thiophenol	5 mol%	81%
7	thiophenol	2 mol%	92%
8	1-butanethiol	2 mol%	97%
9	2-propanethiol	2 mol%	94%
10	1,1-dimethylethanethiol	2 mol%	76%
11	1-dodecanethiol	2 mol%	79% ^b

^a Yield determined by GC. ^b Using 1.2 equiv **1a** and 1.3 equiv Et₃B.

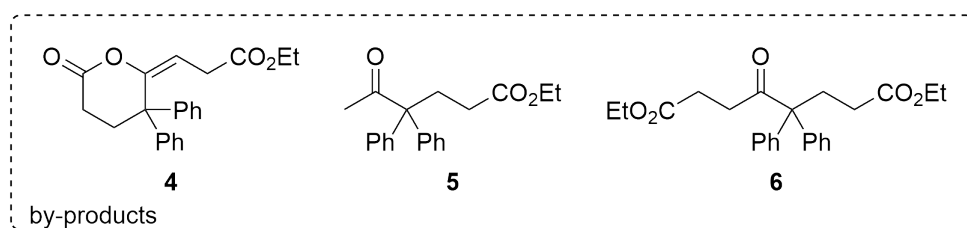
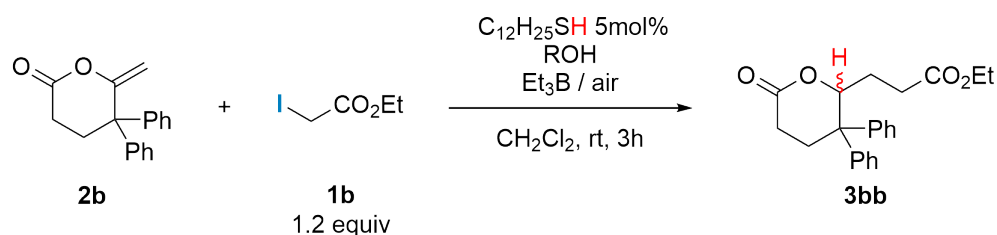
The conditions of entry 11 have been used for the scope and limitation study and is referred as "conditions A".

To a solution of the iodide **1a** (1 mmol), the alkene **2a** (2.5 mmol), thiol (0.1 M in *n*-hexane) and EtOH (0.29 mL, 5 mmol) in CH₂Cl₂ (20.0 mL) under Ar was added the solution of triethylborane (1.2 mL, 1 M in *n*-hexane, 1.2 mmol) slowly while the needle was immersed in solution. The resulting reaction mixture was stirred open to air for 3h at rt with a CaCl₂ guard tube. The crude product was filtered over a small pad of neutral aluminum oxide (2.0 cm) eluting with Et₂O and was then concentrated under reduced pressure. Purification by FC (5:95 Et₂O/pentane) afforded the **3aa** as colorless oil.

benzyl 4,5-dimethylhexanoate (**3aa**)

Colorless oil. *R*_f = 0.38 (6:94 Et₂O/pentane). ¹H NMR (300 MHz, CDCl₃) δ 7.41 – 7.29 (m, 5H), 5.12 (s, 2H), 2.48 – 2.23 (m, 2H), 1.81 – 1.66 (m, 1H), 1.63 – 1.51 (m, 1H), 1.51 – 1.37 (m, 1H), 1.36 – 1.24 (m, 1H), 0.87 (d, *J* = 6.8 Hz, 3H), 0.81 (dd, *J* = 6.8, 1.4 Hz, 6H). ¹³C NMR (75 MHz, CDCl₃) δ 174.1, 136.3, 128.7 (2C), 128.34 (2C), 128.30, 66.2, 38.3, 32.7, 32.0, 29.3, 20.2, 18.1, 15.1. HRMS (ESI): calc. for C₁₅H₂₂O₂ [M+Na]⁺: 257.1512, found: 257.1504. IR (cm⁻¹): 1734, 1379, 1163, 747, 734, 695.

Optimization of the hydroalkylation of the 5-methylenepentanolactone (**2b**) and source of H-atoms



Entry	Equiv 1b	Equiv 2b	Equiv Et ₃ B	Solvent	ROH (equiv)	Yield
1	1	2	1.3	CH ₂ Cl ₂	EtOH (5)	<10%
2	1.2	1	1.3	CH ₂ Cl ₂	EtOH (5)	47%
3	2	1	2.5	CH ₂ Cl ₂	EtOH (5)	54%
4	2	1	2.5	CH ₂ Cl ₂	EtOH (3)	61%
5	2	1	2.5	CH ₂ Cl ₂	H ₂ O (4)	71%
6	2	1	2.5	benzene	H ₂ O (4)	73%
7	2	1	3	benzene	H ₂ O (4)	75%
8	2	1	2.5	CH ₂ Cl ₂	H ₂ O (4)	82% ^a

^a Using thiophenol as a catalyst.

The conditions of entry 5 were selected and will be referred as "conditions B".

The conditions of entry 8 were selected and will be referred as "conditions C".

To a solution of the alkene **2b** (0.5 mmol), iodide **1b**, 1-dodecanethiol (0.5 mL, 0.1 M in n-hexane or CH₂Cl₂, 5 mol%) and ROH in CH₂Cl₂ (4.0 mL) under Ar was added a solution of triethylborane (1 M in n-hexane) slowly while the needle was immersed in solution. The resulting reaction mixture was stirred open to air for 3 h at rt with a CaCl₂ guard tube. The crude product was filtered over a small pad of neutral aluminum oxide (2.0 cm) eluting with EtOAc, concentrated under reduced pressure, and then purified by flash chromatography on silica gel.

ethyl 3-(6-oxo-3,3-diphenyl-tetrahydropyran-2-yl)propanoate (**3bb**)

Colorless oil. *R_f* 0.16 (3:7 Et₂O/pentane). ¹H NMR (300 MHz, CDCl₃) δ 7.34 – 7.12 (m, 10H), 5.24 (dt, *J* = 11.2, 2.3 Hz, 1H), 4.10 (q, *J* = 7.1 Hz, 2H), 2.88 (ddd, *J* = 13.3, 12.0, 6.0 Hz, 1H), 2.66 – 2.36 (m, 4H), 2.14 (ddd, *J* = 18.8, 12.0, 7.2 Hz, 1H), 1.90 (ddt, *J* = 14.5, 11.3, 6.7 Hz, 1H),

1.45 (dtd, $J = 14.8, 7.6, 2.5$ Hz, 1H), 1.23 (t, $J = 7.1$ Hz, 3H). $^{13}\text{C NMR}$ (75 MHz, CDCl_3) δ 173.1, 169.7, 144.04, 144.01, 128.91 (2C), 128.96 (2C), 127.6 (2C), 127.3 (2C), 127.1, 126.9, 83.5, 60.6, 48.0, 30.6, 27.7, 27.5, 27.1, 14.3. **HRMS (ESI)**: calc. for $\text{C}_{22}\text{H}_{24}\text{O}_4$ $[\text{M}+\text{Na}]^+$: 375.1567, found: 375.1562. **IR** (cm^{-1}): 1726, 1176, 1062, 1037, 955, 756, 698.

During the optimization, the compounds **4**, **5** and **6** were isolated as side products. Product **4** would be formed after a SET process. Side products **5** and **6** were observed while using EtOH as source of H-atom, suggesting an ethanolysis process of the starting olefin **2b** and of the unsaturated product **4**, under slightly acidic conditions of the reaction mixture.

ethyl 3-(6-oxo-3,3-diphenyltetrahydro-2H-pyran-2-ylidene)propanoate (**4**)

Colorless oil. R_f 0.19 (2:8 EtOAc/heptanes). $^1\text{H NMR}$ (300 MHz, CDCl_3) δ 7.45 – 7.10 (m, 10H), 4.42 (t, $J = 7.2$ Hz, 1H), 4.14 (q, $J = 7.1$ Hz, 2H), 3.29 (d, $J = 7.2$ Hz, 2H), 2.76 (t, $J = 6.7$ Hz, 2H), 2.58 (t, $J = 6.7$ Hz, 2H), 1.26 (t, $J = 7.2$ Hz, 3H). $^{13}\text{C NMR}$ (75 MHz, CDCl_3) δ 171.4, 167.0, 155.1, 142.3 (2C), 128.8 (4C), 128.6 (4C), 127.5 (2C), 106.3, 60.8, 51.6, 30.4, 30.3, 28.7, 14.3. **HRMS (ESI)**: calc. for $\text{C}_{22}\text{H}_{24}\text{O}_4$ $[\text{M}+\text{Na}]^+$: 373.1410, found: 373.1409. **IR** (cm^{-1}): 1726, 1176, 1062, 1037, 955, 756, 698.

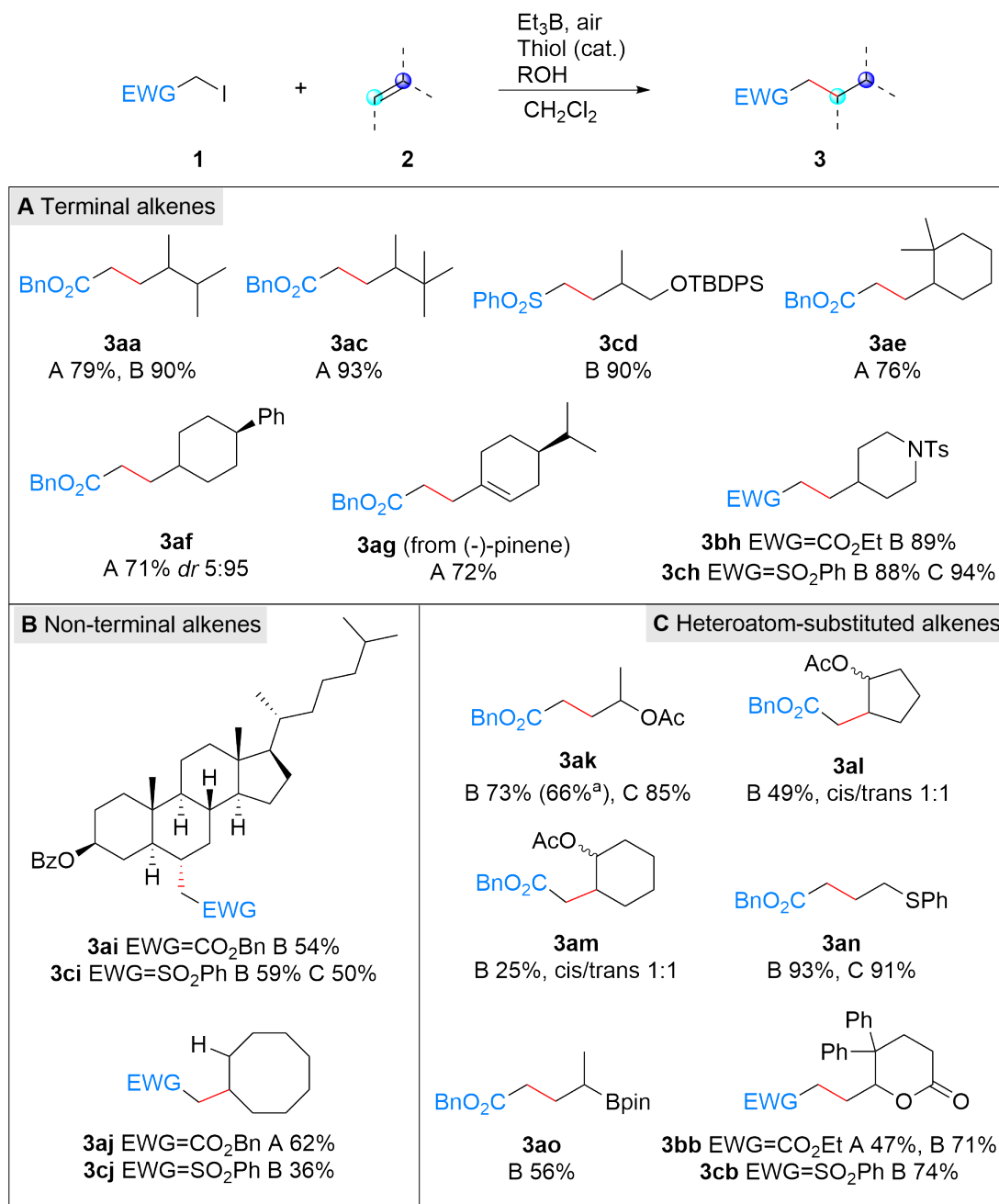
ethyl 5-oxo-4,4-diphenyl-hexanoate (**5**)

Colorless oil. R_f 0.30 (1:9 Et₂O/pentane). $^1\text{H NMR}$ (300 MHz, CDCl_3) δ 7.41 – 7.26 (m, 10H), 4.04 (q, $J = 7.1$ Hz, 2H), 2.71 – 2.61 (m, 2H), 2.12 – 1.97 (m, 5H), 1.20 (t, $J = 7.1$ Hz, 3H). $^{13}\text{C NMR}$ (75 MHz, CDCl_3) δ 207.7, 173.4, 140.7 (2C), 129.3 (4C), 128.6 (4C), 127.3 (2C), 65.7, 60.4, 32.5, 30.5, 27.5, 14.2. **HRMS (ESI)** calc. for $\text{C}_{20}\text{H}_{22}\text{O}_3$ $[\text{M}+\text{H}]^+$: 311.1642, found: 311.1650. **IR** (neat, cm^{-1}): 3058, 3024, 2981, 2936, 1728, 1703, 1494.

diethyl 5-oxo-4,4-diphenyl-octanedioate (**6**)

Whitish sticky solid. R_f 0.48 (2:8 Et₂O/pentane). $^1\text{H NMR}$ (400 MHz, CDCl_3) δ 7.38 – 7.26 (m, 10H), 4.09 (q, $J = 7.2$ Hz, 2H), 4.03 (q, $J = 7.1$ Hz, 2H), 2.70 – 2.64 (m, 4H), 2.38 (t, $J = 6.7$ Hz, 2H), 2.07 – 2.00 (m, 2H), 1.22 (t, $J = 7.2$ Hz, 3H), 1.18 (t, $J = 7.2$ Hz, 3H). $^{13}\text{C NMR}$ (101 MHz, CDCl_3) δ 208.8, 173.5, 172.9, 141.1 (2C), 129.4 (4C), 128.7 (4C), 127.4 (2C), 65.2, 60.7, 60.5, 34.2, 32.7, 30.6, 29.0, 14.3 (2C). **HRMS (ESI)** calc. for $\text{C}_{24}\text{H}_{28}\text{O}_5$ $[\text{M}+\text{Na}]^+$: 419.1829, found: 419.1821. **IR** (neat, cm^{-1}): 2976, 2957, 230, 2864, 1731, 1708, 1596.

Scope and limitation of thiol catalyzed hydroalkylation process



Conditions A:

To a solution of the alkene (1.0 mmol), iodide (1.2 mmol), 1-dodecanethiol (0.2 mL, 0.1 M in n-hexane or CH₂Cl₂, 2 mol%) and EtOH (0.29 mL, 5 mmol) in CH₂Cl₂ (10.0 mL) under Ar was added a solution of triethylborane (1.3 mL, 1 M in n-hexane, 1.3 mmol) slowly while the needle was immersed in solution. The resulting reaction mixture was stirred open to air for 3 h at rt with a CaCl₂ guard tube. The crude product was filtered over a small pad of neutral aluminum oxide (2.0 cm) eluting with EtOAc or Et₂O, concentrated under reduced pressure, and then purified by flash chromatography on silica gel.

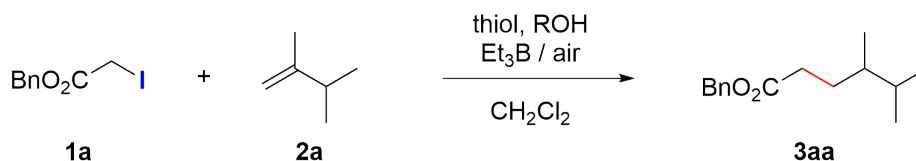
Conditions B:

To a solution of the alkene (0.5 mmol), iodide (1.0 mmol), 1-dodecanethiol (0.25 mL, 0.1 M in n-hexane or CH₂Cl₂, 5 mol%) and H₂O (36 μL, 2.0 mmol) in CH₂Cl₂ (4.0 mL) under Ar was added a solution of triethylborane (1.25 mL, 1 M in n-hexane, 1.25 mmol) slowly while the needle was immersed in solution. The resulting reaction mixture was stirred open to air for 3 h at rt with a CaCl₂ guard tube. The crude product was filtered over a small pad of neutral aluminum oxide (2.0 cm) eluting with EtOAc or Et₂O, concentrated under reduced pressure, and then purified by flash chromatography on silica gel.

Conditions C:

To a solution of the alkene (0.5 mmol), iodide (1.0 mmol), thiophenol (0.25 mL, 0.1 M in n-hexane or CH₂Cl₂, 5 mol%) and H₂O (36 μL, 2.0 mmol) in CH₂Cl₂ (4.0 mL) under Ar was added a solution of triethylborane (1.25 mL, 1 M in n-hexane, 1.25 mmol) slowly while the needle was immersed in solution. The resulting reaction mixture was stirred open to air for 3 h at rt with a CaCl₂ guard tube. The crude product was filtered over a small pad of neutral aluminum oxide (2.0 cm) eluting with EtOAc or Et₂O, concentrated under reduced pressure, and then purified by flash chromatography on silica gel.

benzyl 4,5-dimethylhexanoate (3aa)



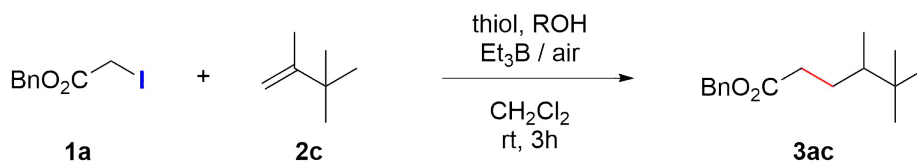
Following **Condition A** with 2,3-dimethyl-1-butene **2a** (84 mg, 1 mmol) and benzyl 2-iodoacetate **1a** (331 mg, 1.2 mmol). Purification by FC (5:95 Et₂O/pentane) delivered the product **3aa** as a colorless oil (185 mg, 79%).

Following **Condition B** with 2,3-dimethylbut-1-ene **2a** (42 mg, 0.5 mmol) and benzyl 2-iodoacetate **1a** (276 mg, 1 mmol) at 0°C. Purification by FC (3:97 EtOAc/heptanes) delivered the product **3aa** as a colorless oil (117 mg, 82% yield after correction, traces of benzyl acetate could not be removed (2%)).

Colorless oil. *R_f* 0.38 (6:94 Et₂O/pentane). ¹H NMR (300 MHz, CDCl₃) δ 7.41 – 7.29 (m, 5H), 5.12 (s, 2H), 2.48 – 2.23 (m, 2H), 1.81 – 1.66 (m, 1H), 1.63 – 1.51 (m, 1H), 1.51 – 1.37 (m, 1H), 1.36 – 1.24 (m, 1H), 0.87 (d, *J* = 6.8 Hz, 3H), 0.81 (dd, *J* = 6.8, 1.4 Hz, 6H). ¹³C NMR (75 MHz, CDCl₃) δ 174.1, 136.3, 128.7 (2C), 128.34 (2C), 128.30, 66.2, 38.3, 32.7, 32.0, 29.3, 20.2, 18.1, 15.1.

Complete characterization data described previously in the optimization part.

benzyl 4,5,5-trimethylhexanoate (**3ac**)



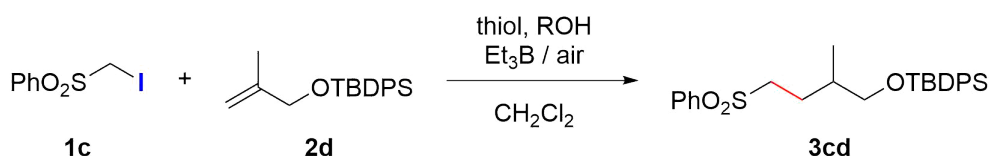
Following **Condition A** with 2,3,3-trimethyl-1-butene **2c** (98 mg, 1 mmol) and benzyl 2-iodoacetate **1a** (331 mg, 1.2 mmol). Purification by FC (5:95 Et₂O/pentane) delivered the product **3ac** as a colorless oil (230 mg, 93%).

Colorless oil. **¹H NMR** (300 MHz, CDCl₃) δ 7.39 – 7.30 (m, 5H), 5.12 (s, 2H), 2.46 (ddd, J = 15.2, 9.7, 5.1 Hz, 1H), 2.26 (ddd, J = 15.7, 8.9, 7.0 Hz, 1H), 2.01 – 1.85 (m, 1H), 1.25 – 1.05 (m, 2H), 0.85 (s, 9H), 0.82 (d, J = 6.5 Hz, 3H). **¹³C NMR** (75 MHz, CDCl₃) δ 174.1, 136.3, 128.7 (2C), 128.4 (2C), 128.3, 66.3, 42.7, 33.6, 33.2, 27.4 (3C), 27.1, 14.0. **HRMS (ESI)** calcd for C₁₆H₂₄O₂ [M+Na]⁺ m/z=271.1669, found 271.1670. **IR** (cm⁻¹): 3033, 2958, 2868, 1734, 1455, 1155.

The physical and spectral data are in accordance with literature data:

Miao, P.; Li, R.; Lin, X.; Rao, L.; Sun, Z. *Green Chemistry*, 2021, 23(4), 1638-1641.

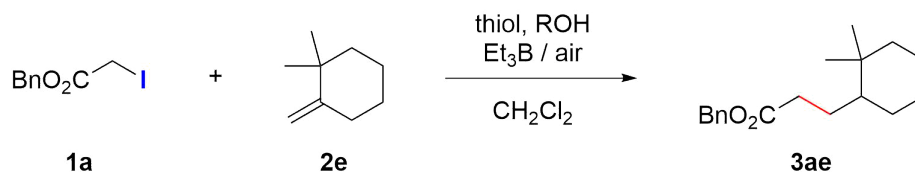
tert-butyl((2-methylpentyl)oxy)diphenylsilane (**3cd**)



Following **Condition B** with iodomethylsulfonamide **1c** (282 mg, 1 mmol) and alkene **2d** (155 mg, 0.5 mmol) at 0°C. Purification by FC (25:75 EtOAc/heptanes) delivered the product **3cd** as colorless oil (210 mg, 90)

Colorless oil. **¹H NMR** (300 MHz, CDCl₃) δ 7.96 – 7.84 (m, 2H), 7.69 – 7.51 (m, 7H), 7.48 – 7.34 (m, 6H), 3.48 (dd, J = 10.1, 5.0 Hz, 1H), 3.39 (dd, J = 10.1, 6.3 Hz, 1H), 3.13 (dd, J = 9.0, 7.4 Hz, 2H), 1.98 – 1.82 (m, 1H), 1.80 – 1.54 (m, 2H), 1.00 (s, 9H), 0.87 (d, J = 6.6 Hz, 3H). **¹³C NMR** (75 MHz, CDCl₃) δ 139.2, 135.7 (2C), 135.6 (2C), 133.7, 133.6, 133.5, 129.8 (2C), 129.3 (2C), 128.2 (2C), 127.8 (4C), 68.2, 54.6, 34.8, 26.9 (3C), 26.5, 19.3, 16.5. **HRMS (ESI)**: calcd for C₂₇H₃₄O₃NaSSi [M+Na]⁺: 489.1890, found: 489.1887. **IR** (cm⁻¹): 1317, 1305, 1145, 1110, 1085, 739, 700, 687.

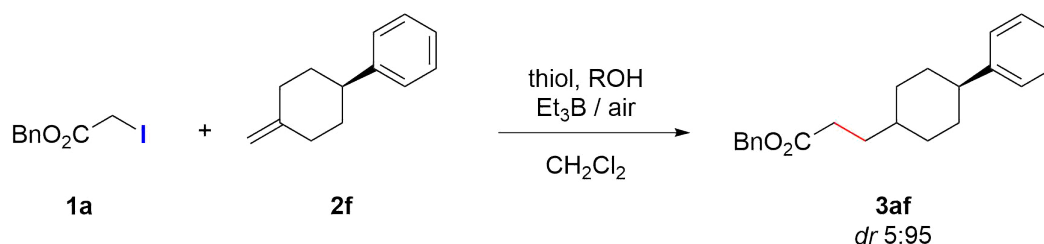
benzyl 3-(4-phenylcyclohexyl)propanoate (**3ae**)



Following **Condition B** with iodomethylsulfonylbenzene **1c** (282 mg, 1 mmol) and alkene **2d** (155 mg, 0.5 mmol) at 0°C. Purification by FC (25:75 EtOAc/heptanes) delivered the product **3cd** as colorless oil (210 mg, 90%).

Colorless oil. ¹H NMR (300 MHz, CDCl₃) δ 7.96 – 7.84 (m, 2H), 7.69 – 7.51 (m, 7H), 7.48 – 7.34 (m, 6H), 3.48 (dd, J = 10.1, 5.0 Hz, 1H), 3.39 (dd, J = 10.1, 6.3 Hz, 1H), 3.13 (dd, J = 9.0, 7.4 Hz, 2H), 1.98 – 1.82 (m, 1H), 1.80 – 1.54 (m, 2H), 1.00 (s, 9H), 0.87 (d, J = 6.6 Hz, 3H). ¹³C NMR (75 MHz, CDCl₃) δ 139.2, 135.7 (2C), 135.6 (2C), 133.7, 133.6, 133.5, 129.8 (2C), 129.3 (2C), 128.2 (2C), 127.8 (4C), 68.2, 54.6, 34.8, 26.9 (3C), 26.5, 19.3, 16.5. HRMS (ESI): calcd for C₂₇H₃₄O₃NaSSi [M+Na]⁺: 489.1890, found: 489.1887. IR (cm⁻¹): 1317, 1305, 1145, 1110, 1085, 739, 700, 687.

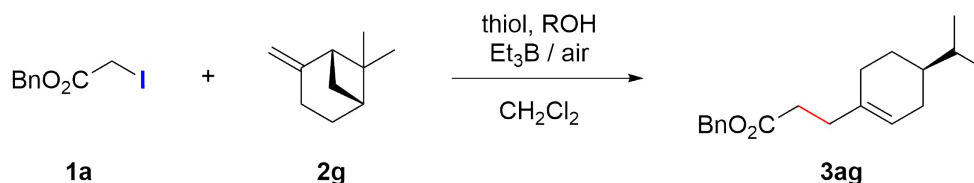
benzyl 3-(4-phenylcyclohexyl)propanoate (**3af**)



Following **Condition A** with (4-methylenecyclohexyl)benzene **2f** (172 mg, 1 mmol) and benzyl 2-iodoacetate **1a** (331 mg, 1.2 mmol). Purification by FC (5:95 Et₂O/pentane) delivered the product **3af** as a yellow oil (230 mg, 71%, dr 5:95).

Yellow oil. ¹H NMR (300 MHz, CDCl₃, major) δ 7.38 – 7.16 (m, 10H), 5.13 (s, 2H), 2.51 – 2.35 (m, 3H), 1.95 – 1.80 (m, 3H), 1.68 – 1.52 (m, 3H), 1.43 (qd, J = 13.7, 13.1, 3.6 Hz, 2H), 1.35 – 1.20 (m, 1H), 1.07 (qd, J = 12.9, 12.1, 3.7 Hz, 2H). ¹³C NMR (75 MHz, CDCl₃, major) δ 174.0, 147.7, 136.3, 128.7 (2C), 128.44 (2C), 128.38 (2C), 128.3, 126.9 (2C), 126.0, 66.3, 44.6, 37.0, 34.2 (2C), 33.3 (2C), 32.4, 32.1. HRMS (ESI) calcd for C₂₂H₂₆O₂ [M+Na]⁺: 345.1825, found 345.1824. IR (cm⁻¹): 3060, 3027, 2919, 2849, 1732, 1601, 1450.

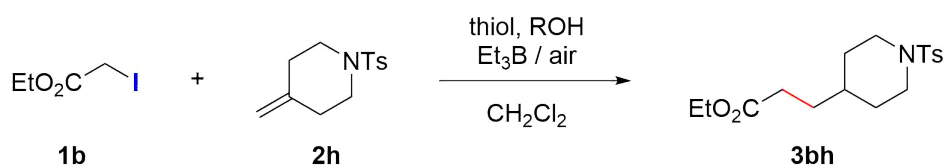
benzyl 3-(4-isopropylcyclohex-1-en-1-yl)propanoate (3ag)



Following **Condition A** with benzyl 2-iodoacetate **1a** (331 mg, 1.2 mmol) and (-)-(*S*)-pinene **2g** (136 mg, 1 mmol). Purification by FC (5:95 Et₂O/pentane) delivered the product **3ag** as colorless oil (205 mg, 72%).

Colorless liquid. ¹H NMR (300 MHz, CDCl₃) δ 7.41 – 7.28 (m, 5H), 5.42 – 5.35 (m, 1H), 5.11 (s, 2H), 2.52 – 2.41 (m, 2H), 2.39 – 2.21 (m, 2H), 2.08 – 1.81 (m, 3H), 1.79 – 1.60 (m, 2H), 1.51 – 1.36 (m, 1H), 1.31 – 1.07 (m, 2H), 0.87 (dd, J = 6.8, 3.8 Hz, 6H). ¹³C NMR (75 MHz, CDCl₃) δ 173.6, 136.3, 135.9, 128.7 (2C), 128.4 (2C), 128.3, 121.7, 66.3, 40.2, 33.1, 32.7, 32.4, 29.1, 29.0, 26.5, 20.1, 19.8. HRMS (ESI) calcd for C₁₉H₂₇O₂ [M+H]⁺: 287.2006, found 287.2008. IR (cm⁻¹): 3033, 2954, 2914, 2870, 2834, 1733, 1455.

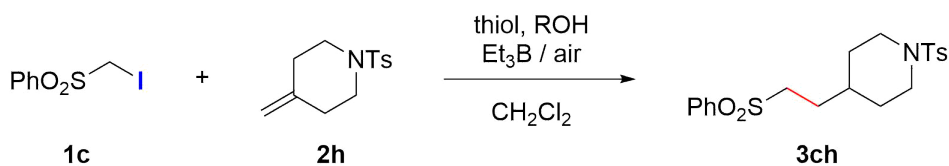
ethyl 3-(1-tosylpiperidin-4-yl)propanoate (3bh)



Following **Condition B** with ethyl iodoacetate **1b** (214 mg, 1 mmol) and alkene **2h** (125 mg, 0.5 mmol) at 0°C. Purification by FC (15:85 EtOAc/heptanes) delivered the product **3bh** as white solid (151 mg, 89% yield).

White solid. **Mp** 80-82°C. ¹H NMR (400 MHz, CDCl₃) δ 7.62 (d, J = 8.1 Hz, 2H), 7.31 (d, J = 8.1 Hz, 2H), 4.09 (qd, J = 7.1, 0.9 Hz, 2H), 3.75 (d, J = 11.7 Hz, 2H), 2.42 (s, 3H), 2.26 (t, J = 7.7 Hz, 2H), 2.24 – 2.16 (m, 2H), 1.79 – 1.65 (m, 2H), 1.55 (q, J = 7.3 Hz, 2H), 1.38 – 1.12 (m, 6H). ¹³C NMR (101 MHz, CDCl₃) δ 173.5, 143.5, 133.3, 129.7 (2C), 127.9 (2C), 60.5, 46.4 (2C), 34.7, 31.6, 31.3 (2C), 31.0, 21.6, 14.3. HRMS (ESI): calcd for C₁₇H₂₅O₄NNaS [M+Na]⁺: 362.1397, found: 362.1386. IR (cm⁻¹): 1729 (s), 1159 (s), 926 (s), 816 (m), 722 (s), 648 (s), 601 (s), 547 (s).

4-(2-(phenylsulfonyl)ethyl)-1-tosylpiperidine (**3ch**)

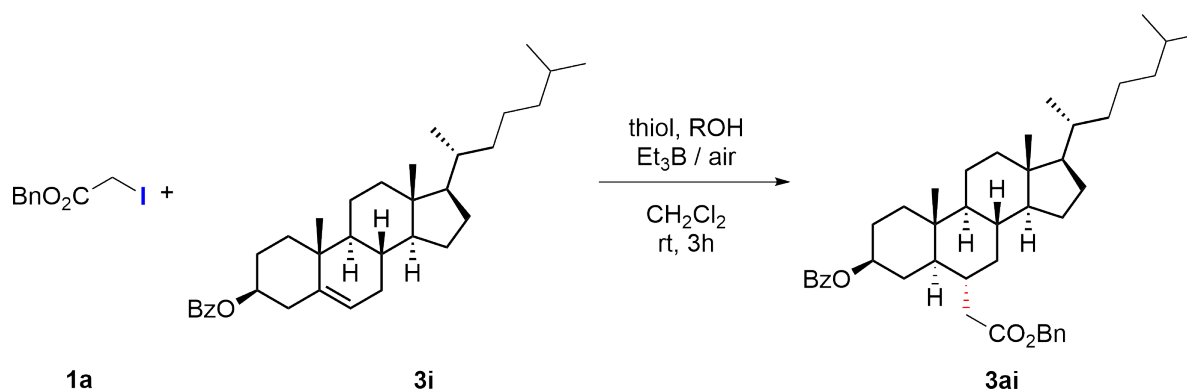


Following **Condition B** with iodomethylsulfonylbenzene **1c** (282 mg, 1 mmol) and alkene **2h** (125 mg, 0.5 mmol) at 0°C. Purification by FC (35:65 EtOAc/heptanes) delivered the product **3ch** as white solid (180 mg, 88% yield).

Following **Condition C** with iodomethylsulfonylbenzene **1c** (282 mg, 2.0 mmol) and alkene **2h** (126 mg, 0.5 mmol) at 0°C. Purification by FC (25:75 EtOAc/heptanes) delivered the product **3ch** as white solid (191 mg, 94% yield).

White solid. **Mp** 103.0-104.7 °C. ¹H NMR (400 MHz, CDCl₃) δ 7.91 – 7.84 (m, 1H), 7.73 – 7.49 (m, 4H), 7.30 (d, J = 8.0 Hz, 2H), 3.87 – 3.63 (m, 2H), 3.09 – 2.93 (m, 2H), 2.31 – 2.07 (m, 2H), 1.74 – 1.56 (m, 3H), 1.43 – 1.17 (m, 2H). ¹³C NMR (101 MHz, CDCl₃) δ 143.7, 139.2, 133.9, 133.2, 129.7 (2C), 129.5 (2C), 128.1 (2C), 127.8 (2C), 53.8, 46.2 (2C), 34.1, 31.1 (2C), 28.7, 21.6. **HRMS** (ESI): calcd for C₂₀H₂₆O₄NS₂ [M+H]⁺: 421.1468, found: 421.1468. **IR** (cm⁻¹): 1726, 1334, 1159, 930, 813, 723, 650, 604, 545.

(3*S*,8*S*,9*S*,10*S*,13*R*,14*S*,17*R*)-6-(2-(benzyloxy)-2-oxoethyl)-10,13-dimethyl-17-((*R*)-6-methylheptan-2-yl)hexadecahydro-1*H*-cyclopenta[*a*]phenanthren-3-yl benzoate (**3ai**)



Following **Condition B** from benzyl 2-iodoacetate **1a** (276 mg, 1.0 mmol) and cholesterol benzoate **3i** (245 mg, 0.5 mmol) at 0°C. Purification by FC (5:95 Et₂O/pentane) delivered the product **3ai** as yellow oil which solidifies upon cooling (172 mg, 54%).

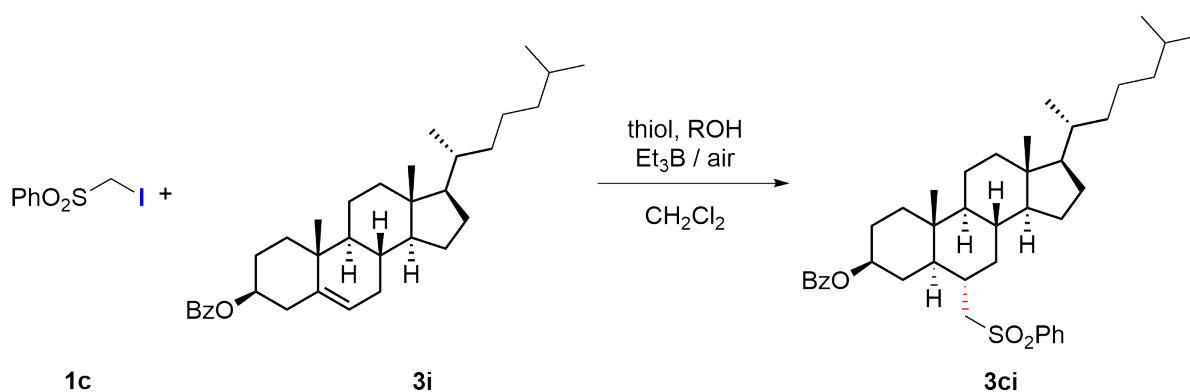
Yellow oil. **R_f** 0.40 (10:90 Et₂O/pentane). ¹H NMR (300 MHz, CDCl₃) δ 8.09 – 8.00 (m, 2H), 7.58 – 7.50 (m, 1H), 7.48 – 7.27 (m, 7H), 5.10 (s, 2H), 5.07 – 4.91 (m, 1H), 2.48 – 2.28 (m, 2H), 2.25 – 2.14 (m, 1H), 2.04 – 1.91 (m, 2H), 1.89 – 0.94 (m, 28H), 0.93 – 0.84 (m, 11H), 0.68 (s,

3H). ^{13}C NMR (75 MHz, CDCl_3) δ 173.8, 166.2, 136.2, 132.8, 130.9, 129.7 (2C), 128.7 (2C), 128.4 (2C), 128.3 (2C), 128.3, 74.7, 66.3, 56.4, 56.0, 54.6, 46.1, 42.7, 40.0, 39.7, 39.3, 36.4, 36.3, 36.0, 35.9 (2C), 34.6, 32.7, 30.9, 28.3, 28.2, 27.8, 24.4, 24.0, 23.0, 22.7, 21.2, 18.8, 16.4, 12.3. **HRMS** (ESI): for $\text{C}_{43}\text{H}_{60}\text{O}_4\text{Na}$ calc. 663.4384, found 663.4381. **IR** (cm^{-1}): 2942, 2932, 2866, 2853, 1711, 1451, 1274, 906, 710.

Physical and spectral data are in accordance with literature data:

Povie, G.; Suravarapu, S.R.; Bircher, M.P.; Mojzes, M.M.; Rieder, S.; Renaud, P. *Science advances*, 2018, 4(7), eaat6031.

(3S,5R,6S,8S,9S,10R,13R,14S,17R)-10,13-dimethyl-17-((R)-6-methylheptan-2-yl)-6-((phenylsulfonyl)methyl)hexadecahydro-1H-cyclopenta[a]phenanthren-3-yl benzoate (3ci**)**



Following **Condition A** from iodomethylsulfonylbenzene **1c** (169 mg, 0.6 mmol) and cholesteryl benzoate **3i** (245 mg, 0.5 mmol) at 0°C . Purification by FC (15:85 EtOAc/heptanes) delivered the product **3ci** as white solid (144 mg, 44%).

Following **Condition B** from iodomethylsulfonylbenzene **1c** (245 mg, 1.0 mmol) and cholesteryl benzoate **3i** (282 mg, 0.5 mmol) at 0°C . Purification by FC (15:85 EtOAc/heptanes) delivered the product **3ci** as white solid (191 mg, 59%).

Following **Condition C** from iodomethylsulfonylbenzene **1c** (245 mg, 1.0 mmol) and cholesteryl benzoate **3i** (282 mg, 0.5 mmol) at 0°C . Purification by FC (15:85 EtOAc/heptanes) delivered the product **3ci** as white solid (162 mg, 50%).

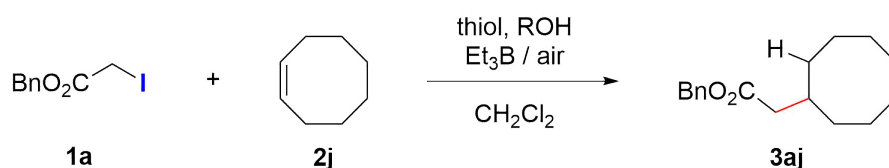
Mixture of diastereoisomers

White solid. **Mp**: $170\text{--}171^\circ\text{C}$. $[\alpha]_D^{23} = -2.9^\circ$ (c 1.0, CHCl_3). ^1H NMR (400 MHz, CDCl_3) δ 8.05 – 7.97 (m, 2H), 7.92 – 7.85 (m, 2H), 7.62 – 7.39 (m, 6H), 4.96 – 4.80 (m, 1H), 3.17 – 3.00 (m, 2H), 2.20 – 2.08 (m, 1H), 2.01 – 1.86 (m, 2H), 1.85 – 1.64 (m, 3H), 1.60 – 0.92 (m, 24H), 0.89 (d, $J = 6.6$ Hz, 3H), 0.86 (dd, $J = 6.6, 1.9$ Hz, 6H), 0.82 (s, 3H), 0.65 (s, 3H). ^{13}C NMR (101 MHz, CDCl_3) δ 166.0, 139.2, 133.8, 132.9, 130.8, 129.6, 129.4, 128.4, 128.4, 74.1, 56.6, 56.3, 55.7,

54.4, 46.0, 42.7, 39.8, 39.6, 38.7, 36.3, 36.0, 35.9, 35.9, 34.0, 32.0, 30.9, 28.3, 28.1, 27.6, 24.3, 23.9, 23.0, 22.7, 21.1, 18.8, 15.8, 12.3. **HRMS** (ESI): calcd for $C_{41}H_{58}O_4NaS$ $[M+Na]^+$: 669.3948, found: 669.3929. **IR** (cm^{-1}): 1701, 1304, 1275, 719, 688.

Stereochemical conformation of major product is in accordance with literature data:
Povie, G.; Suravarapu, S.R.; Bircher, M.P.; Mojzes, M.M.; Rieder, S.; Renaud, P. *Science advances*, 2018, 4(7), eaat6031.

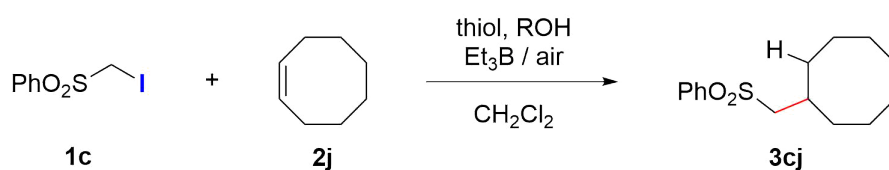
benzyl 2-cyclooctylacetate (**3aj**)



Following **Condition A** with benzyl 2-iodoacetate **1a** (331 mg, 1.2 mmol) and cyclooctene **2j** (116 mg, 1 mmol). Purification by FC (5:95 Et_2O /pentane) delivered the product **3aj** as colorless oil (163 mg, 62%).

Colorless oil. 1H NMR (300 MHz, $CDCl_3$) δ 7.38 – 7.30 (m, 5H), 5.11 (s, 2H), 2.27 (d, $J = 7.3$ Hz, 2H), 2.12 – 2.01 (m, 1H), 1.64 – 1.46 (m, 12H), 1.32 – 1.29 (m, 2H). ^{13}C NMR (75 MHz, $CDCl_3$) δ 173.2, 136.3, 128.6 (2C), 128.22 (2C), 128.17, 66.0, 42.9, 34.7, 32.2 (2C), 27.1 (2C), 26.2, 25.3 (2C). **HRMS** (ESI) calcd for $C_{17}H_{24}NaO_2$ $[M+Na]^+$: 283.1674, found: 283.1663. **IR** (cm^{-1}): 2915, 2845, 1732, 1446, 1374, 1151.

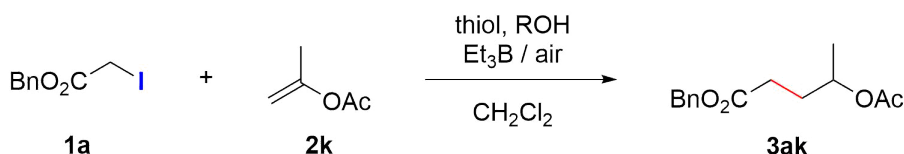
((phenylsulfonyl)methyl)cyclooctane (**3cj**)



Following **Condition B** with iodomethylsulfonylbenzene **1c** (138 mg, 1 mmol) and cyclooctene **2i** (55 mg, 0.5 mmol) at $0^\circ C$. Purification by FC (1:9 $EtOAc$ /heptanes) delivered the product **3ci** as colorless oil (48 mg, 36% yield).

Colorless oil. 1H NMR (300 MHz, $CDCl_3$) δ 8.03 – 7.79 (m, 2H), 7.73 – 7.45 (m, 3H), 3.00 (d, $J = 6.2$ Hz, 2H), 2.37 – 2.11 (m, 1H), 1.88 – 1.29 (m, 14H). ^{13}C NMR (75 MHz, $CDCl_3$) δ 140.4, 133.6, 129.4 (2C), 127.9 (2C), 63.4, 32.8, 32.2 (2C), 27.1 (2C), 26.1, 24.9 (2C). **HRMS** (ESI): calcd for $C_{15}H_{22}O_2NaS$ $[M+Na]^+$: 289.1233, found: 289.1224.

benzyl 4-acetoxypentanoate (3ak)



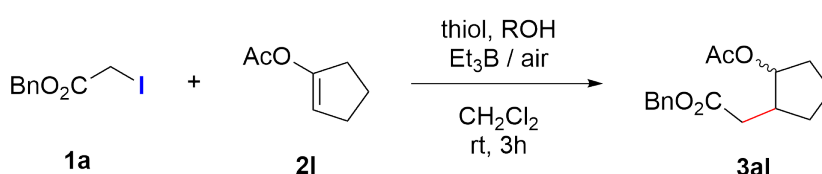
Following **Condition A** with benzyl 2-iodoacetate **1a** (331 mg, 1.2 mmol) and propenyl acetate **2k** (100 mg, 1 mmol) at 0°C. Purification by FC (15:85 Et₂O/pentane) delivered the product **3ak** as colorless oil (180 mg, 72%).

Following **Condition B** with benzyl 2-iodoacetate **1a** (276 mg, 1.0 mmol) and propenyl acetate **2k** (50 mg, 0.5 mmol) at 0°C. Purification by FC (15:85 Et₂O/pentane) delivered the product **3ak** as colorless oil (91 mg, 73%).

Following **Condition C** with benzyl 2-iodoacetate **1a** (276 mg, 1.0 mmol) and propenyl acetate **2k** (50 mg, 0.5 mmol) at 0°C. Purification by FC (15:85 Et₂O/pentane) delivered the product **3ak** as colorless oil (106 mg, 85%).

Colorless oil. ¹H NMR (300 MHz, CDCl₃) δ 7.39 – 7.33 (m, 5H), 5.12 (s, 2H), 4.93 (h, J = 6.2 Hz, 1H), 2.41 (td, J = 7.3, 2.3 Hz, 2H), 2.00 (s, 3H), 1.96 – 1.84 (m, 2H), 1.23 (d, J = 6.2 Hz, 3H). ¹³C NMR (75 MHz, CDCl₃) δ 172.9, 170.7, 136.0, 128.7 (2C), 128.3 (3C), 70.1, 66.5, 31.0, 30.5, 21.3, 20.0. HRMS (ESI): calcd for C₁₄H₁₉O₄ [M+H]⁺: 251.1278, found: 251.1271. IR (cm⁻¹): 1730, 1372, 1237, 1165, 737, 697.

benzyl 2-(2-acetoxycyclopentyl)acetate (3al)



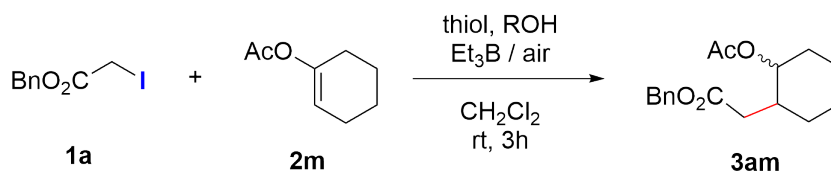
Following the **Conditions A** with the alkene **2l** (63 mg, 0.5 mmol) and benzyl iodoacetate **1a** (276 mg, 1 mmol) at 0°C. The product was purified by flash chromatography on silica gel (heptanes/EtOAc 92.5:7.5) to give the product **3al** as a colorless oil (67 mg, 49% yield, dr 1:1).

Mixture of diastereoisomers

¹H NMR (400 MHz, CDCl₃) δ 7.41 – 7.30 (m, 5H), 5.23 – 5.16 (m, 0.5H), 5.11 (d, J = 2.1 Hz, 2H), 4.87 – 4.77 (m, 0.5H), 2.63 – 2.48 (m, 1H), 2.44 – 2.24 (m, 2H), 2.07 – 1.93 (m, 1H), 2.00 (s, 3H), 1.97 – 1.53 (m, 4H), 1.51 – 1.38 (m, 0.5H), 1.33 – 1.15 (m, 0.5H). ¹³C NMR (101 MHz, CDCl₃) δ 172.7, 172.4, 171.0, 170.7, 136.1, 136.1, 128.7 (2C), 128.40, 128.35 (2C), 128.33, 80.4, 66.4, 66.4, 42.2, 40.3, 38.1, 34.5, 32.5, 31.7, 30.2, 29.8, 22.6, 22.2, 21.3, 21.2. HRMS

(ESI): calcd for $C_{16}H_{20}O_4Na$: 299.1254, found: 299.1242. IR (cm^{-1}): 1729 (s), 1238 (s), 738 (m), 697 (s).

benzyl 2-(2-acetoxycyclohexyl)acetate (**3am**)

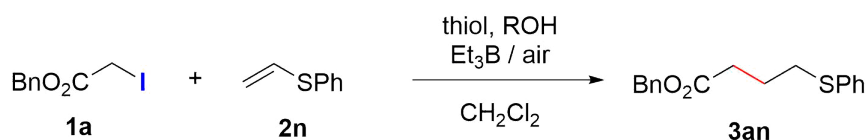


Following the **Conditions A** with the alkene **2m** (70 mg, 0.5 mmol) and benzyl iodoacetate **1a** (276 mg, 1 mmol) at $0^\circ C$. The product was purified by flash chromatography on silica gel (heptanes/EtOAc 92.5:7.5) to give the product **3am** as a colorless oil (37 mg, 26% yield, dr 1:1).

Mixture of diastereoisomers

1H NMR (400 MHz, $CDCl_3$) δ 7.44 – 7.32 (m, 5H), 5.17 – 5.10 (m, 2H), 5.03 (dt, $J = 5.1, 2.3$ Hz, 1H), 4.50 (td, $J = 10.3, 4.3$ Hz, 1H), 2.52 (dd, $J = 15.0, 4.9$ Hz, 1H), 2.42 (dd, $J = 15.4, 6.4$ Hz, 1H), 2.27 (dd, $J = 15.4, 7.9$ Hz, 1H), 2.22 – 2.13 (m, 2H), 2.11 – 1.97 (m, 1H), 2.05 (s, 3H), 2.00 (s, 3H), 1.94 – 1.84 (m, 2H), 1.82 – 1.73 (m, 1H), 1.72 – 1.64 (m, 2H), 1.63 – 1.21 (m, 8H), 1.13 (qd, $J = 12.5, 3.3$ Hz, 1H). ^{13}C NMR (101 MHz, $CDCl_3$) δ 172.63, 172.57, 170.8, 170.6, 136.1, 136.1, 128.7 (2C), 128.4, 128.3 (2C), 76.6, 72.2, 66.4, 66.3, 39.5, 38.2, 37.1, 36.9, 31.9, 31.3, 29.7, 27.5, 24.9 (d, $J = 60.4$ Hz), 21.3, 20.88. HRMS (ESI): calcd. for $C_{17}H_{22}O_4Na$: 313.1410, found: 313.1410. IR (cm^{-1}): 1730 (s), 1233 (s), 738 (m), 696 (m).

benzyl 4-(phenylthio)butanoate (**3an**)



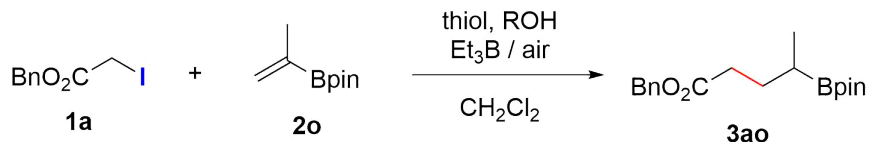
Following **Condition B** with benzyl 2-iodoacetate **1a** (276 mg, 1.0 mmol) and vinylsulfanylbenzene **2n** (68 mg, 0.5 mmol) at $0^\circ C$. Purification by FC (3:97 EtOAc/heptanes) delivered the product **3an** as colorless oil (130 mg, 91%).

Following **Condition C** with benzyl 2-iodoacetate **1a** (276 mg, 1.0 mmol) and propenyl acetate **2n** (68 mg, 0.5 mmol) at $0^\circ C$. Purification by FC (3:97 EtOAc/heptanes) delivered the product **3ak** as colorless oil (129 mg, 90%).

Colorless oil. 1H NMR (400 MHz, $CDCl_3$) δ 7.33 – 7.21 (m, 7H), 7.18 (t, $J = 7.6$ Hz, 2H), 7.08 (t, $J = 7.2$ Hz, 1H), 5.03 (s, 2H), 2.87 (t, $J = 7.1$ Hz, 2H), 2.43 (t, $J = 7.2$ Hz, 2H), 1.89 (p, $J = 7.2$ Hz, 2H). ^{13}C NMR (101 MHz, $CDCl_3$) δ 172.8, 136.1, 136.0, 129.5 (2C), 129.0 (2C), 128.7 (2C), 128.35, 128.31 (2C), 126.1, 66.4, 33.04, 32.98, 24.4. HRMS (ESI) calcd for $C_{17}H_{19}O_2S$:

287.1100, found: 287.1091. IR (cm⁻¹): 1731 (s), 735 (s), 690 (s).

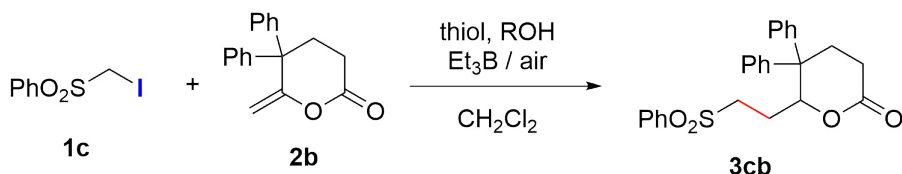
benzyl 4-(4,4,5,5-tetramethyl-1,3,2-dioxaborolan-2-yl)pentanoate (**3ao**)



Following **Condition B** with benzyl 2-iodoacetate **1a** (295 mg, 1.0 mmol) and 2-isopropenyl-4,4,5,5-tetramethyl-1,3,2-dioxaborolane **2o** (83 mg, 0.5 mmol) at 0°C. Purification by FC (4:6 (CH₂Cl₂/pentane/Et₂O 8:1.5:0.5)/pentane, then 1:1) delivered the product **3ao** as colorless oil (82 mg, 53%).

Colorless oil. ¹H NMR (300 MHz, CD₂Cl₂) δ 7.40 – 7.27 (m, 5H), 5.10 (s, 2H), 2.48 – 2.31 (m, 2H), 1.86 – 1.70 (m, 1H), 1.68 – 1.55 (m, 1H), 1.23 (s, 12H), 0.97 (m, 4H). ¹¹B NMR (96 MHz, CD₂Cl₂) δ 34.2. ¹³C NMR (75 MHz, CD₂Cl₂) δ 173.9, 137.0, 128.9 (2C), 128.7 (2C), 128.4, 83.4 (2C), 66.3, 33.9, 28.7, 25.0 (2C), 24.9 (2C), 15.5. HRMS (ESI) calcd for C₁₈H₂₈O₄B: 319.2075, found: 319.2073. IR (cm⁻¹): 1734 (s), 1141(s), 696 (s).

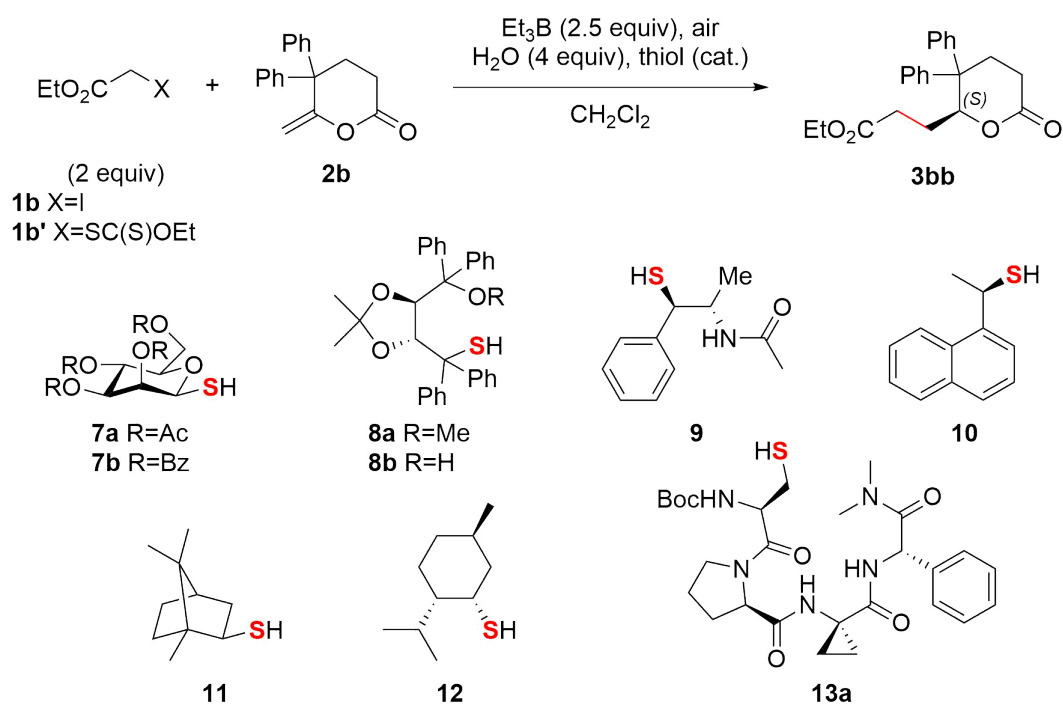
6-[2-(benzenesulfonyl)ethyl]-5,5-diphenyl-tetrahydropyran-2-one (**3cb**)



Following **Condition B** with iodomethylsulfonate **1c** (282 mg, 1.0 mmol) and 6-methylene-5,5-diphenyl-tetrahydropyran-2-one **2b** (132 mg, 0.5 mmol) at 0°C. Purification by FC (4:6 EtOAc/heptanes) delivered the product **3cb** as white solid (156 mg, 74%).

White solid. ¹H NMR (400 MHz, CDCl₃) δ 7.68 – 7.60 (m, 2H), 7.58 – 7.50 (m, 1H), 7.46 – 7.36 (m, 2H), 7.28 – 7.11 (m, 8H), 7.06 – 6.96 (m, 2H), 5.17 (app. dt, J = 11.1, 2.1 Hz, 1H), 3.24 (ddd, J = 14.3, 9.3, 5.4 Hz, 1H), 3.07 (ddd, J = 14.3, 9.0, 6.3 Hz, 1H), 2.78 – 2.62 (m, 1H), 2.48 (ddd, J = 18.4, 5.8, 2.4 Hz, 1H), 2.43 – 2.35 (m, 1H), 2.06 (ddd, J = 18.6, 11.9, 7.0 Hz, 1H), 1.92 (dddd, J = 14.6, 11.1, 9.0, 5.4 Hz, 1H), 1.62 - 1.48 (m, 1H). ¹³C NMR (101 MHz, CDCl₃) δ 169.2, 143.6, 143.3, 139.0, 133.9, 129.4 (2C), 129.11 (2C), 129.06 (2C), 128.1 (2C), 127.52 (2C), 127.49, 127.4 (2C), 127.2, 82.6, 52.9, 48.1, 27.6, 27.3, 26.0. HRMS (ESI): calcd for C₂₅H₂₅O₄S: 421.1468, found: 421.1468. IR (cm⁻¹): 1736 (s), 1295 (s), 1179 (m), 1170 (s), 1132 (s), 1053 (s), 930 (m).

Screening of chiral thiols

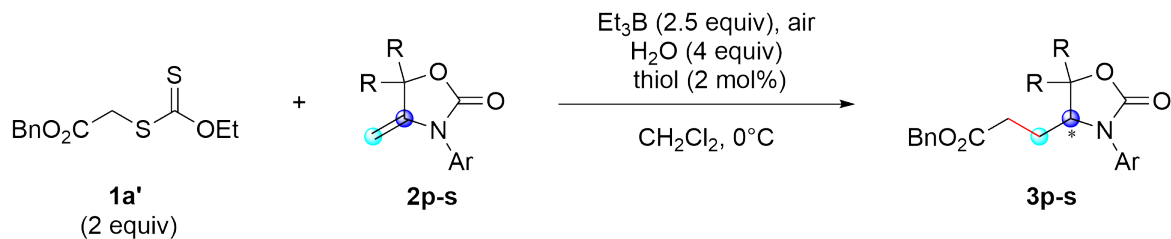


Entry	X	Thiol	T	Yield	E.r.
1	I	7a (5 mol%)	rt	74%	73:27
2	SC(S)OEt	7a (5 mol%)	rt	87%	73:27
3	I	7a (10 mol%)	rt	82%	75:25
4	I	7a (10 mol%)	0 °C	88%	77:23
5	I	7a (10 mol%)	-78 °C	62%	85:15
6	I	7b (10 mol%)	rt	79%	72:28
7	I	8a (5 mol%)	rt	29%	51:49
8	I	8b (5 mol%)	rt	32%	52:48
9	I	9 (5 mol%)	0 °C	79%	70:30
10	I	10 (5 mol%)	0 °C	78%	50:50
11	I	11 (5 mol%)	0 °C	79%	57:43
12	I	12 (5 mol%)	rt	61%	53:47
13	SC(S)OEt	12 (5 mol%)	rt	75%	53:47
14	I	13a (2 mol%)	rt	63%	35:65
15	SC(S)OEt	13a (5 mol%)	rt	81%	35:65
16	SC(S)OEt	13a (2 mol%)	rt	82%	35:65

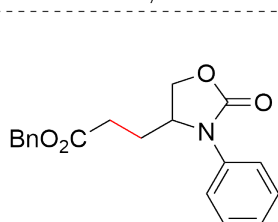
Table 3.4: Screening of chiral thiols.

For synthesis and screening of chiral thiols to see the PhD thesis of V. Soulard.

Hydroalkylation of oxazolidinone derivatives

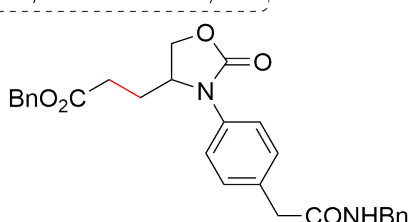


^a 5mol% R*SH; ^b 10mol% R*SH; ^c 1mol% R*SH; ^d rt



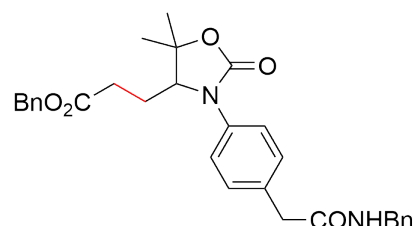
3ap

68%, *er* 51:49 (**7a**)^a
 57%, *er* 51:49 (**9**)^a
 88%, *er* 89:11 (**13a**)
 77%, *er* 91:09 (**13b**)
 80%, *er* 93:07 (**13d**)



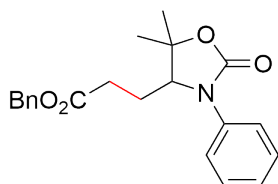
3aq

25%, *er* 53:46 (**7a**)^a
 68%, *er* 51:49 (**9**)^a
 84%, *er* 86:14 (**13a**)



3ar

20%, *er* 53:46 (**7a**)^a
 54%, *er* 59:41 (**9**)^a
 81%, *er* 90:10 (**13a**)
 50%, *er* 90:10 (**13a**)^b
 56%, *er* 87:13 (**13a**)^c



3as

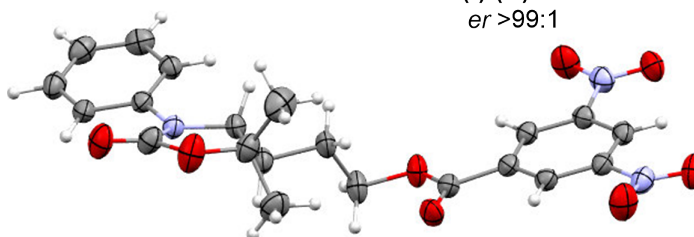
89%, *er* 54:46 (**7a**)^a
 90%, *er* 50:50 (**9**)^a

80%, *er* 91:09 (**13a**)
 84%, *er* 85:15 (**13a**)^d
 92%, *er* 90:10 (**13b**)
 90%, *er* 62:38 (**13c**)
 76%, *er* 92:08 (**13d**)
 63%, *er* 51:49 (**13f**)
 73%, *er* 56:14 (**13g**)
 65%, *er* 67:33 (**13h**)
 67%, *er* 51:49 (**13i**)
 62%, *er* 53:47 (**13j**)
 56%, *er* 50:50 (**13k**)

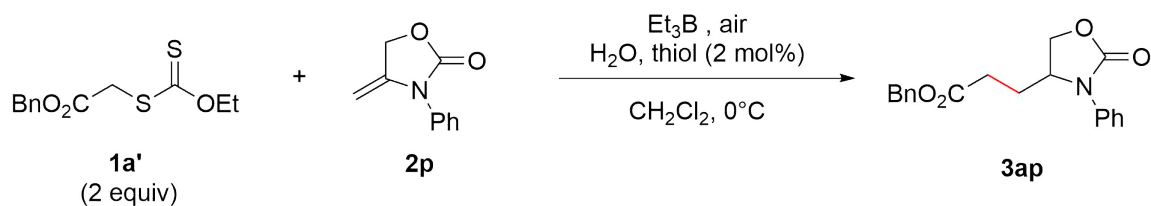


er 98:2

(-)-(R)-14
er >99:1



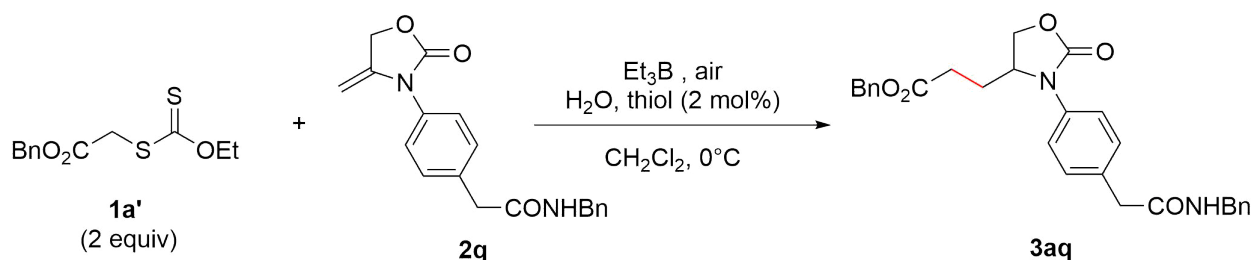
benzyl 3-(2-oxo-3-phenyl-oxazolidin-4-yl)propanoate (3ap)



Following **Condition B** with benzyl 2-ethoxythioacetate **1a'** (278 mg, 1.0 mmol) and oxazolidinone **2p** (91 mg, 0.5 mmol) at 0°C . Purification by FC (8:2 (CH_2Cl_2 /pentane/ Et_2O 8:1.5:0.5)/pentane, then 9:1) delivered the product **3ap** as colorless sticky oil (132 mg, 79%).

Colorless sticky oil. $^1\text{H NMR}$ (400 MHz, CDCl_3) δ 7.48 – 7.43 (m, 2H), 7.40 – 7.30 (m, 7H), 7.21 – 7.16 (m, 1H), 5.10 (s, 2H), 4.58 – 4.48 (m, 2H), 4.19 – 4.07 (m, 1H), 2.46 – 2.30 (m, 2H), 2.21 – 2.10 (m, 1H), 1.95 – 1.83 (m, 1H). $^{13}\text{C NMR}$ (75 MHz, CDCl_3) δ 172.1, 155.7, 136.6, 135.6, 129.5 (2C), 128.8 (2C), 128.7, 128.6 (2C), 125.5, 121.8 (2C), 66.9, 66.6, 55.3, 29.0, 27.2. **HRMS** (ESI): calc. for $\text{C}_{19}\text{H}_{20}\text{NO}_4$: 326.1387, found: 326.1383. **IR** (cm^{-1}): 2919 (w), 1729 (s), 1597 (m), 1499 (s), 1455 (m), 1402 (s), 1297 (m), 1210 (s), 1164 (s), 1124 (s).

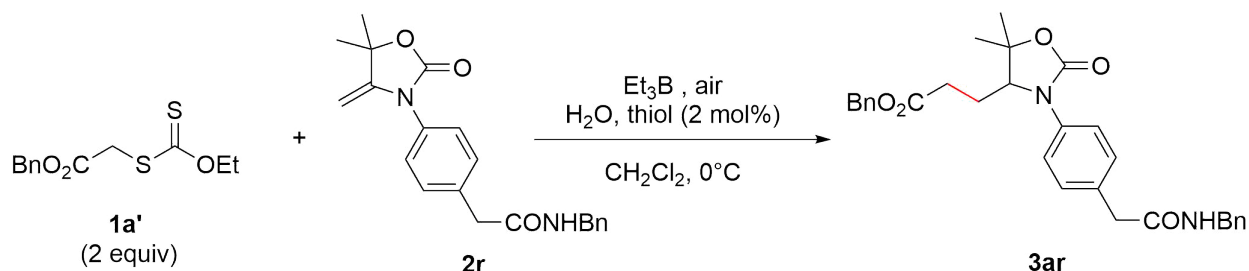
benzyl 3-(3-(4-(2-(benzylamino)-2-oxoethyl)phenyl)-2-oxooxazolidin-4-yl)propanoate (3aq)



Following **Condition B** with benzyl 2-ethoxythioacetate **1a'** (135 mg, 0.5 mmol) and oxazolidinone **2q** (65 mg, 0.25 mmol) at 0°C . Purification by FC (4:1 TBME/acetone) delivered the product **3aq** as pale yellow solid (71 mg, 60%).

Pale yellow solid. **Mp**: $101 - 102^\circ\text{C}$. $^1\text{H NMR}$ (300 MHz, Acetone- d_6) δ 7.53 – 7.50 (m, 2H), 7.38 – 7.30 (m, 7H), 7.28 – 7.18 (m, 5H), 5.10 (s, 2H), 4.74 – 4.66 (m, 1H), 4.56 (t, $J = 8.5\text{Hz}$), 4.38 (s, 2H), 4.28 – 4.23 (m, 1H), 3.55 (s, 2H), 2.53 – 2.46 (m, 2H), 2.19 – 2.09 (m, 1H), 1.95 – 1.85 (m, 1H). $^{13}\text{C NMR}$ (75 MHz, Acetone- d_6) δ 172.0, 170.0, 155.0, 139.4, 136.0, 135.1, 132.8, 129.5, 128.4, 128.2, 128.0, 127.2, 126.7, 121.3, 66.1, 65.6, 54.5, 42.2, 41.7, 28.1, 26.2. **HRMS** (ESI): calc. for $\text{C}_{30}\text{H}_{33}\text{N}_2\text{O}_5$: 501.2384, found: 501.2377. **IR** (cm^{-1}): 3736 (w), 2236 (m), 2157 (w), 2033 (m), 1757 (s), 1727 (s), 1651 (s), 1629 (m), 1511 (m), 1406 (m).

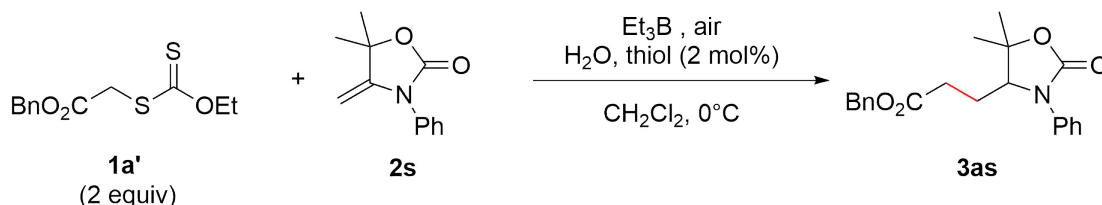
benzyl 3-(3-(4-(2-(benzylamino)-2-oxoethyl)phenyl)-5,5-dimethyl-2-oxooxazolidin-4-yl)propanoate (3ar)



Following **Condition B** with benzyl 2-ethoxycarbothioylsulfanylacetate **1a'** (135 mg, 0.5 mmol) and oxazolidinone **2r** (88 mg, 0.25 mmol) at 0°C . Purification by FC (TBME) delivered the product **3ar** as yellow sticky oil (68 mg, 54%).

Yellow sticky oil. $^1\text{H NMR}$ (300 MHz, CDCl_3) δ 7.39 – 7.20 (m, 14H), 6.03 (br t, $J = 5.1$ Hz, 1H), 5.08 (s, 2H), 4.47 – 4.34 (m, 2H), 4.10 – 4.06 (m, 1H), 3.58 (s, 2H), 2.31 (t, $J = 7.5$ Hz, 2H), 2.10 – 1.89 (m, 2H), 1.50 (d, $J = 14.4$ Hz, 6H). $^{13}\text{C NMR}$ (75 MHz, CDCl_3) δ 172.1, 170.7, 155.1, 138.3, 136.6, 135.6, 132.3, 130.5 (2C), 128.8 (2C), 128.7, 128.6 (2C), 127.8 (2C), 127.6 (2C), 123.3 (2C), 80.5, 66.9, 64.1, 43.8, 43.3, 30.3, 28.7, 27.2, 24.4, 21.9. **HRMS** (ESI): calc. for $\text{C}_{30}\text{H}_{33}\text{N}_2\text{O}_5$: 501.2384, found: 501.2377. **IR** (cm^{-1}): 3736 (w), 2362 (m), 2158 (m), 2033 (w), 1756 (s), 1727 (s), 1651 (m), 1629 (m), 1511 (m), 1406 (m), 1300 (s).

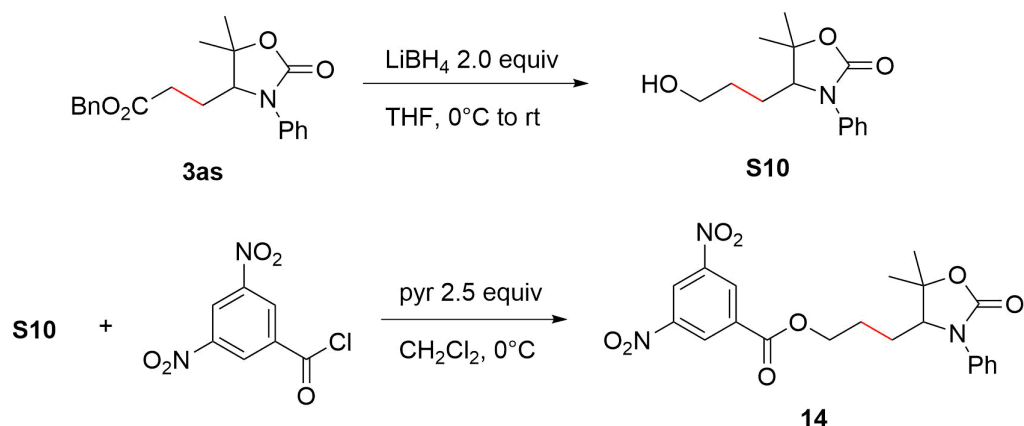
Benzyl 3-(5,5-dimethyl-2-oxo-3-phenyloxazolidin-4-yl)propanoate (3as)



Following **Condition B** with benzyl 2-ethoxycarbothioylsulfanylacetate **1a'** (135 mg, 0.5 mmol) and oxazolidinone **2r** (51 mg, 0.25 mmol) at 0°C . Purification by FC (3:1 TBME/heptane) delivered the product **3as** as colorless sticky oil (63 mg, 71%).

Colorless sticky oil. $^1\text{H NMR}$ (300 MHz, CDCl_3) δ 7.39 – 7.26 (m, 9H), 7.20 – 7.15 (m, 1H), 5.05 (s, 2H), 4.06 (dd, $J_1 = 7.4$ Hz, $J_2 = 5.3$ Hz, 1H), 2.28 (t, $J = 7.6$ Hz, 2H), 2.08 – 1.85 (m, 1H), 1.48 (d, $J = 16.8$ Hz, 6H). $^{13}\text{C NMR}$ (75 MHz, CDCl_3) δ 172.2, 155.1, 137.5, 135.7, 129.5 (2C), 128.8 (2C), 128.7, 128.6 (2C), 125.9, 123.1 (2C), 80.4, 66.8, 64.3, 30.4, 28.7, 24.6, 22.0. **HRMS** (ESI): calc. for $\text{C}_{21}\text{H}_{24}\text{NO}_4$: 354.1700, found: 354.1706. **IR** (cm^{-1}): 3036 (w), 2977(w), 2158 (w), 1731 (s), 1597 (m), 1497 (s), 1395 (s), 1308 (m), 1261 (m), 1168 (s).

3-(5,5-dimethyl-2-oxo-3-phenyl-oxazolidin-4-yl)propyl 3,5-dinitrobenzoate (14)



4-(3-hydroxypropyl)-5,5-dimethyl-3-phenyl-oxazolidin-2-one (**S10**)

To a solution of benzoate **3as** (363 mg, 1.0 mmol) in dry THF (2.5 mL, 0.3M) cooled at 0° was added dropwise LiBH_4 (1.0 mL, 2.0 eq, 2M in THF). The reaction mixture was stirred from 0°C to room temperature overnight. Saturated aqueous NH_4Cl sol. was added to the reaction mixture under cooling with ice. The organic layer was extracted with EtOAc (3 x 10 mL). Combined organic layers were washed with water (until neutral pH) and brine, dried over Na_2SO_4 , filtered and concentrated under reduced pressure. Purification by FC (Et_2O) delivered the alcohol **S10** as colorless oil (236 mg, 92%).

Colorless oil. $^1\text{H NMR}$ (300 MHz, CDCl_3) δ 7.39 – 7.30 (m, 4H), 7.17 (qt, $J = 5.7, 2.7$ Hz, 1H), 4.02 – 3.97 (m, 1H), 3.47 (t, $J = 6.2$ Hz, 2H), 2.19 (s, 1H), 1.71 – 1.61 (m, 2H), 1.51 (s, 3H), 1.44 (s, 3H), 1.48 – 1.37 (m, 2H). $^{13}\text{C NMR}$ (75 MHz, CDCl_3) δ 155.4, 137.3, 129.2 (2C), 125.7, 123.1 (2C), 80.8, 65.4, 62.0, 28.6, 28.6, 25.4, 21.7. **HRMS** (ESI) calc. for $\text{C}_{14}\text{H}_{19}\text{O}_3\text{N}$ $[\text{M}+\text{H}]^+$: 205.1438, found 205.1432. **IR** (cm^{-1}) 3421, 2946, 2871, 1722, 1597, 1397, 1117, 756.

(*R*)-**S10**, major

Following the procedure above with benzoate **3as** (50 mg, 0.14 mmol, er 92:08), THF (1.2 mL, 0.1M) and LiBH_4 (0.14 mL, 2.0 eq, 2M in THF). Purification by FC (Et_2O) delivered the alcohol (*R*)-**S10** as colorless oil (32 mg, 91%).

Characteristic data same as for the racemic **S10**. $\alpha_D^{25} = -20.4^\circ$, $c=0.64$ g/100 mL in CHCl_3 .

3-(5,5-dimethyl-2-oxo-3-phenyl-oxazolidin-4-yl)propyl 3,5-dinitrobenzoate (14)

To a solution of hydroxy-oxazolidinone **S10** (100 mg, 0.4 mmol) in dry CH_2Cl_2 (4.0 mL, 0.1M) cooled at 0°C was added dry pyridine (82 μL , 2.5 equiv) and DMAP (10 mg, 20 mol%) followed by the addition of 3,5-dinitrobenzoyl chloride (185 mg, 2.0 equiv). The reaction mixture was

stirred at 0°C following the conversion by TLC. Upon completion the mixture was diluted with water and extracted with EtOAc (3x 10 mL). Combined organic phases were washed with water and brine, dried over Na₂SO₄, filtered and concentrated under reduced pressure. Purification by FC (7:3 Et₂O/pentane) delivered the derivative **14** as yellowish solid (146 mg, 82%).

Yellowish crystals. *R_f* 0.26 (7:3 Et₂O/pentane); mp 147.7 - 148.3°C, from CH₂Cl₂/pentane. ¹H NMR (300 MHz, CDCl₃) δ 9.23 – 9.19 (m, 1H), 9.07 – 9.03 (m, 2H), 7.46 – 7.32 (m, 4H), 7.20 – 7.13 (m, 1H), 4.40 – 4.30 (m, 2H), 4.12 – 4.04 (m, 1H), 1.86 – 1.74 (m, 4H), 1.59 (s, 3H), 1.53 (s, 3H). ¹³C NMR (75 MHz, CDCl₃) δ 162.4, 155.0, 148.8 (2C, -C-NO₂), 137.3, 133.7, 129.4 (2C), 129.4 (2C), 125.8, 122.8 (2C), 122.6, 80.3, 66.1, 65.0, 28.9, 25.5, 24.8, 21.8. HRMS (ESI) calc. for C₂₁H₂₁O₈N₃ [M+H]⁺: 444.1401, found 444.1395. IR (cm⁻¹) 3100, 2973, 2878, 1728, 1540.

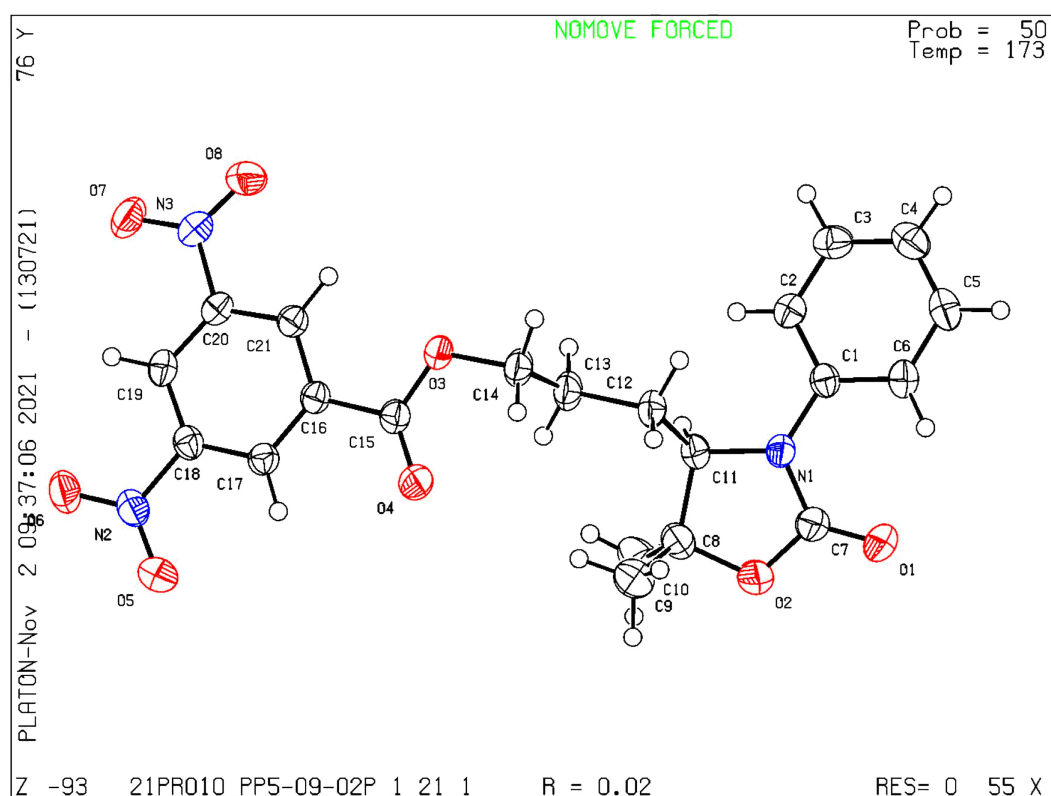
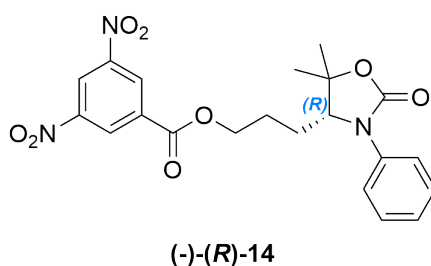
(R)-14, major

Following the procedure above with hydroxy-oxazolidinone **(R)-S10** (32 mg, 0.13 mmol, er 92:08) in dry CH₂Cl₂ (1.3 mL, 0.1M), dry pyridine (26 μL, 2.5 equiv), and 3,5-dinitrobenzoyl chloride (60 mg, 2.0 equiv). Purification by FC (7:3 Et₂O/pentane) delivered the derivative **(R)-14** as yellowish solid (59 mg, quant.).

Characteristic data same as for the racemic **14**. α_D²⁵ = -9.3°, c = 1.14 g/100mL in CHCl₃.

Conform X-ray single crystal diffraction the major isomer possesses the configuration (*R*).

X-ray crystal structure report



Crystal-Structure Determination. A crystal of $C_{21}H_{21}N_3O_8$ immersed in parabar oil was mounted at ambient conditions and transferred into the stream of nitrogen (173 K). All measurements were made on a *RIGAKU Synergy S* area-detector diffractometer¹ using mirror optics monochromated Cu $K\alpha$ radiation ($\lambda = 1.54184$). The unit cell constants and an orientation matrix for data collection were obtained from a least-squares refinement of the setting angles of reflections in the range $3.411^\circ < \theta < 79.547^\circ$. A total of 11112 frames were collected using ω scans, with 0.15 second exposure time (0.4 s for high-angle reflections), a rotation angle of 0.5° per frame, a crystal-detector distance of 34.0 mm, at $T = 173(2)$ K.

Data reduction was performed using the *CrysAlisPro*¹ program. The intensities were corrected for Lorentz and polarization effects, and an absorption correction based on the multi-scan

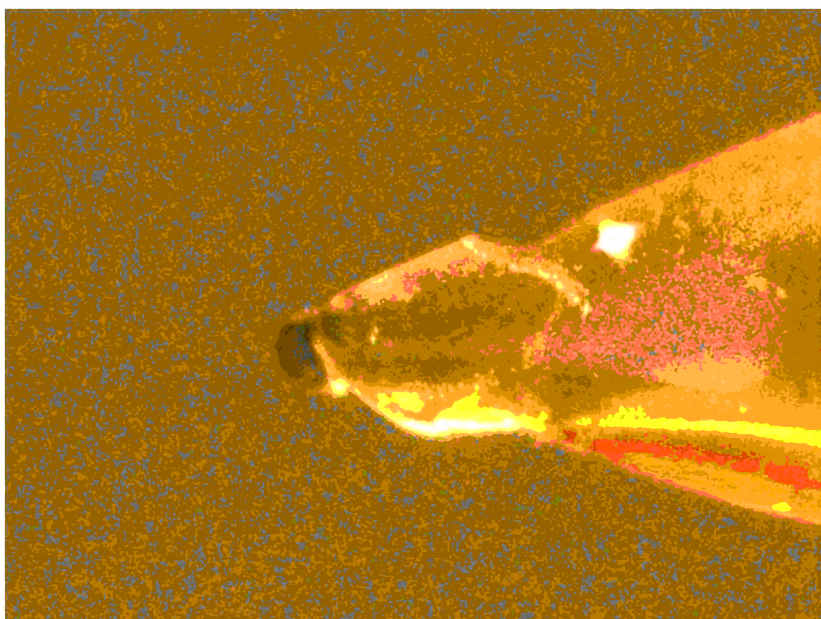
method using SCALE3 ABSPACK in *CrysAlisPro*¹ was applied. Data collection and refinement parameters are given in Table 1 (See the Appendix).

The structure was solved by intrinsic phasing using *SHELXT*², which revealed the positions of all non-hydrogen atoms of the title compound. All non-hydrogen atoms were refined anisotropically. H-atoms were assigned in geometrically calculated positions and refined using a riding model where each H-atom was assigned a fixed isotropic displacement parameter with a value equal to 1.2Ueq of its parent atom (1.5Ueq for methyl groups).

Refinement of the structure was carried out on F^2 using full-matrix least-squares procedures, which minimized the function $\sum w(F_o^2 - F_c^2)^2$. The weighting scheme was based on counting statistics and included a factor to downweight the intense reflections. All calculations were performed using the *SHELXL-2014/7*³ program in *OLEX2*.⁴

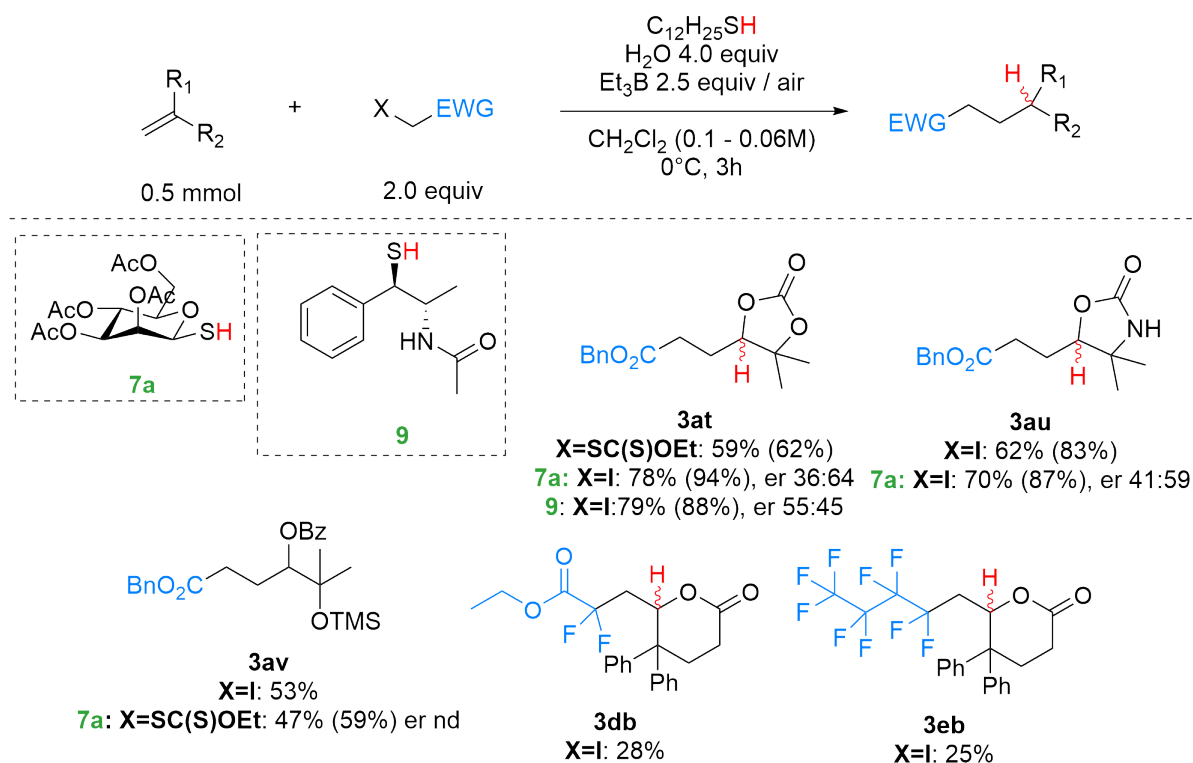
The X-ray crystal structure determination service unit of the Department of Chemistry, Biochemistry and Pharmaceutical Sciences of the University of Bern is acknowledged for measuring, solving, refining and summarizing the structures of compounds XX, YY, ZZ. The Synergy diffractometer was partially funded by the Swiss National Science Foundation (SNF) within the R'Equip programme (project number 206021_177033).

Model has Chirality at C11 (*R*).

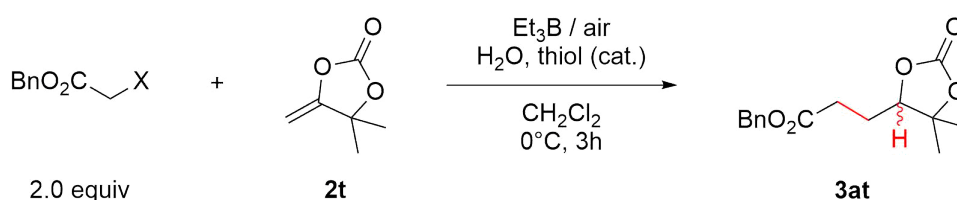


Results not included in this draft

Extension of the substrate scope



benzyl 3-(5,5-dimethyl-2-oxo-1,3-dioxolan-4-yl)propanoate (**3at**)



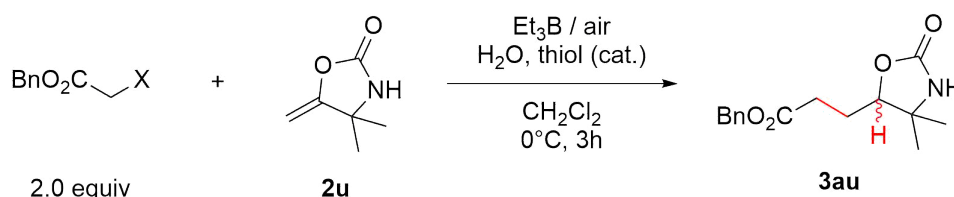
Following **Condition B** with benzyl 2-ethoxycarbothioylsulfanylacetate **1a'** (310 mg, 1.1 mmol) and alkene **2t** (74 mg, 0.57 mmol) at 0°C. Purification by FC (4:6 Et₂O/pentane) delivered the product **3at** as colorless oil (94 mg, 59%, 62% NMR yield).

Following **Condition B** with benzyl 2-iodoacetate **1a** (300 mg, 1.1 mmol), alkene **2t** (71 mg, 0.55 mmol) and mannose thiol **7a** (2 mol%) at 0°C. Purification by FC (4:6 Et₂O/pentane) delivered the product **3at** as colorless oil (119 mg, 78%, 94% NMR yield, er 36:64).

Following **Condition B** with benzyl 2-iodoacetate **1a** (300 mg, 1.1 mmol), dioxolane **2t** (71 mg, 0.55 mmol) and amide thiol **9** (2 mol%) at 0°C. Purification by FC (4:6 Et₂O/pentane) delivered the product **3at** as colorless oil (120 mg, 79%, 88% NMR yield, er 55:45).

Colorless oil. R_f 0.19 (4:6 Et₂O/pentane). ¹H NMR (400 MHz, CDCl₃) δ 7.42 – 7.29 (m, 5H), 5.20 – 5.08 (m, 2H), 4.36 – 4.24 (m, 1H), 2.71 – 2.59 (m, 1H), 2.59 – 2.48 (m, 1H), 2.00 – 1.86 (m, 2H), 1.48 (s, 3H), 1.38 (s, 3H). ¹³C NMR (101 MHz, CDCl₃) δ 172.2, 153.9, 135.7, 128.8 (2C), 128.6, 128.5 (2C), 84.1, 84.0, 66.8, 30.3, 26.2, 24.7, 21.3. IR (neat, cm⁻¹): 3035, 2981, 2937, 1785, 1730, 1349, 1273, 1163. HRMS: calc. for [C₁₅H₁₈O₅Na] 301.1053, found 301.1046.

benzyl 3-(4,4-dimethyl-2-oxooxazolidin-5-yl)propanoate (**3au**)

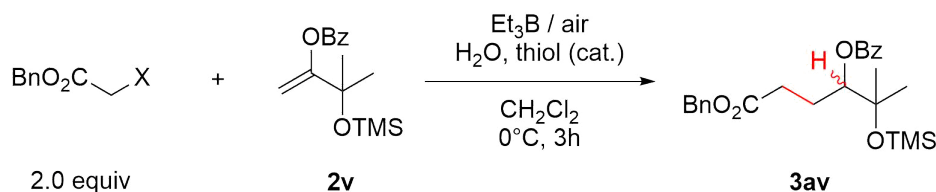


Following **Condition B** with benzyl 2-iodoacetate **1a** (284 mg, 1.0 mmol) and alkene **2u** (66 mg, 0.51 mmol) at 0°C. Purification by FC (Et₂O) delivered the product **3au** as colorless sticky oil (103 mg, 72%, 81% NMR yield).

Following **Condition B** with benzyl 2-iodoacetate **1a** (291 mg, 1.0 mmol), alkene **2u** (67 mg, 0.52 mmol) and mannose thiol **7a** (2 mol%) at 0°C. Purification by FC (Et₂O) delivered the product **3at** as colorless oil (101 mg, 70%, 87% NMR yield, er 41:59).

Colorless sticky oil. R_f 0.25 (Et₂O). ¹H NMR (300 MHz, CD₂Cl₂) δ 7.41 – 7.29 (m, 5H), 5.92 (s, 1H), 5.13 (d, J = 1.4 Hz, 2H), 4.19 – 4.12 (m, 1H), 2.71 – 2.45 (m, 2H), 1.92 (tdd, J = 7.6, 5.4, 2.1 Hz, 2H), 1.29 (s, 3H), 1.20 (s, 3H). ¹³C NMR (75 MHz, CD₂Cl₂) δ 172.8, 158.5, 136.5, 128.9 (2C), 128.6, 128.5 (2C), 85.2, 66.7, 57.9, 31.0, 27.3, 24.9, 22.8. IR 3275, 2970, 2935, 2891, 1728. HRMS: calc. for [C₁₅H₂₀O₄N] 278.1398, found 278.1396.

[4-benzyloxy-1-(1-methyl-1-trimethylsilyloxy-ethyl)-4-oxo-butyl] benzoate (**3av**)

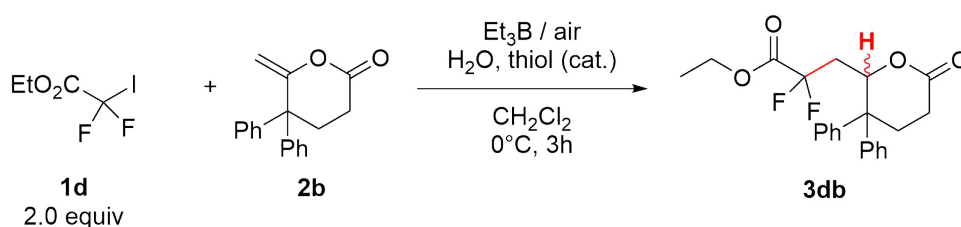


Following **Condition B** with benzyl 2-iodoacetate **1a** (285 mg, 1.0 mmol) and alkene **2v** (145 mg, 0.51 mmol) at 0°C. Purification by FC (5:95 Et₂O/pentane) delivered the product **3av** as colorless oil (121 mg, 53%).

Following **Condition B** with benzyl 2-ethoxycarbothioylsulfanylacetate **1a'** (286 mg, 1.0 mmol), alkene **2v** (149 mg, 0.52 mmol) and mannose thiol **7a** (2 mol%) at 0°C. Purification by FC (5:95 Et₂O/pentane) delivered the product **3av** as colorless oil (109 mg, 47%, 59% NMR yield, er n.d.).

Colorless oil. ¹H NMR (400 MHz, CD₂Cl₂) δ 8.10 – 8.03 (m, 2H), 7.63 – 7.55 (m, 1H), 7.53 – 7.42 (m, 2H), 7.40 – 7.28 (m, 5H), 5.12 – 4.97 (m, 3H), 2.47 – 2.39 (m, 2H), 2.28 – 2.15 (m, 1H), 2.08 – 1.93 (m, 1H), 1.31 (d, J = 9.7 Hz, 6H), 0.14 (s, 9H). ¹³C NMR (101 MHz, CD₂Cl₂) δ 173.3, 166.5, 136.7, 133.4 (2C), 130.9, 130.1 (2C), 128.9 (2C), 128.8 (2C), 128.5 (2C), 80.0, 75.7, 66.5, 31.5, 27.3, 25.9, 25.2, 2.8 (3C).

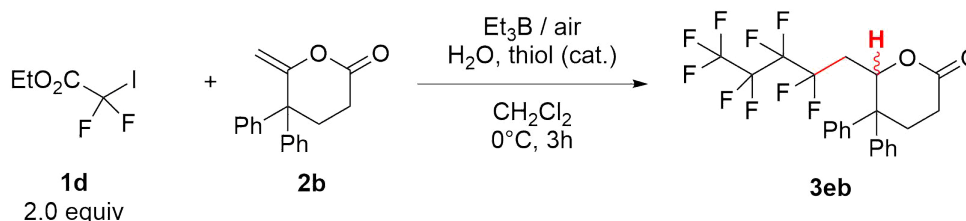
ethyl 2,2-difluoro-3-(6-oxo-3,3-diphenyl-tetrahydropyran-2-yl)propanoate (**3db**)



Following **Condition B** with ethyl 2,2-difluoro-2-iodoacetate **1d** (255 mg, 1.0 mmol) and alkene **2b** (132 mg, 0.50 mmol) at 0°C. Purification by FC (3:7 Et₂O/pentane) delivered the product **3db** as colorless oil (54 mg, 28%).

Colorless oil. *R_f* 0.22 (3:7 Et₂O/pentane). ¹H NMR (400 MHz, CDCl₃) δ 7.39 – 7.14 (m, 10H), 5.51 (dt, J = 11.2, 1.8 Hz, 1H), 4.44 – 4.33 (m, 2H), 2.85 – 2.75 (m, 1H), 2.72 – 2.50 (m, 3H), 2.23 – 2.09 (m, 1H), 1.83 (dddd, J = 14.7, 13.5, 9.4, 2.4 Hz, 1H), 1.38 (t, J = 7.2 Hz, 3H). ¹³C NMR (101 MHz, CDCl₃) δ 168.1, 163.7 (dd, J = 33.1, 30.8 Hz), 143.1, 143.0, 129.2 (2C), 129.1 (2C), 127.6, 127.4 (2C), 127.2, 127.1 (2C), 115.0 (dd, J = 256.1, 246.4 Hz), 78.8 (dd, J = 9.6, 1.9 Hz), 63.6, 47.4, 37.9 (dd, J = 25.9, 23.0 Hz), 27.4, 27.2, 13.9. ¹⁹F NMR (282 MHz, CDCl₃) δ -95.7, -98.8, -99.8, -110.3, -111.3.

6-(2,2,3,3,4,4,5,5,5-nonafluoropentyl)-5,5-diphenyl-tetrahydropyran-2-one (**2eb**)



Following **Condition B** with ethyl 2,2-difluoro-2-iodoacetate **1d** (255 mg, 1.0 mmol) and alkene **2b** (132 mg, 0.50 mmol) at 0°C. Purification by FC (3:7 Et₂O/pentane) delivered the product

3db as colorless oil (54 mg, 28%).

White solid. **Mp.** 108.4° - 109.2°, from CH₂Cl₂. **R_f** 0.19 (3:7 Et₂O/pentane) **¹H NMR** (400 MHz, CDCl₃) δ 7.37 – 7.30 (m, 6H), 7.26 (qt, J = 6.5, 2.2 Hz, 2H), 7.19 – 7.13 (m, 2H), 5.61 (dt, J = 9.3, 1.6 Hz, 1H), 2.74 – 2.58 (m, 3H), 2.46 – 2.19 (m, 2H), 2.07 (dddd, J = 30.7, 15.7, 7.7, 1.6 Hz, 1H). **¹³C NMR** (101 MHz, CDCl₃) δ 168.5, 142.8, 129.3, 129.2, 127.8, 127.5, 127.4, 127.2, 120.2, 119.9, 119.1, 118.8, 118.5, 117.6, 117.3, 117.0, 115.9, 115.6, 114.8, 110.2, 108.5, 77.5, 77.4, 77.4, 76.8, 48.2, 34.4, 34.2, 34.0, 27.9, 27.5. **¹⁹F NMR** (376 MHz, CDCl₃) δ -81.14, -110.86 – -113.00 (m), -114.33 – -116.05 (m), -123.87 – -127.07 (m).

Part II

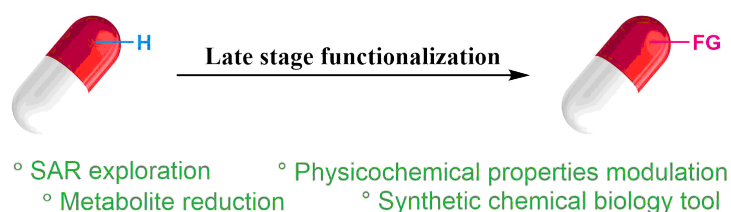
Natural Product Modification by Radical Reactions

4 Late Stage Functionalization in Drug Discovery

*This chapter is dedicated to the introduction to concept of **late stage functionalization** of complex biological relevant compounds, used as a powerful tool in modification of drugs and identification of structure-activity relationships (SARs) in research and development campaigns (R&D).*

4.1 Introduction

In the era of globalization and the outgrowth of pharmacovigilance, the development of high-quality therapeutics at optimum speed and accessible price is the utmost challenge to meet urgent societal needs.^{1–3} Nowadays, drug discovery programs are gradually relying on artificial intelligence and machine learning techniques for decision-making and automation in preclinical studies.^{4–6} As a result, the integration of several fields such as bioinformatics, molecular and clinical biology, medicinal chemistry, chemical biology, and pharmacology can accelerate and increase the positive outcome of drug discovery. Despite such developments, *organic synthesis* is still a key but rate-limiting step.^{7–9} C–H activation is the latest technology added into an organic chemist's toolbox for the rapid construction and late-stage modification of functional molecules to achieve the desired chemical and physical properties. Particularly, late-stage functionalization of privileged medicinal scaffolds expand the chemical space and facilitate the development of structure–activity relationship (SAR) studies,¹⁰ the generation of oxidized metabolites, the blocking of metabolic hot spots and the preparation of biological probes.¹¹



Scheme 4.1: Late stage functionalization.

The term late-stage functionalization (LSF) is now often used in the field of organic methodology development to describe transformations on complex molecules.^{12–14} According to Börgel and Ritter,¹² LSF is defined as a desired chemoselective transformation on a complex molecule to provide at least one analog in sufficient quantity and purity for a given purpose without the necessity for installation of a functional group that exclusively serves the purpose to enable said transformation (Scheme 4.1). The complexity of a molecule often determines the synthetic effort to make it. LSF eases this synthetic effort and can access derivatives that would be substantially more demanding or time consuming to access from simple molecular building blocks. As such, late-stage functionalization can quickly provide access to molecules of potential value, for example, in the area of drug development or material science, that otherwise might not have been available at all or too difficult to make.^{10,11,13,15} Both C–H functionalization reactions^{16,17} and functional-group manipulations^{18–20} can be attributed to LSFs, if they fulfill the requirements of the definition.

Chemoselectivity is a requirement for LSF reactions but not sufficient. A chemoselective reaction is defined as the preferential reaction of a reagent or catalyst with one out of at least two different functional groups in a molecule and as the preferential reaction of a reagent or catalyst with one out of at least two competing molecules.²¹ Complex molecules commonly feature

several distinct functional groups and high level of chemoselectivity referres to functional-group tolerance. Moreover, no required directing or activating group is needed to be installed beforehand.

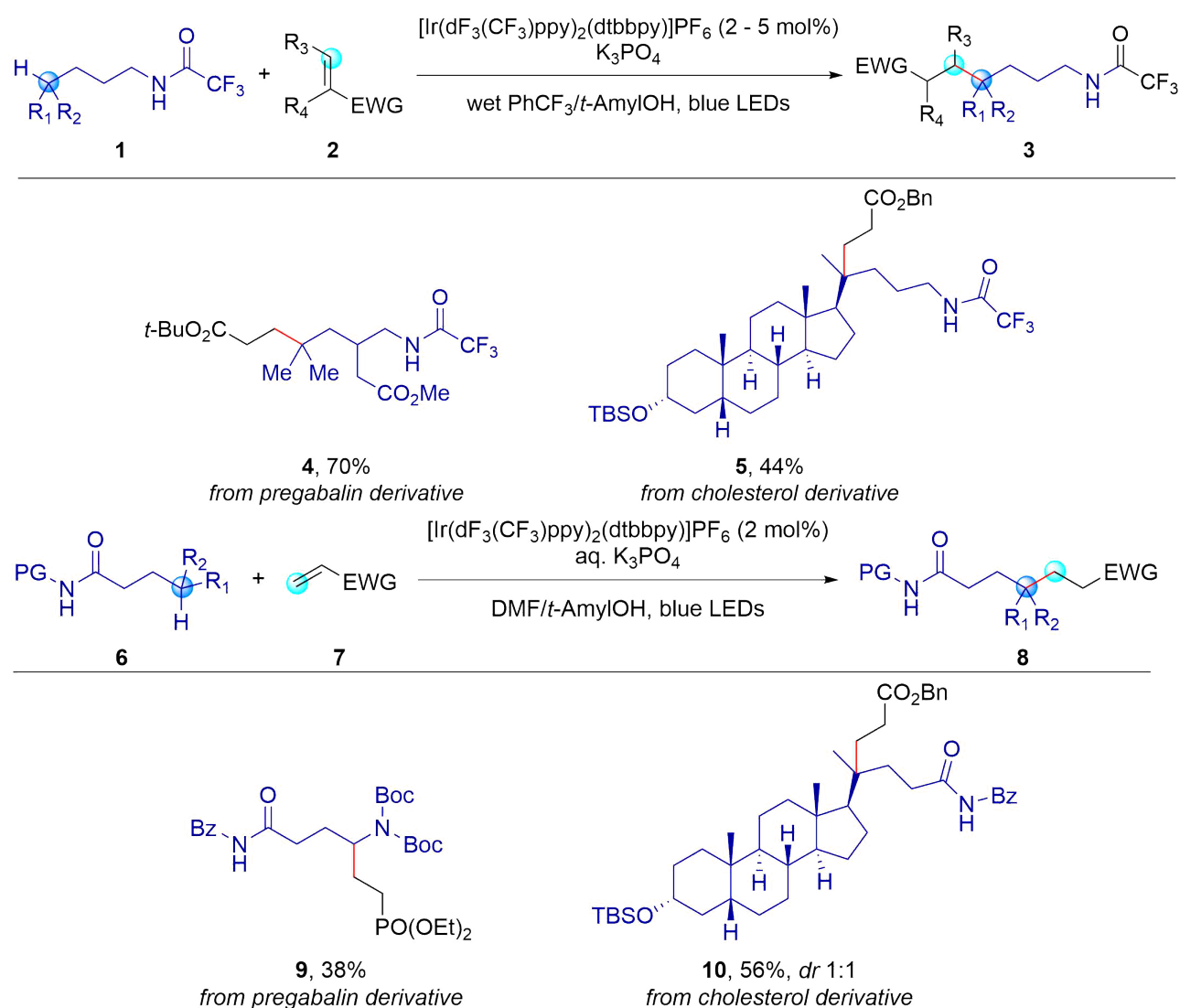
High functional-group tolerance is a requirement for late-stage C–H bond functionalization reactions.^{22–24} Although the definition of LSF does not require distinction between different types of C–H bonds for a C–H functionalization reaction, in practice, it often is desirable because otherwise, the requirement for product isolation in sufficient quantity and purity might not be achievable.¹² Chemoselective aliphatic late-stage C–H bond functionalization is often achieved by methods that proceed via C–H homolysis or C–H insertion steps,^{20,25} and chemoselectivity for stronger C(sp²)-H bonds is most commonly observed in reactions involving their orthogonal π -system.

The level of *site selectivity*, which is synonymous with positional selectivity and regioselectivity, is irrelevant for the classification of a reaction as LSF. Late stage functionalization reactions can be either site selective or not, and both scenarios can be desired and useful.¹² For example, structural optimization of lead compounds in drug discovery can benefit from quick access to various constitutional isomers, so site-unselective introduction of a substituent to access multiple constitutional isomers can be the quickest possible way to access analogs for biological testing, even if purification is difficult.^{11,17,19} It is generally acknowledged that highly site-selective C–H functionalization reactions are inherently valuable, and one set of site-selective C–H functionalization reactions to access each constitutional isomer independently is desirable. Reagent and catalyst control to achieve site selectivity that is not dependent on substrate bias is highly desirable and constitutes an important future objective in the field.^{12,25} Conformational control to induce selectivity can also be used in non-enzymatic systems: the use of supramolecular catalysts that engage in host-guest interactions, for example, is an approach in which the ligand environment of the host can provide high selectivity, distinct from what would be observed by small-molecule catalysts.^{26,27}

Recently, photocatalytic processes have known a tremendous development and applications for the late-stage functionalization of complex molecules.^{13,28–30} Photocatalytic approaches include a catalyst activated by light (also dubbed photocatalyst, PC) that oversees the desired transformation. In such strategies, a huge amount of energy is delivered to the reaction mixture in the form of photons, the PC being in charge of channeling it (upon excitation to PC*) for the selective activation of the reaction partners. Moreover, since photons are made of pure energy, a reduced amount of waste is produced at the end of the process, which significantly improves sustainability. On top of that, these processes are characterized by extremely mild conditions (room temperature, irradiation with soft light sources, etc.) allowing to exert a precise control over the reactivity of the involved radical intermediates.^{13,31} Some selective examples where photocatalytic HAT strategies have been adopted for the selective C–H to C–X conversion in complex substrates will be presented.

4.2 Photocatalytic Promoted 1,5-HAT

The progress of photocatalytic HAT catalysis for the late-stage functionalization of complex molecular architectures, via homolytic cleavage of C(sp³)-H bonds has been recently reviewed by Ravelli and coworkers.¹³ According to the accurate classification reported and based on mechanistic considerations, the formation of C-centered radicals can occur via different classes of HAT processes: *direct processes* (*d*-HAT), *indirect processes* (*i*-HAT), and *remote processes* (*r*-HAT). In *d*-HAT reactions the photocatalyst is able to abstract directly a hydrogen atom from a suitable substrate. *i*-HAT pathways featured the formation of intermediate radical species such as N•, O•, S•, or halogens able to act as the effective hydrogen atom abstractors. The third class - *r*-HAT - can be considered as an intramolecular *i*-HAT catalysis where the generation of a hydrogen atom abstractor via a SET event enables a site-selective functionalization of unactivated C(sp³)-H bonds.^{13,20}



Scheme 4.2: Alkylation of C(sp³)-H bonds.

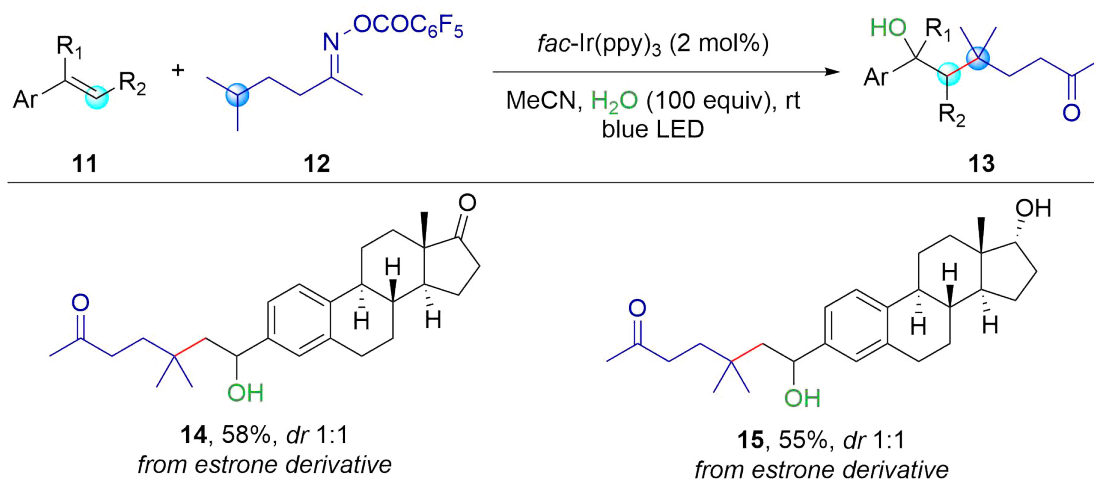
4.2.1 Alkylation

Rovis and coworkers reported the selective alkylation of unactivated C(sp³)-H bonds accomplished by installing either a trifluoroacetamide (**1**)³² or an ethoxycarbonyl protected amide (**6**)³³ at the γ -position (Scheme 4.2).

This functionalization enabled the *in situ* formation of an amidyl radical, able to promote a selective 1,5-HAT thus activating a remote site. The protocol required [Ir(dF(CF₃)ppy)₂(dtbbpy)]PF₆ as the photosensitizer under blue LEDs irradiation. The alkenes scope (**2** and **7**) included both unsubstituted acrylates and those bearing α -substituents, as well as allyl acrylate, methacrylonitrile, and other electron-deficient alkenes such as methyl vinyl ketone, acrylamide, vinyl sulfone and vinyl phosphonate. For the amide scope, substrates with tertiary γ -C-H bonds were well tolerated, while by changing the ratio between the amide and the alkene, secondary C-H bonds can afford either mono- or dialkylated adducts. In case of two different tertiary C-H bonds, the 1,5-HAT occurred with high regioselectivity. Moreover, examples of complex biorelevant substrates, γ -aminobutyric acid derivative - pregabalin, and the steroidal compound gave monoalkylated products **4-5** and **9-10** in moderate to high yields (Scheme 4.2).

4.2.2 Hydroxyalkylation

Ma and co-workers reported the first visible-light driven three-component γ -hydroxyalkylation of ketones under redox neutral conditions.³⁴



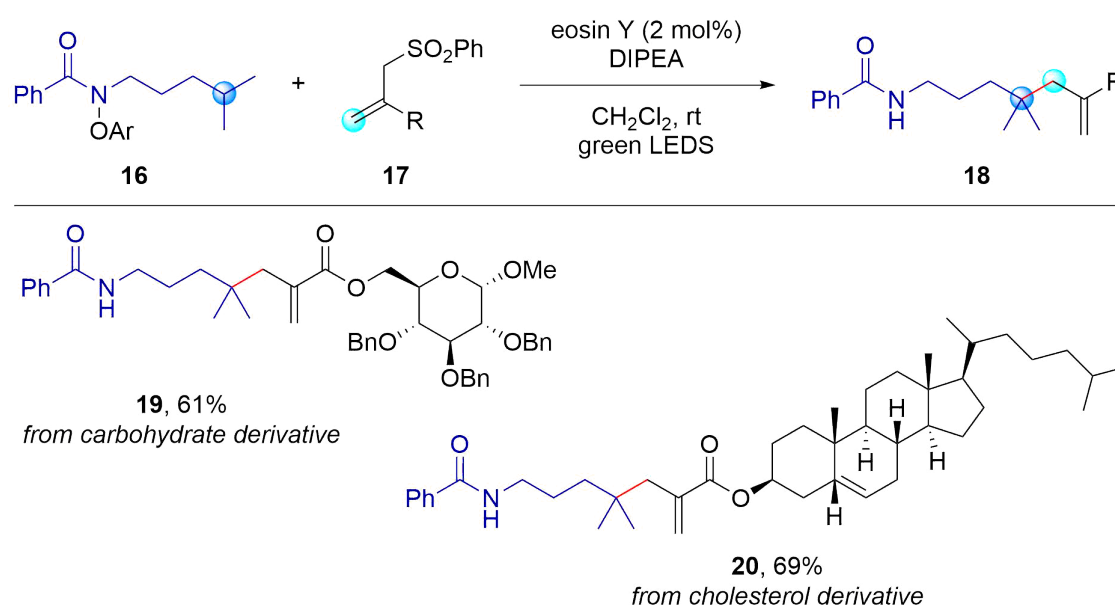
Scheme 4.3: Hydroxyalkylation of olefins.

Styrenes **11** could be hydroxyalkylated with oxime derivative **12** delivering the products **13** (Scheme 4.3). Based on the proposed mechanism, the oxime derivative **12** was able to generate the key iminyl radicals upon single-electron transfer (SET) under visible light irradiation. A subsequent 1,5-HAT generated the C-centered radical, able to add to the olefin double bond, and thus afford a benzyl radical intermediate. Oxidation of the latter to carbocation along with the addition of a molecule of water, and hydrolysis of the iminyl function, provided the final hydroxyalkylketones

13. The reaction was promoted by fac-Ir(ppy)_3 with a 30 W blue LED lamp as the photons' source. The reaction scope was broad with a good functional group tolerance. The reaction was exemplified in the functionalization of the terminal olefins derived from estrone - **14** and **15** (Scheme 4.3).³⁴

4.2.3 Allylation

Wu et.al. developed the visible-light-mediated allylation of unactivated $\text{C(sp}^3\text{)-H}$ bonds, directed by the amidyl radical, which was generated by photocatalytic fragmentation of a pre-functionalized amide precursor.³⁵

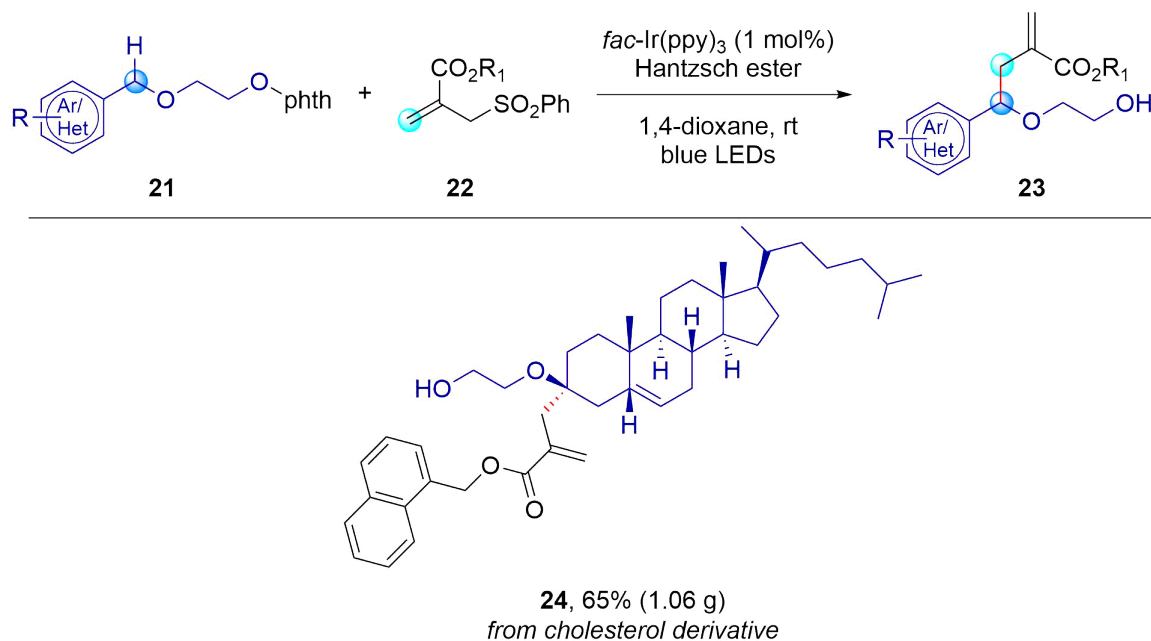


Scheme 4.4: Synthesis of δ -allyl derivatives.

Electron-deficient allyl sulfones **17** can be reacted as δ -carbon radical acceptors generated from aliphatic amide derivatives **16** under photoredox catalytic conditions (Scheme 4.4). In particular, pre-functionalized amides **16**, in the presence of eosin Y as a photocatalyst and green LEDs irradiation, afforded amidyl radicals via a SET reduction. A subsequent 1,5-HAT gave the carbon centered radicals, which added onto alkenes, thus providing δ -allyl-derivatives **18**. Optimized reaction conditions required DIPEA as a sacrificial electron donor to regenerate the photoactive catalyst eosin Y. The scope of the amide enclosed substituted benzoyl-, aromatic-, *N*-acetyl, and *N*-cyclopentyl-carbonyl-substrates, as well as carbamates. Remarkably, a variety of secondary $\text{C(sp}^3\text{)-H}$ bonds were functionalized in excellent yields. Complex substrates such as carbohydrates and cholesterol were easily converted to the corresponding derivatives **19** and **20**, in 61% and 69% yield respectively (Scheme 4.4).³⁵

Zhang et al. reported the remote $\text{C(sp}^3\text{)-H}$ allylation and alkenylation of linear aliphatic alcohols (Scheme 4.5).³⁶ The authors reported for the first time the formation of alkoxy radicals

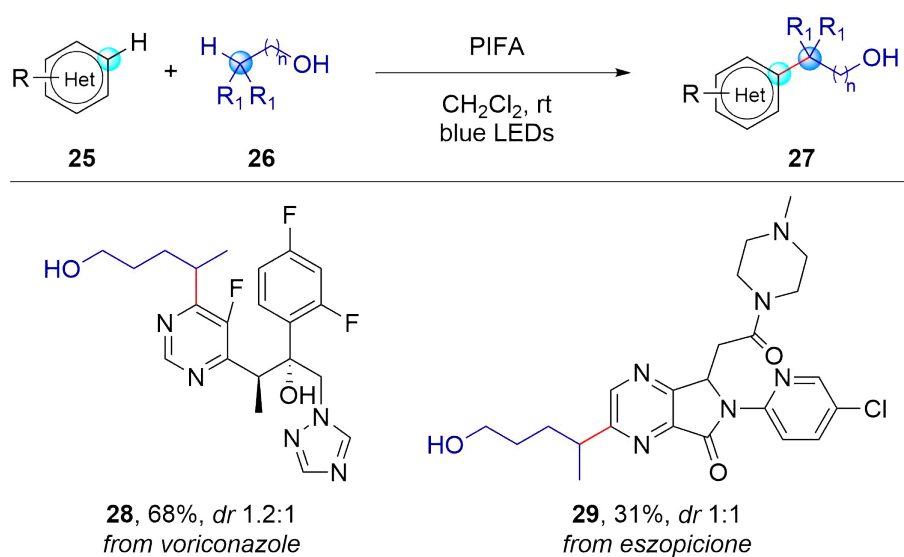
starting from *N*-alkoxyphthalimides **21** under photoredox catalytic conditions. The alkoxy radical, once generated, triggered a 1,5-HAT to form a C-centered radical, which was trapped by either aryl-allyl or vinyl sulfones (**22**). Broad substrate variations, including a structurally complexed steroid **24**, undergo the C(sp³)-H functionalization reaction effectively with high regio- and chemoselectivity (Scheme 4.5).³⁶



Scheme 4.5: Remote C(sp³)-H functionalization of linear aliphatic *N*-alkoxyphthalimides.

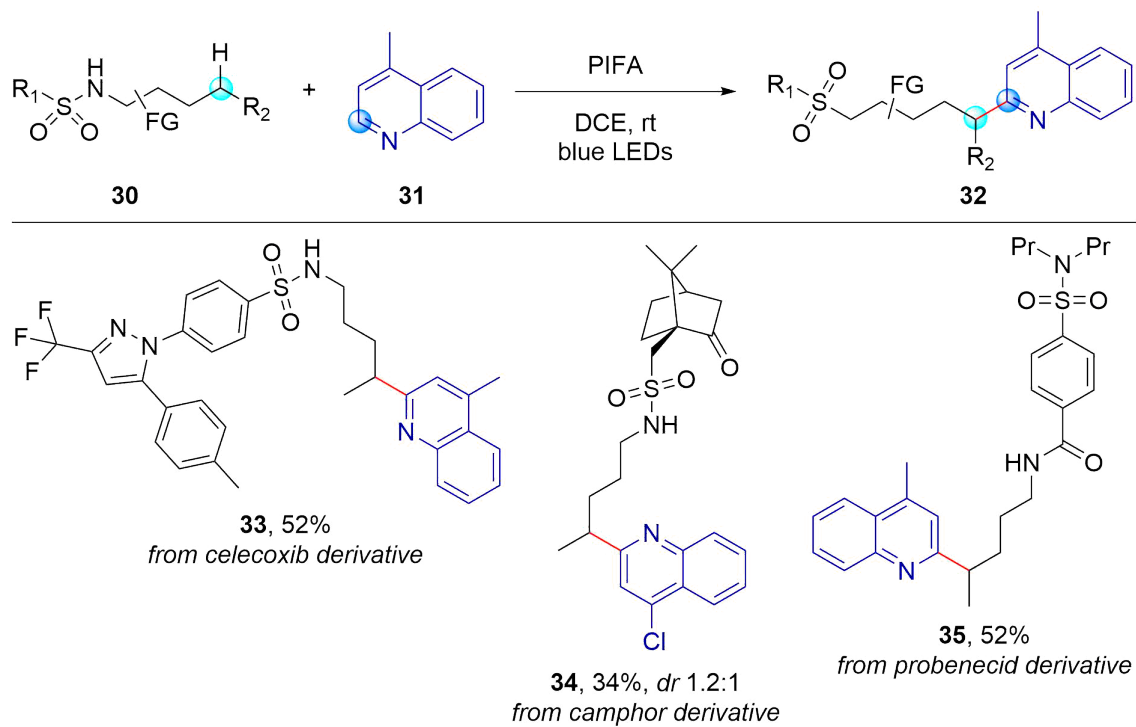
4.2.4 Heteroarylation

Wu and co-workers reported a practical and elusive metal-free alcohol-directed heteroarylation of remote unactivated C(sp³)-H bonds.³⁷ Heteroaryls **25** could be hydroxy-alkylated with aliphatic alcohols **26** delivering derivatives **27**. In this reported case an *in situ* generated alkoxy radical triggered a regioselective HAT event, thereby forming an alkyl radical and enabling a remote C-H bond activation (Scheme 4.6). This challenging transformation (O-H bonds are typically associated with high bond dissociation energies, BDE) was accomplished by using phenyliodine bis(trifluoroacetate) (PIFA) as the only catalyst under visible-light irradiation (100 W blue LEDs). A number of alcohols were shown to be suitable partners, including primary, secondary, and tertiary substrates; in the presence of more reactive benzylic C-H bonds; with a wide range of nitrogen containing heterocycles, such as quinolines, isoquinolines, pyridines, pyrimidines, and pyrazines. The method showed to be compliant also to complex bioactive scaffolds as for voriconazole and eszopiclone, which were converted into their alkyl derivatives **28** and **29** in 68 and 31% yield, respectively (Scheme 4.6).³⁷



Scheme 4.6: Alkylation of heteroarenes.

Tang et al. reported a new and efficient, site-selective heteroarylation of amides via $\text{C}(\text{sp}^3)\text{-H}$ bond functionalization.³⁸ Aliphatic amides (**30**) such as carboxamides, sulfonamides, and phosphoramides can undergo heteroarylation via a direct generation of amidyl radicals from the amide N–H bonds, which triggered a subsequent 1,5-HAT to form a challenging alkyl radical (Scheme 4.7).

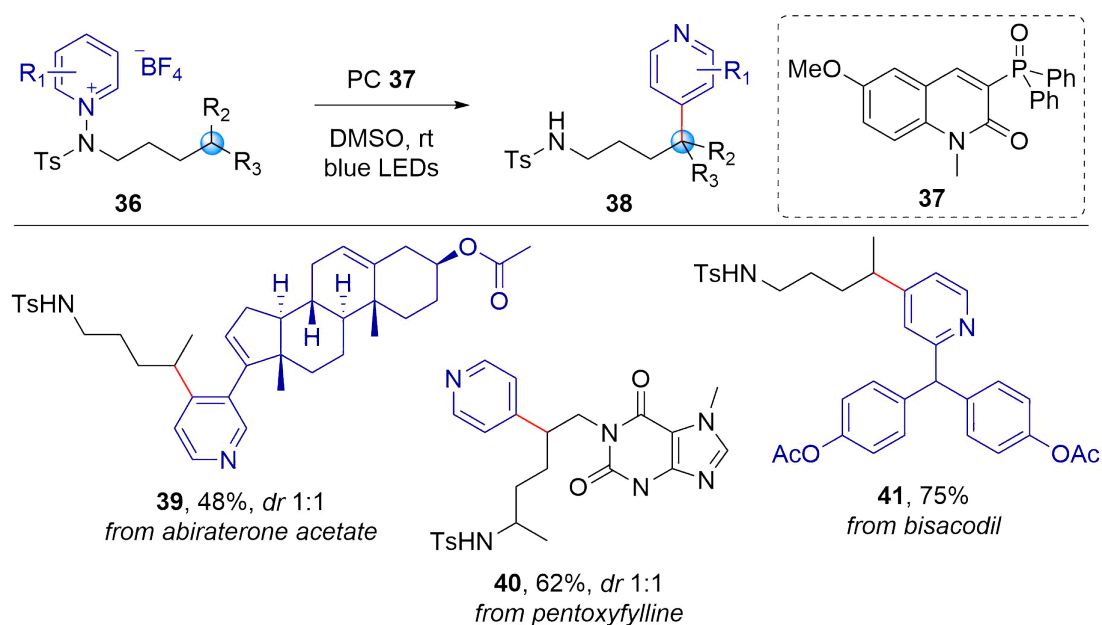


Scheme 4.7: Heteroarylation of $\text{C}(\text{sp}^3)\text{-H}$ bonds.

The transformation required the hypervalent iodine reagent PIFA (phenyliodine bis(trifluoroacetate)) under blue LEDs irradiation. PIFA acted as both the initiator of amidyl radical and the oxidant. The scope of the heteroarene (**31**) included a variety of five- and six-membered-nitrogen-containing heteroarenes (e.g. isoquinolines, phenanthridine, acridine, quinoxaline, thiazoles, benzothiazoles). Both linear and cyclic, primary and secondary, sulfonamides, along with electron-rich or deficient benzamides, phosphoramidate and phosphinamide, were all competent substrates. Complex bioactive scaffolds like celecoxib, camphor, and probenecid - were converted into derivatives **33-35** in moderate yields (Scheme 4.7).³⁸

4.2.5 Pyridylation

Kim et al. reported a similar visible-light induced site-selective C(sp³)-H pyridylation of sulfonamides and carboxamides by using N-amidopyridinium salts **36** (Scheme 4.8).³⁹

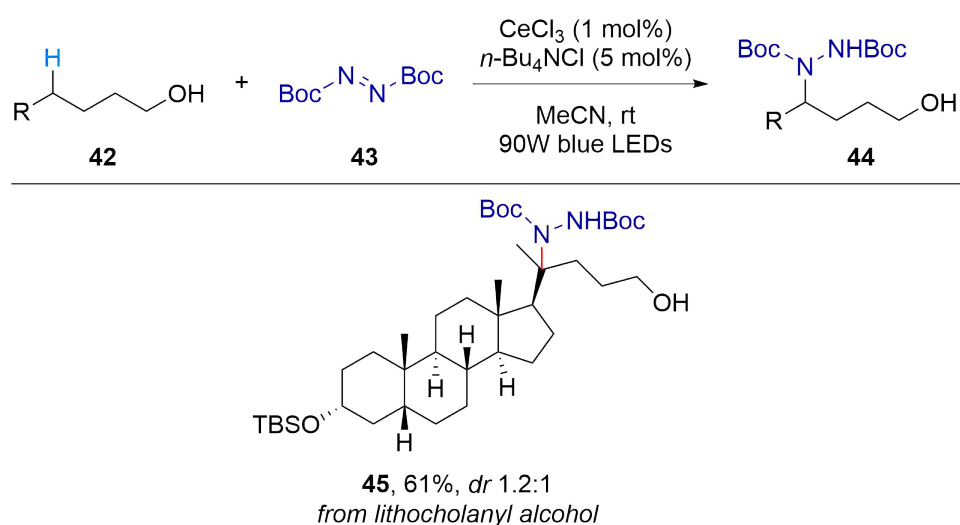


Scheme 4.8: Pyridylation of C(sp³)-H bonds.

Based on the proposed mechanism, the nitrogen-centered radicals generated upon single-electron reduction of the pyridinium salts **36** underwent 1,5-hydrogen atom transfer to form alkyl radical intermediates. Nevertheless, excellent C4-selectivity for the pyridine ring in the radical trapping was observed. Besides the substrate scope exploration with a number of both sulfonamide- and benzamide-pyridinium salts, late-stage functionalization of bisacodyl, abiraterone acetate, and pentoxifylline was achieved in good yields (**39-41**, Scheme 4.8).³⁹

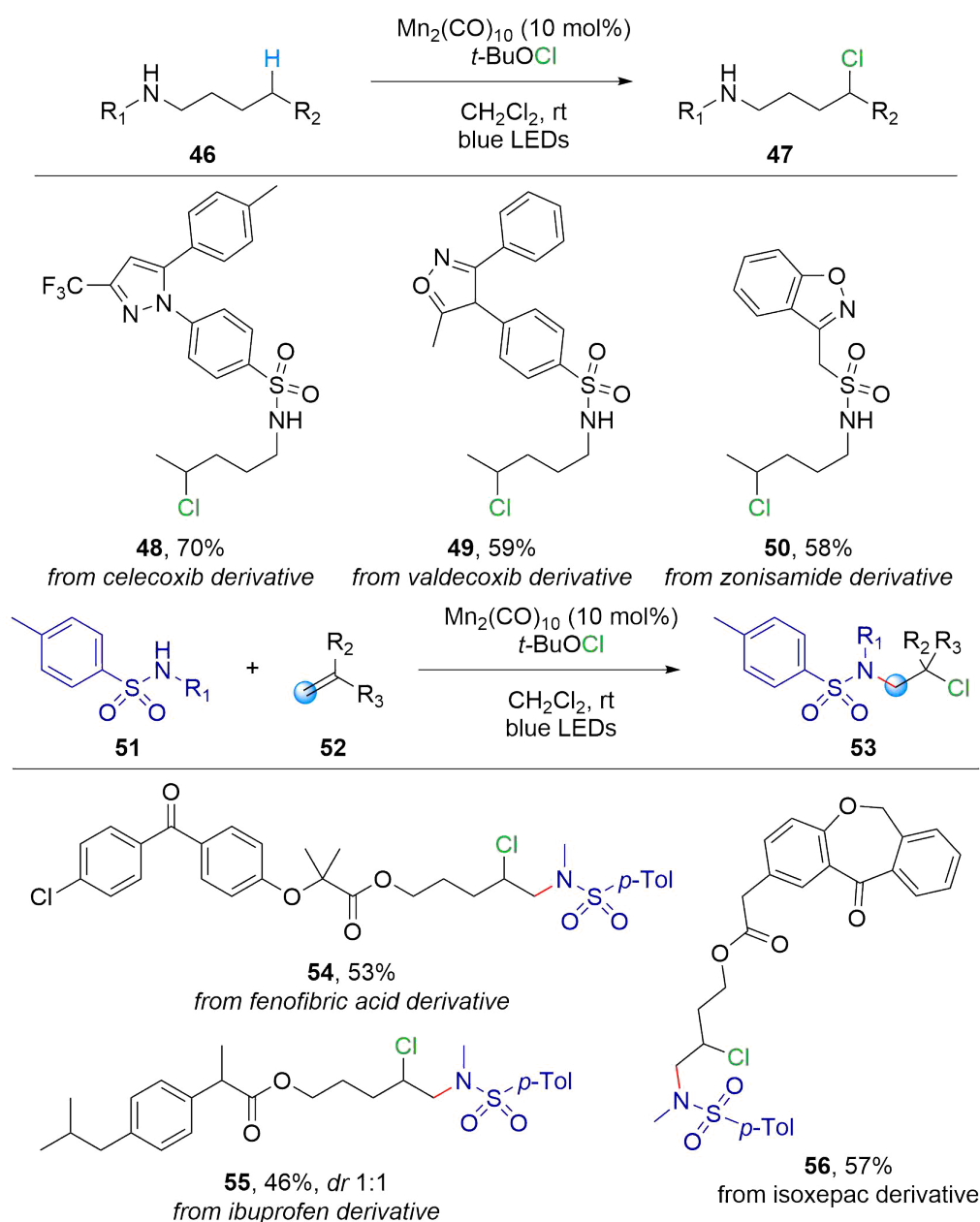
4.2.6 Remote functionalization

The group of Zuo demonstrated the application of ligand-to-metal charge transfer (LMCT) excitation to the direct catalytic generation of energetically challenging alkoxy radicals from alcohols through a coordination-LMCT-homolysis process with an abundant and inexpensive cerium salt as the catalyst.⁴⁰ The formation of a photoactive complex between a cerium(III) catalyst and the aliphatic linear alcohol **42** could trigger the formation of an alkoxy radical, followed by a 1,5-HAT, thus enabling a site-selective remote C(sp³)-H functionalization of linear aliphatic alcohols (Scheme 4.9). In analogy with the cyclic alkanols, the functionalization was accomplished with DBAD (**43**, di-*tert*-butyl azodiformate) delivering the derivatives **44**. The reaction is exemplified for lithocholanyl alcohol derivative **45**.⁴⁰



Scheme 4.9: Remote C(sp³)-H functionalization of linear aliphatic alcohols.

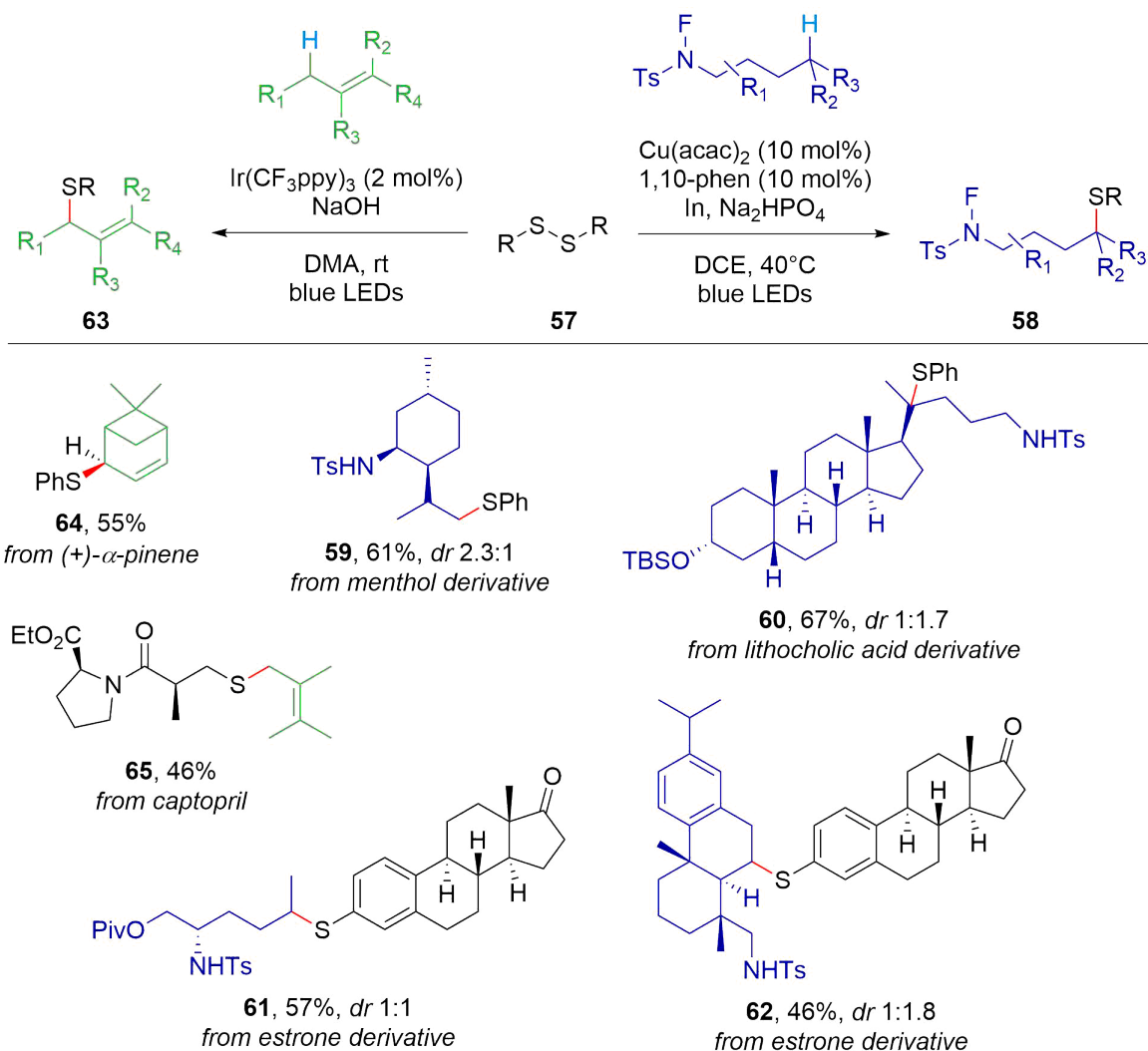
The group of Zhang reported recently the site selective chlorination of unactivated C(sp³)-H bonds of aliphatic amines.⁴¹ Intramolecular and intermolecular chloroaminations of unactivated alkenes could be accomplished through a simple and efficient protocol exploiting the formation of amidyl radicals from amine functionalities under mild reaction conditions (Scheme 4.10). The proposed mechanism relied on a manganese-mediated atom transfer event under visible light irradiation. Thoroughly, *N*-chlorination was performed by using *t*-BuOCl in CH₂Cl₂ at room temperature. The *in situ* addition of Mn₂(CO)₁₀ under blue LEDs irradiation for 1 hour led to remote chlorination, via 1,5-HAT of the amidyl radical to form a C-centered radical. The latter, eventually, underwent a Cl-atom transfer from either the *N*-chlorosulfonamide or a Cl-Mn(CO)₅ formed *in situ*. The application of the mild developed reaction conditions provided access to alkyl chlorides, chlorinated pyrrolidines, and vicinal chloroamine adducts. Late-stage remote chlorination of celecoxib, valdecoxib, and zonisamide, as well as intermolecular chloroamination of alkene-containing complex scaffolds derived from fenofibric acid, ibuprofen, and isoxepac was accomplished in medium to good yields (**48-50** and **54-56**, Scheme 4.10).



Scheme 4.10: Chlorination of C(sp³)-H bonds.

Qin et al. reported the site-selective thiolation of C(sp³)-H bonds via remote functionalization of aliphatic *N*-fluoroamides (Scheme 4.11, **57-58**).⁴² The optimized catalytic system featured Cu(acac)₂ in combination with 1,10-phenanthroline as a ligand, indium powder and Na₂HPO₄ as a base, under blue LEDs irradiation for 9 hours. The reaction mechanism was based on the formation of a photoactive Cu(I) complex with the disulfide **57** (ArS-SAr), which upon excitation induced a reduction of the N-F amide to generate an *N*-centered radical. The latter underwent a 1,5-HAT to form a C-centered radical, which was intercepted by a high-valent Cu(III)-SAr species to give, after further reductive elimination the target thioether compound **58**. The transformation proceeded efficiently with a broad range of aliphatic amides and aro-

matic disulfides, whereas also benzyl disulfide afforded the expected thioether, albeit with a medium yield. C(sp³)-H thiolation of biologically active compounds was shown to be feasible with menthol and lithocholic acid derived N-fluoroamide substrates, and with estrone-derived disulfide (**59-62**, Scheme 4.11).

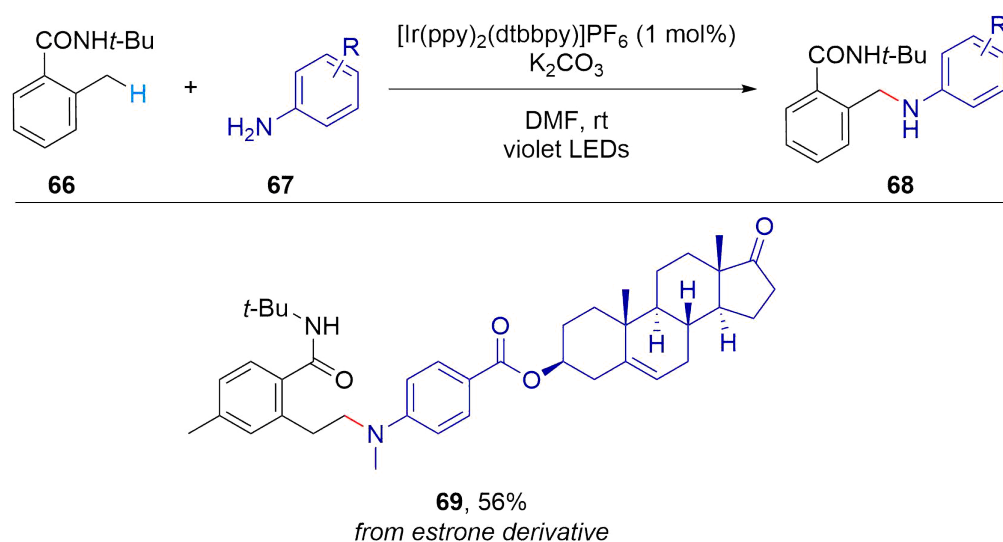


Scheme 4.11: Thiolation of C(sp³)-H bonds

HAT catalysis has been recently exploited to achieve direct allylic C(sp³)-H thiolation with disulfides by Hong and co-workers (Scheme 4.11).²⁶ The Hong protocol enabled the synthesis of allyl thioethers **63** by employing $\text{Ir}(\text{CF}_3\text{ppy})_3$ as a photoredox catalyst and NaOH as a base, under blue LEDs irradiation at room temperature. The role of the base was shown to be critical to route the reaction towards the formation of allylic thioethers circumventing undesired hydrothiolation occurring via thiyl radical addition to olefin. Thoroughly, the formation of such a radical was prevented by immediate deprotonation of thiol, which coupled to photocatalyst-mediated oxidation of allyl radical into an allyl cation, made the reaction pathway an ionic process. A wide range of diaryl sulfides **57** and alkenes afforded the target allyl thioethers **63** with high

efficiency. The scope was extended to unsymmetrical disulfide by synthesizing of various alkyl 2-benzothiazolyl disulfides. The authors demonstrated that the method was concordant to complex bioactive skeletons such as (+)- α -pinene and captopril (**64** and **65**, Scheme 4.11).⁴³

According to Z. Xu and coworkers, alkylation, carboamination, amination of remote C(sp³)-H bonds could be accomplished via a C-C or a C-N cross coupling reaction (Scheme 4.12).⁴⁴



Scheme 4.12: Alkylation of C(sp³)-H bonds.

The carboamination was achieved via the generation of *N*-centered radicals undergoing 1,5-HAT to afford C-centered radicals eventually trapped by α -aminoalkyl radicals, while the alkylation required the use of Hantzsch ester derivatives generating alkyl radicals via 1,2-SET of *N*-centered radicals. The use of primary and secondary anilines as coupling partners provided functionalized tertiary anilines via a direct cross coupling of an *N*-centered radical and an alkyl radical. The amination and carboamination could be performed by using [Ir(ppy)₂(dtbbpy)]PF₆ as a photocatalyst and K₂CO₃ as a base, under violet LED irradiation (390–410 nm) at room temperature. Slight variations of reaction conditions were required to accomplish the alkylation with Hantzsch esters. Representative carboamination of an estrone derivative was carried out in 56% yield (**69**, Scheme 4.12), to proof the robustness of the developed protocol.⁴⁴

4.3 Conclusion

The late-stage functionalization of privileged medicinal scaffolds expand the chemical space and facilitate the development of structure–activity relationship (SAR) studies, the generation of oxidized metabolites, the blocking of metabolic hot spots and the preparation of biological probes. It is a useful synthetic chemical biology tool that allows a fast access to new compounds.

Late-stage functionalization can quickly provide access to molecules of potential value, for example, in the area of drug development or material science, that otherwise might not have been available at all or too difficult to make.

C-H activation and photocatalytic processes have known a tremendous development and applications for the late-stage functionalization of complex molecules in the last years. They offer mild reaction conditions and can be implied in all areas of synthetic organic chemistry.

More efforts need to be made in this direction, since organic synthesis is still the rate-limiting step in drug discovery.

References

- (1) Stewart, D. J.; Stewart, A. A.; Wheatley-Price, P.; Batist, G.; Kantarjian, H. M.; Schiller, J.; Clemons, M.; Bradford, J.-P.; Gillespie, L.; Kurzrock, R. *Cancer Medicine* **2018**, *7*, 1824–1836.
- (2) Cortes, J. et al. *CA: A Cancer Journal for Clinicians* **2020**, *70*, 105–124.
- (3) Gotfrit, J.; Shin, J. J.; Mallick, R.; Stewart, D. J.; Wheatley-Price, P. *The Oncologist* **2020**, *25*, e130–e137.
- (4) Sellwood, M. A.; Ahmed, M.; Segler, M. H.; Brown, N. *Future Medicinal Chemistry* **2018**, *10*, 2025–2028.
- (5) Paul, D.; Sanap, G.; Shenoy, S.; Kalyane, D.; Kalia, K.; Tekade, R. K. *Drug Discovery Today* **2021**, *26*, 80–93.
- (6) Urbina, F.; Lentzos, F.; Invernizzi, C.; Ekins, S. *Nature Machine Intelligence* **2022**, *4*, 189–191.
- (7) Blakemore, D. C.; Castro, L.; Churcher, I.; Rees, D. C.; Thomas, A. W.; Wilson, D. M.; Wood, A. *Nature Chemistry* **2018**, *10*, 383–394.
- (8) Boström, J.; Brown, D. G.; Young, R. J.; Keserü, G. M. *Nature Reviews Drug Discovery* **2018**, *17*, 709–727.
- (9) Campos, K. R.; Coleman, P. J.; Alvarez, J. C.; Dreher, S. D.; Garbaccio, R. M.; Terrett, N. K.; Tillyer, R. D.; Truppo, M. D.; Parmee, E. R. *Science* **2019**, *363*, eaat0805.
- (10) Jana, R.; Begam, H. M.; Dinda, E. *Chemical Communications* **2021**, *57*, 10842–10866.
- (11) Cernak, T.; Dykstra, K. D.; Tyagarajan, S.; Vachal, P.; Krska, S. W. *Chemical Society Reviews* **2016**, *45*, 546–576.
- (12) Börgel, J.; Ritter, T. *Chem* **2020**, *6*, 1877–1887.
- (13) Capaldo, L.; Quadri, L. L.; Ravelli, D. *Green Chemistry* **2020**, *22*, 3376–3396.
- (14) Kumar Hota, S.; Jinan, D.; Prakash Panda, S.; Pan, R.; Sahoo, B.; Murarka, S. *Asian Journal of Organic Chemistry* **2021**, *10*, 1848–1860.
- (15) Wencel-Delord, J.; Glorius, F. *Nature Chemistry* **2013**, *5*, 369–375.
- (16) Dénès, F. *CHIMIA* **2020**, *74*, 23.
- (17) Guillemard, L.; Kaplaneris, N.; Ackermann, L.; Johansson, M. J. *Nature Reviews Chemistry* **2021**, *5*, 522–545.
- (18) Wu, X.; Zhu, C. *Accounts of Chemical Research* **2020**, *53*, 1620–1636.
- (19) Moir, M.; Danon, J. J.; Reekie, T. A.; Kassiou, M. *Expert Opinion on Drug Discovery* **2019**, *14*, 1137–1149.
- (20) Cannalire, R.; Pelliccia, S.; Sancineto, L.; Novellino, E.; Tron, G. C.; Giustiniano, M. *Chemical Society Reviews* **2021**, *50*, 766–897.

- (21) Muller, P. *Pure and Applied Chemistry* **1994**, *66*, 1077–1184.
- (22) Hartwig, J. F. *Accounts of Chemical Research* **2017**, *50*, 549–555.
- (23) Basu, D.; Kumar, S.; V, S. S.; Bandichhor, R. *Journal of Chemical Sciences* **2018**, *130*, 71.
- (24) Wu, Y.; Wan, Y.; Zhang, F. *Current Organic Synthesis* **2018**, *15*, 781–792.
- (25) White, M. C.; Zhao, J. *Journal of the American Chemical Society* **2018**, *140*, 13988–14009.
- (26) Hong, C. M.; Bergman, R. G.; Raymond, K. N.; Toste, F. D. *Accounts of Chemical Research* **2018**, *51*, 2447–2455.
- (27) Bender, T. A.; Bergman, R. G.; Raymond, K. N.; Toste, F. D. *Journal of the American Chemical Society* **2019**, *141*, 11806–11810.
- (28) Nicholls, T. P.; Leonori, D.; Bissember, A. C. *Natural Product Reports* **2016**, *33*, 1248–1254.
- (29) Postigo, A., *Late-stage fluorination of bioactive molecules and biologically-relevant substrates*, OCLC: on1028950993; Elsevier: Amsterdam, Netherlands, 2019; 372 pp.
- (30) Bogdos, M. K.; Pinard, E.; Murphy, J. A. *Beilstein Journal of Organic Chemistry* **2018**, *14*, 2035–2064.
- (31) McAtee, R. C.; McClain, E. J.; Stephenson, C. R. *Trends in Chemistry* **2019**, *1*, 111–125.
- (32) Chu, J. C. K.; Rovis, T. *Nature* **2016**, *539*, 272–275.
- (33) Chen, D.-F.; Chu, J. C. K.; Rovis, T. *Journal of the American Chemical Society* **2017**, *139*, 14897–14900.
- (34) Ma, Z.-Y.; Guo, L.-N.; Gu, Y.-R.; Chen, L.; Duan, X.-H. *Advanced Synthesis & Catalysis* **2018**, *360*, 4341–4347.
- (35) Wu, K.; Wang, L.; Colón-Rodríguez, S.; Flechsig, G.-U.; Wang, T. *Angewandte Chemie* **2019**, *131*, 1788–1792.
- (36) Zhang, J.; Li, Y.; Zhang, F.; Hu, C.; Chen, Y. *Angewandte Chemie International Edition* **2016**, *55*, 1872–1875.
- (37) Wu, X.; Zhang, H.; Tang, N.; Wu, Z.; Wang, D.; Ji, M.; Xu, Y.; Wang, M.; Zhu, C. *Nature Communications* **2018**, *9*, 3343.
- (38) Tang, N.; Wu, X.; Zhu, C. *Chemical Science* **2019**, *10*, 6915–6919.
- (39) Kim, N.; Lee, C.; Kim, T.; Hong, S. *Organic Letters* **2019**, *21*, 9719–9723.
- (40) Hu, A.; Guo, J.-J.; Pan, H.; Tang, H.; Gao, Z.; Zuo, Z. *Journal of the American Chemical Society* **2018**, *140*, 1612–1616.
- (41) Liu, R.-Z.; Li, J.; Sun, J.; Liu, X.-G.; Qu, S.; Li, P.; Zhang, B. *Angewandte Chemie International Edition* **2020**, *59*, 4428–4433.

- (42) Qin, Y.; Han, Y.; Tang, Y.; Wei, J.; Yang, M. *Chemical Science* **2020**, *11*, 1276–1282.
- (43) Kim, J.; Kang, B.; Hong, S. H. *ACS Catalysis* **2020**, *10*, 6013–6022.
- (44) Guo, Q.; Peng, Q.; Chai, H.; Huo, Y.; Wang, S.; Xu, Z. *Nature Communications* **2020**, *11*, 1463.

5 Forskolin Editing via Radical Iodo- and Hydroalkylation

Elena Pruteanu, Nicholas D.C. Tappin, Vladilena Gîrbu, Olga Morărescu, Fabrice Dénès,
Veaceslav Kulcički, Philippe Renaud

Synthesis **2021**, 53(07), 1247 - 1261

Copyright Georg Thieme Verlag KG. Reproduced with permission.

Author contributions

EP and NT contributed equally to the experimental work, VG and OM conducted preliminary experiments. EP, FD, VK and PR were responsible for writing of the article.

Abstract

The modification of highly oxygenated forskolin as well as manoyl and *epi*-manoyl oxide, two less functionalized model substrates sharing the same polycyclic skeleton, via intermolecular carbon-centered radical addition to the vinyl moiety has been investigated. Highly regio- and reasonably stereoselective iodine atom transfer radical addition (ATRA) reactions were developed. Unprotected forskolin afforded an unexpected cyclic ether derivative. Protection of the 1,3-diol as an acetonide led the formation of the iodine ATRA product. Interestingly, by changing the mode of initiation of the radical process, in situ protection of the forskolin 1,3-diol moiety as a cyclic boronic ester took place during the iodine ATRA process without disruption of the radical chain process. This very mild radical-mediated in situ protection of 1,3-diol is expected to be of interest for a broad range of radical and non-radical transformations. Finally, by using our recently developed *tert*-butylcatechol-mediated hydroalkylation procedure, highly efficient preparation of forskolin derivatives bearing an extra ester or sulfone group was achieved.

Key words

radical reaction, natural product modification, alkenes, boronic ester, 1,3-diol protecting group, triethylborane

5.1 Introduction

(–)-Forskolin (**1**; 7 β -acetoxy-1 α ,6 β ,9 α -trihydroxy-8,13-epoxylabd-14-en-11-one) (Figure 5.1), is a polyfunctionalized labdane diterpene presenting the 8,13-epoxylabd-14-en-11-one diterpenoid skeleton¹ and isolated in 1977 from *Coleus forskohlii*, an important medicinal plant which grows in tropical and subtropical regions of Asia and Africa.² *C. forskohlii* is the only species among *Coleus* and *Plectranthus* genera of the *Labiatae* family found to contain forskolin (**1**).³ This natural product is mostly present in the roots, between 0.1% and 2.8% only.⁴ The content in the plant extracts depends on different factors including the genotype,⁴ the biotechnology approaches,^{5,6} the organic and inorganic nutrients,⁷ plant growth hormones,⁸ and the method of extraction.⁹ Presently, plant extracts remain the main source of forskolin: studies to improve the efficiency of its extraction from *C. forskohlii* and that of the plant's growth rate are in progress. Forskolin (**1**) and its water-soluble analogue, colforsin daropate hydrochloride (NKH 477; **2**) (Figure 5.1), possess a wide range of biological effects. The main mechanism of action is based on the direct activation of the adenylate cyclase enzyme,^{10–12} which generates cAMP, a transmitter of intracellular signals that regulates many cellular functions.¹³ Beneficial effects of forskolin (**1**) have been reported in preclinical and clinical studies on the treatment of cystic fibrosis, asthma, cardiovascular diseases, liver fibrosis, and others.¹⁴ Importantly, it has numerous relevant anticancer effects, such as the inhibition of proliferation, motility, and migration in many types of cancer cells, and also the enhancement of the sensitivity to conventional

antineoplastic drugs, which makes forskolin (**1**) a promising molecule for potential application in cancer therapy.^{15–20}

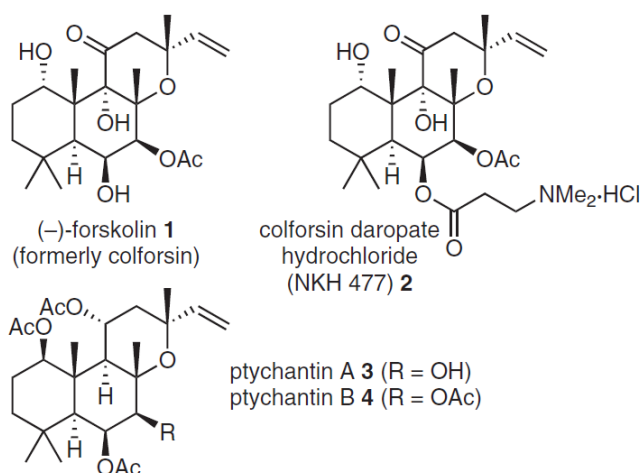


Figure 5.1: (–)-Forskolin (**1**) and related labdane diterpenoids.

Since its isolation, the polyoxygenated, tricyclic skeleton of forskolin (**1**) has stimulated the development of different strategies for its synthesis.^{21,22} Similarly, different routes have been explored for its hemisynthesis. For instance, labdane diterpenoids ptychantin A and B (**3** and **4**, Figure 5.1) are relatively abundant compounds isolated from *Ptychanthus striatus*²³ and they have been used as starting material for the hemisynthesis of (–)-forskolin (**1**).²⁴ In contrast, examples of late-stage functionalization of forskolin (**1**), to prepare analogues for SARs studies or biological applications, are rare. Analogues have been prepared using well established strategies by taking advantage of the free hydroxyl groups in forskolin (**1**) (Figure 5.2). 1-*O*-Propargylforskolin was synthesized and engaged in copper-catalyzed Huisgen cycloaddition to provide analogues containing a triazole moiety such as **5**.²⁵ Other ester analogues have been obtained to prepare, among others, ¹²⁵I-labeled analogues such as **7**.²⁶ Tetracyclic analogue **6** presenting a seven membered-ring carbonate moiety was prepared by König and co-workers by treatment of thionocarbonate **8** (see Scheme 5.1 for structure) with 1,3-dimethyl-2-phenyl-1,3,2-diazaphospholidine (Corey–Winter conditions).²⁷

Despite the fact that unactivated alkenes can serve as an entry to introduce diversity on the skeleton of natural products,²⁸ this opportunity has received only limited attention in the case of forskolin. Simple hydrogenation of forskolin has been carried out to convert the vinyl side chain into the corresponding ethyl group²⁹ as well as for the preparation of the corresponding radioisotopic labeled [³H]-dihydrocolforsin.³⁰ The side chain has been elongated by Lett and Delpech using a sequence involving ozonolysis and subsequent Wittig olefination.³¹ Romo and co-workers showed that alkynyl diazo ester could be employed under rhodium catalysis to form cyclopropane derivatives from forskolin.³² The alkenyl side chain in forskolin was found to participate in 1,3-dipolar additions as illustrated by the formation of bis-cycloadducts as side products in the reaction of 1-*O*-propargylforskolin with oximes aiming at the synthesis of isoxazoles.²⁹

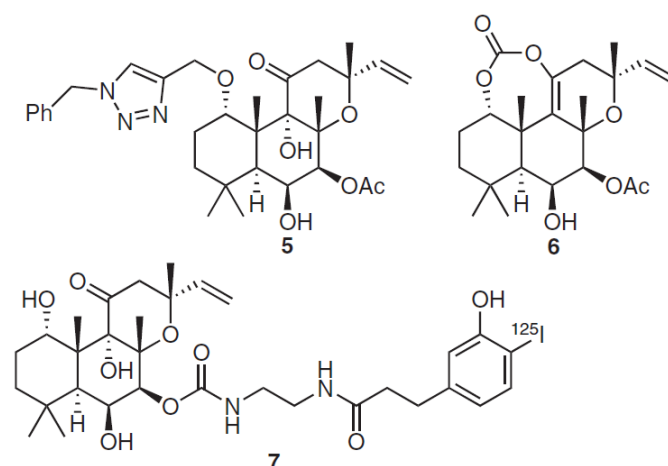
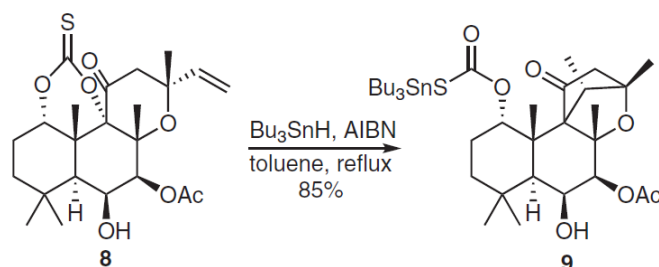


Figure 5.2: Examples of analogues prepared from (-)-forskolin.

In an attempt to remove the 9-hydroxy group via the thiocarbonate **8** under classical radical conditions (Bu_3SnH , AIBN), König and co-workers reported that, instead of the expected deoxygenated product, tetracyclic forskolin analogue **9** was obtained in a highly stereoselective manner, following regioselective cleavage of the thionocarbonate moiety, 5-exo-trig cyclization of the resulting tertiary carbon-centered radical intermediate, and hydrogen atom transfer from the chain carrier reagent (Scheme 5.1).²⁷



Scheme 5.1: König's attempt to prepare deoxygenated (-)-forskolin under radical conditions.

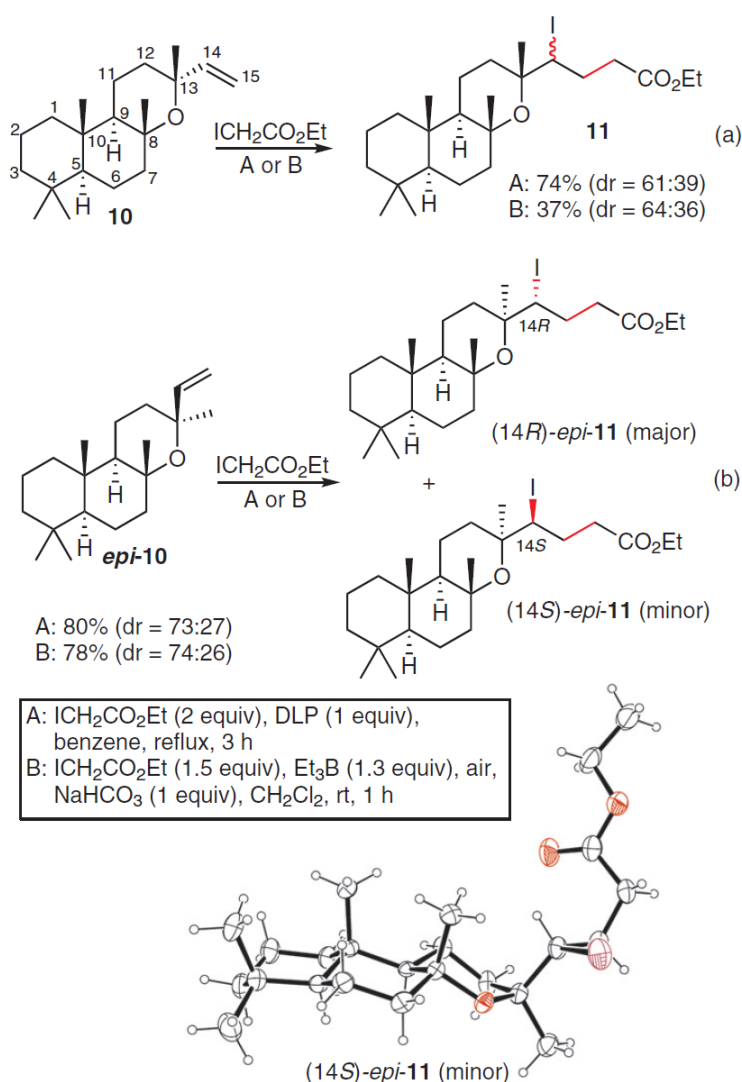
With the exception of this last example, in which the participation of the alkenyl side chain was not originally planned, to our knowledge no effort has been made to use the C=C bond as a partner in radical transformations. Therefore, we decided to explore the reactivity of the pendant terminal alkene in radical C–C bond-forming reactions. Since this allylic ether is electron-rich, radical reactions employing reagents of the general formula I-CH₂-EWG (EWG = electron-withdrawing group) seemed appropriate to achieve this goal. Accordingly, we have selected the atom transfer radical addition (ATRA), pioneered by Kharasch,^{33–38} Curran,³⁹ and others^{40–42} and the hydroalkylation reaction developed by some of us⁴³ to explore the reactivity of the forskolin skeleton under radical conditions. Before tackling the polyhydroxylated skeleton of forskolin, we decided to investigate the reactivity of less functionalized analogues. As model substrates for our study, we first turned our attention to manoyl oxide (**10**) and *epi*-manoyl oxide (*epi*-**10**), which share with forskolin the same tricyclic skeleton, with a terminal alkene in a

sterically hindered environment. These products are easily prepared in one step from sclareol, a readily available natural product from *Salvia sclarea* essential oil production.^{44,45} Diastereomers **10** and *epi*-**10** can be separated by flash column chromatography using 10% AgNO₃ impregnated silica gel.

5.2 Results and Discussion

5.2.1 Iodoalkylation (ATRA reaction) of manoyl and *epi*-manoyl oxide

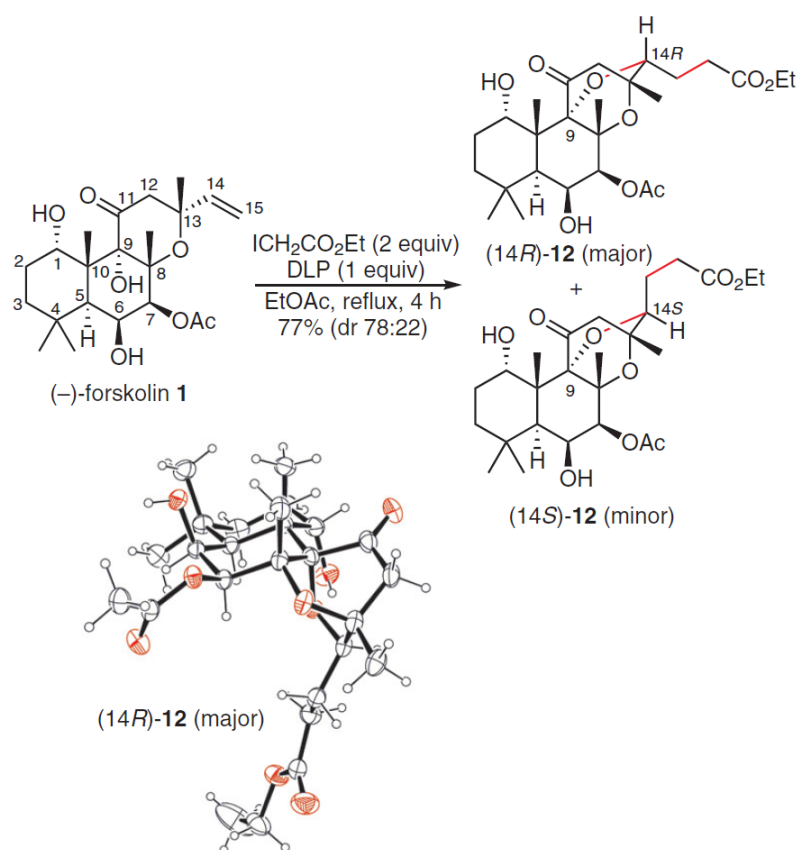
The ATRA was first investigated with ethyl iodoacetate, using dilauroyl peroxide (DLP) as a radical initiator.⁴⁰ Iodoalkylation of manoyl oxide (**10**) with ethyl iodoacetate in the presence of sub-stoichiometric quantities of DLP (5mol% every 2 h) resulted in low conversion and long reaction times (10–18 h, in refluxing benzene). Under these conditions, radical deiodination and ionic elimination side reactions led to the corresponding reduced product and alkenes. Increasing the quantity of DLP (1.0 equiv) led to nearly full conversion of **10** after only 3 hours. Gratifyingly, under these conditions the expected adduct **11** was obtained in 74% yield as a mixture of diastereomers (dr 61:39) (Scheme 5.2a). Longer reaction times and higher loading of initiator resulted in increased amounts of side products, thus reducing the efficiency of the reaction. Surprisingly, the use of milder reaction conditions (Et₃B/air, room temperature) to achieve the iodoalkylation led to an increase in the amount of decomposition products. The presence of an inorganic base as an additive (NaHCO₃) did not significantly improve the yields, the iodinated adduct being isolated in a modest 37% yield (dr 64:36). With *epi*-manoyl oxide (*epi*-**10**) both reaction conditions gave good yields of the ATRA product *epi*-**11** (78–80% yields, Scheme 5.2b), presumably as a result of a slightly higher stability of the iodinated product towards elimination under the reaction conditions. The *S*-configuration at the C-14 position of the minor isomer of *epi*-**11** (EWG = CO₂Et) was unambiguously assigned by single crystal X-ray diffraction data analysis.⁴⁶ Interestingly, the diastereoselectivity of these ATRA reactions remains unusually high for such a transformation, especially in the case of *epi*-manoyl oxide (*epi*-**10**).



Scheme 5.2: Iodoalkylation of manoyl oxide (**10**) and *epi*-manoyl oxide (*epi*-**10**); X-ray single crystal structure of (14*S*)-*epi*-**11** (minor diastereomer) (50% probability ellipsoids).

5.2.2 Iodoalkylation and alkoxyalkylation of (–)-forskolin

Encouraged by our results in the manoyl oxide and *epi*-manoyl series, we undertook the exploration of iodoalkylation to modify the potentially more problematic forskolin. It shares the same skeleton with manoyl oxide but is decorated with one keto group and three hydroxyl groups, one of them being acetylated. (–)-Forskolin (**1**) was first engaged in an iodoalkylation reaction in refluxing ethyl acetate using DLP (1 equiv) as a radical initiator (Scheme 5.3). Under these reaction conditions, a clean reaction took place that delivered the tetracyclic compound **12** in high yield as mixture of diastereomers (dr 78:22) instead of the expected iodoalkylated product. The structure of this new forskolin analogue was determined by careful NMR analysis and unambiguously confirmed by X-ray diffraction data analysis of a single crystal of the major isomer of (14*R*)-**12**. Interestingly, the biological properties of the forskolin analogue 15-hydroxy-9,14-epoxyforskolin presenting a similar tetracyclic skeleton has been previously reported.^{47,48}

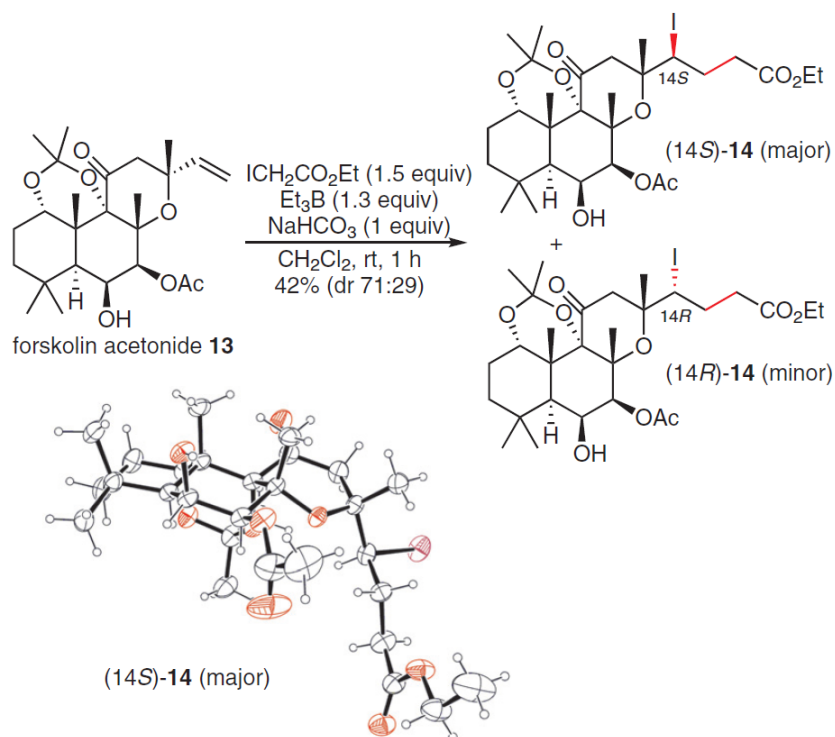


Scheme 5.3: Alkoxyalkylation of (-)-forskolin (**1**) in refluxing EtOAc; X-ray single crystal structure of (14*R*)-**12** (major diastereomer) (50% probability ellipsoids).

The formation of tetracyclic compound **12** arises from the nucleophilic displacement of the iodine atom in the ATRA product intermediate via an intramolecular nucleophilic substitution with inversion. The cyclization of the major isomer appeared to be faster since mainly the major diastereomer of **12** was observed after 2 hours together with the minor diastereomer of the iodoalkylated product. In situ nucleophilic displacement of the iodide atom in I-ATRA products has been reported by using ICH₂CO₂SnBu₃ in refluxing benzene,^{49,50} or with 2-iodoacetamide and 2-iodoacetic acid upon heating in water or ethanol.^{51,52} In the second case, the ATRA reaction with 2-iodoacetic acid led to a mixture of γ -lactone and tetrahydrofuran when carried out on pent-4-en-1-ol, indicating that displacement of the iodide could also be achieved by a free hydroxyl group.^{51,52} Similarly, the reaction of α -iodo esters and α -iodonitriles with allylic alcohols initiated by Et₃B/O₂ and carried out in water, ethanol, or a mixture of both, in the presence of a base, delivered epoxides through the cyclization of the halohydrin intermediates.⁵³ In contrast, no cyclization involving the C–I bond was observed in less polar solvents (1,2-dichloroethane, ethyl acetate, or toluene) by Cordero-Vargas and co-workers. They showed that, upon initiation with DLP in refluxing 1,2-dichloroethane, the ATRA reaction of iodoacetic acid with allylic alcohols exclusively led to γ -iodo- δ -lactones following preferential lactonization of the ATRA products between the carboxylic acid moiety and the free hydroxyl group.⁵⁴ The products resulting from bromine atom transfer are more robust but can nevertheless be converted into

γ -lactones upon heating.³³

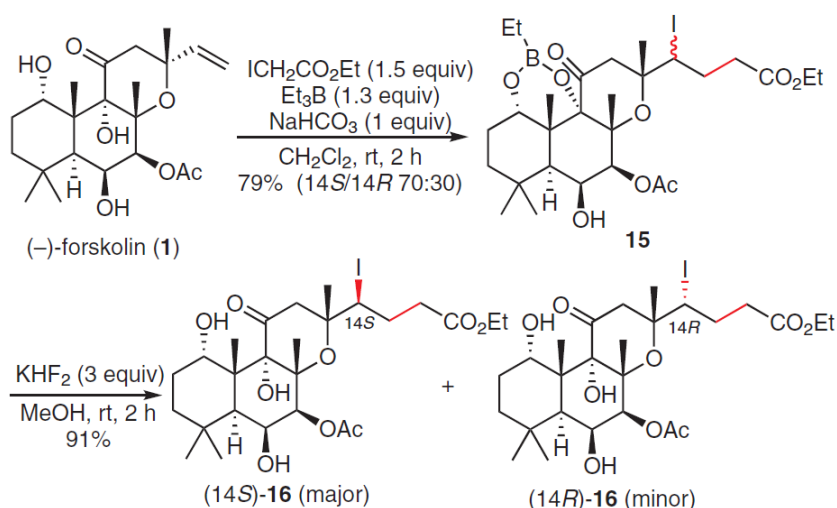
In the conversion of (–)-forskolin into tetracyclic compound **12**, the efficient formation of the ether ring under our reaction conditions is facilitated by the proximity of the OH at C-9 and the iodide at C-14, which favors the nucleophilic substitution reaction.⁵⁵ To prevent the cyclization leading to **12**, we decided to protect (–)-forskolin as forskolin acetonide **13**. This was easily accomplished by protection of the 1,3-diol moiety in (–)-forskolin with 2,2-dimethoxypropane.²² In this case, the I-ATRA reaction was carried out in the presence of a base (NaHCO₃) and gave the corresponding adduct **14** in a moderate isolated yield of 42% (dr 71:29) (Scheme 5.4). The relative configuration at C-14 of the major diastereomer of **14** was assigned by single crystal X-ray diffraction data analysis.⁵⁶



Scheme 5.4: Iodoalkylation of the (–)-forskolin acetonide **13**; X-ray single crystal structure of (14*S*)-**14** (major diastereomer) (50% probability ellipsoids).

The iodoalkylation of unprotected (–)-forskolin (**1**) was then carried out at room temperature in CH₂Cl₂ using 1 equivalent of Et₃B and air to initiate the reaction. Under these reaction conditions, the product of iodoalkylation **15** was obtained in high yield, without subsequent nucleophilic displacement of the iodine atom (Scheme 5.5). Interestingly, **15** was not the expected unprotected iodine ATRA product, but a cyclic boronic ester indicating that in situ protection of the diol is taking place.^{57–60} By monitoring the reaction by ¹H NMR, the formation of the unprotected iodoalkylated product **16** could be observed. After 2 hours, the starting forskolin (**1**) was fully consumed and only the cyclic boronic ester **15** could be isolated. Deprotection of the 1,3-

diol was achieved in a methanolic solution of KHF_2 to afford the sensitive iodide **16** in almost quantitative yield as a 70:30 mixture of diastereomers.^{60,61} The *S*-configuration at C-14 of the major diastereomer of **16** was only tentatively assigned by analogy with the iodoalkylation of forskolin acetonide **13** that proceeds with a comparable diastereoselectivity (see Scheme 5.4). In a pleasing and unplanned way, this approach uses Et_3B not only as a radical initiator but also as a reagent for the protection of the reactive 1,3-diol moiety providing, after easy hydrolysis of the boronic ester, the desired product of iodoalkylation in excellent yield compared to the classical acetonide protection described in Scheme 5.4.

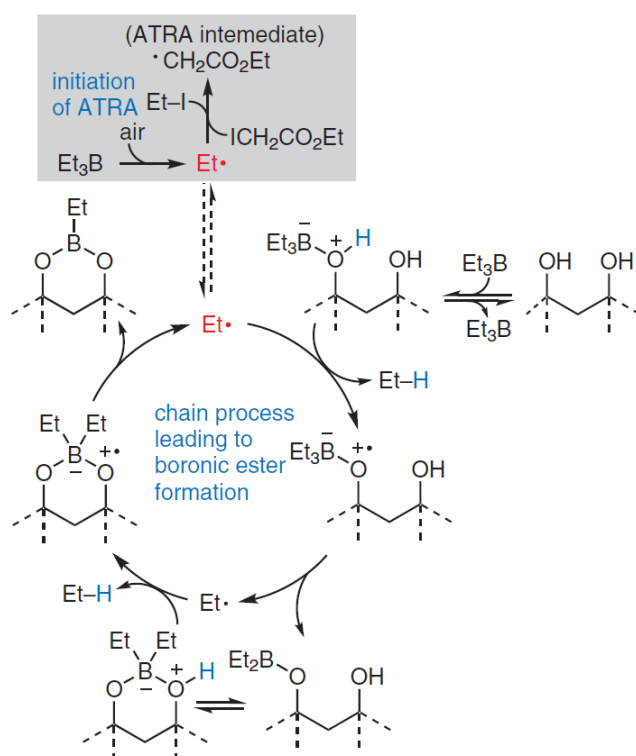


Scheme 5.5: Iodoalkylation of unprotected (-)-forskolin (**1**); configuration at C-14 tentatively assigned by comparison with the product of iodoalkylation of forskolin acetonide **13**.

Guindon and co-workers observed a similar in situ protection of 1,3-diols as boronic esters using Et_3B and air during the generation of α -ester radicals.⁶² However, the mechanism of formation of the cyclic boronic ester was not elucidated. Interestingly, only one equivalent of Et_3B was necessary to protect the 1,3-diol moiety and to initiate the ATRA process. A tentative mechanism involving a radical chain process is proposed in Scheme 5.6. This mechanism is based on the observation that $\text{Et}_3\text{B}\text{-water}$ ^{63–66} and $\text{Et}_3\text{B}\text{-MeOH}$ ^{65–68} complexes are efficient reducing agent for carbon-centered radicals. The rate constant for the hydrogen atom transfer from the complex $\text{Et}_3\text{B}\text{-MeOH}$ to a secondary alkyl radical has been estimated in the $10^6 \text{ M}^{-1} \text{ s}^{-1}$ range.⁶⁸ Remarkably, the formation of the cyclic boronic ester does not compete with the radical initiation process since the ethyl radical (in red) is regenerated during the formation of the boronic ester. This radical can either initiate the iodine ATRA process or be further involved in the boronic ester formation.

5.2.3 Stereoselectivity of the iodoalkylation

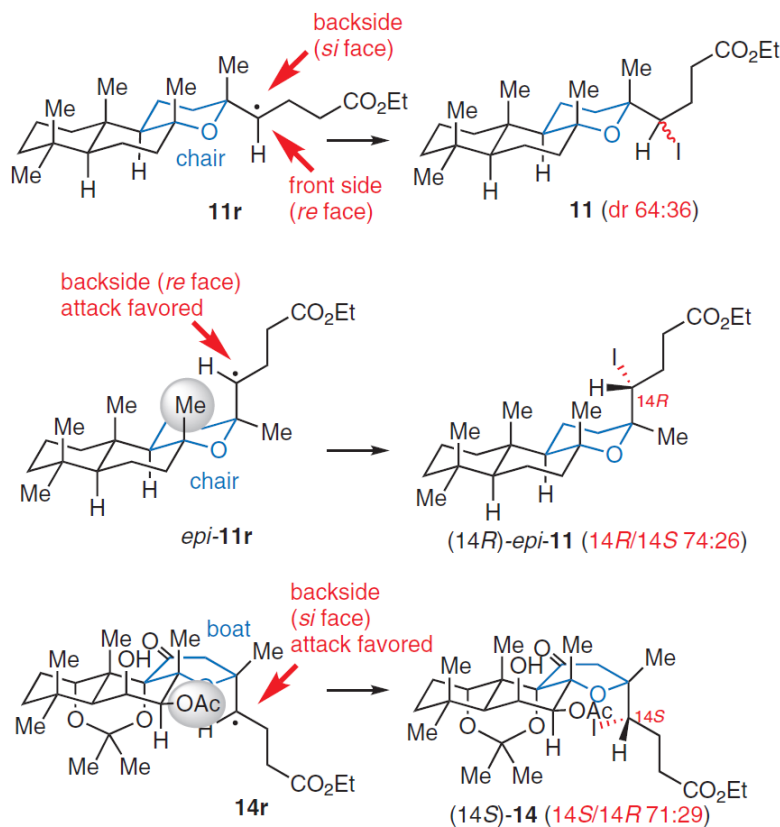
The stereoselectivity of the iodoalkylation deserves some comment as the levels of stereoselectivity are from moderate to unusually high for such an iodine ATRA reaction involving non-



Scheme 5.6: Initiation of ATRA and radical chain mechanism leading to cyclic ethylboronic ester.

stabilized acyclic radicals.^{69,70} The ATRA reaction with manoyl oxide (**10**) goes through the radical adduct **11r** with an all-chair conformation (Scheme 5.7). In this conformation, the radical center is located on an equatorial side chain, far away from the bulky substituents on the polycyclic framework. As a result, a very modest level of stereoselectivity (dr 64:36) was observed (Scheme 5.2a). The iodoalkylation of *epi*-manoyl oxide (*epi*-**10**) gave a higher level of stereocontrol (14*R*/14*S* 74:26, Scheme 5.2b) that can be rationalized by an iodine atom transfer step taking place from the least hindered *re* face of the carbon-centered radical intermediate in the conformation *epi*-**11r** depicted in Scheme 5.7. In this all-chair conformation, the side chain bearing the carbon-centered radical adopts an axial position, the hydrogen atom on the radical pointing towards the tetrahydropyran ring to minimize steric interactions with the angular methyl group. The latter shields the *si* face (front side) of the radical *epi*-**11r** making the *re* face (back side) attack more favored. Despite the same relative configuration at C-13 as manoyl oxide (**10**), (–)-forskolin (**1**) as well as its acetonide **13**, adopt a different conformation. It was demonstrated by NMR analysis that (–)-forskolin (**1**) adopts a flattened boat-like conformation of ring C in solution.⁷¹ A similar boat-like conformation was also observed for in the X-ray single crystal structure of the acetonide **13** (Scheme 5.7). In this conformation, the vinyl side chain adopts a flagpole position with the hydrogen atom at the internal carbon atom of the alkene pointing towards the ring. This is very likely to be the case as well for the secondary carbon-centered radical intermediate **14r**. Iodine atom transfer (i.e., attack) from the *re* face (front side) is partially blocked (or disfavored) by the substituents on the polycyclic framework (axial H-atom

at C-7, axial OR group at C-9 and equatorial OAc group at C-7) and the *si* face (back side) attack becomes the major pathway (14*S*/14*R* 71:29 for **14**), Scheme 5.4). The same model may also explain the stereoselectivity outcome with unprotected forskolin (**1**) and its cyclic boronic ester derivative.

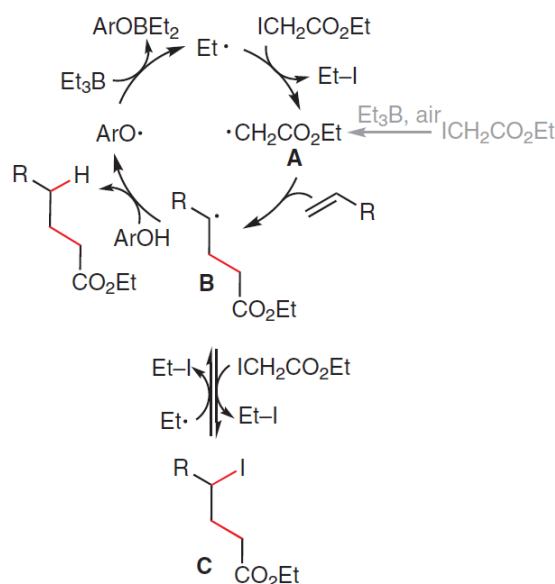


Scheme 5.7: Stereoselectivity of the iodoalkylation of **10**, *epi-10*, and **13**.

5.2.4 Hydroalkylation of manoyl and *epi*-manoyl oxide

Next, we turned our attention to the hydroalkylation reaction developed by some of us that proved to be effective for terminal and non-terminal alkenes.^{43,72–75} The reaction requires the combination of Et_3B and a catechol derivative, which plays the role of hydrogen atom donor. Unlike tin hydride, catechol derivatives are very selective for nucleophilic carbon-centered radicals. As a result of favorable polar effects in the transition state, the hydrogen atom transfer (HAT) from 4-*tert*-butylcatechol (TBC) is about three orders of magnitude faster to secondary alkyl radicals than to ester enolyl radicals ($k_H = 1.3 \times 10^6 \text{ M}^{-1} \text{ s}^{-1}$ at 80°C for secondary alkyl radical; $k_H \approx 2 \times 10^3 \text{ M}^{-1} \text{ s}^{-1}$ at 80°C for an ester enolyl radical).⁴³ This allows for efficient intra- and intermolecular additions to take place with electrophilic carbon-centered radicals and electron-rich alkenes. A simplified mechanism of the hydroalkylation of non-activated alkenes with iodoacetate is depicted in Scheme 5.8. It involves the fast iodine atom abstraction from ethyl iodoacetate by the ethyl radical ($k_{IAT} = 2.6 \times 10^7 \text{ M}^{-1} \text{ s}^{-1}$ in benzene at 50°C)⁷⁶ generated in

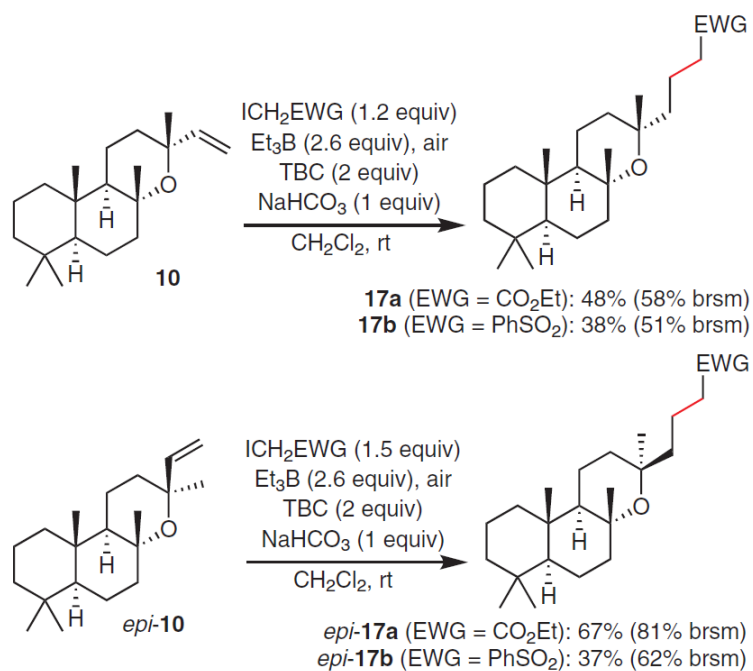
the initiation step from Et_3B by its reaction with molecular oxygen.⁷⁷ The resulting electrophilic enoyl radical **A** adds to the terminal position of the electron-rich alkene to give a secondary alkyl radical **B** that can either be trapped by HAT from the catechol derivative to give the expected product or alternatively, abstracts the iodine atom from ethyl iodoacetate. Based upon the relative rate constants, the second pathway is more likely, at least in the early stage of the reaction. The secondary alkyl iodide **C** formed in the ATRA process can undergo iodine atom abstraction by the ethyl radical to regenerate the secondary alkyl radical **B**. At high conversion, the concentration in ethyl iodoacetate become sufficiently low for the HAT from 4-*tert*-butylcatechol to progressively overcome the conversion of **B** into **C**. The oxygen-centered radical $\text{ArO}\cdot$ generated in the HAT step reacts then with Et_3B to propagate the radical chain. It has also been demonstrated that the exceptional efficacy of the hydroalkylation reaction is also linked to a repair mechanism involving TBC and Et_3B .^{43,78}



Scheme 5.8: Simplified mechanism for the Et_3B -mediated hydroalkylation of alkenes.

A rapid optimization of the previously reported reaction conditions was performed on manoyl oxide (**10**). Based upon our previous work on the iodoalkylation of manoyl oxide, which stressed the relative instability of iodinated products in this series, NaHCO_3 was selected as an additive to trap the hydroiodic acid and/or molecular iodine formed under the reaction conditions and which presumably leads to the decomposition of the product in an autocatalytic process. The hydroalkylation reaction was tested in the manoyl oxide and *epi*-manoyl oxide series (Scheme 5.9) with two different reagents (ethyl iodoacetate and iodomethyl phenyl sulfone). Under standard reaction conditions (1.2 equiv of ethyl iodoacetate and 1.3 equiv of Et_3B), with only 1 equiv of *tert*-butylcatechol (TBC) as a reducing agent, no reduced product was formed and the only product isolated from the reaction mixture was the product of iodoalkylation **11**. Increasing the quantity of TBC to 2 equiv allowed for the isolation of the desired reduced product in low yield (19%). Eventually, a satisfactory 48% yield (58% yield, brsm) of hydroalkylation product **17a** was obtained by using 2.6 equiv of Et_3B (added in two portions) and 2 equiv of

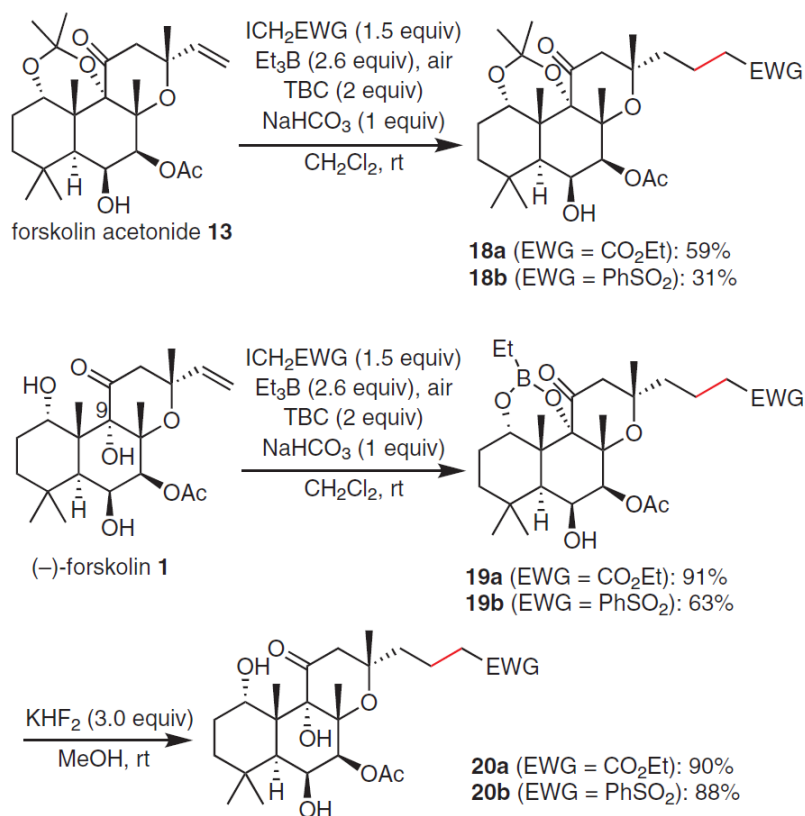
TBC. With these optimized reaction conditions in hand, the reaction was extended to the use of iodomethyl phenyl sulfone, and the corresponding sulfone adduct **17b** was obtained in 38% yield (51% brsm). Similar conditions applied to *epi*-manoyl oxide (*epi*-**10**) led to the corresponding ester *epi*-**17a** and sulfone adduct *epi*-**17b** in 67% (81% brsm) and 37% (62% brsm) yields, respectively. Trace amounts ($\leq 5\%$ in most cases) of uncharacterized olefinic byproducts were observed in all cases.



Scheme 5.9: Hydroalkylation of manoyl oxide (**10**) and *epi*-manoyl oxide (*epi*-**10**).

5.2.5 Hydroalkylation of (–)-forskolin

The hydroalkylation of forskolin acetonide **13** was investigated next. As previously observed in the manoyl oxide series, the formation of non-iodinated products via the hydroalkylation reaction could be achieved in higher yields than the corresponding iodoalkylation, presumably due to the in situ reduction of the sensitive iodides (Scheme 5.10). Hydroalkylation of the acetonide **13** with ethyl iodoacetate and iodomethyl phenyl sulfone under the optimized conditions provided **18a** and **18b** in 59% and 31% yields, respectively. The cleavage of the acetonide moiety in **18a** and **18b** to give **20a** and **20b** was not attempted. Gratifyingly, hydroalkylation of the unprotected (–)-forskolin (**1**) under our optimized reaction conditions gave the corresponding functionalized adducts **19a** in 91% yield (compared to 79% for the iodoalkylation reaction). The hydroalkylation with iodomethyl phenyl sulfone gave the corresponding sulfone adducts **19b** in 63% yield from (–)-forskolin (**1**). The subsequent deprotection of boronic esters **19a** and **19b** was achieved in high yield upon treatment with methanolic KHF_2 at room temperature, delivering the unprotected forskolin adducts **20a** and **20b**.



Scheme 5.10: Hydroalkylation of forskolin (**1**) and its acetonide **13**.

5.3 Conclusion

We have reported examples of functionalization of the forskolin skeleton via intermolecular radical additions to the alkenyl moiety. The studies conducted on manoyl oxide and *epi*-manoyl oxide as model substrates revealed that the iodinated products resulting from an iodine ATRA process were formed with complete regioselectivity in moderate to good yields and stereoselectivities. The use of the recently developed Et₃B/catechol-mediated radical hydroalkylation reaction proved to be particularly well-adapted to access stable functionalized derivatives in these series. The highly oxygenated skeleton of (–)-forskolin, with its free hydroxyl group at C-9, led to the formation of an interesting cyclic ether during initial attempts to run the iodoalkylation in refluxing ethyl acetate. This tetracyclic product results formally from an alkoxyalkylation of the vinyl moiety and involving an iodine ATRA followed by an intramolecular nucleophilic substitution process. As anticipated, the ionic substitution in forskolin could be avoided by running the reaction with an acetonide-protected derivative. Deploying Et₃B as a radical initiator circumnavigated the necessity for a protecting group installation prior to ATRA functionalization, thanks to the in situ formation of a cyclic boronic ester intermediate which acts as a protecting group for the free hydroxyl groups. Thus, the iodinated compounds could be isolated in excellent yields. This unexpected in situ protection of diols under mild radical conditions may be of general interest for radical reactions (and probably other concerted ionic reactions) involving 1,3-diols. Finally, the hydroalkylation of forskolin proceeds efficiently and demonstrates further the potential of this method to introduce functionalized side chain in natural products containing alkene residues. The mild radical chemistry reported here offers many opportunities to prepare elaborated analogues for biological studies that are not accessible by conventional methods.

For details of techniques, materials, and instrumentation, see the Supporting Information. [Compounds characterization is included in the Experimental part only].

Funding Information

This work was funded by the Swiss National Science Foundation: project IZ73Z0_152346/1 (SCOPES program involving VK and PR) and project 200020_172621 (PR). EP and VG were both partly supported by the State Secretariat for Education and Innovation (SERI) via a Swiss Government Excellence Scholarships for Foreign Scholars and Artists.

Acknowledgment

We thank the group of Chemical Crystallography of the University of Bern (Prof. Dr. P. Macchi, PD Dr. Simon Grabowsky and Dr. Michal Andrzejewski) for measuring, solving, refining, and summarizing the X-ray structures.

Supporting Information

Sup. info. for this article is available online at <https://doi.org/10.1055/s-0040-1706003>.

References

- (1) Alasbahi, R.; Melzig, M. *Planta Medica* **2010**, *76*, 653–661.
- (2) Bhat, S.; Bajwa, B.; Dornauer, H.; do Scusa, N.; Fehlhaber, H.-W. *Tetrahedron Letters* **1977**, *18*, 1669–1672.
- (3) Shah, V.; Bhat, S.; Bajwa, B.; Dornauer, H.; de Souza, N. *Planta Medica* **1980**, *39*, 183–185.
- (4) Vishwakarma, R.; Tyagi, B.; Ahmed, B.; Husain, A. *Planta Medica* **1988**, *54*, 471–472.
- (5) Jha, S.; Bandyopadhyay, M.; Chaudhuri, K. N.; Ghosh, S.; Ghosh, B. *Plant Genetic Resources* **2005**, *3*, 101–115.
- (6) Veeresham, C.; Reddy, C.; Praveena, C. *International Journal of Pharmaceutical Sciences and Nanotechnology* **2012**, *5*, 1720–1726.
- (7) Nadukeri, S.; Kattimani, K. N.; Kolakar, S. S. *Internat. J. agric. Sci.* **2014**, *10*, 119–123.
- (8) Choudhary, A.; Upadhayaya, S.; Sharma, A.; Raidas, D. *Journal of Pharmacognosy and Phytochemistry* **2019**, 686–688.
- (9) Singh, P.; Suryanarayana, M. A. *Indian Journal of Pharmaceutical Sciences* **2019**, *81*.
- (10) Seamon, K. B.; Daly, J. W. *Trends in Pharmacological Sciences* **1983**, *4*, 120–123.
- (11) Forte, L. R. *Archives of Biochemistry and Biophysics* **1983**, *225*, 898–905.
- (12) Sengupta, S.; Mehta, G. *Organic & Biomolecular Chemistry* **2018**, *16*, 6372–6390.
- (13) Dessauer, C. W.; Watts, V. J.; Ostrom, R. S.; Conti, M.; Dove, S.; Seifert, R. *Pharmacological Reviews* **2017**, *69*, ed. by Ohlstein, E. H., 93–139.
- (14) Salehi, B.; Staniak, M.; Czopek, K.; Stępień, A.; Dua, K.; Wadhwa, R.; Kumar Chellappan, D.; Sytar, O.; Brestic, M.; Ganesh Bhat, N.; Venkatesh Anil Kumar, N.; del Mar Contreras, M.; Sharopov, F.; C. Cho, W.; Sharifi-Rad, J. *Applied Sciences* **2019**, *9*, 4089.
- (15) Follin-Arbelet, V.; Misund, K.; Hallan Naderi, E.; Ugland, H.; Sundan, A.; Kiil Blomhoff, H. *Scientific Reports* **2015**, *5*, 13001.
- (16) Quinn, S. N.; Graves, S. H.; Dains-McGahee, C.; Friedman, E. M.; Hassan, H.; Witkowski, P.; Sabbatini, M. E. *Molecular Carcinogenesis* **2017**, *56*, 1344–1360.
- (17) Sapio, L.; Gallo, M.; Illiano, M.; Chiosi, E.; Naviglio, D.; Spina, A.; Naviglio, S. *Journal of Cellular Physiology* **2017**, *232*, 922–927.
- (18) Illiano, M.; Sapio, L.; Salzillo, A.; Capasso, L.; Caiafa, I.; Chiosi, E.; Spina, A.; Naviglio, S. *Biochemical Pharmacology* **2018**, *152*, 104–113.
- (19) Wang, H.; Lou, C.; Ma, N. *Cancer Management and Research* **2019**, *Volume 11*, 1685–1696.
- (20) Shen, L.; Yuan, F.; Hong, Y.; Xu, M.; Hu, Y.; Liu, Y. *Journal of Molecular Cell Biology* **2020**, *12*, ed. by Li, J., 245–248.

- (21) Colombo, M. I.; Zinczuk, J.; Rúveda, E. A. *Tetrahedron* **1992**, *48*, 963–1037.
- (22) Hylse, O.; Maier, L.; Kučera, R.; Perečko, T.; Svobodová, A.; Kubala, L.; Paruch, K.; Švenda, J. *Angewandte Chemie International Edition* **2017**, *56*, 12586–12589.
- (23) Hashimoto, T.; Horie, M.; Toyota, M.; Taira, Z.; Takeda, R.; Tori, M.; Asakawa, Y. *Tetrahedron Letters* **1994**, *35*, 5457–5460.
- (24) Hagiwara, H.; Takeuchi, F.; Kudou, M.; Hoshi, T.; Suzuki, T.; Hashimoto, T.; Asakawa, Y. *The Journal of Organic Chemistry* **2006**, *71*, 4619–4624.
- (25) Koteswara Reddy, M.; Santosh Kumar, K.; Sreenivas, P.; David Krupadanam, G.; Janardhan Reddy, K. *Tetrahedron Letters* **2011**, *52*, 6537–6540.
- (26) Appel, N. M.; Robbins, J. D.; De Souza, E. B.; Seamon, K. B. *Journal of Pharmacology and Experimental Therapeutics* **1992**, *263*, 1415–1423.
- (27) Egger, M.; Maity, P.; Hübner, M.; Seifert, R.; König, B. *European Journal of Organic Chemistry* **2009**, *2009*, 3613–3618.
- (28) Cristina Silva Costa, D. *Arabian Journal of Chemistry* **2020**, *13*, 799–834.
- (29) Burra, S.; Voora, V.; Rao, C. P.; Vijay Kumar, P.; Kancha, R. K.; David Krupadanam, G. *Bioorganic & Medicinal Chemistry Letters* **2017**, *27*, 4314–4318.
- (30) Orphanos, D.; Filer, C. N. *Applied Radiation and Isotopes* **2016**, *107*, 203–205.
- (31) Delpech, B.; Lett, R. *Tetrahedron Letters* **1987**, *28*, 4061–4064.
- (32) Robles, O.; Serna-Saldívar, S. O.; Gutiérrez-Urbe, J. A.; Romo, D. *Organic Letters* **2012**, *14*, 1394–1397.
- (33) Kharasch, M. S.; Skell, P. S.; Fisher, P. *Journal of the American Chemical Society* **1948**, *70*, 1055–1059.
- (34) Kharasch, M. S.; Jensen, E. V.; Urry, W. H. *Science* **1945**, *102*, 128–128.
- (35) Kharasch, M. S.; Urry, W. H.; Jensen, E. V. *Journal of the American Chemical Society* **1945**, *67*, 1626–1626.
- (36) Kharasch, M. S.; Jensen, E. V.; Urry, W. H. *Journal of the American Chemical Society* **1946**, *68*, 154–155.
- (37) Kharasch, M. S.; Jensen, E. V.; Urry, W. H. *Journal of the American Chemical Society* **1947**, *69*, 1100–1105.
- (38) Kharasch, M. S.; Reinmuth, O.; Urry, W. H. *Journal of the American Chemical Society* **1947**, *69*, 1105–1110.
- (39) Curran, D. P. In *Free Radicals in Synthesis and Biology*, Minisci, F., Ed.; Springer Netherlands: Dordrecht, 1989, pp 37–51.
- (40) Ollivier, C.; Bark, T.; Renaud, P. *Synthesis* **2000**, *2000*, 1598–1602.
- (41) Tappin, N. D. C.; Renaud, P. *Advanced Synthesis & Catalysis* **2021**, *363*, 275–282.

- (42) *Radicals in organic synthesis*, 1st ed; Renaud, P., Sibi, M. P., Eds., OCLC: ocm48574823; Wiley-VCH: Weinheim ; New York, 2001, 2 pp.
- (43) Povie, G.; Suravarapu, S. R.; Bircher, M. P.; Mojzes, M. M.; Rieder, S.; Renaud, P. *Science Advances* **2018**, *4*, eaat6031.
- (44) Vlad, P. F.; Ungur, N. D.; Barba, A. N.; Korchagina, D. V.; Bagryanskaya, I. Y.; Gatilov, Y. V.; Gatilova, V. P.; Barkhash, V. A. *Chemistry of Natural Compounds* **1988**, *24*, 166–170.
- (45) Alvarez-Manzaneda, E.; Chaboun, R.; Alvarez, E.; Cabrera, E.; Alvarez-Manzaneda, R.; Haidour, A.; Ramos, J. *Synlett* **2006**, *2006*, 1829–1834.
- (46) CCDC 2025764, 2025762, 2025760, and 2025765 contain the supplementary crystallographic data for compound (14S)-epi- 11, (14R)-12, 13, and (14S)-14, respectively. These data can be obtained free of charge from The Cambridge Crystallographic Data Centre via <http://www.ccdc.cam.ac.uk/getstructures>.
- (47) Bhat, S. V.; Bajwa, B. S.; Dornauer, H.; de Souza, N. J. *Journal of the Chemical Society, Perkin Transactions 1* **1982**, 767.
- (48) Bhat, S. V.; Dohadwalla, A. N.; Bajwa, B. S.; Dadkar, N. K.; Dornauer, H.; De Souza, N. J. *Journal of Medicinal Chemistry* **1983**, *26*, 486–492.
- (49) Kraus, G. A.; Landgrebe, K. *Tetrahedron Letters* **1984**, *25*, 3939–3942.
- (50) Kraus, G. A.; Landgrebe, K. *Tetrahedron* **1985**, *41*, 4039–4046.
- (51) Yorimitsu, H.; Wakabayashi, K.; Shinokubo, H.; Oshima, K. *Tetrahedron Letters* **1999**, *40*, 519–522.
- (52) Yorimitsu, H.; Wakabayashi, K.; Shinokubo, H.; Oshima, K. *Bulletin of the Chemical Society of Japan* **2001**, *74*, 1963–1970.
- (53) Peralta-Hernández, E.; Cortezano-Arellano, O.; Cordero-Vargas, A. *Tetrahedron Letters* **2011**, *52*, 6899–6902.
- (54) León-Rayó, D. F.; Morales-Chamorro, M.; Cordero-Vargas, A. *European Journal of Organic Chemistry* **2016**, *2016*, 1739–1750.
- (55) The major ATRA adduct cyclizes significantly faster than the minor isomer. The cyclization via inversion of the stereocenter at the C–I bond was confirmed by the stereoselective cyclization of the minor isomer of **16** (isolated from another experiment) to the minor isomer of **12**, as well as the comparison between the diastereomeric ratio obtained for the ATRA reaction leading to **16** and the formation of tetracyclic **12**.
- (56) CCDC 2025764, 2025762, 2025760, and 2025765 contain the supplementary crystallographic data for compound (14S)-epi- 11, (14R)-12, 13, and (14S)-14, respectively. These data can be obtained free of charge from The Cambridge Crystallographic Data Centre via <http://www.ccdc.cam.ac.uk/getstructures>.
- (57) Someya, H.; Itoh, T.; Aoki, S. *Molecules* **2017**, *22*, 1650.

- (58) Nazari, S. H.; Forson, K. G.; Martinez, E. E.; Hansen, N. J.; Gassaway, K. J.; Lyons, N. M.; Kenney, K. C.; Valdivia-Berroeta, G. A.; Smith, S. J.; Michaelis, D. J. *Organic Letters* **2019**, *21*, 9589–9593.
- (59) Wein, L. A.; Wurst, K.; Angyal, P.; Weisheit, L.; Magauer, T. *Journal of the American Chemical Society* **2019**, *141*, 19589–19593.
- (60) Shimada, N.; Urata, S.; Fukuhara, K.; Tsuneda, T.; Makino, K. *Organic Letters* **2018**, *20*, 6064–6068.
- (61) Churches, Q. I.; Hooper, J. F.; Hutton, C. A. *The Journal of Organic Chemistry* **2015**, *80*, 5428–5435.
- (62) Bouvier, J.-P.; Jung, G.; Liu, Z.; Guérin, B.; Guindon, Y. *Organic Letters* **2001**, *3*, 1391–1394.
- (63) Medeiros, M. R.; Schacherer, L. N.; Spiegel, D. A.; Wood, J. L. *Organic Letters* **2007**, *9*, 4427–4429.
- (64) Davy, J. A.; Mason, J. W.; Moreau, B.; Wulff, J. E. *The Journal of Organic Chemistry* **2012**, *77*, 6332–6339.
- (65) Allais, F.; Boivin, J.; Nguyen, V. T. *Beilstein Journal of Organic Chemistry* **2007**, *3*, DOI: 10.1186/1860-5397-3-46.
- (66) Jin, J.; Newcomb, M. *The Journal of Organic Chemistry* **2007**, *72*, 5098–5103.
- (67) Jin, J.; Newcomb, M. *The Journal of Organic Chemistry* **2008**, *73*, 4740–4742.
- (68) Povie, G.; Marzorati, M.; Bigler, P.; Renaud, P. *The Journal of Organic Chemistry* **2013**, *78*, 1553–1558.
- (69) Porter, N. A.; Giese, B.; Curran, D. P. *Accounts of Chemical Research* **1991**, *24*, 296–304.
- (70) Curran, D. P.; Porter, N. A.; Giese, B., *Stereochemistry of radical reactions: concepts, guidelines, and synthetic applications*; VCH: Weinheim ; New York, 1996; 280 pp.
- (71) Kogler, H.; Fehlhäber, H.-W. *Magnetic Resonance in Chemistry* **1991**, *29*, 993–998.
- (72) Suravarapu, S. R.; Peter, B.; Renaud, P. *Science China Chemistry* **2019**, *62*, 1504–1506.
- (73) Giese, B.; Kopping, B.; Chatgililoglu, C. *Tetrahedron Letters* **1989**, *30*, 681–684.
- (74) Chatgililoglu, C. *Accounts of Chemical Research* **1992**, *25*, 188–194.
- (75) Ryu, I.; Uehara, S.; Hirao, H.; Fukuyama, T. *Organic Letters* **2008**, *10*, 1005–1008.
- (76) Curran, D. P.; Bosch, E.; Kaplan, J.; Newcomb, M. *The Journal of Organic Chemistry* **1989**, *54*, 1826–1831.
- (77) Ollivier, C.; Renaud, P. *Chemical Reviews* **2001**, *101*, 3415–3434.
- (78) Povie, G.; Tran, A.-T.; Bonnaffé, D.; Habegger, J.; Hu, Z.; Le Narvor, C.; Renaud, P. *Angewandte Chemie International Edition* **2014**, *53*, 3894–3898.

5.4 Experimental Section

General Information

Techniques

All reactions requiring anhydrous conditions were performed in flame dried glassware under an argon atmosphere. Silica gel 60Å(40–63 μm) from *Silicycle* was used for flash column chromatography (FCC). Thin layer chromatography (TLC) was performed on *Silicycle* silica gel 60 F254 plates, visualization under UV light (254 nm) and by dipping in a solution of cerium ammonium molybdate - $(\text{NH}_4)_2\text{MoO}_4$ (15.0 g), $\text{Ce}(\text{SO}_4)_2$ (0.5 g), H_2O (90 mL), conc. H_2SO_4 (10 mL) - and subsequent heating. Silver nitrate impregnated silica gel was prepared according to ratio: SiO_2 (50 g), AgNO_3 (5.5 g) and H_2O (30 mL) for flash column chromatography and AgNO_3 (1 g), H_2O (2.5 mL) and acetone (10 mL) for TLC, followed by activation at 105–110 $^\circ\text{C}$ (light sensitive, to be covered with aluminium foil and/or stored in the dark). Anhydrous sodium sulfate was used as drying reagent.

Materials

Commercial reagents were used without further purification unless otherwise stated. Dry solvents for reactions were filtered over columns of dried alumina under a positive pressure of argon and/or stored over 3Å molecular sieves. Solvents for extractions (Et_2O , *n*-pentane, CH_2Cl_2 , AcOEt) and flash column chromatography were of technical grade and distilled prior to use.

Instrumentation

^1H and ^{13}C NMR spectra were recorded on a *Bruker Avance IIIHD-300* spectrometer operating at 300 MHz for ^1H and 75 MHz for ^{13}C at rt (24–25 $^\circ\text{C}$) unless otherwise stated. Some ^1H and ^{13}C NMR spectra were recorded on a *Bruker Avance IIIHD-400* or a *Bruker Avance II-400* spectrometer (^1H : 400 MHz; ^{13}C : 100 MHz). Chemical shifts (δ) are reported in parts per million (ppm) downfield from tetramethylsilane $\text{Si}(\text{CH}_3)_4$ ($\delta = 0.00$ for ^1H NMR spectra) using residual solvent signal as an internal standard: δ singlet 7.26 (^1H), triplet 77.0 (^{13}C) for CDCl_3 or δ singlet 7.16 (^1H), triplet 128.0 (^{13}C) for C_6D_6 . Multiplicities are given as s (singlet), d (doublet), t (triplet), q (quadruplet), m (multiplet), and br (broad). Coupling constants (*J*) are reported in Hz. In ^{13}C -NMR spectra, the peak positions are reported on one decimal unless the difference in chemical shift between two signals is small and required two decimals. Due to coupling to the quadrupolar ^{11}B and ^{10}B nuclei, the carbons linked to boron atoms generally give a broad signal in ^{13}C NMR, sometimes not detected.

Diastereomeric ratio were determined by NMR on crude reaction mixtures.

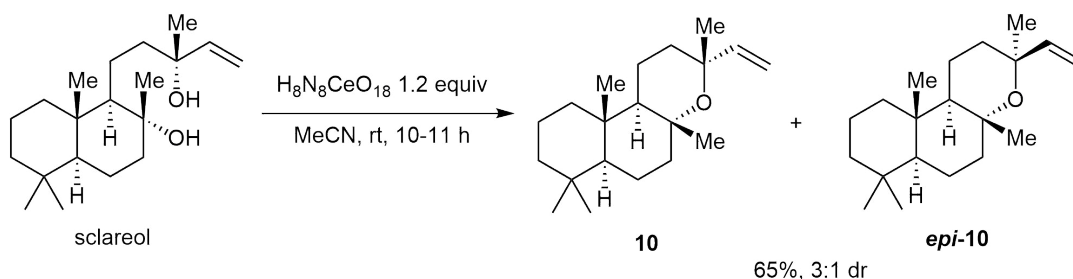
Infrared spectra were recorded on a *Jasco FT-IR-460* plus spectrometer equipped with a *Specac MKII Golden Gate Single Reflection Diamond ATR* system and are reported in wave numbers (cm^{-1}). At maximum, the ten most prominent peaks are reported. HRMS analyses and accurate mass determinations were performed on a *Thermo Scientific LTQ Orbitrap XL* mass spectrometer using ESI mode (positive ion mode). Melting points were measured on a *Büchi B545* apparatus.

Specific rotation $[\alpha]_D^{20}$ are expressed in $\text{deg}\cdot\text{mL}\cdot\text{g}^{-1}\cdot\text{dm}^{-1}$. The concentration c is in $\text{g}/100\text{ mL}$ and the path length l is in decimeters. The units of the specific rotation, $\text{deg}\cdot\text{mL}\cdot\text{g}^{-1}\cdot\text{dm}^{-1}$, are implicit and are not included with the reported value.

Synthesis

Preparation of the reagents

Manoyl oxide (10) and *epi*-manoyl oxide (*epi*-10)



To a solution of sclareol (3.0 g, 9.72 mmol) in deoxygenated dry MeCN (90 mL) under an inert atmosphere was added cerium ammonium nitrate (6.4 g, 1.2 equiv). The mixture was stirred at rt and monitored by TLC. Upon completion (10–11 h), the solvent was removed under reduced pressure. The mixture was diluted with water and extracted with Et₂O (2 ×). The combined organic phases were washed successively with sat. aq NaHCO₃ soln, water, and brine, dried (Na₂SO₄), filtered, and concentrated under reduced pressure. The crude was purified by flash column chromatography (Et₂O/pentane 1:99) to afford the mixture of manoyl oxide (**10**) and its 13-epimer *epi*-**10** (2.10 g, 65%, dr 3:1). The diastereomers were isolated individual on a 10% AgNO₃ impregnated silica gel flash column chromatography (Et₂O/pentane from 1:99 to 3:97) to afford the 13-*epi*-manoyl oxide (*epi*-**10**; 0.5 g) and manoyl oxide (**10**; 1.4 g). Physical and spectral data are in accordance with literature data.¹

Manoyl Oxide (10)

Colorless oil (white solid at 4 °C). $R_f = 0.6$ (Et₂O/pentane 5:95) and $R_f = 0.31$ (AgNO₃/silica 1:10; Et₂O/pentane 5:95).

¹H NMR (CDCl₃, 300 MHz): $\delta = 5.87$ (dd, $J = 17.4, 10.7$ Hz, 1 H), 5.14 (dd, $J = 17.4, 1.6$ Hz, 1 H), 4.91 (dd, $J = 10.7, 1.6$ Hz, 1 H), 1.86–1.71 (m, 2 H), 1.69–1.31 (m, 11 H), 1.29 (d, $J = 1.1$ Hz, 3 H), 1.27 (s, 3 H), 1.26–1.05 (m, 2 H), 0.93 (dd, $J = 12.2, 2.5$ Hz, 1 H), 0.85 (s, 3 H), 0.79 (s, 3 H), 0.78 (s, 3 H).

¹³C NMR (CDCl₃, 75 MHz): $\delta = 148.1, 110.4, 75.2, 73.4, 56.6, 55.8, 43.4, 42.2, 39.1, 37.1, 35.8, 33.5, 33.4, 28.7, 25.7, 21.5, 20.1, 18.7, 15.6, 15.4$.

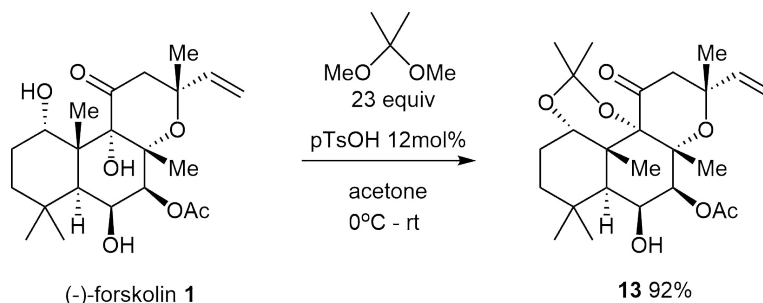
13-*epi*-Manoyl Oxide (*epi*-10)

White powder. $R_f = 0.6$ (Et₂O/pentane 5:95) and $R_f = 0.62$ (AgNO₃/silica 1:10; Et₂O/pentane 5:95); **m.p.** 95.5–97.3 °C (Et₂O/pentane) (Lit.⁵⁴ mp 96 °C).

¹H NMR (CDCl₃, 300 MHz): $\delta = 6.00$ (dd, $J = 17.9, 11.0$ Hz, 1 H), 5.01–4.86 (m, 2 H), 2.27–2.13 (m, 1 H), 1.76 (dt, $J = 11.2, 3.0$ Hz, 1 H), 1.63 (ddt, $J = 10.0, 6.3, 3.7$ Hz, 3 H), 1.56–1.32 (m, 7 H), 1.32–1.07 (m, 3 H), 1.22 (s, 3 H), 1.12 (s, 3 H), 0.94 (dd, $J = 12.1, 2.5$ Hz, 1 H), 0.84 (s, 3 H), 0.77 (s, 3 H), 0.71 (s, 3 H).

^{13}C NMR (CDCl_3 , 75 MHz): δ = 147.8, 109.6, 76.2, 73.4, 58.6, 56.6, 43.2, 42.3, 39.5, 36.9, 35.0, 33.47, 33.41, 32.8, 24.1, 21.4, 20.0, 18.8, 16.01, 15.99.

1,9-acetonide-forskolin (**13**)



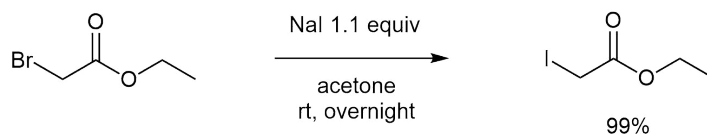
To a solution of forskolin (**1**; 616 mg, 1.5 mmol) in acetone (30 mL, 0.05 M) at 0 °C under an inert atmosphere was added 2,2-dimethoxypropane (4.3 mL, 23 equiv) and *p*-TsOH (32 mg, 12 mol%). The mixture was stirred at rt and monitored by TLC. Upon completion (6 h), a saturated aqueous solution of NaHCO_3 soln was added and the mixture was extracted with Et_2O (2 \times). The combined organic phases were washed with water and brine, dried (Na_2SO_4), filtered, and concentrated under reduced pressure. The crude was purified by flash column chromatography (EtOAc/heptane 1:5) to afford **13** (620 mg, 92%) as a white powder. Physical and spectral data are in accordance with literature data.²

White powder; R_f = 0.54 (EtOAc/heptane 3:7); **mp** 207.9–210.3 °C (Et_2O /pentane) (Lit. m.p. 224–225 °C).

^1H NMR (CDCl_3 , 300 MHz): δ = 5.91 (dd, J = 17.1, 10.6 Hz, 1 H), 5.33 (d, J = 3.7 Hz, 1 H), 5.25 (dd, J = 17.1, 1.6 Hz, 1 H), 4.92 (dd, J = 10.6, 1.6 Hz, 1 H), 4.43 (s, 1 H), 4.28 (dd, J = 3.9, 2.0 Hz, 1 H), 2.95 (d, J = 19.4 Hz, 1 H), 2.63 (d, J = 19.4 Hz, 1 H), 2.22 (d, J = 2.5 Hz, 1 H), 2.14 (s, 3 H), 2.13–2.00 (m, 1 H), 1.78 (td, J = 13.5, 4.2 Hz, 1 H), 1.70 (br s, 1 H), 1.60 (s, 3 H), 1.47 (s, 3 H), 1.42–1.07 (m, 1 H), 1.39 (s, 3 H), 1.27 (s, 3 H), 1.26 (m, 7 H), 1.09–1.02 (m, 1 H), 1.01 (s, 3 H).

^{13}C NMR (CDCl_3 , 75 MHz): δ = 207.4, 169.8, 147.1, 110.6, 99.9, 81.0, 80.1, 76.7, 73.8, 70.2, 70.1, 50.1, 42.7, 37.8, 36.2, 34.4, 33.6, 33.3, 31.6, 25.1, 23.7, 22.9, 22.3, 21.3, 17.6.

Ethyl iodoacetate



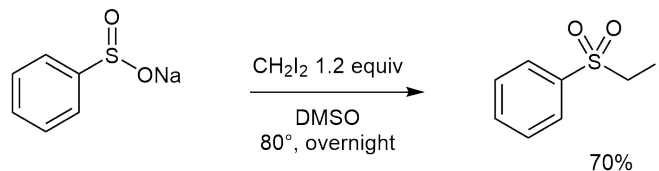
To a stirred solution of sodium iodide (49.5 g, 330 mmol, 1.1 equiv) in acetone (500 mL) was added ethyl 2-bromoacetate (49.5 g, 300 mmol) at room temperature. The formed suspension was allowed to stir at room temperature overnight in the dark. The suspension was filtrated, and the filtrate evaporated under reduced pressure. The residue was diluted with water (150 mL) and extracted with pentane (300/150 mL). The organic layers were washed successively with a 5% sodium thiosulfate solution (150 mL) and water (150 mL), dried over Na₂SO₄, filtered and concentrated to give ethyl 2-iodoacetate (63.4 g, 99%). Physical and spectral data are in accordance with literature data.³ The compound was used without any further purification.

Yellowish liquid.

¹H NMR (CDCl₃, 300 MHz): δ = 4.21 (q, J = 7.1 Hz, 2H), 3.69 (s, 2H), 1.29 (t, J = 7.1 Hz, 3H).

¹³C NMR (CDCl₃, 75 MHz): δ = 168.8, 62.1, 13.9, -5.2.

Iodomethyl phenylsulfone



To a solution of sodium sulfinate (3.0 g, 18 mmol) in dry DMSO (72 mL) under inert atmosphere was added dropwise diiodomethane (1.76 mL, 2.15 mmol, 1.2 eq) at room temperature. The reaction mixture was stirred at 80°C overnight. The reaction mixture was cooled down to room temperature and diluted with water. The solid was filtrated and washed with water. The crude product was purified by crystallization in pentane to give iodomethyl phenylsulfone (3.55 g, 70%) as a white solid. Physical and spectral data are in accordance with literature data.⁴

White solid; R_f = 0.63 (AcOEt/heptane 3:7); mp: 58.6–60.1 °C, pentane (lit. m.p.: 64 °C, EtOH/hexane).⁴

¹H NMR (CDCl₃, 300 MHz): δ = 8.00–7.91 (m, 2H), 7.70 (t, J = 7.4 Hz, 1H), 7.59 (m, 2H), 4.46 (s, 2H).

¹³C NMR (CDCl₃, 75 MHz): δ = 136.0, 134.6, 129.4 (2C), 129.0 (2C), 16.9.

Iodo-alkylation of manoyl and *epi*-manoyl oxide **10** and *epi*-**10**

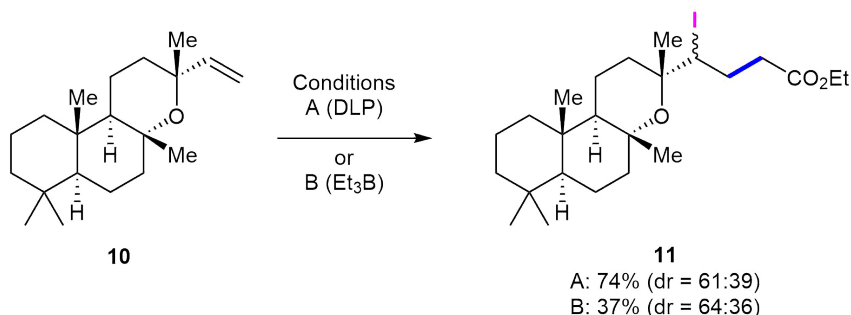
General Procedure A (GP A): Carboiodination initiated by dilauroyl peroxide DLP

To a mixture of alkene (**10**; 1.0 equiv) and NaHCO₃ (1.0 equiv) in dry benzene or EtOAc (0.1 M to alkene) under an inert atmosphere were added sequentially the alkylating reagent (2.0 equiv) and DLP (1.0 equiv). The mixture was warmed up to reflux (90 °C bath temperature) and monitored by TLC. After completion (3 h), the mixture was diluted with deionized water and extracted with Et₂O (3 ×). The combined organic phases were washed with water and brine, dried (Na₂SO₄), filtered, and concentrated under reduced pressure (with a low bath temperature).

General Procedure B (GP B): Carboiodination initiated by triethylborane Et₃B

To a mixture of alkene (**10**; 1.0 equiv) and NaHCO₃ (1.0 equiv) in dry CH₂Cl₂ (0.1 M to alkene) under inert atmosphere were added, sequentially the alkylating reagent (1.2–1.5 equiv) and Et₃B (1.3 equiv, 1.15 M in dry benzene). The mixture was opened to air with a CaCl₂ guard tube, protected from light, and stirred vigorously at rt and monitored by TLC. After completion (1 h), the mixture was diluted with deionized water and extracted with Et₂O (3 ×). The combined organic phases were washed with brine, dried (Na₂SO₄), filtered, and concentrated under reduced pressure (with a low bath temperature). In order to remove borane residues, the mixture was then filtered through a short pad of neutral alumina (eluting with Et₂O) and concentrated under reduced pressure.

Ethyl (13*R*,14*R/S*)-14-Iodo-8,13-epoxylabdan-15-ylacetate (**11**)



According to **GPA** from manoyl oxide (**10**; 64 mg, 0.22 mmol), NaHCO₃ (18 mg, 0.216 mmol), ethyl iodoacetate (94 mg, 0.43 mmol), and DLP (91 mg, 0.22 mmol) in dry benzene (2.0 mL). The crude mixture was purified by flash column chromatography (Et₂O/pentane 2:98) to afford an inseparable mixture of diastereomers **11** (81 mg, 74%, dr 61:39).

According to **GPB** from manoyl oxide (**10**; 73 mg, 0.25 mmol), NaHCO₃ (21 mg, 1.0 equiv), ethyl iodoacetate (80 mg, 1.5 equiv), and Et₃B (0.28 mL, 1.15 M in C₆D₆) in dry CH₂Cl₂ (1.3 mL). The crude mixture was purified by flash column chromatography (Et₂O/pentane 2:98) to afford an inseparable mixture of diastereomers **11** (46 mg, 37%, dr 64:36).

Colorless oil; $R_f = 0.3$ (Et₂O/pentane 5:95).

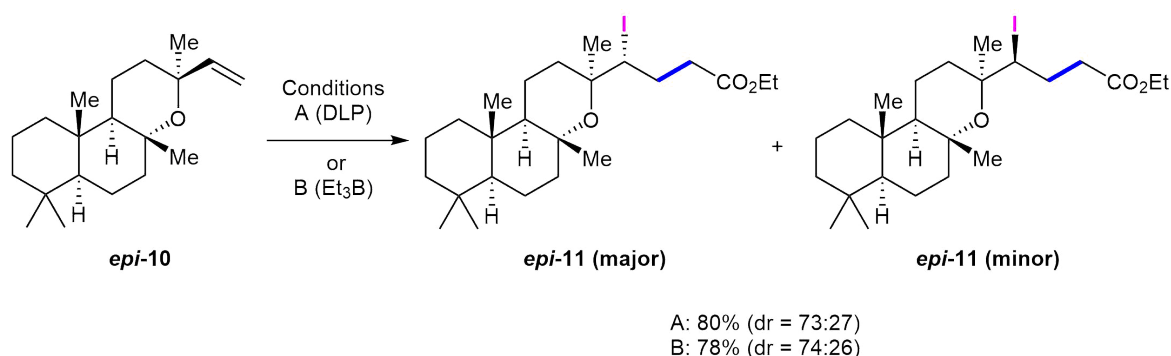
IR: 2977, 2924, 2864, 1733, 1464, 1375, 1180, 1116, 956, 497 cm⁻¹.

¹H NMR (mixture, C₆D₆, 300 MHz): major (selected peaks) $\delta = 4.08$ –4.00 (m, 1 H), 3.92 (q, $J = 7.1$ Hz, 2 H), 2.70–0.62 (m, 20 H), 1.28 (s, 3 H), 1.07 (s, 3 H), 0.940 (t, $J = 7.1$ Hz, 3 H), 0.81 (s, 3 H), 0.75 (s, 3 H), 0.61 (s, 3 H); minor (selected peaks) $\delta = 4.08$ –4.00 (m, 1 H), 3.92 (q, $J = 7.1$ Hz, 2 H), 2.70–0.62 (m, 20 H), 1.28 (s, 3 H), 1.12 (s, 3 H), 0.937 (t, $J = 7.1$ Hz, 3 H), 0.79 (s, 3 H), 0.75 (s, 3 H), 0.62 (s, 3 H). **¹³C NMR** (major, C₆D₆, 75 MHz): $\delta = 172.2, 76.0, 74.1, 60.2, 57.7, 56.5, 54.2, 43.1, 42.4, 39.2, 36.9, 36.6, 35.4, 33.5, 33.4, 30.6, 24.6, 22.9, 21.5, 20.1, 19.0, 15.9, 15.8, 14.3$.

¹³C NMR (minor, C₆D₆, 75 MHz): $\delta = 172.5, 75.8, 74.0, 60.2, 58.1, 56.4, 55.1, 43.0, 42.3, 39.2, 39.1, 36.9, 35.4, 33.4, 33.4, 30.5, 25.4, 24.7, 21.5, 20.1, 19.0, 16.0, 15.9, 14.3$.

HRMS (ESI): m/z [M + H]⁺ calcd for C₂₄H₄₂IO₃: 505.2179; found: 505.2155.

Ethyl (13*S*,14*R/S*)-14-Iodo-8,13-epoxylabdan-15-ylacetate (*epi*-11)



According to **GPA** from *epi*-manoyl oxide (*epi*-10; 51 mg, 0.172 mmol), NaHCO₃ (15 mg, 0.172 mmol), ethyl iodoacetate (75 mg, 0.344 mmol), and DLP (72 mg, 0.172 mmol) in dry benzene (1.7 mL). The crude mixture was purified by flash column chromatography (Et₂O/pentane 2:98) to afford the mixture of diastereomers (69 mg, 80%, dr 73:27).

According to **GPB** from *epi*-manoyl oxide (*epi*-10; 69 mg, 0.233 mmol), NaHCO₃ (20 mg, 1.0 equiv), ethyl iodoacetate (75 mg, 1.5 equiv), and Et₃B (0.27 mL, 1.3 equiv, 1.15 M in dry C₆D₆) in dry CH₂Cl₂ (1.3 mL). The crude mixture was purified by flash column chromatography (Et₂O/pentane, gradient from 2:98 to 3:97) to afford a mixture of diastereomers (92 mg, 78%, dr 74:26).

The mixture of diastereomers was purified by flash column chromatography (Et₂O/pentane, gradient from 0:100 to 3:97), to afford clean fraction of major *epi*-11 and enriched fraction of minor *epi*-11 (80%). The enriched fraction of the minor diastereomer recrystallized at 4 °C (Et₂O/pentane 1:5; fridge, sensitive to light) to give a single crystal suitable for X-ray diffraction analysis.

(14R)-*epi*-11 (major)

Colorless oil; $R_f = 0.32$ (Et₂O/pentane 5:95); $[\alpha]_D^{20} +25$ (c 1.0, CH₂Cl₂).

IR: 2979, 2923, 2866, 1733, 1457, 1374, 1179, 1073, 957, 593 cm⁻¹.

¹H NMR (C₆D₆, 300 MHz): $\delta = 4.24$ (dd, $J = 11.3, 1.7$ Hz, 1 H), 3.95 (q, $J = 7.1$ Hz, 2 H), 2.83–2.68 (m, 2 H), 2.42–2.33 (m, 1 H), 2.28–2.10 (m, 2 H), 1.80–1.66 (m, 2 H), 1.40 (s, 3 H), 1.58–1.25 (m, 7 H), 1.22–1.02 (m, 4 H), 1.01 (d, $J = 1.0$ Hz, 3 H), 0.98–0.93 (m, 3 H), 0.79 (s, 3 H), 0.74 (dd, $J = 12.4, 2.3$ Hz, 1 H), 0.74 (s, 3 H), 0.63 (dd, $J = 12.5, 4.1$ Hz, 1 H), 0.59 (s, 3 H).

¹³C NMR (C₆D₆, 75 MHz): $\delta = 172.2, 75.8, 75.0, 60.3, 56.5, 55.2, 49.3, 43.6, 42.3, 39.0, 37.1, 36.4, 35.4, 33.5, 33.3, 30.8, 25.7, 25.1, 21.5, 20.2, 18.9, 15.4, 15.1, 14.3$.

HRMS (ESI): m/z [M + Na]⁺ calcd for C₂₄H₄₁IO₃Na: 527.1998; found: 527.1964.

(14S)-*epi*-11 (minor)

White powder; $R_f = 0.29$ (Et₂O/pentane 5:95); **mp** 65.4–67.9 °C (Et₂O/pentane).

IR: 2977, 2923, 2865, 2844, 1731, 1456, 1375, 1260, 961 cm⁻¹.

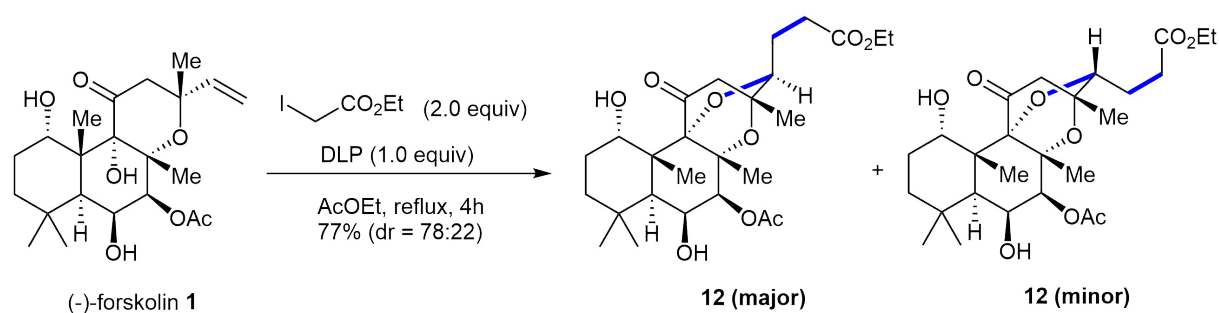
¹H NMR (C₆D₆, 300 MHz, selected peaks): $\delta = 4.40$ (dd, $J = 11.4, 2.1$ Hz, 1 H), 3.93 (q, $J = 7.1$ Hz, 2 H), 2.61–2.50 (m, 2 H), 2.13–1.96 (m, 2 H), 1.95–1.87 (m, 1 H), 1.34 (m, 6 H), 0.95 (t, $J = 7.1$ Hz, 3 H), 0.79 (s, 3 H), 0.74 (s, 3 H), 0.65 (s, 3 H).

¹³C NMR (C₆D₆, 75 MHz): $\delta = 172.5, 76.0, 74.6, 60.3, 56.6, 55.2, 54.9, 43.9, 42.4, 39.2, 37.2, 35.4, 33.5, 33.3, 31.9, 30.7, 28.7, 24.7, 21.5, 20.2, 18.9, 15.5, 15.4, 14.3$.

HRMS (ESI): m/z [M + Na]⁺ calcd for C₂₄H₄₁IO₃Na: 527.1998; found: 527.1964.

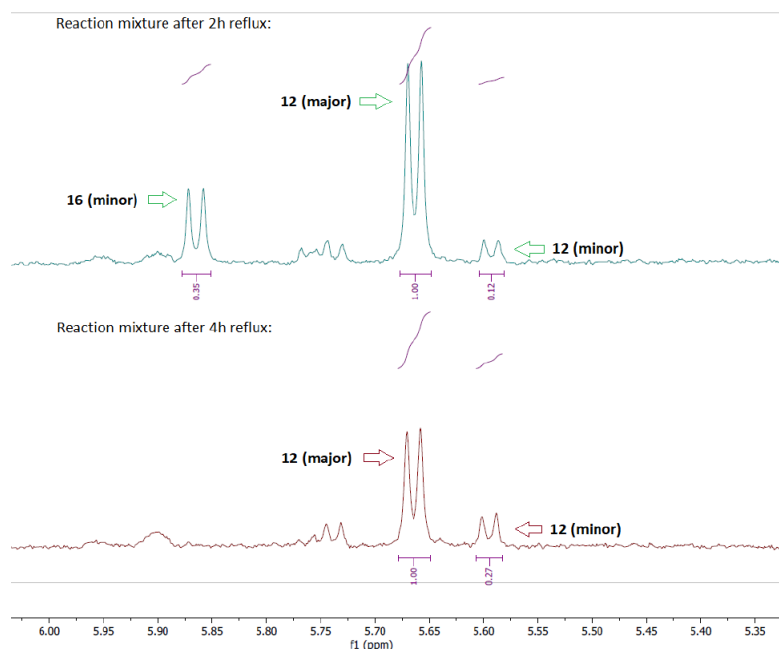
Iodo-alkylation of (-)-forskolin 1

Ethyl (13*R*,14*R/S*)-7-Acetoxy-1,6-dihydroxy-11-oxo-8,13:9,14-diepoxyabdan-15-ylacetate (12)



According to **GPA** from forskolin (**1**; 85 mg, 0.207 mmol), ethyl iodoacetate (89 mg, 0.414 mmol), and DLP (83 mg, 0.207 mmol) in dry EtOAc (2.0 mL). The crude mixture was purified by flash column chromatography (EtOAc/heptane 1:4) to isolate a mixture of diastereomers **12** (79 mg, 77%, dr 78:22). A clean fraction of each diastereomer was identified and concentrated for full characterization. Major isomer (14*R*)-**12** crystallized from Et₂O/pentane (1:5) to give a single crystal suitable for X-ray diffraction analysis.

Upon monitoring the reaction mixture by ¹H NMR (C₆D₆) the formation of minor-**16** was identified, which later converted into the minor isomer (14*S*)-**12**:



(14S)-12 (minor)

Yellowish oil; $R_f = 0.42$ (EtOAc/heptanes 6:4); $[\alpha]_D^{20} -47$ (c 0.7, CH₂Cl₂).

IR: 3489, 3421, 2978, 2928, 2869, 2856, 1733, 1446, 1371, 989 cm⁻¹.

¹H NMR (CDCl₃, 400 MHz): $\delta = 5.32$ (d, $J = 3.8$ Hz, 1 H), 4.44 (t, $J = 3.3$ Hz, 1 H), 4.31 (t, $J = 2.7$ Hz, 1 H), 4.18–4.09 (m, 3 H), 2.65 (d, $J = 19.2$ Hz, 1 H), 2.57–2.38 (m, 3 H), 2.18 (s, 3 H), 2.11 (d, $J = 2.8$ Hz, 1 H), 2.07–1.85 (m, 3 H), 1.67–1.56 (m, 1 H), 1.50 (s, 3 H), 1.49 (s, 3 H), 1.50–1.43 (m, 1 H), 1.26 (s, 3 H), 1.25 (t, $J = 7.2$ Hz, 3 H), 1.15 (s, 3 H), 1.05 (s, 3 H), 1.07–1.01 (m, 1 H).

¹³C NMR (CDCl₃, 101 MHz): $\delta = 201.0, 172.5, 170.1, 85.4, 81.4, 79.4, 77.1, 73.1, 72.9, 69.9, 60.9, 46.0, 43.9, 42.9, 36.1, 34.8, 33.2, 30.7, 27.6, 25.9, 25.1, 24.9, 21.8, 21.3, 19.9, 14.3$.

HRMS (ESI): m/z [M + H]⁺ calcd for C₂₆H₄₁O₉: 497.2751; found: 496.2723.

(14R)-12 (major)

White powder; $R_f = 0.36$ (EtOAc/heptanes 6:4); **mp** 127.5–128.2 °C (TBME/heptanes 1:4); $[\alpha]_D^{20} -9$ (c 1.5, CH₂Cl₂).

IR: 3481, 3434, 2977, 2929, 2869, 1731, 1446, 1372, 990 cm⁻¹.

¹H NMR (CDCl₃, 300 MHz): $\delta = 5.44$ (d, $J = 3.8$ Hz, 1 H), 4.40 (t, $J = 3.3$ Hz, 1 H), 4.34–4.31 (m, 1 H), 4.14 (q, $J = 7.2$ Hz, 2 H), 3.91 (dd, $J = 10.8, 3.4$ Hz, 1 H), 2.62 (d, $J = 18.9$ Hz, 1 H), 2.60–2.32 (m, 3 H), 2.38 (d, $J = 18.9$ Hz, 1 H), 2.17 (s, 3 H), 2.04 (d, $J = 2.6$ Hz, 1 H), 2.00–1.82 (m, 3 H), 1.49 (s, 3 H), 1.49–1.44 (m, 1 H), 1.47 (s, 3 H), 1.25 (s, 3 H), 1.24 (t, $J = 7.2$ Hz, 3 H), 1.10 (s, 3 H), 1.04 (s, 3 H), 1.03–0.99 (m, 1 H).

¹³C NMR (CDCl₃, 75 MHz): $\delta = 201.5, 173.0, 169.9, 84.7, 80.0, 79.2, 76.9, 73.1, 70.7, 69.7, 60.8, 50.6, 43.6, 43.0, 35.9, 34.7, 33.5, 29.6, 25.8, 25.14, 25.10, 24.6, 21.5, 21.3, 19.6, 14.3$.

HRMS (ESI): m/z [M + H]⁺ calcd for C₂₆H₄₁O₉: 497.2751; found: 497.2745.

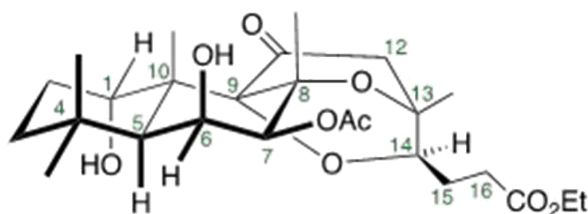
Full NMR Assignment for (14*R*)-12 (major):

Assignments were made with the aid of Kogler's forskolin assignments,⁵ and numerations therein were duplicated. For reported major diastereoisomer - complete assignments were made with full consistency in the ²D NMRs (COSY, HSQC, and HMBC, see tables for details; and NOESY spectra), and the relative stereochemistry of H-14 in the major diastereoisomer was confirmed with ¹D NOESY: no nOe response between H-14 and H-7 α and 4% between H-14 and H-12 α .

D₂O exchange and their COSY correlations:

Complete disappearance of $\delta = 1.74$ (br ddd, 1H) = 6 β -OH, COSY to 4.42 (m, 1H) = H-6 α

Splitting and shift altered of $\delta = 4.89$ (br d, 1H) = 1 α -OH, COSY to half of an ABq at 2.00 ppm (H-2 α or β).



¹³C-NMR

signal	Shift iocsp1 TMS=0 (CDCl ₃) Forskolin- ICH ₂ CO ₂ Et	DEPT -135	HSQC correlation (vic- ² J _{C-H})	HMBC correlation (dist- ⁿ J _{C-H})	assignment
a	201.4	Cq	None	2.64 (d, H-12 β); 2.40 (d, H-12 α)	C-11
b	172.9	Cq	None	4.15 (q, ethyl-CH ₂); 2.60 – 2.45 (m, H-16A and B)	Ethyl ester
c	169.8	Cq	None	2.19 (s, acetyl-CH ₃); 5.46 (d, H-7 α)	Acetyl-CO
d	84.6	Cq	None	1.51 (s, 8 β -CH ₃) strong; 1.48 (s, 10 β -CH ₃) strong	C-9
e	79.9	CH	3.92 (dd, H-14)	2.64 (d, H-12 β); 1.11 (s, 13 α -CH ₃)	C-14
f	79.1	Cq	None	1.51 (s, 8 β -CH ₃); 5.46 (d, H-7 α)	C-8
g	76.8	CH	5.46 (d, H-7 α)	1.51 (s, 8 β -CH ₃)	C-7
h	73.0	CH	4.34 (br ddd, H-1 β)	4.89 (br d, 1 α -OH) weak; 1.48 (s, 10 β -CH ₃) strong; 1.06 (s, 4 α -CH ₃)	C-1 (switched c.f. forsk)

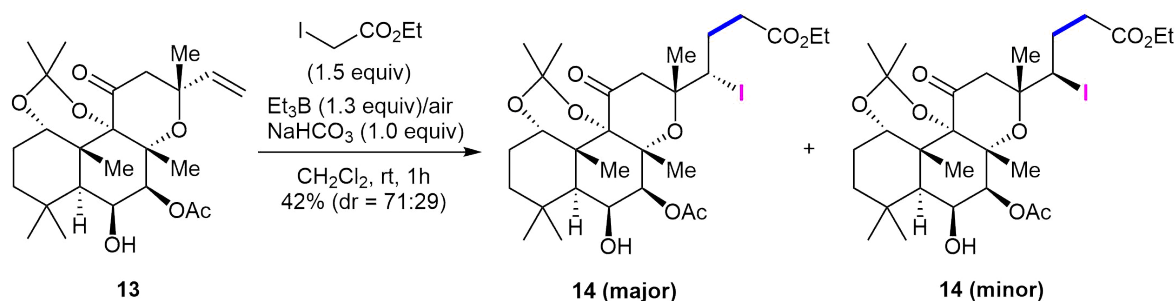
signal	Shift iocsp1 TMS=0 (CDCl ₃) Forskolin- ICH ₂ CO ₂ Et	DEPT -135	HSQC correlation (vic- ² J _{C-H})	HMBC correlation (dist- ⁿ J _{C-H})	assignment
i	70.6	Cq	None	1.11 (s, 13β-CH ₃); 2.64 (d, H-12β) strong; 2.40 (d, H-12α) weak	C-13
j	69.7	CH	4.42 (br ddd, H-6α)	None! 5 and 7 too close, rest quats.	C-6 (switched c.f. forsk)
k	60.7	CH ₂	4.15 (q, ethyl-CH ₂)	1.26 (t, ethyl-CH ₃)	Ethyl-CH ₂
l	50.6	CH ₂	2.64 (d, H-12α); 2.40 (d, H-12β)	1.11 (s, 13β-CH ₃)	C-12
m	43.5	Cq	None	4.89 (br d, 1α-OH) weak; 2.06 (dd, H-5α); 1.48 (s, 10β-CH ₃)	C-10
n	43.0	CH	2.06 (dd, H-5α)	4.34 (ddd, H-1β) weak; 1.74 (br dd, 6β-OH); 1.27 (s, 4β-CH ₃); 1.06 (s, 4α-CH ₃)	C-5
o	35.8	CH ₂	2.04 – 1.84 (m, H-3α); 1.10 – 1.00 (H-3β)	1.27 (s, 4β-CH ₃); 1.06 (s, 4α-CH ₃)	C-3
p	34.6	Cq	None	2.06 (m, H-5α); 1.27 (s, 4β-CH ₃); 1.06 (s, 4α-CH ₃)	C-4
q	33.5	CH ₃	1.06 (s, 4α-CH ₃)	1.27 (s, 4β-CH ₃)	4α-CH ₃
r	29.5	CH ₂	2.60 – 2.45 (m, H-16A and H-16B)	None!	C-16
s	25.7	CH ₂	2.07 – 1.92 (m, H-2β); 1.55 – 1.45 (m, H-2α)	4.89 (br d, 1α-OH)	C-2
t	25.00	CH ₃	1.27 (s, 4β-CH ₃)	1.06 (s, 4α-CH ₃) strong; 2.06 (dd, H-5α); 2.04 – 1.84 (m, H-2β and/or H-3α); 1.55 – 1.45 (m, H-2α)	4β-CH ₃
u	24.96	CH ₃	1.51 (s, 8β-CH ₃)	5.46 (d, H-7α); 1.48 (s, 10β-CH ₃)	8β-CH ₃
v	24.5	CH ₂	2.47 – 2.34 (m, H-15A); 1.97 – 1.84 (m, H-15B)	2.60 – 2.45 (m, H-16A and H-16B)	C-15
w	21.4	CH ₃	1.11 (s, 13β-CH ₃)	2.64 (d, H-12β); 2.40 (d, H-12α)	13β-CH ₃
x	21.2	CH ₃	2.19 (s, acetyl-CH ₃)	None	Acetyl-CH ₃
y	19.5	CH ₃	1.48 (s, 10β-CH ₃)	2.06 (dd, 2.06, H-5α) strong; 1.51 (s, 8β-CH ₃)	10β-CH ₃
z	14.2	CH ₃	1.26 (t, ethyl-CH ₃)	4.15 (q, ethyl-CH ₂)	Ethyl-CH ₃

¹H-NMR

signal	δ	Observed multiplicity	HSQC correlation (δ /ppm)	Proton-proton coupling (coupling partner)	Comparison to Kogel's Forskolol assignments
H-1 β	4.36 – 4.32 or 4.34	m or ddd	C-1 (73.0)	2.0 Hz (H-1 β ; 4.89 in COSY) ~2.5 Hz (H-2 β ; ~2.0 in COSY) ~2.5 Hz (H-2 α ; ~1.5 in COSY)	4.54 (ddd, J = 3.0 (H-2 β), 2.5 (H-2 α), 2.5 (1 β -OH) Hz)
1 α -OH	4.89	br d	None (OH)	2.0 Hz (H-1b; not in COSY)	3.4 (d, J = 2.5 (H-1 β) Hz)
H-2 β	2.07 – 1.92	m	C-2 (25.7)	? Hz (H-3 α ; 1.00-1.10 in COSY) ? Hz (H-3 β ; 2.47-2.34 in COSY) ? Hz (H-1 β ; 4.34 in COSY) ? Hz (H-2 β ; 1.55-1.45 in COSY)	2.16 (dddd, J = 15.0 (H-2 α), 13.3 (H-3 α), 4.0 (H-3 β), 2.5 (H-1 β) Hz)
H-2 α	1.55 – 1.45	m	C-2 (25.7)	/	1.42 (dddd, J = 15.0 (H-2 β), 3.5 (H-3 α), 3.0 (H-3 β), 3.0 (H-1 α) Hz)
H-3 β	1.10 – 1.00	m	C-3 (35.8)		1.09 (ddd, J = 13.4 (H-3 α), 3.0 (H-2 β), 4.0 (H-2 α) Hz)
H-3 α	2.04 – 1.84	m	C-3 (35.8)		1.76 (ddd, J = 13.4 (H-3 β), 13.3 (H-2 β), 3.5 (H-2 α) Hz)
H-5 α	2.06	dd	C-5 (43.0)	2.8 Hz (H-6 α ; 4.42 in COSY) 1.3 Hz (6 β -OH; 1.74 in COSY) 0 (?-CH ₃ ; 1.05 in COSY) 0 (?-CH ₃ ; 1.11 in COSY)	2.15 (dd, J = 3.2 (H-6 α), 1.8 (6 β -OH), 0 (4 β -CH ₃), 0 (10-CH ₃) Hz)
6 β -OH	1.74	br dd	None (OH)	2.3 Hz (H-6 α ; 2.06 in COSY) 1.3 Hz (H-5 α ; 2.06 in COSY) 0 Hz (H-7 α ; 5.46 in COSY)	1.9 (dd, J = 1.8 (H-5 α), 2.8 (H-6 α) Hz)
H-6 α	4.42	br ddd	C-7 (69.7)	3.8 Hz (H-7 α ; 5.46 in COSY) 2.8 Hz (H-5 α ; 2.06 in COSY) 2.3 Hz (6 β -OH; 1.74 in COSY)	4.44 (ddd, J = 4.3 (H-7 α), 3.2 (H-5 α), 2.8 (6 β -OH) Hz)
H-7 α	5.46	d	C-7 (76.8)	3.8 Hz (H-6 α ; 4.42 in COSY)	5.46 (d, J = 4.3 (H-6 α), 0 (8 β -CH ₃) Hz)
H-12 α	2.40	d, (ABq, $\Delta\delta = 0.23$)	C-12 (50.6)	18.8 Hz (H-12 β ; 2.40 in COSY)	3.17 (d, J = 17.3 (H-12 β), 0 (8 β -CH ₃), 0 (13 β -CH ₃) Hz)
H-12 β	2.64	d, (ABq, $\Delta\delta = 0.23$)	C-12 (50.6)	18.8 Hz (H-12 α ; 2.64 in COSY)	2.38 (d, J = 17.3 (H-12 α), 0 (13 β -CH ₃) Hz)
H-14	3.93	br dd	C-14 (79.9)	10.8 Hz (H-15(A); 2.43 in COSY) 3.3 Hz (H-15(A); 1.90 in COSY) Broadening and difference in J-values suggest C-14 - C-15 has mostly restricted rotation	5.93 (vinylic, reacted group)
H-15A	2.47 – 2.34	m	C-15 (24.5)		4.97 (vinylic, reacted group)
H-15B	1.97 – 1.84	m	C-15 (24.5)		5.28 (vinylic, reacted group)
H-16A	2.60 – 2.45	m	C-16 (29.4)		n/a
H-16B	2.60 – 2.45	m	C-16 (29.4)		n/a
13 β -CH ₃	1.11	s	13 β -CH ₃ (21.4)		1.33 (s, J = 0 (H-12 α), 0 (12 β -CH ₃), 0 (H-14), 0 (H-15 trans) Hz)
8 β -CH ₃	1.51	s	8 β -CH ₃ (24.96)		1.70 (s, J = 0 (H-7 α), 0 (9 α -OH), 0 (H-12 α) Hz)
4 α -CH ₃	1.06	s	4 α -CH ₃ (33.5)		1.02 (s, J = 0 (4 β -CH ₃) Hz)

signal	δ	Observed multiplicity	HSQC correlation (δ /ppm)	Proton-proton coupling (coupling partner)	Comparison to Kogel's Forskolin assignments
4 β -CH ₃	1.27	s	4 β -CH ₃ (25.00)		1.25 (s, $J = 0$ (4 α -CH ₃), 0 (H-3 α), 0 (H-5 α) Hz)
10 β -CH ₃	1.48	s	10 β -CH ₃ (19.5)		1.42 (s, $J = 0$ (H-5 α) Hz)
Acetyl-CH ₃	2.19	s	Acetyl-CH ₃ (21.2)	none	2.16 (s)
Ethyl-CH ₂	4.15	q	Ethyl-CH ₂ (60.7)	7.1 Hz (Ethyl-CH ₃ ; 1.26 in COSY)	n/a
Ethyl-CH ₃	1.26	t	Ethyl-CH ₃ (14.2)	7.1 Hz (Ethyl-CH ₂ ; 1.26 in COSY)	n/a

Ethyl (13*R*,14*R*/*S*)-7-Acetoxy-6-hydroxy-1,9-(isopropylidenedioxy)- 14-iodo-11-oxo-8,13-epoxylabdan-15-ylacetate (14**)**



According to **GPB** from forskolin 1,9-acetonide (**13**; 79 mg, 0.17 mmol), NaHCO₃ (15 mg, 1.0 equiv), ethyl iodoacetate (56 mg, 1.5 equiv), and Et₃B (0.2 mL, 1.15 M in dry C₆D₆) in dry CH₂Cl₂ (1.0 mL). The crude mixture was purified by flash column chromatography (Et₂O/pentane 1:4) to afford **14** as a mixture of diastereomers (44 mg, 42%, dr 71:29). Individual fractions of each diastereomer were isolated for characterization.

(14*R*)-14 (minor)

Colorless oil; $R_f = 0.44$ (Et₂O/pentane 4:6); $[\alpha]_D^{20} -19$ (c 1.05, CH₂Cl₂).

IR: 3503, 2977, 2928, 2858, 1726, 1715, 1456, 1374, 1249, 907 cm⁻¹.

¹H NMR (CDCl₃, 400 MHz): $\delta = 5.30$ (d, $J = 3.9$ Hz, 1 H), 4.44 (t, $J = 3.4$ Hz, 1 H), 4.25–4.20 (m, 1 H), 4.16–4.14 (m, 1 H), 4.13 (q, $J = 7.2$ Hz, 2 H), 3.40 (d, $J = 16.5$ Hz, 1 H), 2.63–2.49 (m, 2 H), 2.50 (d, $J = 16.5$ Hz, 1 H), 2.25 (d, $J = 2.8$ Hz, 1 H), 2.23–2.15 (m, 1 H), 2.14 (s, 3 H), 2.08 (tdd, $J = 14.3, 4.5, 2.0$ Hz, 1 H), 1.92–1.82 (m, 1 H), 1.78 (td, $J = 13.5, 4.3$ Hz, 1 H), 1.65 (s, 3 H), 1.50 (s, 3 H), 1.49–1.40 (m, 1 H), 1.46 (s, 3 H), 1.44 (s, 3 H), 1.43 (s, 3 H), 1.26 (t, $J = 7.2$ Hz, 3 H), 1.26 (s, 3 H), 1.05 (ddd, $J = 13.1, 4.3, 2.4$ Hz, 1 H), 1.00 (s, 3 H).

¹³C NMR (CDCl₃, 101 MHz): $\delta = 208.2, 172.9, 169.6, 100.2, 81.9, 81.7, 76.3, 76.0, 70.2, 70.1, 60.7, 51.1, 47.5, 42.8, 38.2, 36.4, 34.5, 34.3, 33.5, 31.5, 30.7, 29.3, 25.2, 23.8, 23.1, 22.1, 21.5, 17.6, 14.4$.

HRMS (ESI): m/z [M + Na]⁺ calcd for C₂₉H₄₅IO₉Na: 687.2006; found: 687.2009.

(14S)-14 (major)

Colorless crystals; $R_f = 0.33$ (Et₂O/pentane 4:6); mp 147.7–151.9 °C (Et₂O/pentane); $[\alpha]_D^{20} -48.17$ (c 1.85, CH₂Cl₂).

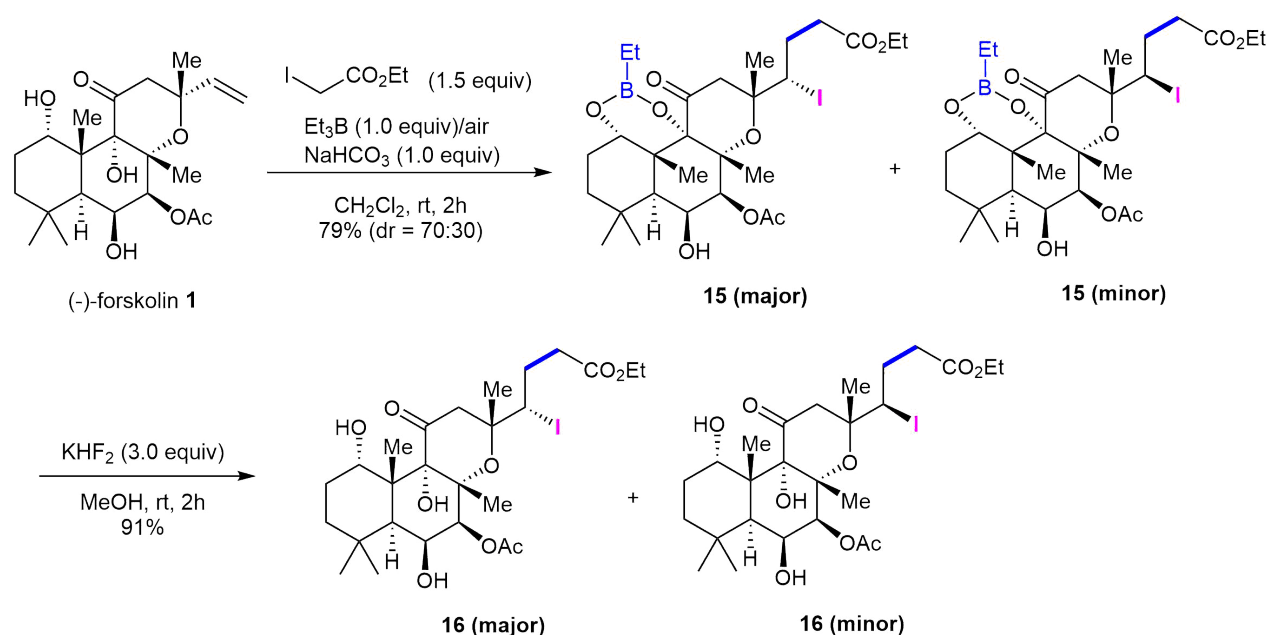
IR: 3447, 2976, 2933, 2860, 1735, 1715, 1445, 1374, 1250, 1116 cm⁻¹.

¹H NMR (CDCl₃, 400 MHz): $\delta = 5.26$ (d, $J = 3.8$ Hz, 1 H), 4.48 (dd, $J = 10.8, 2.1$ Hz, 1 H), 4.39 (t, $J = 3.3$ Hz, 1 H), 4.23 (dd, $J = 3.9, 2.0$ Hz, 1 H), 4.15 (q, $J = 7.2$ Hz, 2 H), 3.49 (d, $J = 19.0$ Hz, 1 H), 2.65–2.57 (m, 1 H), 2.54 (d, $J = 19.0$ Hz, 1 H), 2.49–2.39 (m, 1 H), 2.39–2.29 (m, 1 H), 2.18 (d, $J = 2.6$ Hz, 1 H), 2.13 (s, 3 H), 2.07 (tdd, $J = 14.8, 4.6, 2.3$ Hz, 1 H), 2.01–1.92 (m, 1 H), 1.77 (td, $J = 13.5, 4.3$ Hz, 1 H), 1.55 (s, 3 H), 1.50–1.40 (m, 1 H), 1.47 (s, 3 H), 1.46 (s, 3 H), 1.45 (s, 3 H), 1.37 (s, 3 H), 1.27 (t, $J = 7.1$ Hz, 3 H), 1.25 (s, 3 H), 1.05 (ddd, $J = 13.0, 4.3, 2.4$ Hz, 1 H), 0.99 (s, 3 H).

¹³C NMR (CDCl₃, 101 MHz): $\delta = 206.8, 172.8, 169.4, 100.0, 81.9, 81.4, 76.05, 76.02, 70.3, 70.2, 60.5, 52.2, 50.9, 42.7, 38.0, 36.2, 35.6, 34.4, 33.6, 31.9, 30.2, 28.0, 25.1, 23.7, 22.7, 22.2, 21.3, 17.6, 14.4$.

HRMS (ESI): m/z [M + Na]⁺ calcd for C₂₉H₄₅O₉Na: 687.2006; found: 687.2009.

Ethyl (13R,14R/S)-7-Acetoxy-1,6,9-trihydroxy-11-oxo-8,13-epoxylabdan- 15-ylacetate (16)



According to **GPB** from forskolin (**1**; 100 mg, 0.241 mmol), NaHCO₃ (21 mg, 0.241 mmol), ethyl iodoacetate (77 mg, 0.362 mmol), and Et₃B (0.21 mL, 0.241 mmol, 1.15 M in dry C₆D₆) in dry CH₂Cl₂ (1.5 mL). The mixture was stirred at rt for 2 h (for complete formation of boronic ester derivative; more stable). The crude mixture was purified by flash column chromatography (Et₂O/pentane 3:7) to afford **15** as a mixture of diastereomers (118 mg, 79%, dr 70:30). Enriched fractions of each diastereomer were collected for individual characterization.

(14S)-15 (major)

Whitish oil; $R_f = 0.36$ (Et₂O/pentane 1:1).

IR: 3470, 2975, 2952, 2933, 2874, 1721, 1441, 1374, 1342, 1213 cm⁻¹.

¹H NMR (C₆D₆, 400 MHz): $\delta = 5.47$ (d, $J = 4.0$ Hz, 1 H), 4.58 (d, $J = 3.1$ Hz, 1 H), 4.48 (dd, $J = 10.8, 1.8$ Hz, 1 H), 4.23 (dt, $J = 4.3, 2.3$ Hz, 1 H), 3.96 (q, $J = 7.1$ Hz, 2 H), 3.39 (d, $J = 16.4$ Hz, 1 H), 2.74–2.64 (m, 2 H), 2.53–2.44 (m, 1 H), 2.37 (d, $J = 16.4$ Hz, 1 H), 2.24–2.12 (m, 1 H), 1.92–1.84 (m, 1 H), 1.83 (s, 3 H), 1.62 (s, 3 H), 1.61–1.51 (m, 2 H), 1.50 (s, 3 H), 1.49 (d, $J = 2.8$ Hz, 1 H), 1.30 (s, 3 H), 1.21 (s, 3 H), 1.04 (t, $J = 7.7$ Hz, 3 H), 0.97 (t, $J = 7.1$ Hz, 3 H), 0.94–0.89 (m, 1 H), 0.86–0.79 (m, 2 H), 0.80 (s, 3 H).

¹³C NMR (C₆D₆, 101 MHz): $\delta = 201.3, 171.2, 168.9, 81.9, 81.8, 77.5, 75.9, 73.4, 70.1, 60.3, 51.4, 50.4, 43.4, 40.1, 36.4, 35.2, 34.2, 32.9, 30.9, 27.5, 24.6, 23.8, 22.9, 20.7, 18.9, 14.3, 8.3, 7.3$ (broad signal). **¹¹B NMR** (C₆D₆, 96 MHz): $\delta = 31.8$.

HRMS (ESI): m/z [M + H]⁺ calcd for C₂₈H₄₅BiO₉: 663.2201; found: 663.2196.

(14R)-15 (minor)

Whitish oil; $R_f = 0.45$ (Et₂O/pentane 1:1).

IR: 3515, 2975, 2951, 2933, 2874, 1721, 1374, 1342, 1211, 1056 cm⁻¹.

¹H NMR (C₆D₆, 400 MHz): $\delta = 5.52$ (d, $J = 3.9$ Hz, 1 H), 4.58 (t, $J = 2.9$ Hz, 1 H), 4.40 (dd, $J = 11.4, 1.8$ Hz, 1 H), 4.36 (t, $J = 3.1$ Hz, 1 H), 3.93 (q, $J = 7.1$ Hz, 2 H), 3.28 (d, $J = 15.7$ Hz, 1 H), 2.50–2.44 (m, 2 H), 2.25 (d, $J = 15.7$ Hz, 1 H), 2.05–1.95 (m, 1 H), 1.94–1.86 (m, 1 H), 1.85 (s, 3 H), 1.75 (ddt, $J = 11.5, 9.1, 5.7$ Hz, 1 H), 1.67 (s, 3 H), 1.62 (s, 3 H), 1.65–1.56 (m, 2 H), 1.55 (d, $J = 2.9$ Hz, 1 H), 1.24 (s, 3 H), 1.22 (s, 3 H), 1.09 (t, $J = 7.7$ Hz, 3 H), 0.96 (t, $J = 7.2$ Hz, 3 H), 0.96–0.91 (m, 1 H), 0.93–0.87 (m, 2 H), 0.85 (s, 3 H).

¹³C NMR (C₆D₆, 101 MHz): $\delta = 202.9, 172.8, 168.9, 81.65, 81.56, 77.0, 76.2, 73.4, 70.0, 60.4, 50.9, 46.8, 43.4, 41.0, 37.1, 34.3, 34.2, 32.9, 30.9, 28.3, 24.7, 23.9, 23.4, 21.0, 18.9, 14.2, 8.3, 7.3$ (broad signal).

¹¹B NMR (C₆D₆, 96 MHz): $\delta = 31.7$.

HRMS (ESI): m/z [M + H]⁺ calcd for C₂₈H₄₅BiO₉: 663.2201; found: 663.2197.

To a solution of iodoboronic esters **15** (120 mg, 0.181 mmol) in MeOH (3.6 mL, 0.05 M) was added to KHF₂ (43 mg, 0.544 mmol, 3.0 equiv) at rt. The mixture was stirred for 2 h at rt, then concentrated in vacuo. The residue was diluted with Et₂O, filtered, and concentrated under reduced pressure. The crude mixture was purified by flash column chromatography (EtOAc/heptane 23:77) to afford **16** (102 mg, 91%, dr 68:32) as an inseparable mixture of diastereomers.

(14S)-16 (major):

According to procedure above, major isomer (14S)-**16** (17 mg, 87%) was obtained from major isomer (14S)-**15** (21 mg, 0.03 mmol) and KHF₂ (8 mg, 0.09 mmol) in MeOH (1.0 mL) for individual characterization.

colorless oil; $R_f = 0.49$ (EtOAc/heptane 4:6).

IR: 3480, 3406, 2980, 2927, 2870, 2856, 1715, 1372, 1235, 1037 cm^{-1} .

$^1\text{H NMR}$ (C_6D_6 , 400 MHz): $\delta = 5.81$ (d, $J = 4.1$ Hz, 1 H), 4.75–4.71 (m, 1 H), 4.45 (s, 1 H), 4.30 (d, $J = 3.6$ Hz, 1 H), 3.97 (q, $J = 7.1$ Hz, 2 H), 3.77 (d, $J = 16.4$ Hz, 1 H), 2.78 (dddd, $J = 16.5, 8.3, 6.3, 2.2$ Hz, 1 H), 2.67 (ddd, $J = 16.2, 9.7, 4.6$ Hz, 1 H), 2.52–2.41 (m, 1 H), 2.44 (d, $J = 16.3$ Hz, 1 H), 2.25–2.13 (m, 1 H), 2.10 (d, $J = 3.3$ Hz, 1 H), 2.00–1.88 (m, 1 H), 1.83 (s, 3 H), 1.57–1.47 (m, 1 H), 1.54 (s, 3 H), 1.52 (s, 3 H), 1.38 (s, 3 H), 1.27 (s, 3 H), 0.99 (t, $J = 7.1$ Hz, 3 H), 0.93–0.85 (m, 2 H), 0.85–0.83 (m, 3 H).

$^{13}\text{C NMR}$ (C_6D_6 , 101 MHz): $\delta = 205.2, 172.2, 168.6, 104.3, 82.9, 82.5, 77.3, 76.7, 74.8, 70.3, 60.2, 51.4, 51.3, 43.3, 43.1, 36.3, 35.3, 34.4, 32.8, 30.9, 27.0, 24.3, 23.5, 20.8, 20.3, 14.3$.

HRMS (ESI): m/z $[\text{M} + \text{Na}]^+$ calcd for $\text{C}_{26}\text{H}_{41}\text{IO}_9\text{Na}$: 647.1693; found: 647.1662.

(14*R*)-16 (minor):

According to procedure above, minor isomer (14*R*)-**16** (18 mg, quant) was obtained from minor isomer (14*R*)-**15** (20 mg, 0.03 mmol) and KHF_2 (8 mg, 0.09 mmol) in MeOH (1.0 mL) for individual characterization;

whitish oil; $R_f = 0.49$ (EtOAc/heptanes 4:6).

IR: 3455, 3267, 2952, 2923, 2855, 1712, 1443, 1374, 1258, 1035 cm^{-1} .

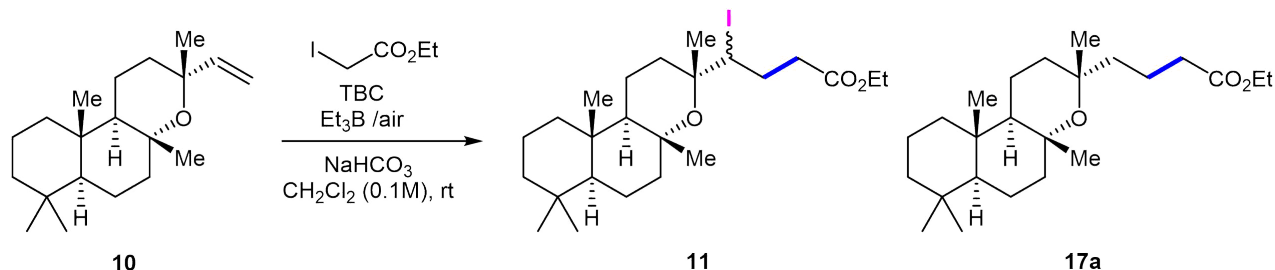
$^1\text{H NMR}$ (C_6D_6 , 400 MHz): $\delta = 5.86$ (d, $J = 4.3$ Hz, 1 H), 4.46 (dd, $J = 11.4, 2.0$ Hz, 1 H), 4.39 (t, $J = 3.6$ Hz, 1 H), 4.36 (s, 1 H), 3.91 (qd, $J = 7.1, 1.5$ Hz, 2 H), 3.63 (d, $J = 14.8$ Hz, 1 H), 2.52 (ddd, $J = 16.9, 7.9, 5.1$ Hz, 1 H), 2.40 (dt, $J = 16.5, 7.7$ Hz, 1 H), 2.30 (d, $J = 14.9$ Hz, 1 H), 2.21–2.13 (m, 1 H), 2.12 (d, $J = 2.9$ Hz, 1 H), 2.00–1.92 (m, 1 H), 1.92–1.86 (m, 1 H), 1.86 (s, 3 H), 1.64 (s, 3 H), 1.58 (s, 3 H), 1.48 (td, $J = 14.6, 3.6$ Hz, 1 H), 1.28 (br s, 2×3 H), 0.95 (t, $J = 7.1$ Hz, 3 H), 0.89–0.81 (m, 2 H), 0.86 (s, 3 H).

$^{13}\text{C NMR}$ (C_6D_6 , 101 MHz): $\delta = 207.0, 172.5, 169.1, 82.8, 82.7, 77.5, 77.0, 74.6, 70.3, 60.3, 51.8, 46.7, 43.3, 43.2, 36.3, 34.7, 34.4, 32.7, 30.9, 28.6, 27.0, 24.3, 24.0, 21.0, 20.2, 14.2$.

HRMS (ESI): m/z $[\text{M} + \text{H}]^+$ calcd for $\text{C}_{26}\text{H}_{42}\text{IO}_9$: 625.1874; found: 625.1848.3.

Hydroalkylation of manoyl and *epi*-manoyl oxide **10** and *epi*-**10**

Short optimization of standard conditions



Entry	$\text{ICH}_2\text{CO}_2\text{Et}$	Et_3B	TBC	Time, h	Product (yield)
1.	1.2 eq	1.3 eq	1.0 eq	2	11 (65%)
2.	1.2 eq	1.3 eq	2.0 eq	3	17a (19%)
3.	1.2 eq	1.3 eq x2	1.0 eq x2	3	17a (48%, 58% brsm)

A rapid optimization of the previously reported reaction conditions was performed on manoyl oxide **10**. NaHCO_3 (1.0 equiv) was selected as an additive to trap the hydroiodic acid and/or molecular iodine formed under the reaction conditions and which presumably leads to the decomposition of the product in an autocatalytic process. Under standard reaction conditions (Entry 1), with only one equivalent of tert-butyl catechol (TBC) as a reducing agent, no reduced product was formed and the only product isolated from the reaction mixture was the product of iodo-alkylation **11**. Increasing the quantity of TBC to two equivalents (Entry 2) allowed for the isolation of the desired reduced product in low yield (19%). Eventually, a satisfactory 48% yield (58% yield, brsm) of hydro-alkylation product **17a** was obtained by using 2.6 equivalents of Et_3B (added in two portions) and 2 equivalents of TBC (added in 2 portions) (Entry 3).

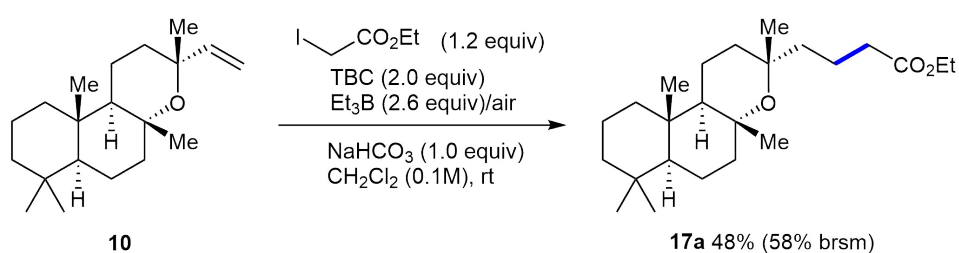
General Procedure C (GP C): Hydroalkylation

To a solution of alkene (1.0 equiv) and NaHCO_3 (1.0 equiv) in dry CH_2Cl_2 (0.1 M to alkene) under an inert atmosphere were added sequentially the alkylating reagent (1.2–1.5 equiv), 4-tert-butylcatechol (1.0 equiv), and Et_3B (1.3 equiv, 1.15 M in benzene). The mixture was opened to air with a CaCl_2 guard tube, covered from light, and stirred vigorously at rt. After 1 h, 4-tert-butylcatechol (1.0 equiv) and Et_3B (1.3 equiv) were added to the mixture. After completion (3 h), the mixture was diluted with sat. aq $\text{Na}_2\text{S}_2\text{O}_3$ soln and extracted with Et_2O (3 ×). The combined organic phases were washed successively with deionized water and brine, dried (Na_2SO_4), filtered, and concentrated under atmospheric pressure. The crude was passed through a short pad of neutral alumina (elution with Et_2O) in order to remove borane residues and concentrated under reduced pressure. The crude mixture was then purified by flash column chromatography. *If required, removal of the olefinic side products (elimination products) possessing same R_f value as the hydroalkylation product was done by epoxidation on the crude mixture (see below).*

General Procedure D (GP D): Epoxidation with meta-chloroperbenzoic acid (*m*-CPBA)

To a solution of mixture composed of the hydroalkylation product and olefinic side products (0.05–0.1 mmol) in CH₂Cl₂ (0.5–1 mL, 0.1 M) were added NaHCO₃ (1.0 equiv) and *m*-CPBA (1.0 equiv) at 0 °C. The mixture was stirred at rt under inert atmosphere until completion (1–3 h). The mixture was diluted with sat. aq NaHCO₃ soln and extracted with Et₂O (3 ×). The combined organic phases were washed successively with water and brine, dried (Na₂SO₄), filtered, and concentrated under reduced pressure. The crude mixture was purified by flash column chromatography.

Ethyl (13*R*)-8,13-Epoxyabdan-15-ylacetate (**17a**)



According to **GPC** from manoyl oxide (**10**; 52 mg, 0.177 mmol), NaHCO₃ (15 mg, 0.177 mmol), ethyl iodoacetate (46 mg, 0.213 mmol), *tert*-butylcatechol (2 portions, 2 × 30 mg, 2 × 0.177 mmol), and Et₃B (2 portions, 2 × 0.2 mL, 2 × 0.230 mmol, 1.15 M in benzene) in dry CH₂Cl₂ (1.0 mL). The crude was subjected to epoxidation (according to GPD) and then purified by flash column chromatography (EtOAc/heptane 4:96) to give **17a** (32 mg, 48%, 58% brsm) as a colorless oil.

R_f = 0.42 (Et₂O/pentane 1:9); [α]_D²⁰ +3 (c 1.03, CH₂Cl₂).

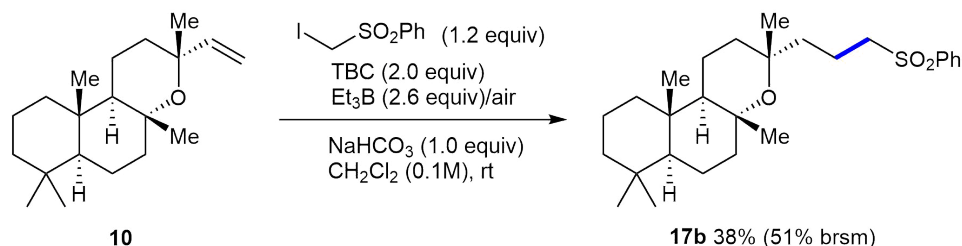
IR: 2981, 2935, 2925, 2868, 1737, 1463, 1373, 1235, 1044, 847, 634 cm⁻¹.

¹H NMR (CDCl₃, 300 MHz): δ = 4.11 (q, *J* = 7.1 Hz, 2 H), 2.26 (td, *J* = 7.5, 2.6 Hz, 2 H), 1.75–1.57 (m, 4 H), 1.53 (m, 3 H), 1.48–1.28 (m, 5 H), 1.28–1.20 (m, 2 H), 1.25 (s, 3 H), 1.24 (t, *J* = 7.1 Hz, 3 H), 1.20 (s, 3 H), 1.17–1.03 (m, 3 H), 0.92 (dd, *J* = 12.3, 3.0 Hz, 1 H), 0.88–0.83 (m, 1 H), 0.84 (s, 3 H), 0.82–0.78 (m, 1 H), 0.78 (s, 3 H), 0.75 (s, 3 H).

¹³C NMR (CDCl₃, 75 MHz): δ = 174.1, 74.8, 72.7, 60.2, 58.4, 56.5, 45.1, 43.2, 42.3, 39.3, 37.0, 36.4, 34.9, 33.47, 33.42, 27.7, 25.0, 21.4, 20.0, 19.5, 18.8, 15.9, 15.5, 14.4.

HRMS (ESI): *m/z* [M + H]⁺ calcd for C₂₄H₄₃O₃: 379.3212; found: 379.3209.

(13*R*)-8,13-Epoxyabdan-15-ylmethyl Phenyl Sulfone (**17b**)



According to **GPC** from manoyl oxide (**10**; 52 mg, 0.179 mmol), NaHCO₃ (15 mg, 0.179 mmol), iodomethyl phenyl sulfone (62 mg, 0.215 mmol), *tert*-butylcatechol (2 portions, 2 × 30 mg, 2 × 0.179 mmol), and Et₃B (2 portions, 2 × 0.2 mL, 2 × 0.230 mmol, 1.15 M in benzene) in dry CH₂Cl₂ (1.0 mL). The crude was subjected to epoxidation (according to GPD) and then purified by flash column chromatography (EtOAc/heptane 7:93) to give **17b** (30 mg, 38%, 51% brsm) as a colorless sticky oil.

$R_f = 0.28$ (EtOAc/heptanes 2:8); $[\alpha]_D^{20} -5$ (c 0.7, CH₂Cl₂).

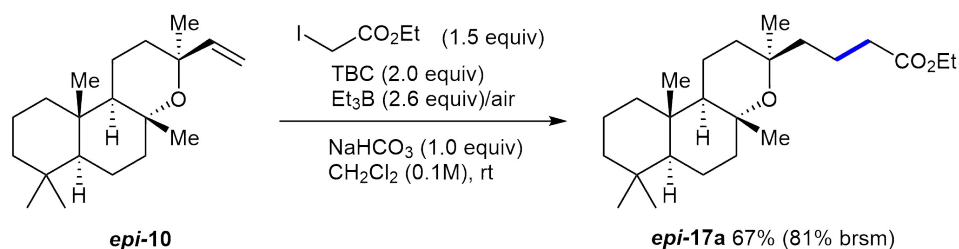
IR: 2992, 2921, 2862, 1446, 1375, 1305, 1147, 959, 597, 529 cm⁻¹.

¹H NMR (CDCl₃, 300 MHz): $\delta = 7.94\text{--}7.88$ (m, 2 H), 7.68–7.61 (m, 1 H), 7.56 (dd, $J = 8.3, 6.6$ Hz, 2 H), 3.16–3.08 (m, 2 H), 1.86–1.73 (m, 2 H), 1.67–1.55 (m, 4 H), 1.54–1.23 (m, 10 H), 1.21 (s, 3 H), 1.19–1.15 (m, 1 H), 1.14 (s, 3 H), 1.12–0.88 (m, 2 H), 0.90–0.79 (m, 1 H), 0.86 (s, 3 H), 0.78 (s, 3 H), 0.73 (s, 3 H).

¹³C NMR (CDCl₃, 75 MHz): $\delta = 139.5, 133.6, 129.3$ (2 C), 128.2 (2 C), 74.9, 72.6, 58.4, 57.0, 56.5, 43.4, 43.1, 42.3, 39.2, 36.9, 36.4, 33.46, 33.41, 27.9, 24.8, 21.4, 19.9, 18.7, 17.4, 15.9, 15.4.

HRMS (ESI): m/z [M + H]⁺ calcd for C₂₇H₄₃O₃S: 447.2933; found: 447.2926.

Ethyl (13*S*)-8,13-Epoxyabdan-15-ylacetate (*epi*-**17a**)



According to **GPC** from *epi*-manoyl oxide (*epi*-**10**; 64 mg, 0.216 mmol), NaHCO₃ (18 mg, 0.216 mmol), ethyl iodoacetate (70 mg, 0.324 mmol), *tert*-butylcatechol (2 portions, 2 × 36 mg, 2 × 0.216 mmol), and Et₃B (2 portions, 2 × 0.24 mL, 2 × 0.281 mmol, 1.15 M in benzene) in dry CH₂Cl₂ (1.2 mL). The crude was purified by flash column chromatography (EtOAc/heptane 4:96) to give *epi*-**17a** (55 mg, 67%, 81% brsm) as a colorless oil.

$R_f = 0.35$ (EtOAc/heptanes 1:9); $[\alpha]_D^{20} +16$ (c 1.5, CH₂Cl₂).

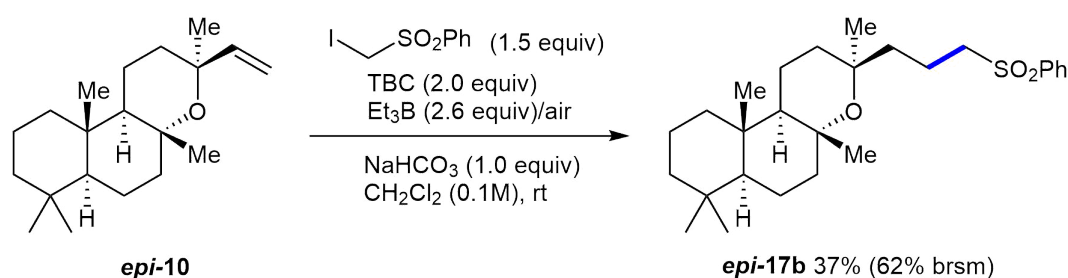
IR: 2937, 2866, 1736, 1464, 1373, 1235, 1044, 963, 846, 607 cm⁻¹.

¹H NMR (CDCl₃, 400 MHz): $\delta = 4.11$ (q, $J = 7.1$ Hz, 2 H), 2.26 (td, $J = 7.3, 1.8$ Hz, 2 H), 1.80–1.28 (m, 15 H), 1.25–1.21 (m, 1 H), 1.24 (t, $J = 7.2$ Hz, 3 H), 1.23 (s, 3 H), 1.21–1.17 (m, 1 H), 1.14 (dd, $J = 13.2, 4.3$ Hz, 1 H), 1.10 (s, 3 H), 0.93 (dd, $J = 12.0, 2.5$ Hz, 1 H), 0.88–0.79 (m, 1 H), 0.84 (s, 3 H), 0.78 (s, 3 H), 0.75 (s, 3 H).

¹³C NMR (CDCl₃, 101 MHz): $\delta = 173.8, 75.0, 73.1, 60.3, 57.7, 56.6, 43.7, 42.3, 40.8, 39.3, 37.4, 37.1, 35.1, 33.48, 33.39, 30.2, 24.4, 21.4, 20.4, 20.1, 18.7, 15.8, 15.4, 14.4$.

HRMS (ESI): m/z [M + Na]⁺ calcd for C₂₄H₄₂O₃Na: 401.3032; found: 401.3026.

(13S)-8,13-Epoxyabdan-15-ylmethyl Phenyl Sulfone (*epi-17b*)



According to **GPC** from *epi*-manoyl oxide (*epi-10*; 63 mg, 0.213 mmol), NaHCO₃ (18 mg, 0.213 mmol), iodomethyl phenyl sulfone (92 mg, 0.319 mmol), *tert*-butylcatechol (2 portions, 2 × 35 mg, 2 × 0.213 mmol), and Et₃B (2 portions, 2 × 0.24 mL, 2 × 0.276 mmol, 1.15 M in benzene) in dry CH₂Cl₂ (1.4 mL). The crude was purified by flash column chromatography (EtOAc/heptane 7:93) to give *epi-17b* (35 mg, 37%, 62% brsm) as a white sticky oil.

$R_f = 0.27$ (EtOAc/heptanes 2:8); $[\alpha]_D^{20} +20$ (c 1.05, CH₂Cl₂).

IR: 2923, 2864, 1736, 1446, 1373, 1235, 1044, 962, 635, 598 cm⁻¹.

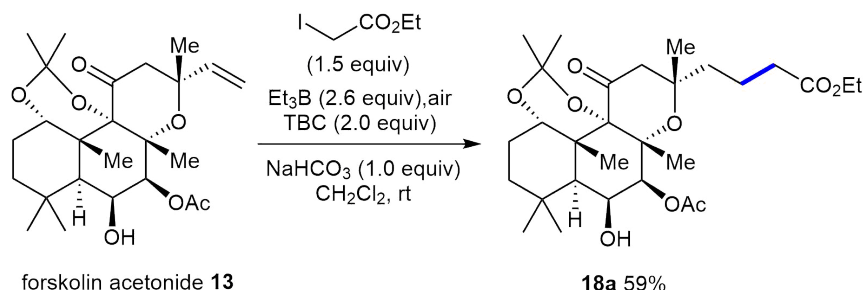
¹H NMR (CDCl₃, 400 MHz): $\delta = 7.93$ –7.89 (m, 2 H), 7.68–7.62 (m, 1 H), 7.56 (ddt, $J = 8.3, 6.5, 1.5$ Hz, 2 H), 3.07 (t, $J = 7.7$ Hz, 2 H), 1.86–1.17 (m, 17 H), 1.14 (dd, $J = 13.3, 3.7$ Hz, 1 H), 1.09 (s, 3 H), 1.05 (s, 3 H), 0.91 (dd, $J = 12.1, 2.5$ Hz, 1 H), 0.87–0.82 (m, 1 H), 0.84 (s, 3 H), 0.77 (s, 3 H), 0.73 (s, 3 H).

¹³C NMR (CDCl₃, 101 MHz): $\delta = 139.3, 133.7, 129.4$ (2 C), 128.2 (2 C), 75.1, 72.6, 57.2, 57.0, 56.6, 43.6, 42.2, 39.9, 39.3, 37.1, 37.0, 33.5, 33.4, 30.1, 24.2, 21.4, 20.1, 18.7, 18.2, 15.8, 15.3.

HRMS (ESI): m/z [M + H]⁺ calcd for C₂₇H₄₃O₃: 447.2933; found: 447.2927.

Hydroalkylation of (-)-forskolin 1

Ethyl (13*R*)-7-Acetoxy-6-hydroxy-1,9-(isopropylidenedioxy)-11-oxo-8,13-epoxylabdan-15-ylacetate (18a)



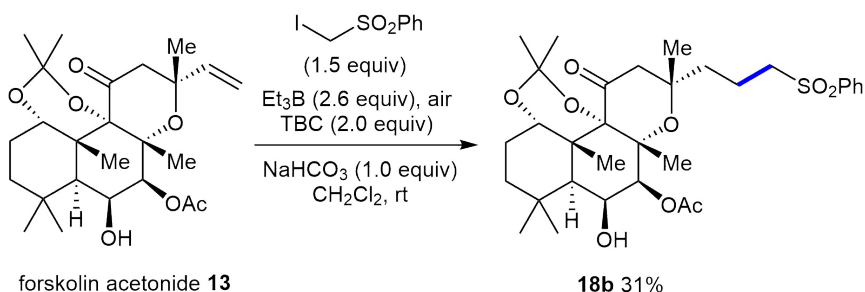
According to **GPC** from forskolin 1,9-acetonide (**13**; 100 mg, 0.22 mmol), NaHCO₃ (19 mg, 0.22 mmol), ethyl iodoacetate (71 mg, 0.33 mmol), *tert*-butylcatechol (2 portions, 2 × 37 mg, 2 × 0.22 mmol), and Et₃B (2 portions, 2 × 0.25 mL, 2 × 0.286 mmol, 1.15 M in benzene) in dry CH₂Cl₂ (1.4 mL). The crude was purified by flash column chromatography (EtOAc/heptane 1:5) to give **18a** (70 mg, 59%) as a white powder.

R_f = 0.35 (EtOAc/heptanes 3:7); **mp** 119.7–122.8 °C (Et₂O/pentane); [α]_D²⁰ -35 (c 1.48, CH₂Cl₂). **IR**: 3519, 2933, 1731, 1712, 1456, 1372, 1241, 1046, 961, 789, 508 cm⁻¹.

¹H NMR (CDCl₃, 300 MHz): δ = 5.22 (d, *J* = 3.8 Hz, 1 H), 4.41 (t, *J* = 3.3 Hz, 1 H), 4.23–4.17 (m, 1 H), 4.11 (q, *J* = 7.1 Hz, 2 H), 3.01 (d, *J* = 17.7 Hz, 1 H), 2.37 (d, *J* = 17.7 Hz, 1 H), 2.29 (td, *J* = 7.1, 5.1 Hz, 2 H), 2.21 (d, *J* = 2.7 Hz, 1 H), 2.12 (s, 3 H), 2.04 (ddd, *J* = 14.2, 4.3, 2.0 Hz, 1 H), 1.84–1.59 (m, 5 H), 1.57 (s, 3 H), 1.55–1.49 (m, 1 H), 1.47 (s, 3 H), 1.44 (s, 3 H), 1.37 (s, 3 H), 1.25 (s, 3 H), 1.24 (t, *J* = 6.9 Hz, 3 H), 1.23 (s, 3 H), 1.09–1.00 (m, 1 H), 0.99 (s, 3 H).

HRMS (ESI): *m/z* [M + Na]⁺ calcd for C₂₉H₄₆O₉Na: 561.3040; found: 561.3009.

(13*R*)-7-Acetoxy-6-hydroxy-1,9-(isopropylidenedioxy)-11-oxo-8,13-epoxylabdan-15-ylmethyl Phenyl Sulfone (18b)



According to **GPC** from forskolin 1,9-acetonide (**13**; 97 mg, 0.213 mmol), NaHCO₃ (18 mg, 0.213 mmol), iodomethyl phenyl sulfone (92 mg, 0.320 mmol), *tert*-butylcatechol (2 portions, 2 × 36 mg, 2 × 0.213 mmol), and Et₃B (2 portions, 2 × 0.24 mL, 2 × 0.277 mmol, 1.15 M

in benzene) in dry CH₂Cl₂ (1.6 mL). The crude was purified by flash column chromatography (EtOAc/heptane 1:3) to give **18b** (40 mg, 31%) as a white powder.

R_f = 0.23 (EtOAc/heptanes 4:6); **mp** 171.1–175.2 °C (Et₂O/pentane); [α]_D²⁰ –18 (c 1.0, CH₂Cl₂).

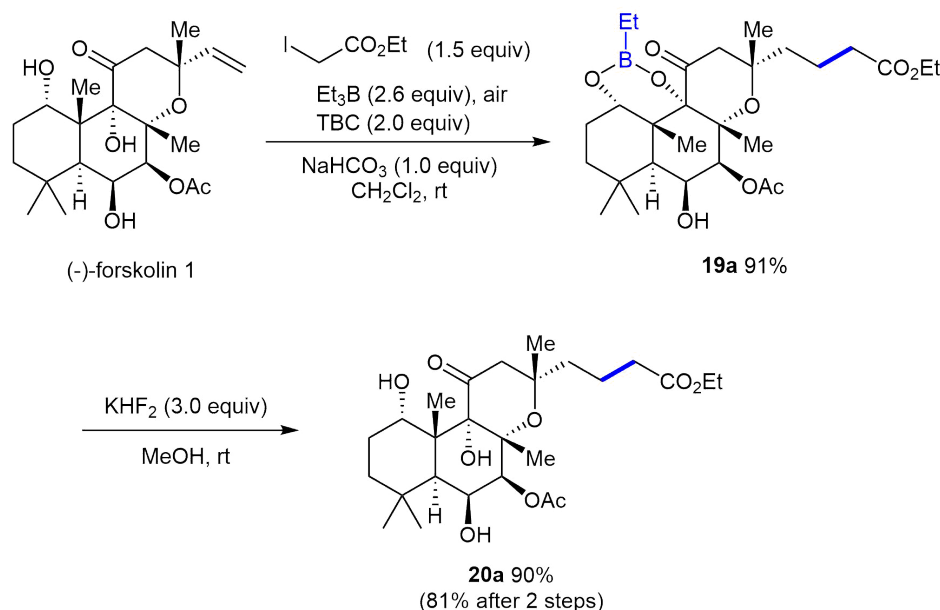
IR: 3514, 2930, 1712, 1447, 1373, 1304, 1148, 961, 745, 690 cm⁻¹.

¹H NMR (CDCl₃, 400 MHz): δ = 7.96–7.91 (m, 2 H), 7.68–7.62 (m, 1 H), 7.60–7.54 (m, 2 H), 5.18 (d, *J* = 3.8 Hz, 1 H), 4.39 (t, *J* = 3.5 Hz, 1 H), 4.20 (dd, *J* = 3.9, 1.9 Hz, 1 H), 3.20 (dt, *J* = 14.5, 7.7 Hz, 1 H), 3.09 (dt, *J* = 14.5, 7.1 Hz, 1 H), 2.92 (d, *J* = 17.8 Hz, 1 H), 2.41 (d, *J* = 17.7 Hz, 1 H), 2.18 (d, *J* = 2.7 Hz, 1 H), 2.10 (s, 3 H), 2.04 (ddd, *J* = 14.2, 4.3, 2.0 Hz, 1 H), 1.94–1.57 (m, 4 H), 1.59–1.53 (m, 1 H), 1.56 (s, 3 H), 1.47 (s, 3 H), 1.45–1.40 (m, 1 H), 1.39 (s, 3 H), 1.34 (s, 3 H), 1.25 (s, 3 H), 1.21 (s, 3 H), 1.04 (ddd, *J* = 13.1, 4.3, 2.5 Hz, 1 H), 0.99 (s, 3 H).

¹³C NMR (CDCl₃, 75 MHz): δ = 208.3, 169.5, 139.7, 133.6, 129.3 (2 C), 128.2 (2 C), 99.9, 81.8, 80.6, 76.2, 74.4, 70.2, 70.1, 56.7, 50.7, 44.3, 42.7, 38.0, 36.2, 34.5, 33.5, 31.8, 31.0, 25.2, 23.7, 22.9, 22.5, 21.3, 17.6, 17.5.

HRMS (ESI): *m/z* [M + H]⁺ calcd for C₃₂H₄₇O₉S: 607.2941; found: 607.2935.

Ethyl (13*R*)-7-Acetoxy-1,6,9-trihydroxy-11-oxo-8,13-epoxylabdan- 15-ylacetate (**20a**)



According to **GPC** from forskolin (**1**; 95 mg, 0.23 mmol), NaHCO₃ (19 mg, 0.23 mmol), ethyl iodoacetate (74 mg, 0.344 mmol), *tert*-butylcatechol (2 portions, 2 × 38 mg, 2 × 0.23 mmol), and Et₃B (2 portions, 2 × 0.26 mL, 2 × 0.3 mmol, 1.15 M in benzene) in dry CH₂Cl₂ (1.3 mL). The crude was purified by flash column chromatography (EtOAc/heptane 28:72) to give boronic ester **19a** (112 mg, 91%) as a whitish oil.

R_f = 0.63 (EtOAc/heptanes 1:1).

IR: 3480, 2975, 2930, 2869, 2857, 1733, 1713, 1458, 1373, 1059 cm^{-1} .

$^1\text{H NMR}$ (CDCl_3 , 400 MHz): δ = 5.21 (d, J = 4.0 Hz, 1 H), 4.40 (dt, J = 4.5, 2.5 Hz, 1 H), 4.35 (t, J = 3.0 Hz, 1 H), 4.10 (q, J = 7.1 Hz, 2 H), 3.03 (d, J = 15.8 Hz, 1 H), 2.28 (dt, J = 11.4, 7.2 Hz, 2 H), 2.21 (d, J = 15.8 Hz, 1 H), 2.14 (s, 3 H), 2.05 (tdd, J = 14.3, 4.1, 2.6 Hz, 1 H), 1.82–1.79 (m, 1 H), 1.78–1.64 (m, 2 H), 1.62 (s, 3 H), 1.62–1.57 (m, 1 H), 1.54 (s, 3 H), 1.53–1.44 (m, 2 H), 1.42 (d, J = 2.6 Hz, 1 H), 1.26–1.22 (m, 9 H), 1.09 (dt, J = 13.0, 3.4 Hz, 1 H), 0.96 (s, 3 H), 0.93 (t, J = 7.8 Hz, 3 H), 0.75 (m, 2 H).

$^{13}\text{C NMR}$ (CDCl_3 , 101 MHz): δ = 205.0, 173.9, 169.7, 81.6, 80.4, 76.5, 76.1, 73.2, 69.7, 60.2, 49.5, 45.3, 43.1, 39.8, 36.3, 34.6, 34.3, 33.1, 30.2, 24.5, 23.9, 23.3, 21.2, 19.2, 18.8, 14.4, 8.0, 6.9 (broad signal).

$^{11}\text{B NMR}$ (CDCl_3 , 96 MHz): δ = 31.6.

HRMS (ESI): m/z $[\text{M} + \text{Na}]^+$ calcd for $\text{C}_{28}\text{H}_{45}\text{BO}_9\text{Na}$: 559.3054; found: 559.3036.

To a solution of boronic ester **19a** (40 mg, 0.07 mmol) in MeOH (1.0 mL) was added KHF_2 (18 mg, 0.22 mmol, 3.0 equiv) at rt. The mixture was stirred at rt for 2 h. The mixture was concentrated in vacuo, diluted with Et_2O , filtered, and concentrated under reduced pressure. The crude mixture was purified by flash column chromatography (EtOAc/ heptane 1:4) to give **20a** (33 mg, 90%) as a white powder.

R_f = 0.46 (EtOAc/heptanes 1:1); mp 46.3–50.8 $^\circ\text{C}$ (Et_2O); $[\alpha]_D^{20}$ -6 (c 0.6, CH_2Cl_2).

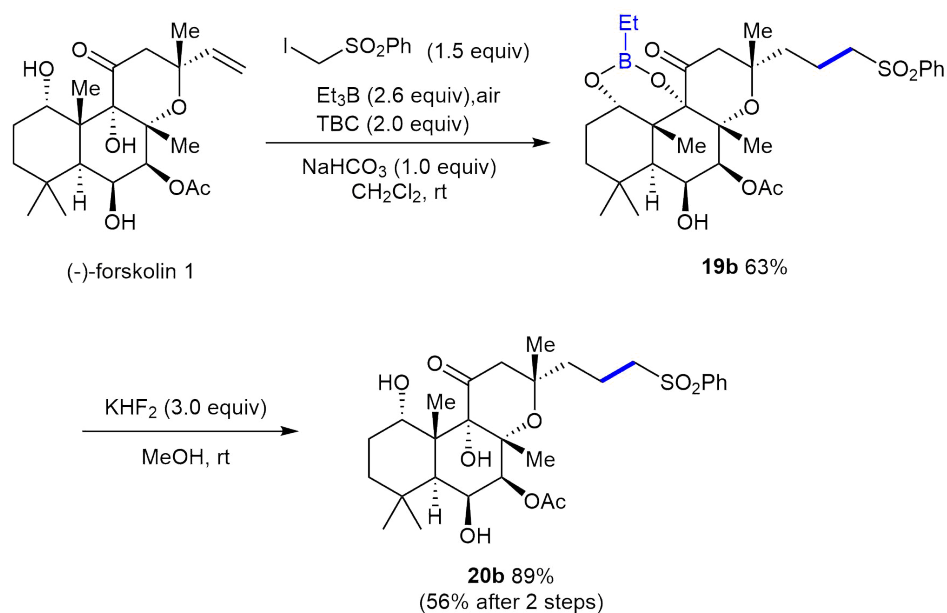
IR: 3431, 3254, 2974, 2930, 2867, 2857, 1731, 1710, 1445, 1373 cm^{-1} .

$^1\text{H NMR}$ (CDCl_3 , 400 MHz): δ = 6.50 (br s, 1 H, OH), 5.44 (d, J = 4.2 Hz, 1 H), 4.54 (t, J = 2.9 Hz, 1 H), 4.44 (dd, J = 4.3, 2.9 Hz, 1 H), 4.11 (q, J = 7.1 Hz, 2 H), 3.25 (d, J = 15.8 Hz, 1 H), 2.51 (br s, 1 H, OH), 2.36–2.18 (m, 5 H), 2.15 (s, 3 H), 1.80–1.66 (m, 4 H), 1.62 (s, 3 H), 1.56–1.47 (m, 1 H), 1.45 (s, 3 H), 1.40 (dq, J = 15.0, 3.4 Hz, 1 H), 1.256 (s, 3 H), 1.248 (s, 3 H), 1.245 (t, J = 7.1 Hz, 3 H), 1.12 (dt, J = 13.3, 3.4 Hz, 1 H), 1.02 (s, 3 H).

$^{13}\text{C NMR}$ (CDCl_3 , 101 MHz): δ = 208.2, 174.1, 169.8, 82.9, 81.5, 77.0, 76.2, 74.7, 70.0, 60.3, 49.8, 45.3, 43.1, 36.3, 34.51, 34.47, 33.0, 30.1, 27.1, 24.3, 23.7, 21.3, 20.1, 19.2 (2 C), 14.4.

HRMS (ESI): m/z $[\text{M} + \text{H}]^+$ calcd for $\text{C}_{26}\text{H}_{43}\text{O}_9$: 499.2907; found: 499.2902.

(13*R*)-7-Acetoxy-1,6,9-trihydroxy-11-oxo-8,13-epoxylabdan-15-ylmethyl Phenyl Sulfone (20b)



According to **GPC** from forskolin (**1**; 100 mg, 0.244 mmol), **NaHCO₃** (21 mg, 0.244 mmol), iodomethyl phenyl sulfone (105 mg, 0.365 mmol), **tert**-butylcatechol (2 portions, 2 × 41 mg, 2 × 0.244 mmol), and **Et₃B** (2 portions, 2 × 0.28 mL, 2 × 0.32 mmol, 1.15 M in benzene) in dry **CH₂Cl₂** (2.0 mL). The crude was purified by flash column chromatography (**EtOAc**/heptane 1:3) to give boronic ester **19b** (56 mg, 63%) as a colorless oil.

R_f = 0.53 (**EtOAc**/heptanes 1:1).

IR: 3517, 2974, 2949, 2933, 2870, 2856, 1718, 1446, 1304, 1145 cm⁻¹.

¹H NMR (**CDCl₃**, 300 MHz): δ = 7.97–7.86 (m, 2 H), 7.68–7.57 (m, 1 H), 7.61–7.47 (m, 2 H), 5.12 (d, *J* = 4.0 Hz, 1 H), 4.35 (dd, *J* = 6.5, 2.6 Hz, 2 H), 3.26–3.14 (m, 1 H), 3.11–2.99 (m, 2 H), 2.90 (d, *J* = 16.0 Hz, 1 H), 2.22 (d, *J* = 15.9 Hz, 1 H), 2.14–2.10 (m, 1 H), 2.10 (s, 3 H), 2.09–1.96 (m, 1 H), 1.95–1.68 (m, 3 H), 1.60 (s, 3 H), 1.58–1.41 (m, 1 H), 1.51 (s, 3 H), 1.36 (d, *J* = 2.7 Hz, 1 H), 1.22 (s, 3 H), 1.20 (s, 3 H), 1.07 (dt, *J* = 13.4, 3.5 Hz, 1 H), 0.94 (s, 3 H), 0.89–0.80 (m, 3 H), 0.64 (dt, *J* = 7.9, 6.9 Hz, 2 H).

¹³C NMR (**CDCl₃**, 75 MHz): δ = 204.2, 169.7, 139.4, 133.6, 129.3 (2 C), 128.1 (2 C), 81.5, 80.5, 76.0, 75.7, 73.1, 69.5, 56.5, 49.7, 44.5, 44.0, 43.0, 39.7, 36.1, 34.2, 33.0, 29.9, 24.4, 23.8, 23.2, 21.2, 18.7, 17.4, 8.0, 6.8 (broad signal).

¹¹B NMR (**CDCl₃**, 96 MHz): δ = 31.5.

HRMS (ESI): *m/z* [**M** + **Na**]⁺ calcd for **C₃₁H₄₅BO₉SNa**: 627.2775; found: 627.2767.

To a solution of boronic ester **19b** (35 mg, 0.06 mmol) in **MeOH** (1.0 mL) was added **KHF₂** (14 mg, 0.17 mmol, 3.0 equiv) at rt. The mixture was stirred at rt for 2 h. The mixture was concentrated in vacuo, diluted with **Et₂O**, filtered, and concentrated under reduced pressure. The

crude mixture was purified by flash column chromatography (EtOAc/ heptane 35:65) to give **20b** (31 mg, 89%) as a colorless oil.

$R_f = 0.28$ (EtOAc/heptanes 1:1); $[\alpha]_D^{20} +3$ (c 0.5, CH₂Cl₂).

IR: 3463, 3278, 2976, 2947, 2930, 2869, 2856, 1737, 1714, 1144 cm⁻¹.

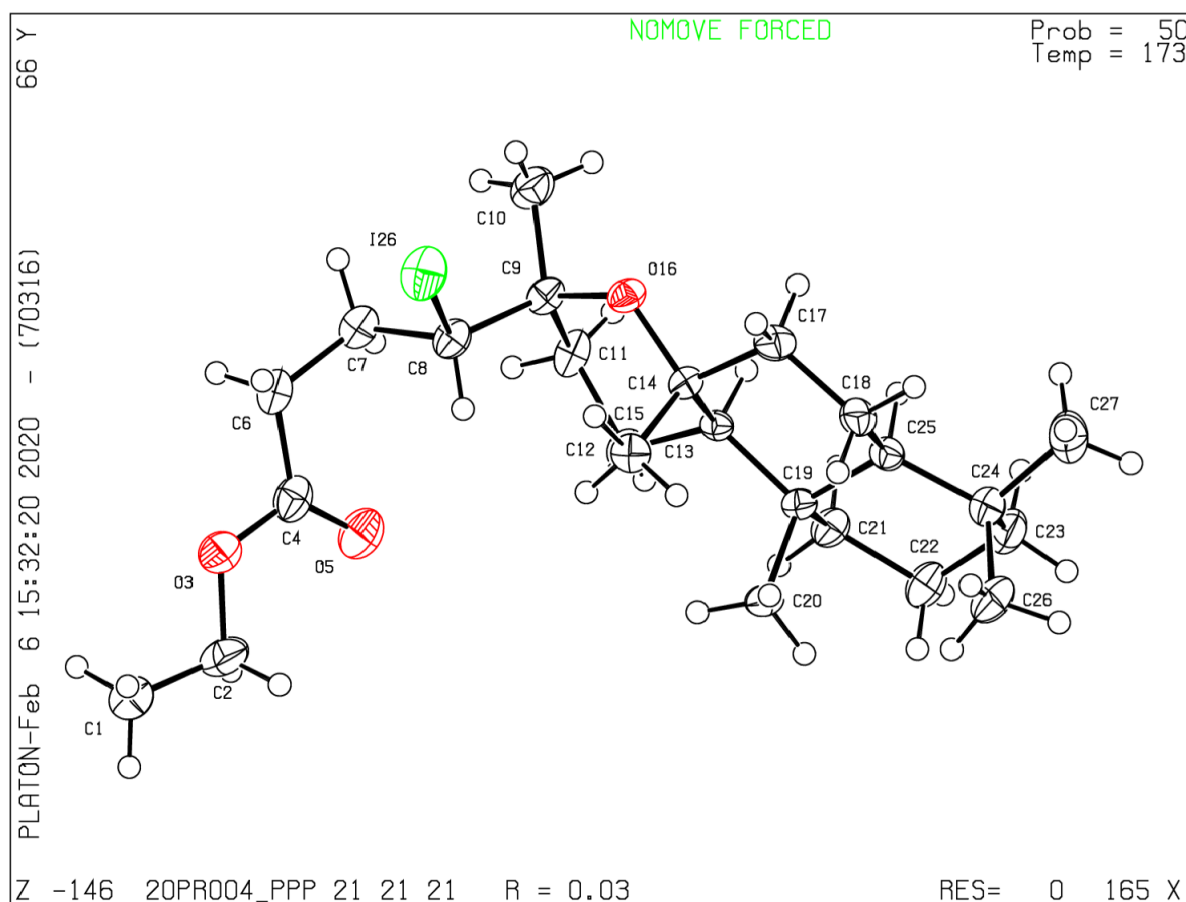
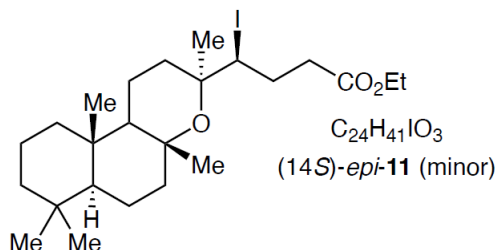
¹H NMR (CDCl₃, 400 MHz): $\delta = 7.93$ – 7.88 (m, 2 H), 7.69 – 7.62 (m, 1 H), 7.56 (dd, $J = 8.4, 7.0$ Hz, 2 H), 6.64 (br s, 1 H, OH), 5.80 (dd, $J = 4.7, 2.9$ Hz, 1 H), 4.59 (d, $J = 2.9$ Hz, 1 H), 4.15 (d, $J = 4.7$ Hz, 1 H), 3.24 – 3.14 (m, 3 H), 2.26 (d, $J = 2.9$ Hz, 1 H), 2.22 – 2.14 (m, 2 H), 2.09 (s, 3 H), 1.98 – 1.88 (m, 2 H), 1.81 – 1.54 (m, 3 H), 1.49 (s, 3 H), 1.4 – 1.36 (m, 1 H), 1.41 (s, 3 H), 1.26 (s, 3 H), 1.14 (dt, $J = 13.5, 3.4$ Hz, 1 H), 1.08 (s, 3 H), 0.98 (s, 3 H).

¹³C NMR (CDCl₃, 101 MHz): $\delta = 207.8, 171.0, 139.4, 133.8, 129.3$ (2 C), 128.3 (2 C), $82.5, 82.2, 76.2, 74.7, 73.7, 71.4, 56.7, 49.0, 43.4, 43.3, 42.4, 36.5, 34.1, 33.0, 30.8, 27.1, 23.3, 22.7, 21.8, 19.8, 17.7$.

HRMS (ESI): m/z [M + H]⁺ calcd for C₂₉H₄₃O₉S: 567.2628; found: 567.2622.

X-ray crystal data reports

Epi-11a (minor):



Crystal-Structure Determination. A crystal of $C_{24}H_{41}IO_3$ was mounted in air at ambient conditions. All measurements were made on a *Oxford Diffraction SuperNova* area-detector diffractometer⁶ using mirror optics monochromated Mo $K\alpha$ radiation ($\lambda = 0.71073 \text{ \AA}$) and Al filtered.⁷ The unit cell constants and an orientation matrix for data collection were obtained from a least-squares refinement of the setting angles of reflections in the range $4.048^\circ < 2\theta < 56.42^\circ$. A total of 549 frames were collected using ω scans, with 3+3 seconds exposure time, a rotation angle of 1.0° per frame, a crystal-detector distance of 65.0 mm, at $T = 173(2) \text{ K}$.

Data reduction was performed using the *CrysAlisPro*⁶ program. The intensities were corrected

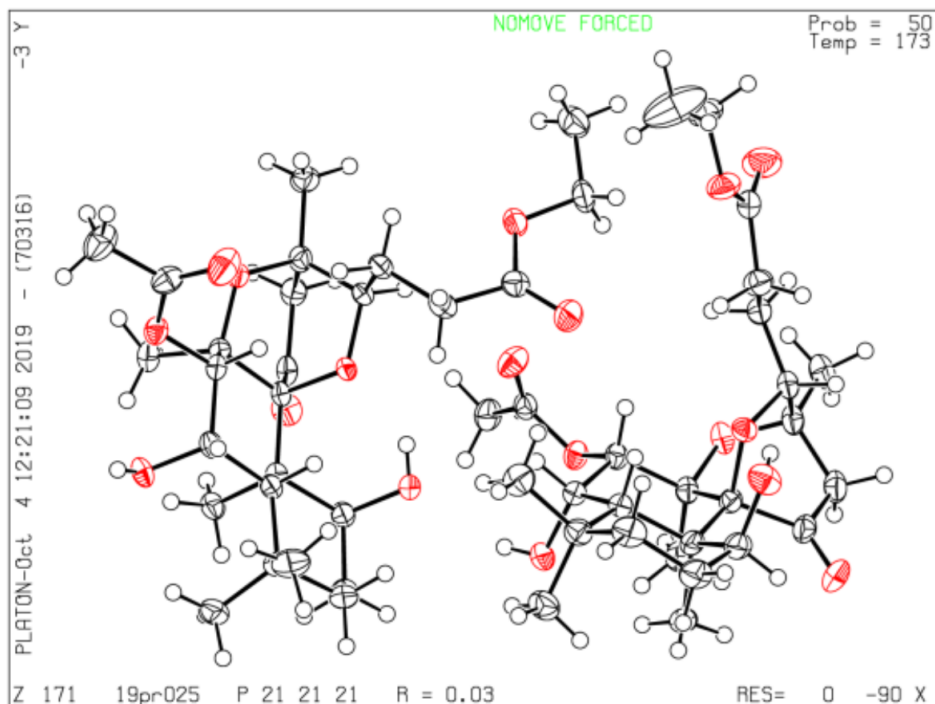
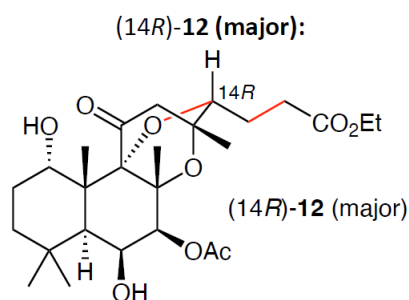
for Lorentz and polarization effects, and an absorption correction based on the multi-scan method using SCALE3 ABSPACK in *CrysAlisPro*⁶ was applied.

The structure was solved by direct methods using *SHELXT*,⁸ which revealed the positions of all non-hydrogen atoms of the title compound. All non-hydrogen atoms were refined anisotropically, and H-atoms were assigned in geometrically calculated positions and refined using a riding model where each H-atom was assigned a fixed isotropic displacement parameter with a value equal to 1.2Ueq of its parent atom (1.5Ueq for methyl groups).

Refinement of the structure was carried out on F^2 using full-matrix least-squares procedures, which minimized the function $\sum w(F_o^2 - F_c^2)^2$. The weighting scheme was based on counting statistics and included a factor to downweight the intense reflections. All calculations were performed using the *SHELXL-2014/7*⁹ program in OLEX2.¹⁰



Single crystal of the compound mounted on a glass fiber.



Crystal-Structure Determination. A crystal of $C_{26}H_{40}O_9$ was mounted in air at ambient conditions. All measurements were made on a *RIGAKU Synergy S* area-detector diffractometer⁶ using mirror optics monochromated Cu $K\alpha$ radiation ($\lambda = 1.54184\text{\AA}$).⁷ The unit cell constants and an orientation matrix for data collection were obtained from a least-squares refinement of the setting angles of reflections in the range $3.532^\circ < \theta < 71.535^\circ$. A total of 5724 frames were collected using ω scans, with 0.05 and 0.17 (for high angle reflections) seconds exposure time, a rotation angle of 0.5° per frame, a crystal-detector distance of 65.0 mm, at $T = 173(2)$ K.

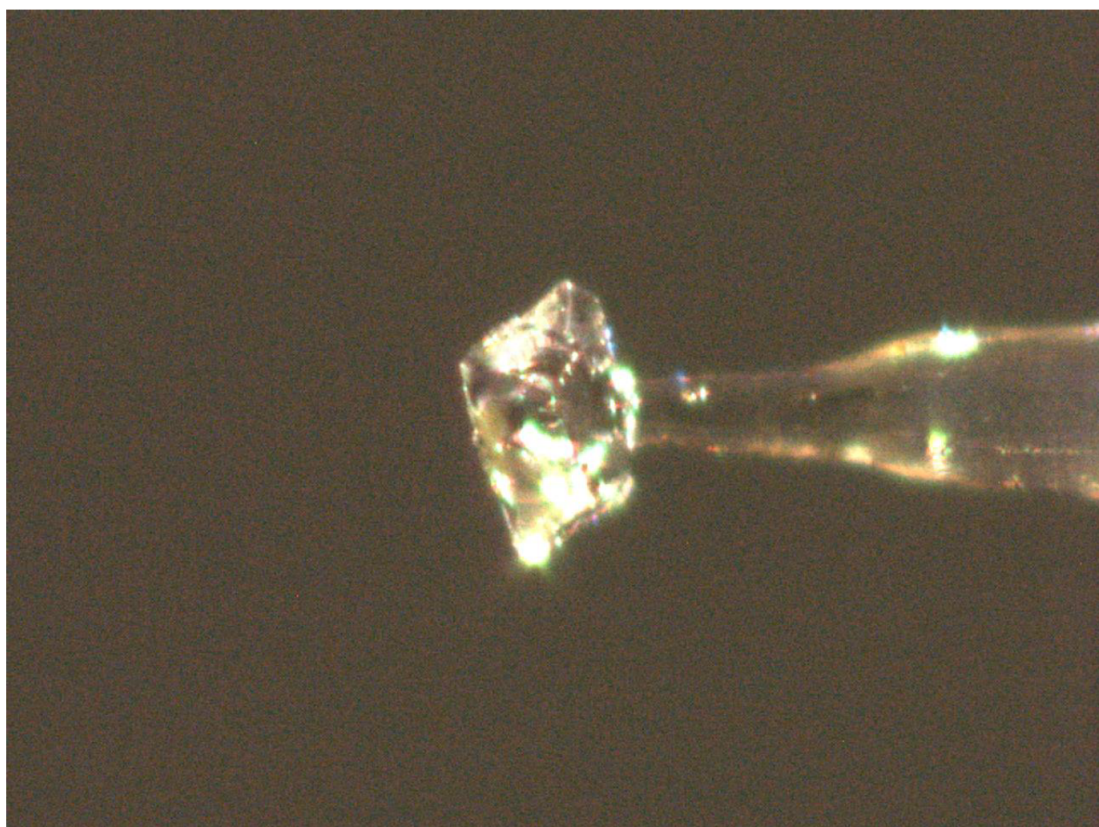
Data reduction was performed using the *CrysAlisPro*⁶ program. The intensities were corrected for Lorentz and polarization effects, and an absorption correction based on the multi-scan method using SCALE3 ABSPACK in *CrysAlisPro*⁶ was applied.

The structure was solved by direct methods using *SHELXT*,⁸ which revealed the positions of all non-hydrogen atoms of the title compound. All non-hydrogen atoms were refined anisotropically. H-atoms were assigned in geometrically calculated positions and refined using a riding model where each H-atom was assigned a fixed isotropic displacement parameter with a value

equal to 1.2Ueq of its parent atom (1.5Ueq for methyl groups).

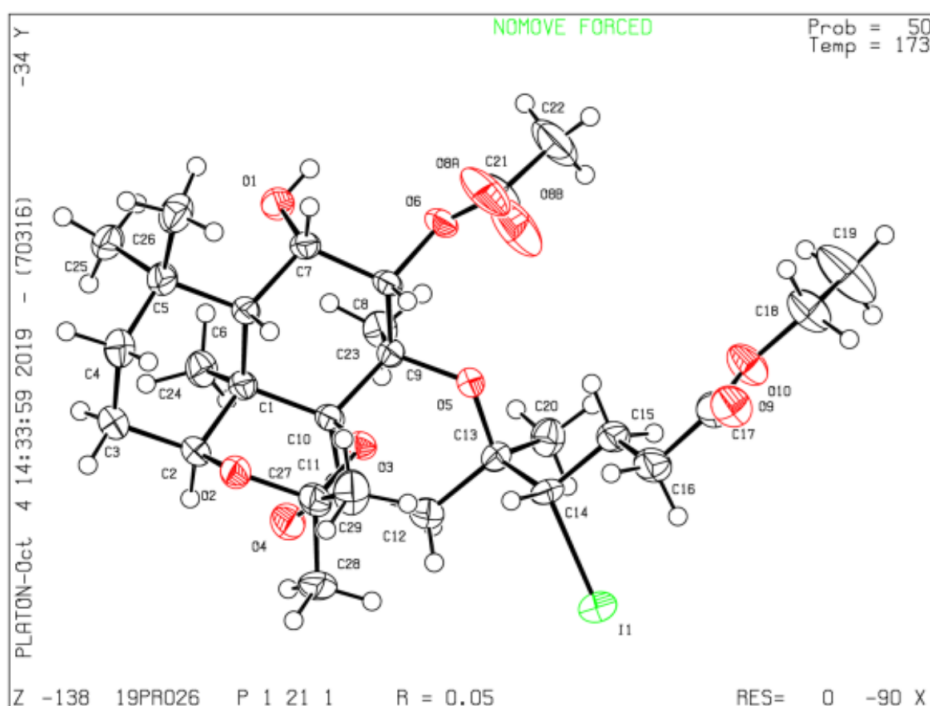
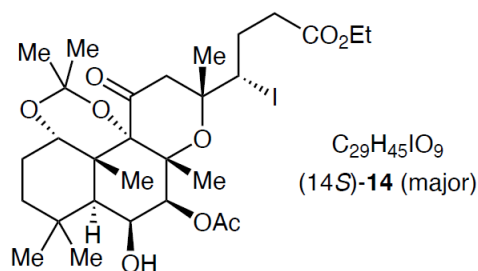
Refinement of the structure was carried out on F^2 using full-matrix least-squares procedures, which minimized the function $\sum w(F_o^2 - F_c^2)^2$. The weighting scheme was based on counting statistics and included a factor to downweight the intense reflections. All calculations were performed using the *SHELXL-2014/7*⁹ program in OLEX2.¹⁰

The structure contains two molecules in the independent part of the unit cell and for this reason atoms were denoted as A and B. Both C14A and C14B have R configuration.



A single crystal of the compound mounted on a glass fiber.

(14*S*)-14 (major):



Crystal-Structure Determination. A crystal of C₂₉H₄₅IO₉ was mounted in air at ambient conditions. All measurements were made on a *RIGAKU Synergy S* area-detector diffractometer⁶ using mirror optics monochromated Cu K α radiation ($\lambda = 1.54184 \text{ \AA}$).⁷ The unit cell constants and an orientation matrix for data collection were obtained from a least-squares refinement of the setting angles of reflections in the range $2.717^\circ < \theta < 71.485^\circ$. A total of 10232 frames were collected using ω scans, with 0.06 seconds exposure time, a rotation angle of 0.5° per frame, a crystal-detector distance of 65.0 mm, at $T = 173(2) \text{ K}$.

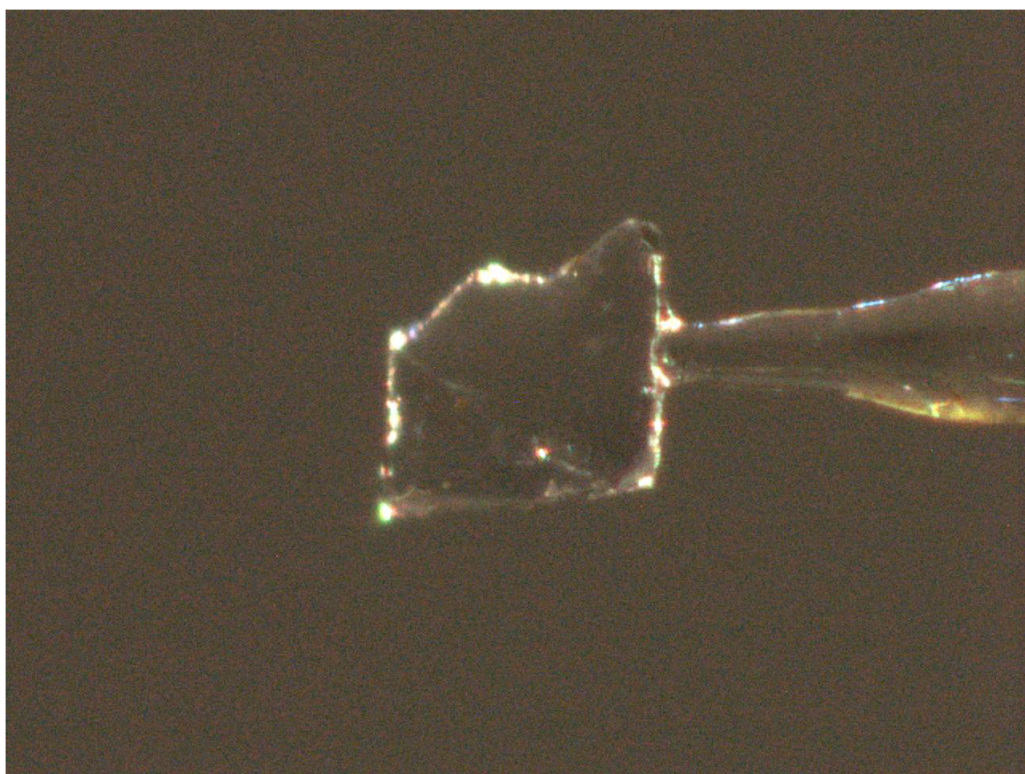
Data reduction was performed using the *CrysAlisPro*⁶ program. The intensities were corrected for Lorentz and polarization effects, and an absorption correction based on the multi-scan method using SCALE3 ABSPACK in *CrysAlisPro*⁶ was applied.

The structure was solved by direct methods using *SHELXT*,⁸ which revealed the positions of all non-hydrogen atoms of the title compound. All non-hydrogen atoms were refined anisotropically. H-atoms were assigned in geometrically calculated positions and refined using a riding

model where each H-atom was assigned a fixed isotropic displacement parameter with a value equal to 1.2Ueq of its parent atom (1.5Ueq for methyl groups).

Refinement of the structure was carried out on F^2 using full-matrix least-squares procedures, which minimized the function $\sum w(F_o^2 - F_c^2)^2$. The weighting scheme was based on counting statistics and included a factor to downweight the intense reflections. All calculations were performed using the *SHELXL-2014/7*⁹ program in OLEX2.¹⁰

The structure contains disordered atom O8, which was been refined into two positions with 0.6 and 0.4 occupancies, respectively.



A single crystal of the compound mounted on a glass fiber.

References

- (1) (a) Alvarez-Manzaneda, E. J.; Chaboun, R.; Alvarez, E.; Cabrera, E.; Alvarez-Manzaneda, R.; Haidour, A.; Ramos, J.M. *Synlett* **2006**, 1829. (b) Koval'skaya, S. S.; Kozlov, N. G.; Kulcitki, V.; Aricu, A.; Ungur, N. *Russ. J. Org. Chem.* **2013**, 49, 303. (c) Moulines, J.; Lamidey, A.-M.; Bats, J.-P.; Morisson, V. *Synth. Commun.* **1993**, 23, 2991.
- (2) (a) Lal, B.; Gidwani, R. M.; Rupp, R. H. *Synthesis* **1989**, 711. (b) Hylse, O.; Maier, L.; Kučera, R.; Perečko, T.; Svobodová, A.; Kubala, L.; Paruch, K.; Švenda, J. *Angew. Chem. Int. Ed.* **2017**, 56, 12586.
- (3) Meyer, D.; Vin, E.; Wyler, B.; Lapointe, G.; Renaud, P. *Synlett* **2016**, 27, 745.
- (4) Imamoto, T.; Koto, H. *Synthesis* **1985**, 982.
- (5) Kogler, H.; Fehlhaber, H.-W. *Magnet. Res. Chem.* **1991**, 29, 993.
- (6) Oxford Diffraction (**2018**). CrysAlisPro (Version 1.171.40.37a). Oxford Diffraction Ltd., Yarnton, Oxfordshire, UK.ed.
- (7) Macchi, P.; Burgi, H.-B.; Chimpri, A. S.; Hauser, J.; Gal, Z. *J. Appl. Cryst.* **2011**, 44, 763.
- (8) Sheldrick, G. *Acta Cryst.* **2015**, A71, 3.
- (9) Sheldrick, G. *Acta Cryst.* **2015**, C71, 3.
- (10) Dolomanov, O. V.; Bourhis, L. J.; Gildea, R. J.; Howard, J. A. K.; Puschmann, H. *J. Appl. Cryst.* **2009**, 42, 339.

6 C–H Functionalization of Manoyl Oxide Derivatives via Selective 1,5-HAT

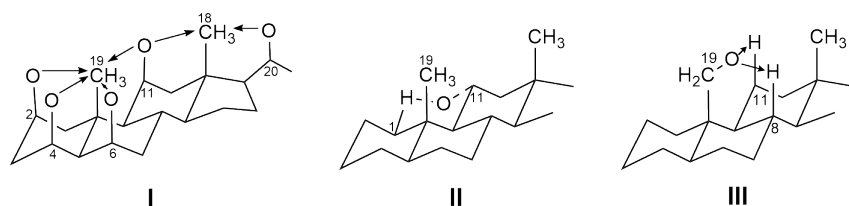
This chapter is dedicated to the investigation of remote C-H functionalization of natural scaffolds (steroids and labdane diterpenoids) via long range 1,5-HAT (up to 3 consecutive shifts), called as "billiard reaction" or "travelling radical". Manoyl oxide and its 13-epimer were used as main substrates in the study.

The project was initiated by Dr. O. Morărescu-Chețraru under the supervision of Prof. Dr. V. Kulçitki, in the collaboration with Prof. Dr. P. Renaud (SCOPES program). Their contribution is greatly acknowledged and some of their results are included in this chapter.

Personal contribution includes: the reactions under dibenzoyl peroxide initiation, derivatization and preparation of the single crystal for X-ray structure confirmation, derivatization using different radical traps.

6.1 Introduction

Direct functionalization of an unactivated sp^3 C–H bond has a large potential in changing classical methodologies in organic chemistry.^{1–3} Transition metal-catalyzed reactions have become the mainstream of C–H activation chemistry in the last years,^{4–7} but metal free reagents would be more efficient from environmental and economical point of view.^{8,9} Among the various approaches to transition metal-free sp^3 C–H functionalization, methods involving radical species have been developed over the past century.^{10,11}



Scheme 6.1: Dreiding models for atom distances determinations in steroids.

Steroids, and other natural products, are particularly favoured class of compounds for studying long-range effects and introduction of a functional group onto a remote non-activated carbon center. Their rigid framework of the carbon skeleton permits reasonably precise knowledge about inter-group distances and spatial arrangements. These effects are classified as: (1) inductive effects, (2) electrostatic field effects, (3) conformational transmission, and (4) direct interaction. The last one, includes those groups that can come close enough to interact with each other or with the reagent simultaneously.¹² Intramolecular abstraction of hydrogen corresponds to the transfer of a hydrogen atom to an attacking free radical in the same molecule, and hence to a 1,5-hydrogen shift, via the most favorable 6-membered ring in the chair form transition state.

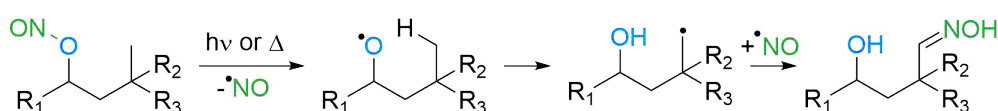
The steric requirements and the influence of neighboring groups determine the course of intramolecular radical reactions. The relative position of reaction centers are very easily assigned in the case of fused ring cyclohexane derivatives, since the spatial arrangement of the ring members and the distances between substituents are fixed in these compounds. Steroids are used as substrates for these reactions, since here the spatial arrangement of the ring members and the distances between substituents are strongly fixed. Particularly alicyclic natural products, such as steroids or terpenoids, exhibit considerable rigidity owing to the fused rings of their skeleton.

Structures **I** to **III** (Scheme 6.1) demonstrate the importance of steric requirements for successful intramolecular radical reactions. The values for internuclear distances between the oxygen atoms and the carbon atoms carrying hydrogen are of 2.5 to 2.7 Å, corresponding very closely to the O–O distances in compounds of the type O–H...O (compounds with hydrogen bridges). For intramolecular hydrogen bridges between C–H groups and oxygen atoms, the C–O distances have been found to be 2.6 to 3.0 Å. The distance between the C-20 oxygen atom and the C-18 carbon in **I** can be reduced to about 2.0 Å, depending on the configuration of the side chain.

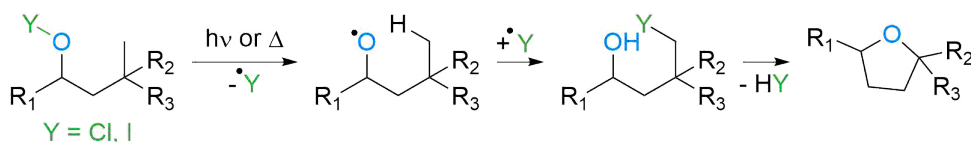
It was concluded that the activation energy for the intramolecular abstraction of hydrogen in fixed systems with an O-C distance of 2.5 to 2.7 Å, in the starting material, reaches a minimum and are so much more rapid than intermolecular ones, then that for distances exceeding 2.8 Å.¹³

Introduction of a functional group onto a remote non-activated carbon center is an particularly prominent radical reaction which has been successfully applied in organic synthesis, especially for functionalization of inaccessible angular methyl groups in steroid molecules and other natural products.^{13–16} The most common reactions of this class are the *Barton reaction*, the *hypohalite reaction* and the *Hofmann-Löffler-Freytag reaction*.¹⁰

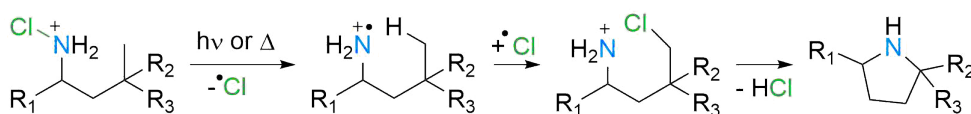
1960, Barton



1963, Hypohalite reaction



1963, Hoffmann-Löffler-Freytag reaction



Scheme 6.2: Radical C-H functionalization methods.

Barton and co-workers^{17,18} reported introduction of an oxime group into an unactivated methyl group using a photolysis reaction of a nitrite compound in studies on steroid chemistry. Photolysis of the nitrite compound generates the corresponding highly reactive alkoxy radical, and it transformed a methyl group into an oxime group via 1,5-hydrogen shift followed by trapping of the resultant radical by nitrogen oxide or to form a tetrahydrofuran derivative (Scheme 6.2). Despite the fact that the *Barton reaction* has often suffered from low yield of the product, it has been indisputable as a valuable synthetic method for a direct functionalization on an unactivated alkyl group.¹⁹

The photolysis of a tertiary hypohalite (readily prepared from the corresponding alcohol) generates alkoxy radical, which abstracts hydrogen from δ -carbon to produce an alkyl radical. The resulting alkyl radical abstracts halogen atom from a second molecule of the hypohalite to give δ -haloalcohol, which is cyclized in presence of a base to form a tetrahydrofuran derivative²⁰ (Scheme 6.2).

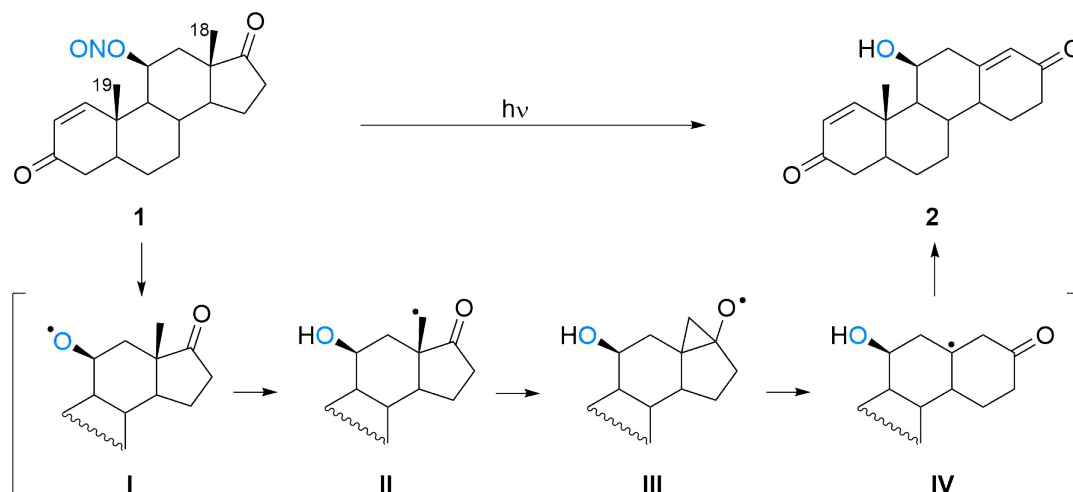
The Hofmann-Löffler-Freytag reaction proceeds via homolytic cleavage of protonated halo-

generated amine to a nitrogen cation-radical, which undergoes an intramolecular abstraction of hydrogen atom from the δ -carbon via a six-membered cyclic transition state to form an alkyl radical. The resulting alkyl radical abstracts a halogen atom from another molecule of halogenated amine to form a protonated δ -halo amine, which on basification undergoes intramolecular cyclization and elimination of hydrohalic acid to form pyrrolidine derivative²¹ (Scheme 6.2).

6.2 Literature Precedents

6.2.1 Steroid and related natural scaffolds modifications

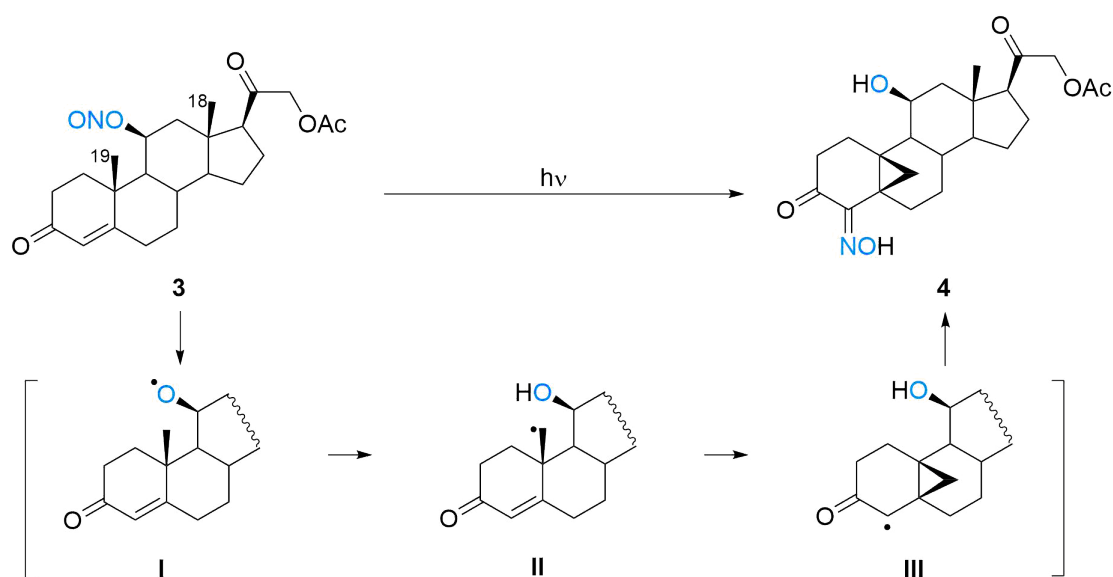
In 1961, Barton et al.²² published the article entitled "A novel rearrangement of the steroid nucleus. Synthesis of 18-nor-D-Homosteroids" which included the first example of the "traveling radical". It was reported the photolytic conversion of steroid 11 β -hydroxy-17-keto nitrite ester **1** to 18-nor-D-homo-4,13-(17 α)-androstadiene-11 β -ol-3,17-dione **2**.



Scheme 6.3: Photolysis of steroid 11 β -hydroxy-17-keto nitrite ester.

The authors explained the free radical rearrangement as a Wagner-Meerwein formally type. The carbon radical at the C-18 methyl group **II**, generated by 1,5-hydrogen shift of the alkoxy radical **I** in the photolysis of nitrite **1**, undergoes a 3-exocyclisation with the adjacent carbonyl group to give a cyclopropyloxy radical **III**.²³ From the carbon radical **IV**, formed by a subsequent cyclopropane ring opening, hydrogen elimination and D-ring enlargement occurs affording the conjugated ketone **2** (Scheme 6.3).

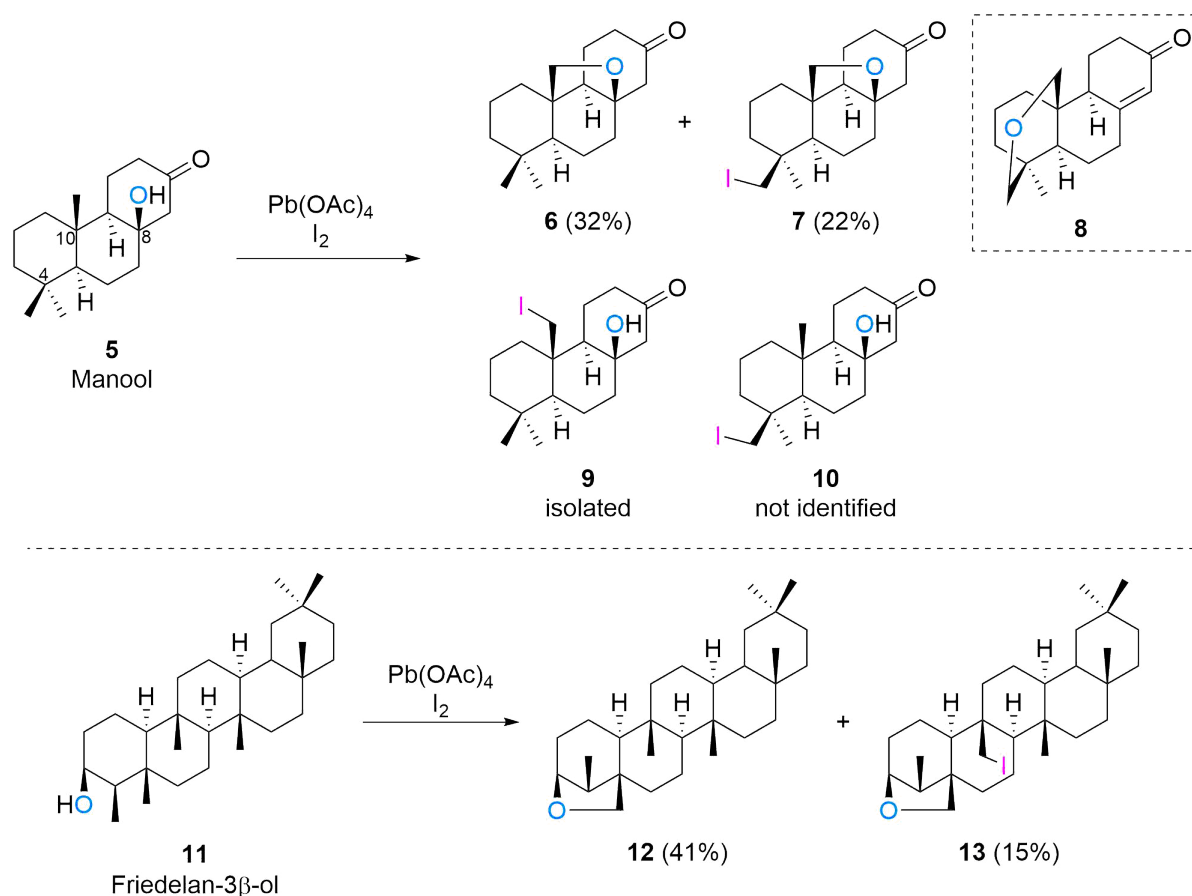
δ -Carbon radicals generated in the Barton photolysis of alkyl nitrites, under certain structural conditions find more stabilisation and deliver rearranged products. Thus, Barton²⁴ reported the photolysis of steroidal nitrites such as corticosterone-11 β -nitrite-21-acetate **3**. In addition to the expected products of functionalization of the angular C-18 methyl group, the 5-oximinosteroid compound **4** was also obtained. The formation of **4** involves an intramolecular 1,5-hydrogen abstraction of the 11 β -alkoxy radical **I** from the C-19 methyl group, thus generating the δ -carbon radical **II**, which is a 3-butenyl-type radical. The electron-deficient olefinic bond is present in the appropriate position and it undergoes a 3-exo-cyclisation to give the radical **III** which was quenched by the nitroso radical to give the 5-oximinosteroid compound **4** (Scheme 6.4).²⁴



Scheme 6.4: Photolysis of Corticosterone-11 β -nitrite-21-acetate.

Few years later, Wenkert and Mylari²⁵ reported the application of lead tetraacetate oxidation of alcohols for the functionalization of saturated hydrocarbon centers (especially methyl groups) in close proximity to the original hydroxy functions. When manool **5** was exposed to hypoiodite oxidation in cyclohexane or benzene solution, the expected ketooxide **6** (32%) was obtained together with the iodoketooxide **7** (22%), which would be generated after a two oxidations of **5**. Rigorous proof of the structure of iodoketooxide **7** was obtained from its treatment with sodium bicarbonate in dimethyl sulfoxide, delivering the product **8**. In order to understand the formation of **7** different reaction conditions were screened (reduction of reaction time, concentration of oxidizing agents). The unstable iodohydrin **9** was isolated, however no traces of primary intermediate **10** was found. Short heating of a pyridine solution of **9** yielded the ketooxide **6**, while lead tetraacetate-iodine oxidation gave the iodo compound **7** (51%) (Scheme 6.5). The novel long-range oxidation appears to consist of two consecutive alkoxy radical generated 1,5-hydrogen shifts, the second of which represents a intramolecular hydrogen abstraction from a saturated carbon-hydrogen bond site by a carbon radical. The exclusivity of iodination of the 4 β -methyl group is probably a reflection of the steric congestion at the 10 β -iodomethyl location.²⁵

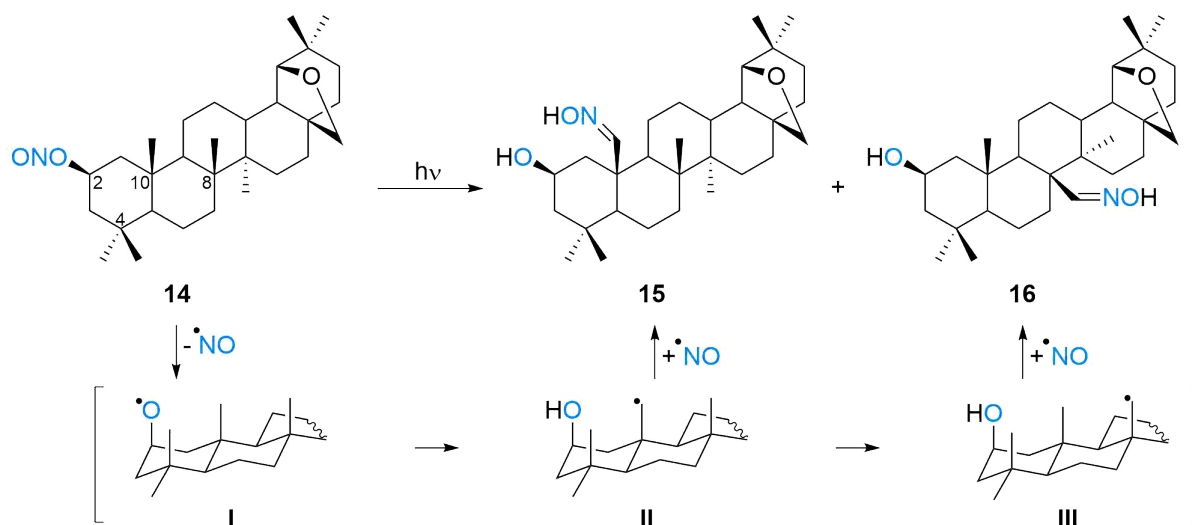
A second example of the "billiard reaction" reported by Wenkert and Mylari²⁵ is the lead tetraacetate oxidation of friedelan-3 β -ol **11**. Compounds **12** and **13** were identified as major products of the reaction, with 41 and 15% yield respectively (Scheme 6.5). Although the palladium-induced hydrogenolysis of the iodide **13** yielded **12** and the mechanistic interpretations supporting the most likely structure, there is no rigorous proof of the structure of **13**. Considering that the friedanol skeleton should permit three 1,5-hydrogen shifts to take place, no products of overoxidation of demonstrated constitution derived from such changes have been isolated and characterized. However, two of the minor products, may be such representatives.²⁵



Scheme 6.5: Lead tetraacetate oxidation of Manool and Friedelan-3 β -ol.

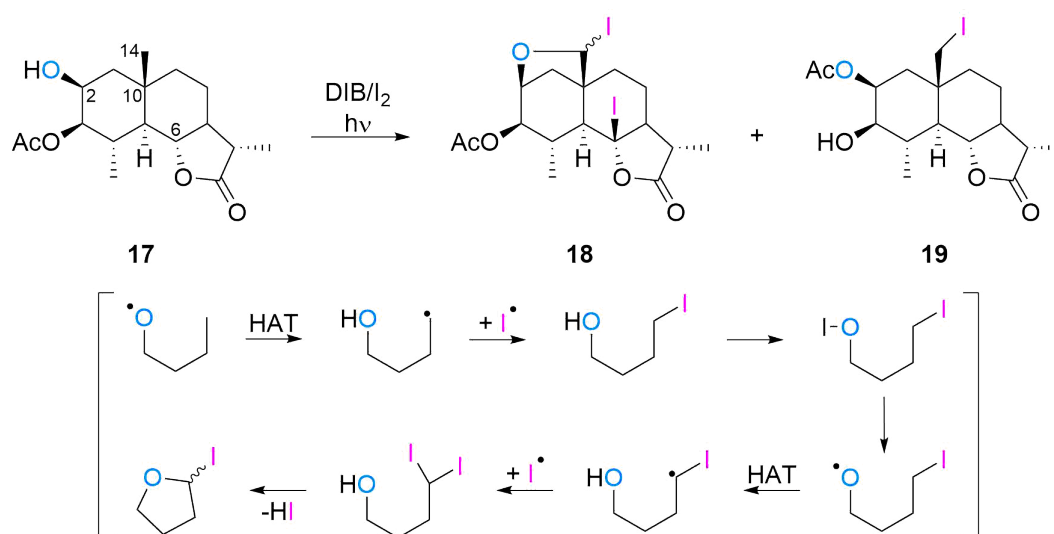
Sejbal and co-workers^{26–28} were interested in study the directed functionalization of oleanane type triterpenoids: which of the 2 axial methyl groups - 4 β and 10 β (close to the 2 β -hydroxy group) - will be attacked and how the functionalization is influenced by substituents on the ring A. A remarkable photolytic transformation under Barton condition of 2-nitrite **14** lead to the formation of two regioisomeric oximes **15** and **16** (Scheme 6.6).

The functionalization of the rather distant 8 β -methyl group in the photolysis can be explained by two consecutive 1,5-hydrogen shifts between the 1,3-*syn*-axial groups. The first consists in H \cdot radical transfer from the 10 β -methyl group to the oxygen radical **I** generated by homolytic cleavage of the 2 β -nitrite **14** forming intermediate **II**. The second is a transfer from the 8 β -methyl group to the radical at C-25 to give **III**. Final recombination with the NO \cdot radical gives the desired oximes **15** and **16** (Scheme 6.6). Products of functionalization in the 4 β -position have not been detected, which indicated that the distance between the hydrogen atom of the 10 β -methyl group and the 2 β -oxygen atom is shorter than in the case of the 4 β -methyl group. The remotely functionalized C-25 and C-26 oximes were further converted into corresponding nitriles. Similar transformations could be performed on ursane, hopane and lupane skeletons.²⁶ Hernandez et al.²⁹ reported the cascade of 1,5-shifts on vernolepin derived scaffold. Irradiation



Scheme 6.6: Functionalization of Oleanane triterpenoids.

of the hydroxy acetate **17** in cyclohexane, in the presence of (diacetoxyiodo)benzene (DIB) (1.5 equiv) and iodine (0.5 equiv), with two tungsten-filament lamps at 40 °C for 10.5 h, gave a mixture of compounds in moderate overall yield. Worth to mention the formation of diiodo derivative **18** and iodohydrin **19** (Scheme 6.7).

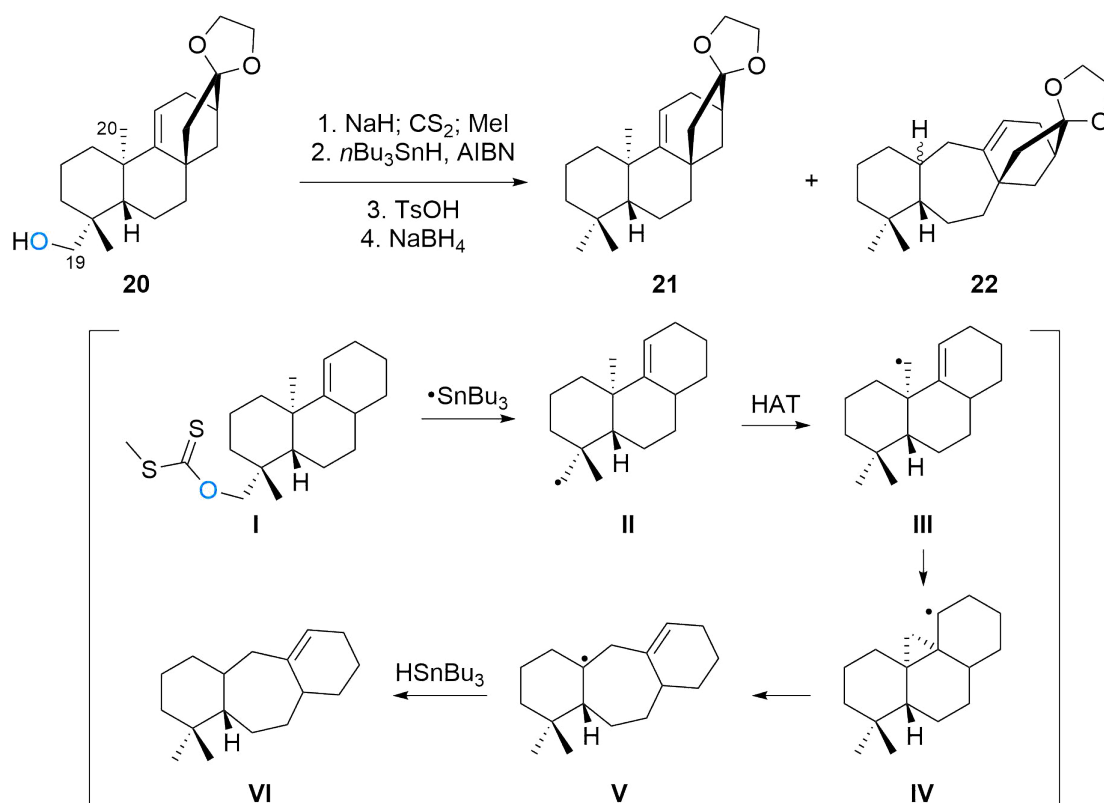


Scheme 6.7: Functionalization of Vernolepin derivative.

The author²⁹ explained that the diiodo derivative **18** is probably produced by intramolecular hydrogen abstraction of the C-6 β hydrogen from the initially formed C-14 radical and two consecutive hydrogen abstractions at C-14 hydrogens from the C-2 alkoxy radical with subsequent cyclization to the iodotetrahydrofuran group¹⁵ (Scheme 6.7). Iodohydrin **19** can be produced by 1,2-alkoxy radical rearrangement via an orthoacetate radical intermediate.

The beyerane and kaurane diterpenoids derivatives were as well submitted to functionalization

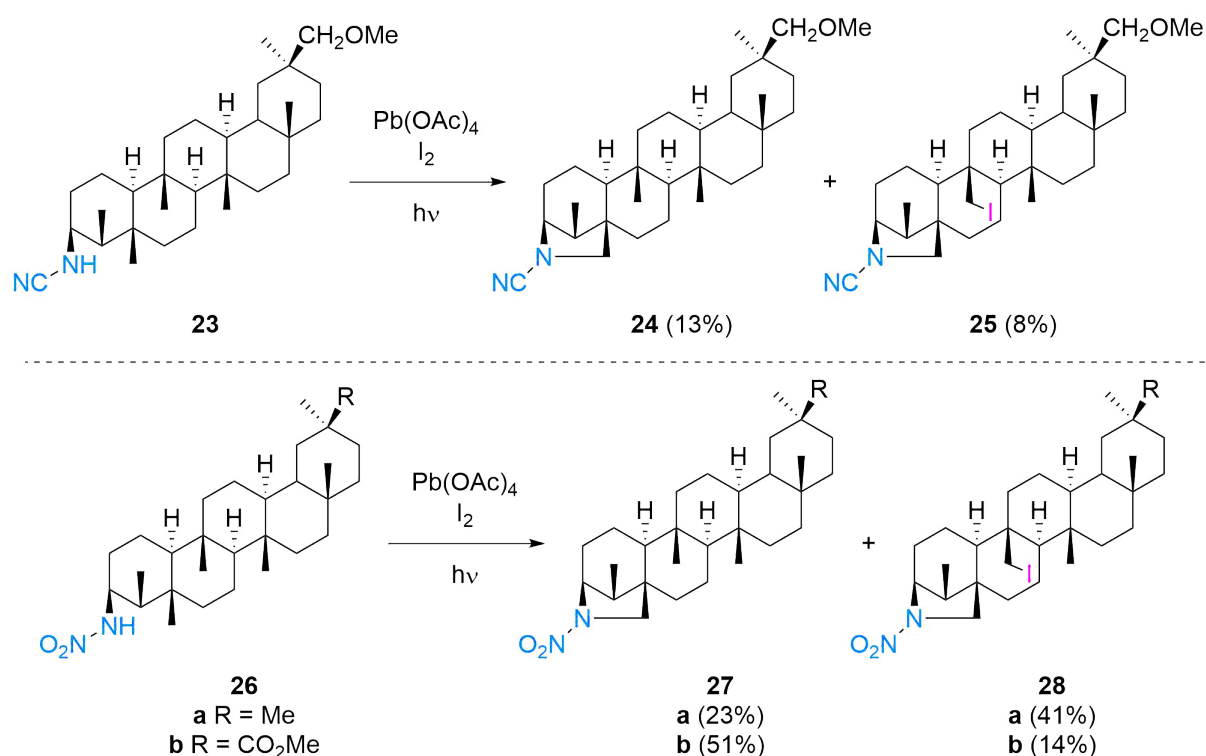
of angular methyl groups under radical conditions.^{30,31} Zhang³² reported an interesting example of rearrangement on the kaurane scaffold via a xanthate intermediate. The alcohol **20** was derivatized to the xanthate **I** and treated with tri-*n*-butyl-stannane and AIBN as radical initiator. To facilitate the separation, the obtained mixture was reduced with sodium borohydride. Together with the expected major product **21**, the rearranged by-product **22** was identified. The authors³² concluded that the intermediate C-19-yl radical **II** had undergone a 1,5-transannular shift to form the C-20-yl radical **III**, which then isomerised to **VI** via the cyclopropylcarbinyl radical **IV**. The final radical **VI** is later reduced by tributyltin hydride and sustain the chain (Scheme 6.8). The 1,5 shift could also have occurred in the saturated substrate, but could not have led to rearrangement and would therefore not have been apparent.



Scheme 6.8: Rearrangement on the Kaurane skeleton.

Intramolecular functionalizations due to alkoxy radicals have been exhaustively studied, however little attention has been devoted to those promoted by nitrogen radicals. Based on the Hofmann-Loeffler-Freytag reaction, cyclic amines can be prepared by thermal or photochemical fragmentation of *N*-haloamines. As occurs with the alkoxy radical, the mechanism for the hydrogen abstraction involves formation of a neutral radical which is obtained by photolysis of the corresponding *N*-iodo derivative generated in situ by reaction of the cyanamide with iodine and lead tetraacetate or diacetoxyiodobenzene as oxidative agents.^{33,34}

The group of Suarez was specialized on functionalization of non-activated carbon atoms initiated by neutral aminyl radicals (produced by photolysis of the corresponding *N*-iodonitroamines, *N*-iodophosphoramidates, or *N*-iodocyanamide). In 1987,³³ they described the synthesis of



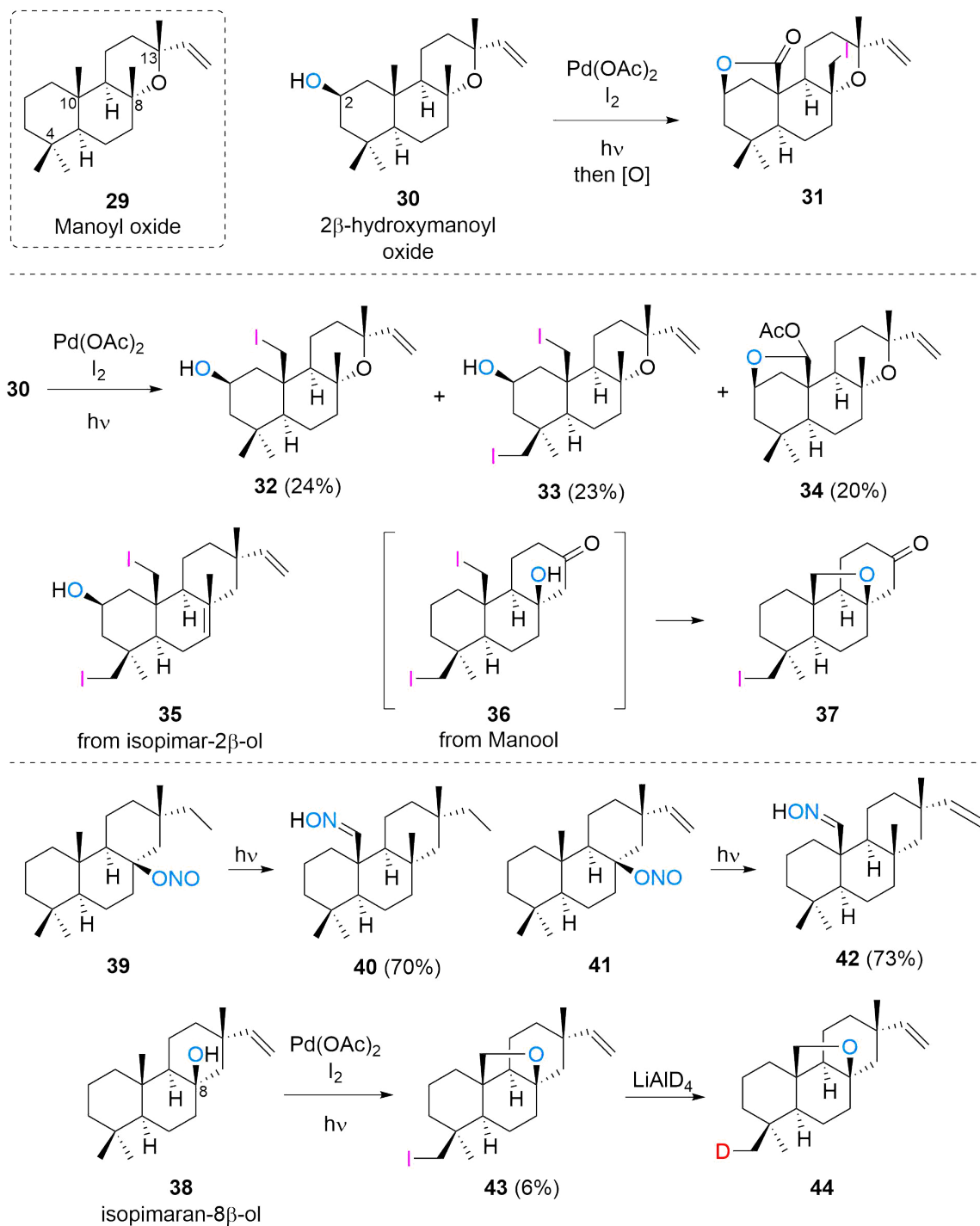
Scheme 6.9: Functionalization of triterpenoids via aminyl radical formation.

several steroidal and terpenic *N*-cyanoepimino compounds from the corresponding cyanamides. An interesting case was the photolysis of 29-methoxyfriedelan-3 β -ylcyanamide **23** which resulted in the formation of epimines **24** (13%) and **25** (8%) as by-products (Scheme 6.9). Formation of **24** was agreed with expectation. To produce **25**, two consecutive hydrogen abstractions were needed in a manner similar to that previously reported for friedelan-3 β -ol **11** (Scheme 6.5).²⁵

Another "billiard reaction" via aminyl radical, was reported by the same group one year later. de Armas et al.³⁴ described the photolysis of the nitroamino-friedelane derivatives **26a, b** under lead tetraacetate and iodine oxidation conditions. Two types of compounds were formed in each case, the expected *N*-nitroimines **27a, b** and the iodo compounds **28a, b** (derived from two consecutive 1,5 hydrogen abstractions) (Scheme 6.9).

6.2.2 Manoyl oxide derivatives functionalization

Manoyl oxide **29** and its derivatives were as well involved in long-range functionalization studies (Scheme 6.10). The advantage of this scaffold is that its rigid structure increases the proximity between the 4 β -, 8 β -, 10 β - and 13 β -methyl groups.



Scheme 6.10: Functionalization of Manoyl oxide and Isopimarane derivatives.

The first report was published in 1967, by Wenkert and Mylari.²⁵ The authors mentioned briefly

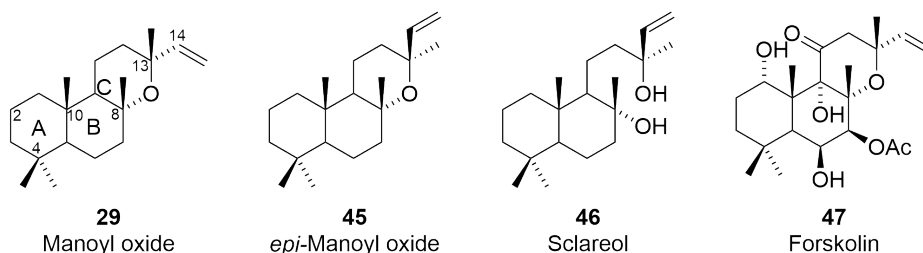
the formation of compound **32** upon lead tetraacetate-iodine oxidation followed by Jones oxidation of 2β -hydroxymanoyl oxide **30**. Few years later, Ceccherelli et al.³⁵ reported the same oxidation of the alcohol **30** upon lead tetraacetate and iodine in benzene, however three different compounds were reported: iodohydrin **32**, diiodohydrin **33**, and acetoxytetrahydrofuran **34** in 24%, 23%, and 20% yields respectively (Scheme 6.10). The structures of the three products of oxidation of alcohol **30** were characterized by NMR spectroscopy and reveal that the 10β -methyl moiety is more vulnerable to free-radical oxidation than the 4β -methyl group, a fact ascribable to the angular methyl function being in the midst of the rigid ring skeleton. Ceccherelli et al.³⁵ observed the same behaviour upon oxidative conditions for isopimarane and manool scaffolds (Scheme 6.10, **35-37**), showing the generality of the oxidation reaction.

Corbett and Wilkins¹⁴ were investigating the functionalization of angular methyl groups in isopimarane diterpenoids (analogues of manoyl oxide). The authors report the photolysis of nitrite esters **39** and **41** that delivered only the oximes **40** and **42** respectively. The oxidation of Isopimarane- 8β -ol **38** with lead tetraacetate and iodine delivered the iodo-compound **43** in a low yield. Reduction of **43** with lithium aluminium deuteride gave the deuterio-labeled derivative **44** confirming the structure (Scheme 6.10).

Functionalization of the 13β -methyl group did not appear to occur, and the vinylic group did not effect the course of this reaction. They explained that the relationship of the 10β -methyl to the 8β -hydroxy group is rigidly fixed by the carbon framework, and that the 13β -methyl group is not in a true 1,3-diaxial relation to the 8β -hydroxy group. Rings **A** and **C** show to be more flexible than ring **B** and that any distortion or flattening of these rings would affect the 13β - and 4β -methyl groups. The over-oxidative functionalization of the 4β -methyl group indicates that ring **A** does not deviate significantly from the chair conformation, which is different with the ring **C**. The later one, must be appreciably flattened, thus moving the 13β -methyl group away from its theoretical 1,3-diaxial relation to the 8β -hydroxy group.¹⁴ Later, the authors extended the long-range functionalization studies on the hopane triterpenoid derivatives.

6.3 Results and Discussion

We have initiated a program of modification of available terpenic scaffolds by ATRA and related radical reactions.^{36,37} These transformations are very efficient and can be run under mild reaction conditions. It represents an ideal tool for late-stage structure modification and molecular editing within SAR studies of complex molecules.

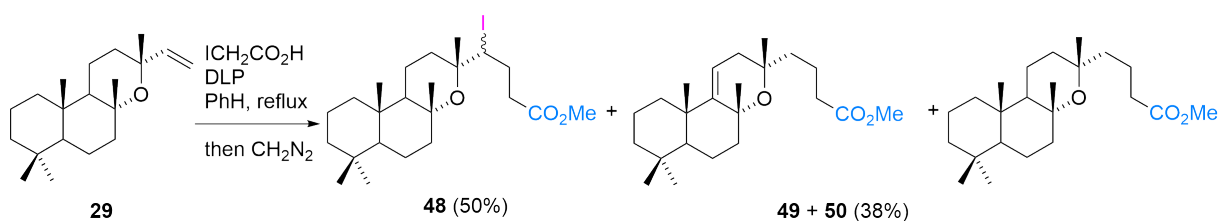


Scheme 6.11: Labdanic diterpenoids.

A special case of the studies is represented by the labdanic diterpenoids manoyl oxide **29** and *epi*-manoyl oxide **45**. Both substrates can be easily obtained from commercial sclareol **46**, and represent the carbon skeleton of forskolin **47** (Scheme 6.11). The vinyl lateral chain of compounds **29** and **45** presents interest for free radical functionalization and introduction of diverse functional groups.

6.3.1 Manoyl oxide modifications

At the beginning we attempted to perform the ATRA reaction on manoyl oxide **29** using several halogenated alkylating agents with electron-accepting functional groups and dilauroyl peroxide (DLP) as radical initiator.³⁸

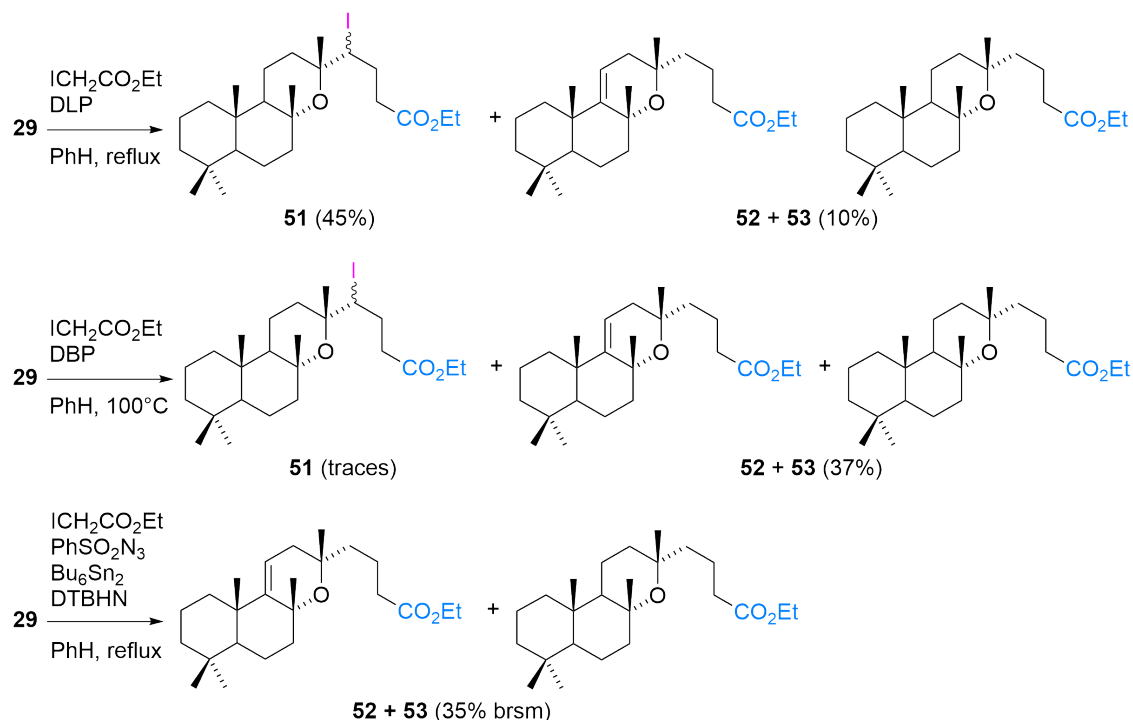


Scheme 6.12: ATRA reaction on manoyl oxide using iodoacetic acid.

Treatment of **29** with iodoacetic acid $\text{ICH}_2\text{CO}_2\text{H}$ led to the quick consumption of the starting material in the presence of dilauroyl peroxide in refluxing benzene. The reaction product represented a rather complex mixture. A tentative separation by flash chromatography failed, and in order to reduce the tail effect of the free carboxylic acids, methylation with an ethereal solution of diazomethane was performed. Chromatographic separation of obtained methyl esters resulted in the isolation of the expected 1,2-addition product **48** and also a fraction containing alkylated compounds which lack the iodine in their structure (Scheme 6.12). A careful examination of NMR data led to the conclusion that this fraction represents a mixture of two compounds, the

major one being olefin **49**, which could be possibly formed after a 1,5-radical migration, followed by elimination. The structure of the other component of the isolated fraction was tentatively assigned as **50**, which can be derived from a reductive hydrogen radical abstraction (Scheme 6.12).

The complex nature of reaction products suggested a parallel substrate reactivity, due to acid catalyzed transformations induced by free iodoacetic acid. In order to diminish this effect, reaction of **29** with ethyl iodoacetate $\text{ICH}_2\text{CO}_2\text{Et}$ under the same conditions has been investigated (Scheme 6.13).



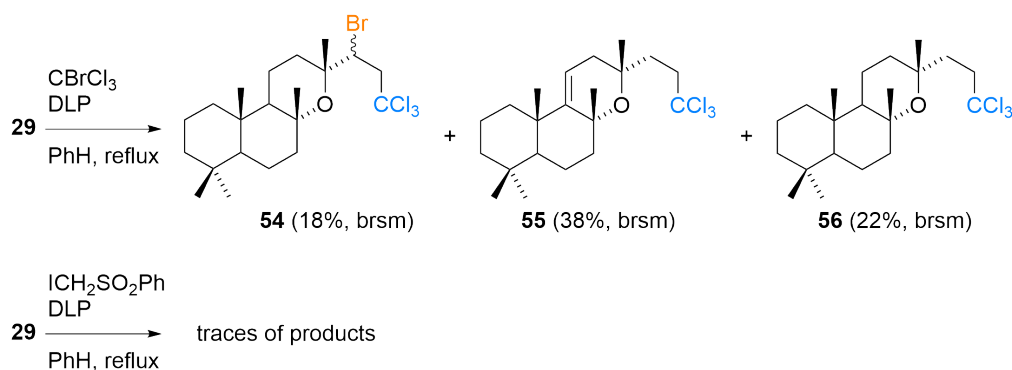
Scheme 6.13: ATRA reaction and carboazidation attempt on manoyl oxide using ethyl iodoacetate.

The conversion rate was slightly slower in this case, but reaction selectivity was much better. The main reaction product was isolated by flash chromatography and according to NMR data its structure assigned as iodide **51** (Scheme 6.13). A minor fraction was also isolated and the NMR data showed a mixture of esters **52** and **53**, similar to esters **49** and **50** derived from reaction of **29** with iodoacetic acid. All attempts to separate individual **52** and **53** failed.

Dibenzoyl peroxide (DBP) was tried as radical initiator due to its higher oxidation potential and higher temperature required for decomposition.^{39,40} Performing the reaction of **29** with ethyl iodoacetate under DBP conditions in PhH at 100°C , a mixture of products **52** and **53** in 37% yield (4:6 ratio) was obtained (Scheme 6.13). Traces of ATRA product **51** was identified, that could be associated with decomposition of iodides at this high temperature.

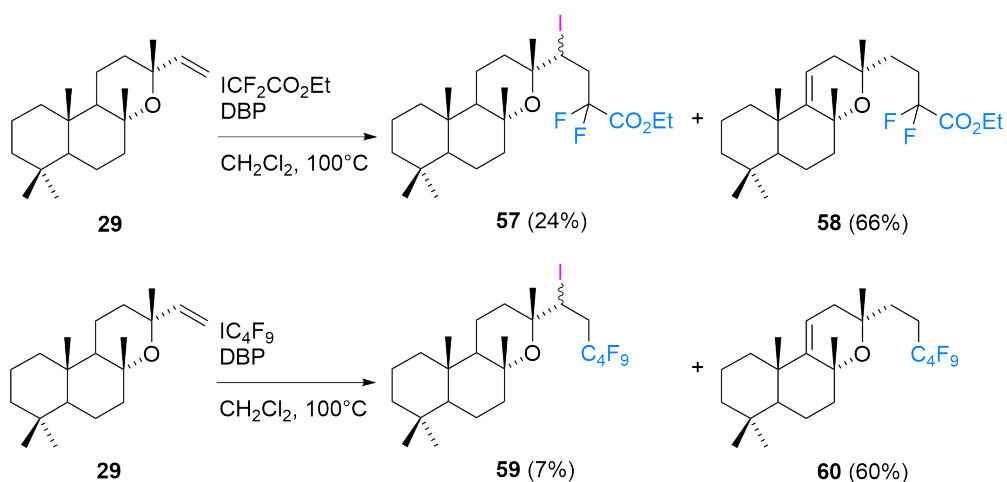
On the other hand, the reaction of the same substrate under carboazidation conditions with

ethyl iodoacetate and phenylsulfonyl azide as azide source led to the same mixture of esters **52** and **53** and no azide radical transfer was observed (Scheme 6.13).



Scheme 6.14: ATRA reaction on manoyl oxide using bromotrichloromethane.

Manoyl oxide **29** reacted with bromotrichloromethane CBrCl_3 with a different selectivity. Bromide **54**, the product of 1,2-addition, was minor in this case and the predominating products **55** and **56** have been isolated in individual form (Scheme 6.14). Their structure was assigned univocally on the basis of 2D-NMR spectra. The difference in the reaction selectivity of the same substrate with different alkylating agents can be explained by the lower transfer rate of bromine radical vs. iodine (2.7×10^4 vs. 2.6×10^7).⁴¹ In line with this conclusion, using the massive iodomethyl phenyl sulfone⁴² as alkylating agent resulted in a very sluggish reaction and complex reaction product profile. No individual reaction product was isolated (Scheme 6.14).



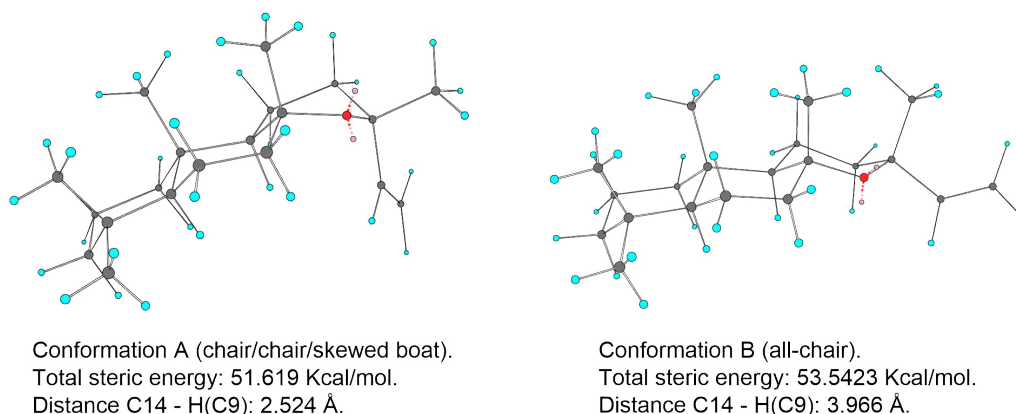
Scheme 6.15: ATRA reaction on manoyl oxide using fluorinated alkylating agents.

Reaction of **29** with ethyl iododifluoroacetate $\text{ICF}_2\text{CO}_2\text{Et}$ in CH_2Cl_2 at 100°C delivered the clean product **58** in 66% yield together with 18% of ATRA product **57**. Reaction of **29** with perfluorobutyl iodide IC_4F_9 delivered the clean product **60** in 60% yield and 7% of ATRA product **59**

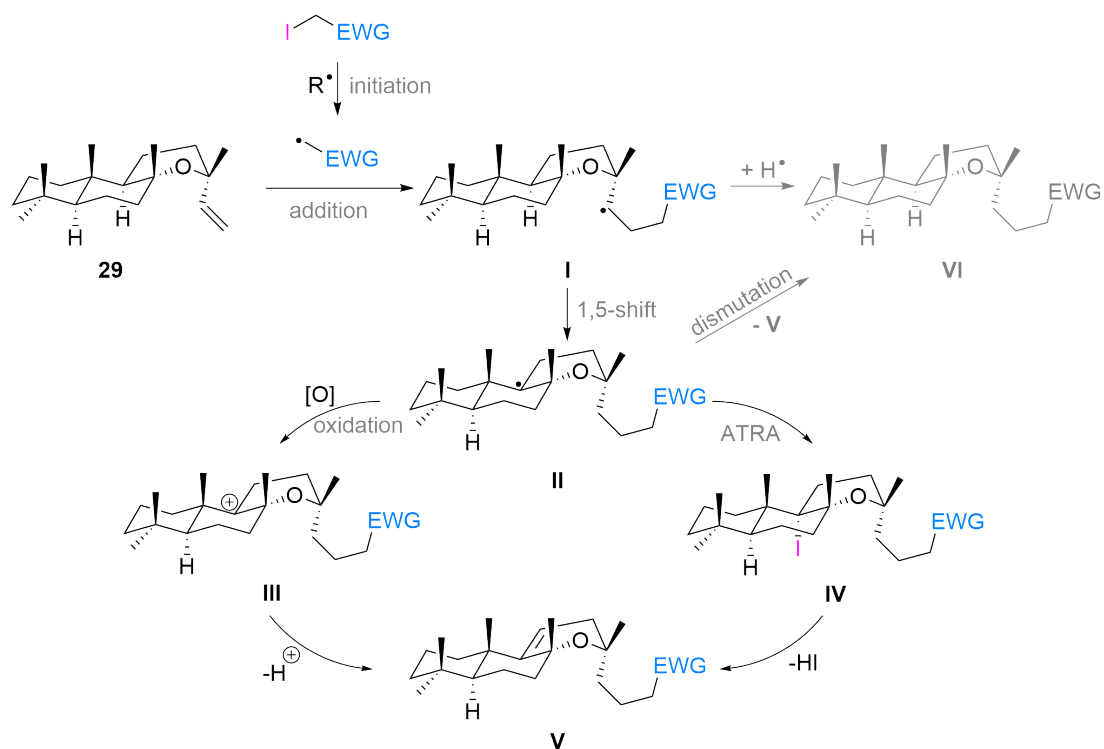
(Scheme 6.15). This results are in accordance with a fast 1,5-hydrogen shift and exclusive formation of the HAT product.

The most interesting aspect of these transformations is represented by manoyl oxide derivatives with the unsaturation in the cycle C. Formation of compounds **49**, **52**, **55**, **58** and **60** - can be accounted for a radical translocation mechanism leading to a formal remote functionalization. 1,5-Translocations are known phenomena in radical chemistry (Chapter 6.2) and include generation of a carbon or heteroatom centered radical, followed by a 1,5-hydrogen atom transfer and trapping of the translocated radical by either intramolecular or intermolecular processes. This pathway represents a very important approach for remote functionalization of unactivated C-H bonds and the reported procedures basing on this strategy rely upon different methods of initial radical generation.

The structure of substrate **29**, with a rigid condensed cyclic system, favors intramolecular radical translocation, leading to a formal remote C-H functionalization. An examination of molecular models revealed that a favorable steric arrangement of the lateral chain so that the distance between the radical center at C-14 and the hydrogen at C-9 to be abstracted shorter than 3\AA ⁴³ can be achieved. The corresponding conformation of **29** (Conformation A, Scheme 6.16) has the oxacycle in a skewed-boat and the calculated total steric energy is 51.619 Kcal/mol.²⁶ The other stable conformation of this molecule which is all-chair (conformation B, Scheme 6.16), has a slightly higher steric energy of 53.5423 Kcal/mol and a much longer distance between the C-14 and the hydrogen at C-9. This data support a 1,5-HAT mechanism following the radical additions to manoyl oxide **29**, leading to isolated products **49**, **52**, **55**, **58** and **60**.

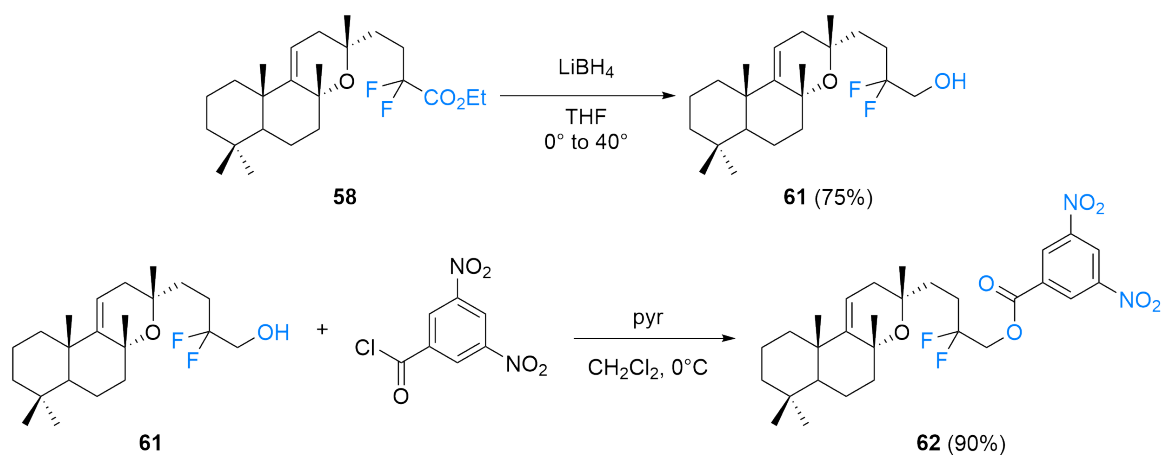


Scheme 6.16: Optimized conformation of manoyl oxide **29**.



Scheme 6.17: Proposed mechanism for the 1,5-HAT on manoyl oxide.

From the mechanistic point of view the 1,5 hydrogen atom transfer on manoyl oxide scaffold can be explained with the represented Scheme 6.17. The secondary carbon center radical **I** formed after the radical addition of the radical precursor on the olefin, will perform the 1,5-hydrogen abstraction and deliver the tertiary carbon center radical **II**. The tertiary carbon center radical would rather get oxidized by DLP or DBP⁴⁴ to form the tertiary carbon cation **III** or to undergo iodine atom transfer to form the unstable intermediate **IV**. Both intermediates, **III** and **IV**, would then deliver the unsaturated final product via an H^+ or HI elimination. The formation of the hydroalkylated species **VI** almost in a 1:1 mixture with **V** could be explained by disproportionation of **II** or by a competitive intermolecular HAT involving radical **I**^{45,46} (Scheme 6.17).



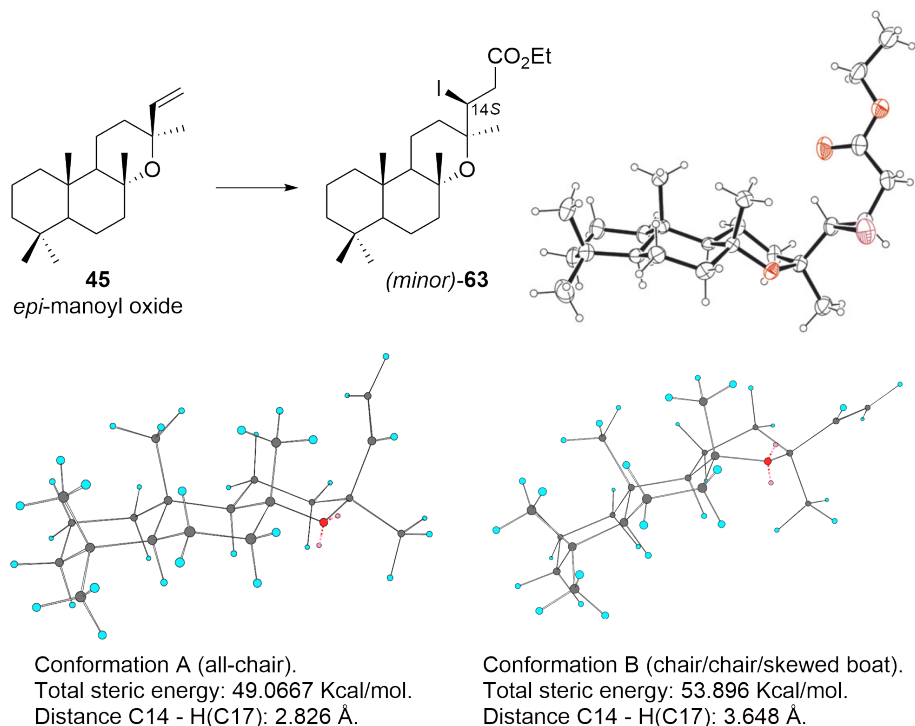
Scheme 6.18: Derivatization to form crystalline derivatives for X-ray single crystal analysis.

From the structure confirmation point of view, functionalization to a crystalline derivative was performed. Compound **58** was reduced to the alcohol **55**, which was subject to esterification with *p*-nitrobenzoyl chloride affording the compound **56** as yellowish solid (Scheme 6.18). Crystallization attempts are on going.

6.3.2 *epi*-Manoyl oxide modifications

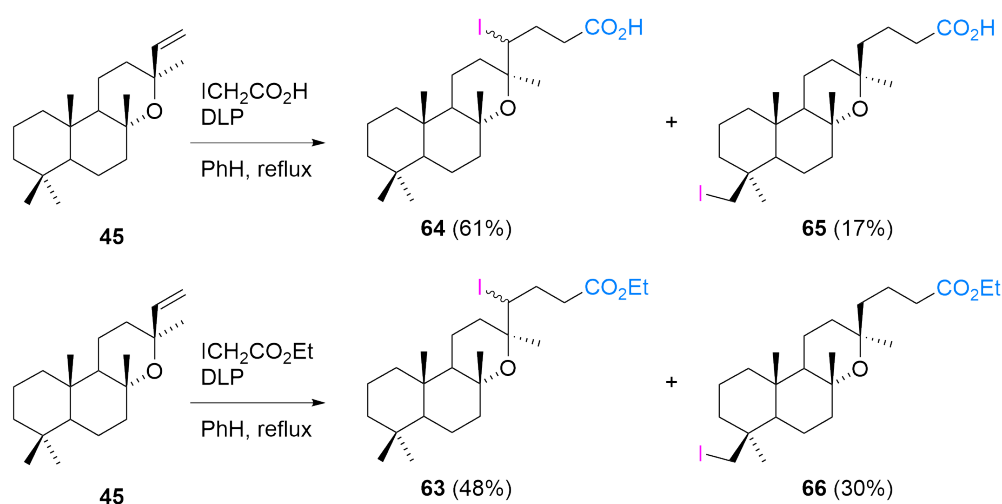
Inspired by the result for the manoyl oxide **29**, we further continued to investigate the ATRA reactions on epimeric oxide **45**. In the first attempts it showed the same good reactivity under the conditions reported above and that the conversion rate and product distribution is strongly dependent on the alkylation agent used.

Conformational studies on substrate **45**, showed that the all-chair conformation is the most stable and ensures a shorter distance between radical translocation centers (Scheme 6.19, Conformation A). The other chair/chair/skewed boat conformation is unfavorable to 1,5-HAT and less stable, due to the higher steric energy (Scheme 6.19, Conformation B). The all-chair conformation was confirmed by the X-ray measurement of the minor iodoalkylated product of *epi*-manoyl oxide **45** reported in the previous work.³⁷ One could imagine that 3 consecutive 1,5-hydrogen shifts are possible on this skeleton.



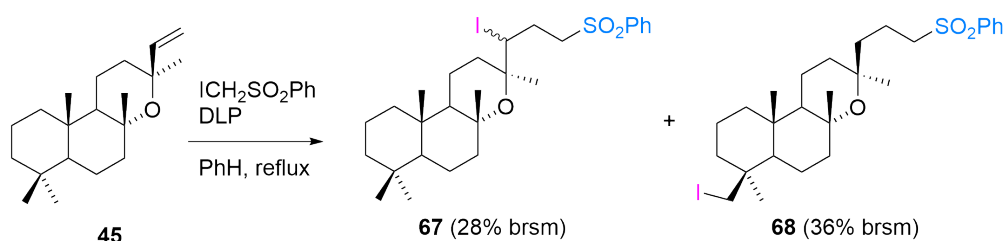
Scheme 6.19: Optimized conformation of *epi*-manoyl oxide **45**.

Performing iodoalkylation of **45** with iodoacetic acid and its ethyl ester under the DLP initiation conditions resulted in the formation of similar iodides **63-64** as major reaction products (Scheme 6.20). Along with these major products, a minor fraction of iodides has been also isolated and its structural characterization led us to the conclusion of final addition of iodine at the distal methyl from cycle A of substrate. These distal iodides **65** and **66** have been identified in the reaction products derived from all involved alkylation agents, but their yield was different. The highest yield of the distal iodide **66** was observed when ethyl iodoacetate was used, and lower yield for iodoacetic acid promoted alkylation and formation of **65**.



Scheme 6.20: ATRA on *epi*-manoyl oxide using iodoacetic acid and its ethyl ester.

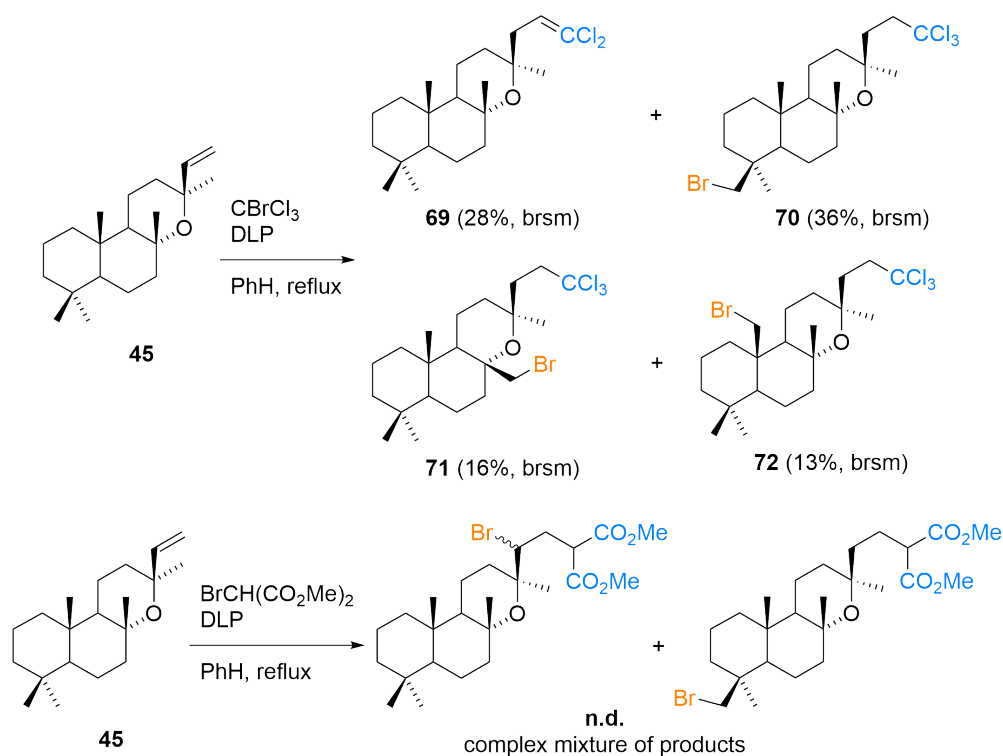
Following our assumption that radical stability govern the radical translocations, we investigated alkylation of *epi*-manoyl oxide **45** with iodomethyl phenyl sulfone. In this case the reaction was much more sluggish showing a modest conversion rate of 25% due to less efficient iodine atom transfer. However, the product distribution was in favor of the distal iodide **68**, which was formed along with expected iodoalkylated product **67** (Scheme 6.21).



Scheme 6.21: ATRA on *epi*-manoyl oxide using iodomethyl phenyl sulfone.

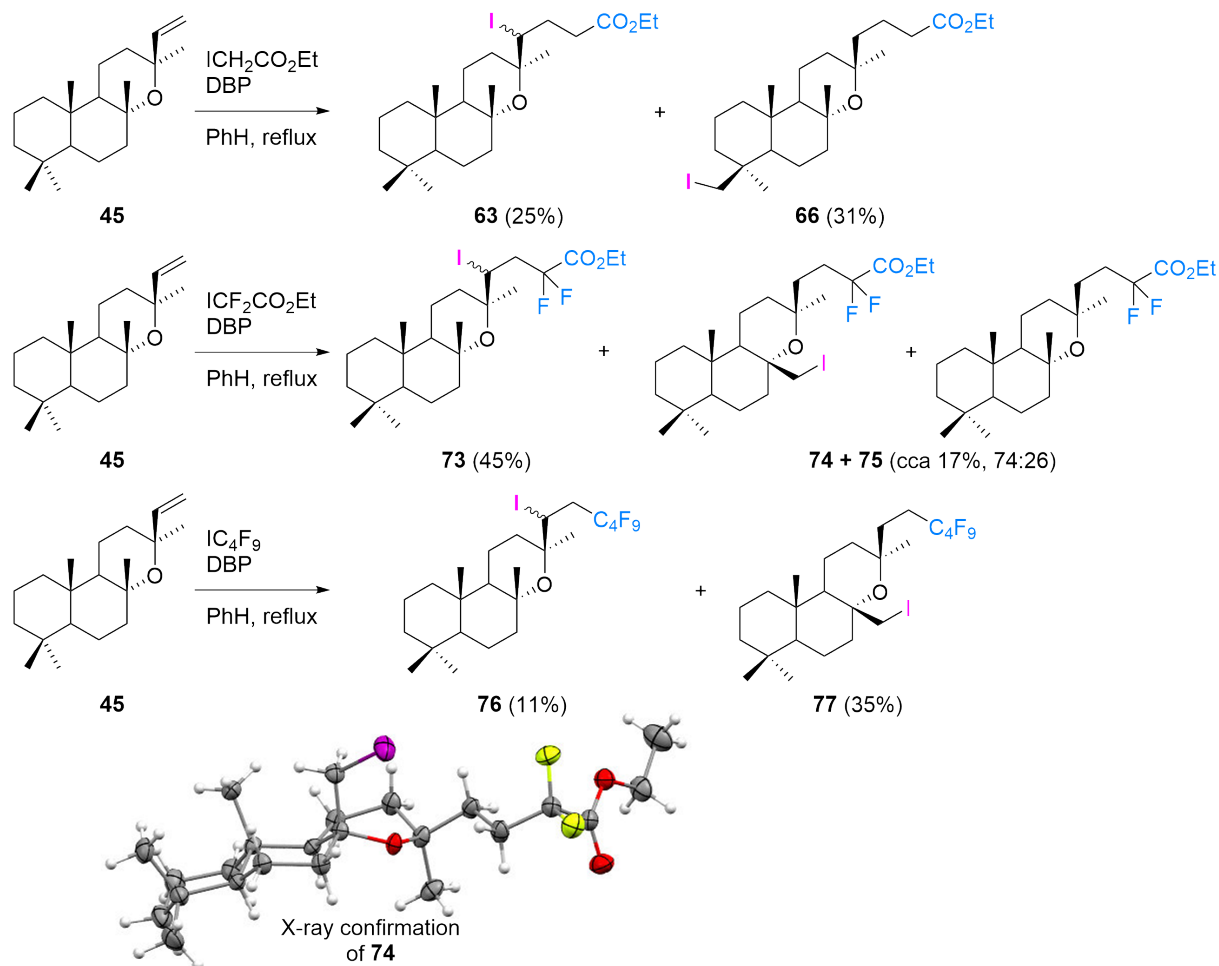
Switching to the CBrCl_3 alkylation, a better overall yield of radical translocation products was observed. Moreover, the identification of products **71** and **72** derived from all successive radical shifts was made possible by a careful HPLC of the reaction products and following NMR studies. In fact, the yield of these intermediate-translocated bromides was quite substantial. Their identification represents a solid proof to the reaction mechanism which involves a sequence of three

1,5-HAT (Scheme 6.22). These results represent the longest ever observed 1,5-HAT sequence. It is also noteworthy mentioning, that formation of vinylic dichloride **69** involves a combined 1.5-HAT + 1.6 HAT,⁴³ followed by the ease of HCl elimination. When bromo dimethylmalonate was tried as alkylating agent, complex mixture of unseparable products was obtained. Based on crude NMR, defined peaks for ATRA and HAT products were observed.



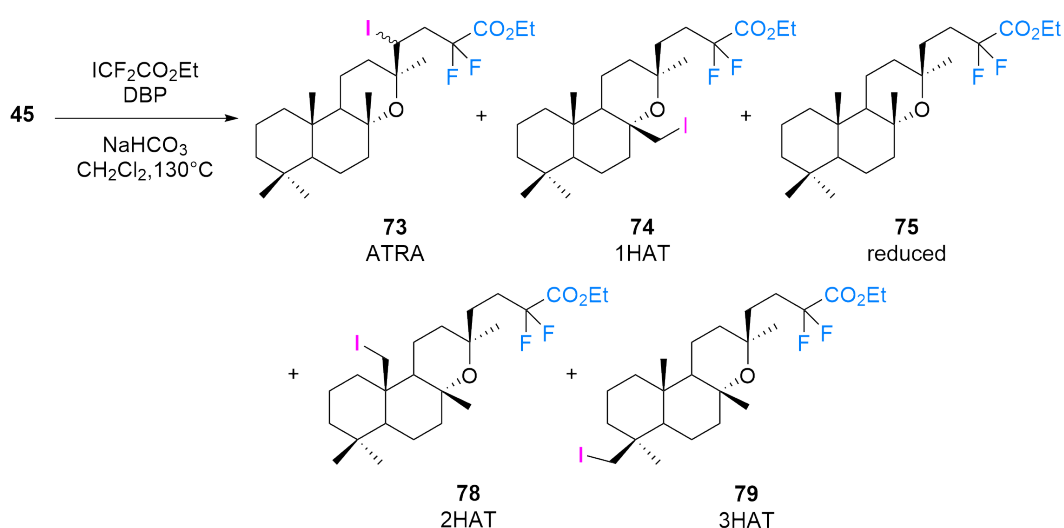
Scheme 6.22: Bromoalkylation of *epi*-manoyl oxide **45**.

For a better control of the reactive species in the reaction mixture, the iodoalkylation of *epi*-manoyl oxide **45** using a syringe pump was investigated. The reactions were performed in a sealed tube allowing to reach 100°C and connected to the syringe pump apparatus. No big change in yield was observed to the desired compounds - 31% for the formation of **60** which is comparable with the result obtained under the DLP conditions. Regarding to the fluorinated radical precursors, promising results were obtained (up to 35% for **77**), however problem of conversion of starting material was noted. A side interaction between perfluoroalkyl radical and the solvent (in this case benzene)^{47,48} was concluded. Using another solvent was proposed in order to understand the reactivity. From another hand, upon using fluorinated radical precursors the 8β-methyl functionalization products were identified (Scheme 6.23, **74** and **77**). This could be explained by the fast Iodine Atom Transfer (ATRA) from this radical precursors and fast trapping of just one 1,5-shift primary radical intermediate. The structure of **74** was confirmed by the X-ray diffraction on the single crystal, obtained from crystallization of the mixture with the hydroalkylated compound **75** (Scheme 6.23).



Scheme 6.23: Iodoalkylation using syringe pump addition.

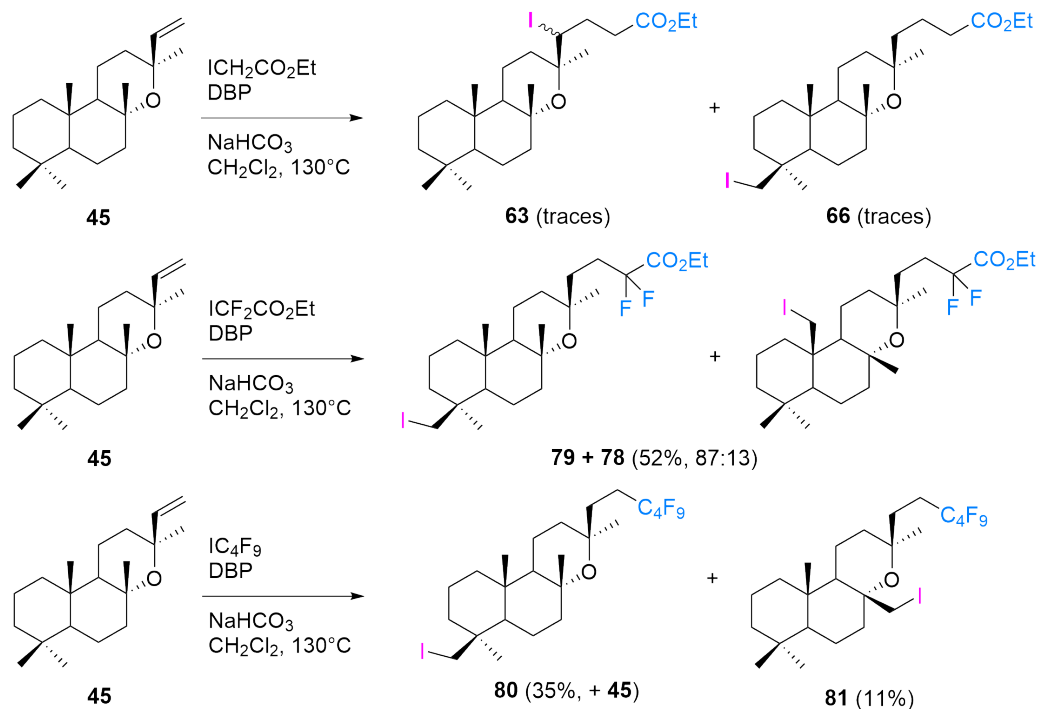
A small optimization of reaction conditions were performed on *epi*-manoyl oxide **45** using ethyl difluoroiodoacetate as alkylating agent (Scheme 6.24). Solvent change from benzene to dichloromethane afforded full conversion of starting olefin (Entry 1, Scheme 6.24). In order to achieve the high temperatures for dichloromethane, the reactions were performed in closed system using a sealed tube. The system can be heated up to 130°C during 1h. When the reaction was tried with an equal amount of initiator and alkylating agent, at 130°C, 55% of reduced product was isolated (Entry 2, Scheme 6.24). This can be explain that in the absence of the iodo precursor in the mixture, the obtained radical intermediates will have to abstract a hydrogen from the solvent or other species delivering the hydroalkylated product. Diminishing the initiator amount compared to the alkylating agent (Entry 3-6, Scheme 6.24), the reaction proceeded with full conversion and in a good yield for the expected products. The reaction showed an excellent chain efficiency, while the products were obtained in the same ratios. Without initiator no conversion of starting olefin to the desired products occurs (Entry 7, Scheme 6.24), concluding that the iodide dissociation promoted by high temperature does not take place.



Entry	DBP, equiv	I-R _f , equiv	Temp, °C	45	73	74+75	78+79
1	1.0	2.0	100	-	-	30%+12%	37% (15:85)
2	1.0	1.0	130	-	-	0%+55%	-
3	0.2	1.0	130	-	17%	19%+12%	47% (17:82)
4	0.1	1.0	130	-	17%	16%+10%	45% (16:83)
5	0.05	1.0	130	9%	18%	16%+14%	44% (18:81)
6	0.02	1.0	130	25%	17%	18%+4%	31% (16:83)
7	-	1.0	130	80%	-	-	-

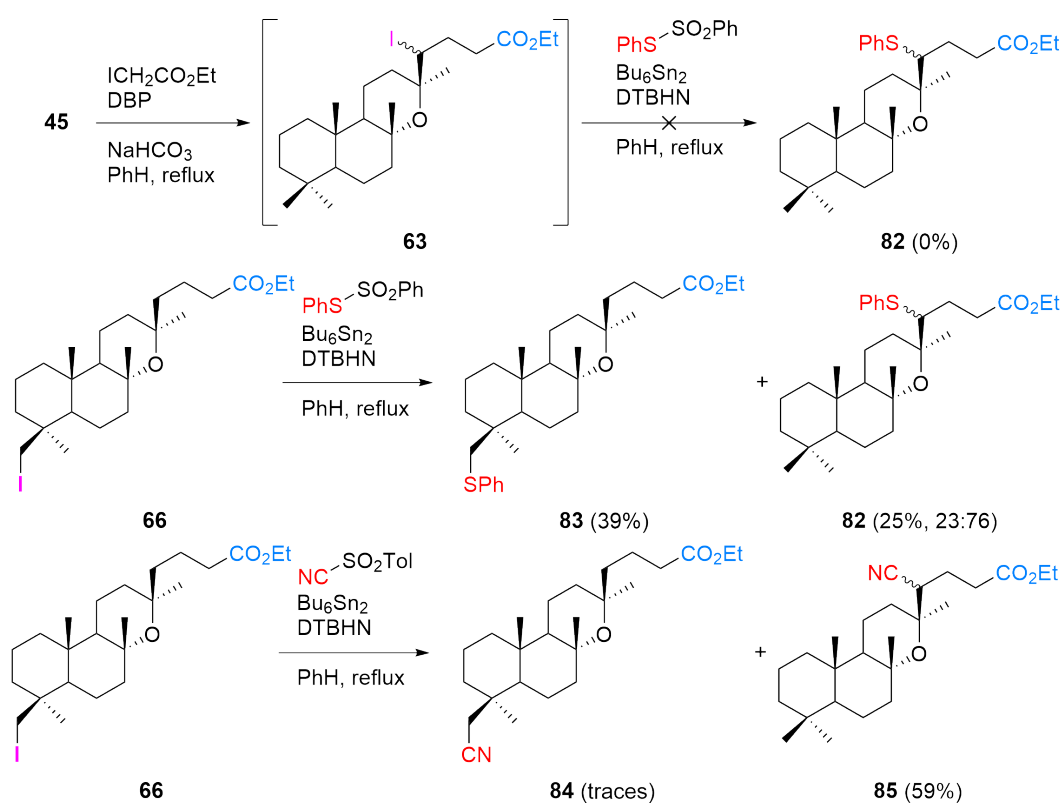
Scheme 6.24: Conversion control under different amounts of initiator.

The iodoalkylation of **45** was retried under the best conditions (Scheme 6.25). Good results were obtained, however the individual isolation of desired products still remains a problem. Due to same chemical behaviour, the products are isolated in a mixture either with their analogue, either with the hydroalkylated product, or with unconsumed starting material. Surprisingly, the reaction using ethyl iodoacetate in dichloromethane as solvent, delivered traces of desired products (Scheme 6.25, **63** and **66**). A reason could be the unstability of the secondary iodinated intermediates or of the ethyl iodoacetate itself at this high temperature, comparing to the fluorinated products that showed a much better stability under this conditions. Fluorinated alkylating agents delivered 3 and 2 consecutive HAT derivatives as major products under this conditions (Scheme 6.25).



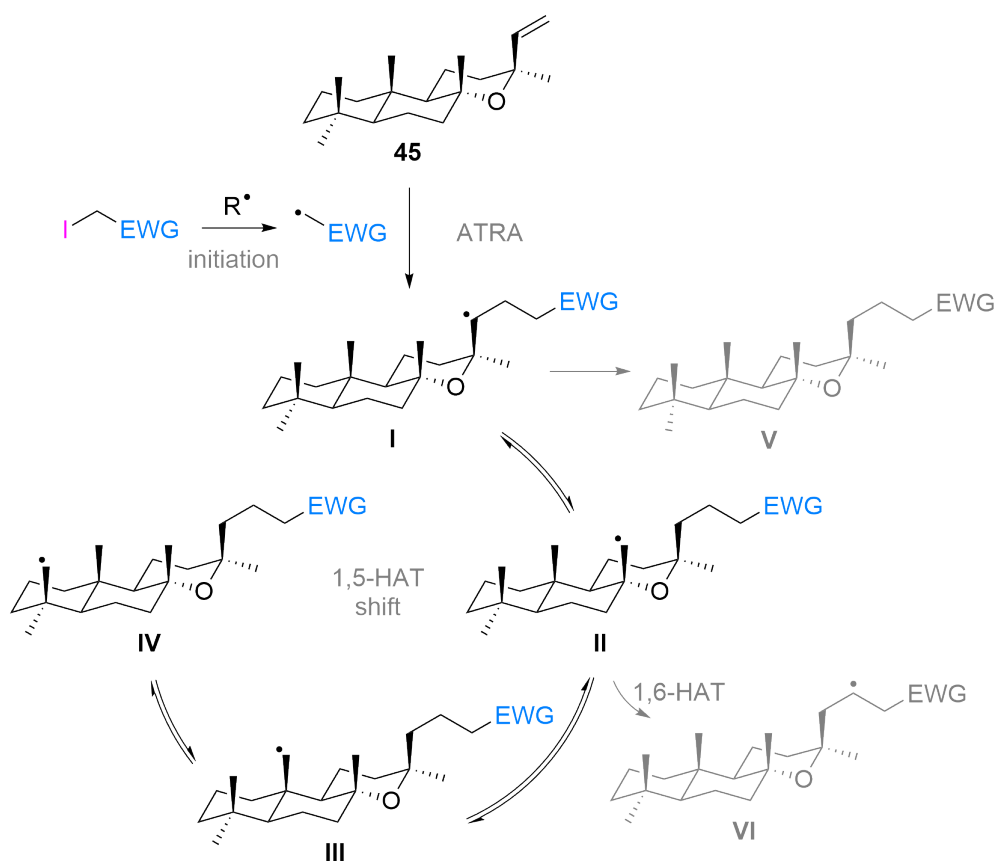
Scheme 6.25: Iodoalkylation in dichloromethane as solvent.

In order to perform further functionalizations of iodinated products, the thiophenylation and cyanation reactions were investigated. Performing a one pot protocol starting from the olefin and later adding the *S*-phenyl benzenethiosulfonate trap, no desired thiophenylated product **82** was obtained (Scheme 6.26). The secondary iodide intermediate **63** was identified by NMR after the first sequence. However no functionalization took place and just decompositions were noted. When the thiophenylation was repeated starting from the C-19 iodinated compound **66**, 2 major products were isolated. One is expected to be the direct C-19 thiophenylated product **83**, and the second one corresponds to the C-14 functionalized product **82** in a diastereomeric ratio of 23:76. This ratio corresponds to the previously observed one for the iodoalkylation of *epi*-manoyl oxide.³⁷ In case of the cyanation reaction, no C-19 functionalized product **84** was isolated, just the C-14 cyanated product **85** with 59% yield (Scheme 6.26). This results showed that the 1,5-HAT process is in equilibrium and can go back from the primary carbon center radical to the secondary one. Depending on the trap used the reaction mixture delivers different products.



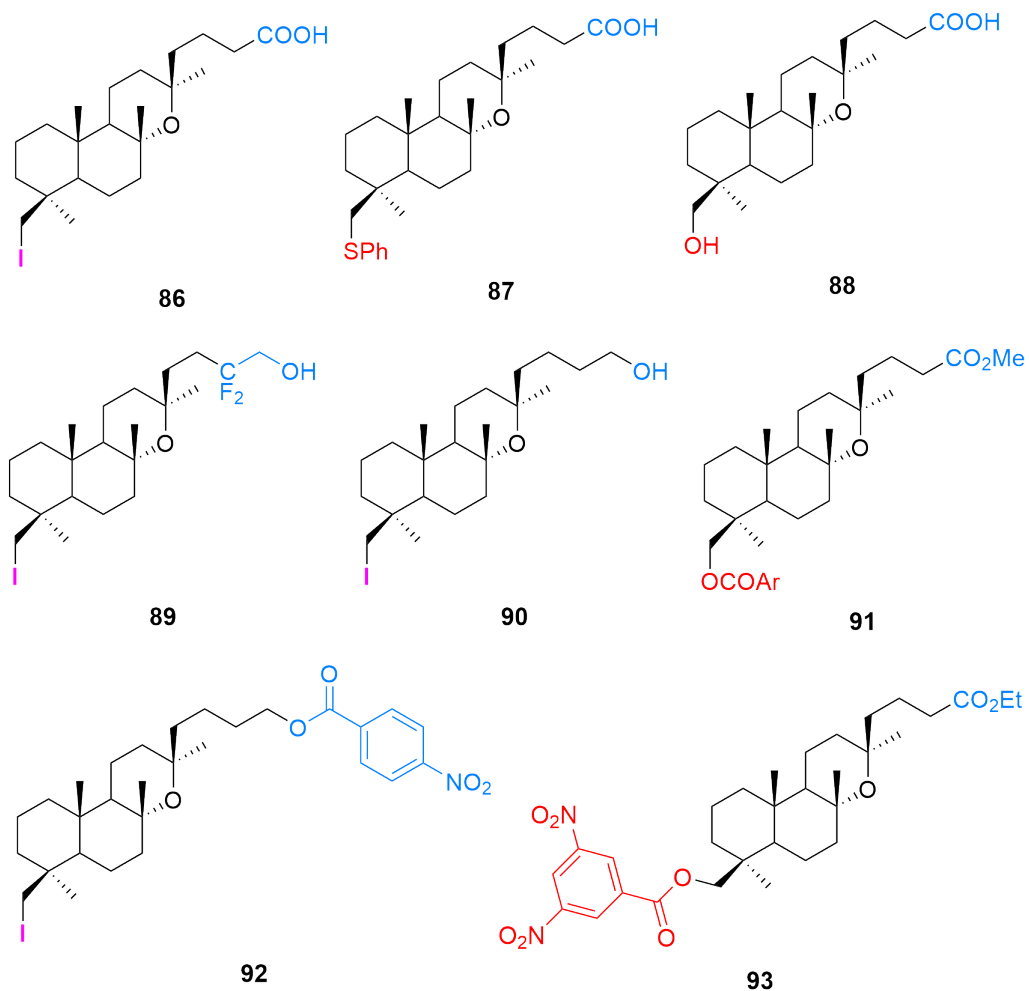
Scheme 6.26: Derivatization of iodinated derivative **66** using PhSSO_2Ph or TolSO_2CN as radical traps.

The proposed mechanism of functionalization of *epi*-manoyl oxide **45** scaffold is represented in the Scheme 6.27. Upon addition on the double bond of the primary carbon center radical bearing a electron withdrawing group (generated after the initiation step), the intermediate **I** is formed. This secondary center radical can either abstract an iodine atom from the radical precursor and sustain the chain or enter the 1,5-HAT shift. The obtained result showed that the hydrogen translocation is not unidirectional and can go back from the C-19 primary radical intermediate **IV** to the secondary radical **I**. Each radical species **I-IV** present in the mixture can be reduced delivering the hydroalkylated product **V**, perform the iodine abstraction to form the iodoalkylated products or be trapped by different radical traps to get functionalized products. A 1,6-HAT is possible from **II**, leading to the formation of the intermediate **VI**.



Scheme 6.27: Proposed mechanism for iodoalkylation of *epi*-manoyl oxide **45**.

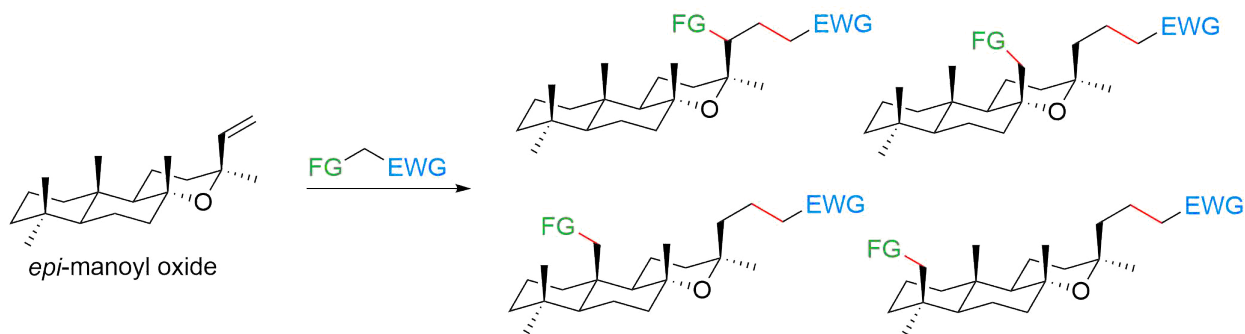
To be able to confirm the formation of the C-19 iodoalkylated products, a series of solid compounds was synthesized (Scheme 6.28). Crystallization attempts to form a single crystal are on going.



Scheme 6.28: Derivatization to form crystalline derivatives for X-ray single crystal analysis.

6.4 Conclusion

The present work demonstrates application of the free radical transformations for efficient structural modification of manoyl oxide and its 13-epimer. We demonstrate the first example of an ATRA reaction that is accompanied by radical translocation via successive 1,5-HAT which lead to remote functionalization of the terpenic scaffold.



The triple 1,5-HAT sequence is totally unprecedented radical remote functionalizations. Resulting advanced functionalization can lead to biological activities which could be complementary to other relevant representatives of manoyl oxides family. In particular, the observed radical translocations for both investigated substrates open the possibility to introduce additional functional groups in cycle A and B basing on a remote functionalization strategy. This “abnormal” reaction course of ATRA can provide an unique opportunity to functionalize with heteroatoms the hardly available C19 methyl group of manoyl oxide framework.

Acknowledgements

The presented work was performed within the project “Radical mediated modifications of natural products” supported financially by the Swiss National Science Foundation (SCOPES program, project No. IZ73Z0_152346/1).

References

- (1) Newhouse, T.; Baran, P. S. *Angewandte Chemie International Edition* **2011**, *50*, 3362–3374.
- (2) Cao, H.; Tang, X.; Tang, H.; Yuan, Y.; Wu, J. *Chem Catalysis* **2021**, *1*, 523–598.
- (3) Capaldo, L.; Ravelli, D.; Fagnoni, M. *Chemical Reviews* **2022**, *122*, 1875–1924.
- (4) Doyle, M. P.; Duffy, R.; Ratnikov, M.; Zhou, L. *Chemical Reviews* **2010**, *110*, 704–724.
- (5) Ackermann, L. *Chemical Reviews* **2011**, *111*, 1315–1345.
- (6) Li, B.; Ali, A. I.; Ge, H. *Chem* **2020**, *6*, 2591–2657.
- (7) Lu, X.; He, S.-J.; Cheng, W.-M.; Shi, J. *Chinese Chemical Letters* **2018**, *29*, 1001–1008.
- (8) Song, S.-Z.; Meng, Y.-N.; Li, Q.; Wei, W.-T. *Advanced Synthesis & Catalysis* **2020**, *362*, 2120–2134.
- (9) Batra, A.; Singh, K. N. *European Journal of Organic Chemistry* **2020**, *2020*, 6676–6703.
- (10) Dinda, B. In *Essentials of Pericyclic and Photochemical Reactions*, Series Title: Lecture Notes in Chemistry; Springer International Publishing: Cham, 2017, pp 301–313.
- (11) Stateman, L.; Nakafuku, K.; Nagib, D. *Synthesis* **2018**, *50*, 1569–1586.
- (12) Blickenstaff, R.; Sophasan, K. *Tetrahedron* **1972**, *28*, 1945–1953.
- (13) Heusler, K.; Kalvoda, J. *Angewandte Chemie International Edition in English* **1964**, *3*, 525–538.
- (14) Corbett, R. E.; Wilkins, A. L. *J. Chem. Soc., Perkin Trans. 1* **1975**, 710–716.
- (15) Majetich, G.; Wheless, K. *Tetrahedron* **1995**, *51*, 7095–7129.
- (16) Čeković, Ž. *Tetrahedron* **2003**, *59*, 8073–8090.
- (17) Barton, D. H. R.; Beaton, J. M.; Geller, L. E.; Pechet, M. M. *Journal of the American Chemical Society* **1960**, *82*, 2640–2641.
- (18) Barton, D. H. R.; Beaton, J. M.; Geller, L. E.; Pechet, M. M. *American Chemical Society* **1961**, *83*, 4076–4083.
- (19) Taniguchi, T.; Sugiura, Y.; Hatta, T.; Yajima, A.; Ishibashi, H. *Chemical Communications* **2013**, *49*, 2198.
- (20) Walling, C.; Padwa, A. *Journal of the American Chemical Society* **1963**, *85*, 1597–1601.
- (21) Corey, E. J.; Hertler, W. R. *Journal of the American Chemical Society* **1960**, *82*, 1657–1668.
- (22) Reimann, H.; Capomaggi, A. S.; Strauss, T.; Oliveto, E. P.; Barton, D. H. R. *Journal of the American Chemical Society* **1961**, *83*, 4481–4482.
- (23) Nonhebel, D. C. *Chemical Society Reviews* **1993**, *22*, 347.

- (24) Barton, D. H. R.; Beaton, J. M. *Journal of the American Chemical Society* **1962**, *84*, 199–204.
- (25) Wenkert, E.; Mylari, B. L. *Journal of the American Chemical Society* **1967**, *89*, 174–176.
- (26) Sejbal, J.; Klinot, J.; Vystrčil, A. *Collection of Czechoslovak Chemical Communications* **1988**, *53*, 118–131.
- (27) Sejbal, J.; Klinot, J.; Buděšínský, M. *Collection of Czechoslovak Chemical Communications* **1991**, *56*, 1732–1743.
- (28) Sejbal, J.; Klinot, J.; Buděšínský, M. *Collection of Czechoslovak Chemical Communications* **1996**, *61*, 1360–1370.
- (29) Hernández, R.; Velázquez, S. M. *J. Org. Chem* **1994**, *59*, 6395–6403.
- (30) Hanson, J. *Tetrahedron* **1967**, *23*, 793–799.
- (31) Hanson, J. *Tetrahedron* **1970**, *26*, 2711–2715.
- (32) Zhang, H.; Wynne, G.; Mander, L. N. *Arkivoc* **2001**, *VIII*, 40–58.
- (33) Carrau, R.; Hernandez, R.; Betancor, C. *Journal of the Chemical Society, Perkin Transactions 1* **1987**, 937–943.
- (34) De Armas, P.; Francisco, C. G.; Hernandez, R.; Salazar, J. A. *Journal of the Chemical Society, Perkin Transactions 1* **1988**, 3255–3265.
- (35) Ceccherelli, P.; Curini, M.; Marcotullio, M. C.; Mylari, B. L.; Wenkert, E. *The Journal of Organic Chemistry* **1986**, *51*, 1505–1509.
- (36) Pruteanu, E.; Gîrbu, V.; Ungur, N.; Persoons, L.; Daelemans, D.; Renaud, P.; Kulcički, V. *Molecules* **2021**, *26*, 4549.
- (37) Pruteanu, E.; Tappin, N. D. C.; Gîrbu, V.; Morarescu, O.; Dénès, F.; Kulcički, V.; Renaud, P. *Synthesis* **2021**, *53*, 1247–1261.
- (38) Charrier, N. In *Encyclopedia of Reagents for Organic Synthesis*, John Wiley & Sons, Ltd., Ed.; John Wiley & Sons, Ltd: Chichester, UK, 2007, rn00698.
- (39) Walling, C. *Tetrahedron* **1985**, *41*, 3887–3900.
- (40) RajanBabu, T. V. (; Gagosz, F. In *Encyclopedia of Reagents for Organic Synthesis*, John Wiley & Sons, Ltd., Ed.; John Wiley & Sons, Ltd: Chichester, 2005, rd022.
- (41) Curran, D. P.; Bosch, E.; Kaplan, J.; Newcomb, M. *The Journal of Organic Chemistry* **1989**, *54*, 1826–1831.
- (42) Masuyk, M. *Tetrahedron Letters* **1997**, *38*, 879–882.
- (43) Nechab, M.; Mondal, S.; Bertrand, M. P. *Chemistry - A European Journal* **2014**, *20*, 16034–16059.
- (44) Guerrero, M. A.; Cruz-Almanza, R.; Miranda, L. D. *Tetrahedron* **2003**, *59*, 4953–4958.
- (45) Khudyakov, I. V.; Kuz'min, V. A. *Russian Chemical Reviews* **1978**, *47*, 22–42.

- (46) Denisov, E. T.; Khudyakov, I. V. *Chemical Reviews* **1987**, *87*, 1313–1357.
- (47) Birchall, J. M.; Irvin, G. P.; Boyson, R. A. *Journal of the Chemical Society, Perkin Transactions 2* **1975**, 435.
- (48) Brace, N. O. *Journal of Fluorine Chemistry* **2001**, *108*, 147–175.

6.5 Experimental Section

General Information

Techniques

All reactions requiring anhydrous conditions were performed in flame dried glassware under an argon atmosphere. Silica gel 60Å(40–63 μm) from *Silicycle* was used for flash column chromatography (FCC). Thin layer chromatography (TLC) was performed on *Silicycle* silica gel 60 F254 plates, visualization under UV light (254 nm) and by dipping in a solution of cerium ammonium molybdate - $(\text{NH}_4)_2\text{MoO}_4$ (15.0 g), $\text{Ce}(\text{SO}_4)_2$ (0.5 g), H_2O (90 mL), conc. H_2SO_4 (10 mL) - and subsequent heating. Silver nitrate impregnated silica gel was prepared according to ratio: SiO_2 (50 g), AgNO_3 (5.5 g) and H_2O (30 mL) for flash column chromatography and AgNO_3 (1 g), H_2O (2.5 mL) and acetone (10 mL) for TLC, followed by activation at 105–110 $^\circ\text{C}$ (light sensitive, to be covered with aluminium foil and/or stored in the dark). Anhydrous sodium sulfate was used as drying reagent.

Materials

Commercial reagents were used without further purification unless otherwise stated. Dry solvents for reactions were filtered over columns of dried alumina under a positive pressure of argon and/or stored over 3Å molecular sieves. Solvents for extractions (Et_2O , *n*-pentane, CH_2Cl_2 , AcOEt) and flash column chromatography were of technical grade and distilled prior to use.

Instrumentation

^1H and ^{13}C NMR spectra were recorded on a *Bruker Avance IIIHD-300* spectrometer operating at 300 MHz for ^1H and 75 MHz for ^{13}C at rt (24–25 $^\circ\text{C}$) unless otherwise stated. Some ^1H and ^{13}C NMR spectra were recorded on a *Bruker Avance IIIHD-400* or a *Bruker Avance II-400* spectrometer (^1H : 400 MHz; ^{13}C : 100 MHz). Chemical shifts (δ) are reported in parts per million (ppm) downfield from tetramethylsilane $\text{Si}(\text{CH}_3)_4$ ($\delta = 0.00$ for ^1H NMR spectra) using residual solvent signal as an internal standard: δ singlet 7.26 (^1H), triplet 77.0 (^{13}C) for CDCl_3 or δ singlet 7.16 (^1H), triplet 128.0 (^{13}C) for C_6D_6 . Multiplicities are given as s (singlet), d (doublet), t (triplet), q (quadruplet), m (multiplet), and br (broad). Coupling constants (*J*) are reported in Hz. In ^{13}C -NMR spectra, the peak positions are reported on one decimal unless the difference in chemical shift between two signals is small and required two decimals. Due to coupling to the quadrupolar ^{11}B and ^{10}B nuclei, the carbons linked to boron atoms generally give a broad signal in ^{13}C NMR, sometimes not detected.

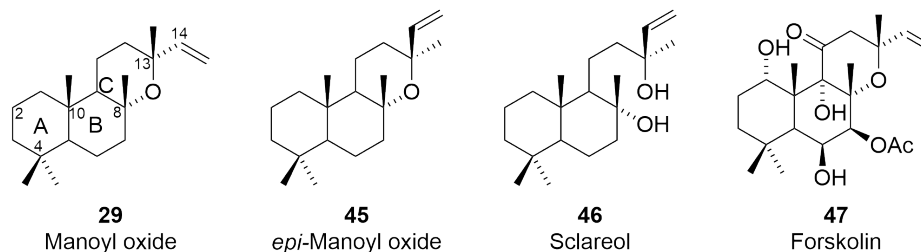
Diastereomeric ratio were determined by NMR on crude reaction mixtures.

Infrared spectra were recorded on a *Jasco FT-IR-460* plus spectrometer equipped with a *Specac MKII Golden Gate Single Reflection Diamond ATR* system and are reported in wave numbers (cm^{-1}). At maximum, the ten most prominent peaks are reported. HRMS analyses and accurate mass determinations were performed on a *Thermo Scientific LTQ Orbitrap XL* mass spectrometer using ESI mode (positive ion mode). Melting points were measured on a *Büchi B545* apparatus.

Specific rotation $[\alpha]_D^{20}$ are expressed in $\text{deg}\cdot\text{mL}\cdot\text{g}^{-1}\cdot\text{dm}^{-1}$. The concentration c is in $\text{g}/100\text{ mL}$ and the path length l is in decimeters. The units of the specific rotation, $\text{deg}\cdot\text{mL}\cdot\text{g}^{-1}\cdot\text{dm}^{-1}$, are implicit and are not included with the reported value.

Synthesis

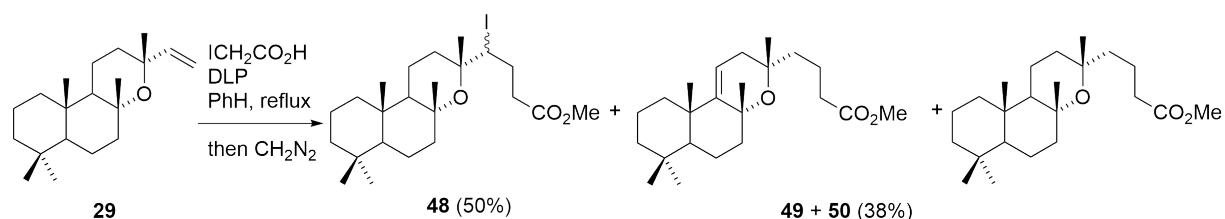
Modifications of manoyl oxide



DLP induced carbohalogenation. To a solution of substrate (1 mmol) in dry benzene (15 mL) the corresponding halide (1 mmol) was added under nitrogen atmosphere, followed by 0.25 equiv. of DLP, every 2 hours, until TLC shows an optimal conversion. Upon completion, the solvent was removed under reduced pressure to provide the crude reaction product.

DBP induced carbohalogenation. To a sealed tube charged with the solution of substrate (0.5 mmol) in dry CH_2Cl_2 (10.0 mL, 0.05M) was added NaHCO_3 (1.0 equiv), DBP (0.1 equiv) followed by the corresponding halide (1.1 equiv). Upon completion of addition, the tube was sealed and heated up to 130° using a pre-heated oil bath and stirred for 0.5h. Then, it was let to cool to rt, treated with water and extracted with Et_2O (3 x 10 mL). Combined organic phases were washed with 5% $\text{Na}_2\text{S}_2\text{O}_3$ sol., then water and brine, dried over Na_2SO_4 , filtered and concentrated under reduced pressure to give the crude reaction product.

Carboiodination of manoyl oxide with iodoacetic acid followed by methylation.



The crude reaction product obtained according to the general procedure from 40 mg (0.14 mmol) of manoyl oxide **29**, 26 mg (0.14 mmol) iodoacetic acid and 12 mg DLP (0.03 mmol) at reflux (8h) was methylated with an ethereal solution of diazomethane. The methylated product was submitted to flash chromatography on a silica gel column under gradient petroleum ether/EtOAc elution (0.5% EtOAc – 1.5% EtOAc) and gave the mixture of esters **49** and **50** (19 mg, 38%, 7:8=1:3, ^1H NMR), along with 44 mg of a complex mixture containing 75% (^1H NMR) of iodides **48**. This mixture was submitted to HPLC to give a pure sample of iodides **48**.

(13R)-14-iodo-8,13-epoxy-labdanyl-methylacetate (48) (mixture of epimers, 1:1).

Pale-yellow viscous liquid, IR (ν , cm^{-1}): 2947, 2925, 2864, 2324, 2077, 1741, 1462, 1440,

1388, 1377, 1262, 1195, 1176, 1119, 1098, 10791053, 1033, 996, 963. ¹H NMR: 3.93 and 3.96 (t, 1H, H-14, J=2.7 Hz), 3.677 and 3.683 (s, 3H, CO₂Me), 2.63-2.75 (m, 1H), 2.18-2.50 (m, 3H), 1.38 and 1.39 (s, 3H, Me-16), 1.24 and 1.25 (s, 3H, Me-17), 0.85 (s, 3H, Me-18), 0.79 (s, 3H, Me-19), 0.75 (s, 3H, Me-20). ¹³C NMR: 173.53, 173.34 (s, C(O)O); 76.04, 75.85 (s, C-8); 73.94 (s, C-13); 57.82, 57.43 (d, C-9); 56.49, 56.43 (d, C-5); 54.03, 53.92 (d, C-14); 51.56 (q, OMe), 42.74, 42.69 (t, C-7), 42.19, 42.18 (t, C-3); 39.17 (t, C-1); 36.87, 36.86 (s, C-10); 37.95, 35.71, (t, C-12); 35.18, 35.10 (t, C-21); 33.31, 33.29 (q, C-18, overlap with s, C-4); 30.17, 30.11 (t, C-15); 25.88, 23.04 (q, C-16); 24.57, 24.47 (q, C-17); 21.28 (q, C-19); 19.90, 19.86 (t, C-6); 18.62, 18.61 (t, C-2); 15.73, 15.69 (q, C-20); 15.66, 15.57 (t, C-11).

Mixture of (13R)- 8,13-epoxy-labda-9,11-enyl-methylacetate (49) and (13R)- 8,13-epoxy-labdanyl-methylacetate (50).

Colorless viscous liquid, IR (ν , cm⁻¹): 2928, 2867, 2309, 1741, 1460, 1441, 1388, 1376, 1255, 1194, 1171, 1119, 1101, 1080, 1047, 1029, 972, 960.

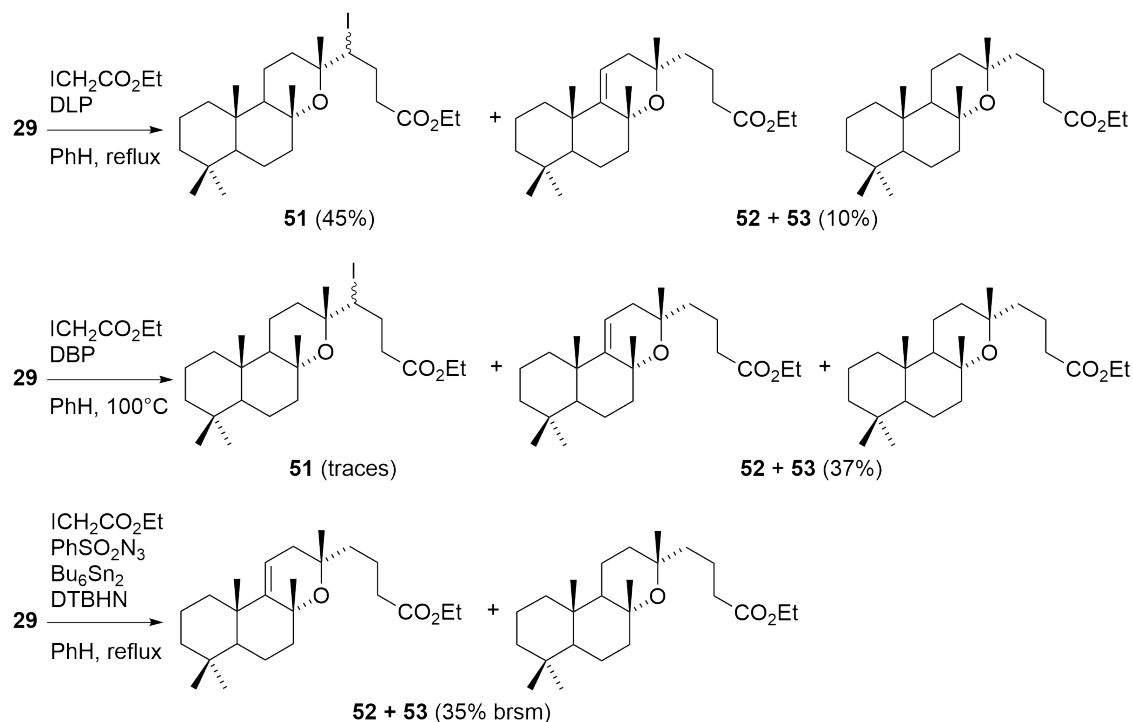
(13R)- 8,13-epoxy-labda-9,11-enyl-methylacetate (48) (minor compound, 25%).

¹H NMR*: 0.83 (s, 3H, Me-19), 0.86 (s, 3H, Me-18), 1.06 (s, 3H, Me-20), 1.20 (s, 3H, Me-16), 1.40 (s, 3H, Me-17), 1.94 (dd, 1H, H-12, AMX, JAM = 16.3, JMX = 3.7 Hz), 2.10 (dd, 1H, H-12, AMX, JAM = 16.3, JAX = 6.00 Hz), 2.27-2.31 (m, 2H, H-21), 3.66 (s, 3H, CO₂Me), 5.46 (dd, 1H, H-11, J = 6.3; 3.8 Hz). ¹³C NMR*: 174.39 (s, C(O)O), 152.41 (s, C-9), 112.64 (d, C-11), 74.22 (s, C-8), 71.78 (s, C-13), 54.19 (d, C-5), 51.37 (q, OMe), 43.21 (t, C-7), 42.04 (t, C-3), 41.00 (t, C-14), 39.67 (s, C-10), 38.72 (t, C-1), 35.15 (t, C-12), 34.65 (t, C-21), 33.78 (s, C-4), 33.32 (q, C-18), 30.57 (q, C-17), 28.27 (q, C-16), 22.27 (q, C-20), 21.65 (q, C-19), 20.21 (t, C-6), 19.97 (t, C-15), 19.13 (q, C-2).

(13R)- 8,13-epoxy-labdanyl-methylacetate (50) (major compound, 75%).

¹H NMR*: 0.75 (s, 3H, Me-20), 0.78 (s, Me-19), 0.85 (s, Me-18), 1.20 (s, Me-16), 1.26 (s, Me-17), 2.27-2.31 (m, 2H, H-21), 3.66 (s, 3H, CO₂Me). ¹³C NMR*: 174.39 (s, C-22), 74.68 (s, C-8), 72.59 (s, C-13), 58.29 (d, C-9), 56.50 (d, C-5), 51.35 (q, OMe), 45.02 (t, C-14), 43.15 (t, C-7), 42.25 (t, C-3), 39.24 (t, C-1), 36.92 (s, C-10), 36.43 (t, C-12), 34.57 (t, C-21), 33.34 (s, C-4), 33.32 (q, C-18), 27.59 (q, C-16), 24.83 (q, C-17), 21.28 (q, C-19), 19.89 (t, C-6), 19.37 (t, C-15), 18.66 (t, C-2), 15.74 (q, C-20), 15.43 (t, C-11).

Carboiodination of manoyl oxide with ethyl iodoacetate.



The crude reaction product obtained according to the general procedure from 98 mg (0.33 mmol) of manoyl oxide **29**, 70 mg (0.33 mmol) ethyliodoacetate and 50 mg DLP (0.126 mmol) at reflux (18h) was submitted to flash chromatography on a silica gel column under gradient elution with petroleum ether/EtOAc (0.5% EtOAc – 1.5% EtOAc) and gave individual epimer **51** (63 mg, 36%) along with the mixture of esters **52** and **53** (13 mg, 10%, 10:11=6:4, $^1\text{H NMR}$).

(13R)-14-iodo-8,13-epoxy-labdanyl-ethylacetate (**51**).

Pale-yellow viscous liquid. $[\alpha]_D^{20} = 0.64$ (*c* 0.28, MeOH). **IR** (ν , cm^{-1}): 3450, 2925, 2867, 1736, 1459, 1376, 1177, 1031. **NMR** – see table 6.1, Appendix. Anal. Calcd for $\text{C}_{24}\text{H}_{41}\text{IO}_3$ (504.49): C, 57.14; H, 8.19. Found: C, 57.22; H, 8.25.

Mixture of (13R)-8,13-epoxy-labda-9,11-enyl-ethylacetate (**52**) (60%) and (13R)-8,13-epoxy-labdanyl-ethylacetate (**53**) (40%).

Colorless viscous liquid, **IR** (ν , cm^{-1}): 3902, 3741, 3590, 3463, 3361, 3238, 2944, 2632, 2494, 2333, 2191, 2080, 1984, 1737, 1692, 1457, 1377, 1264, 1180, 1030.

(13R)-8,13-epoxy-labda-9,11-enyl-ethylacetate (**52**) (major compound, 60%).

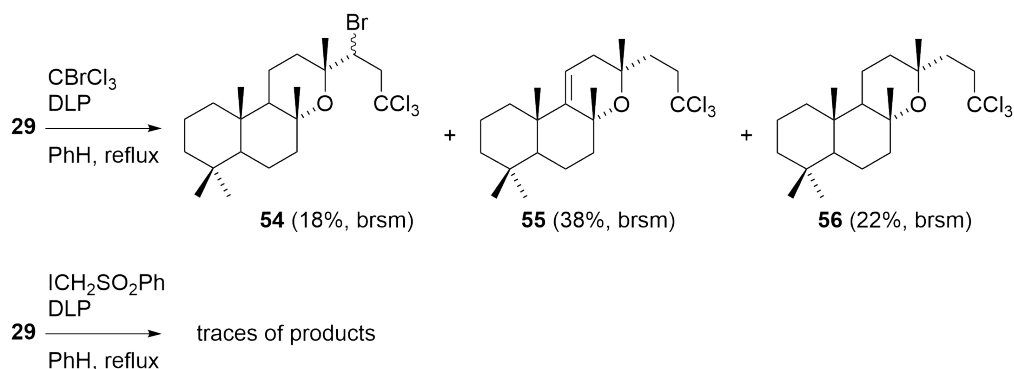
$^1\text{H NMR}$: 0.83 (s, 3H, Me-19), 0.86 (s, 3H, Me-18), 1.06 (s, 3H, Me-20), 1.20 (s, 3H, Me-16), 1.25 (t, 3H, CO_2Et , $J = 7.1$ Hz), 1.39 (s, 3H, Me-17), 1.83 (m, 1H, H-7), 1.94 (dd, 1H, H-12, AMX, JAM = 16.2 Hz, JMX = 4 Hz), 2.10 (dd, 1H, H-12, AMX, JAM = 16.2 Hz, JAX = 6 Hz), 2.28 (t, 2H, H-21, $J = 7.6$ Hz), 4.11 (q, 2H, CO_2Et , $J = 7.1$ Hz), 5.46 (dd, 1H, H-11, $J_1 = 6$ Hz, $J_2 = 4$ Hz). $^{13}\text{C NMR}^*$: 173.72 (s, C=O), 152.36 (s, C9), 112.61 (d, C11), 74.17 (s, C7), 71.76 (s,

C13), 60.08 (t, OCH₂-), 54.13 (d, C5), 43.17 (t, C7), 41.98 (t, C3), 40.97 (t, C14), 38.66 (t, C1), 35.08 (t, C12), 34.88 (t, C21), 33.74 (s, C4), 33.27 (q, C18), 30.53 (q, C17), 28.24 (q, C16), 22.24 (q, C20), 21.62 (q, C19), 20.17 (t, C6), 19.95 (t, C15), 19.09 (t, C2), 14.26 (q, -CH₃ (Et)).

(13R)- 8,13-epoxy-labdanyl-ethylacetate (53) (minor compound, 40%).

¹H NMR: 0.76 (s, 3H, Me-20), 0.78 (s, 3H, Me-19), 0.85 (s, 3H, Me-18), 1.20 (s, 3H, Me-16), 1.25 (t, 3H, CO₂Et, J = 7.1 Hz), 1.26 (s, 3H, Me-17), 2.27 (t, 2H, H-21, J = 7.5 Hz), 4.11 (q, 2H, CO₂Et, J = 7.1 Hz). ¹³C NMR*: 173.93 (s, C=O), 74.63 (s, C8), 72.56 (s, C13), 60.05 (t, OCH₂-), 58.23 (d, C9), 56.45 (d, C5), 44.99 (t, C14), 43.14 (t, C17), 42.20 (t, C3), 39.63 (s, C10), 39.19 (t, C1), 36.38 (t, C12), 34.78 (t, C21), 33.30 (q, C18), 27.53 (q, C16), 24.79 (q, C17), 21.24 (q, C19), 19.85 (t, C6), 19.33 (t, C15), 18.61 (t, C2), 15.70 (q, C20), 15.38 (t, C11), 14.26 (q, -CH₃ (Et)).

Carbobromination of manoyl oxide with CBrCl₃. Compounds 54-56.



The crude reaction product (43.6 mg) obtained according to the general procedure from 29 mg (0.1 mmol) of manoyl oxide **29**, 20 mg (0.1 mmol) bromotrichloromethane and 10 mg DLP (0.025 mmol) at reflux (10h) was submitted to HPLC. Separation gave 9 mg (31%) unreacted starting material, epimeric bromides **54** (5.2 mg, 15%) along with pure **55** (10.2 mg, 38%, brsm) and **56** (8.2 mg, 30%).

(13R)-14-bromo-8,13-epoxy-15-trichloromethyl-labdane (54) (major epimer, 75%).

Colorless viscous liquid, $[\alpha]_D^{20} = 7.33^\circ$ (*c* 0.03, CHCl₃). IR (ν , cm⁻¹): 2948, 2866, 1463, 1379, 1119, 1099, 1079, 1032, 959. NMR – see table 6.1, Appendix. Anal. Calcd for C₂₁H₃₄BrCl₃O (488.76): C, 51.61; H, 7.01. Found: C, 51.70; H, 7.11.

(13R)-14-bromo-8,13-epoxy-15-trichloromethyl-labdane (54) (minor epimer, 25%).

Identified in the mixture of epimers.

IR (ν , cm⁻¹): 2926, 2668, 1463, 1388, 1378, 1120, 1108, 1078, 1056, 1033, 996, 967, 796.

¹H NMR (subtracted from the spectrum of the mixture containing the major epimer): 0.76 (s, 3H, Me-20), 0.79 (s, 3H, Me-19), 0.86 (s, 3H, Me-18), 1.40 (s, 3H, Me-17), 1.47 (s, 3H, Me-16), 3.18 (dd, 1H, H-15, J = 8.9; 7.1 Hz), 3.73 (d, 1H, H-15, J = 15.9 Hz), 3.95 (dd, 1H, H-14, J = 7.1;

1.4 Hz). ^{13}C NMR (subtracted from the spectrum of the mixture containing the major epimer): 98.52 (s, C-21), 76.34 (s, C-8), 75.19 (s, C-13), 58.59 (d, C-5), 58.50 (t, C-15), 58.13 (t, C-14), 56.51 (d, C-5), 42.73 (t, C-7), 42.14 (t, C-3), 39.15 (t, C-1), 36.95 (t, C-10), 34.3 (s, C-4), 33.28 (q, C-18), 27.40 (t, C-12), 26.40 (q, C-16), 24.42 (q, C-17), 21.27 (q, C-19), 19.84 (t, C-6), 18.6 (t, C-2), 15.17 (q, C-11).

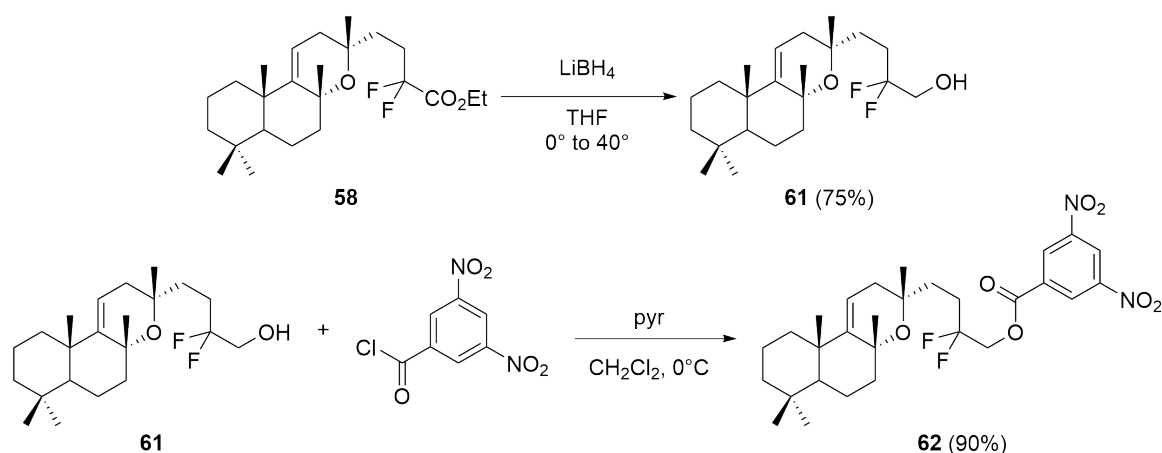
(13R)-8,13-epoxy-15-trichloromethyl-labd-9,11-ene (55).

Colorless viscous liquid, $[\alpha]_D^{20} = 3.18^\circ$ (c 0.54, CHCl_3). IR (ν , cm^{-1}): 2928, 2868, 1714, 1459, 1388, 1376, 1341, 1282, 1261, 1139. NMR – see table 6.1, Appendix. Anal. Calcd for $\text{C}_{21}\text{H}_{33}\text{Cl}_3\text{O}$ (407.84): C, 61.84; H, 8.16. Found: C, 61.92; H, 8.27.

(13R)-8,13-epoxy-15-trichloromethyl-labdane (56).

Colorless viscous liquid, $[\alpha]_D^{20} = 0.80^\circ$ (c 0.20, CHCl_3). IR (ν , cm^{-1}): 2927, 2866, 1465, 1446, 1388, 1377, 1120, 1102, 1079, 1045. NMR – see table 6.1, Appendix. Anal. Calcd for $\text{C}_{21}\text{H}_{35}\text{Cl}_3\text{O}$ (409.86): C, 61.54; H, 8.61. Found: C, 61.61; H, 8.69.

Derivatization to 3,5-dinitrobenzoyl ester 62



4-[(3S,4aR,10aS)-3,4a,7,7,10a-pentamethyl-5,6,6a,8,9,10-hexahydro-2H-benzo[f]chromen-3-yl]-2,2-difluoro-butan-1-ol (61)

To a 10 mL rbf charged with MO-ester (413 mg, 1.0 mmol) in dry THF (2.3 mL, 0.3M) was added at 0° , LiBH_4 (1.0 mL, 2.0 eq, 2M in THF). The reaction mixture was stirred for 10 min at 0° , then warmed up to 40° and stirred overnight. Upon completion, the mixture was diluted with Et_2O , and treated with water at 0° , extracted 3 times, treated with water and brine, then dried over Na_2SO_4 , filtered and concentrated under reduced pressure to deliver the crude product. FC (2:8 Et_2O /pentane) delivered the product as colorless oil (278 mg, 75% yield).

^1H NMR (300 MHz, CDCl_3) δ 5.46 (dd, $J = 5.2, 4.1$ Hz, 1H), 3.73 (t, $J = 12.7$ Hz, 2H), 2.19 – 0.74 (m, 17H), 1.43 (s, 4H), 1.22 (s, 3H), 1.06 (d, $J = 1.0$ Hz, 3H), 0.85 (s, 3H), 0.83 (s, 3H). ^{13}C NMR (75 MHz, CDCl_3) δ 152.1, 124.05 (t, $J = 241.9$ Hz), 112.4, 77.6, 76.7, 74.8, 71.4, 64.09 (t, $J = 32.3$ Hz), 54.4, 43.1, 42.1, 39.8, 38.7, 35.6, 33.6, 33.53 (t, $J = 4.2$ Hz), 33.4, 30.5, 27.97

(t, J = 24.1 Hz), 22.2, 21.8, 20.2, 19.2.

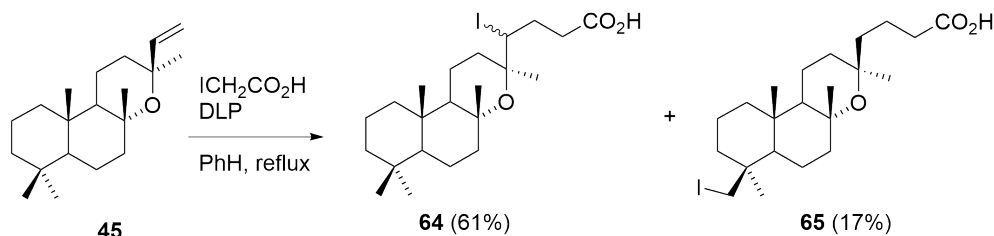
[4-[(3S,4aR,10aS)-3,4a,7,7,10a-pentamethyl-5,6,6a,8,9,10-hexahydro-2H-benzo[f]chromen-3-yl]-2,2-difluoro-butyl] 3,5-dinitrobenzoate (62)

To a 10 mL rbf charged with hydroxy-manoyl derivative (195 mg, 0.53 mmol) in dry CH₂Cl₂ (5.8 mL, 0.1M) cooled to 0°C, was added pyridine (0.11 mL, 2.5 equiv) followed by 3,5-dinitrobenzoyl chloride (243 mg, 2.0 equiv). The resulting mixture was stirred at 0°C, and monitored by TLC upon completion. The reaction mixture was diluted with EtOAc, treated with sat sol NH₄Cl (15 mL) and transferred to the separating funnel. The organic phase was extracted with EtOAc (3x 10mL). Combined organic phases were treated with water and brine, dried over Na₂SO₄, filtered and concentrated under reduced pressure. FC (1:9 Et₂O/pentane) delivered the product as yellowish solid (267 mg, 90% yield).

¹H NMR (300 MHz, CDCl₃) δ 9.25 (t, J = 2.1 Hz, 1H), 9.16 (d, J = 2.2 Hz, 2H), 5.47 (dd, J = 5.7, 3.8 Hz, 1H), 4.67 – 4.53 (m, 2H), 2.23 – 1.93 (m, 4H), 1.87 – 0.78 (m, 30H), 1.39 (s, 4H), 1.22 (s, 3H), 1.05 (s, 4H), 0.83 (s, 3H), 0.82 (s, 3H). ¹³C NMR (75 MHz, CDCl₃) δ 161.8, 152.7, 148.9, 133.0, 129.7, 123.0, 121.7, 112.4, 77.6, 76.7, 74.5, 70.8, 65.66 (t, J = 32.3 Hz), 54.3, 43.2, 42.0, 39.7, 38.7, 35.6, 33.8, 33.4, 33.2, 30.5, 29.06 (t, J = 23.5 Hz), 28.4, 22.3, 21.7, 20.2, 19.2.

Modifications of *epi*-manoyl oxide

Carboiodination of *epi*-manoyl oxide with iodoacetic acid



The crude reaction product obtained according to the general procedure from 50 mg (0.17 mmol) of *epi*-manoyl oxide **45**, 32 mg (0.17 mmol), iodoacetic acid and 14 mg DLP (0.034 mmol) at reflux (8h) was submitted to flash chromatography on a silica gel column under gradient elution with petroleum ether/EtOAc (7% EtOAc – 10% EtOAc) and gave individual epimers of **64** (36 mg major epimer, 44% and 13 mg minor epimer, 16%), along with an unresolved complex polar mixture.

(13S)-14-iodo-8,13-epoxy-labdanyl-acetic acid (**64**) (major epimer).

Pale yellow viscous liquid, $[\alpha]_D^{20} = 41.5^\circ$ (c 0.21, MeOH), **IR** (ν , cm^{-1}): 2980, 2924, 2870, 1709, 1456, 1446, 1388, 1377, 1133, 1073, 1060, 986, 958. **NMR** – see table 6.2, Appendix. Anal. Calcd for $\text{C}_{22}\text{H}_{37}\text{IO}_3$ (476.44): C, 55.46; H, 7.83. Found: C, 55.49; H, 7.92.

(13S)-14-iodo-8,13-epoxy-labdanyl-acetic acid (**64**) (minor epimer).

Pale yellow viscous liquid, $[\alpha]_D^{20} = 8.6^\circ$ (c 0.52, MeOH). **IR** (ν , cm^{-1}): 2923, 2870, 1708, 1457, 1446, 1388, 1377, 1144, 1125, 1092, 1076, 1043, 1026, 989, 963. **NMR** – see table 6.2, Appendix. Anal. Calcd for $\text{C}_{22}\text{H}_{37}\text{IO}_3$ (476.44): C, 55.46; H, 7.83. Found: C, 55.40; H, 7.87.

Carboiodination of *epi*-manoyl oxide with iodoacetic acid followed by methylation.

The crude reaction product obtained according to the general procedure from 104 mg (0.36 mmol) of *epi*-manoyl oxide **45**, 67 mg (0.36 mmol) iodoacetic acid, 29 mg DLP (0.072 mmol) at reflux (8h) mg was methylated with an ethereal solution of diazomethane. The methylated product was submitted to flash chromatography on a silica gel column under gradient petroleum ether/EtOAc elution (0.5% EtOAc – 1.5% EtOAc) and gave individual epimers of **64'** (70 mg major epimer, 41% and 27 mg minor epimer, 18%), followed by iodide **65'** (25 mg, 17%).

(13S)-14-iodo-8,13-epoxy-labdanyl-methylacetate (**64'**) (major epimer)

Pale-yellow viscous liquid. $[\alpha]_D^{20} = 28.4^\circ$ (c 0.34, MeOH). **IR** (ν , cm^{-1}): 2946, 2990, 2870, 1741, 1448, 1388, 1378, 1362, 1143, 1073. **NMR** – see table 6.2, Appendix. Anal. Calcd for $\text{C}_{23}\text{H}_{39}\text{IO}_3$ (490.47): C, 55.32; H, 8.02. Found: C, 55.36; H, 8.10.

(13S)-14-iodo-8,13-epoxy-labdanyl-methylacetate (64') (minor epimer)

Pale-yellow viscous liquid. $[\alpha]_D^{20} = 4.4^\circ$ (*c* 0.14, MeOH). **IR** (ν , cm^{-1}): 2924, 2854, 1742, 1458, 1439, 1377, 1156, 1077. **NMR** – see table 6.2, Appendix. Anal. Calcd for $\text{C}_{23}\text{H}_{39}\text{IO}_3$ (490.47): C, 55.32; H, 8.02. Found: C, 55.34; H, 8.09.

(13R)-19-iodo-8,13-epoxy-labdanyl-methylacetate (65')

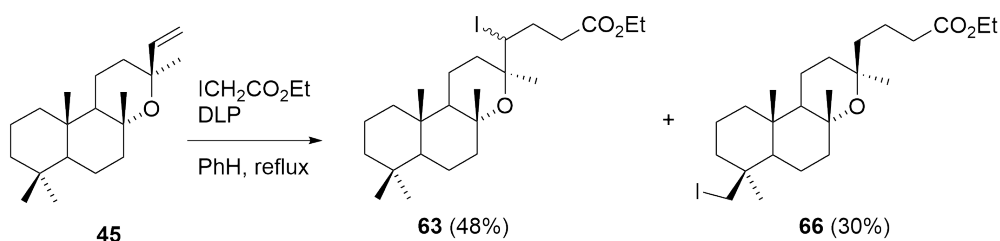
Colorless viscous liquid. $[\alpha]_D^{20} = 28.4^\circ$ (*c* 0.34, MeOH). **IR** (ν , cm^{-1}): 2977, 2942, 2872, 1740, 1451, 1376, 1202, 1164, 1142, 1134. **NMR** – see table 6.3, Appendix. Anal. Calcd for $\text{C}_{23}\text{H}_{39}\text{IO}_3$ (490.47): C, 55.32; H, 8.02. Found: C, 55.37; H, 8.01.

Hydrolysis of iodide (65'). (13R)-19-iodo-8,13-epoxy-labdanyl-acetic acid (65).

To the cold solution (0 °C) of compound **65'** (8.4 mg, 0.02 mmol) in THF (0.9 mL) was slowly added the aqueous solution (0.3 mL) of LiOH (0.96 mg, 0.04 mmol), then the ice bath has been removed and the reaction allowed to stir at room temperature 24h. The reaction was monitored by TLC. After the usual workup, extraction with Et_2O (3 × 2 mL), drying over Na_2SO_4 , 8.9 mg of a crude residue was obtained which was purified on a silica gel column under elution with petroleum ether/EtOAc (25%) to give acid **18** (4.2 mg, 52%).

Colorless viscous liquid. $[\alpha]_D^{20} = 4.2^\circ$ (*c* 0.15, MeOH). **IR** (ν , cm^{-1}): 2972, 2926, 2870, 1734, 1708, 1457, 1377, 1142, 1079, 1043. **NMR** – see table 6.3, Appendix. Anal. Calcd for $\text{C}_{22}\text{H}_{37}\text{IO}_3$ (476.44): C, 55.46; H, 7.83. Found: C, 55.51; H, 7.91.

Carboiodination of *epi*-manoyl oxide with ethyl iodoacetate.



The crude reaction product obtained according to the general procedure from 153 mg (0.53 mmol) of *epi*-manoyl oxide **45**, 169 mg (0.53 mmol), ethyl iodoacetate and 53 mg DLP (0.13 mmol) at reflux (10 h) was submitted to flash chromatography on a silica gel column under gradient elution with petroleum ether/EtOAc (0.5% EtOAc – 1.5% EtOAc) and gave individual epimers of **63** (84 mg major epimer, 32% and 43 mg minor epimer, 16%) along with iodide **66** (79 mg, 30%).

(13S)-14-iodo-8,13-epoxy-labdanyl-ethylacetate (63) (major epimer)

Pale-yellow viscous liquid. $[\alpha]_D^{20} = 1.07$ (*c* 0.13, MeOH). **IR** (ν , cm^{-1}): 3670, 2967, 2298, 1737, 1454, 1441, 1407, 1376, 1242, 1171, 1066, 1050, 882. **NMR** – see table 6.3, Appendix. Anal. Calcd for $\text{C}_{24}\text{H}_{47}\text{IO}_3$ (504.21): C, 57.14; H, 8.19. Found: C, 57.11; H, 8.23.

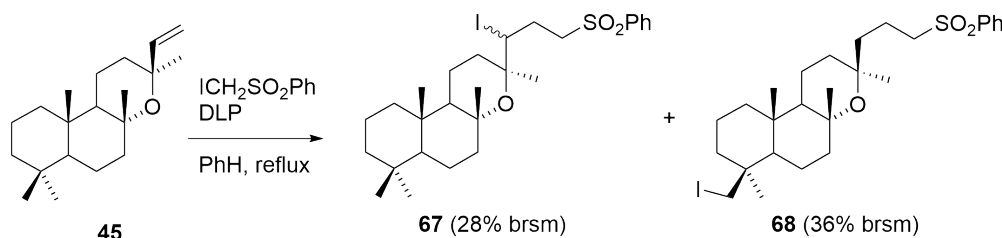
(13S)-14-iodo-8,13-epoxy-labdanyl-ethylacetate (63) (minor epimer)*.

Pale-yellow viscous liquid. $[\alpha]_D^{20} = 17.72$ (*c* 0.32, MeOH). **IR** (ν , cm^{-1}): 2980, 2936, 2869, 2342, 1734, 1461, 1444, 1388, 1376, 1182, 1125, 1094, 1078, 1034, 991. **NMR** – see table 6.3, Appendix. Anal. Calcd for $\text{C}_{24}\text{H}_{47}\text{IO}_3$ (504.21): C, 57.14; H, 8.19. Found: C, 57.20; H, 8.25.

(13R)-19-iodo-8,13-epoxy-labdanyl-ethylacetate (66).

Colorless viscous liquid. $[\alpha]_D^{20} = -1.32$ (*c* 0.47, MeOH). **IR** (ν , cm^{-1}): 2965, 2927, 2870, 1735, 1463, 1452, 1375, 1260, 1203, 1192, 1164, 1129, 1102, 1080, 1042, 1023, 989. **NMR** – see table 6.4, Appendix. Anal. Calcd for $\text{C}_{24}\text{H}_{47}\text{IO}_3$ (504.21): C, 57.14; H, 8.19. Found: C, 57.19; H, 8.26.

Carboiodination of *epi*-manoyl oxide with iodomethyl sulfonyl benzene.



The crude reaction product obtained according to the general procedure from 51 mg (0.179 mmol) of *epi*-manoyl oxide **45**, 50.6 mg (0.179 mmol) iodomethyl sulfonyl benzene, and 18 mg DLP (0.045 mmol) at reflux (10 h) was submitted to flash chromatography on a silica gel column under gradient elution with petroleum ether/EtOAc (3% EtOAc – 7% EtOAc) and gave 42 mg (75%) of unreacted starting material along with iodide **67** (4.7 mg, 28% brsm) and iodide **68** (6.2 mg, 36% brsm).

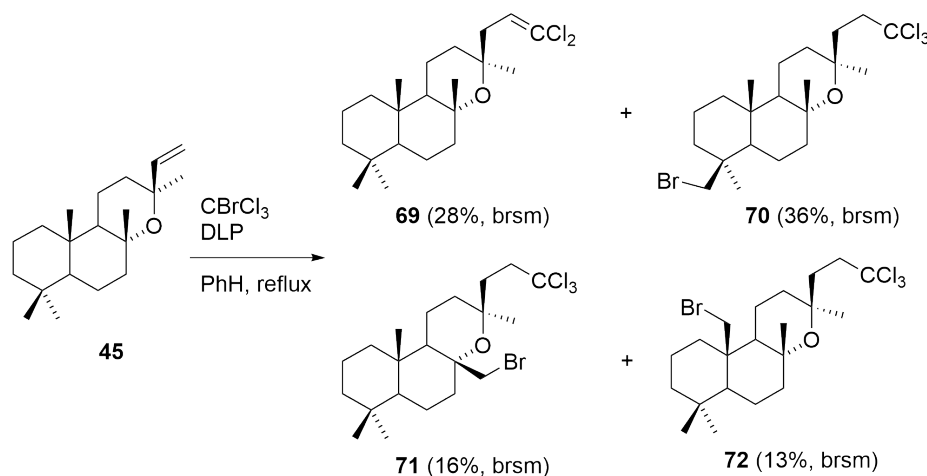
(13S)-16-iodo-8,13-epoxy-15-(phenylsulfonyl)methylabdane (67)

Pale-yellow viscous liquid. $[\alpha]_D^{20} = 45.6$ (*c* 0.24, MeOH). **IR** (ν , cm^{-1}): 2925, 2857, 1447, 1321, 1308, 1149, 1087, 1073. **NMR** – see table 6.4, Appendix. Anal. Calcd for $\text{C}_{27}\text{H}_{41}\text{IO}_3\text{S}$ (572.59): C, 56.64; H, 7.22. Found: C, 56.71; H, 7.31.

(13S)-19-iodo-8,13-epoxy-15-(phenylsulfonyl)methylabdane (68)

Colorless viscous liquid, $[\alpha]_D^{20} = -0.2$ (*c* 1.26, MeOH), **IR** (ν , cm^{-1}): 3388, 2921, 2850, 1708, 1667, 1628, 1449, 1216, 1072, 1052, 908, 855. **NMR** – see table 6.4, Appendix. Anal. Calcd for $\text{C}_{27}\text{H}_{41}\text{IO}_3\text{S}$ (572.59): C, 56.64; H, 7.22. Found: C, 56.68; H, 7.30.

Carbobromination of *epi*-manoyl oxide with CBrCl₃. Compounds 69-72



The crude reaction product obtained according to the general procedure from 93.6 mg (0.32 mmol) of *epi*-manoyl oxide **45**, 63.5 mg (0.32 mmol) and 32 mg DLP (0.08 mmol) at reflux (10 h) bromotrichloromethane was submitted to HPLC (following a percolation on a short silicagel column) under elution with 1% EtOAc in petroleum ether and gave dichloride **69** (10 mg, 10% brsm), bromide **71** (22 mg, 16%), bromide **72** (17 mg, 13%) and bromide **70** (48 mg, 36%), along with 15% (14 mg) of recovered starting material.

(13S)-8,13-epoxy-15-dichloromethyl-labd-15-ene (**69**).

Colorless viscous liquid. $[\alpha]_D^{20} = 20.1^\circ$ (*c* 0.15, CHCl₃). IR (ν , cm⁻¹): 2926, 2866, 1737, 1465, 1376, 1096, 1078, 991. NMR – see table 6.5, Appendix. Anal. Calcd for C₂₁H₃₄Cl₂O (372.20): C, 67.55; H, 9.18. Found: C, 67.61; H, 9.24.

(13S)-16-bromo-8,13-epoxy-15-trichloromethyl-labdane (**71**).

Colorless viscous liquid. $[\alpha]_D^{20} = -14.2^\circ$ (*c* 0.17, CHCl₃). IR (ν , cm⁻¹): 2925, 2869, 2850, 1731, 1463, 1376, 1041, 787, 693. NMR – see table 6.5, Appendix. Anal. Calcd for C₂₁H₃₄BrCl₃O (488.76): C, 51.61; H, 7.01. Found: C, 51.65; H, 7.09.

(13S)-20-bromo-8,13-epoxy-15-trichloromethyl-labdane (**72**).

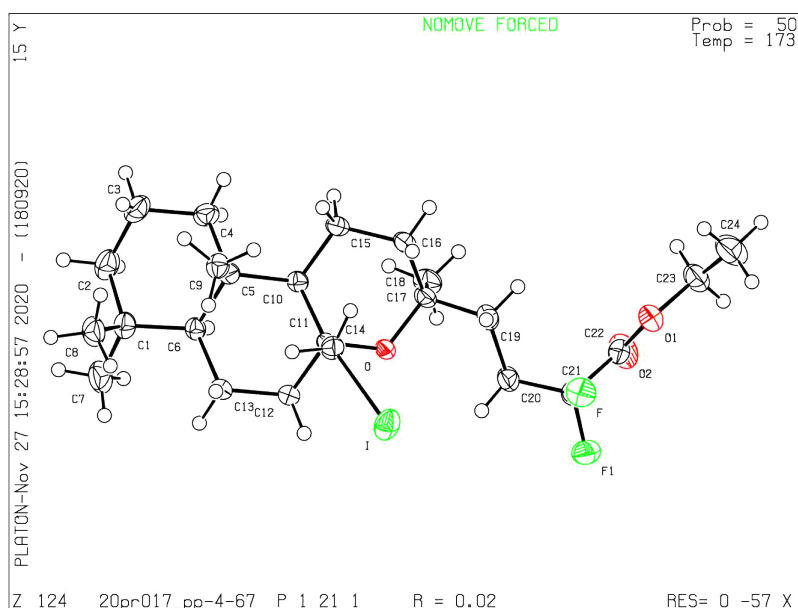
Colorless viscous liquid. $[\alpha]_D^{20} = 7.37^\circ$ (*c* 0.16, CHCl₃), IR (ν , cm⁻¹): 2972, 2929, 2866, 1465, 1452, 1377, 1104, 1080, 1042, 995, 790. ¹H NMR (400 MHz): 0.84 (s, 3H, Me-19), 0.90 (s, 3H, Me-18), 1.13 (s, 3H, Me-16), 1.53 (s, 3H, Me-17), 3.65 (dd, 1H, H-20, *J* = 11.3; 1.7 Hz), 3.92 (dd, 1H, H-20, *J* = 11.3; 1.2 Hz). ¹³C NMR: 100.71 (s, C-21), 75.01 (s, C-8), 72.52 (s, C-13), 59.62 (d, C-9), 58.09 (d, C-5), 50.95 (t, C-15), 41.69 (t, C-3), 41.00 (s, C-10), 40.57 (t, C-12), 36.60 (s, C-14), 36.34 (t, C-20), 35.93 (t, C-1), 34.27 (q, C-18), 33.14 (s, C-4), 30.56 (q, C-16), 23.51 (q, C-17), 22.26 (q, C-18), 19.78 (t, C-11), 18.52 (t, C-11), 17.95 (q, C-2).

(13S)-19-bromo-8,13-epoxy-15-trichloromethyl-labdane (**70**).

Colorless viscous liquid. $[\alpha]_D^{20} = 9.0^\circ$ (*c* 0.26, CHCl₃). IR (ν , cm⁻¹): 2970, 2930, 2865, 1465,

1452, 1377, 1105, 1080, 1041, 994, 787, 692. **NMR** – see table 6.5, Appendix. Anal. Calcd for $C_{21}H_{34}BrCl_3O$ (488.76): C, 51.61; H, 7.01. Found: C, 51.58; H, 7.10.

X-ray crystal structure report



Crystal-Structure Determination. A crystal of $C_{24}H_{39}F_2IO_3$ immersed in parabar oil was mounted at ambient conditions and transferred into the stream of nitrogen (173 K). All measurements were made on a *RIGAKU Synergy S* area-detector diffractometer¹ using mirror optics monochromated Cu $K\alpha$ radiation ($\lambda = 1.54184$ Å). The unit cell constants and an orientation matrix for data collection were obtained from a least-squares refinement of the setting angles of reflections in the range $3.411^\circ < \theta < 79.547^\circ$. A total of 11112 frames were collected using ω scans, with 0.15 second exposure time (0.4 s for high-angle reflections), a rotation angle of 0.5° per frame, a crystal-detector distance of 34.0 mm, at $T = 173(2)$ K.

Data reduction was performed using the *CrysAlisPro*¹ program. The intensities were corrected for Lorentz and polarization effects, and an absorption correction based on the multi-scan method using SCALE3 ABSPACK in *CrysAlisPro*¹ was applied. Data collection and refinement parameters are given in Table 1 (See the Appendix).

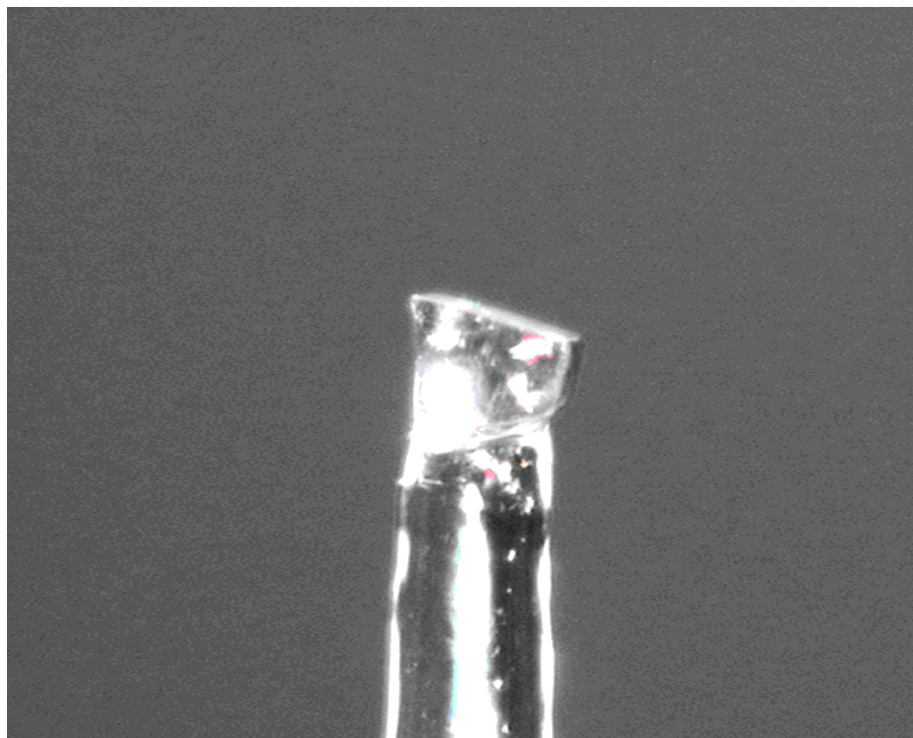
The structure was solved by intrinsic phasing using *SHELXT*², which revealed the positions of all non-hydrogen atoms of the title compound. All non-hydrogen atoms were refined anisotropically. H-atoms were assigned in geometrically calculated positions and refined using a riding model where each H-atom was assigned a fixed isotropic displacement parameter with a value equal to 1.2Ueq of its parent atom (1.5Ueq for methyl groups).

Refinement of the structure was carried out on F^2 using full-matrix least-squares procedures, which minimized the function $\sum w(F_o^2 - F_c^2)^2$. The weighting scheme was based on counting statistics and included a factor to downweight the intense reflections. All calculations were performed using the *SHELXL-2014/7*³ program in *OLEX2*.⁴

The X-ray crystal structure determination service unit of the Department of Chemistry, Bio-

chemistry and Pharmaceutical Sciences of the University of Bern is acknowledged for measuring, solving, refining and summarizing the structures of compounds XX, YY, ZZ. The Synergy diffractometer was partially funded by the Swiss National Science Foundation (SNF) within the R'Equip programme (project number 206021_177033).

Model has Chirality at C11 (*R*).



Single crystal of the compound mounted on a glass fiber.

7 Appendix

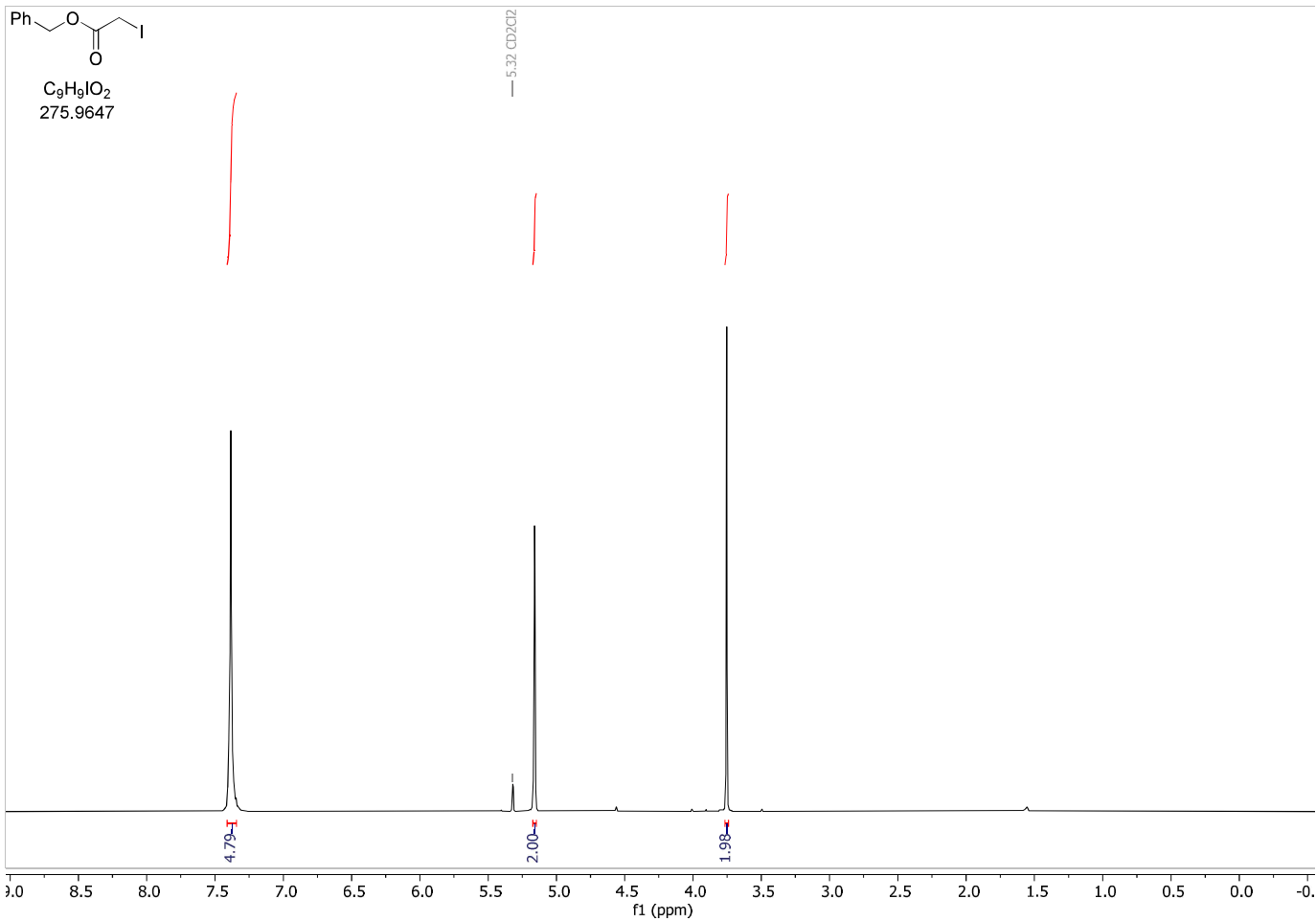
NMR Spectra

7.1 NMR and X-ray Chapter 3

Thiol Catalysed Enantioselective Hydroalkylation

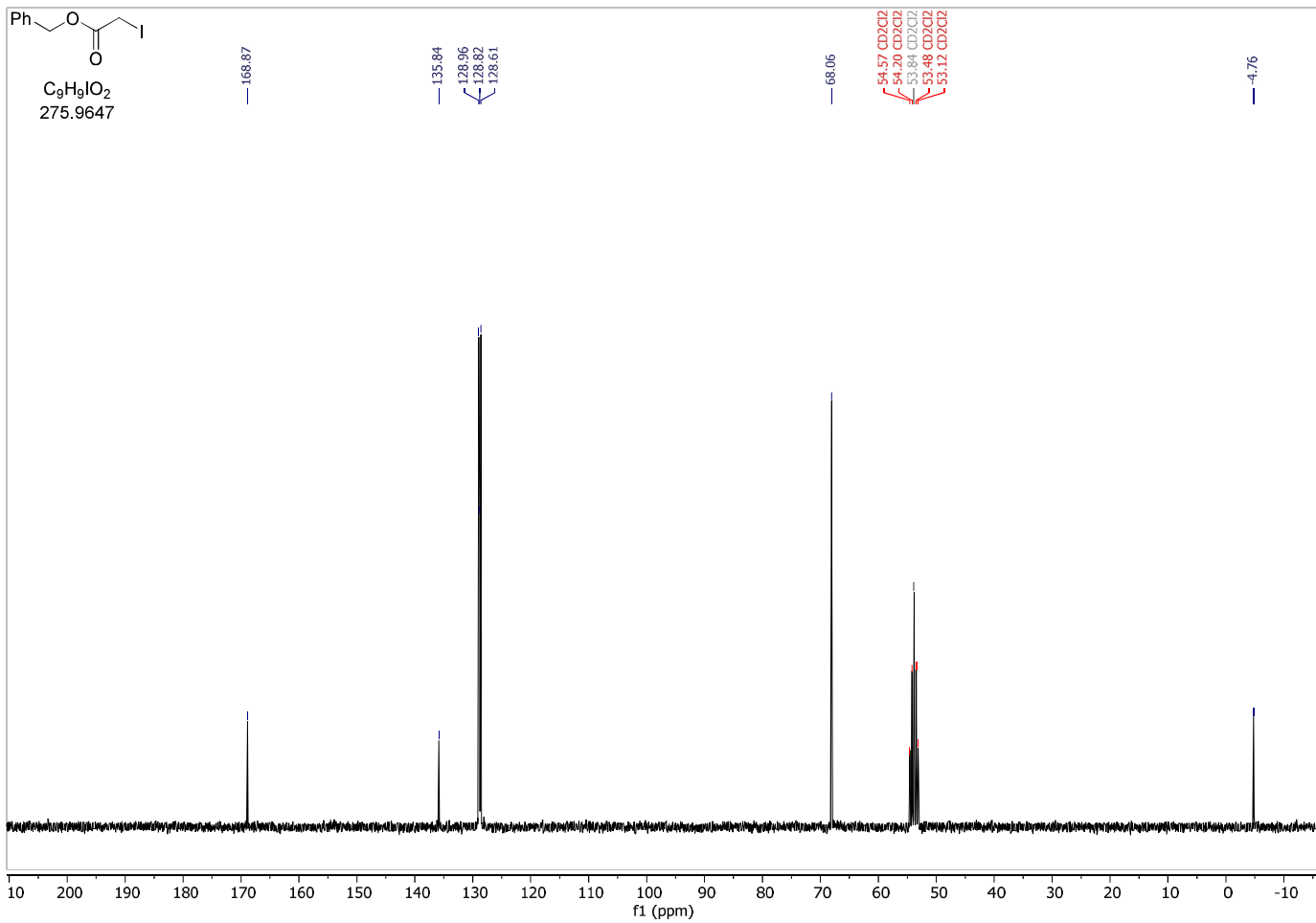
benzyl 2-iodoacetate (1a)

$^1\text{H-NMR}$ (300 MHz, CD_2Cl_2)

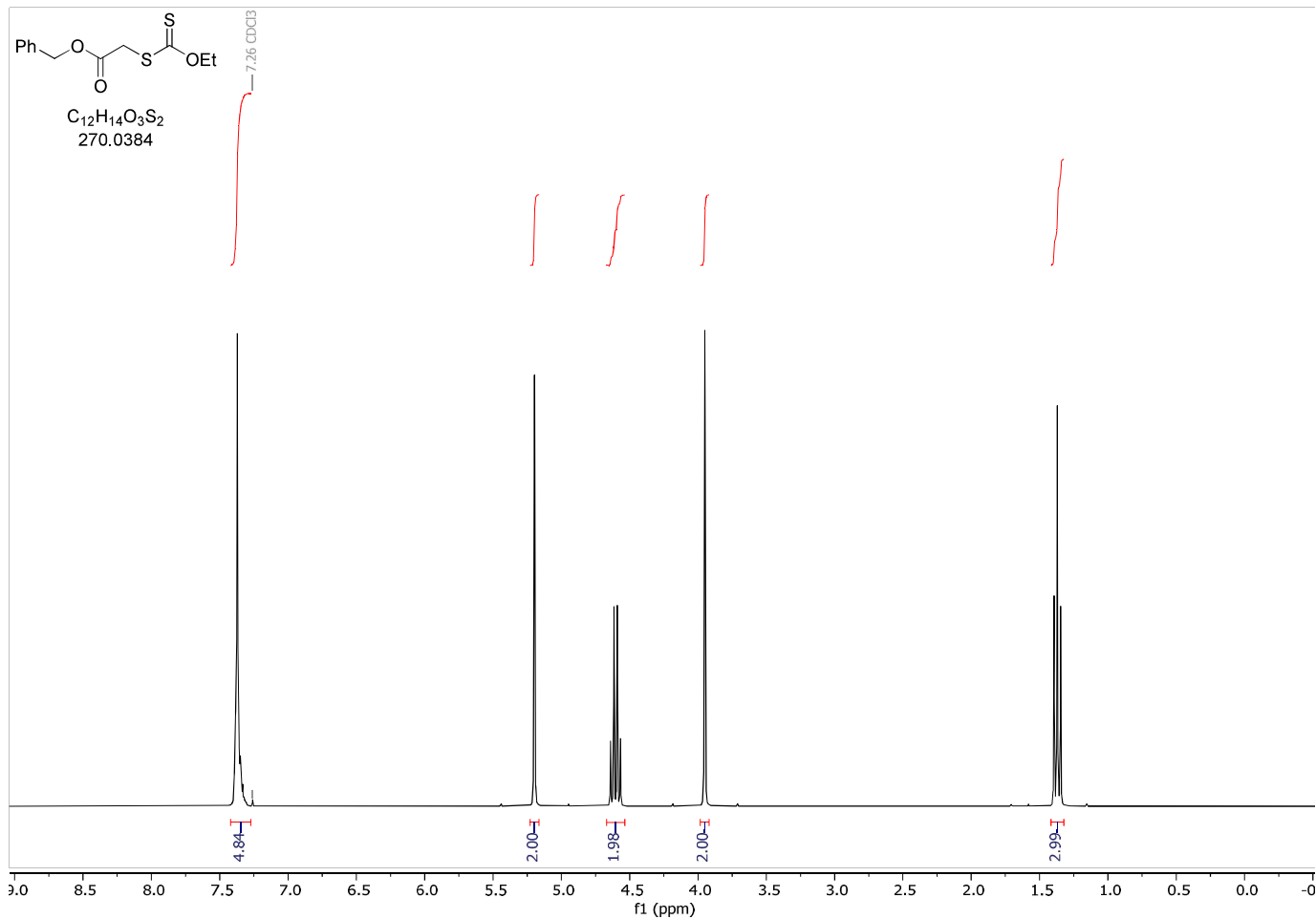


benzyl 2-iodoacetate (1a)

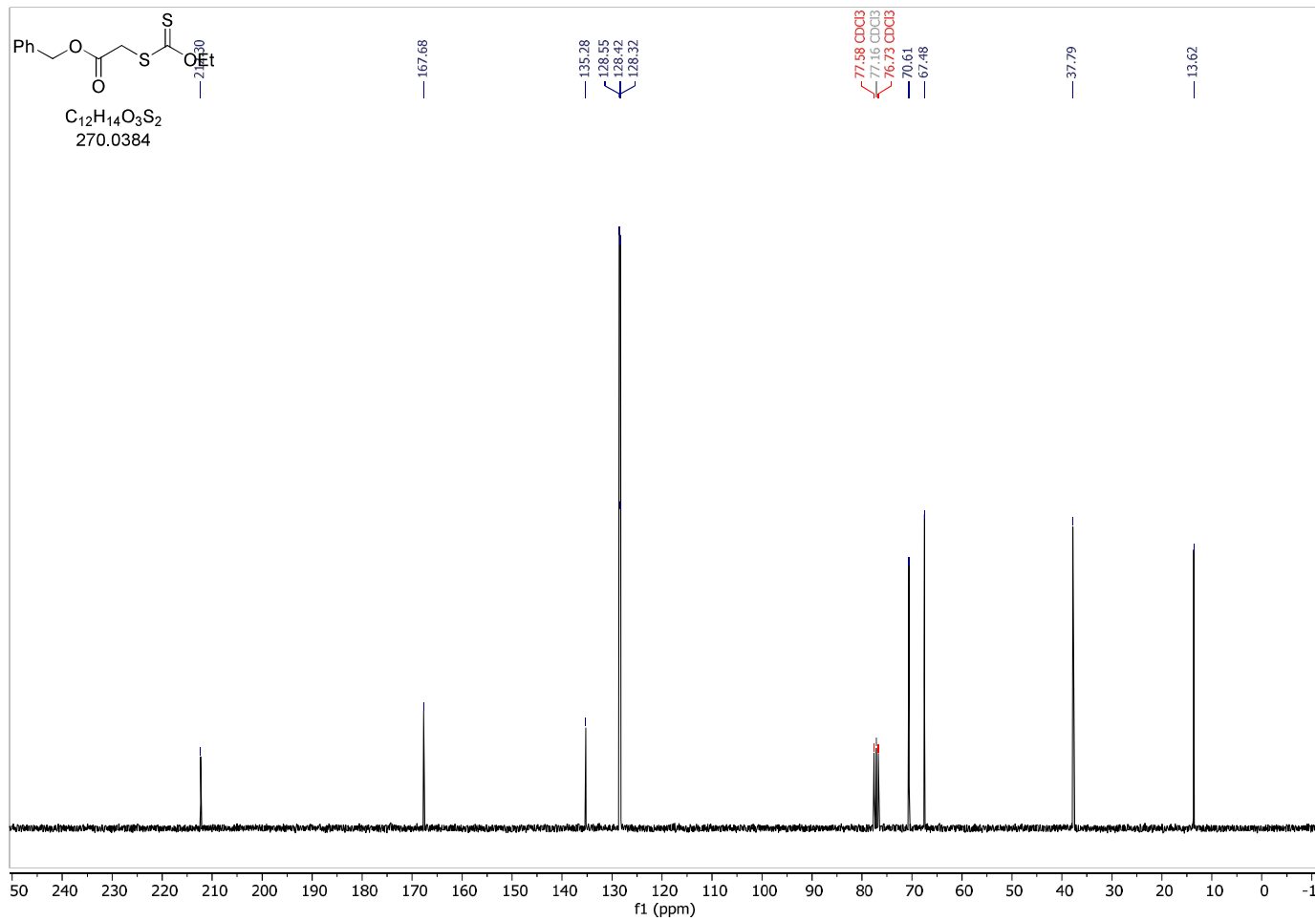
$^{13}\text{C-NMR}$ (75 MHz, CD_2Cl_2)



benzyl 2-((ethoxycarbonthioyl)thio)acetate (1a')

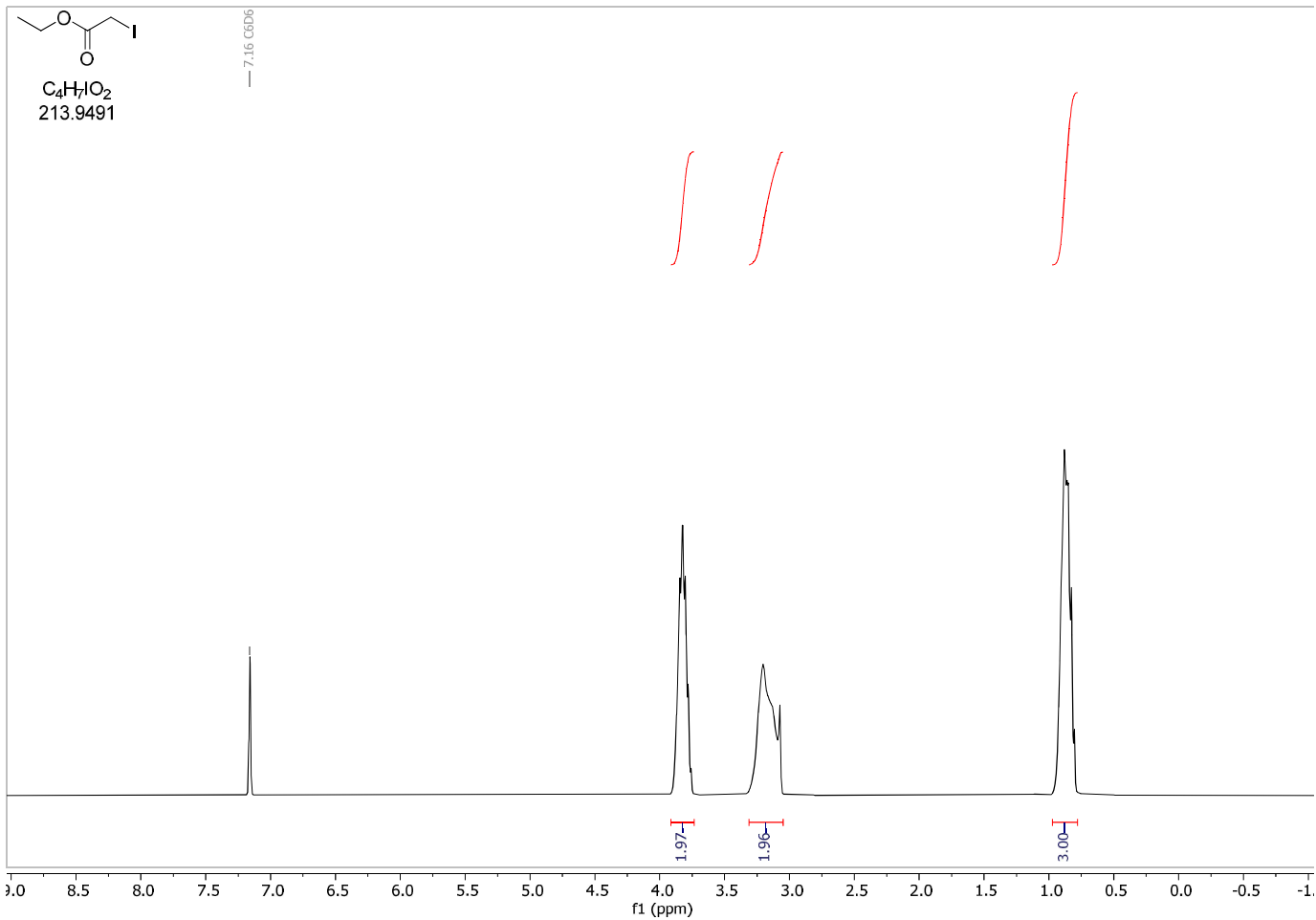
 $^1\text{H-NMR}$ (300 MHz, CDCl_3)

benzyl 2-((ethoxycarbonthioyl)thio)acetate (1a')

 $^{13}\text{C-NMR}$ (75 MHz, CDCl_3)

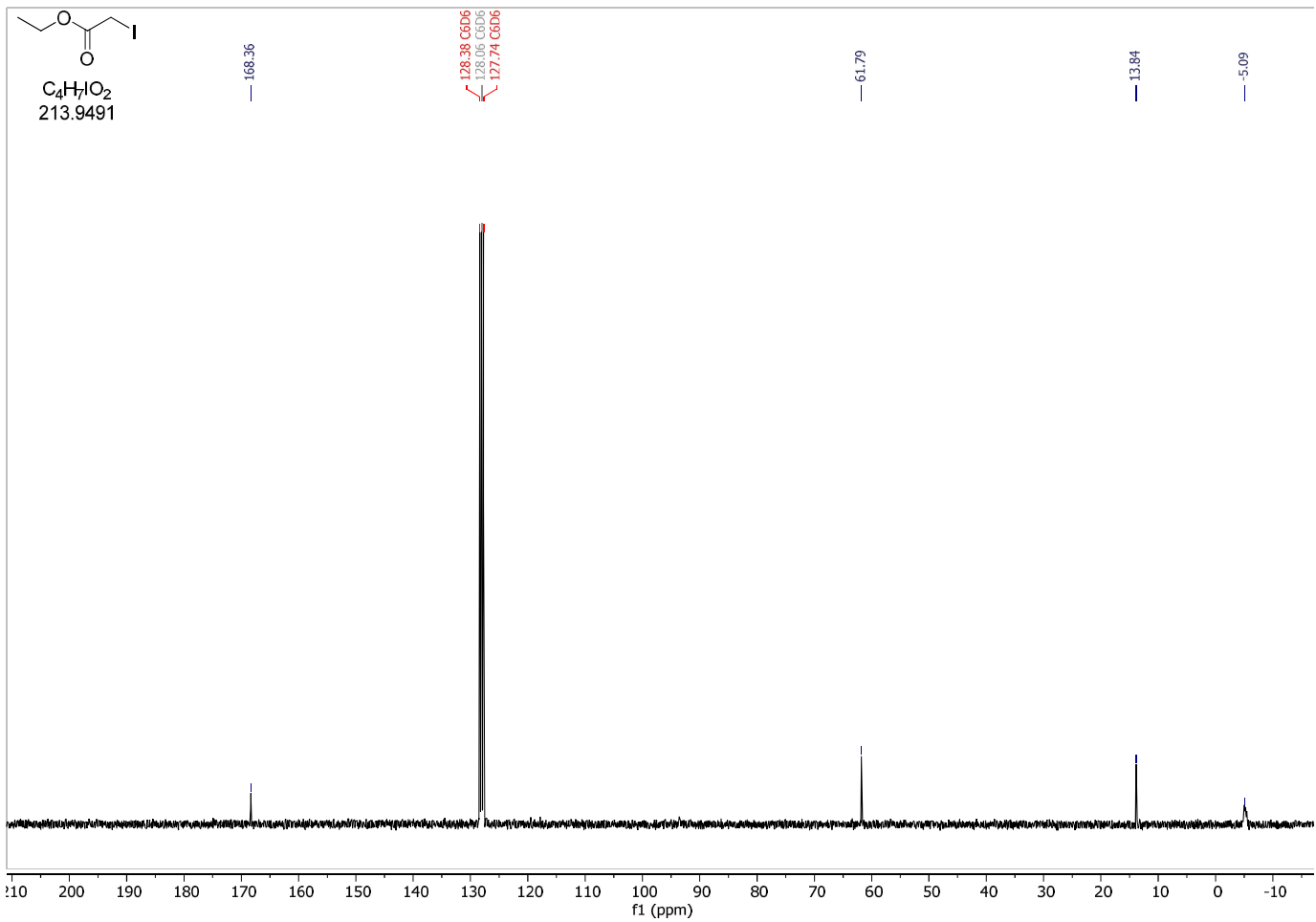
ethyl 2-iodoacetate (1b)

$^1\text{H-NMR}$ (300 MHz, C_6D_6)



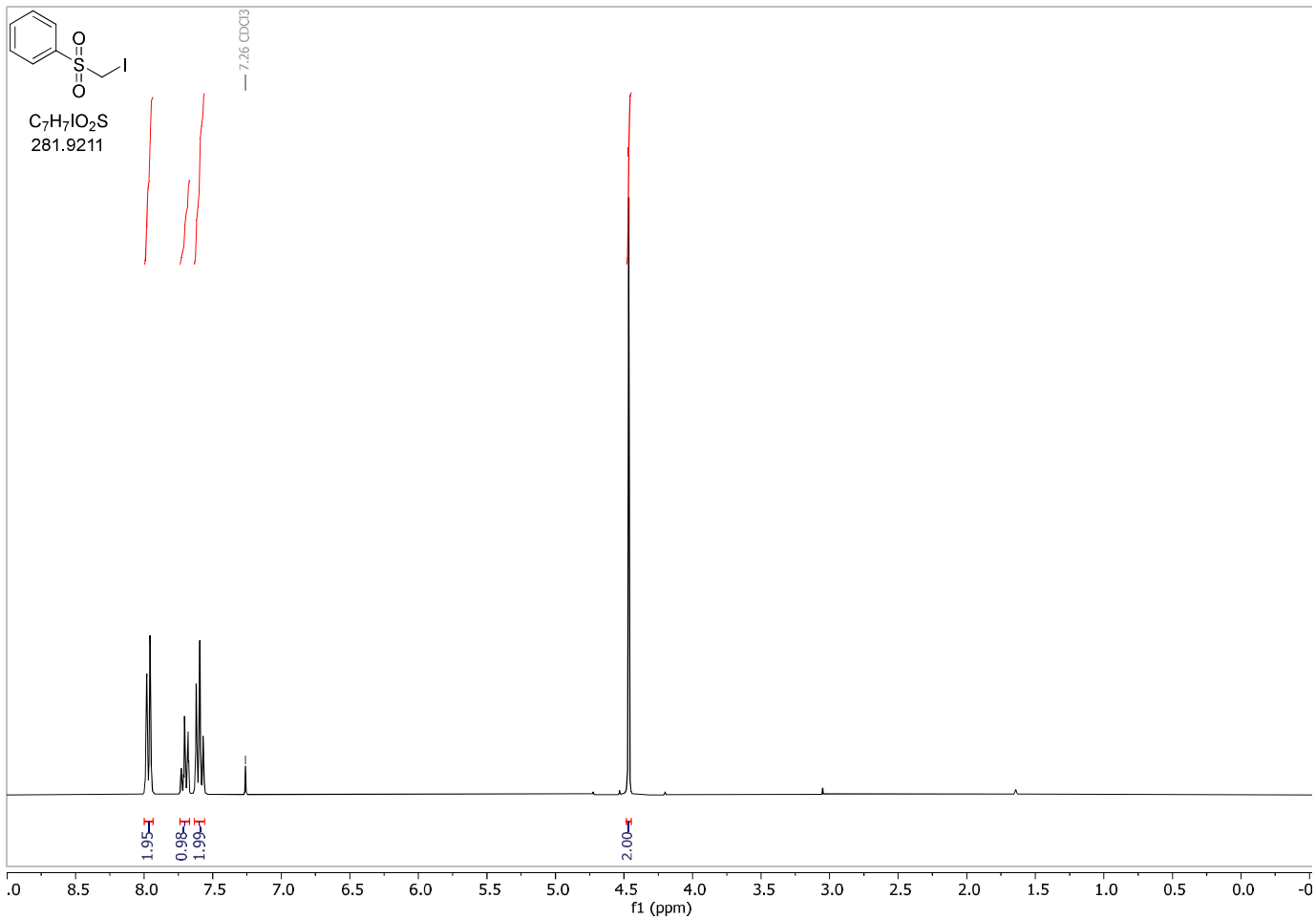
ethyl 2-iodoacetate (1b)

$^{13}\text{C-NMR}$ (75 MHz, C_6D_6)



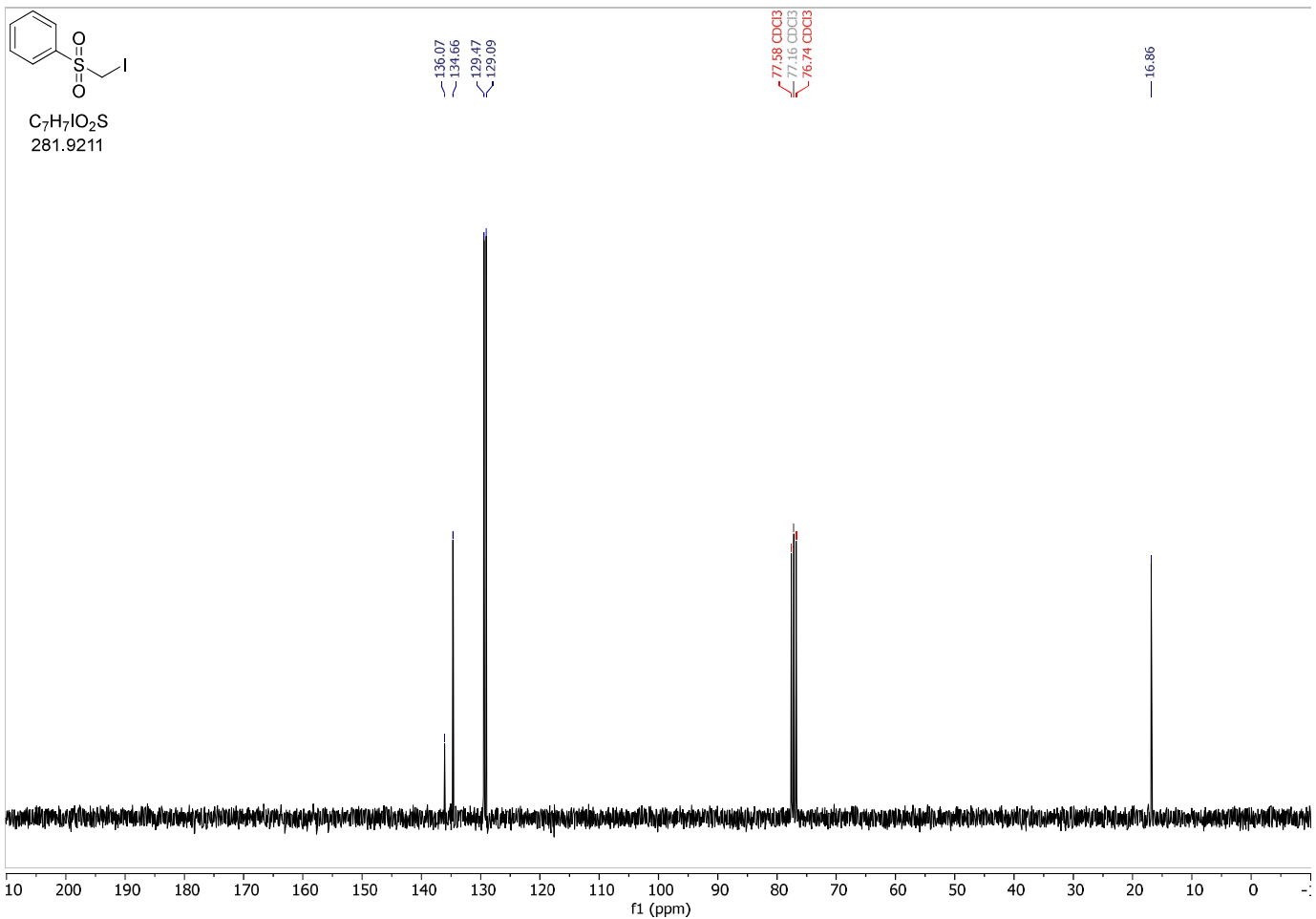
Iodomethylsulfonylbenzene (1c)

¹H-NMR (300 MHz, CD₂Cl₂)

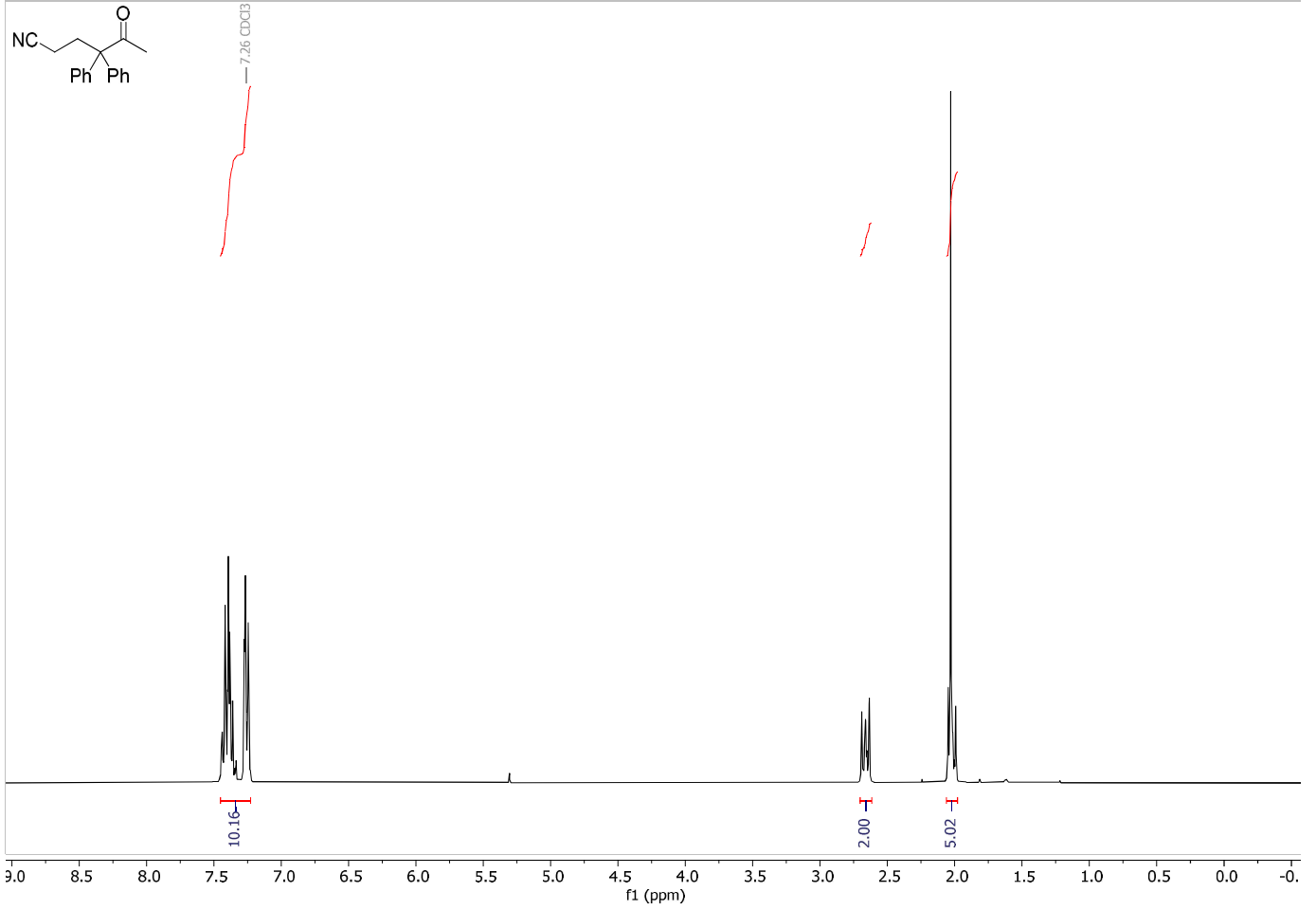


Iodomethylsulfonylbenzene (1c)

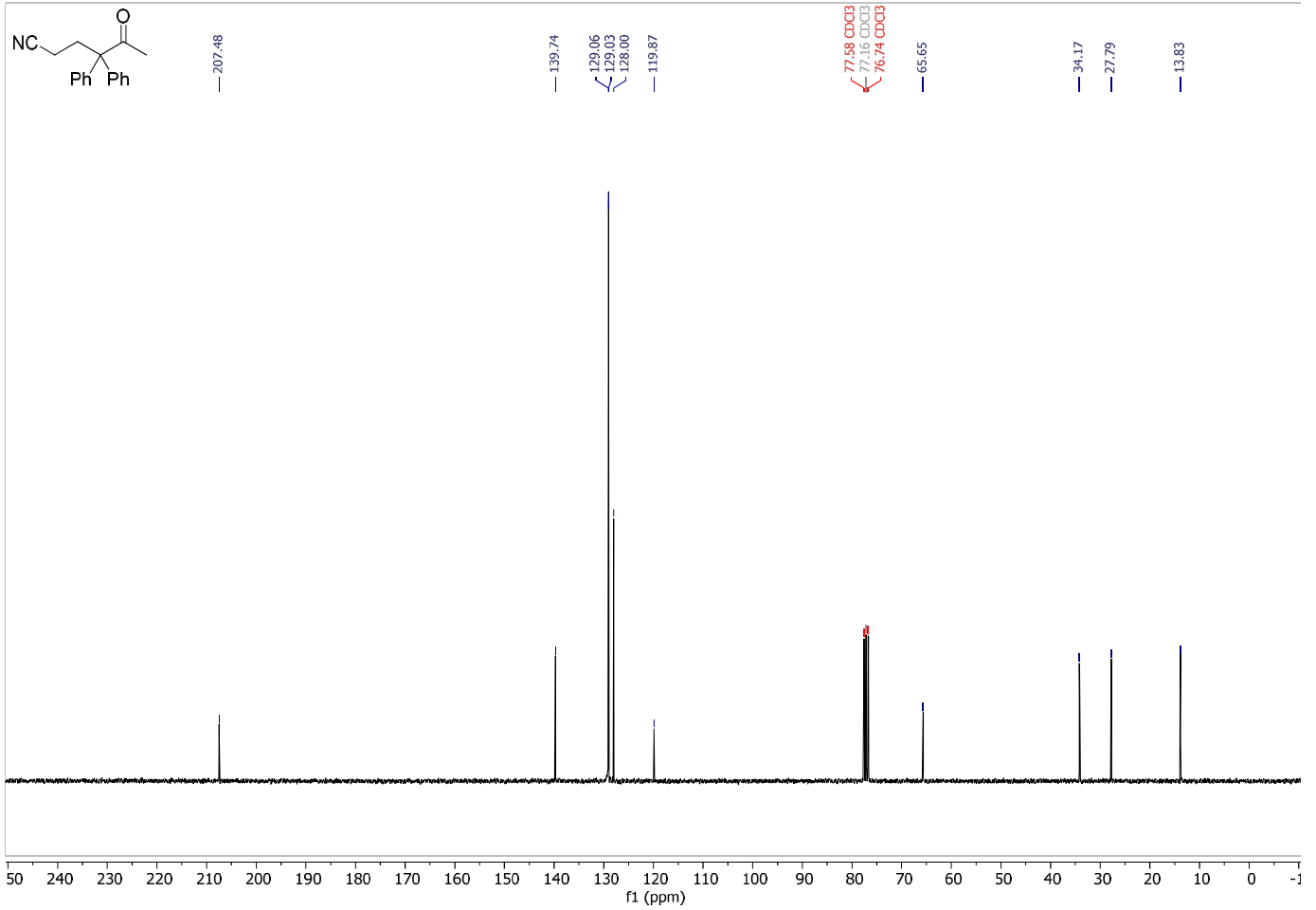
¹³C-NMR (300 MHz, CD₂Cl₂)



5-oxo-4,4-diphenylhexanenitrile (S1)

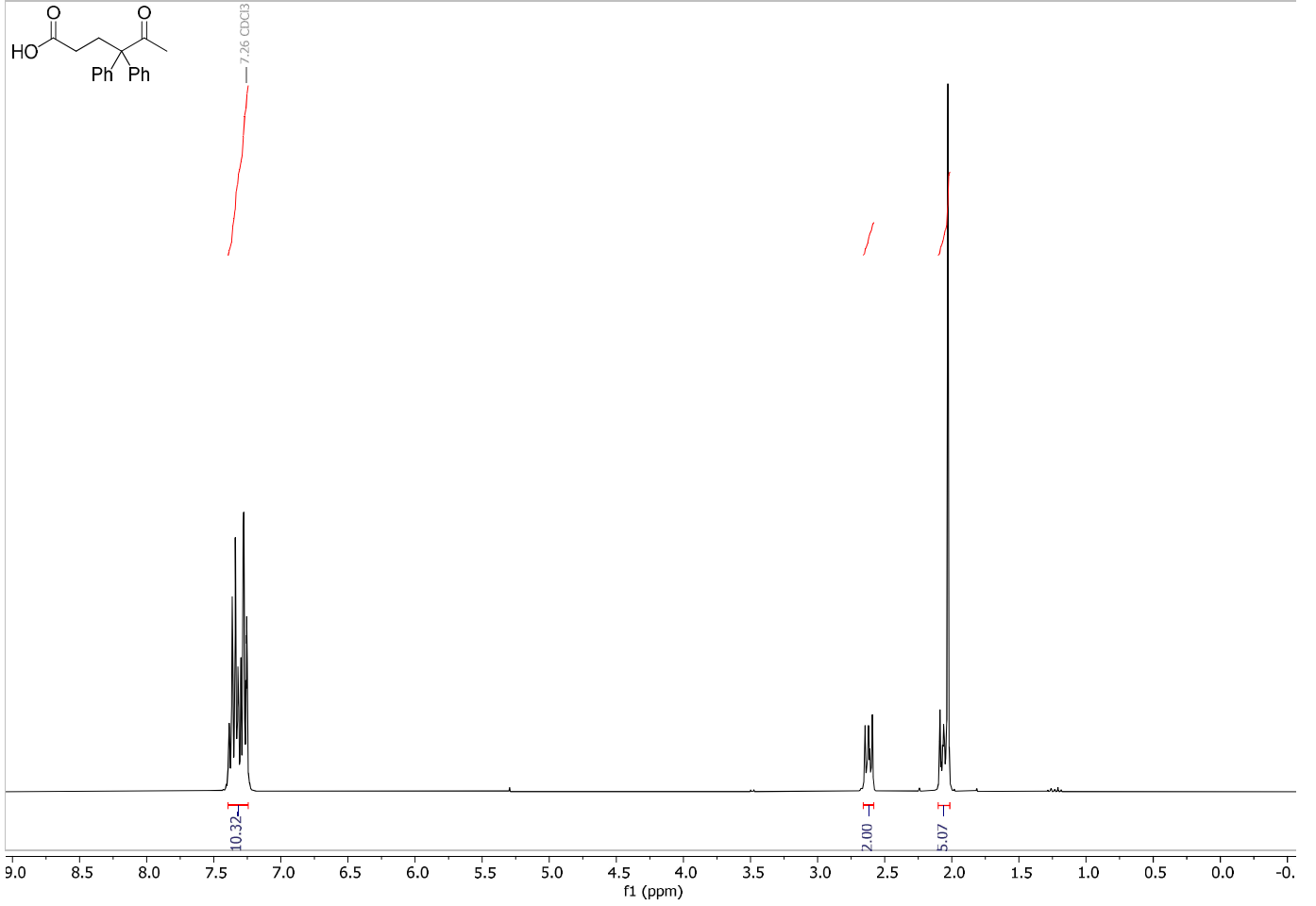
 $^1\text{H-NMR}$ (300 MHz, CDCl_3)

5-oxo-4,4-diphenylhexanenitrile (S1)

 $^{13}\text{C-NMR}$ (75 MHz, CDCl_3)

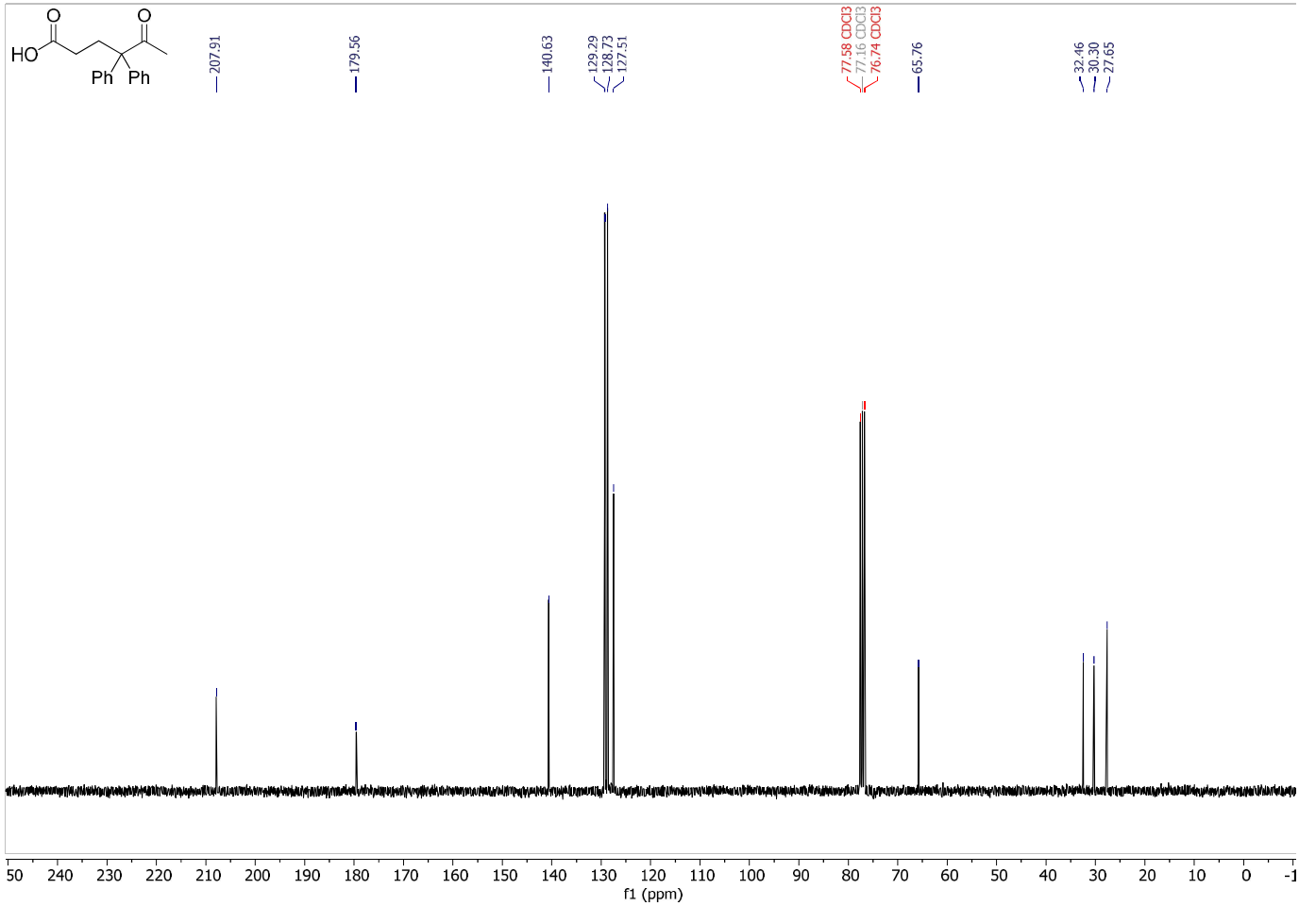
5-oxo-4,4-diphenylhexanoic acid (S2)

¹H-NMR (300 MHz, CDCl₃)

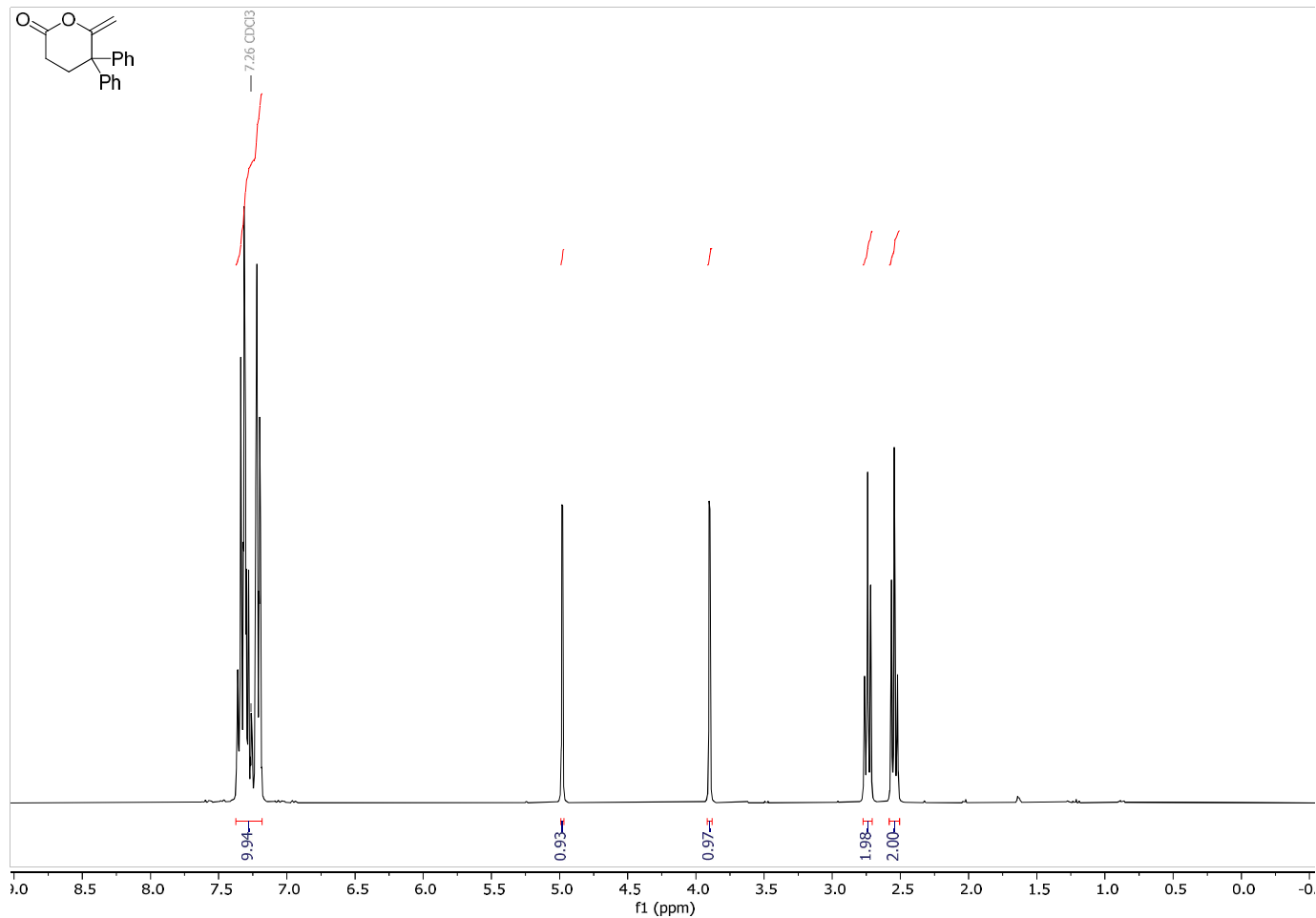


5-oxo-4,4-diphenylhexanoic acid (S2)

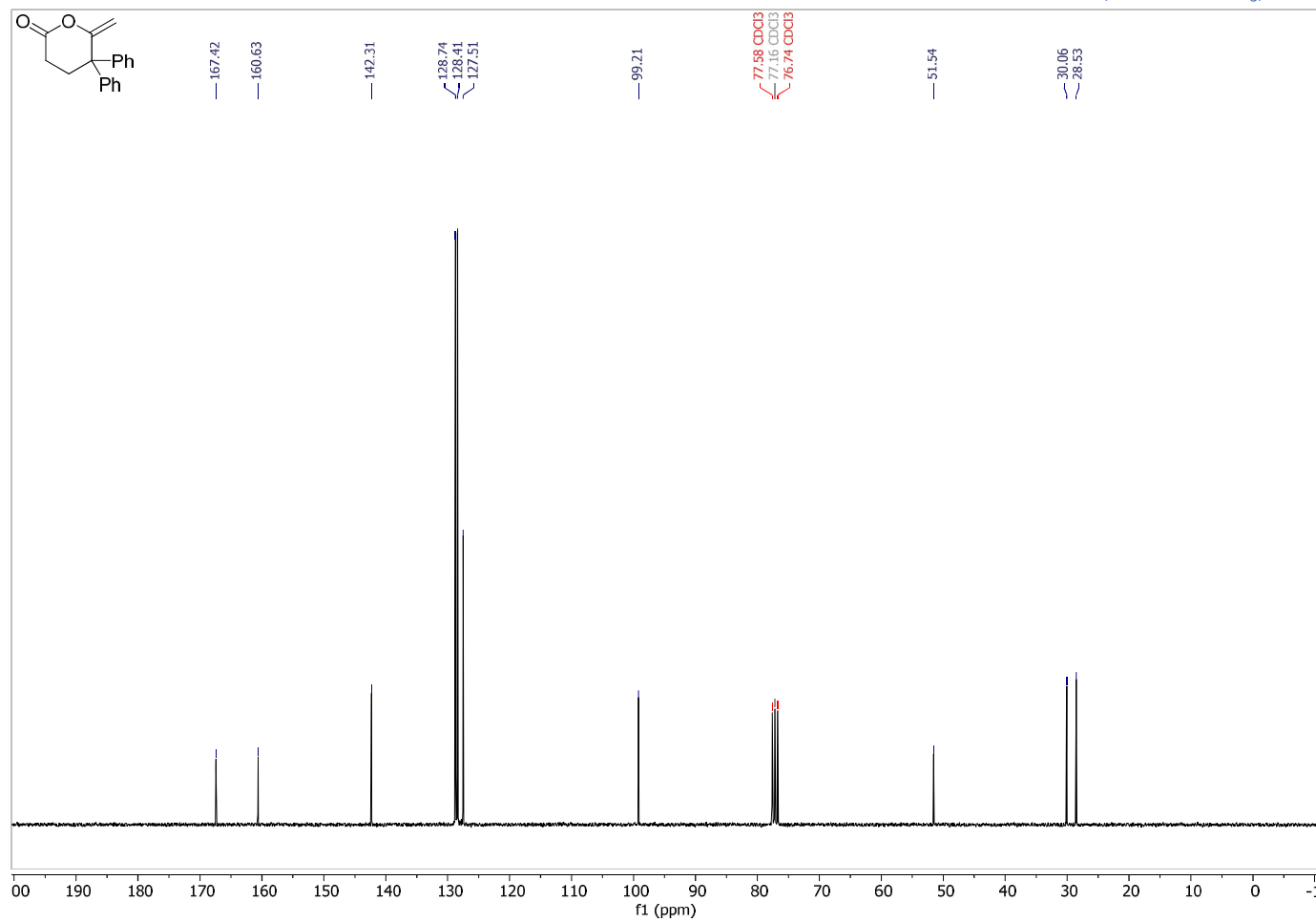
¹³C-NMR (75 MHz, CDCl₃)



6-methylene-5,5-diphenyltetrahydro-2H-pyran-2-one (2b)

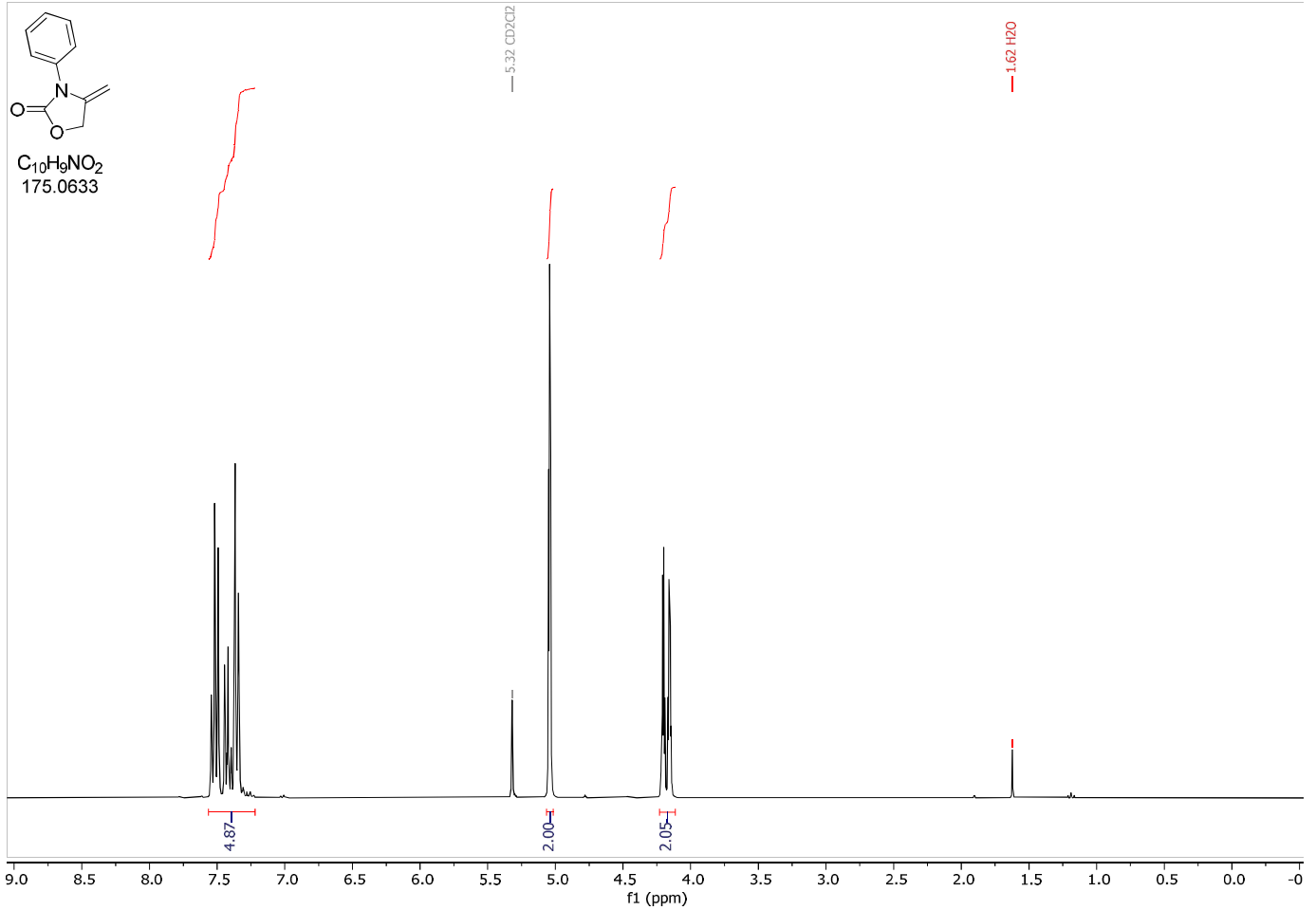
 $^1\text{H-NMR}$ (300 MHz, CDCl_3)

6-methylene-5,5-diphenyltetrahydro-2H-pyran-2-one (2b)

 $^{13}\text{C-NMR}$ (75 MHz, CDCl_3)

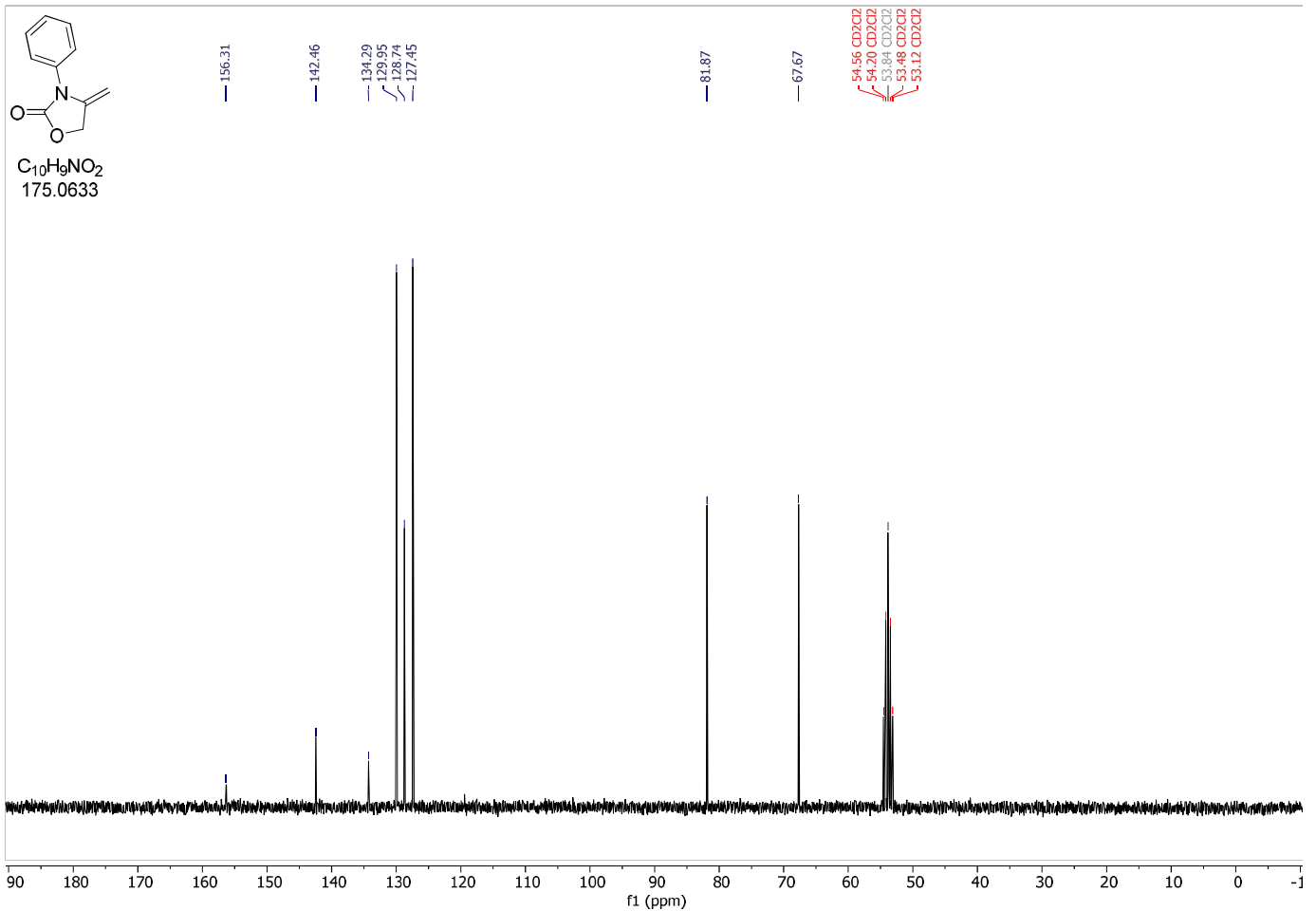
4-methylene-3-phenyl-oxazolidin-2-one (2p)

¹H-NMR (300 MHz, CD₂Cl₂)



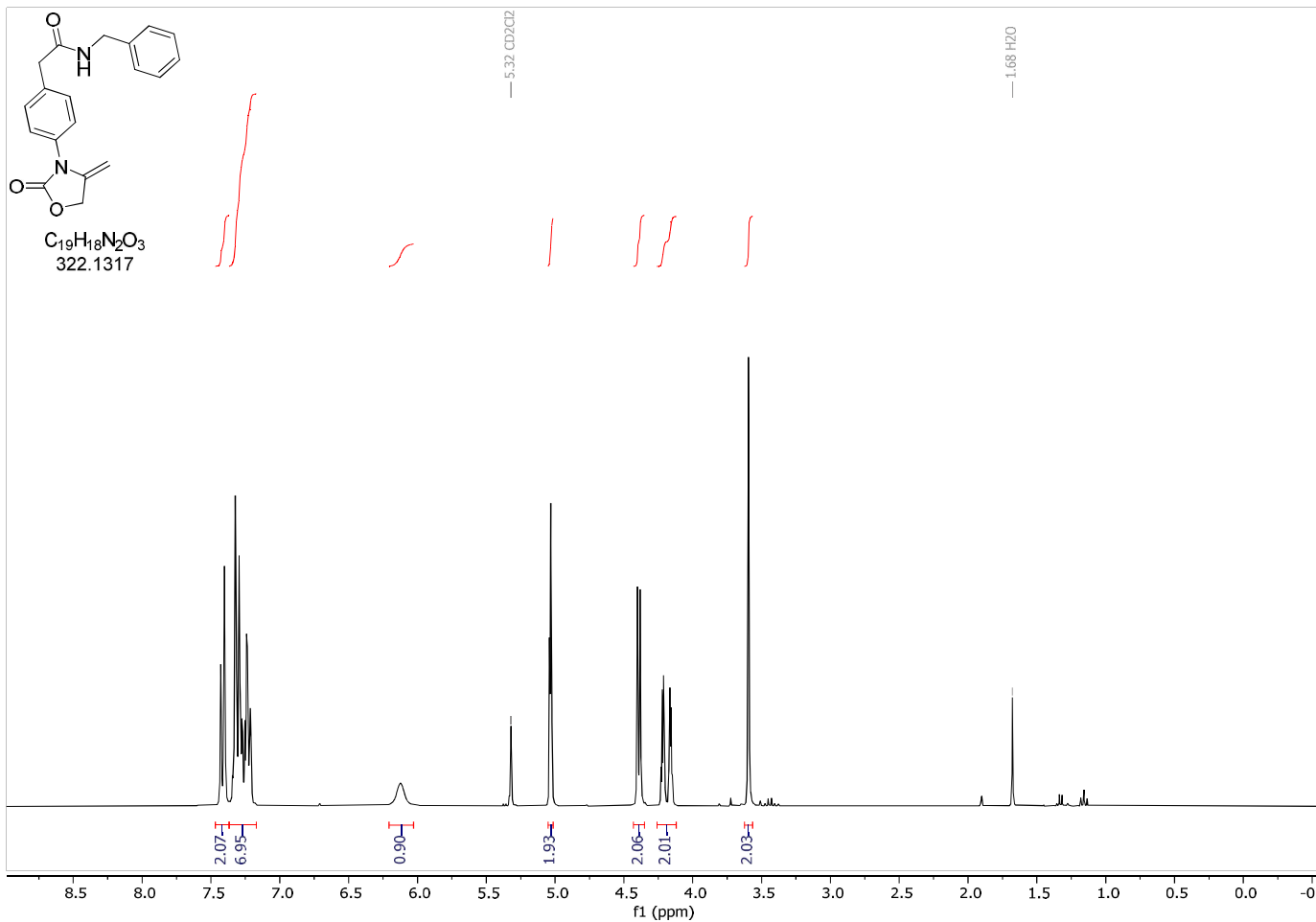
4-methylene-3-phenyl-oxazolidin-2-one (2p)

¹³C-NMR (75 MHz, CD₂Cl₂)



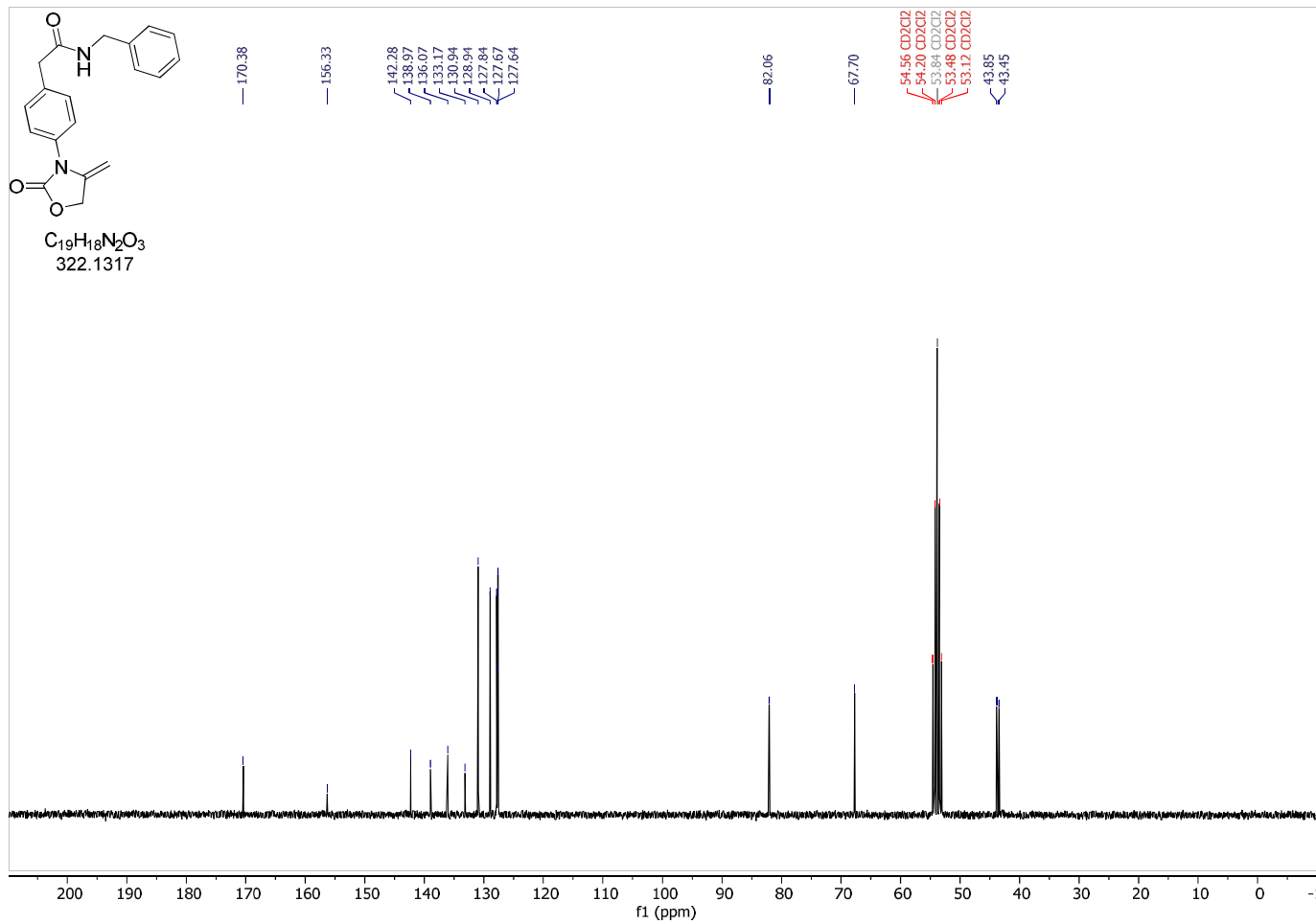
N-Benzyl-2-(4-(4-methylene-2-oxooxazolidin-3-yl)phenyl)acetamide (2q)

¹H-NMR (300 MHz, CD₂Cl₂)



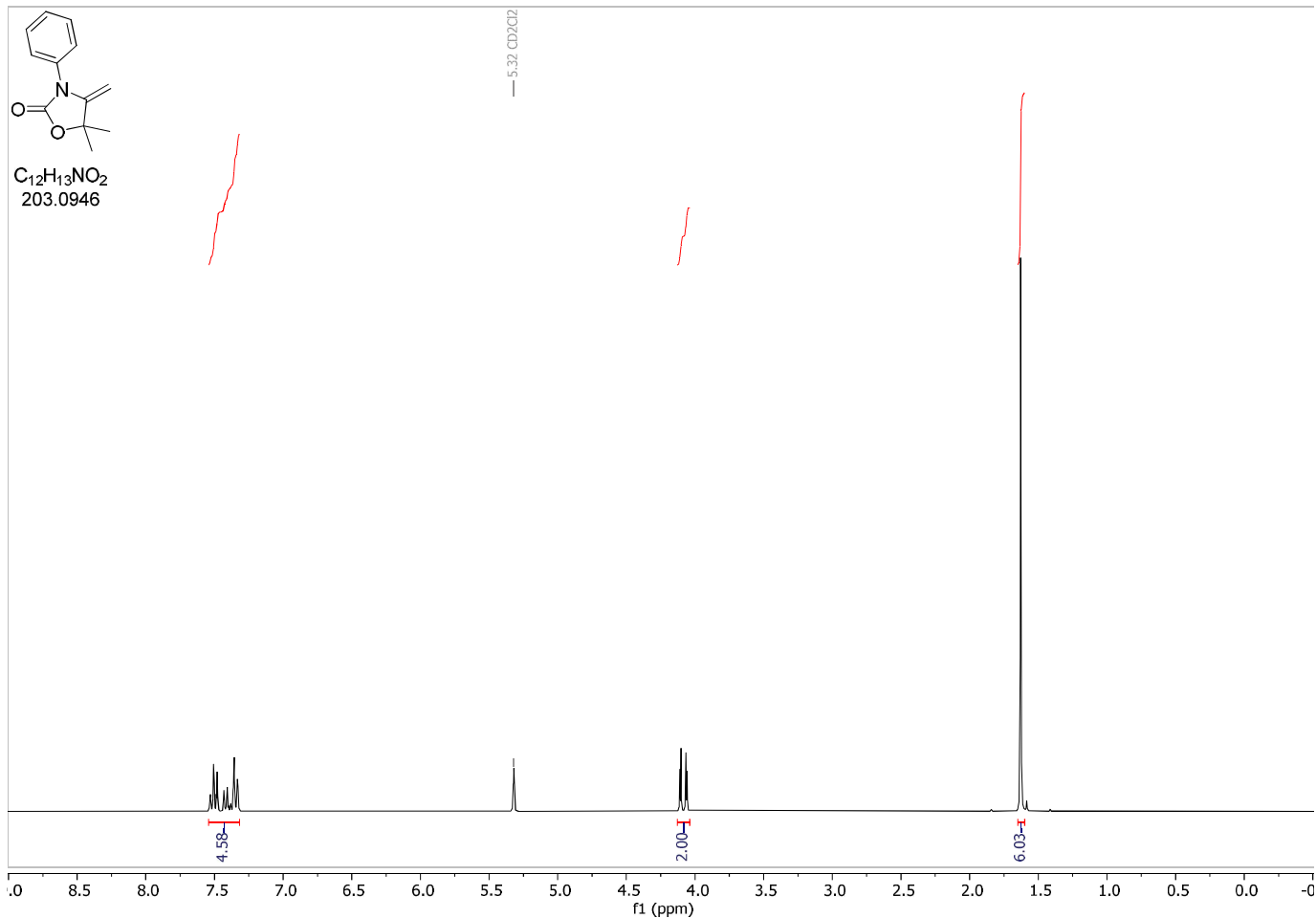
N-Benzyl-2-(4-(4-methylene-2-oxooxazolidin-3-yl)phenyl)acetamide (2q)

¹³C-NMR (75 MHz, CD₂Cl₂)



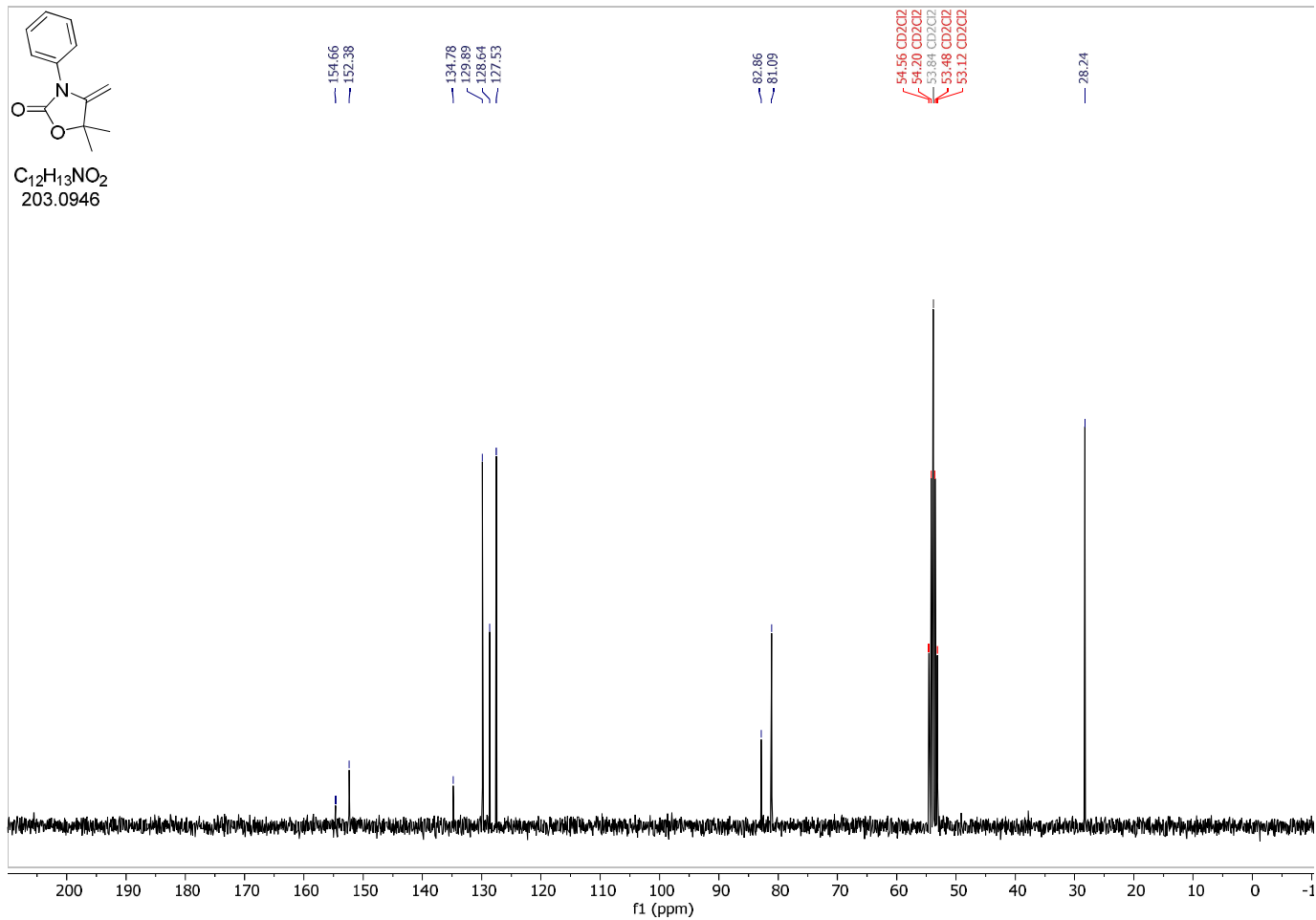
5,5-dimethyl-4-methylene-3-phenyl-oxazolidin-2-one (2s)

¹H-NMR (300 MHz, CD₂Cl₂)



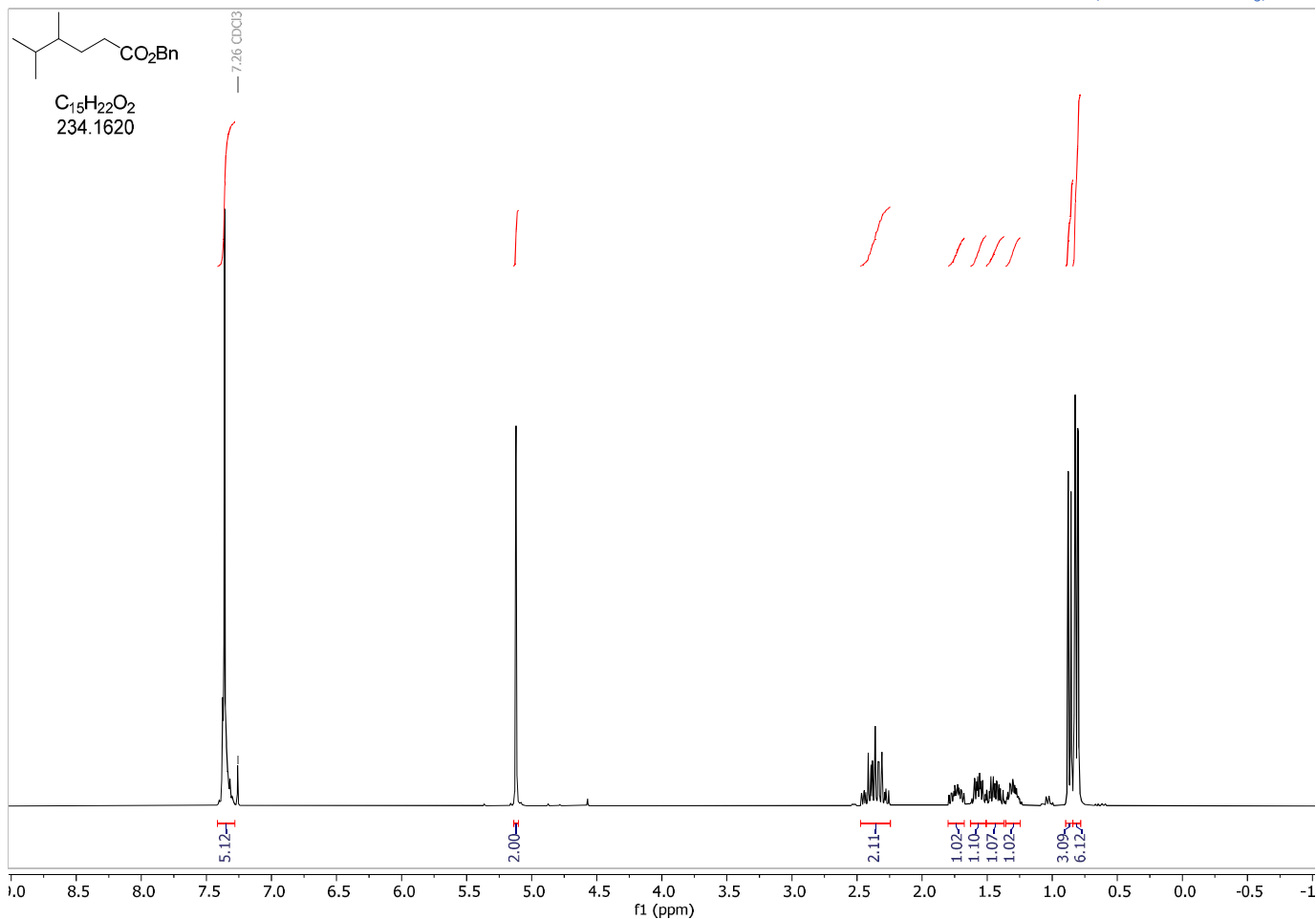
5,5-dimethyl-4-methylene-3-phenyl-oxazolidin-2-one (2s)

¹³C-NMR (75 MHz, CD₂Cl₂)



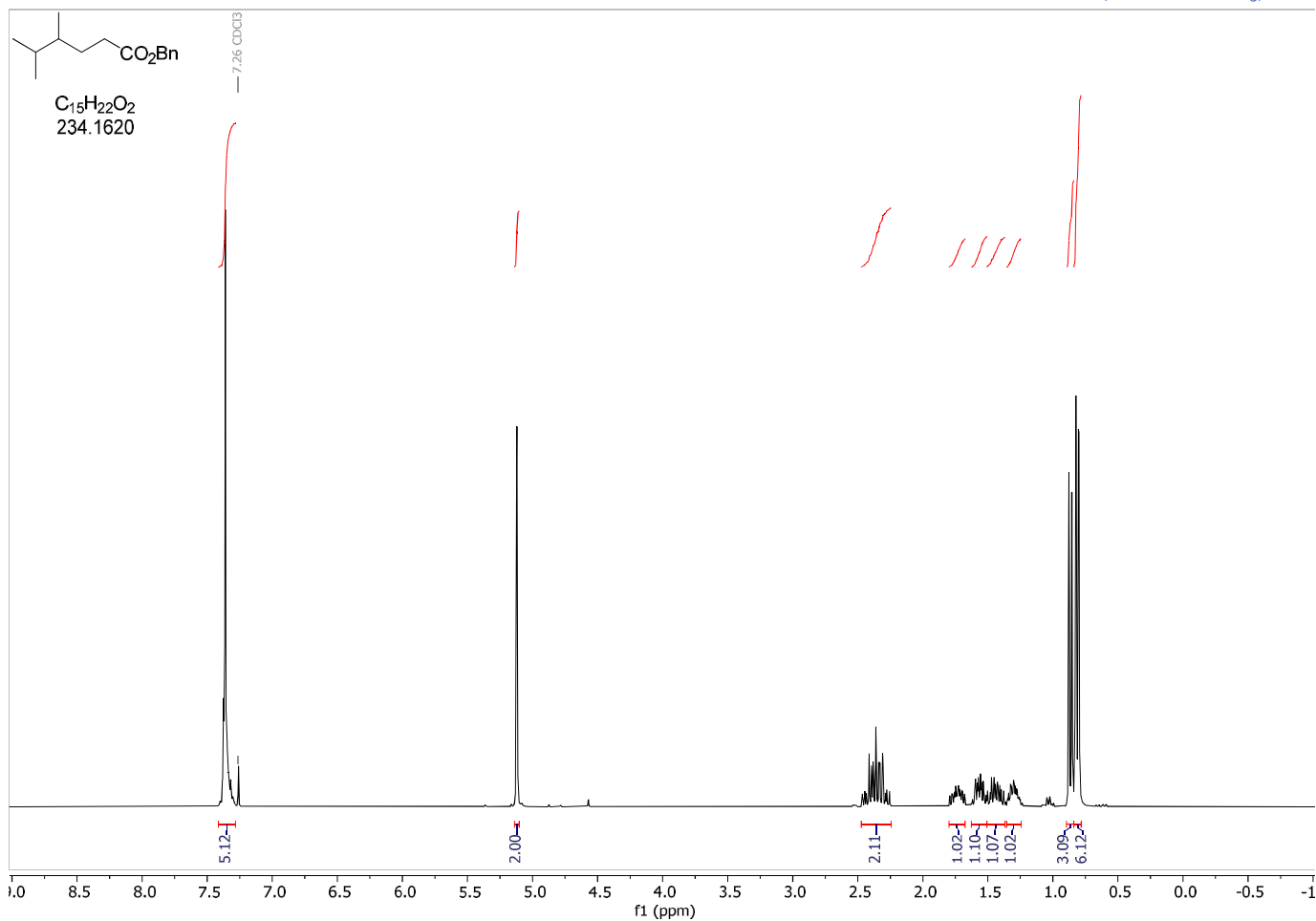
benzyl 4,5-dimethylhexanoate (3aa)

¹H-NMR (300 MHz, CDCl₃)

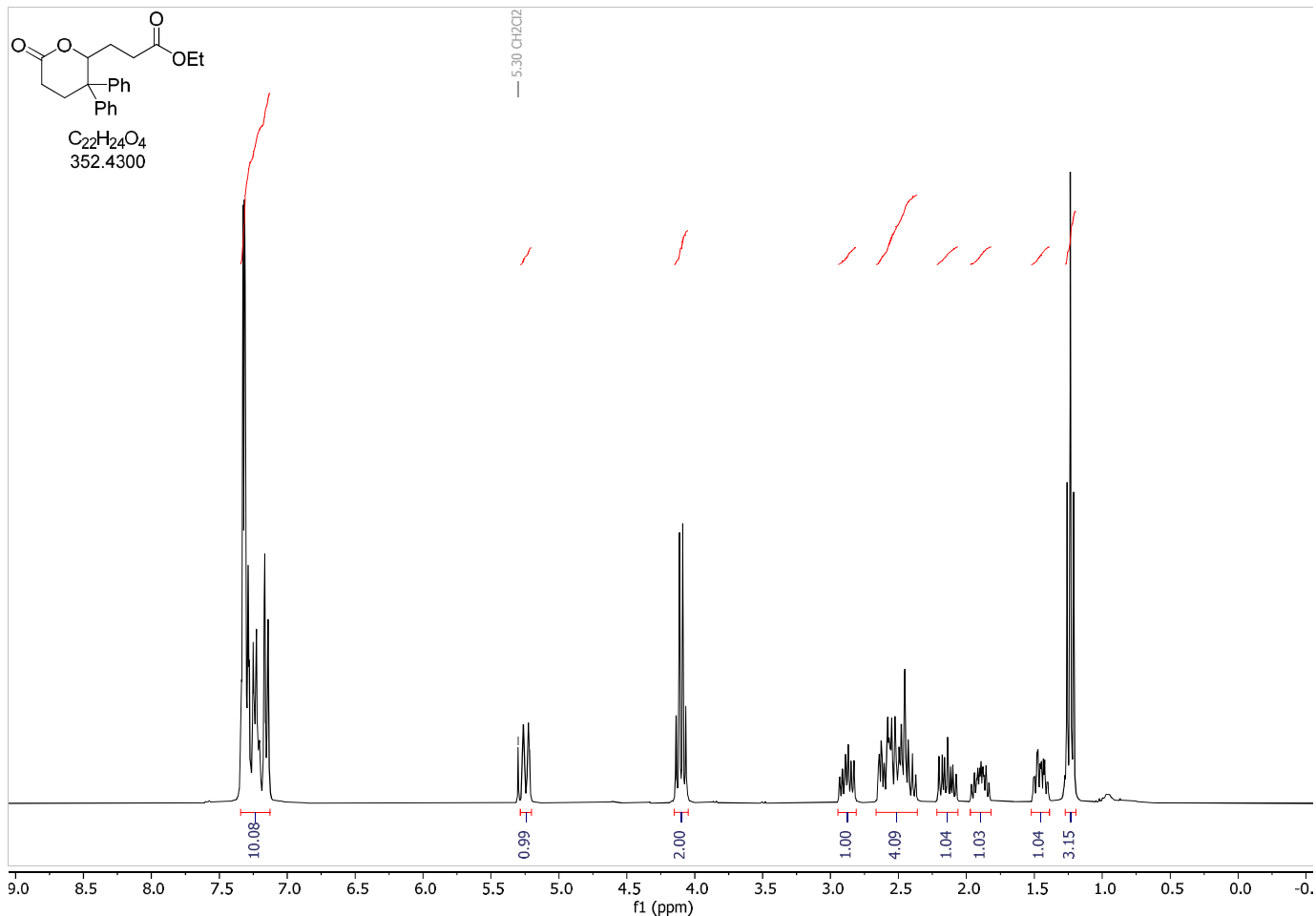


benzyl 4,5-dimethylhexanoate (3aa)

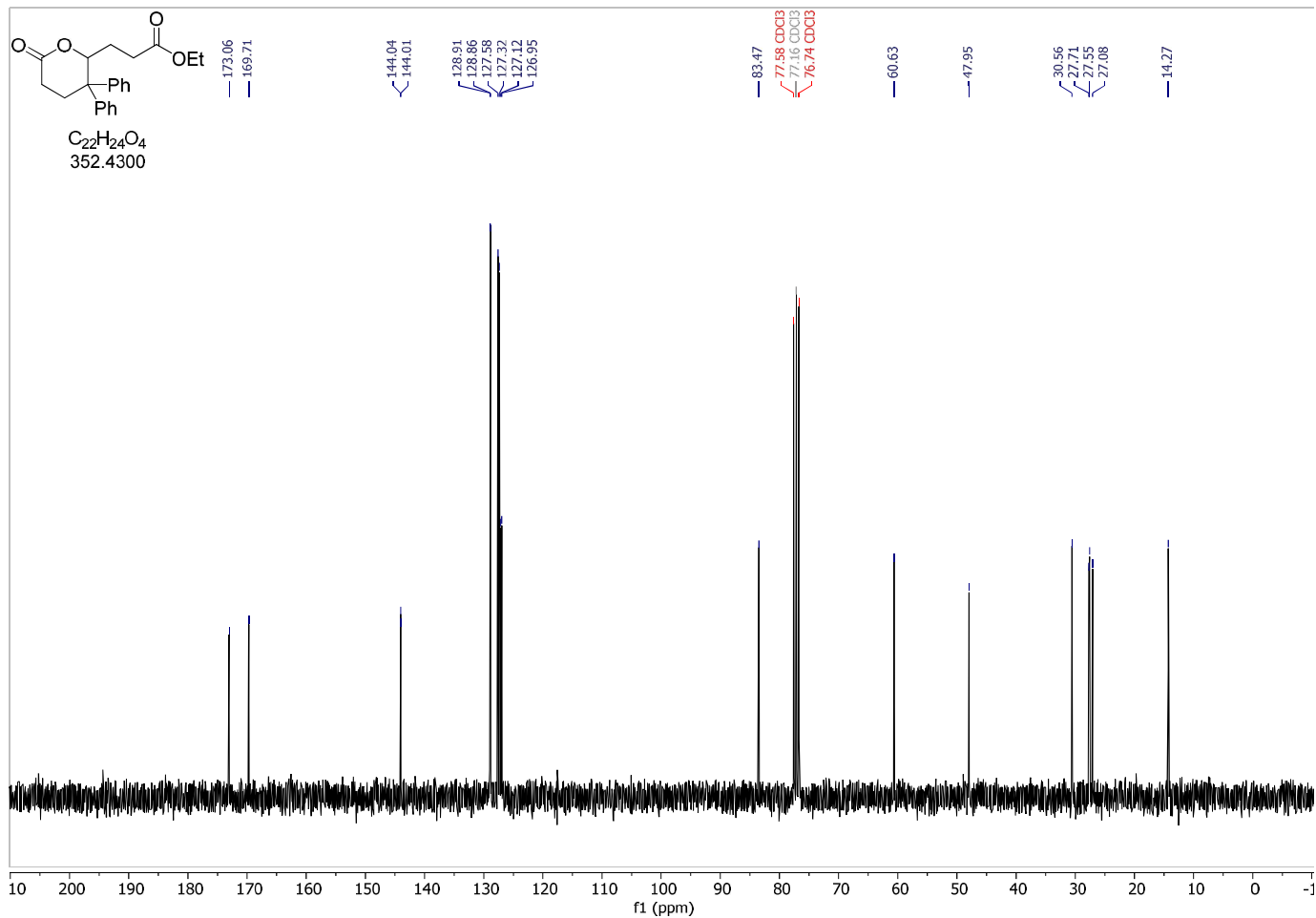
¹³C-NMR (75 MHz, CDCl₃)



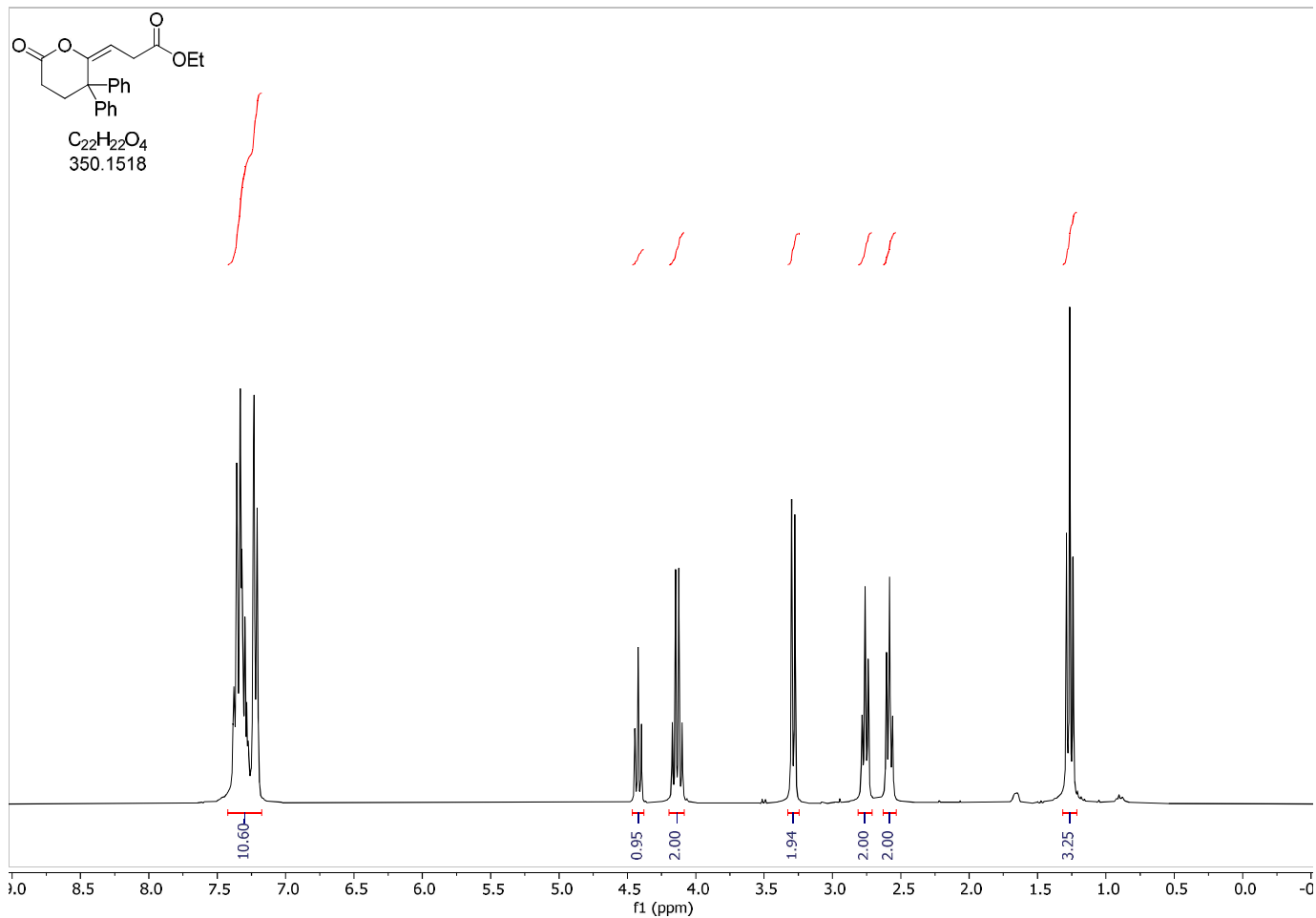
ethyl 3-(6-oxo-3,3-diphenyl-tetrahydropyran-2-yl)propanoate (3bb)

 $^1\text{H-NMR}$ (300 MHz, CDCl_3)

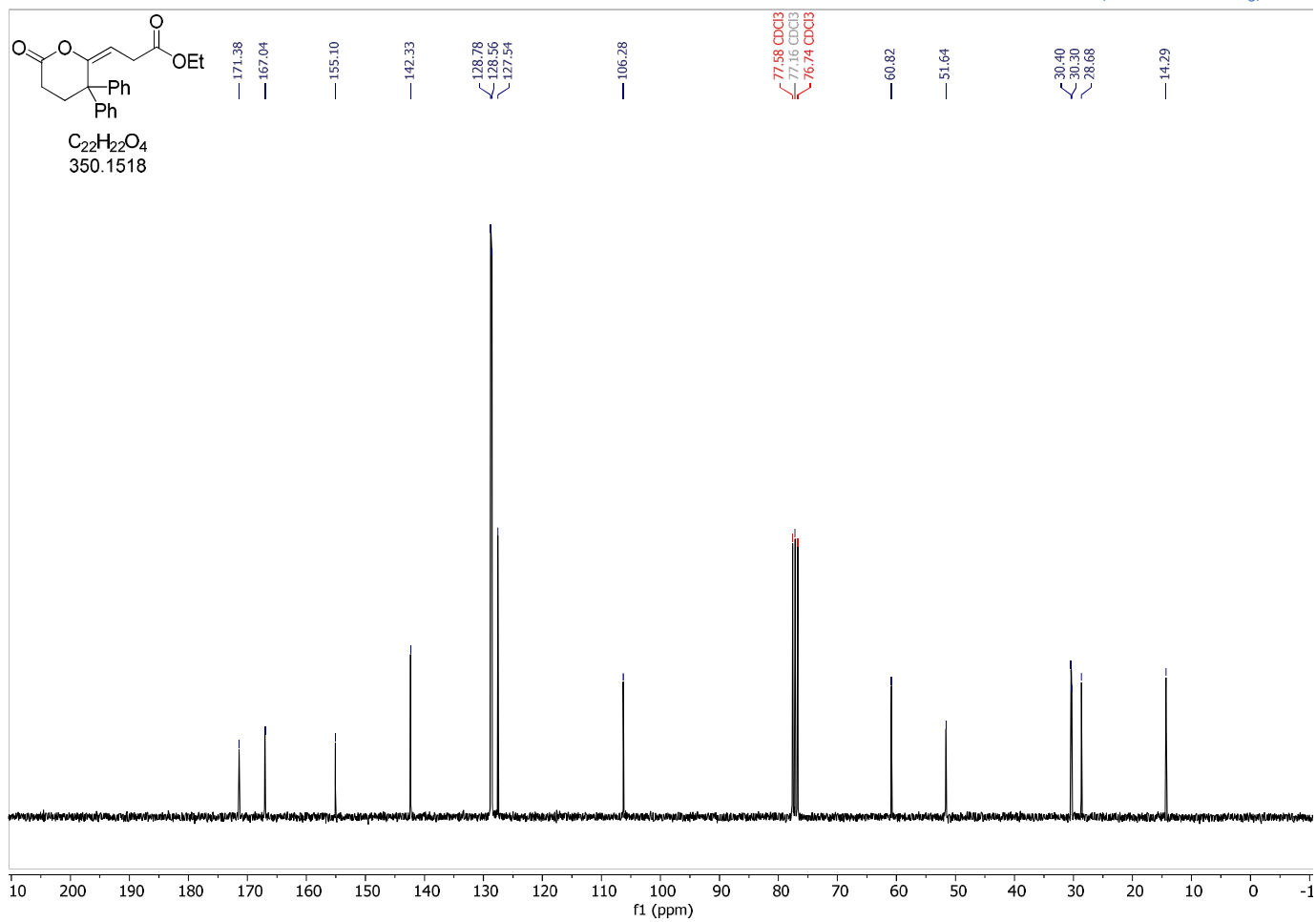
ethyl 3-(6-oxo-3,3-diphenyl-tetrahydropyran-2-yl)propanoate (3bb)

 $^{13}\text{C-NMR}$ (75 MHz, CDCl_3)

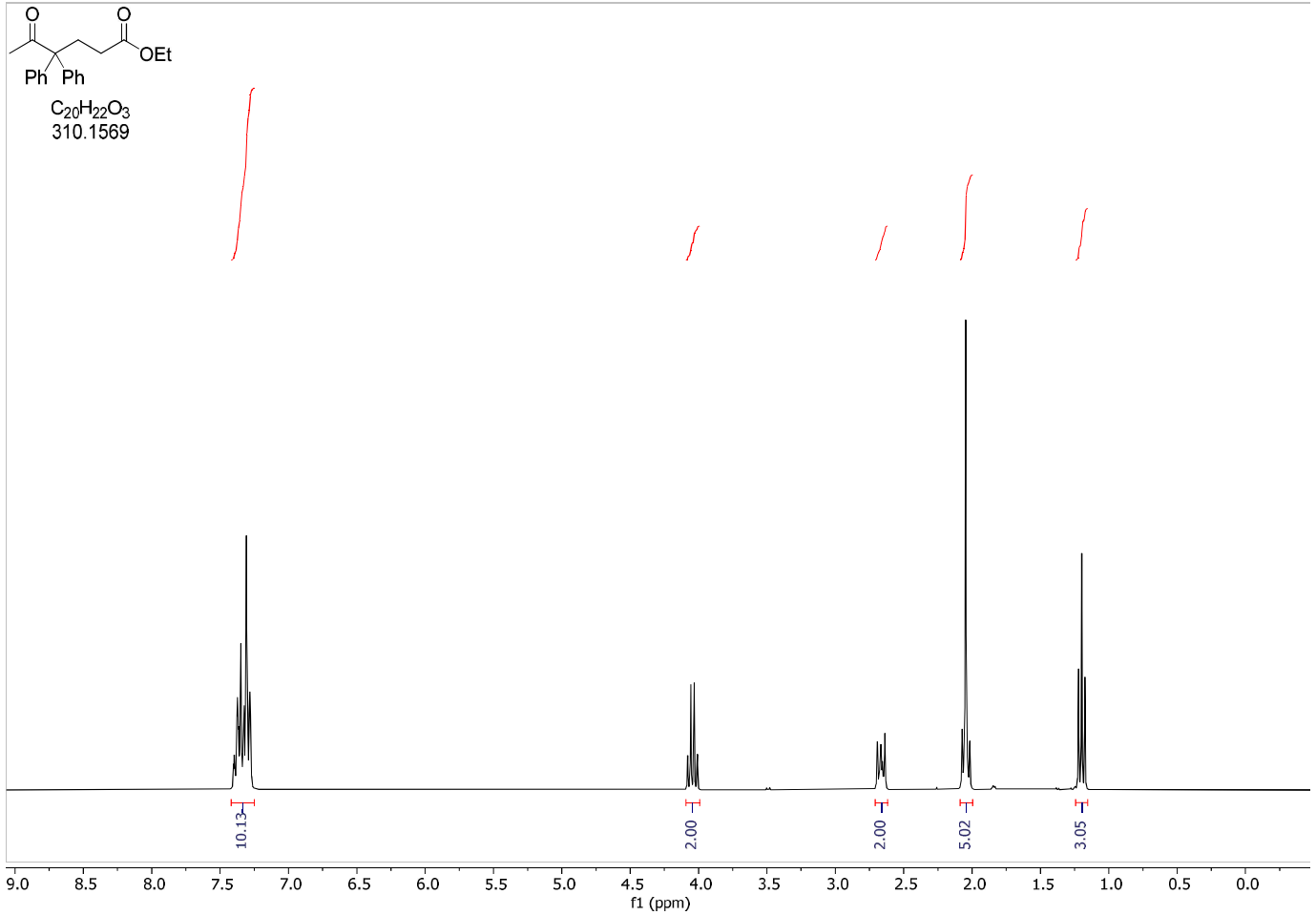
ethyl 3-(6-oxo-3,3-diphenyltetrahydro-2H-pyran-2-ylidene)propanoate (4)

 $^1\text{H-NMR}$ (300 MHz, CDCl_3)

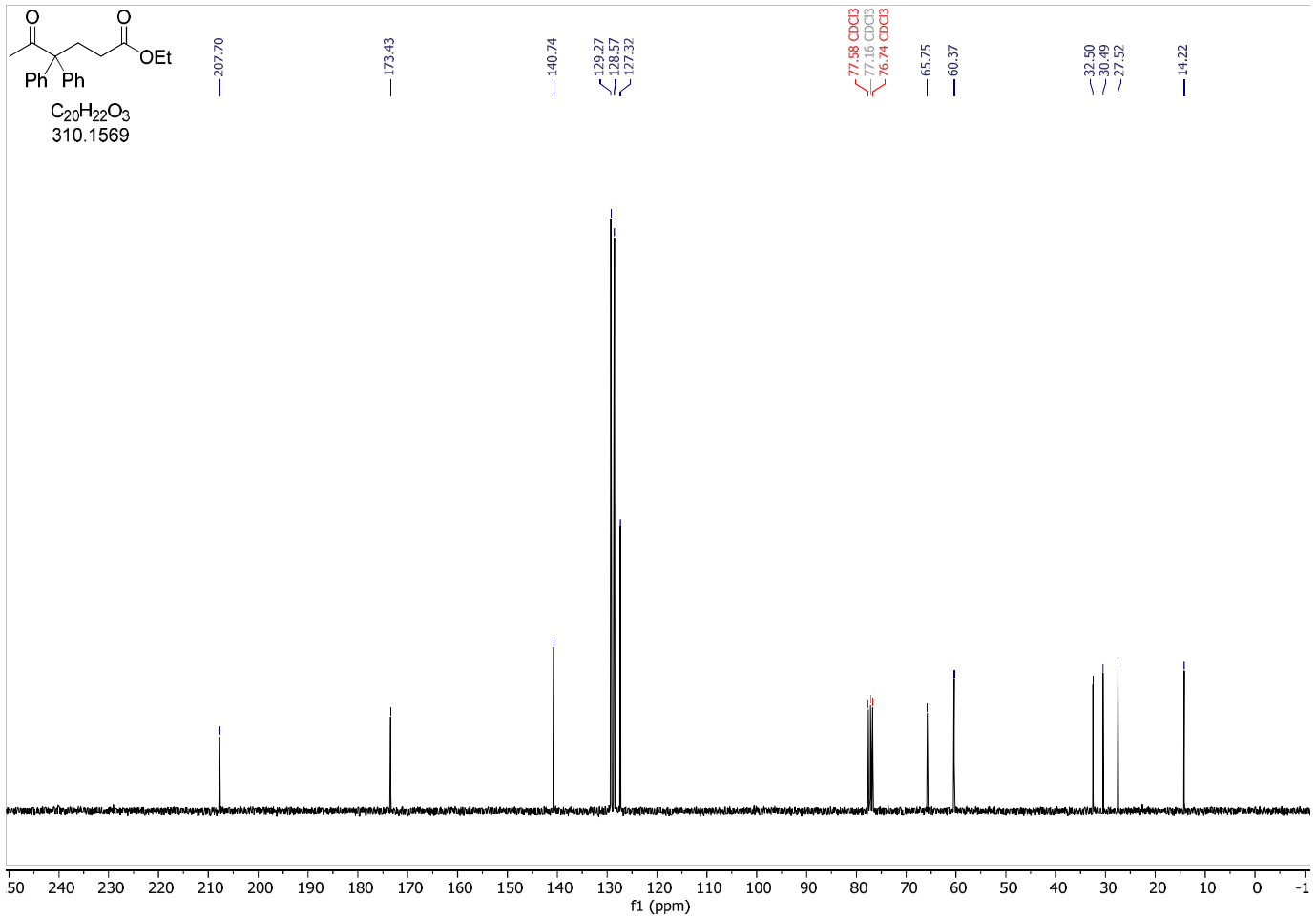
ethyl 3-(6-oxo-3,3-diphenyltetrahydro-2H-pyran-2-ylidene)propanoate (4)

 $^{13}\text{C-NMR}$ (75 MHz, CDCl_3)

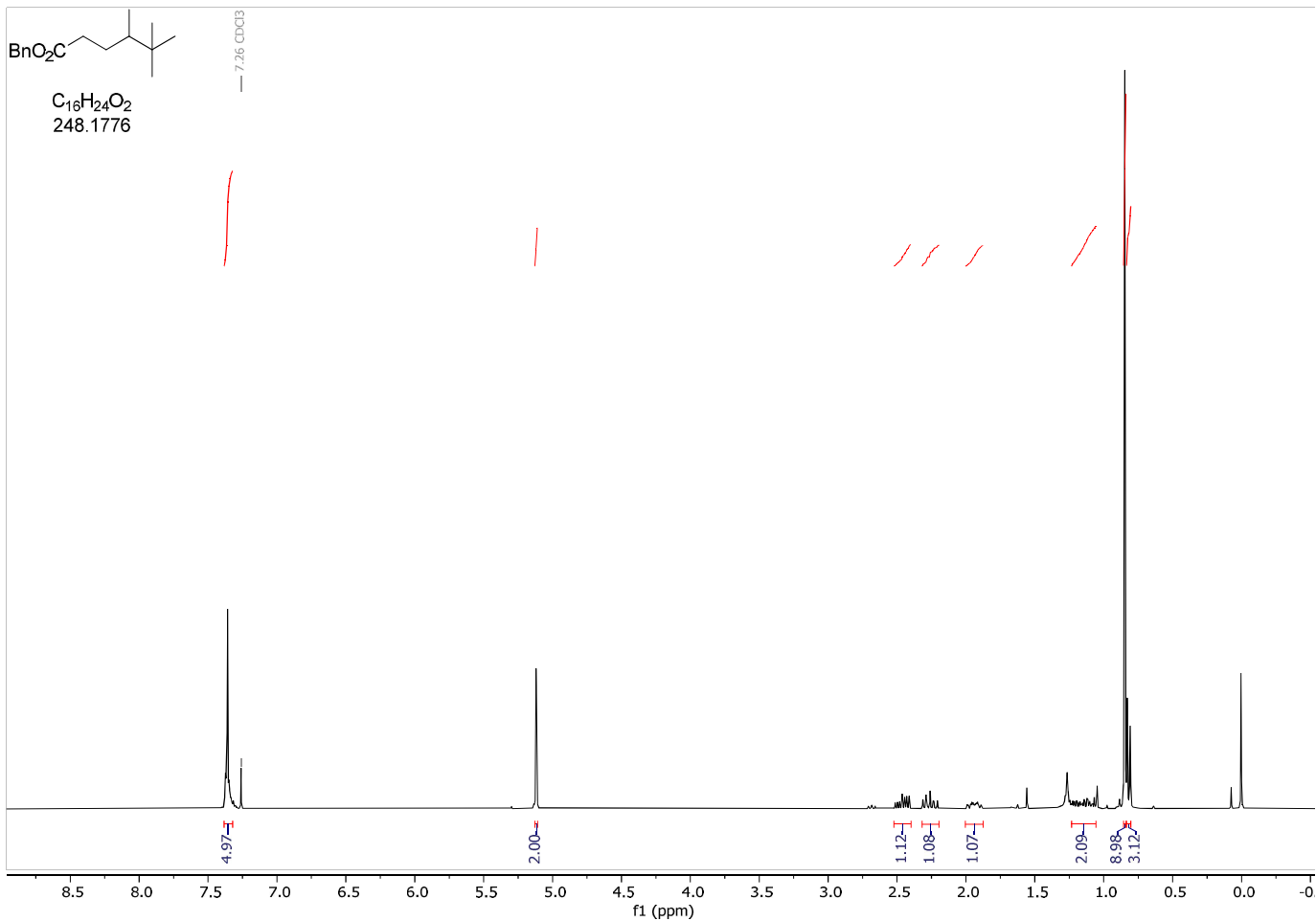
ethyl 5-oxo-4,4-diphenyl-hexanoate (5)

 $^1\text{H-NMR}$ (300 MHz, CDCl_3)

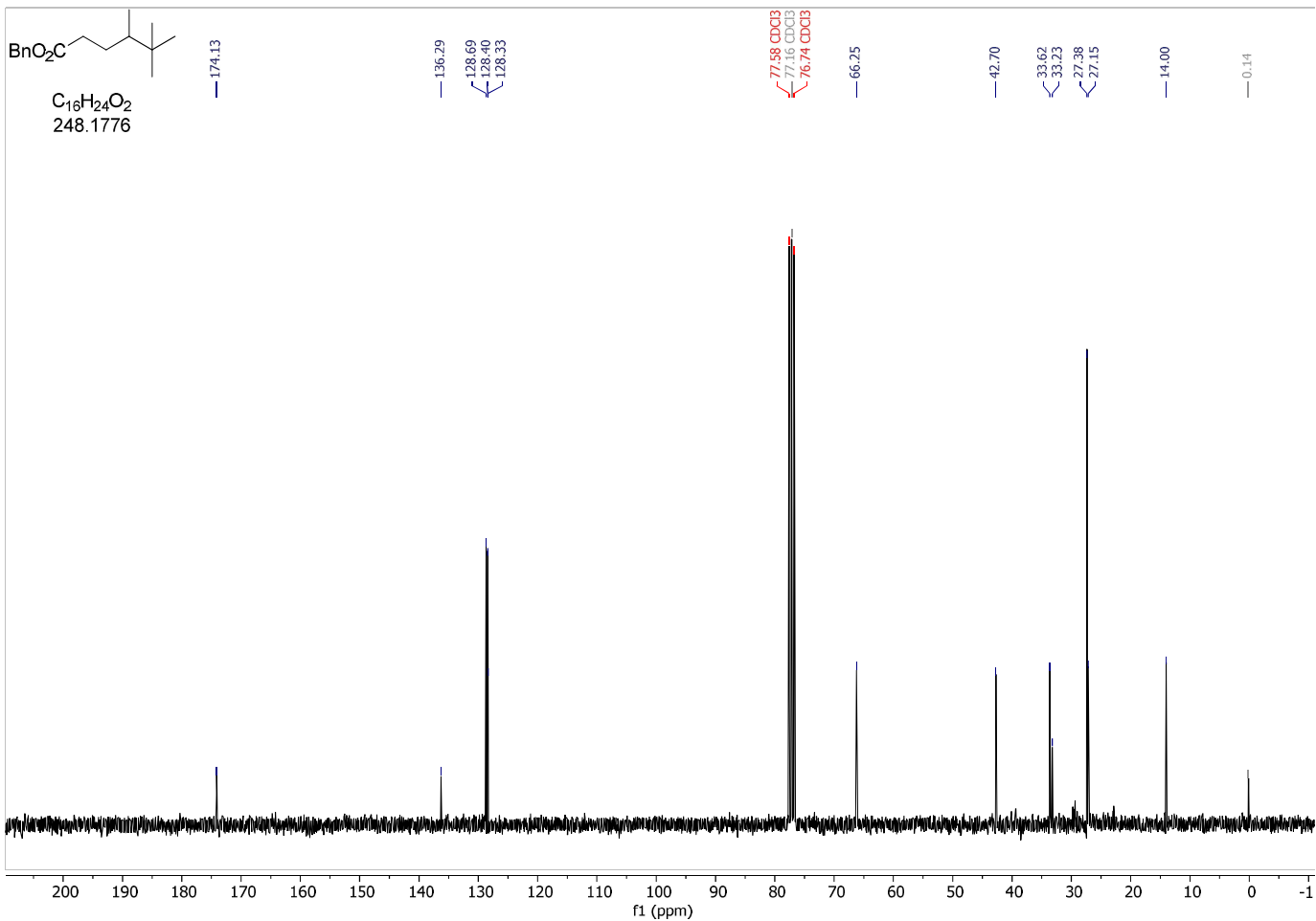
ethyl 5-oxo-4,4-diphenyl-hexanoate (5)

 $^{13}\text{C-NMR}$ (75 MHz, CDCl_3)

benzyl 4,5,5-trimethylhexanoate (3ac)

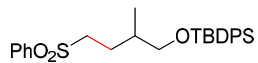
 $^1\text{H-NMR}$ (300 MHz, CDCl_3)

benzyl 4,5,5-trimethylhexanoate (3ac)

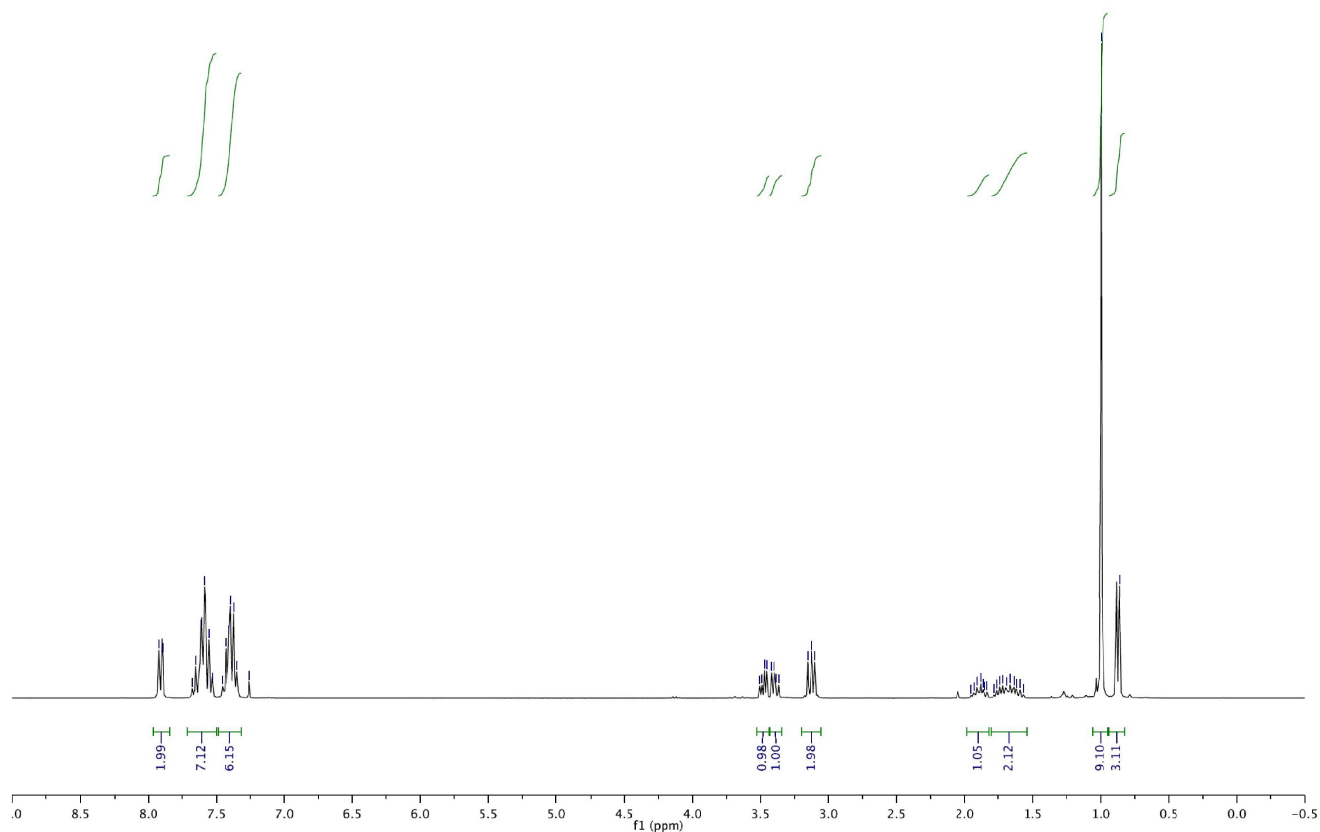
 $^{13}\text{C-NMR}$ (75 MHz, CDCl_3)

tert-butyl((2-methylpentyl)oxy)diphenylsilane (3cd)

¹H-NMR (300 MHz, CDCl₃)

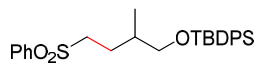


C₂₇H₃₄O₃SSi
466.1998

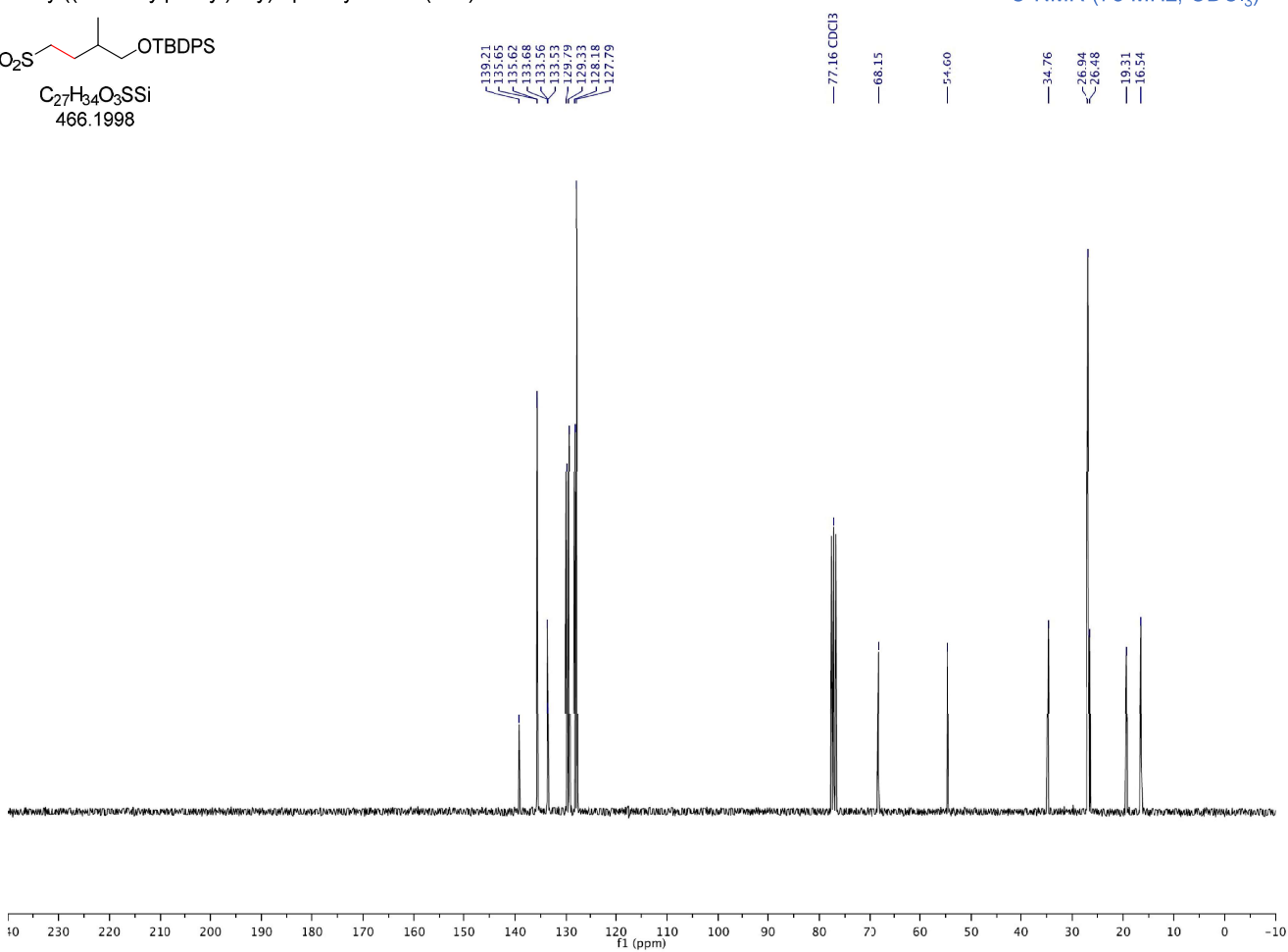


tert-butyl((2-methylpentyl)oxy)diphenylsilane (3cd)

¹³C-NMR (75 MHz, CDCl₃)

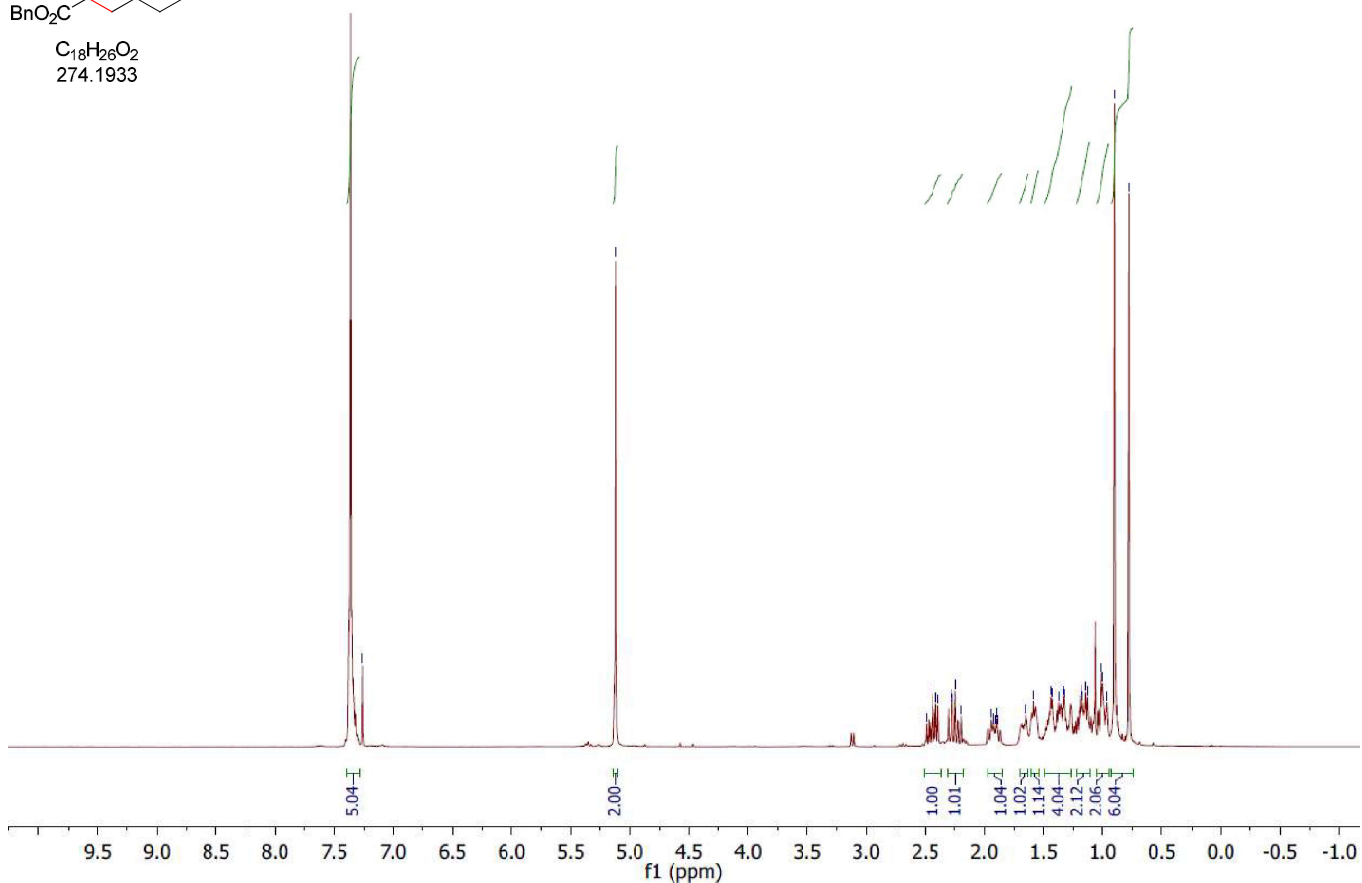
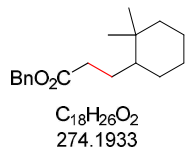


C₂₇H₃₄O₃SSi
466.1998



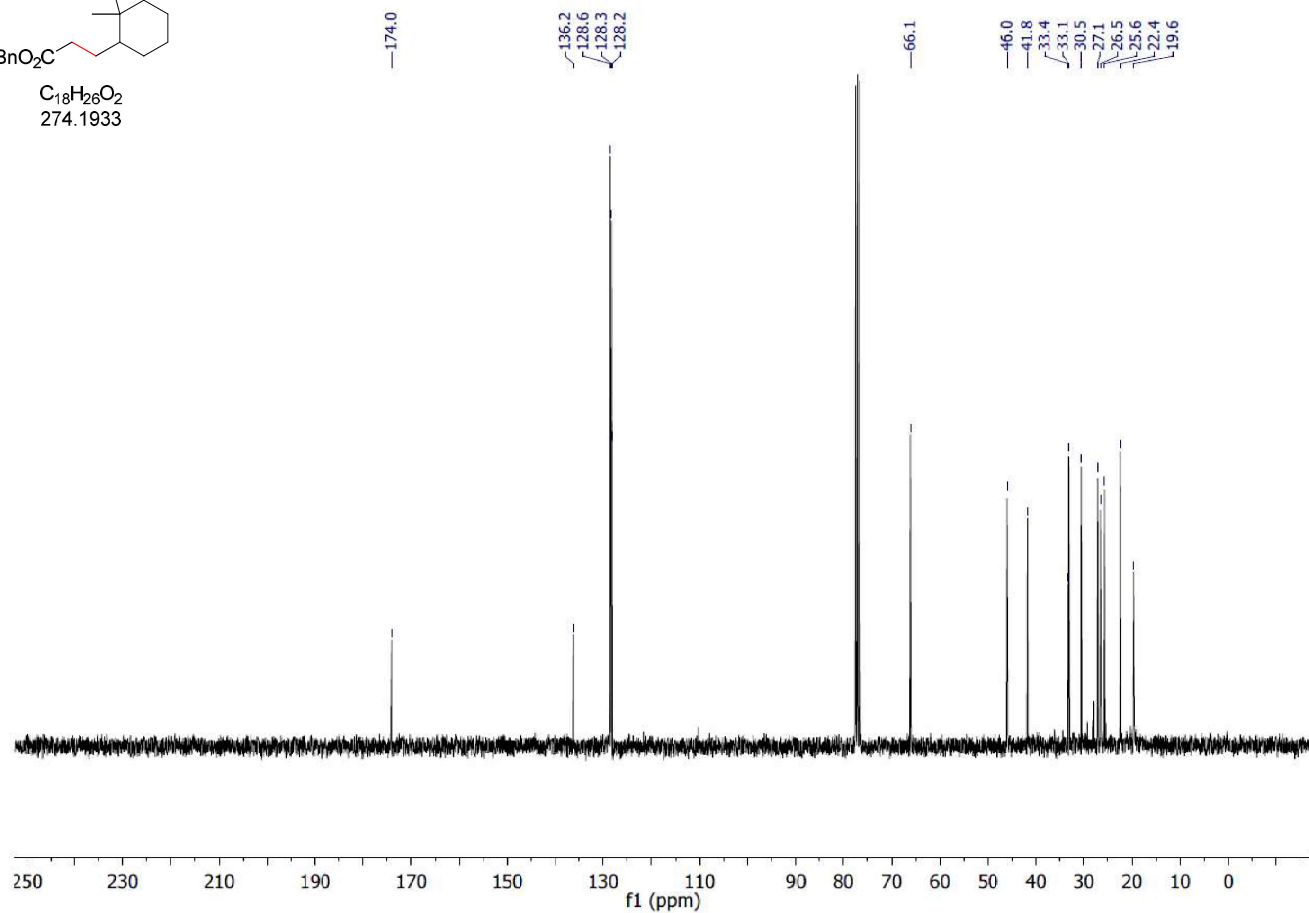
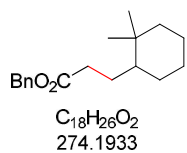
benzyl 3-(2,2-dimethylcyclohexyl)propanoate (3ae)

$^1\text{H-NMR}$ (300 MHz, CDCl_3)



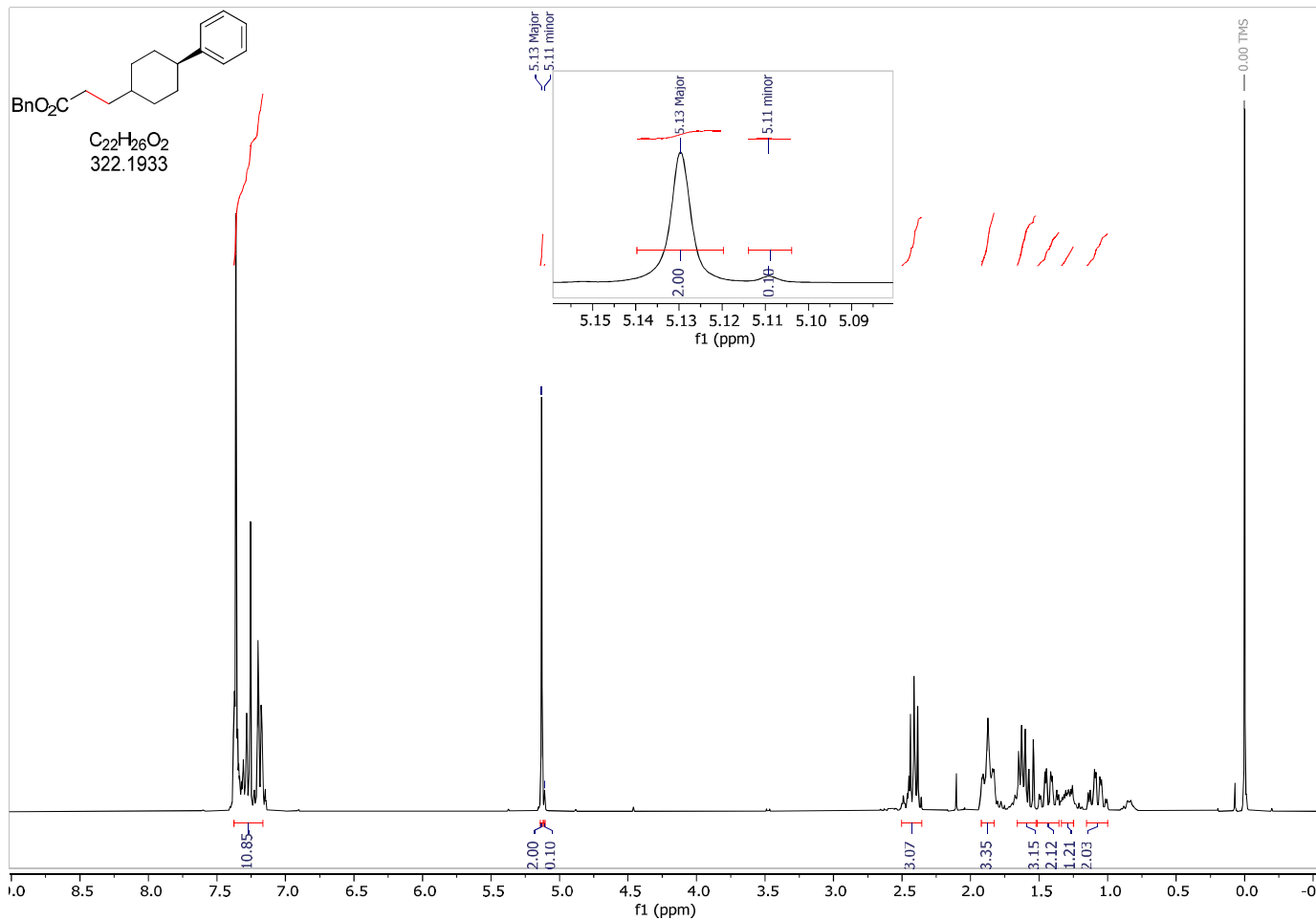
benzyl 3-(2,2-dimethylcyclohexyl)propanoate (3ae)

$^{13}\text{C-NMR}$ (75 MHz, CDCl_3)



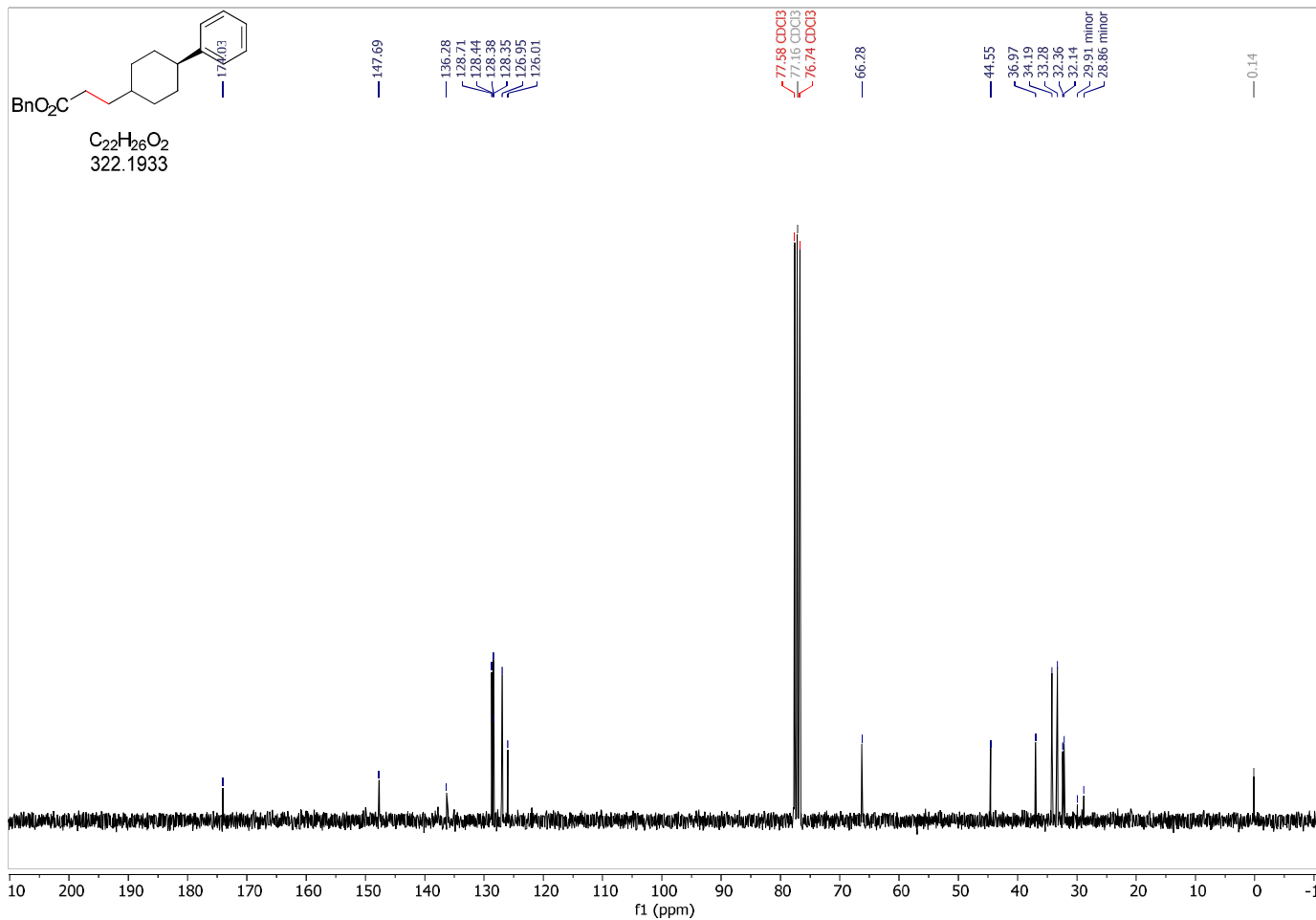
benzyl 3-(4-phenylcyclohexyl)propanoate (3af)

¹H-NMR (300 MHz, CDCl₃)

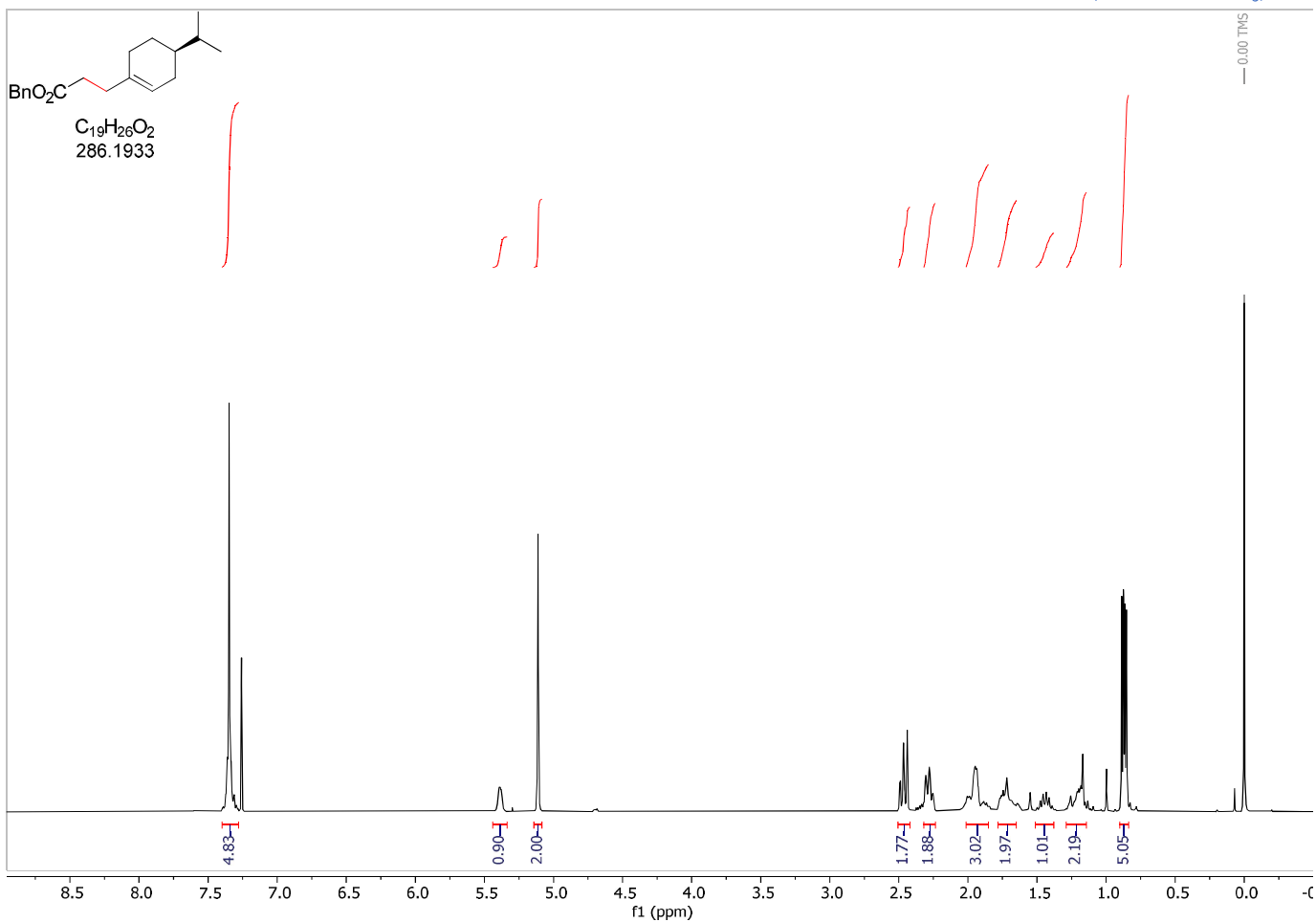


benzyl 3-(4-phenylcyclohexyl)propanoate (3af)

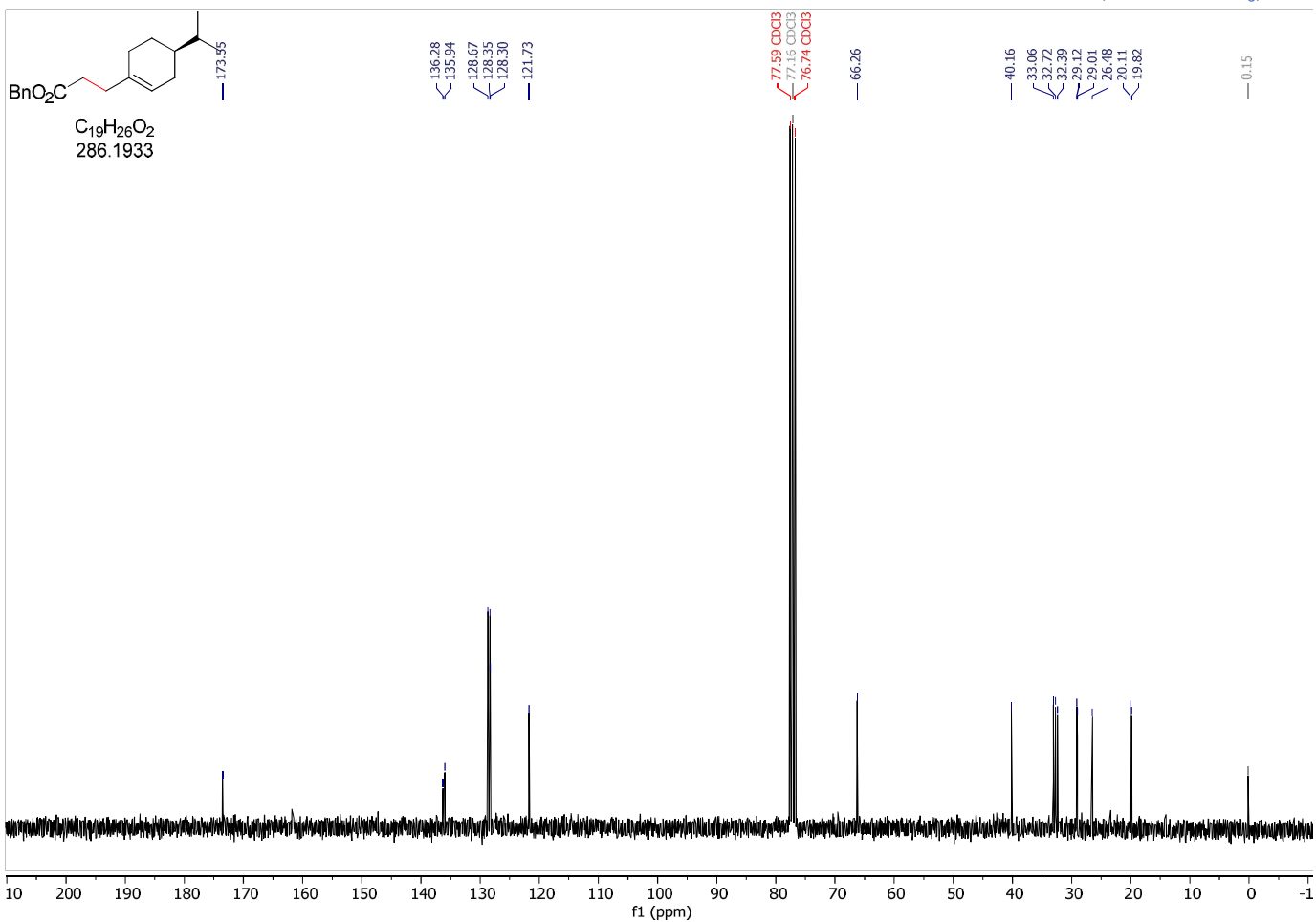
¹³C-NMR (75 MHz, CDCl₃)



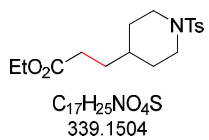
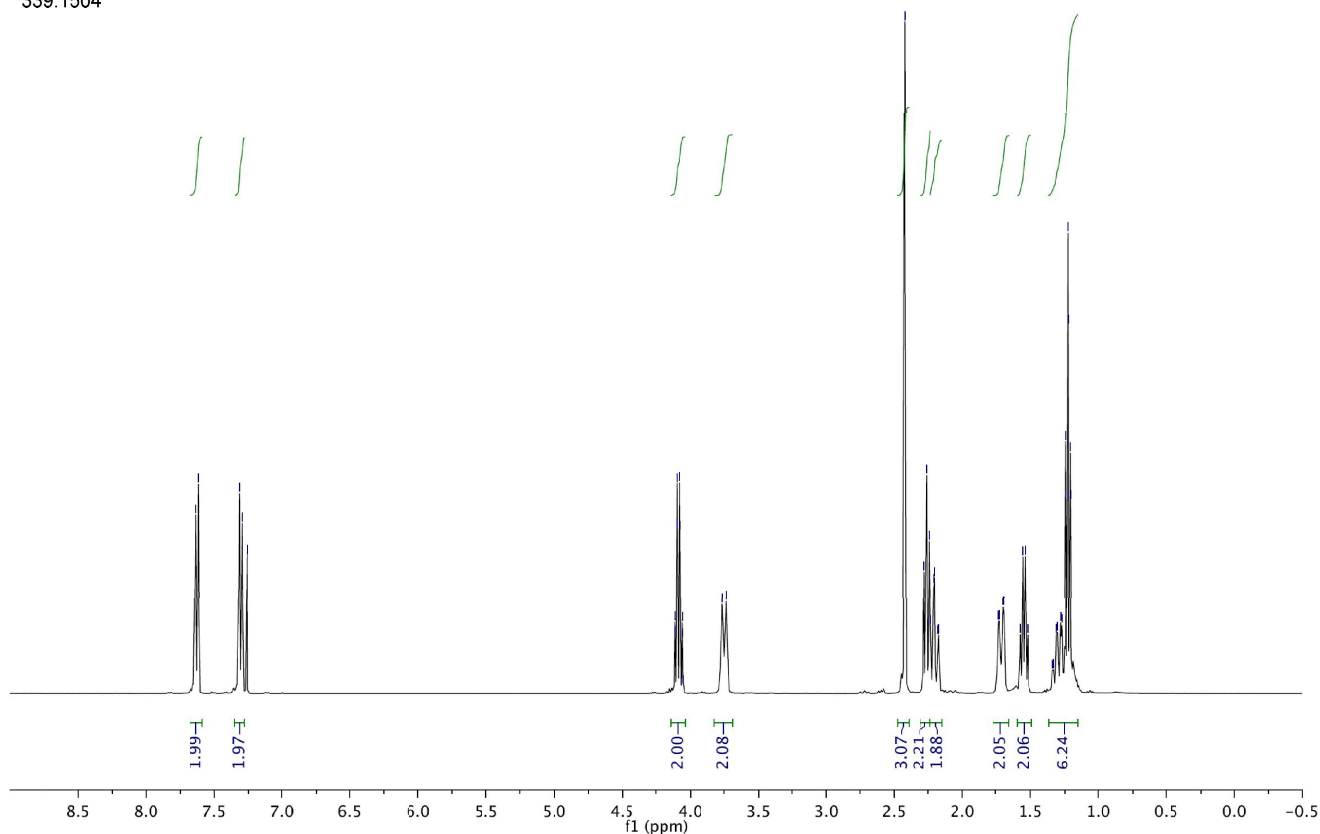
benzyl 3-(4-isopropylcyclohex-1-en-1-yl)propanoate (3ag)

 $^1\text{H-NMR}$ (300 MHz, CDCl_3)

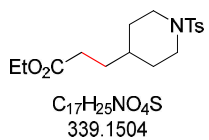
benzyl 3-(4-isopropylcyclohex-1-en-1-yl)propanoate (3ag)

 $^{13}\text{C-NMR}$ (75 MHz, CDCl_3)

ethyl 3-(1-tosylpiperidin-4-yl)propanoate (3bh)

 $^1\text{H-NMR}$ (400 MHz, CDCl_3)7.26 CDCl_3 

ethyl 3-(1-tosylpiperidin-4-yl)propanoate (3bh)

 $^{13}\text{C-NMR}$ (101 MHz, CDCl_3)

173.53

143.51

133.29

129.69

127.85

77.16 CDCl_3

60.49

46.44

34.69

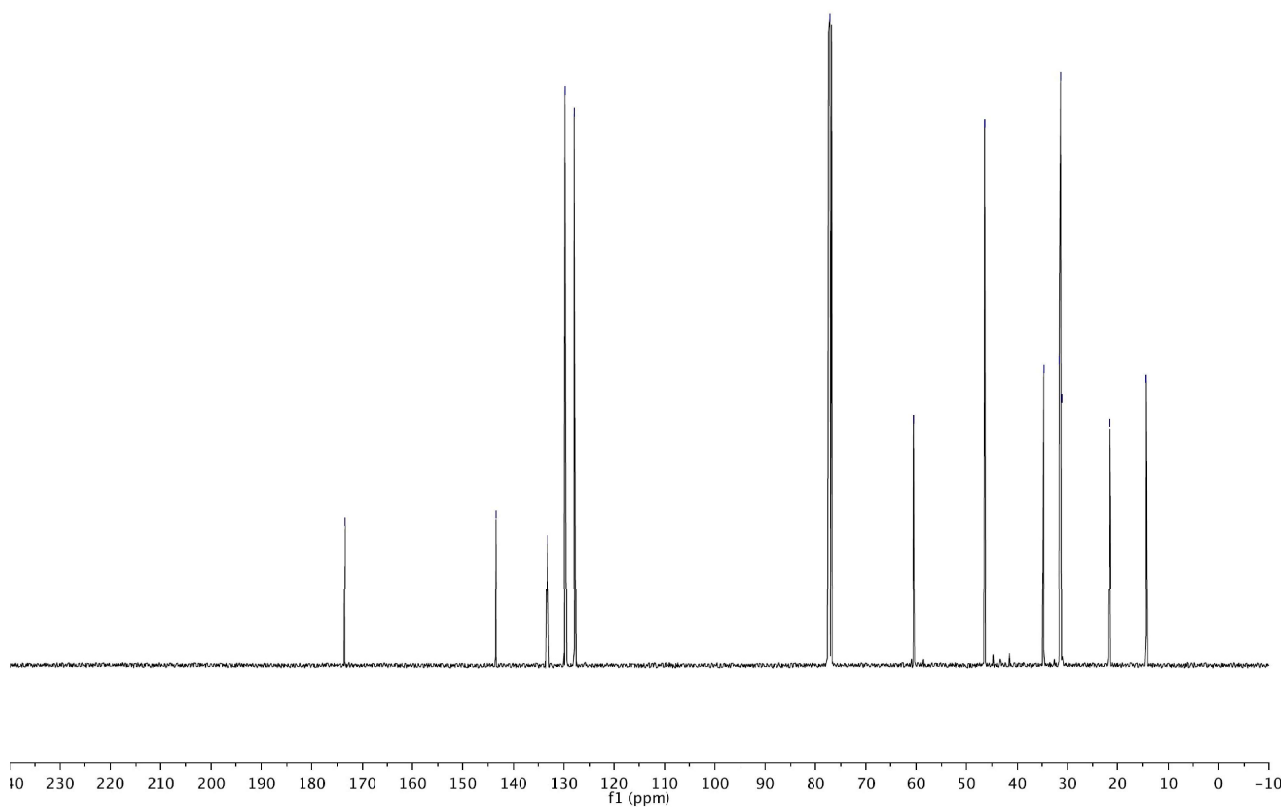
31.57

31.29

31.04

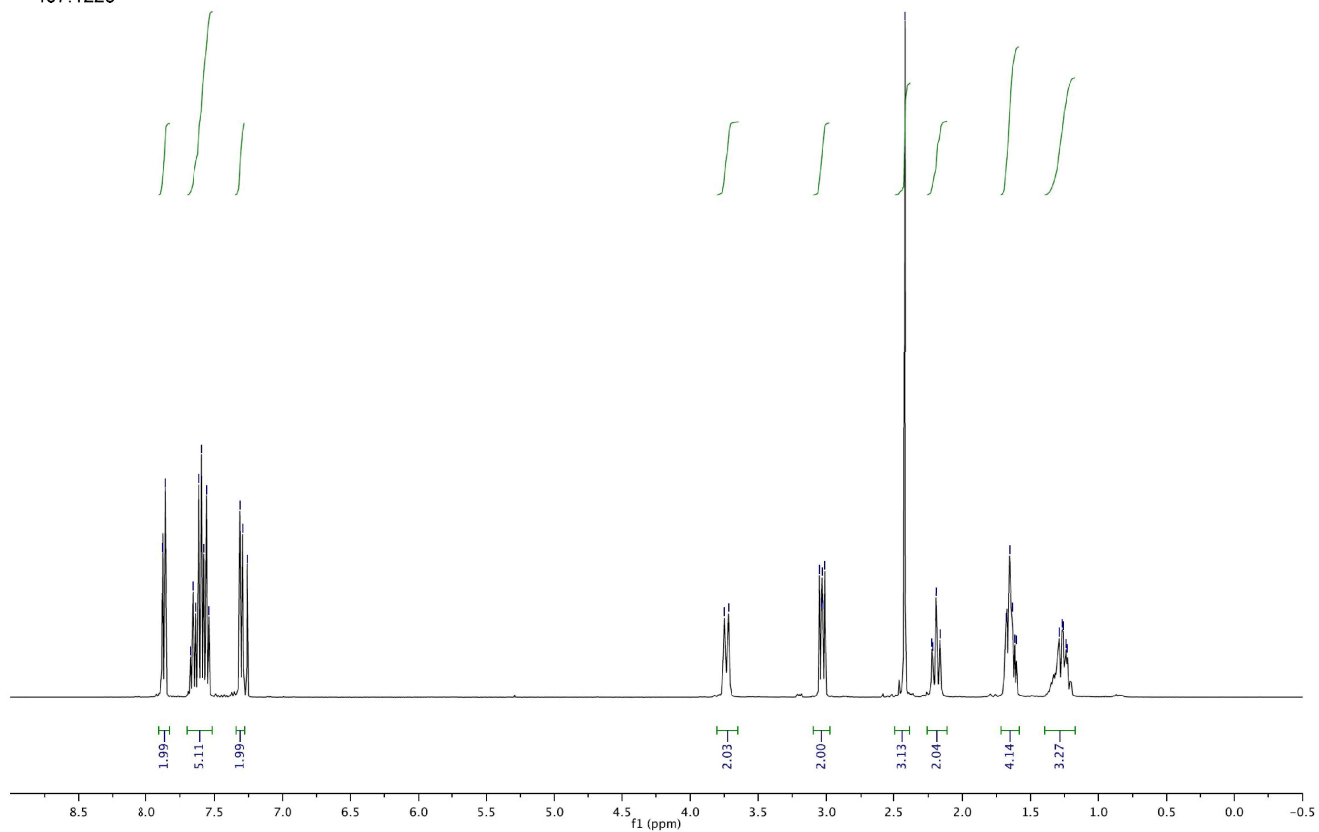
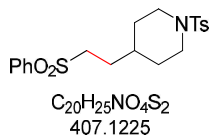
21.64

14.34



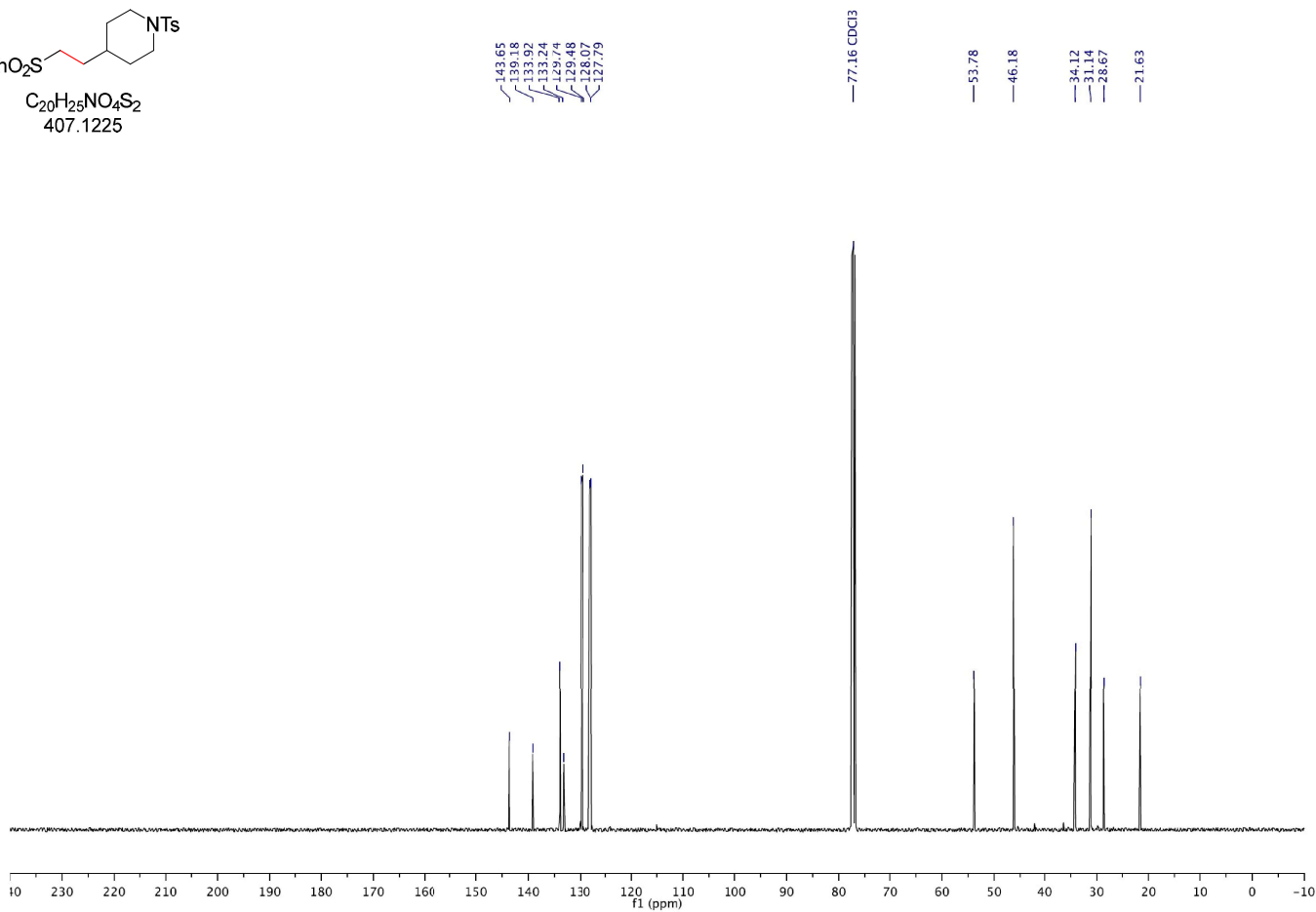
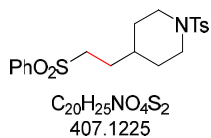
4-(2-(phenylsulfonyl)ethyl)-1-tosylpiperidine (3ch)

¹H-NMR (400 MHz, CDCl₃)



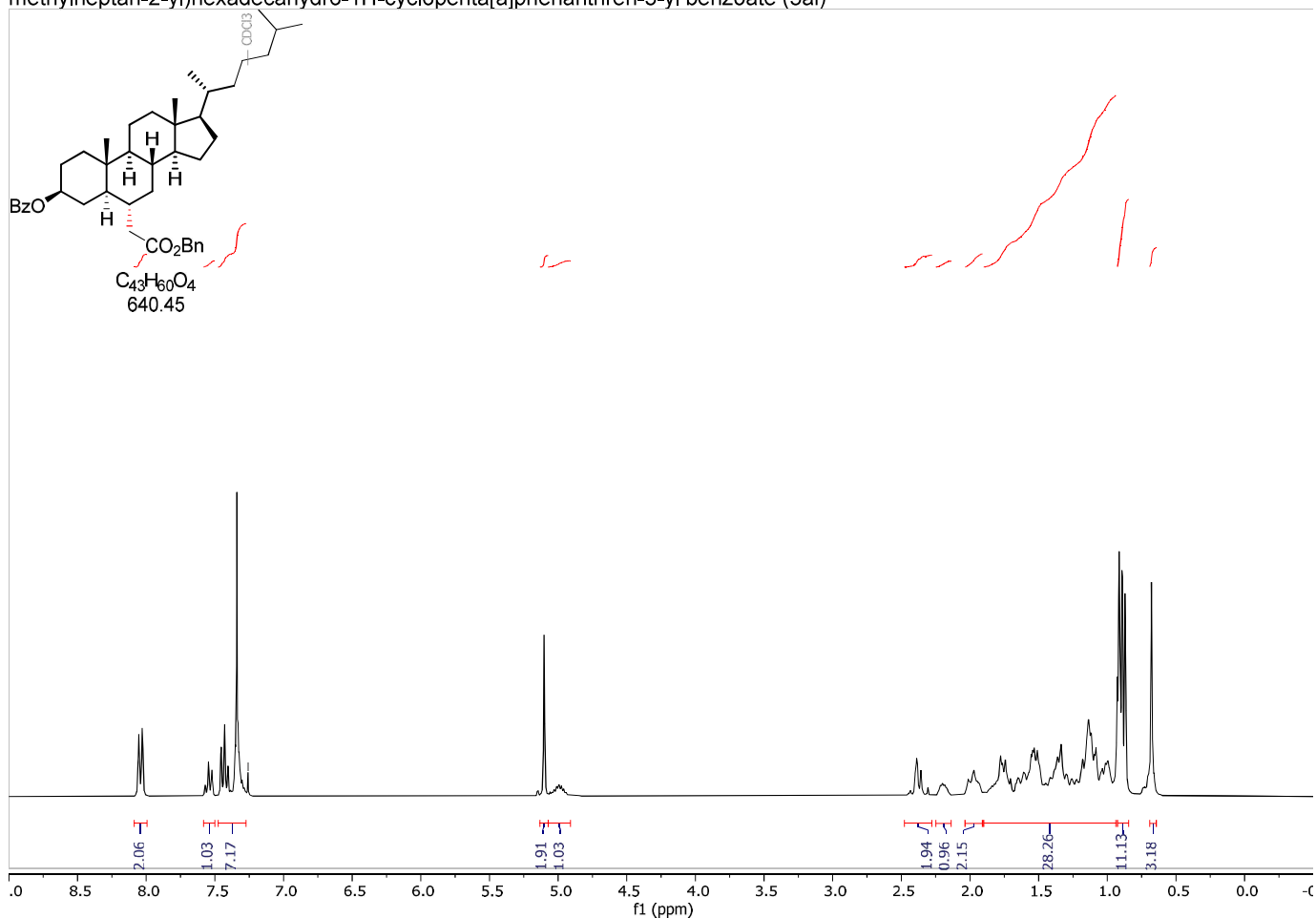
4-(2-(phenylsulfonyl)ethyl)-1-tosylpiperidine (3ch)

¹³C-NMR (101 MHz, CDCl₃)



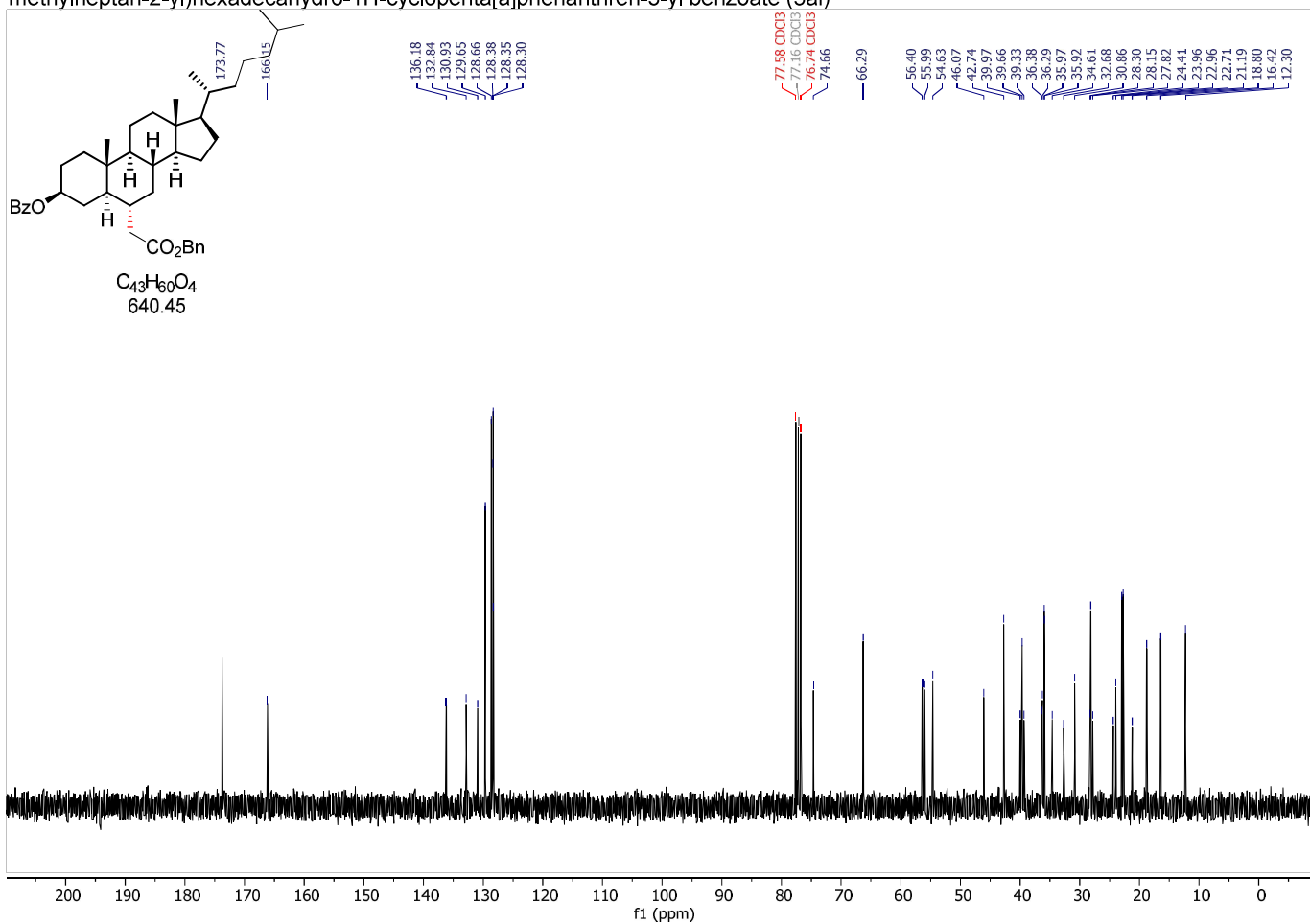
(3S,8S,9S,10S,13R,14S,17R)-6-(2-(benzyloxy)-2-oxoethyl)-10,13-dimethyl-17-((R)-6-methylheptan-2-yl)hexadecahydro-1H-cyclopenta[a]phenanthren-3-yl benzoate (3ai)

$^1\text{H-NMR}$ (300 MHz, CDCl_3)



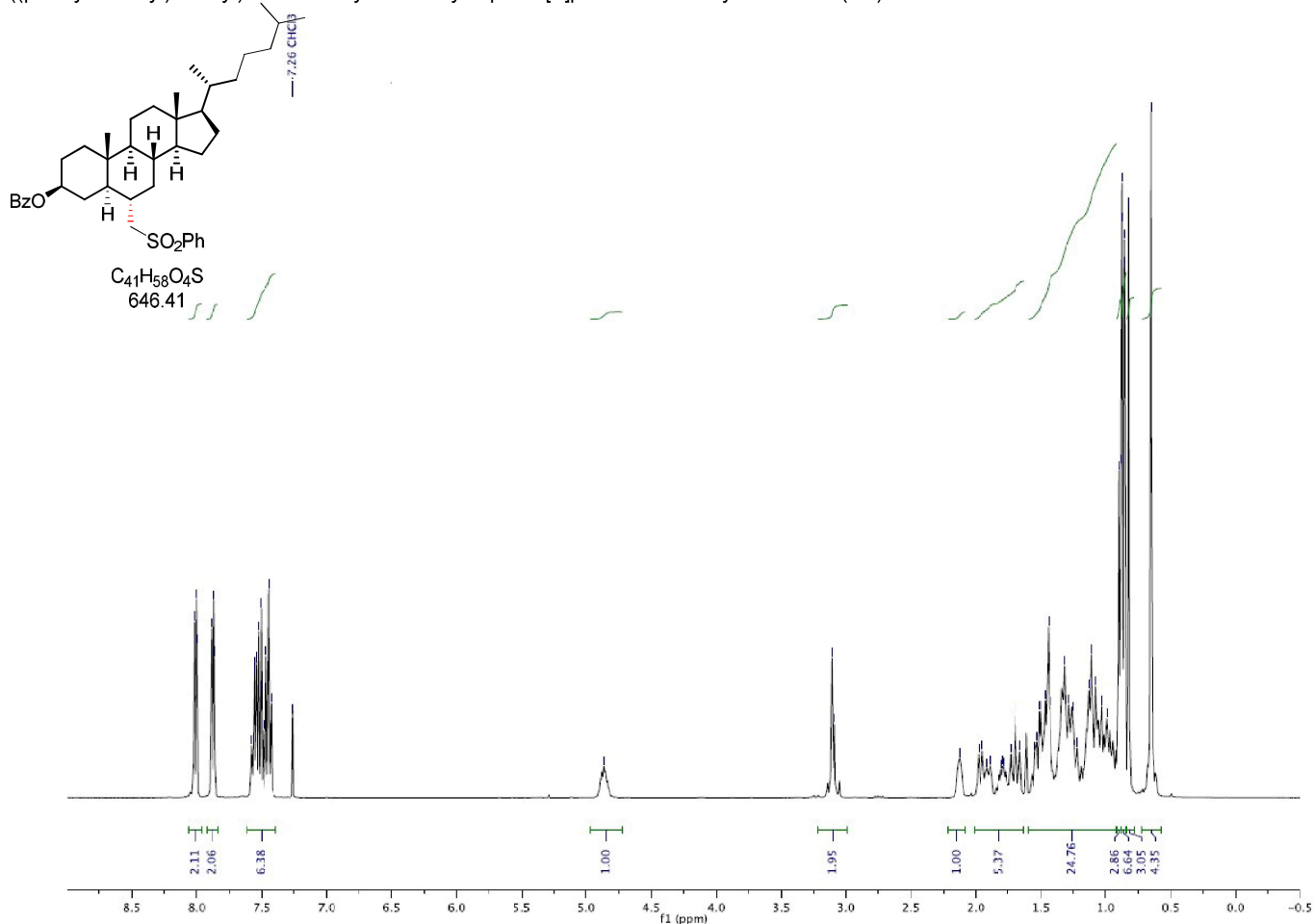
(3S,8S,9S,10S,13R,14S,17R)-6-(2-(benzyloxy)-2-oxoethyl)-10,13-dimethyl-17-((R)-6-methylheptan-2-yl)hexadecahydro-1H-cyclopenta[a]phenanthren-3-yl benzoate (3ai)

$^{13}\text{C-NMR}$ (75 MHz, CDCl_3)



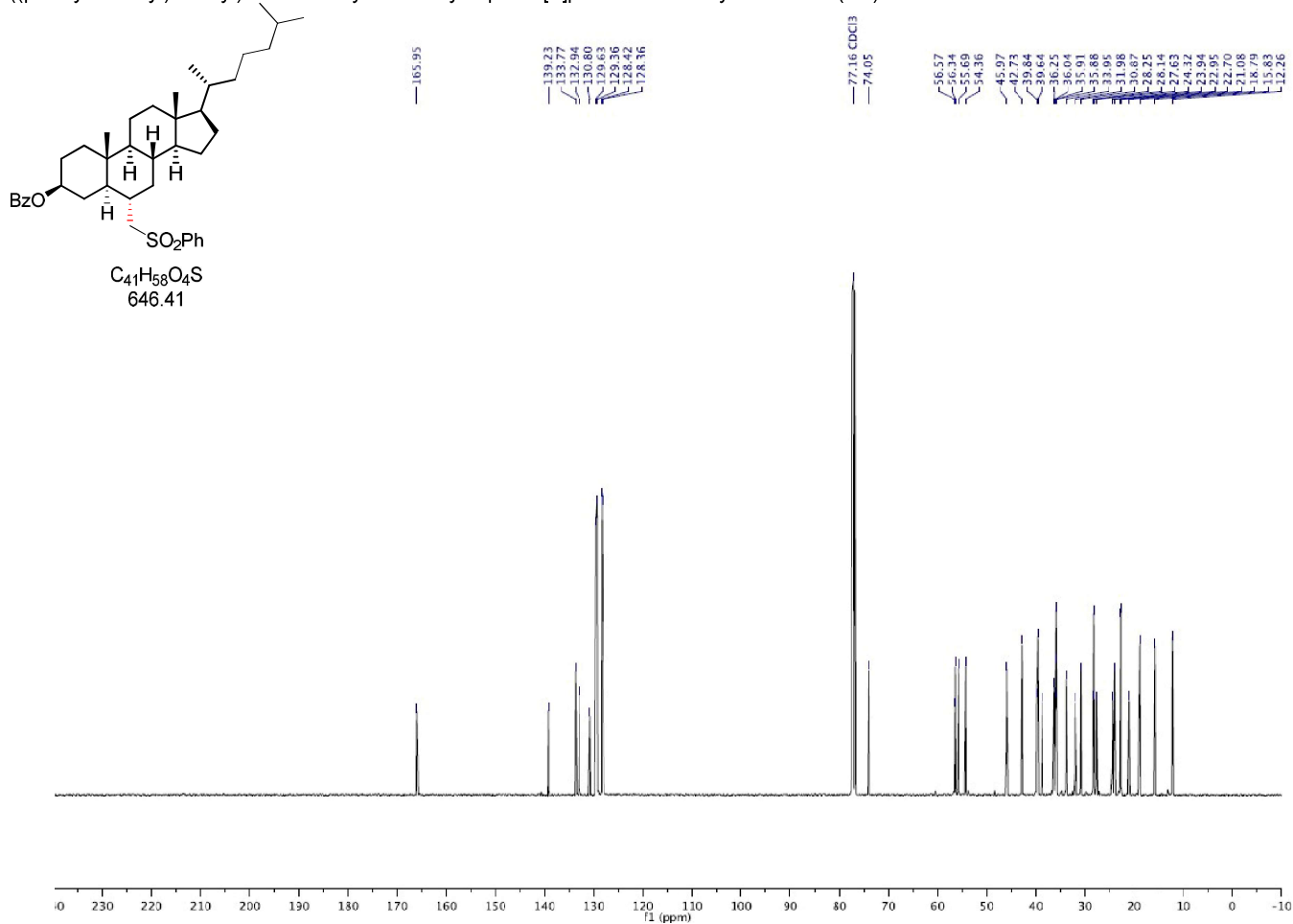
(3S,5R,6S,8S,9S,10R,13R,14S,17R)-10,13-dimethyl-17-((R)-6-methylheptan-2-yl)-6-((phenylsulfonyl)methyl)hexadecahydro-1H-cyclopenta[a]phenanthren-3-yl benzoate (3ci)

$^1\text{H-NMR}$ (400 MHz, CDCl_3)

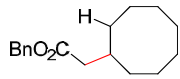


(3S,5R,6S,8S,9S,10R,13R,14S,17R)-10,13-dimethyl-17-((R)-6-methylheptan-2-yl)-6-((phenylsulfonyl)methyl)hexadecahydro-1H-cyclopenta[a]phenanthren-3-yl benzoate (3ci)

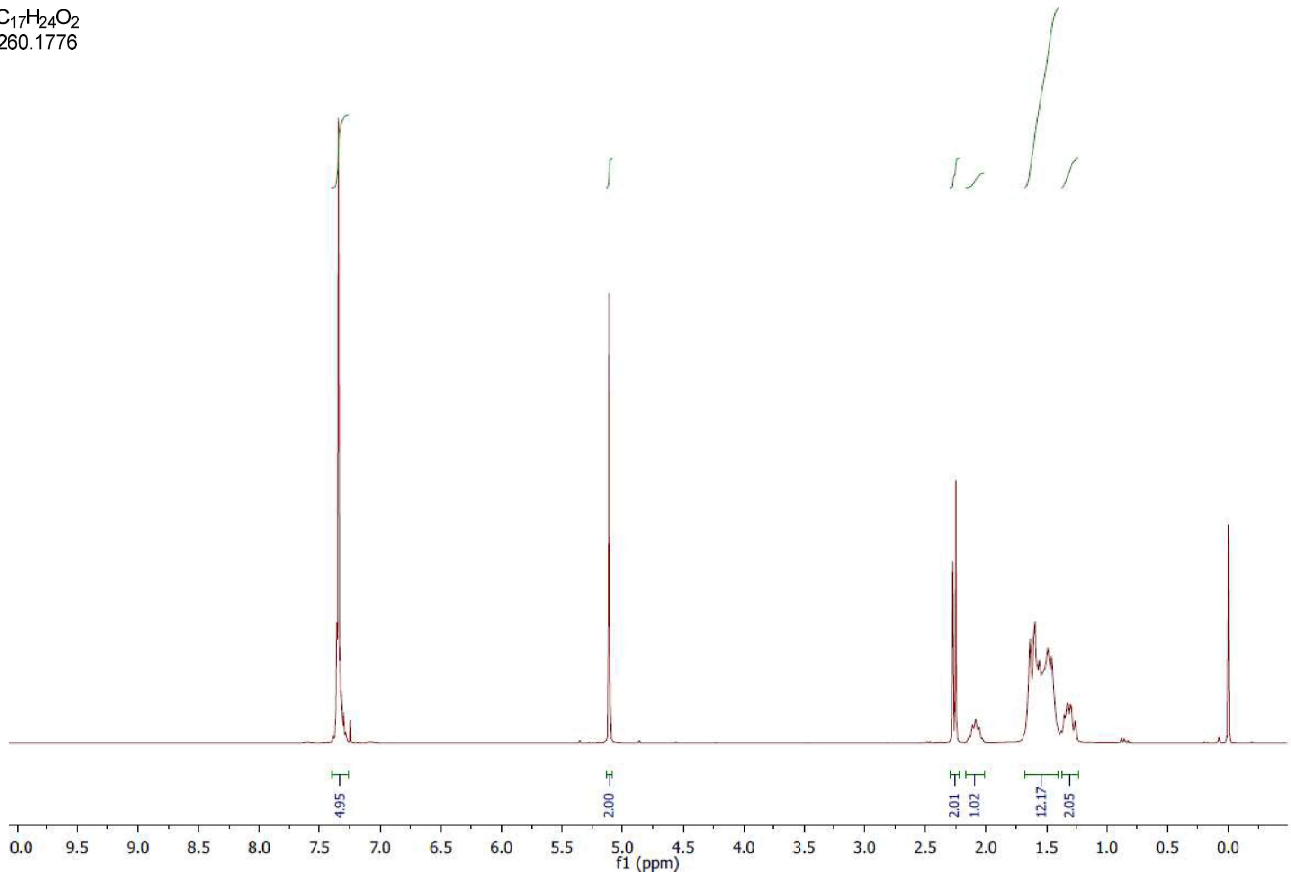
$^{13}\text{C-NMR}$ (101 MHz, CDCl_3)



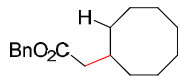
benzyl 2-cyclooctylacetate (3aj)

 $^1\text{H-NMR}$ (300 MHz, CDCl_3)

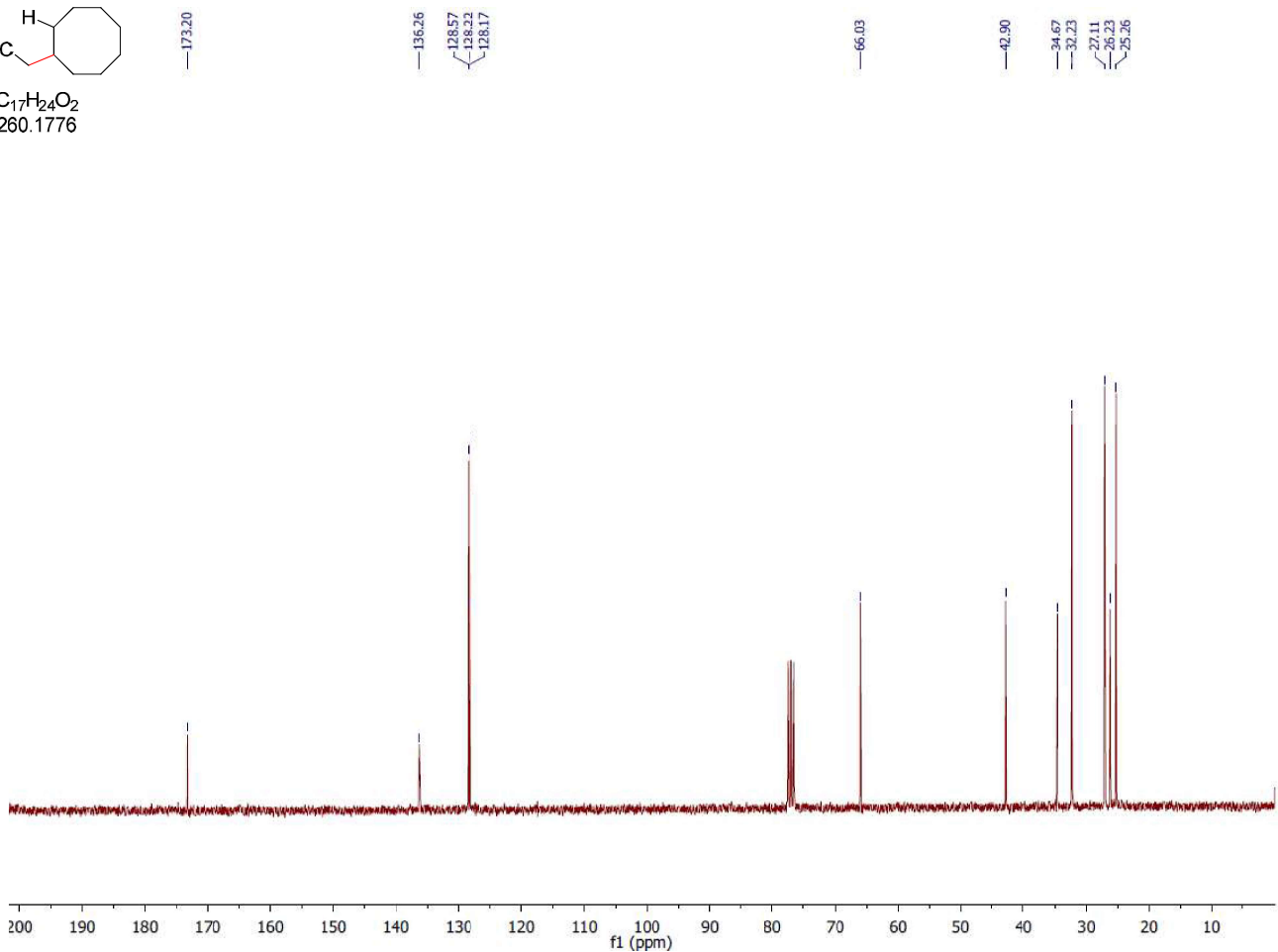
$\text{C}_{17}\text{H}_{24}\text{O}_2$
260.1776



benzyl 2-cyclooctylacetate (3aj)

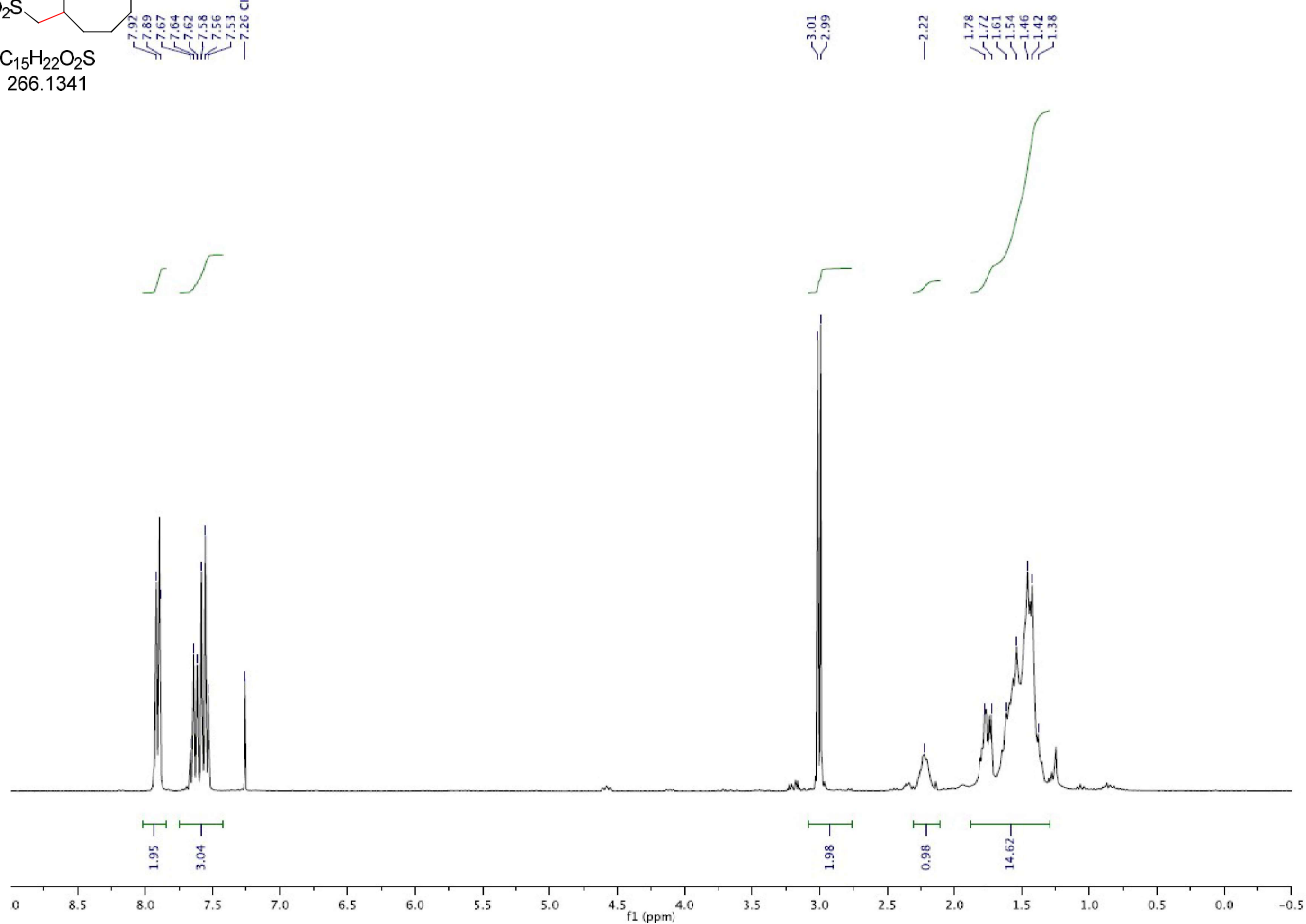
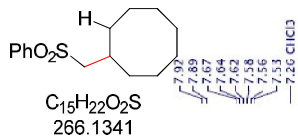
 $^{13}\text{C-NMR}$ (75 MHz, CDCl_3)

$\text{C}_{17}\text{H}_{24}\text{O}_2$
260.1776



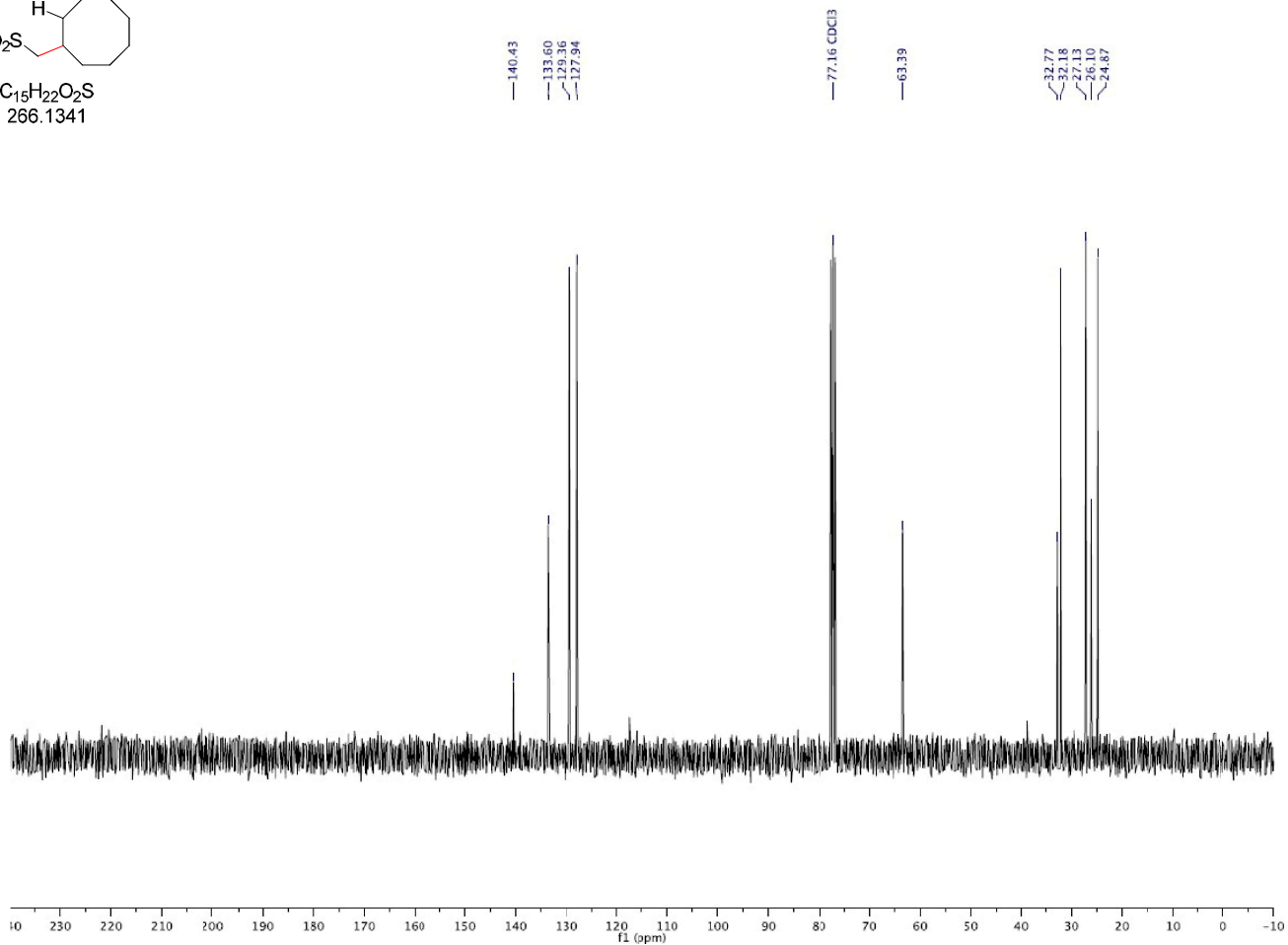
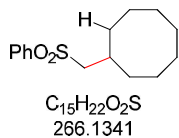
((phenylsulfonyl)methyl)cyclooctane (3cj)

$^1\text{H-NMR}$ (300 MHz, CDCl_3)

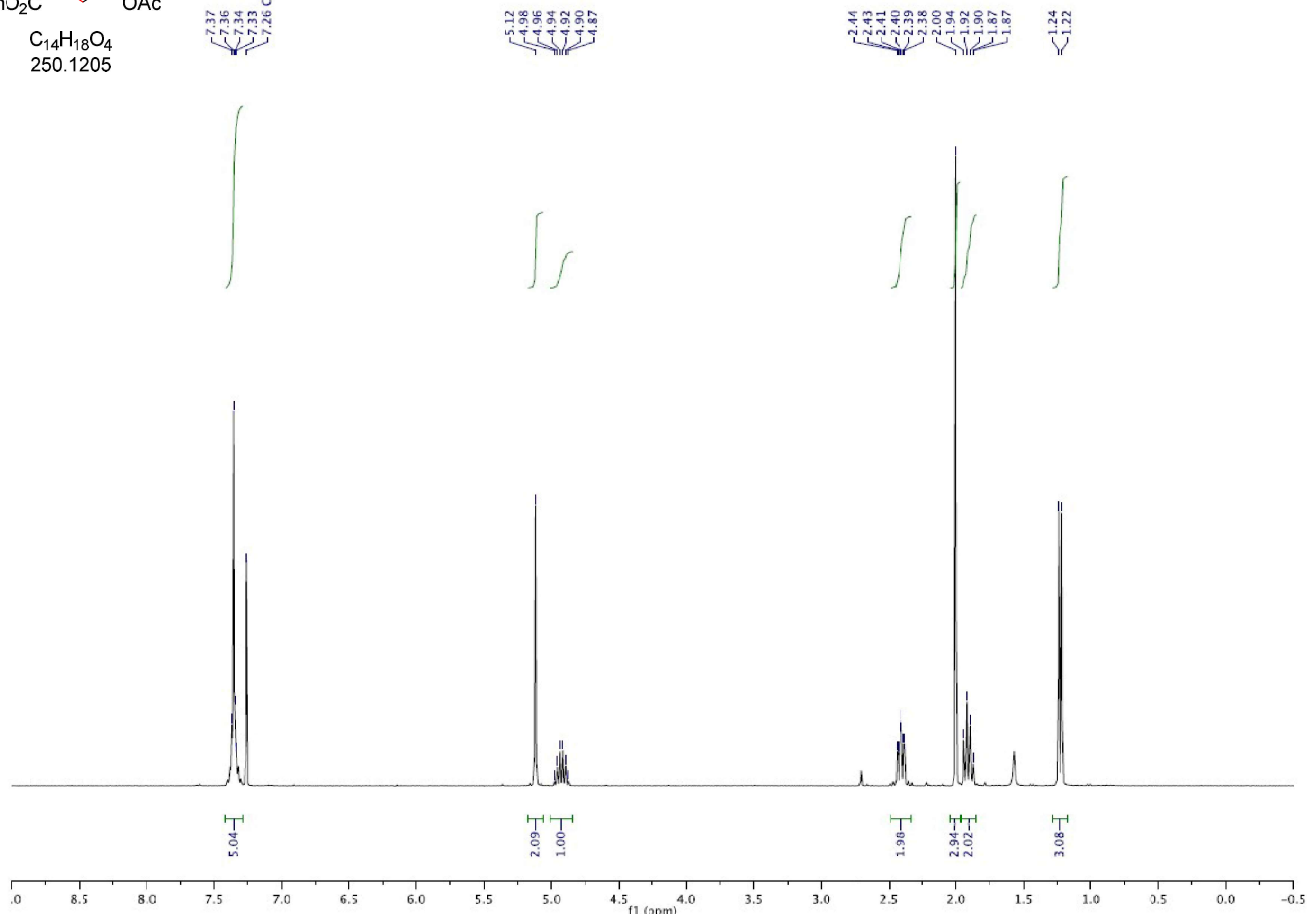
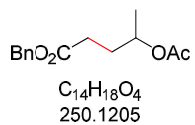


((phenylsulfonyl)methyl)cyclooctane (3cj)

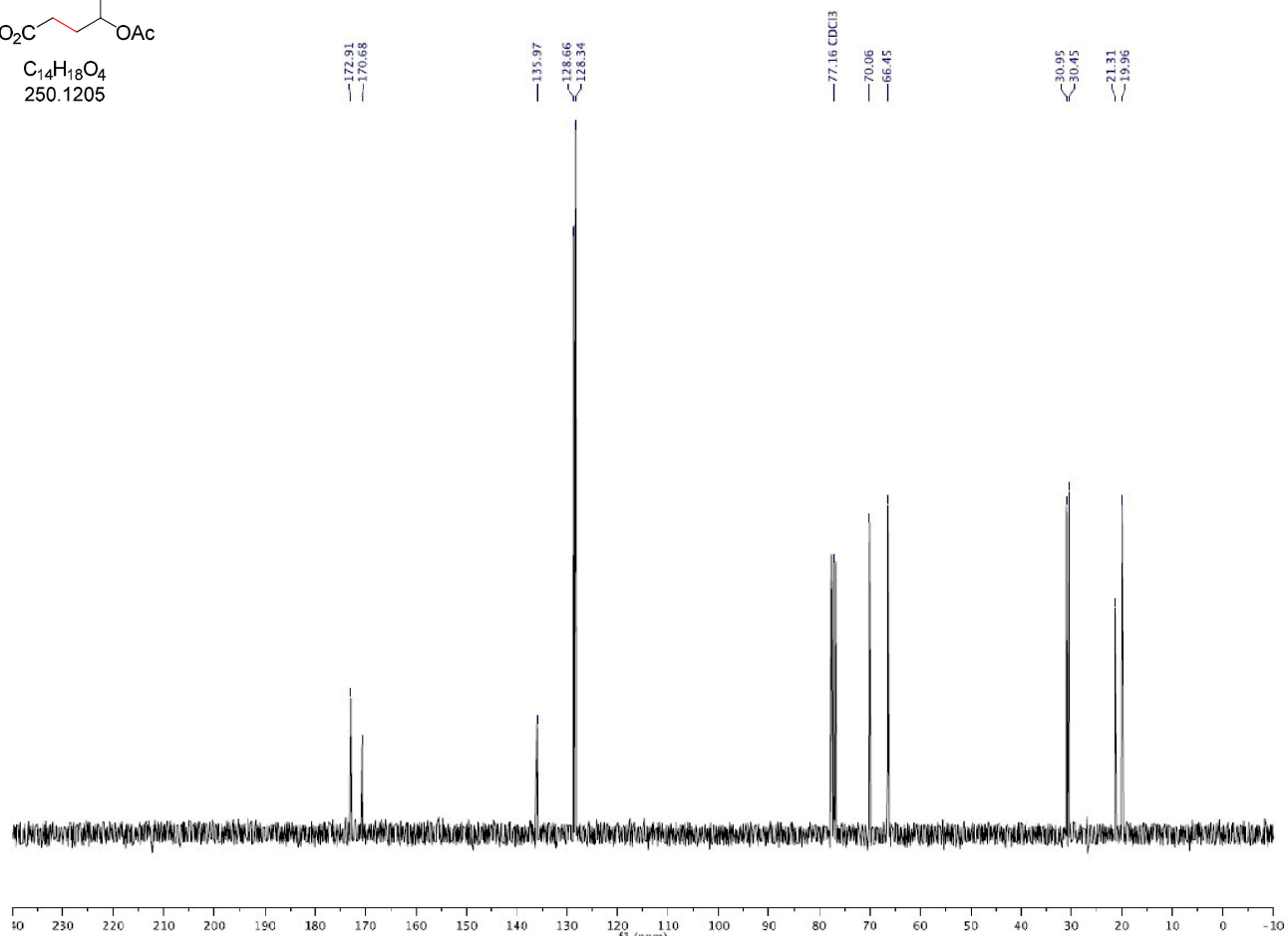
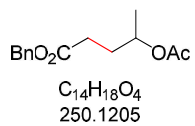
$^{13}\text{C-NMR}$ (75 MHz, CDCl_3)



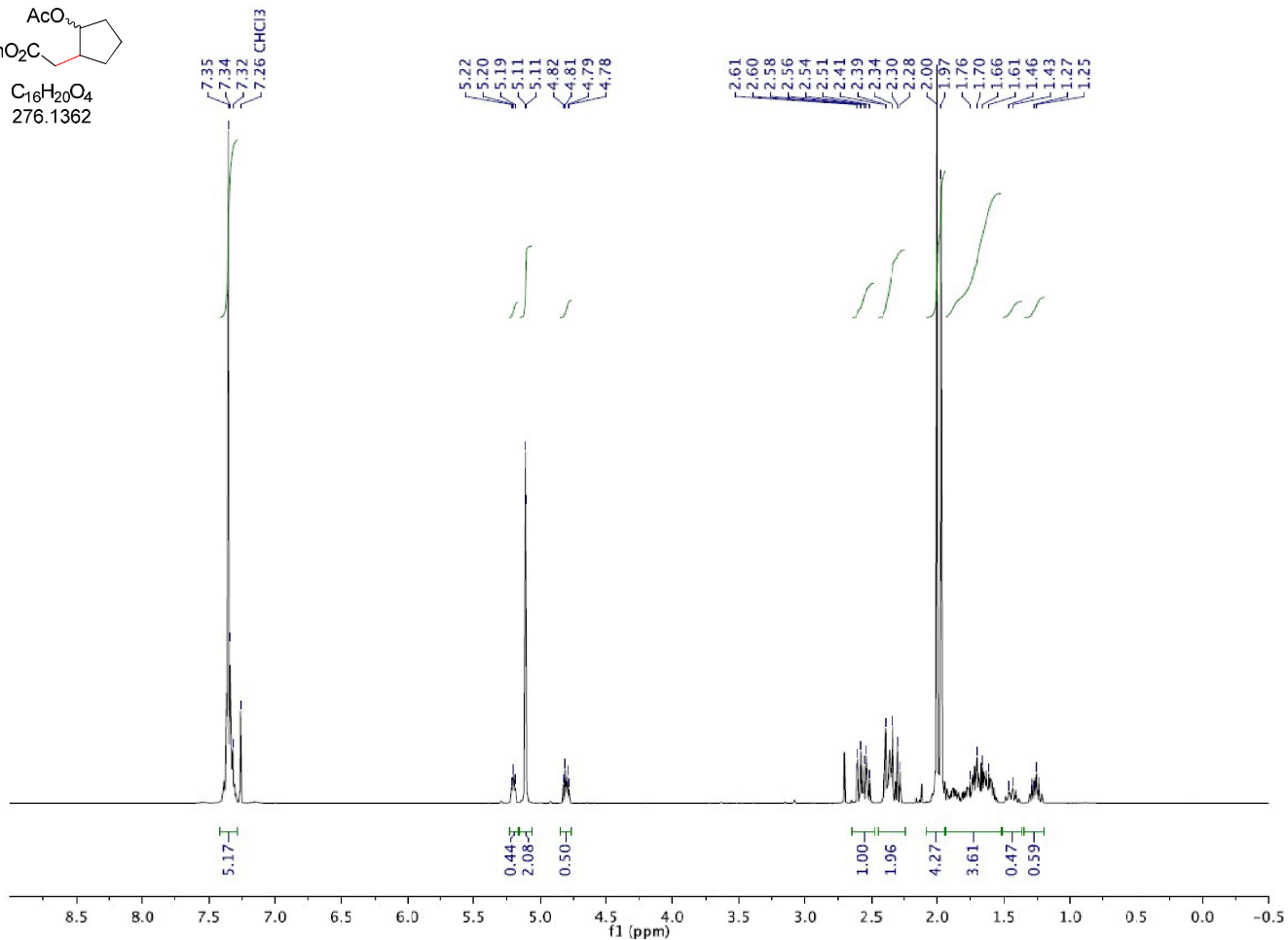
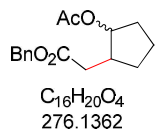
benzyl 4-acetoxypentanoate (3ak)

 $^1\text{H-NMR}$ (300 MHz, CDCl_3)

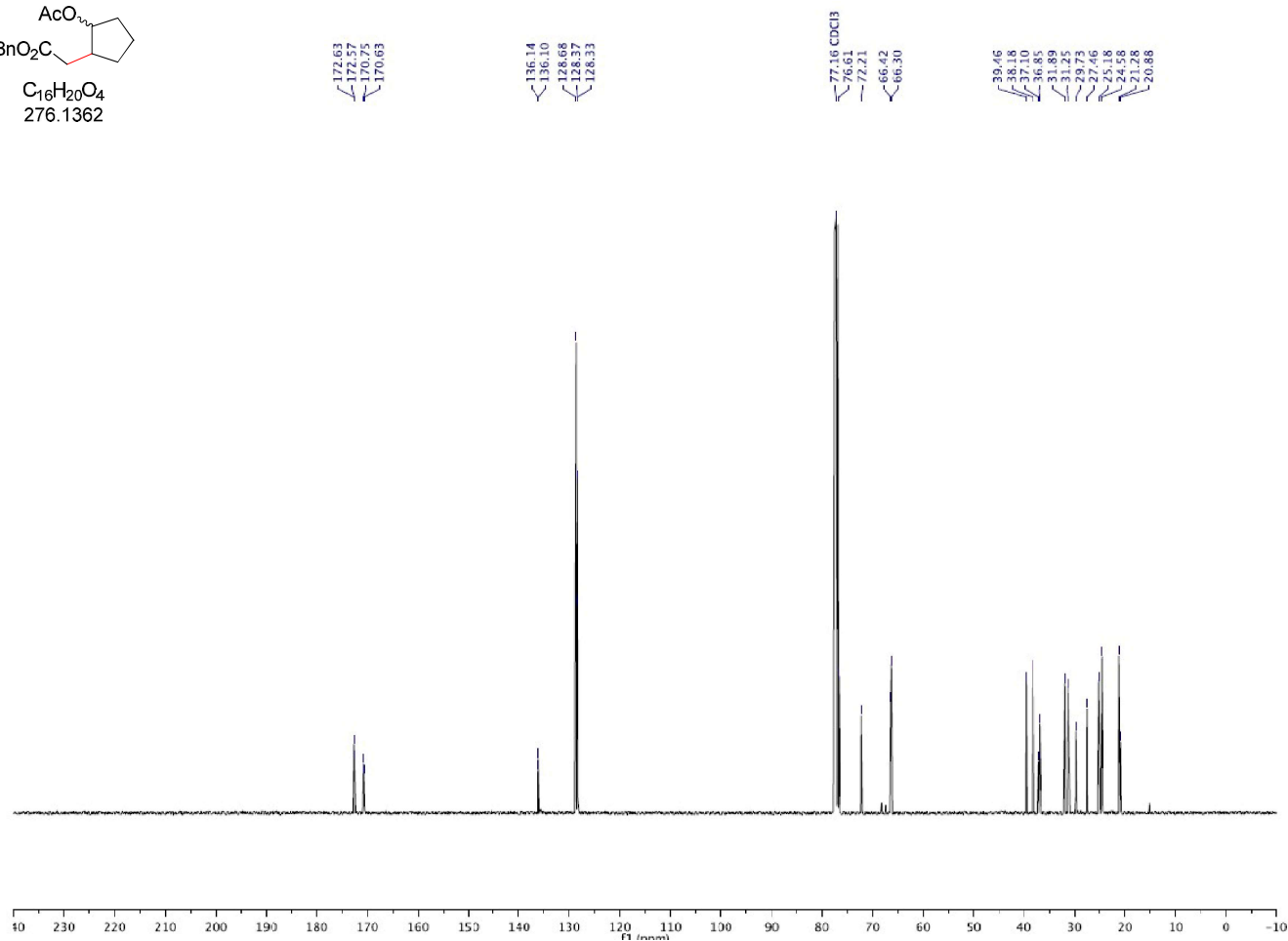
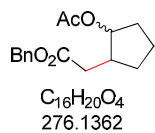
benzyl 4-acetoxypentanoate (3ak)

 $^{13}\text{C-NMR}$ (75 MHz, CDCl_3)

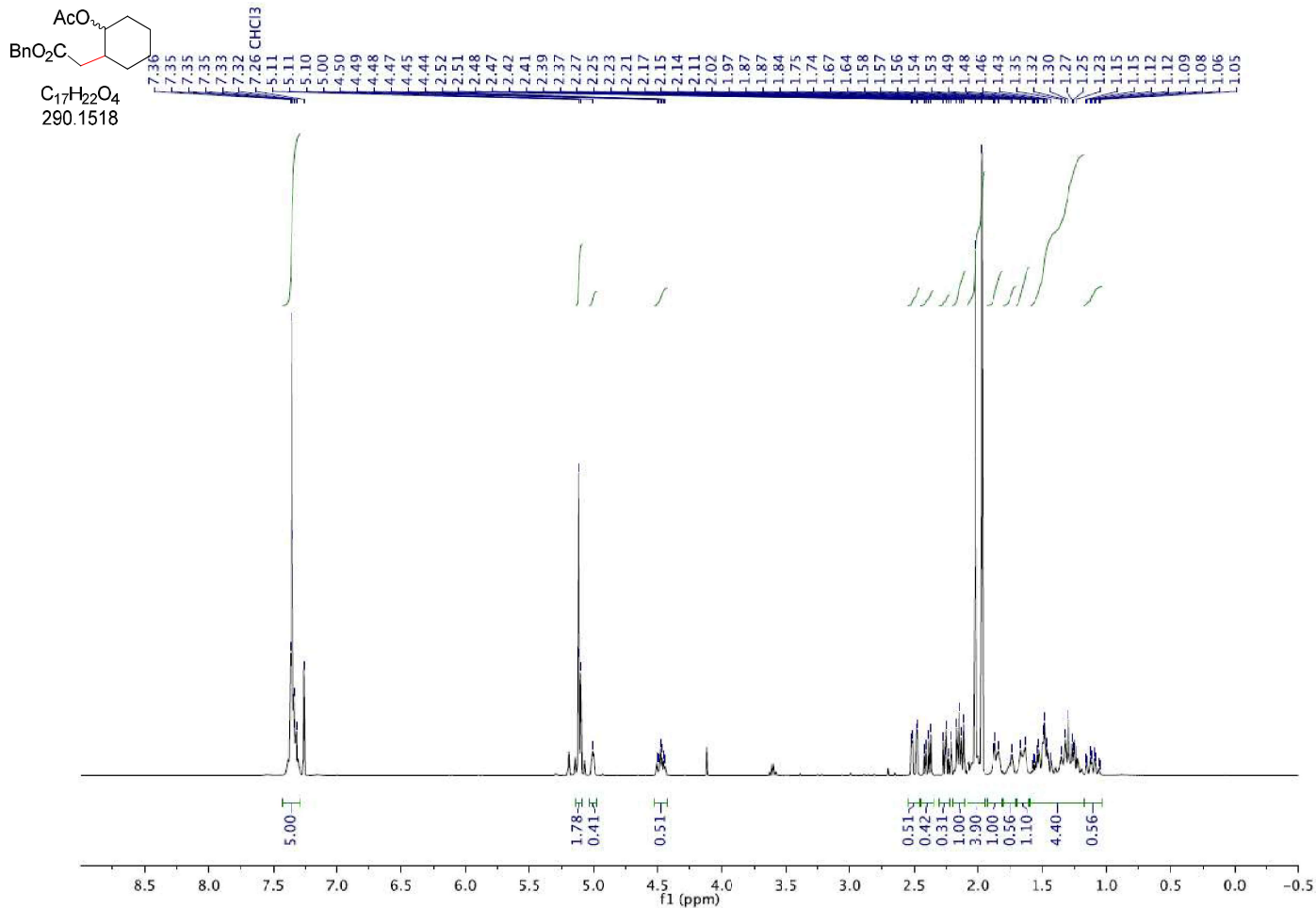
benzyl 2-(2-acetoxycyclopentyl)acetate (3a)

 $^1\text{H-NMR}$ (400 MHz, CDCl_3)

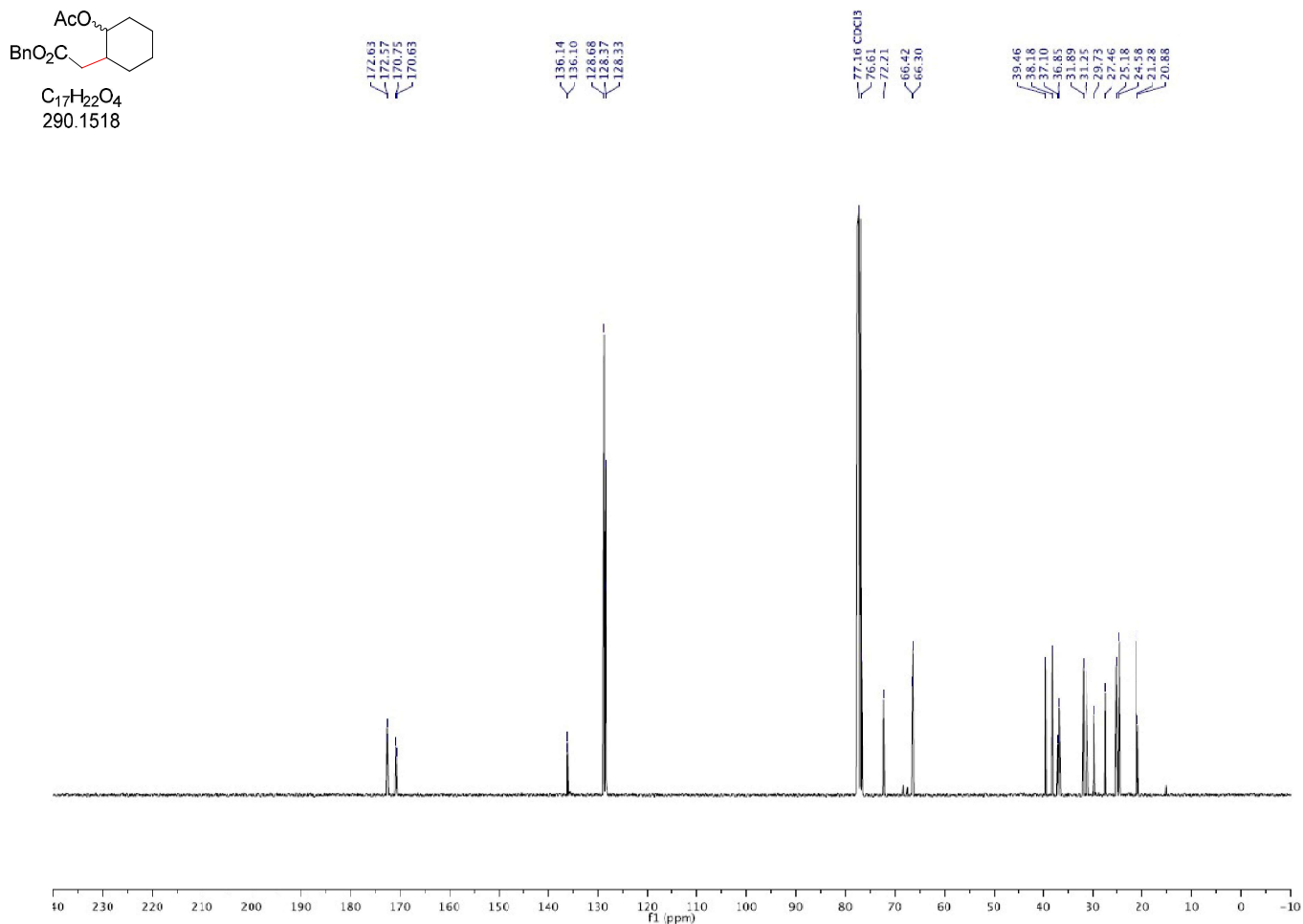
benzyl 2-(2-acetoxycyclopentyl)acetate (3a)

 $^{13}\text{C-NMR}$ (101 MHz, CDCl_3)

benzyl 2-(2-acetoxycyclohexyl)acetate (3am)

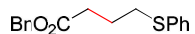
 $^1\text{H-NMR}$ (400 MHz, CDCl_3)

benzyl 2-(2-acetoxycyclohexyl)acetate (3am)

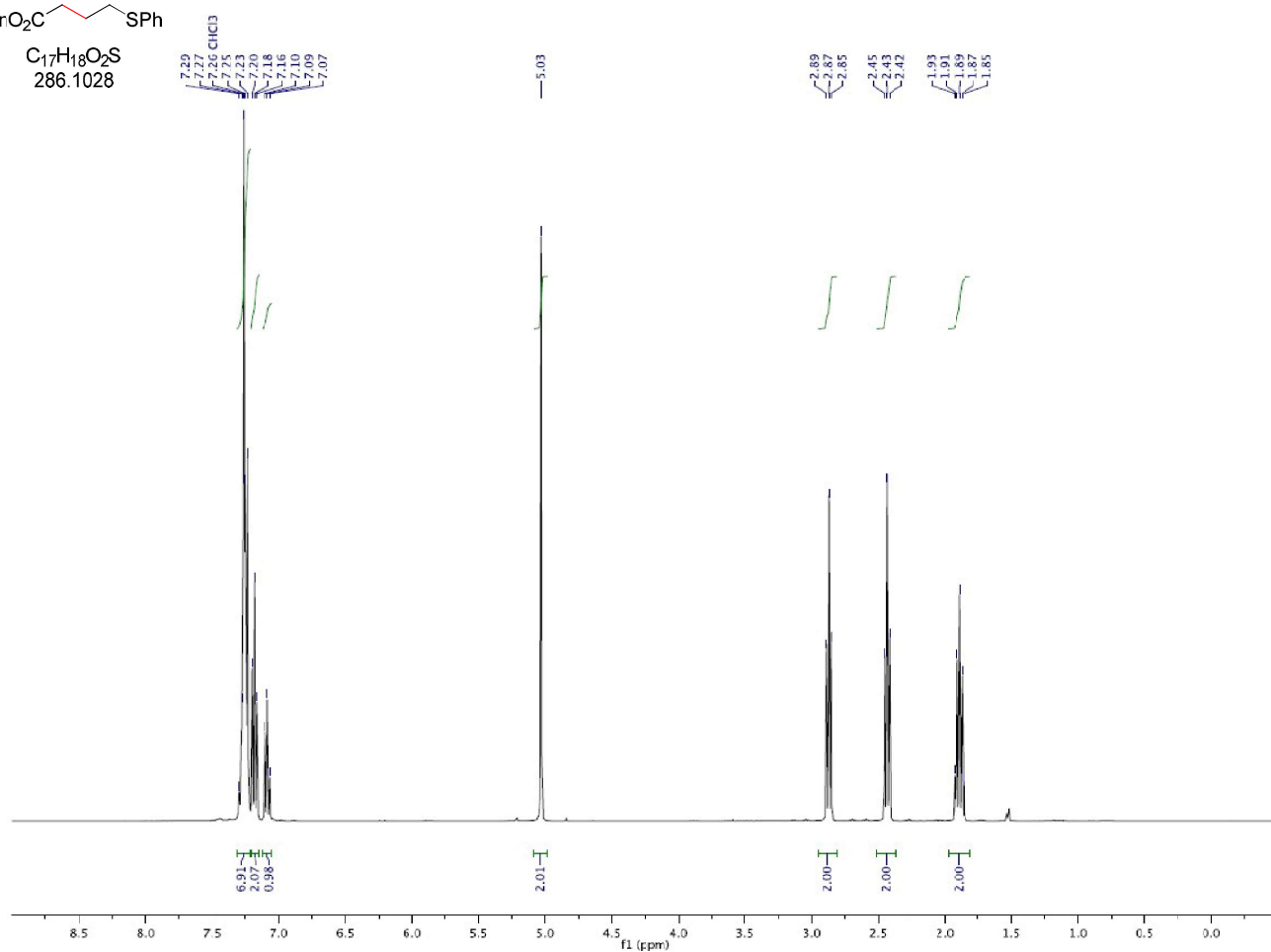
 $^{13}\text{C-NMR}$ (101 MHz, CDCl_3)

benzyl 4-(phenylthio)butanoate (3an)

¹H-NMR (300 MHz, CDCl₃)

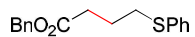


C₁₇H₁₈O₂S
286.1028

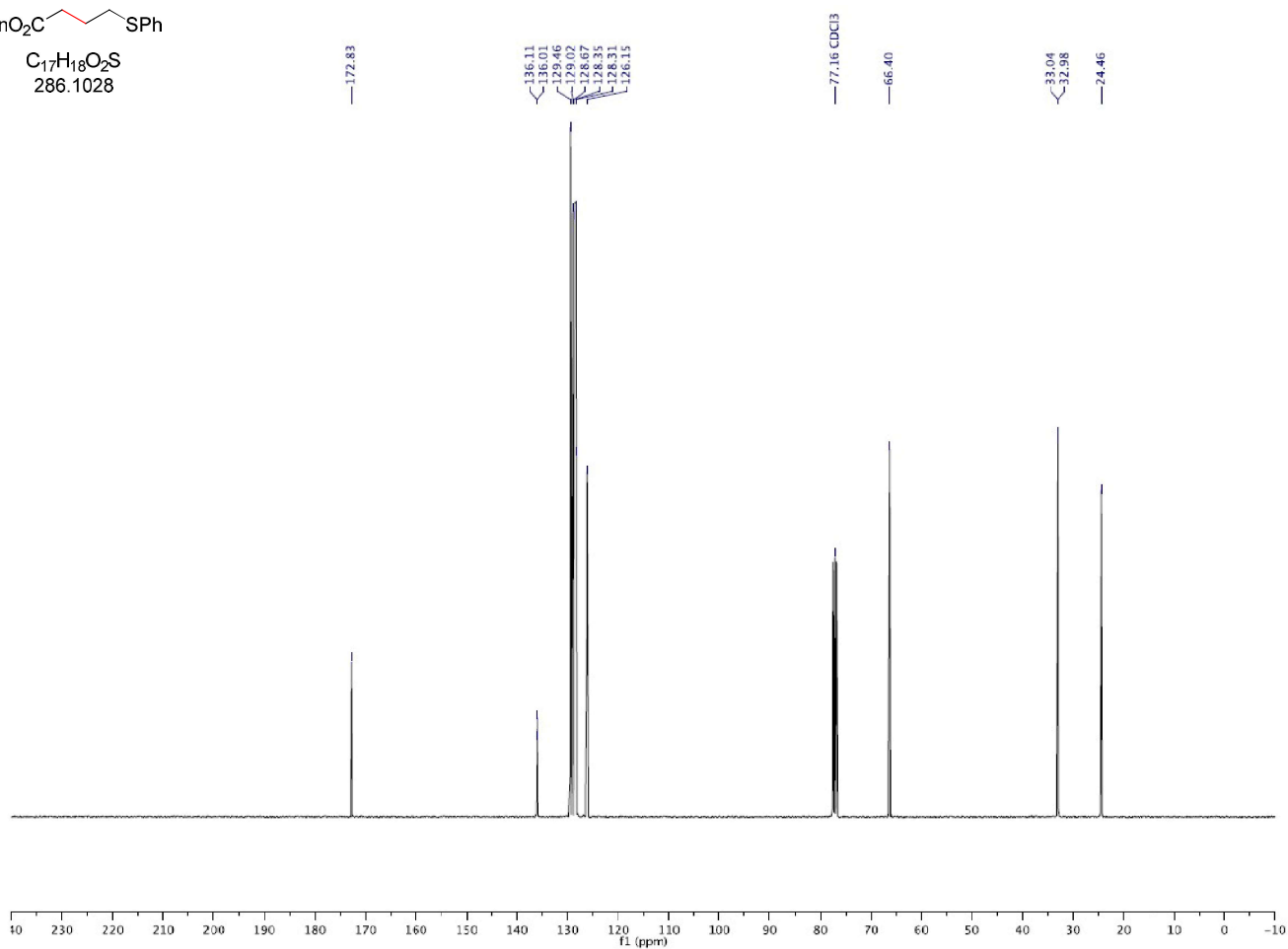


benzyl 4-(phenylthio)butanoate (3an)

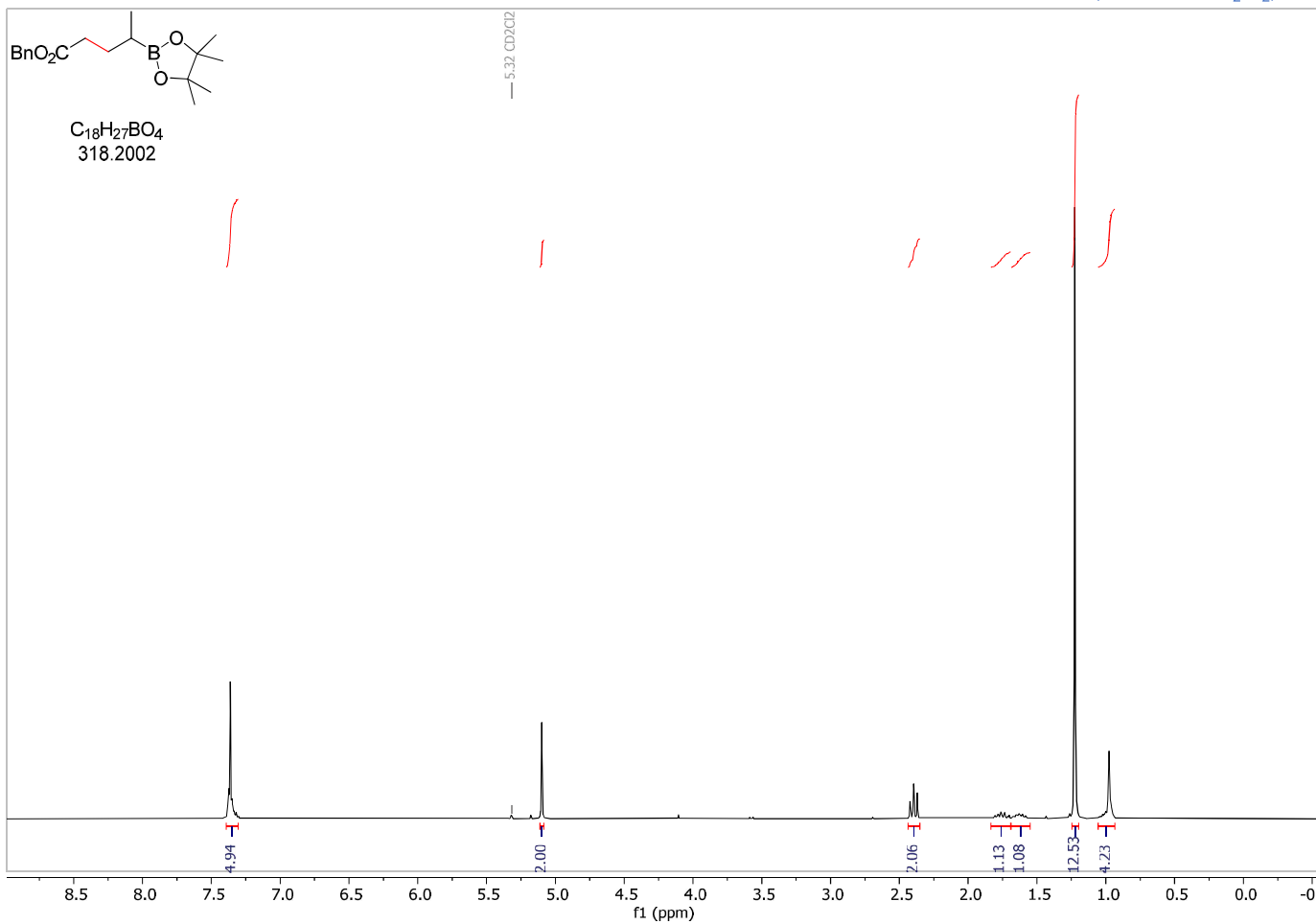
¹³C-NMR (75 MHz, CDCl₃)



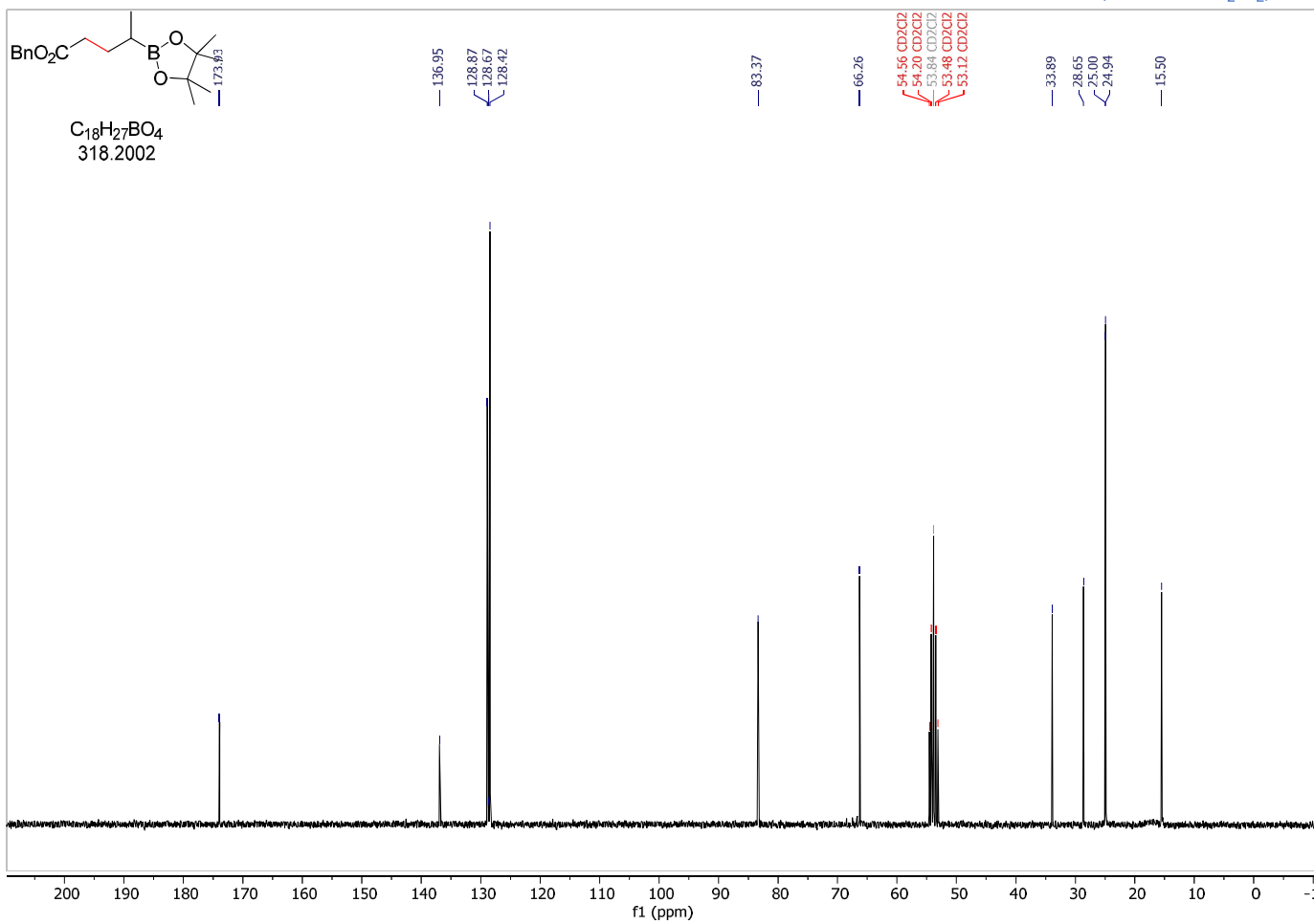
C₁₇H₁₈O₂S
286.1028

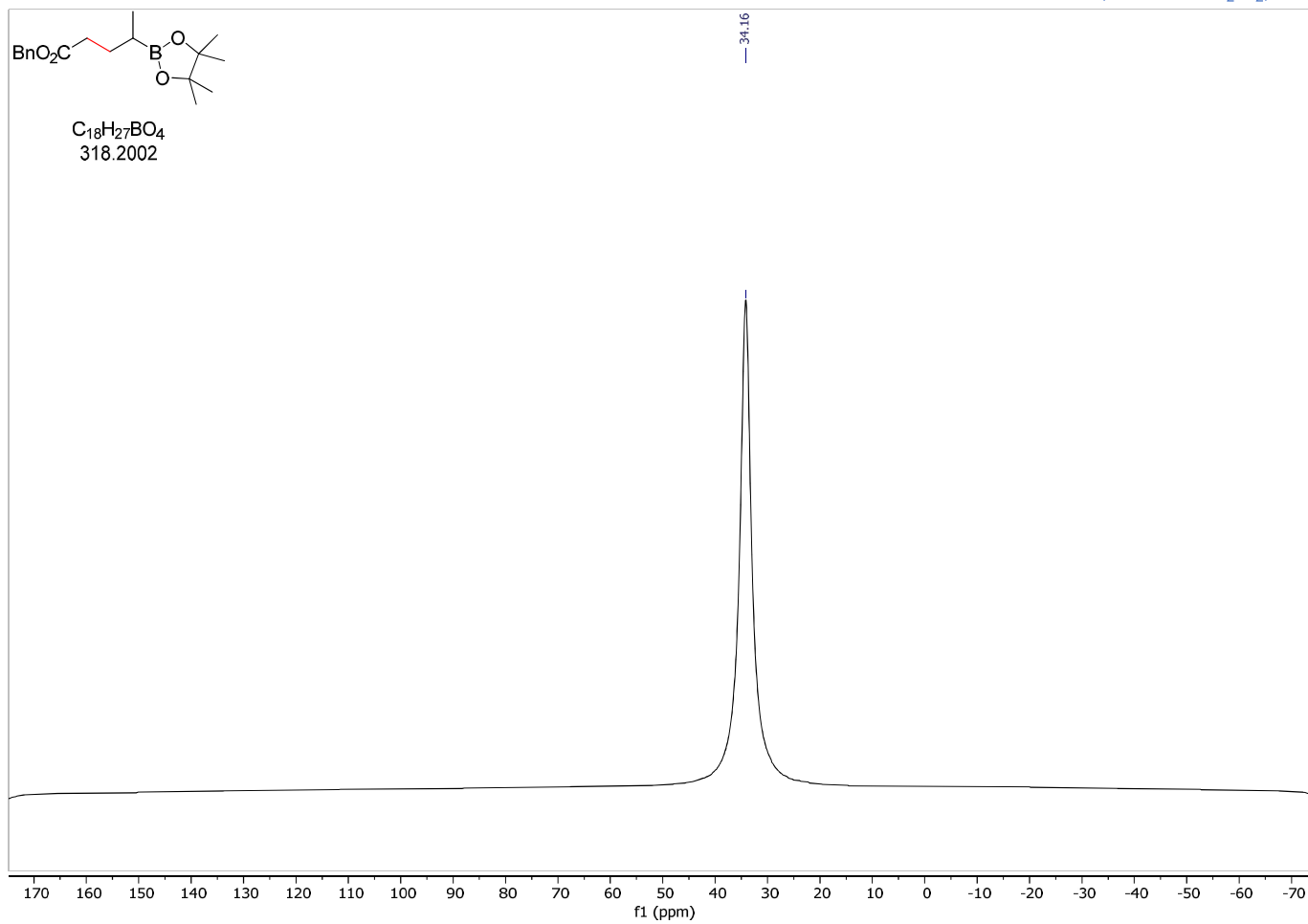


benzyl 4-(4,4,5,5-tetramethyl-1,3,2-dioxaborolan-2-yl)pentanoate (3ao)

 $^1\text{H-NMR}$ (300 MHz, CD_2Cl_2)

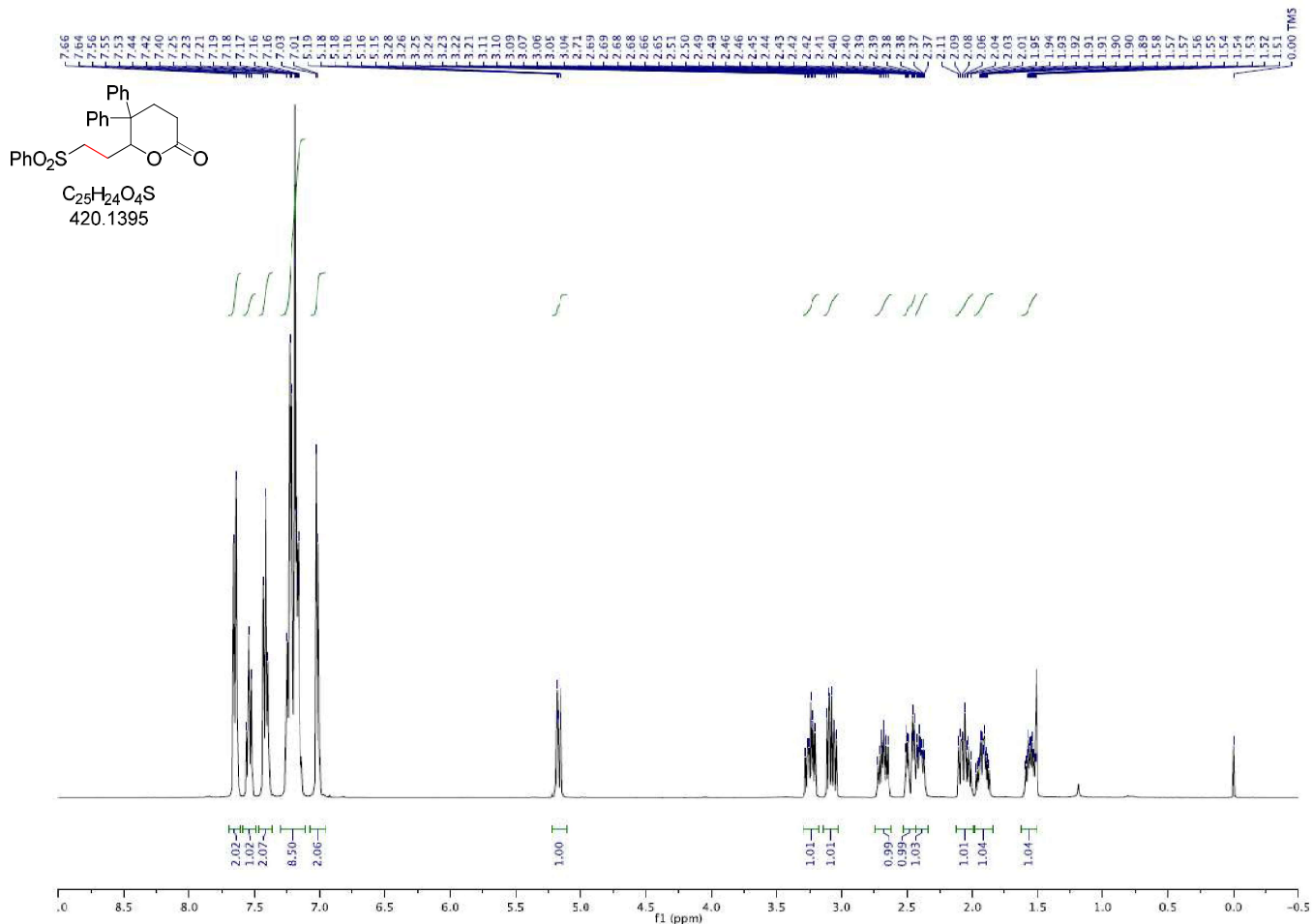
benzyl 4-(4,4,5,5-tetramethyl-1,3,2-dioxaborolan-2-yl)pentanoate (3ao)

 $^{13}\text{C-NMR}$ (75 MHz, CD_2Cl_2)



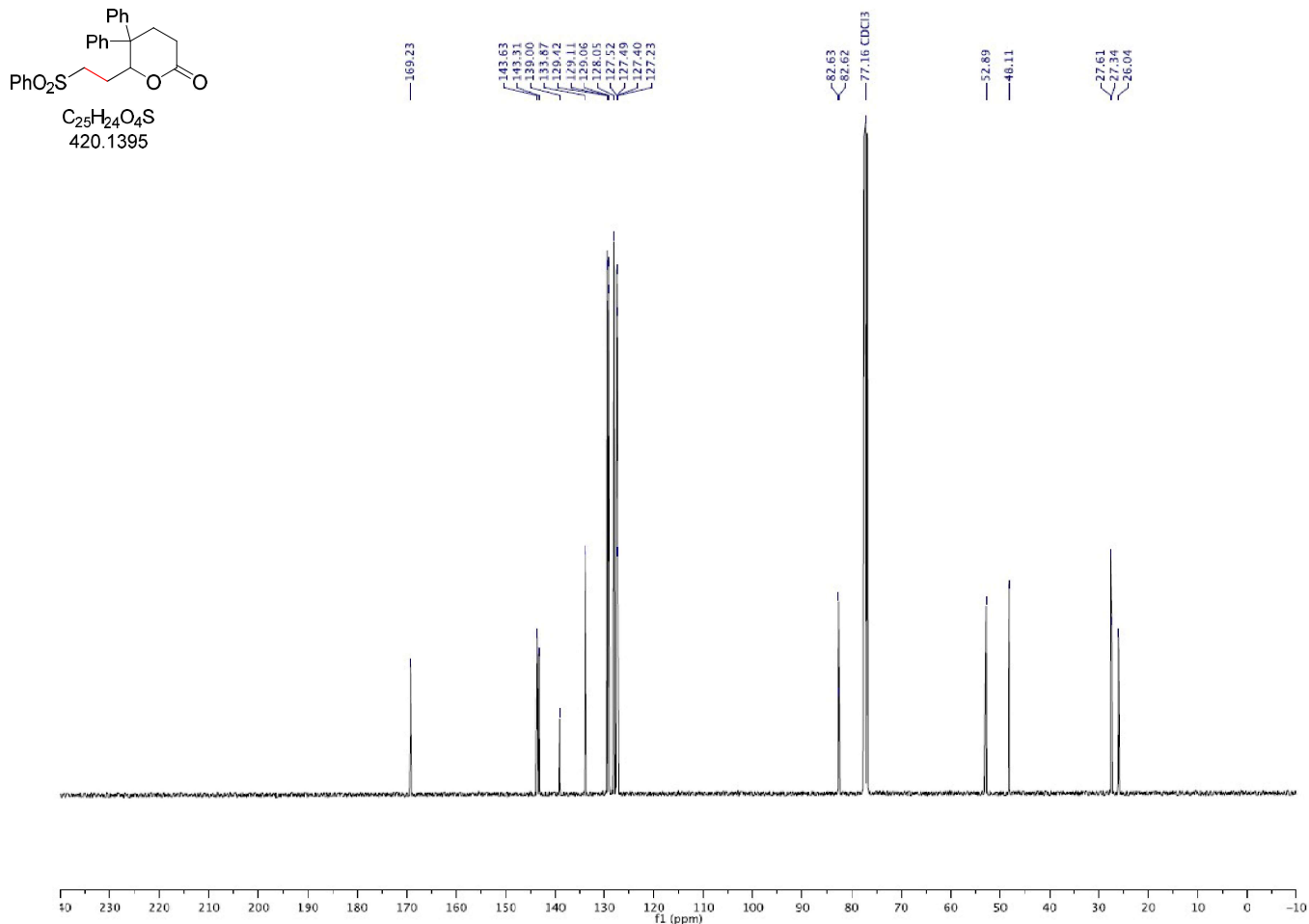
6-[2-(benzenesulfonyl)ethyl]-5,5-diphenyl-tetrahydropyran-2-one (3cb)

$^1\text{H-NMR}$ (300 MHz, CDCl_3)

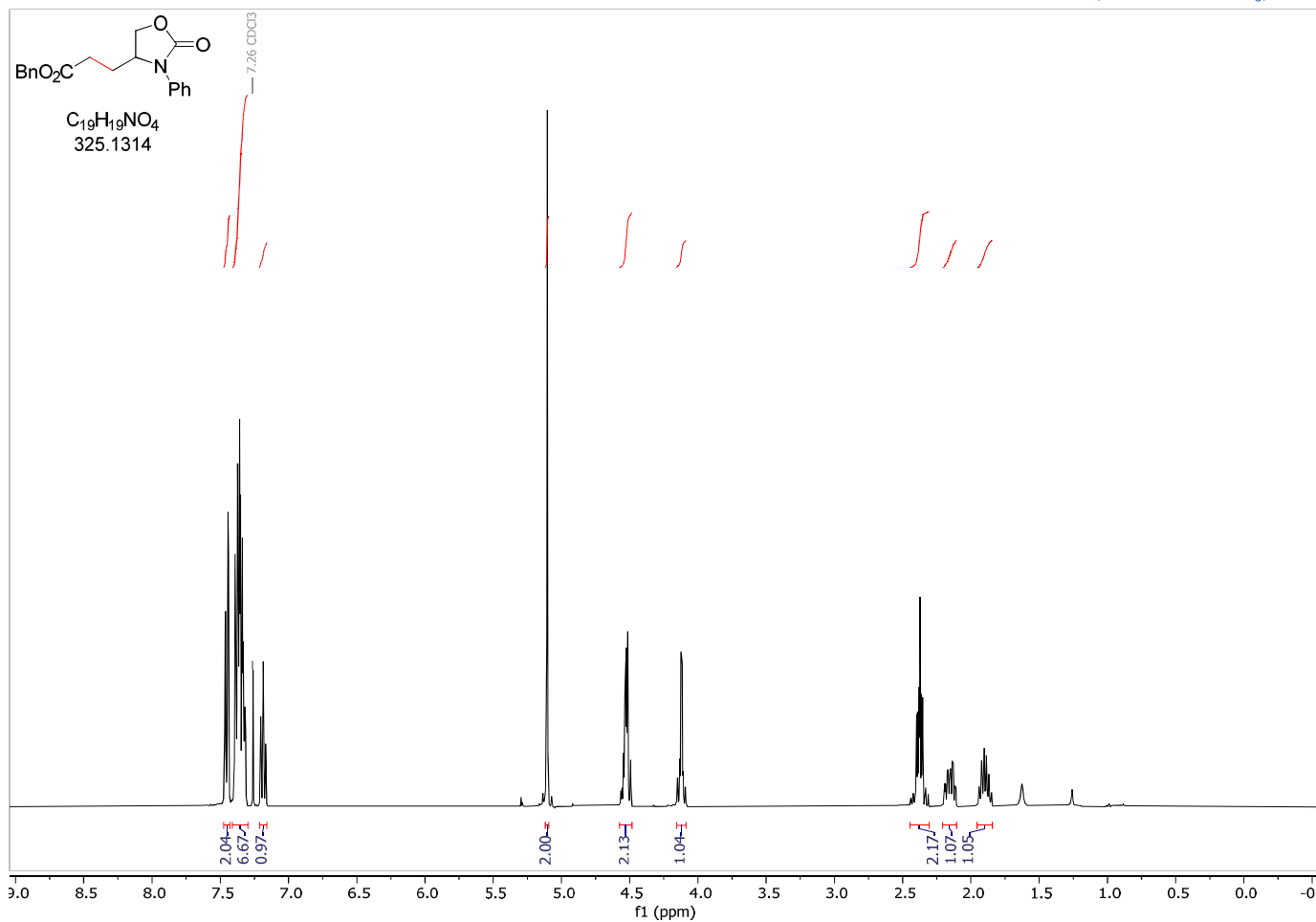


6-[2-(benzenesulfonyl)ethyl]-5,5-diphenyl-tetrahydropyran-2-one (3cb)

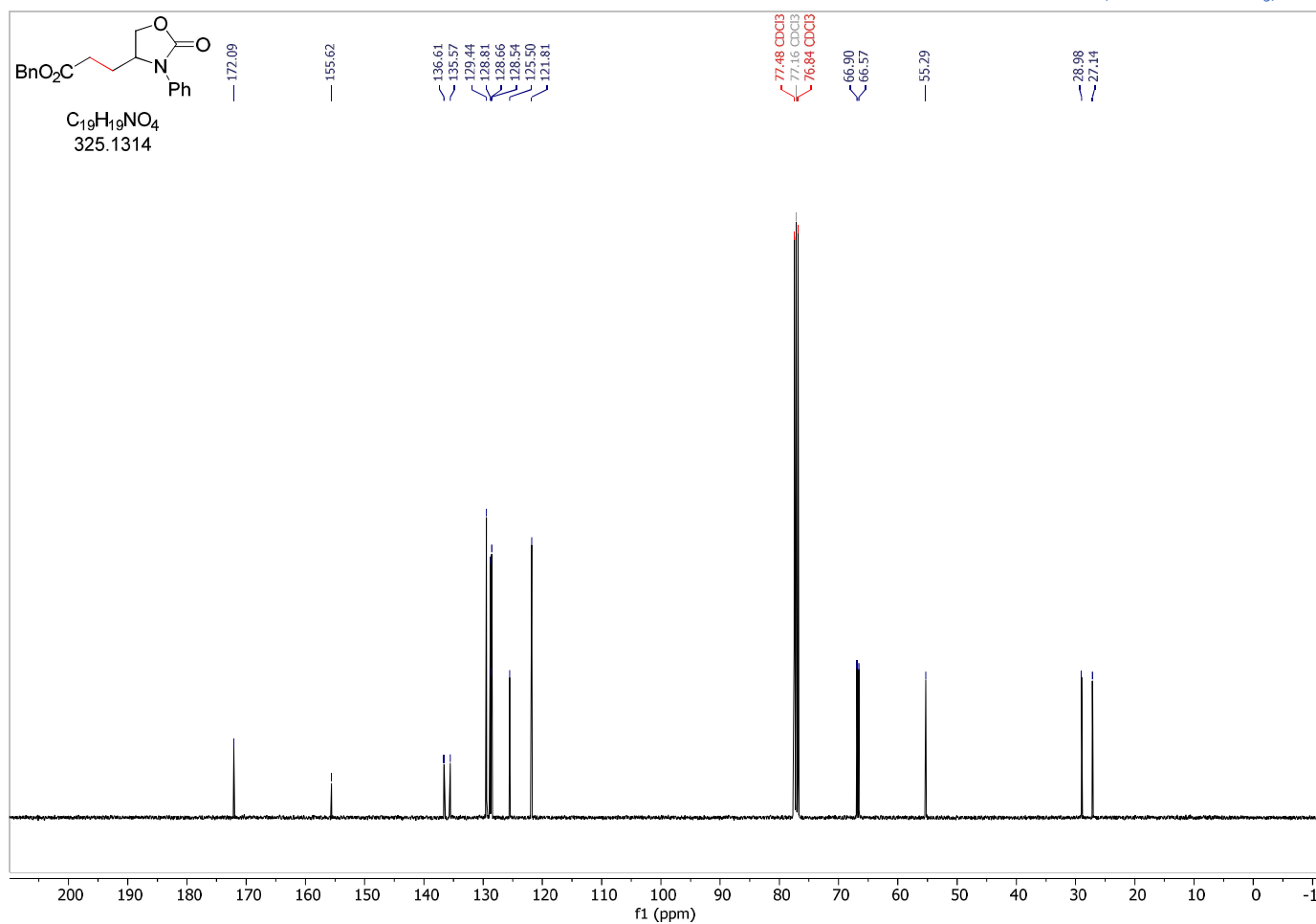
$^{13}\text{C-NMR}$ (75 MHz, CDCl_3)



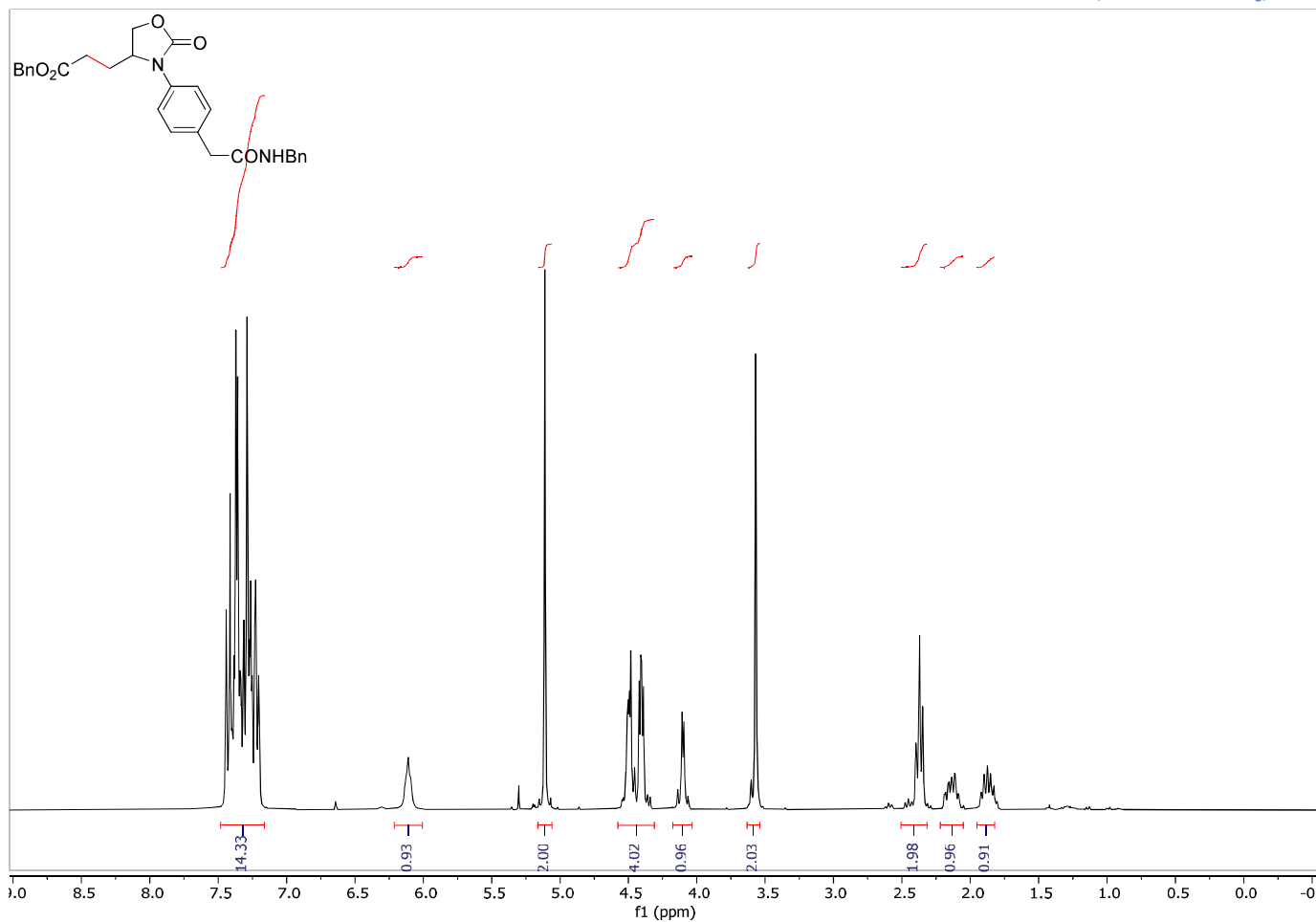
benzyl 3-(2-oxo-3-phenyl-oxazolidin-4-yl)propanoate (3ap)

 $^1\text{H-NMR}$ (400 MHz, CDCl_3)

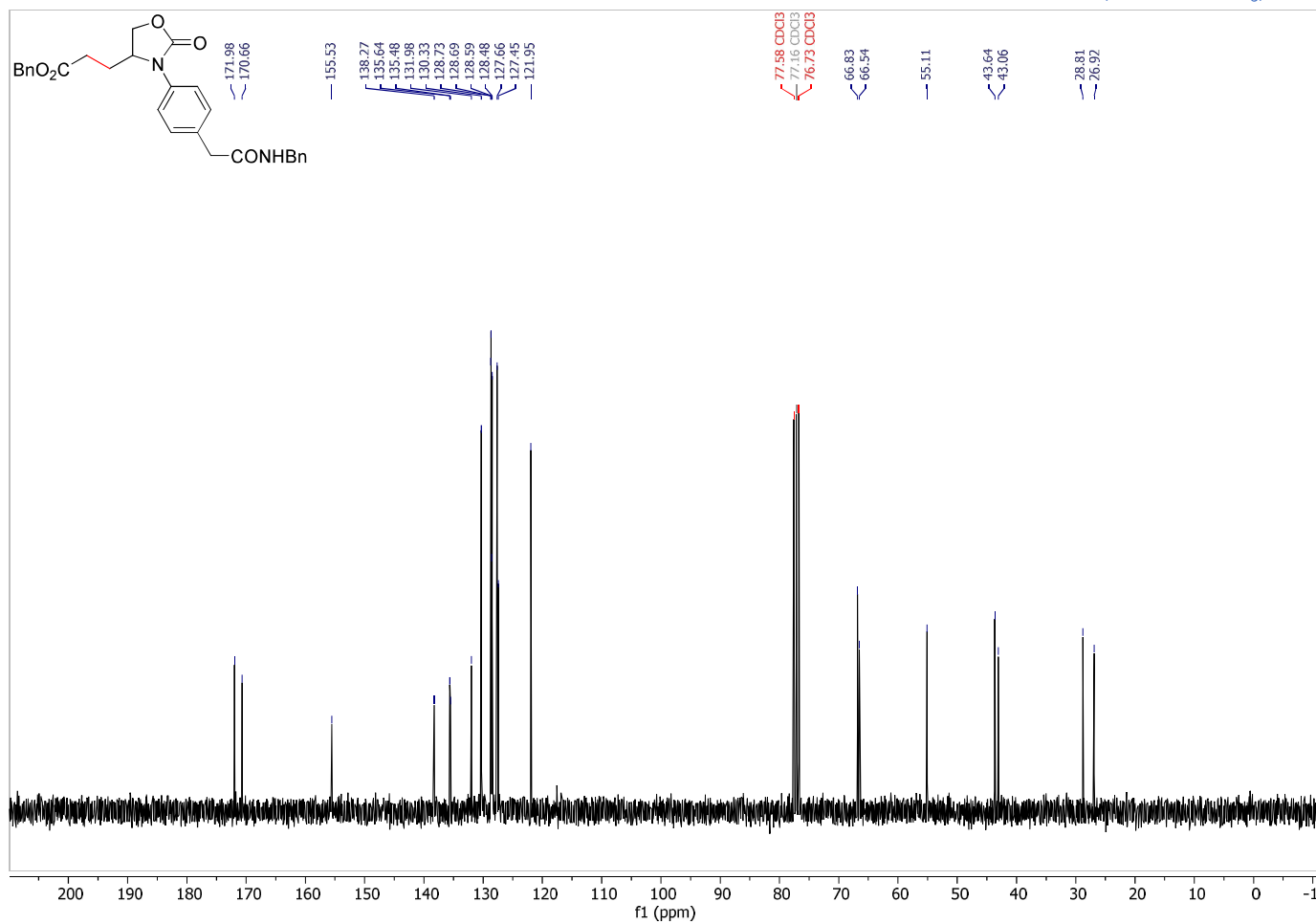
benzyl 3-(2-oxo-3-phenyl-oxazolidin-4-yl)propanoate (3ap)

 $^{13}\text{C-NMR}$ (100 MHz, CDCl_3)

benzyl 3-(3-(4-(2-(benzylamino)-2-oxoethyl)phenyl)-2-oxooxazolidin-4-yl)propanoate (3aq)

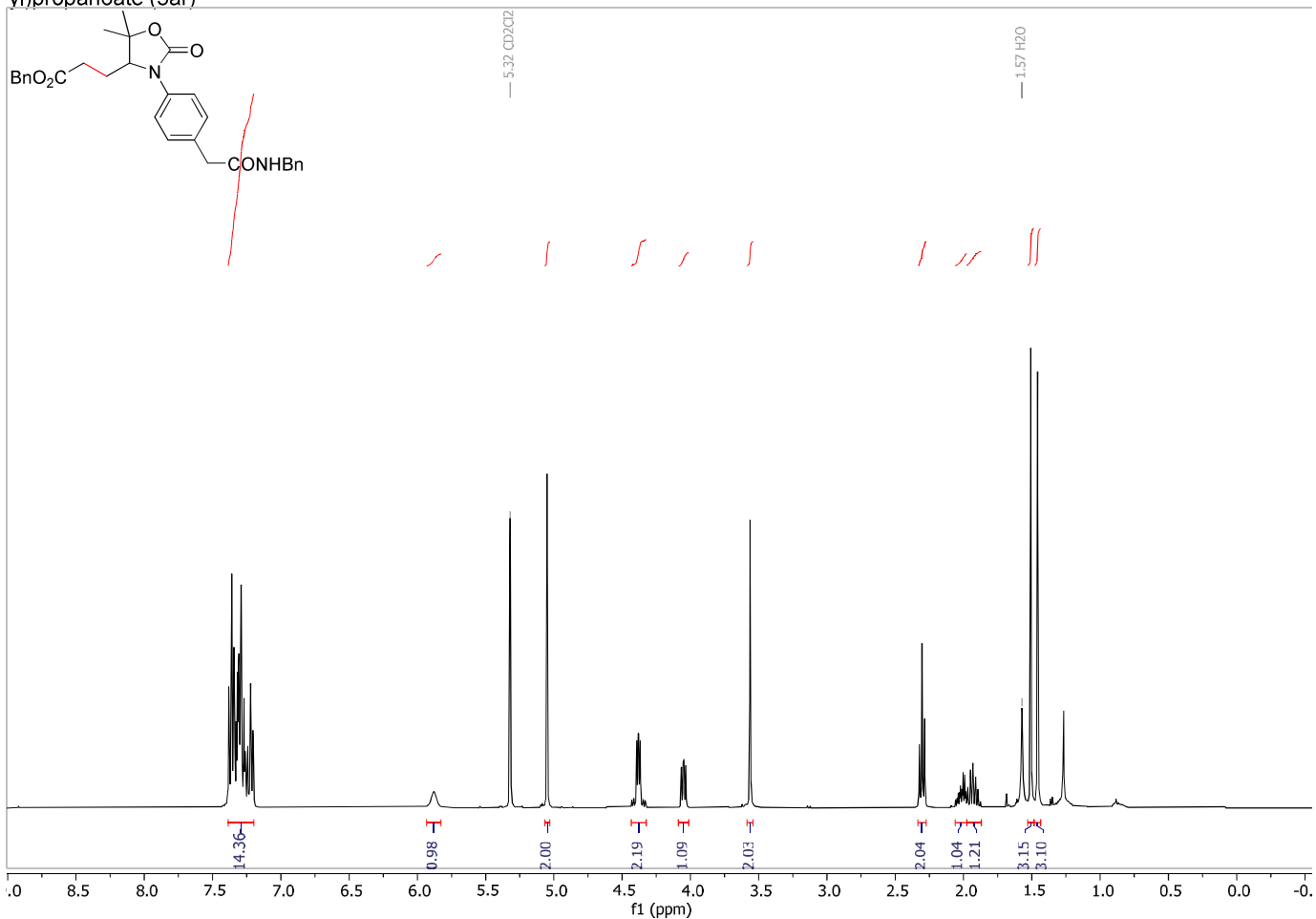
¹H-NMR (300 MHz, CDCl₃)

benzyl 3-(3-(4-(2-(benzylamino)-2-oxoethyl)phenyl)-2-oxooxazolidin-4-yl)propanoate (3aq)

¹³C-NMR (75 MHz, CDCl₃)

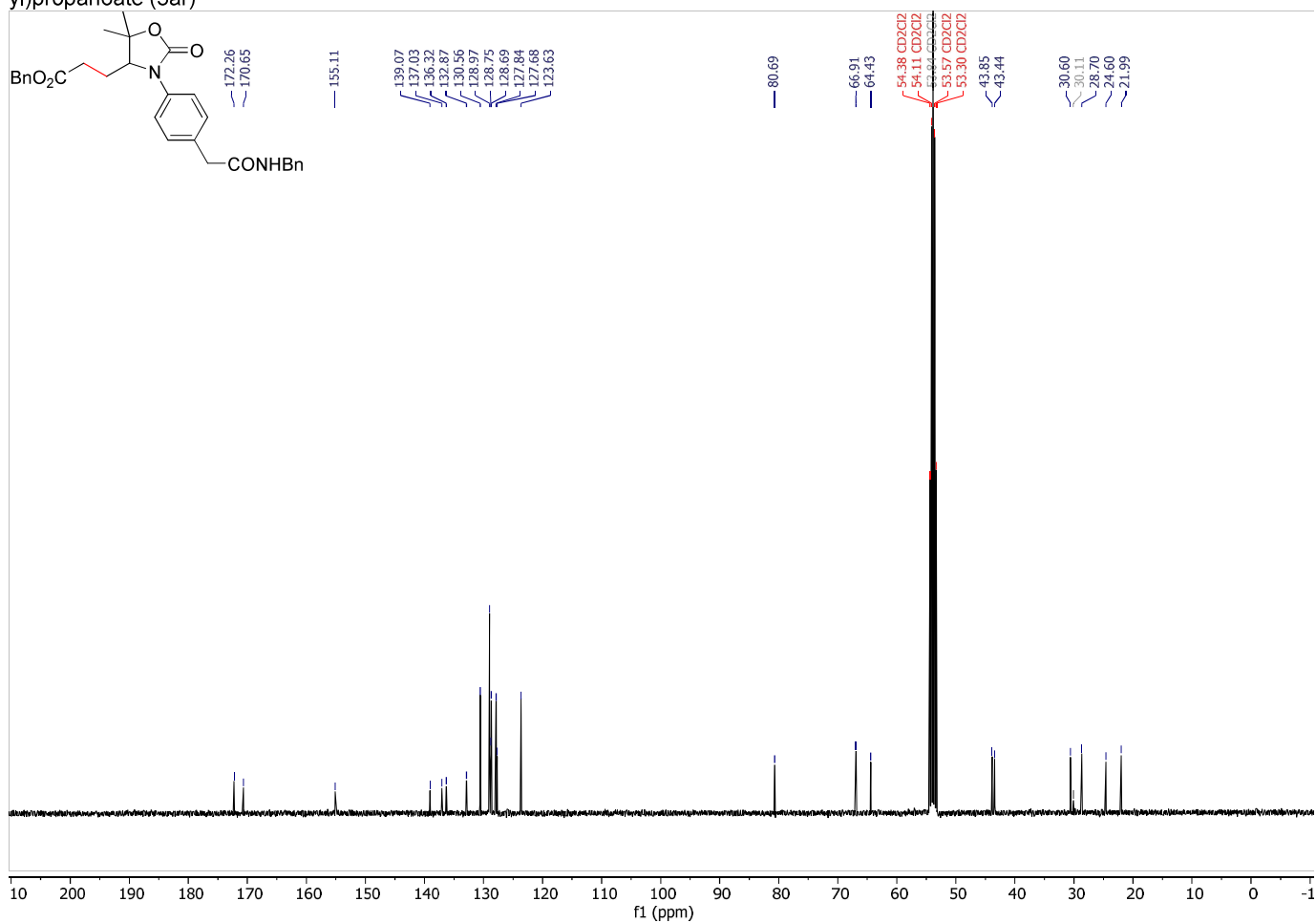
benzyl 3-(3-(4-(2-(benzylamino)-2-oxoethyl)phenyl)-5,5-dimethyl-2-oxooxazolidin-4-yl)propanoate (3ar)

¹H-NMR (400 MHz, CD₂Cl₂)

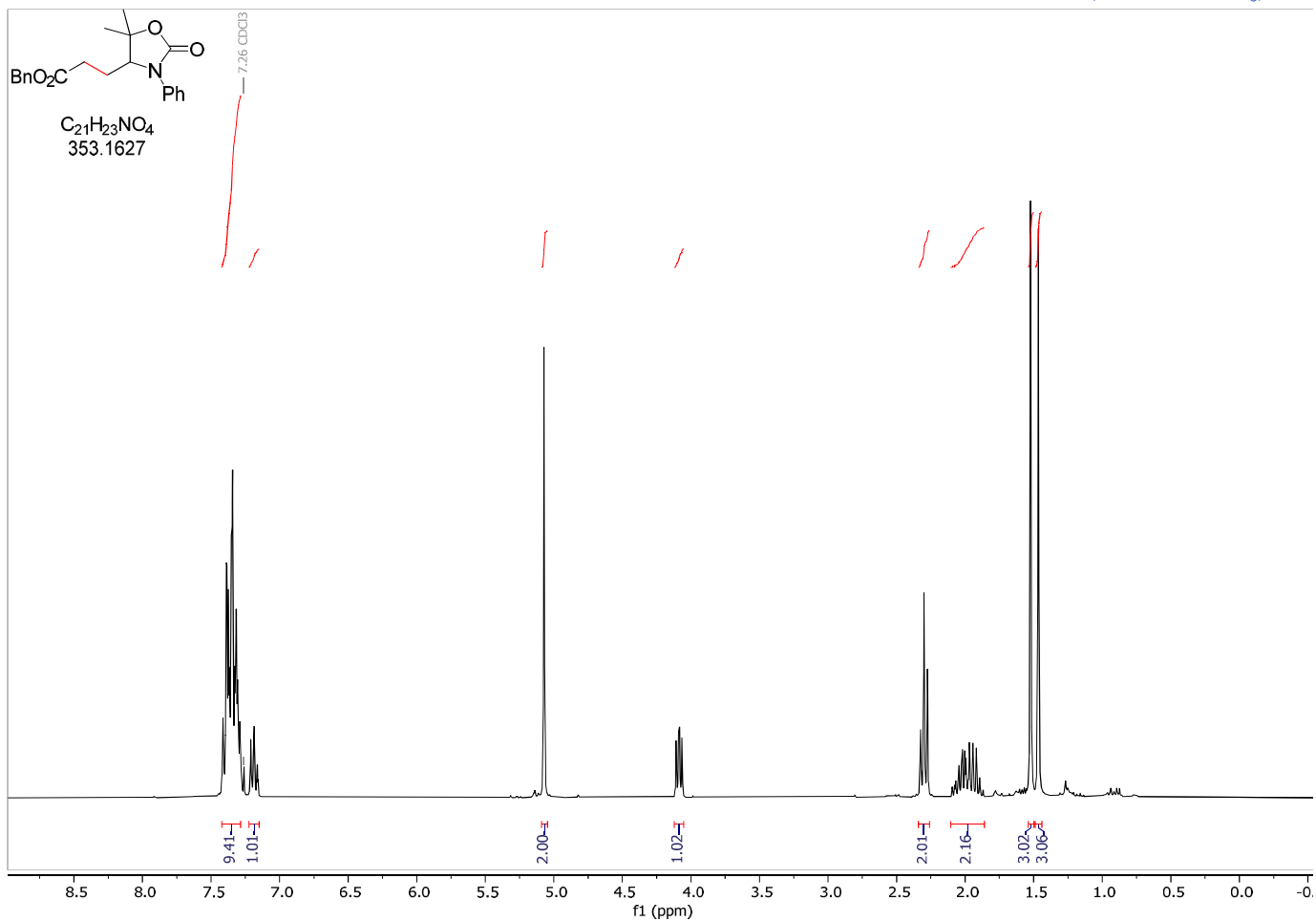


benzyl 3-(3-(4-(2-(benzylamino)-2-oxoethyl)phenyl)-5,5-dimethyl-2-oxooxazolidin-4-yl)propanoate (3ar)

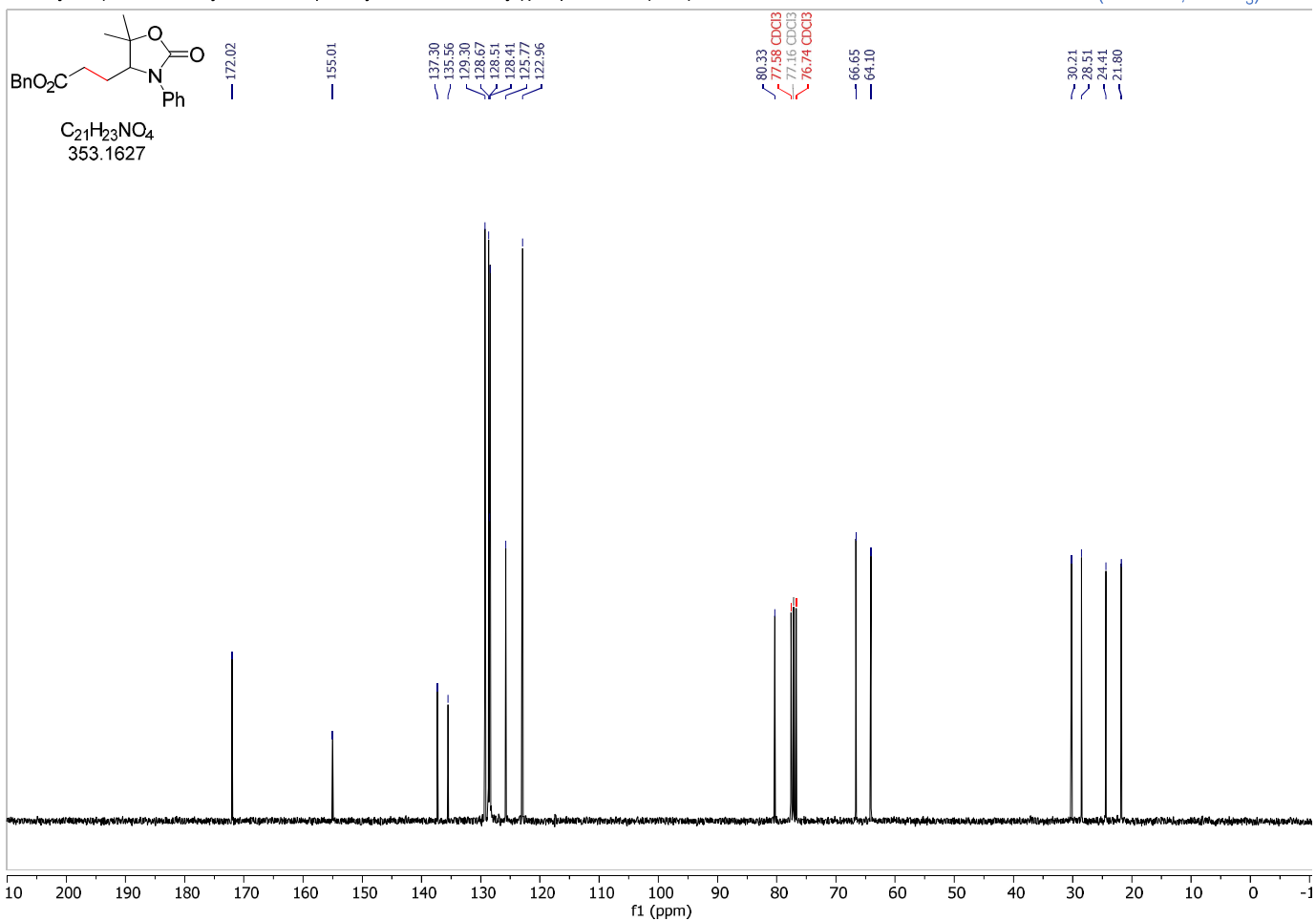
¹³C-NMR (101 MHz, CD₂Cl₂)



benzyl 3-(5,5-dimethyl-2-oxo-3-phenyloxazolidin-4-yl)propanoate (3as)

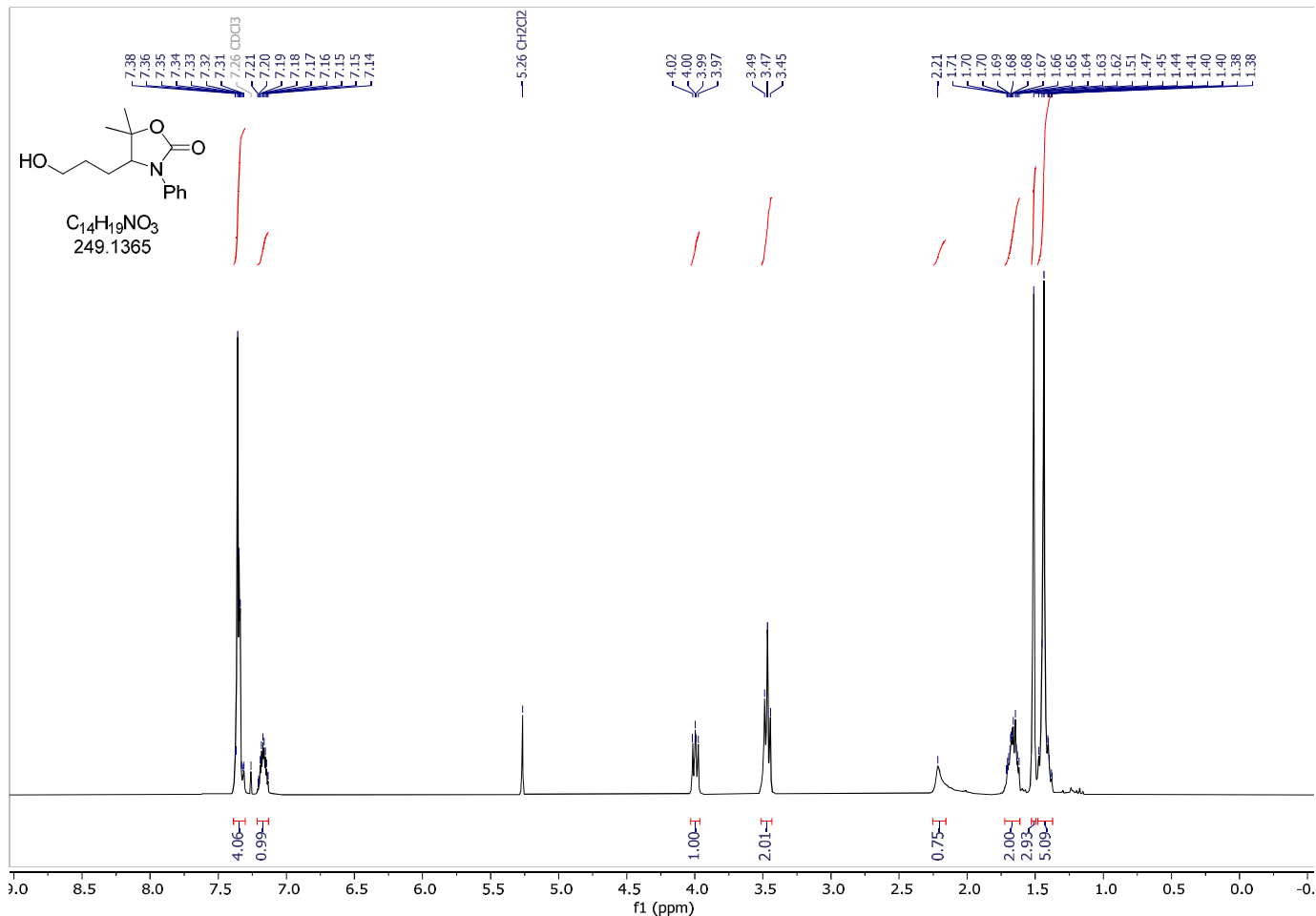
 $^1\text{H-NMR}$ (300 MHz, CDCl_3)

benzyl 3-(5,5-dimethyl-2-oxo-3-phenyloxazolidin-4-yl)propanoate (3as)

 $^{13}\text{C-NMR}$ (75 MHz, CDCl_3)

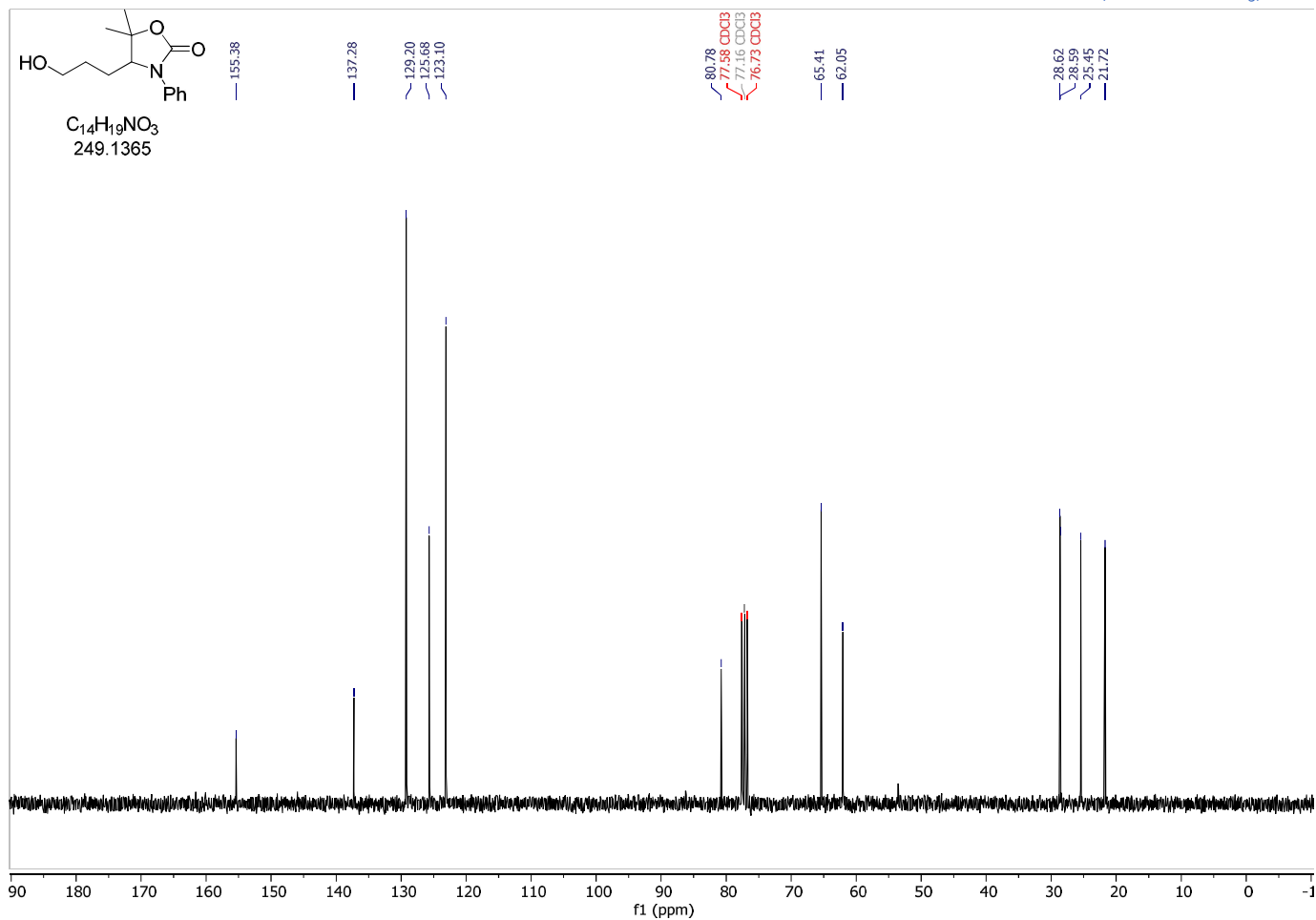
4-(3-hydroxypropyl)-5,5-dimethyl-3-phenyl-oxazolidin-2-one (S10)

¹H-NMR (300 MHz, CDCl₃)

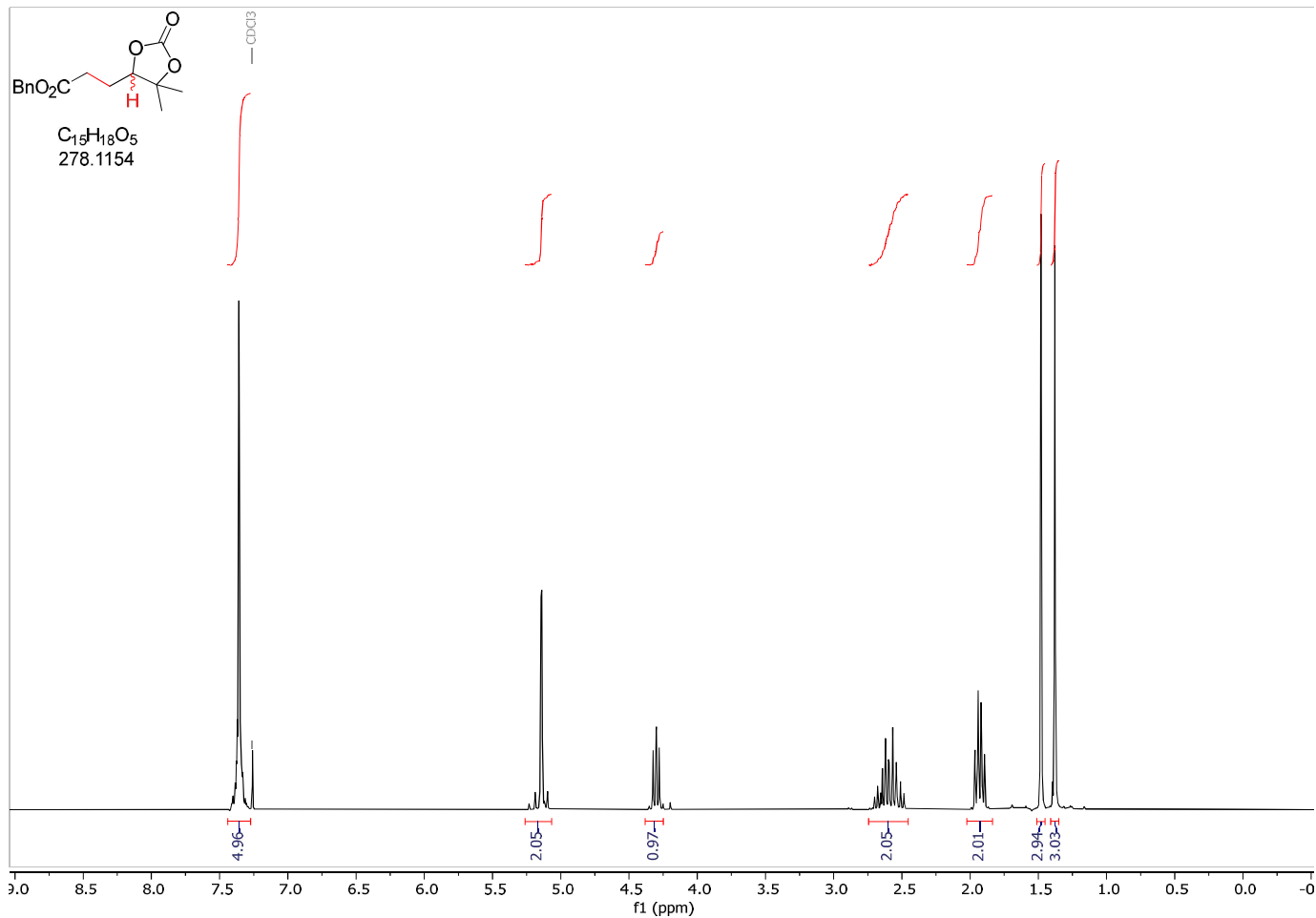


4-(3-hydroxypropyl)-5,5-dimethyl-3-phenyl-oxazolidin-2-one (S10)

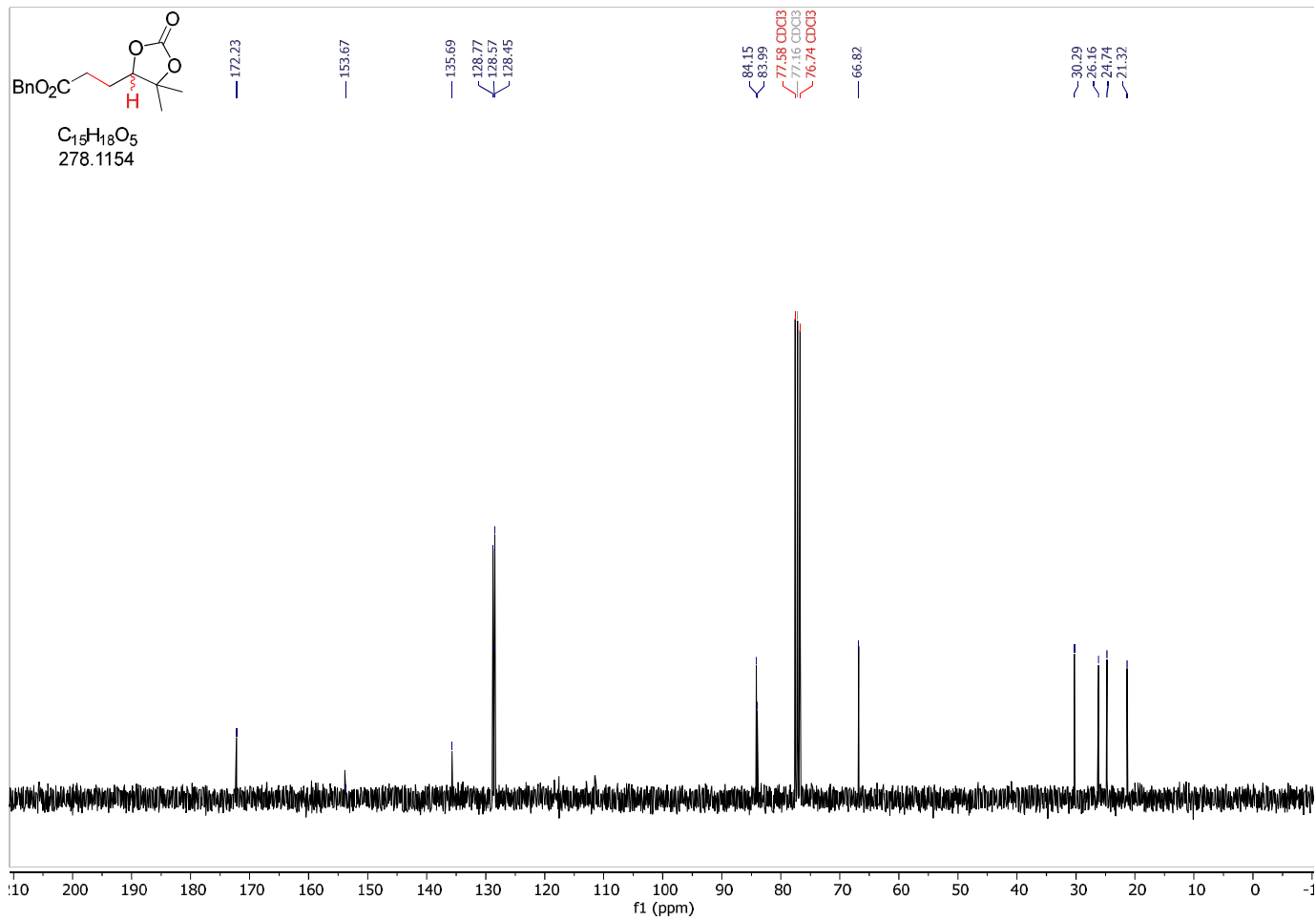
¹³C-NMR (75 MHz, CDCl₃)



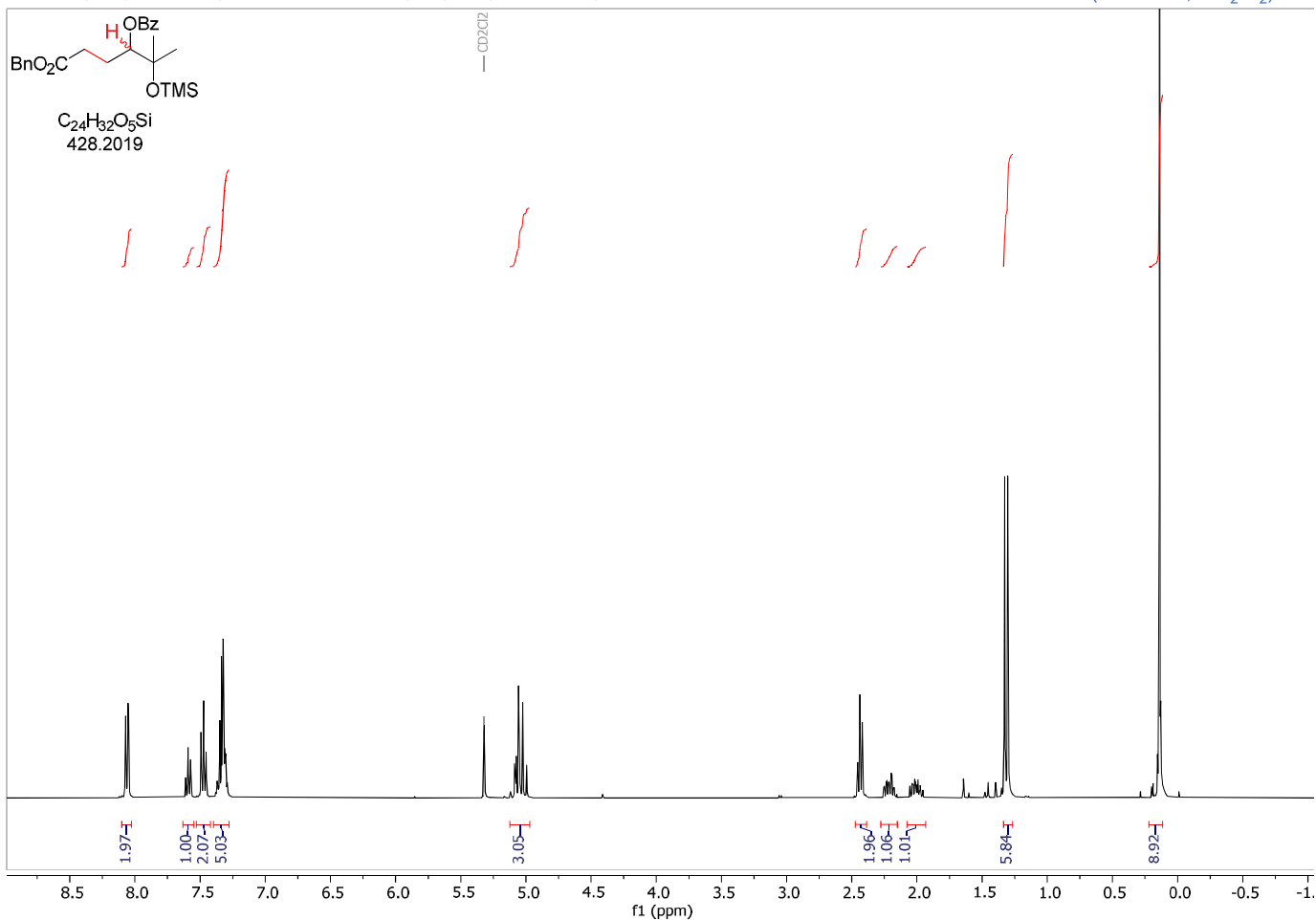
benzyl 3-(5,5-dimethyl-2-oxo-1,3-dioxolan-4-yl)propanoate (3at)

 $^1\text{H-NMR}$ (300 MHz, CDCl_3)

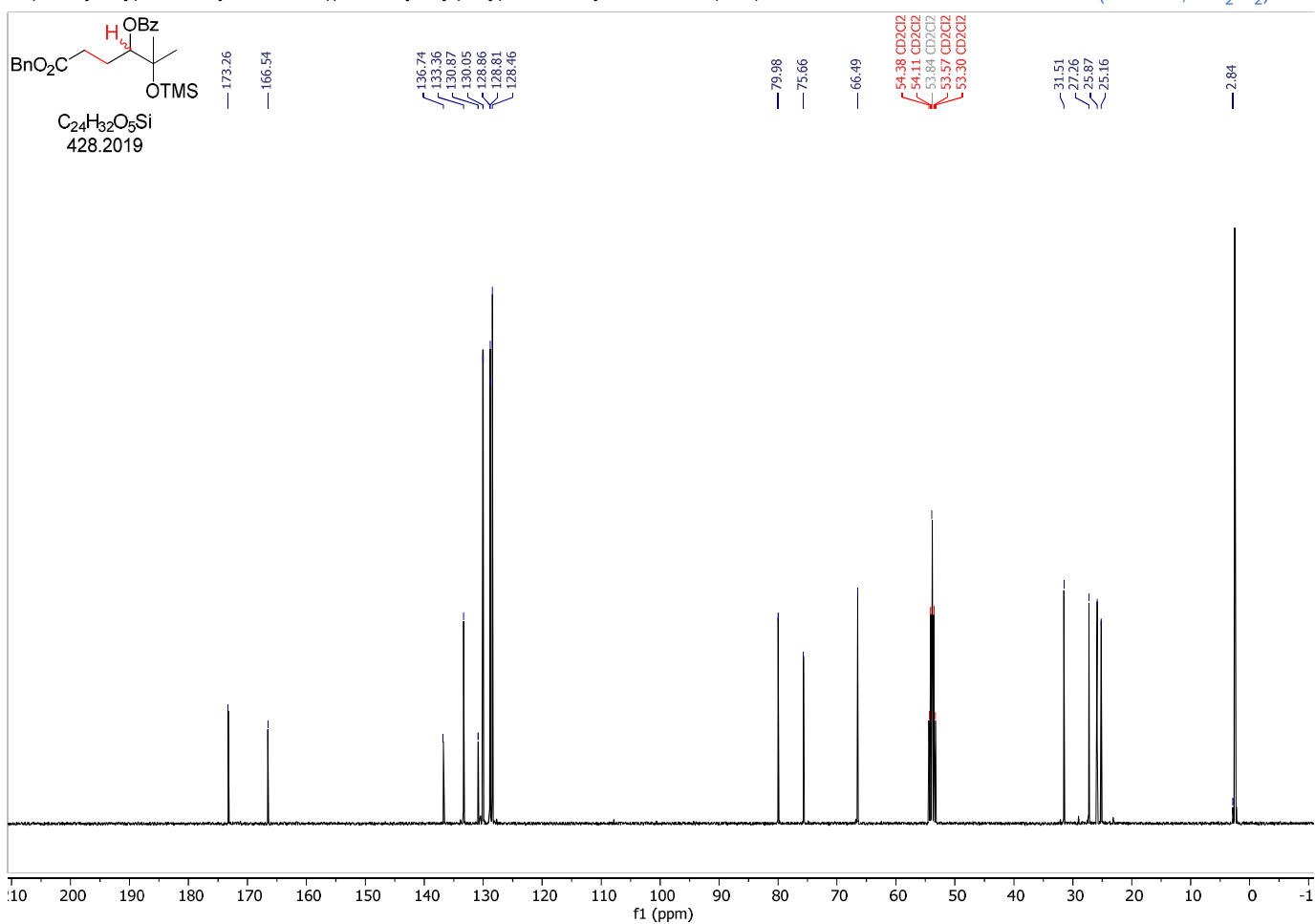
benzyl 3-(5,5-dimethyl-2-oxo-1,3-dioxolan-4-yl)propanoate (3at)

 $^{13}\text{C-NMR}$ (75 MHz, CDCl_3)

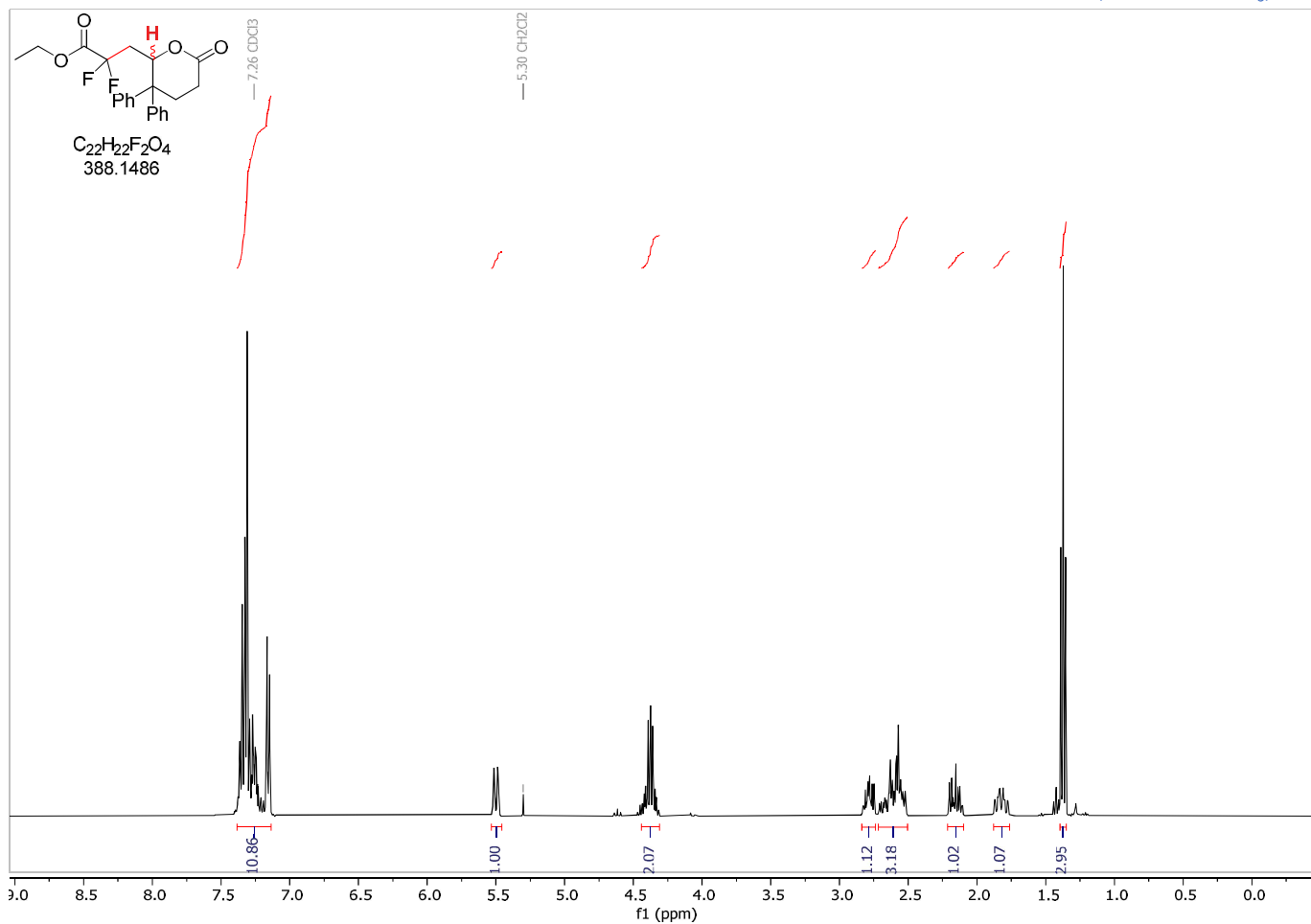
6-(benzyloxy)-2-methyl-6-oxo-2-((trimethylsilyloxy)hexan-3-yl benzoate (3av)

 $^1\text{H-NMR}$ (300 MHz, CD_2Cl_2)

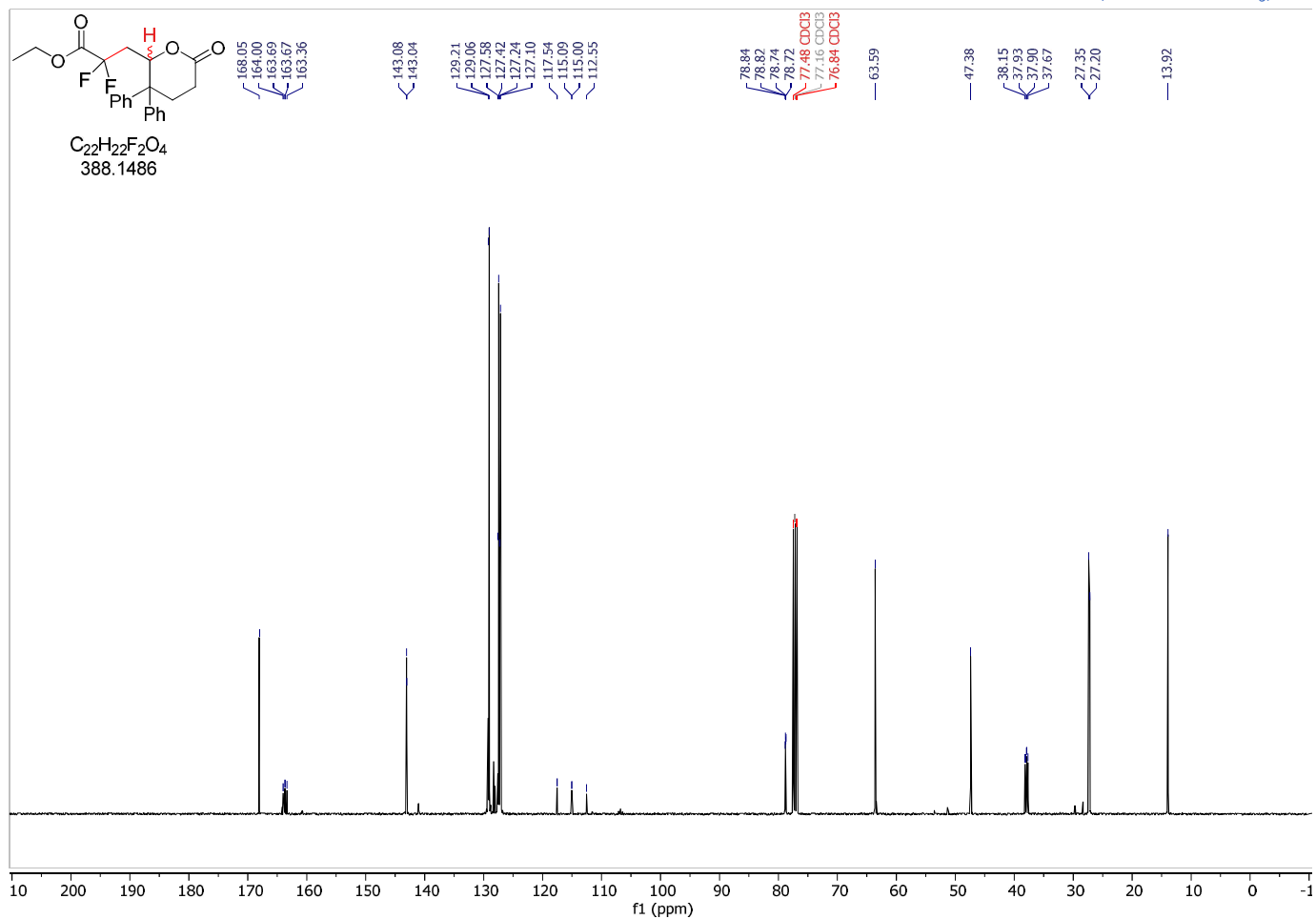
6-(benzyloxy)-2-methyl-6-oxo-2-((trimethylsilyloxy)hexan-3-yl benzoate (3av)

 $^{13}\text{C-NMR}$ (75 MHz, CD_2Cl_2)

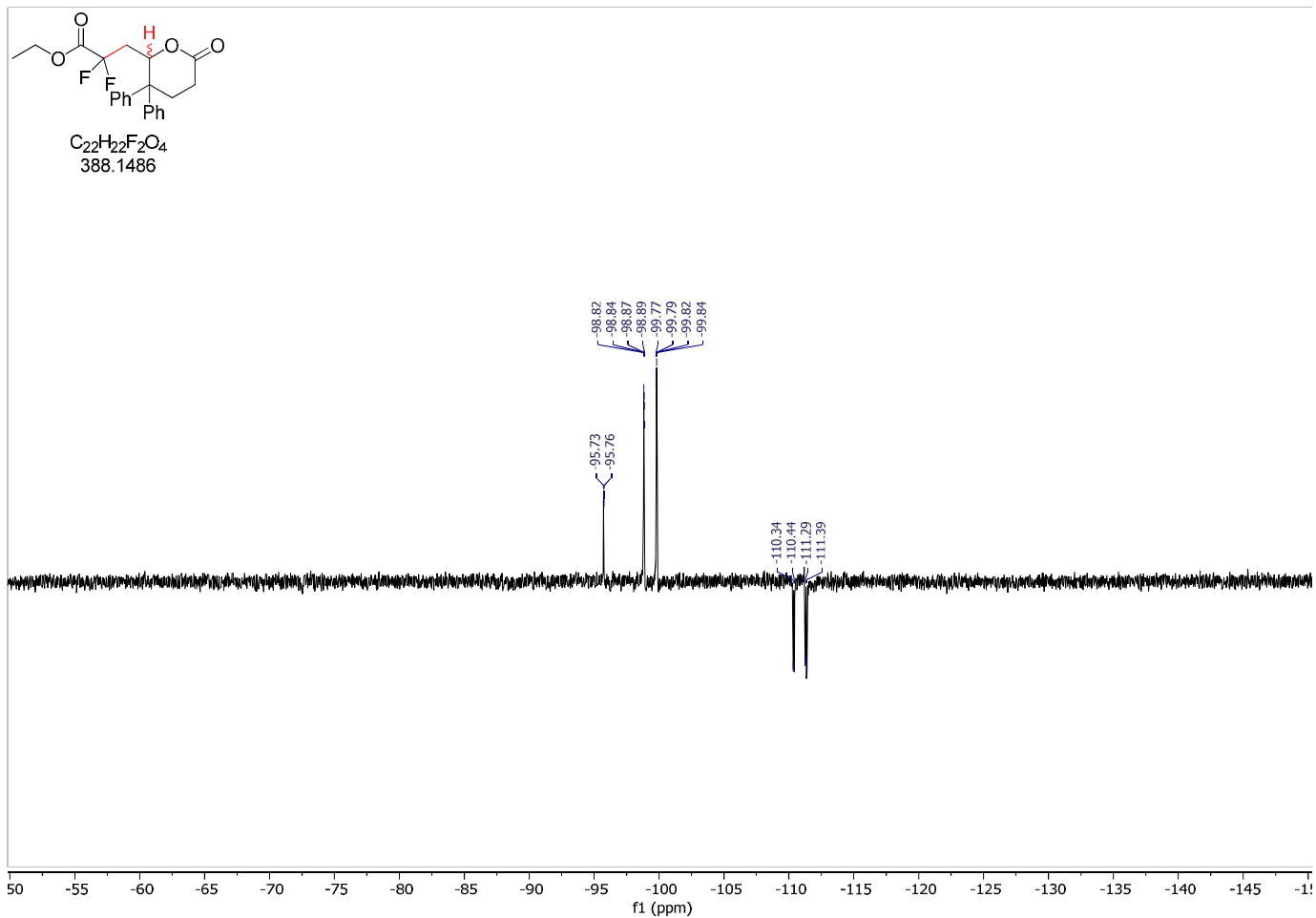
ethyl 2,2-difluoro-3-(6-oxo-3,3-diphenyltetrahydro-2H-pyran-2-yl)propanoate (3db)

 $^1\text{H-NMR}$ (400 MHz, CDCl_3)

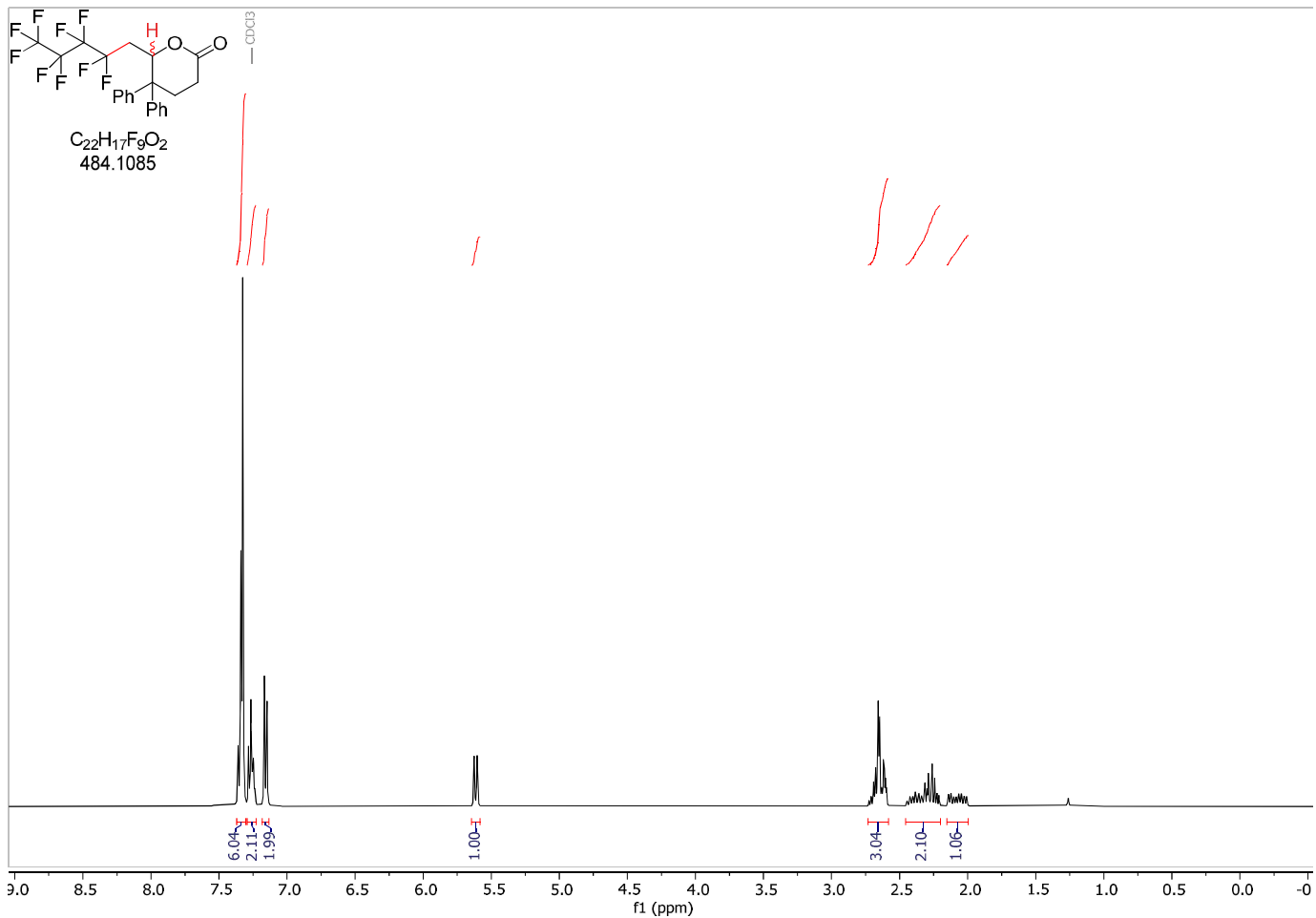
ethyl 2,2-difluoro-3-(6-oxo-3,3-diphenyltetrahydro-2H-pyran-2-yl)propanoate (3db)

 $^{13}\text{C-NMR}$ (100 MHz, CDCl_3)

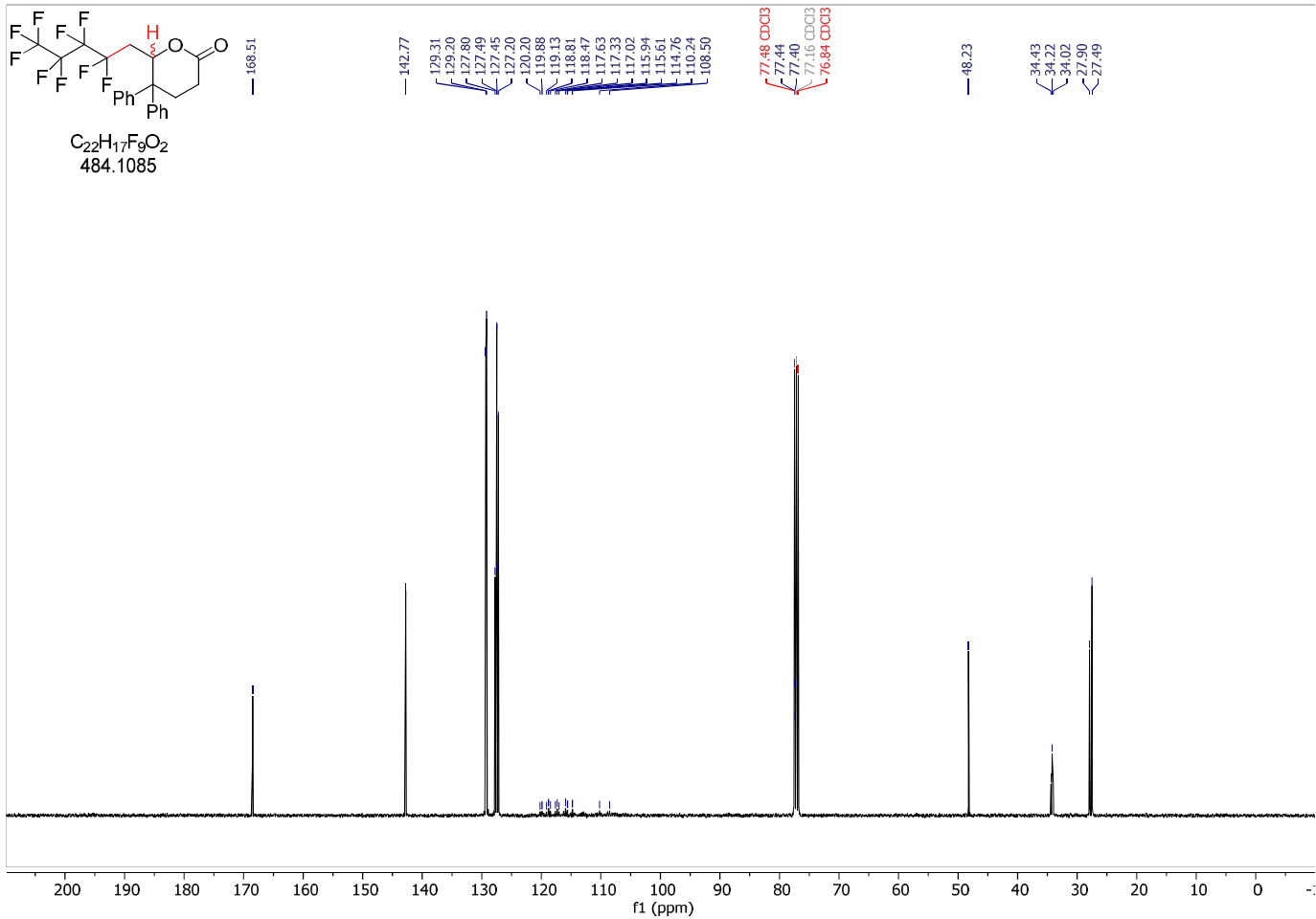
ethyl 2,2-difluoro-3-(6-oxo-3,3-diphenyltetrahydro-2H-pyran-2-yl)propanoate (3db)

 ^{19}F -NMR (282 MHz, CDCl_3)

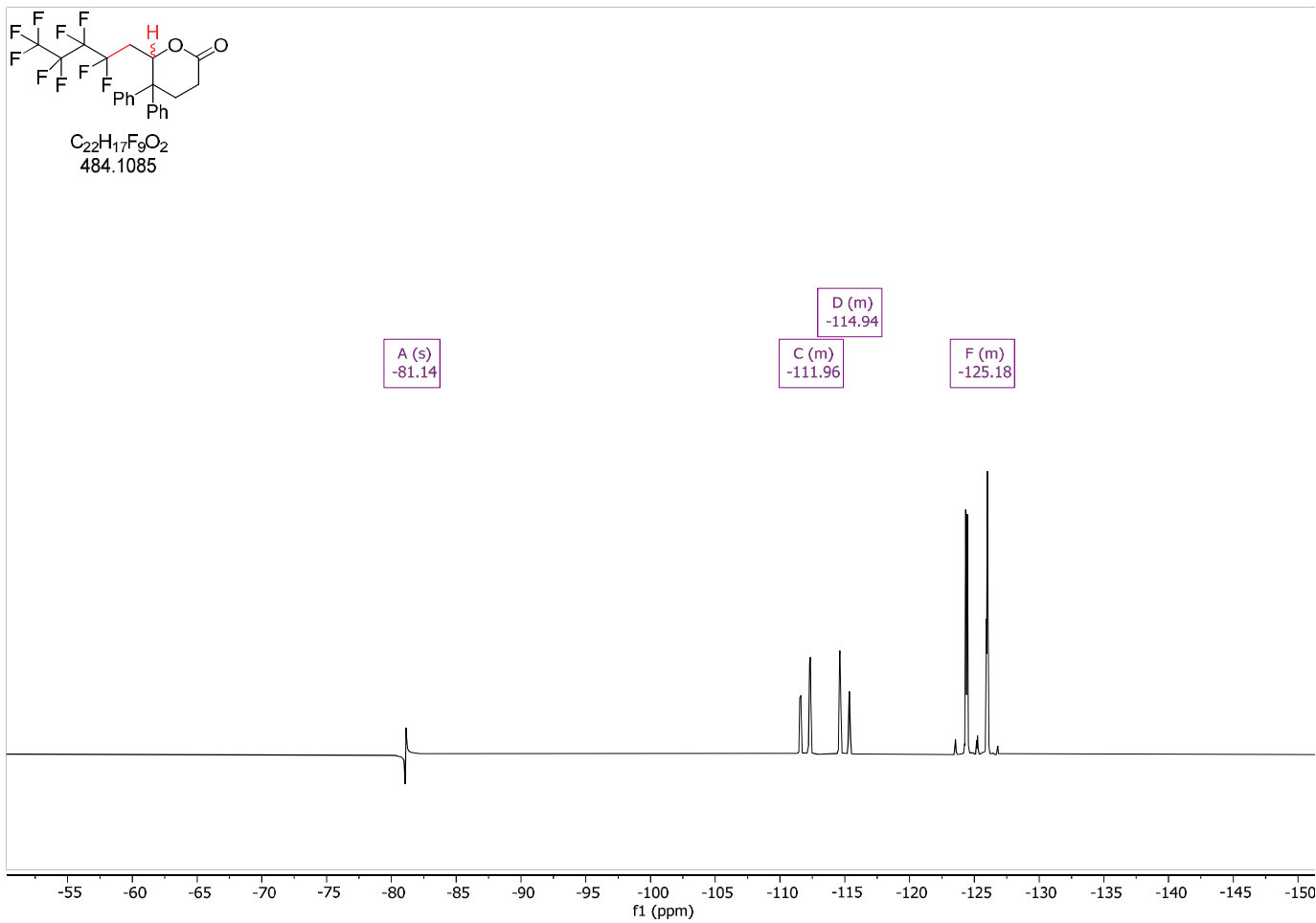
6-(2,2,3,3,4,4,5,5,5-nonafluoropentyl)-5,5-diphenyl-tetrahydropyran-2-one (2eb)

 ^1H -NMR (400 MHz, CDCl_3)

6-(2,2,3,3,4,4,5,5,5-nonafluoropentyl)-5,5-diphenyl-tetrahydropyran-2-one (2eb)

 ^{13}C -NMR (100 MHz, CDCl_3)

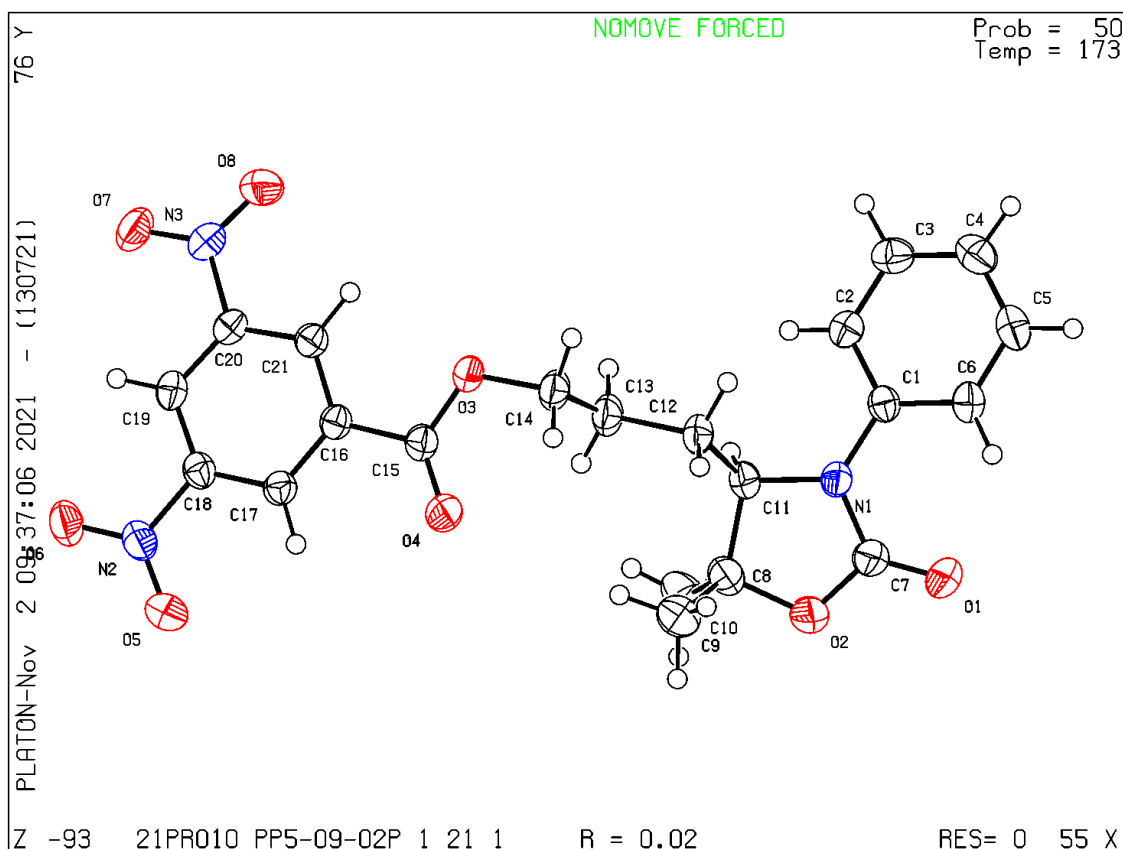
6-(2,2,3,3,4,4,5,5,5-nonafluoropentyl)-5,5-diphenyl-tetrahydropyran-2-one (2eb)

 ^{19}F -NMR (282 MHz, CDCl_3)

Department of Chemistry, Biochemistry
and Pharmaceutical Sciences
Universität Bern
Chemische Kristallographie
Freiestrasse 3, CH-3012 Bern, Switzerland

Dr. Lorraine Andrade Malaspina
Tel: +41 (0)31 684 4390
e-mail: lorraine.malaspina@unibe.ch

X-RAY CRYSTAL STRUCTURE REPORT



EXPERIMENTAL

Crystal-Structure Determination. A crystal of $C_{21}H_{21}N_3O_8$ immersed in parabar oil was mounted at ambient conditions and transferred into the stream of nitrogen (173 K). All measurements were made on a *RIGAKU Synergy S* area-detector diffractometer¹ using mirror optics monochromated Cu $K\alpha$ radiation ($\lambda = 1.54184 \text{ \AA}$). The unit cell constants and an orientation matrix for data collection were obtained from a least-squares refinement of the setting angles of reflections in the range $3.411^\circ < \theta < 79.547^\circ$. A total of 11112 frames were collected using ω scans, with 0.15 second exposure time (0.4 s for high-angle reflections), a rotation angle of 0.5° per frame, a crystal-detector distance of 34.0 mm, at $T = 173(2) \text{ K}$.

Data reduction was performed using the *CrysAlisPro*¹ program. The intensities were corrected for Lorentz and polarization effects, and an absorption correction based on the multi-scan method using SCALE3 ABSPACK in *CrysAlisPro*¹ was applied. Data collection and refinement parameters are given in *Table 1*.

The structure was solved by intrinsic phasing using *SHELXT*², which revealed the positions of all non-hydrogen atoms of the title compound. All non-hydrogen atoms were refined anisotropically. H-atoms were assigned in geometrically calculated positions and refined using a riding model where each H-atom was assigned a fixed isotropic displacement parameter with a value equal to 1.2U_{eq} of its parent atom (1.5U_{eq} for methyl groups).

Refinement of the structure was carried out on F^2 using full-matrix least-squares procedures, which minimized the function $\sum w(F_o^2 - F_c^2)^2$. The weighting scheme was based on counting statistics and included a factor to downweight the intense reflections. All calculations were performed using the *SHELXL-2014/7*³ program in OLEX2.⁴

Model has Chirality at C11 (R).

The X-ray crystal structure determination service unit of the Department of Chemistry, Biochemistry and Pharmaceutical Sciences of the University of Bern is acknowledged for measuring, solving, refining and summarizing the structures of compounds XX, YY, ZZ. The Synergy diffractometer was partially funded by the Swiss National Science Foundation (SNF) within the R'Equip programme (project number 206021_177033).



A single crystal of the compound mounted on a loop.

REFERENCES (In case this structure is submitted for publication, please use these references in the main text of a publication)

- 1) Oxford Diffraction (2018). *CrysAlisPro* (Version 1.171.40.37a). Oxford Diffraction Ltd., Yarnton, Oxfordshire, UK.
- 2) Sheldrick, G. M. (2015). *Acta Cryst.* **A71**, 3-8.
- 3) Sheldrick, G. M. (2015). *Acta Cryst.* **C71**, 3-8.
- 4) Dolomanov, O.V., Bourhis, L.J., Gildea, R.J, Howard, J.A.K. & Puschmann, H. (2009), *J. Appl. Cryst.* 42, 339-341.

Table 1 Crystal data and structure refinement for 21PR010_PP5-09-02.

Identification code	21PR010_PP5-09-02
Empirical formula	C ₂₁ H ₂₁ N ₃ O ₈
Formula weight	443.41
Temperature/K	173.1(6)
Crystal system	monoclinic
Space group	P2 ₁
a/Å	7.31172(6)
b/Å	12.98641(9)
c/Å	10.92635(8)
α/°	90
β/°	100.7537(7)
γ/°	90
Volume/Å ³	1019.270(13)
Z	2
ρ _{calc} /cm ³	1.445
μ/mm ⁻¹	0.952
F(000)	464.0
Crystal size/mm ³	0.373 × 0.245 × 0.087
Radiation	Cu Kα (λ = 1.54184)
2θ range for data collection/°	8.236 to 149.984
Index ranges	-9 ≤ h ≤ 9, -16 ≤ k ≤ 16, -13 ≤ l ≤ 13
Reflections collected	39493
Independent reflections	4190 [R _{int} = 0.0357, R _{sigma} = 0.0128]
Data/restraints/parameters	4190/1/374
Goodness-of-fit on F ²	1.049
Final R indexes [I ≥ 2σ (I)]	R ₁ = 0.0249, wR ₂ = 0.0647
Final R indexes [all data]	R ₁ = 0.0250, wR ₂ = 0.0650
Largest diff. peak/hole / e Å ⁻³	0.14/-0.11
Flack parameter	0.01(4)

Table 2 Fractional Atomic Coordinates (×10⁴) and Equivalent Isotropic Displacement Parameters (Å²×10³) for 21PR010_PP5-09-02. U_{eq} is defined as 1/3 of of the trace of the orthogonalised U_{ij} tensor.

Atom	x	y	z	U(eq)
O3	9562 (2)	5528.9 (10)	6522.9 (12)	39.9 (3)
O4	9346 (2)	4393.7 (10)	8045.2 (13)	42.8 (3)
O7	8125 (2)	9725.2 (11)	8885.6 (15)	48.3 (3)
O2	5517 (2)	960.4 (12)	4436.4 (14)	55.1 (4)
O6	8280 (2)	7386.6 (13)	12347.0 (13)	50.7 (4)
O8	8317 (3)	9111.2 (12)	7072.5 (14)	54.5 (4)
O1	5365 (2)	276.5 (11)	2552.9 (14)	52.4 (4)

Table 2 Fractional Atomic Coordinates ($\times 10^4$) and Equivalent Isotropic Displacement Parameters ($\text{\AA}^2 \times 10^3$) for 21PR010_PP5-09-02. U_{eq} is defined as 1/3 of of the trace of the orthogonalised U_{ij} tensor.

Atom	x	y	z	U(eq)
N1	6232 (2)	1983.0 (11)	2965.3 (13)	31.6 (3)
N2	8282 (2)	6641.8 (14)	11669.4 (14)	38.1 (3)
O5	8122 (3)	5753.7 (13)	11996.7 (14)	58.1 (4)
N3	8344 (2)	9014.6 (12)	8194.4 (15)	38.0 (3)
C19	8435 (2)	7832.0 (14)	9955.9 (17)	32.7 (3)
C15	9303 (2)	5260.1 (14)	7658.6 (16)	32.5 (3)
C1	6211 (2)	2344.0 (14)	1734.8 (15)	30.0 (3)
C16	8955 (2)	6174.3 (13)	8416.3 (16)	29.4 (3)
C20	8581 (2)	7972.3 (13)	8722.5 (16)	31.4 (3)
C21	8871 (2)	7169.1 (13)	7945.6 (16)	30.5 (3)
C18	8491 (2)	6829.8 (14)	10371.3 (16)	31.6 (4)
C6	6449 (2)	1669.1 (15)	777.6 (16)	34.6 (4)
C7	5682 (3)	1011.4 (15)	3235.0 (17)	39.9 (4)
C17	8722 (2)	5995.4 (13)	9632.0 (16)	31.0 (3)
C2	5962 (2)	3393.3 (14)	1465.0 (17)	34.2 (4)
C12	8141 (3)	3292.1 (14)	4316.2 (17)	34.6 (4)
C11	6321 (2)	2686.6 (14)	4025.8 (15)	32.0 (4)
C14	9818 (3)	4663.9 (15)	5713.0 (19)	41.5 (4)
C8	5926 (3)	1946.7 (16)	5071.2 (18)	41.6 (4)
C13	7946 (3)	4214.7 (14)	5155.0 (18)	39.3 (4)
C5	6399 (3)	2044.8 (17)	-415.4 (18)	41.8 (4)
C3	5915 (3)	3749.0 (16)	260.1 (19)	41.3 (4)
C4	6121 (3)	3081.1 (18)	-685.9 (19)	43.8 (4)
C9	7540 (4)	1746 (2)	6133 (2)	54.2 (5)
C10	4209 (4)	2265 (3)	5559 (2)	61.8 (7)

Table 3 Anisotropic Displacement Parameters ($\text{\AA}^2 \times 10^3$) for 21PR010_PP5-09-02. The Anisotropic displacement factor exponent takes the form: - $2\pi^2[h^2a^{*2}U_{11}+2hka^*b^*U_{12}+\dots]$.

Atom	U_{11}	U_{22}	U_{33}	U_{23}	U_{13}	U_{12}
O3	58.2 (8)	30.2 (6)	34.3 (6)	-8.3 (5)	15.8 (6)	-9.8 (6)
O4	59.7 (8)	29.9 (6)	38.3 (7)	0.0 (5)	7.3 (6)	8.3 (6)
O7	59.1 (8)	29.1 (6)	55.6 (9)	-9.6 (6)	8.2 (7)	-0.8 (6)
O2	81.7 (11)	46.9 (8)	38.5 (8)	-1.6 (6)	15.7 (7)	-24.4 (8)
O6	63.6 (9)	55.1 (9)	36.6 (7)	-13.7 (7)	17.7 (6)	-10.8 (7)
O8	82.8 (11)	37.9 (7)	45.7 (8)	8.3 (6)	20.0 (7)	5.9 (7)
O1	74.1 (10)	35.3 (7)	45.3 (8)	-6.2 (6)	4.4 (7)	-15.8 (7)
N1	35.8 (7)	28.8 (7)	28.8 (7)	-3.5 (6)	3.0 (6)	-1.0 (6)
N2	38.3 (7)	46.0 (9)	30.7 (7)	-4.3 (7)	7.9 (6)	-4.6 (7)
O5	88.9 (12)	48.8 (9)	39.9 (8)	5.1 (7)	20.5 (8)	-6.8 (8)

Table 3 Anisotropic Displacement Parameters ($\text{\AA}^2 \times 10^3$) for 21PR010_PP5-09-02. The Anisotropic displacement factor exponent takes the form: - $2\pi^2[h^2a^{*2}U_{11}+2hka^*b^*U_{12}+\dots]$.

Atom	U_{11}	U_{22}	U_{33}	U_{23}	U_{13}	U_{12}
N3	39.8 (8)	29.2 (7)	44.7 (8)	-1.4 (6)	7.2 (6)	-1.8 (6)
C19	29.6 (8)	33.5 (9)	34.6 (8)	-8.6 (7)	5.0 (6)	-3.0 (7)
C15	33.3 (8)	31.3 (8)	31.7 (8)	-3.6 (7)	3.1 (6)	-0.7 (7)
C1	26.9 (7)	34.4 (8)	28.1 (7)	-3.2 (7)	3.3 (6)	-0.6 (6)
C16	27.7 (7)	29.6 (8)	29.7 (8)	-2.8 (6)	2.6 (6)	-1.9 (6)
C20	29.7 (8)	27.1 (8)	36.8 (9)	-2.2 (7)	4.3 (6)	-2.0 (6)
C21	30.2 (8)	30.7 (8)	30.3 (8)	-1.3 (6)	4.6 (6)	-3.1 (6)
C18	29.0 (7)	37.3 (9)	28.1 (8)	-3.2 (7)	4.1 (6)	-2.7 (6)
C6	31.9 (8)	37.2 (10)	33.4 (9)	-7.2 (7)	2.5 (6)	1.8 (7)
C7	46.1 (10)	36.8 (10)	35.1 (9)	0.0 (8)	3.2 (7)	-7.6 (8)
C17	31.3 (8)	30.0 (9)	30.3 (8)	-0.6 (7)	2.3 (6)	-1.9 (6)
C2	34.4 (8)	31.5 (8)	36.7 (9)	-3.0 (7)	7.0 (7)	0.0 (7)
C12	37.4 (9)	34.6 (9)	32.7 (8)	-10.1 (7)	8.6 (7)	-1.3 (7)
C11	34.5 (8)	34.2 (9)	27.9 (8)	-5.0 (6)	7.2 (6)	2.1 (7)
C14	53.5 (11)	35.3 (10)	39.7 (10)	-14.0 (8)	19.3 (9)	-10.7 (8)
C8	46.8 (10)	46.6 (11)	31.5 (9)	-1.7 (8)	7.8 (8)	-6.8 (8)
C13	48.3 (10)	33.7 (9)	35.1 (9)	-10.5 (7)	5.9 (8)	3.9 (8)
C5	39.1 (9)	54.6 (12)	32.4 (9)	-9.5 (8)	8.0 (7)	-1.9 (8)
C3	39.0 (9)	40.1 (10)	44.6 (10)	6.6 (8)	7.4 (8)	-4.3 (8)
C4	40.8 (10)	57.3 (12)	33.8 (9)	3.7 (8)	7.9 (7)	-6.0 (9)
C9	66.0 (14)	52.0 (13)	40.7 (11)	5.7 (10)	-0.2 (10)	0.9 (11)
C10	55.4 (13)	92 (2)	43.7 (12)	1.7 (13)	23.6 (10)	-6.0 (13)

Table 4 Bond Lengths for 21PR010_PP5-09-02.

Atom	Atom	Length/ \AA	Atom	Atom	Length/ \AA
O3	C15	1.336 (2)	C15	C16	1.496 (2)
O3	C14	1.464 (2)	C1	C6	1.400 (2)
O4	C15	1.200 (2)	C1	C2	1.399 (3)
O7	N3	1.222 (2)	C16	C21	1.388 (2)
O2	C7	1.342 (2)	C16	C17	1.390 (2)
O2	C8	1.461 (2)	C20	C21	1.386 (2)
O6	N2	1.218 (2)	C18	C17	1.381 (2)
O8	N3	1.229 (2)	C6	C5	1.386 (3)
O1	C7	1.206 (2)	C2	C3	1.389 (3)
N1	C1	1.421 (2)	C12	C11	1.527 (2)
N1	C7	1.373 (2)	C12	C13	1.531 (2)
N1	C11	1.468 (2)	C11	C8	1.560 (3)
N2	O5	1.220 (2)	C14	C13	1.508 (3)
N2	C18	1.475 (2)	C8	C9	1.515 (3)
N3	C20	1.469 (2)	C8	C10	1.511 (3)

Table 4 Bond Lengths for 21PR010_PP5-09-02.

Atom	Atom	Length/Å	Atom	Atom	Length/Å
C19	C20	1.384 (2)	C5	C4	1.385 (3)
C19	C18	1.376 (3)	C3	C4	1.379 (3)

Table 5 Bond Angles for 21PR010_PP5-09-02.

Atom	Atom	Atom	Angle/°	Atom	Atom	Atom	Angle/°
C15	O3	C14	114.67 (15)	C19	C18	N2	118.13 (15)
C7	O2	C8	111.93 (15)	C19	C18	C17	123.27 (16)
C1	N1	C11	122.18 (14)	C17	C18	N2	118.59 (16)
C7	N1	C1	123.66 (14)	C5	C6	C1	119.81 (18)
C7	N1	C11	111.99 (14)	O2	C7	N1	109.79 (16)
O6	N2	O5	124.16 (16)	O1	C7	O2	121.56 (18)
O6	N2	C18	117.72 (17)	O1	C7	N1	128.65 (17)
O5	N2	C18	118.12 (15)	C18	C17	C16	118.56 (16)
O7	N3	O8	124.04 (17)	C3	C2	C1	120.18 (17)
O7	N3	C20	118.20 (15)	C11	C12	C13	110.65 (14)
O8	N3	C20	117.70 (15)	N1	C11	C12	113.16 (13)
C18	C19	C20	116.27 (16)	N1	C11	C8	101.98 (14)
O3	C15	C16	112.01 (15)	C12	C11	C8	115.99 (15)
O4	C15	O3	124.96 (17)	O3	C14	C13	109.42 (16)
O4	C15	C16	123.03 (16)	O2	C8	C11	103.99 (14)
C6	C1	N1	121.28 (16)	O2	C8	C9	105.89 (18)
C2	C1	N1	119.91 (15)	O2	C8	C10	107.33 (19)
C2	C1	C6	118.80 (16)	C9	C8	C11	116.25 (18)
C21	C16	C15	122.27 (15)	C10	C8	C11	111.67 (19)
C21	C16	C17	120.34 (15)	C10	C8	C9	110.9 (2)
C17	C16	C15	117.39 (15)	C14	C13	C12	111.47 (16)
C19	C20	N3	118.63 (15)	C4	C5	C6	121.33 (18)
C19	C20	C21	123.09 (16)	C4	C3	C2	120.94 (19)
C21	C20	N3	118.24 (15)	C3	C4	C5	118.91 (18)
C20	C21	C16	118.35 (15)				

Table 6 Hydrogen Bonds for 21PR010_PP5-09-02.

D	H	A	d(D-H)/Å	d(H-A)/Å	d(D-A)/Å	D-H-A/°
C17H17	O7 ¹		0.94 (2)	2.53 (2)	3.044 (2)	114.6 (14)
C6 H6	O1		0.97 (3)	2.27 (2)	2.870 (3)	119.0 (17)
C19H19	O4 ²		0.94 (2)	2.50 (2)	3.193 (2)	130.3 (16)

¹2-X,-1/2+Y,2-Z; ²2-X,1/2+Y,2-Z

Table 7 Torsion Angles for 21PR010_PP5-09-02.

A	B	C	D	Angle/°	A	B	C	D	Angle/°
O3	C15	C16	C21	1.6(2)	C20	C19	C18	N2	178.16(14)
O3	C15	C16	C17	178.07(14)	C20	C19	C18	C17	1.4(2)
O3	C14	C13	C12	178.96(15)	C21	C16	C17	C18	-2.9(2)
O4	C15	C16	C21	178.60(18)	C18	C19	C20	N3	174.03(15)
O4	C15	C16	C17	1.7(2)	C18	C19	C20	C21	-3.5(2)
O7	N3	C20	C19	3.8(2)	C6	C1	C2	C3	1.3(2)
O7	N3	C20	C21	178.58(16)	C6	C5	C4	C3	0.8(3)
O6	N2	C18	C19	-8.1(2)	C7	O2	C8	C11	2.3(2)
O6	N2	C18	C17	172.32(17)	C7	O2	C8	C9	-120.7(2)
O8	N3	C20	C19	173.78(17)	C7	O2	C8	C10	120.7(2)
O8	N3	C20	C21	3.8(2)	C7	N1	C1	C6	-29.3(2)
N1	C1	C6	C5	179.25(16)	C7	N1	C1	C2	151.22(17)
N1	C1	C2	C3	179.13(16)	C7	N1	C11	C12	131.08(17)
N1	C11	C8	O2	-4.62(18)	C7	N1	C11	C8	5.77(19)
N1	C11	C8	C9	111.33(19)	C17	C16	C21	C20	1.0(2)
N1	C11	C8	C10	120.04(19)	C2	C1	C6	C5	-1.2(2)
N2	C18	C17	C16	178.76(14)	C2	C3	C4	C5	-0.7(3)
O5	N2	C18	C19	171.90(18)	C12	C11	C8	O2	128.05(16)
O5	N2	C18	C17	-7.7(2)	C12	C11	C8	C9	-12.1(3)
N3	C20	C21	C16	175.21(15)	C12	C11	C8	C10	116.5(2)
C19	C20	C21	C16	2.3(2)	C11	N1	C1	C6	168.84(15)
C19	C18	C17	C16	1.6(2)	C11	N1	C1	C2	-10.7(2)
C15	O3	C14	C13	80.7(2)	C11	N1	C7	O2	-4.7(2)
C15	C16	C21	C20	178.67(15)	C11	N1	C7	O1	175.2(2)
C15	C16	C17	C18	176.82(15)	C11	C12	C13	C14	165.77(17)
C1	N1	C7	O2	168.24(16)	C14	O3	C15	O4	3.1(3)
C1	N1	C7	O1	11.7(3)	C14	O3	C15	C16	177.12(15)
C1	N1	C11	C12	-65.1(2)	C8	O2	C7	O1	-178.6(2)
C1	N1	C11	C8	169.57(14)	C8	O2	C7	N1	1.3(2)
C1	C6	C5	C4	0.2(3)	C13	C12	C11	N1	163.69(15)
C1	C2	C3	C4	-0.4(3)	C13	C12	C11	C8	-78.9(2)

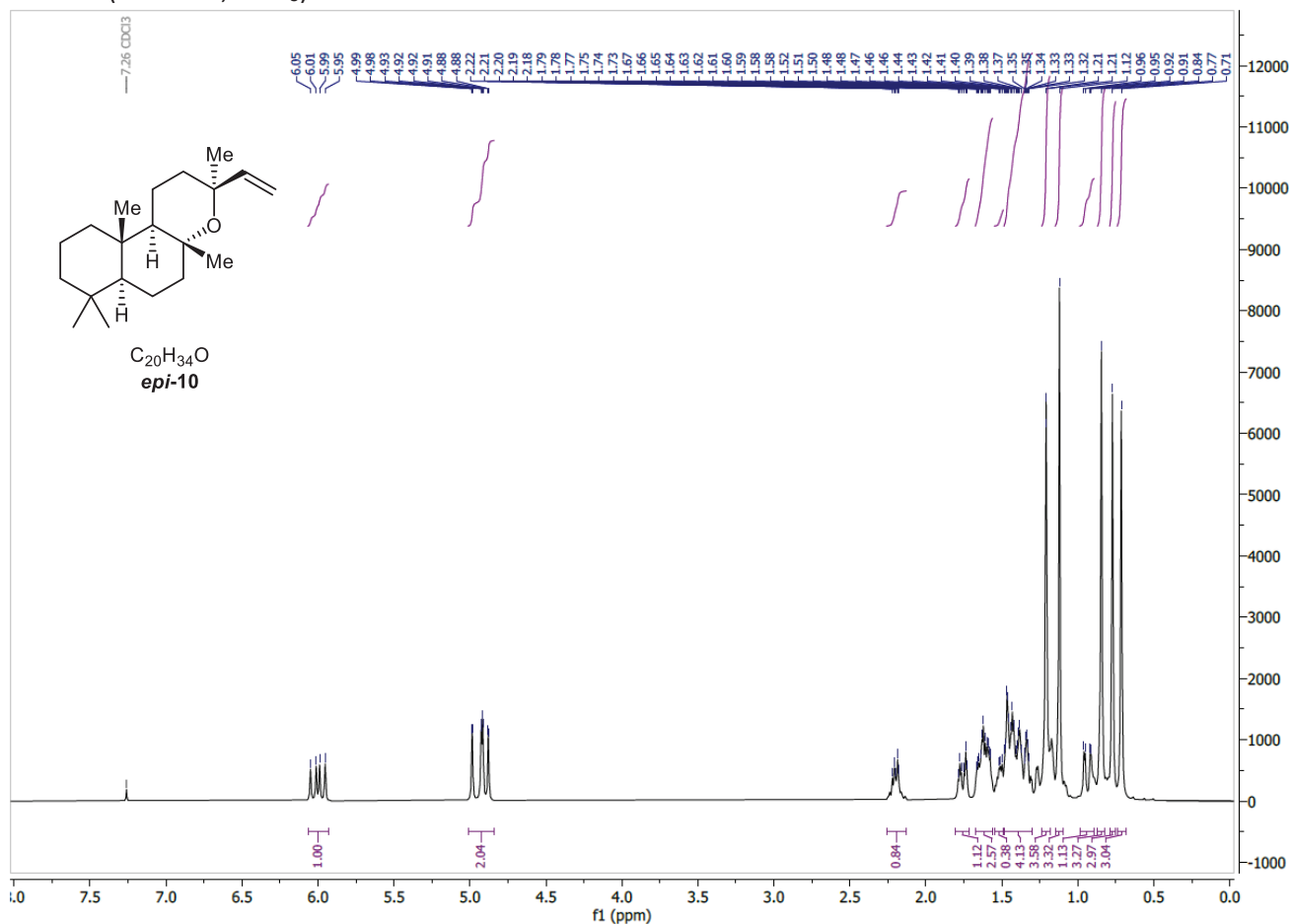
Table 8 Hydrogen Atom Coordinates ($\text{\AA}\times 10^4$) and Isotropic Displacement Parameters ($\text{\AA}^2\times 10^3$) for 21PR010_PP5-09-02.

Atom	x	y	z	U(eq)
H12A	9180 (30)	2849 (19)	4690 (20)	38 (5)
H10A	4400 (40)	2940 (20)	5940 (30)	54 (7)
H12B	8490 (30)	3529 (19)	3540 (20)	36 (5)
H17	8730 (30)	5325 (17)	9959 (18)	28 (5)
H6	6660 (30)	950 (20)	1000 (20)	43 (6)
H10B	3110 (50)	2360 (30)	4830 (30)	76 (9)
H11	5290 (30)	3187 (16)	3840 (19)	32 (5)
H9A	8600 (40)	1500 (20)	5830 (30)	59 (7)
H13A	7340 (30)	4024 (19)	5840 (20)	41 (6)
H3	5730 (30)	4500 (20)	100 (20)	44 (6)
H2	5780 (30)	3854 (19)	2110 (20)	40 (6)
H9B	7800 (40)	2390 (20)	6640 (30)	58 (7)
H13B	7170 (40)	4750 (20)	4650 (30)	57 (7)
H14A	10650 (30)	4120 (20)	6240 (20)	42 (6)
H9C	7160 (40)	1190 (20)	6680 (30)	70 (8)
H14B	10410 (40)	4970 (20)	5100 (30)	55 (7)
H21	8980 (30)	7321 (18)	7080 (20)	37 (5)
H19	8290 (30)	8398 (19)	10460 (20)	36 (5)
H4	6060 (40)	3290 (20)	-1520 (20)	54 (7)
H5	6570 (40)	1550 (20)	-1070 (30)	55 (7)
H10C	3940 (40)	1760 (30)	6160 (30)	72 (9)

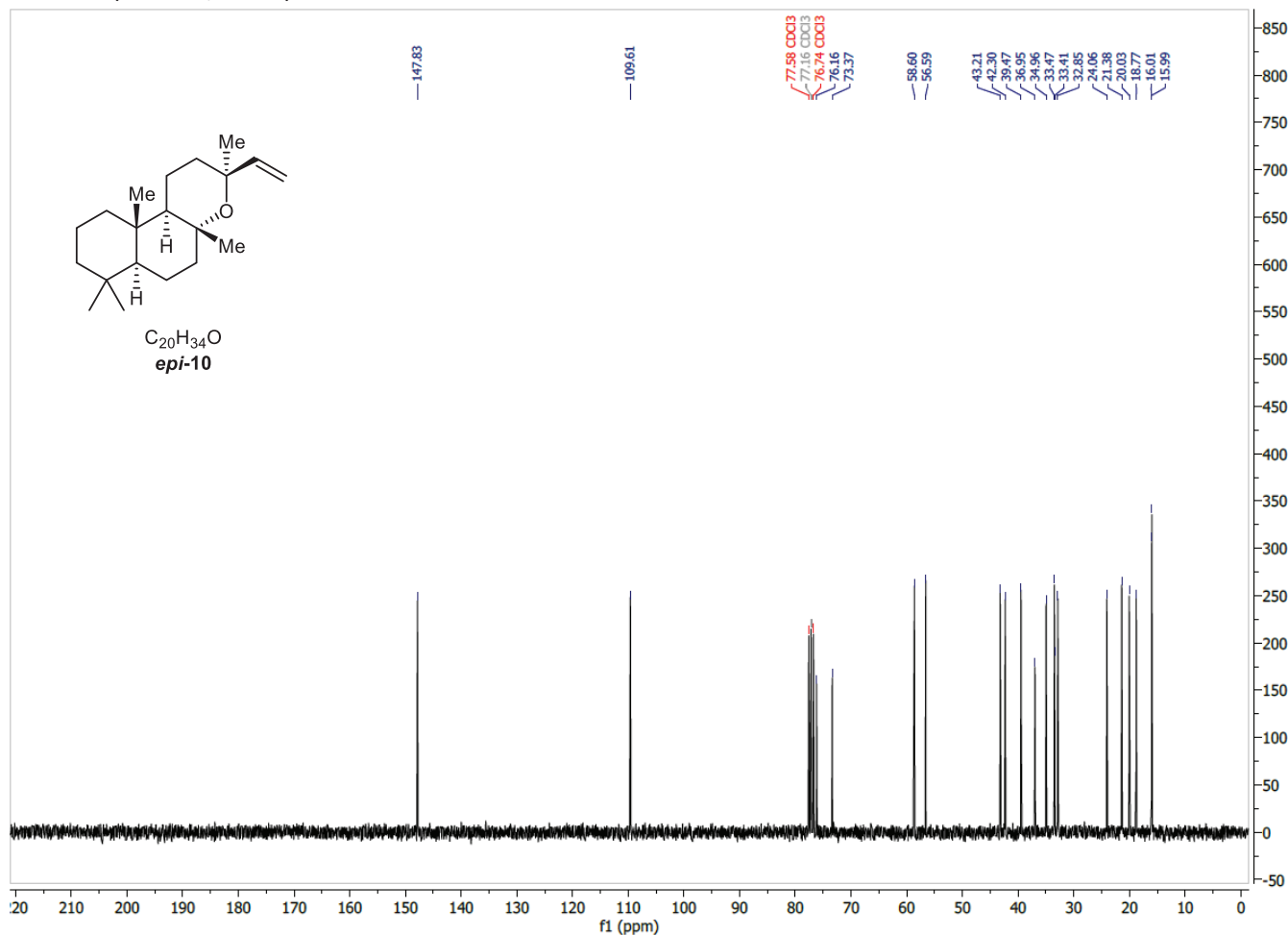
7.2 NMR and X-ray Chapter 5

Forskolin Editing via Radical Iodo- and Hydroalkylation

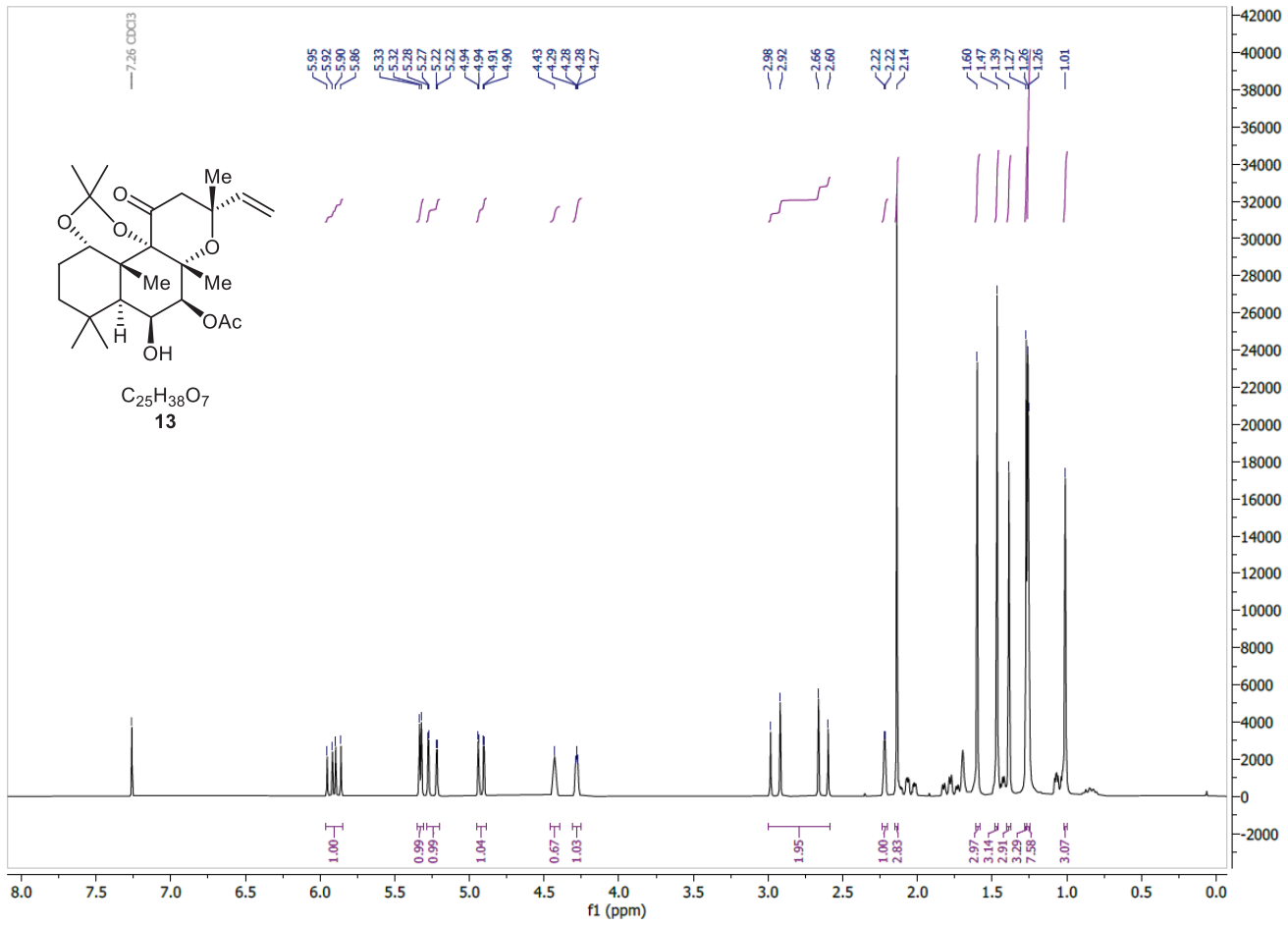
¹H NMR (300 MHz, CDCl₃)



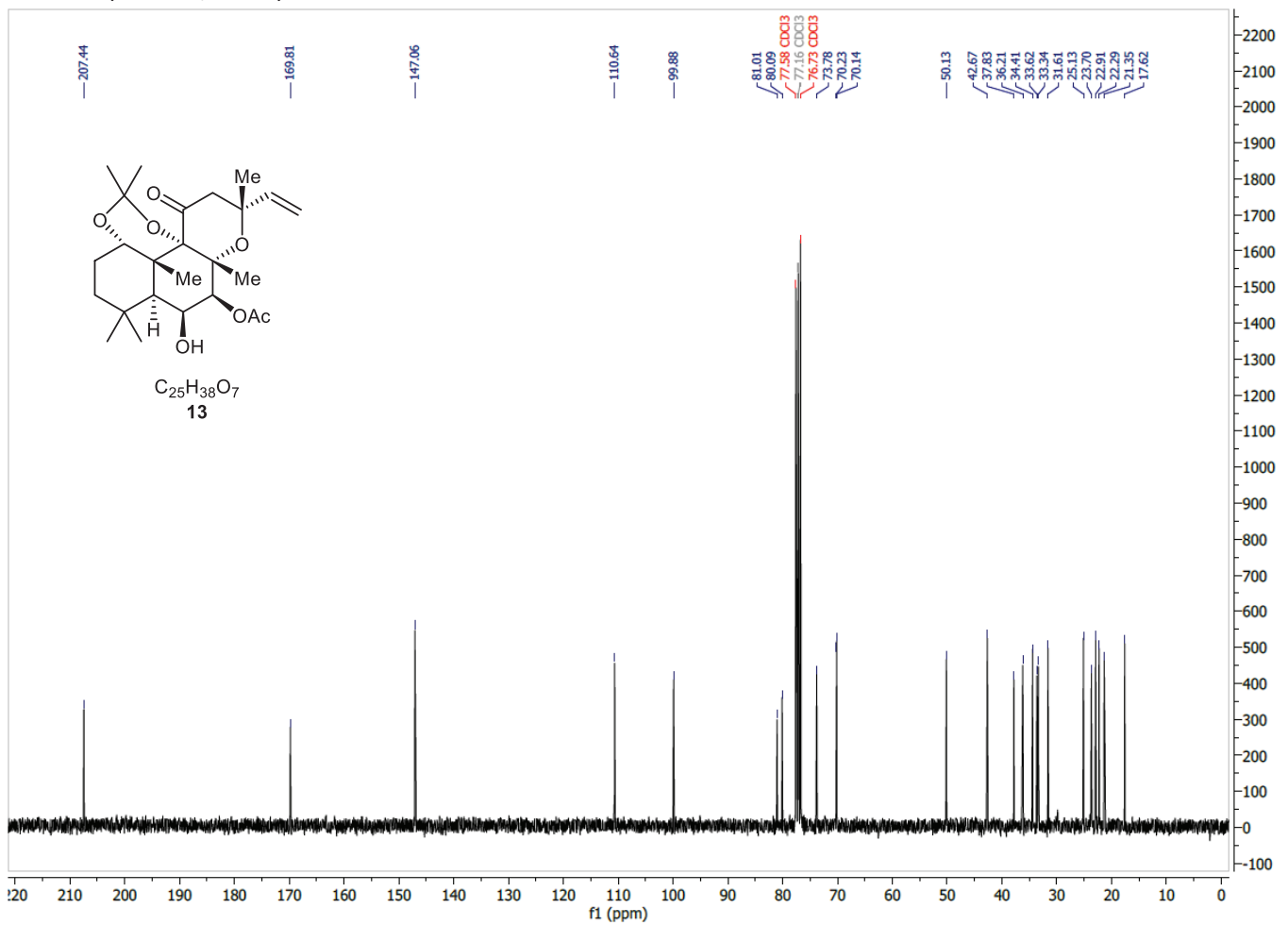
¹³C NMR (75 MHz, CDCl₃)



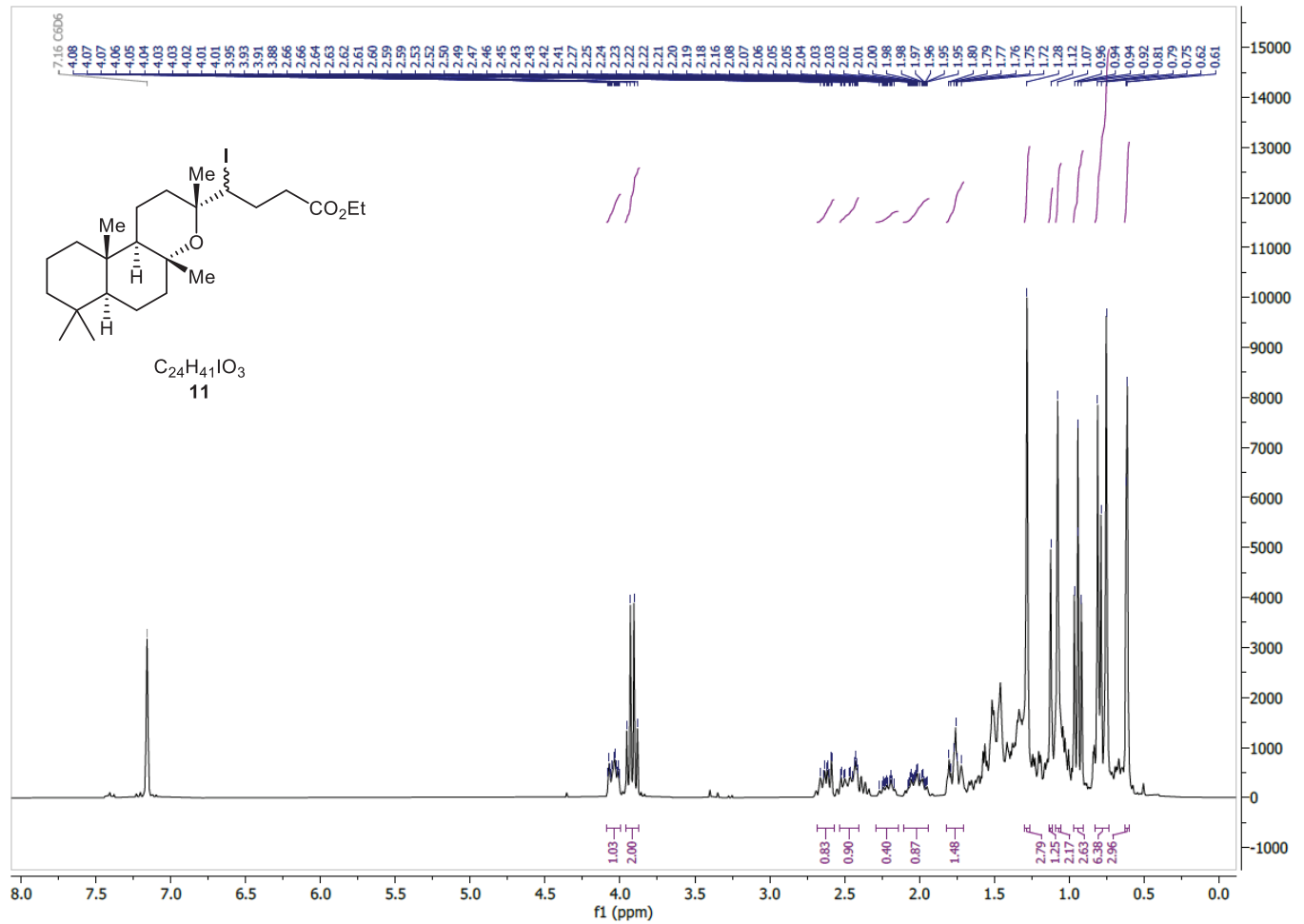
^1H NMR (300 MHz, CDCl_3)



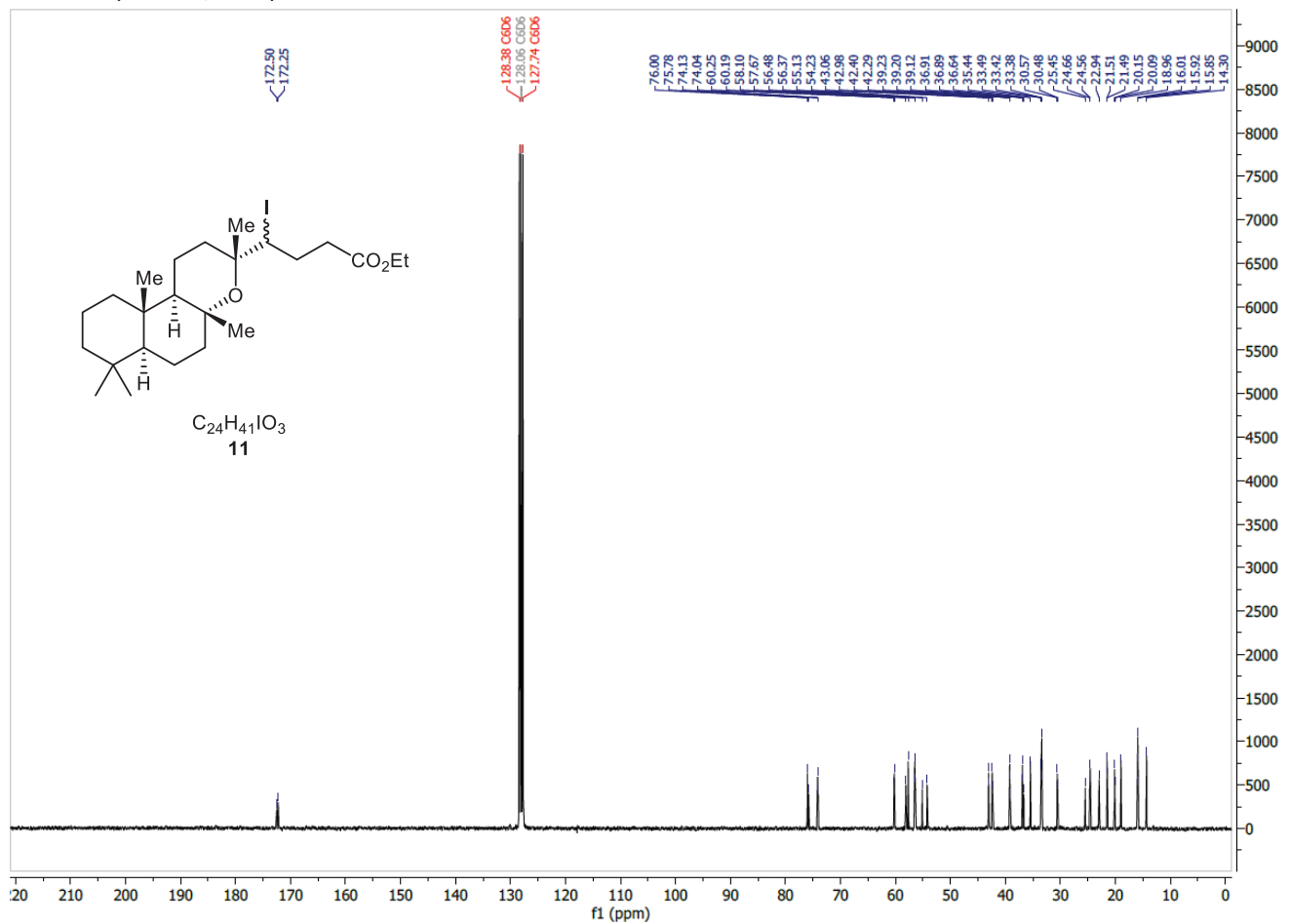
^{13}C NMR (75 MHz, CDCl_3)



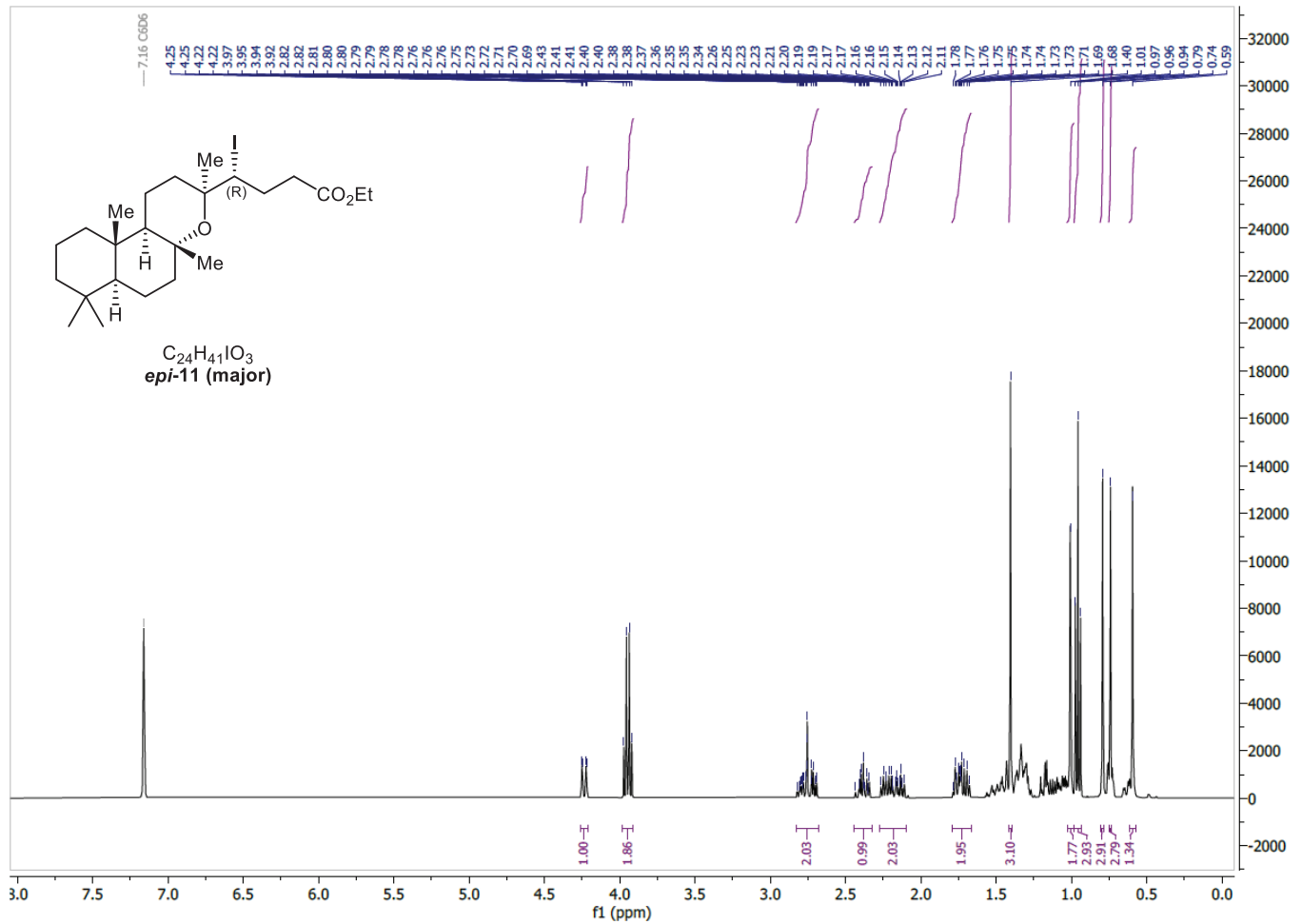
^1H NMR (300 MHz, C_6D_6)



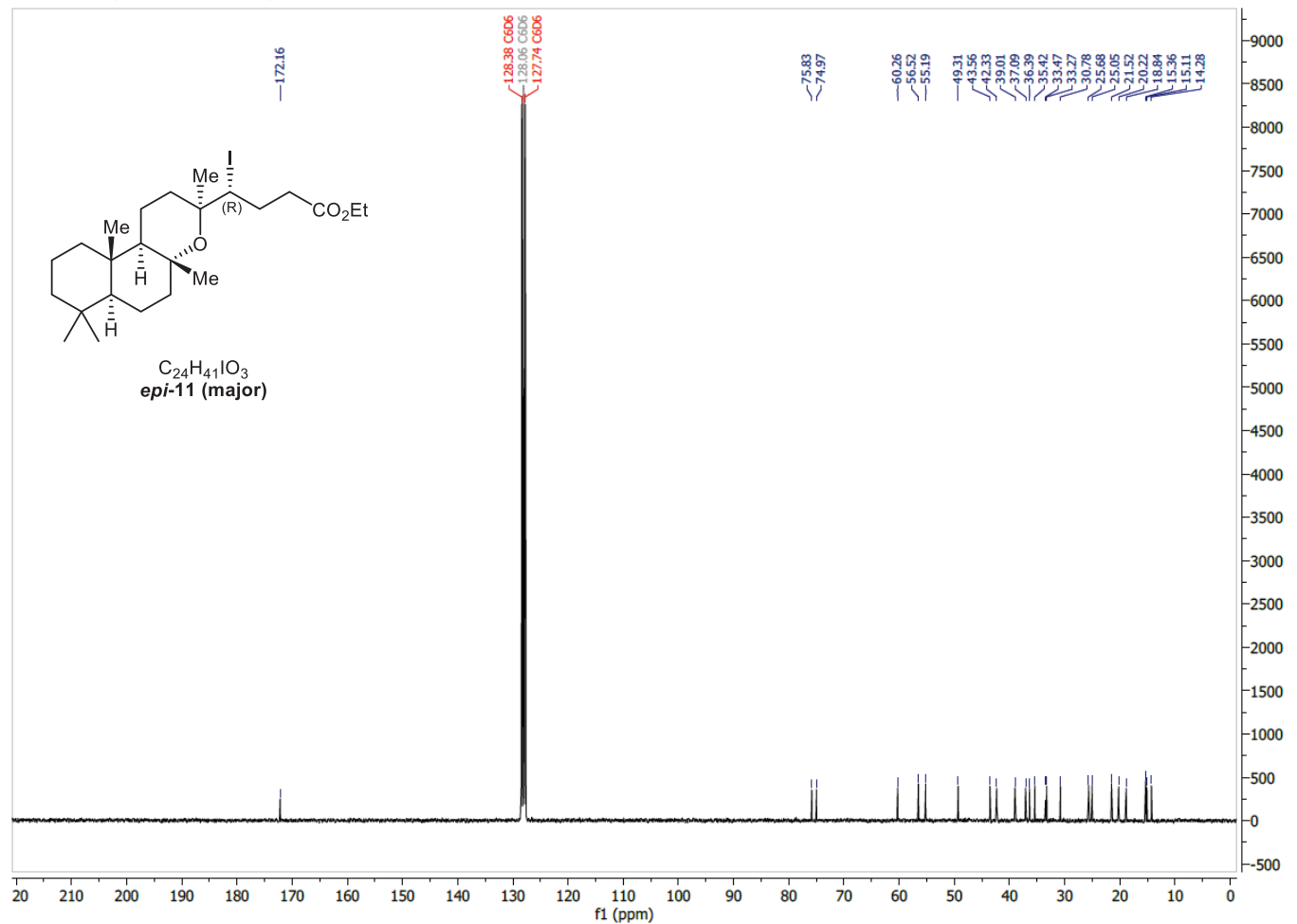
^{13}C NMR (75MHz, C_6D_6)



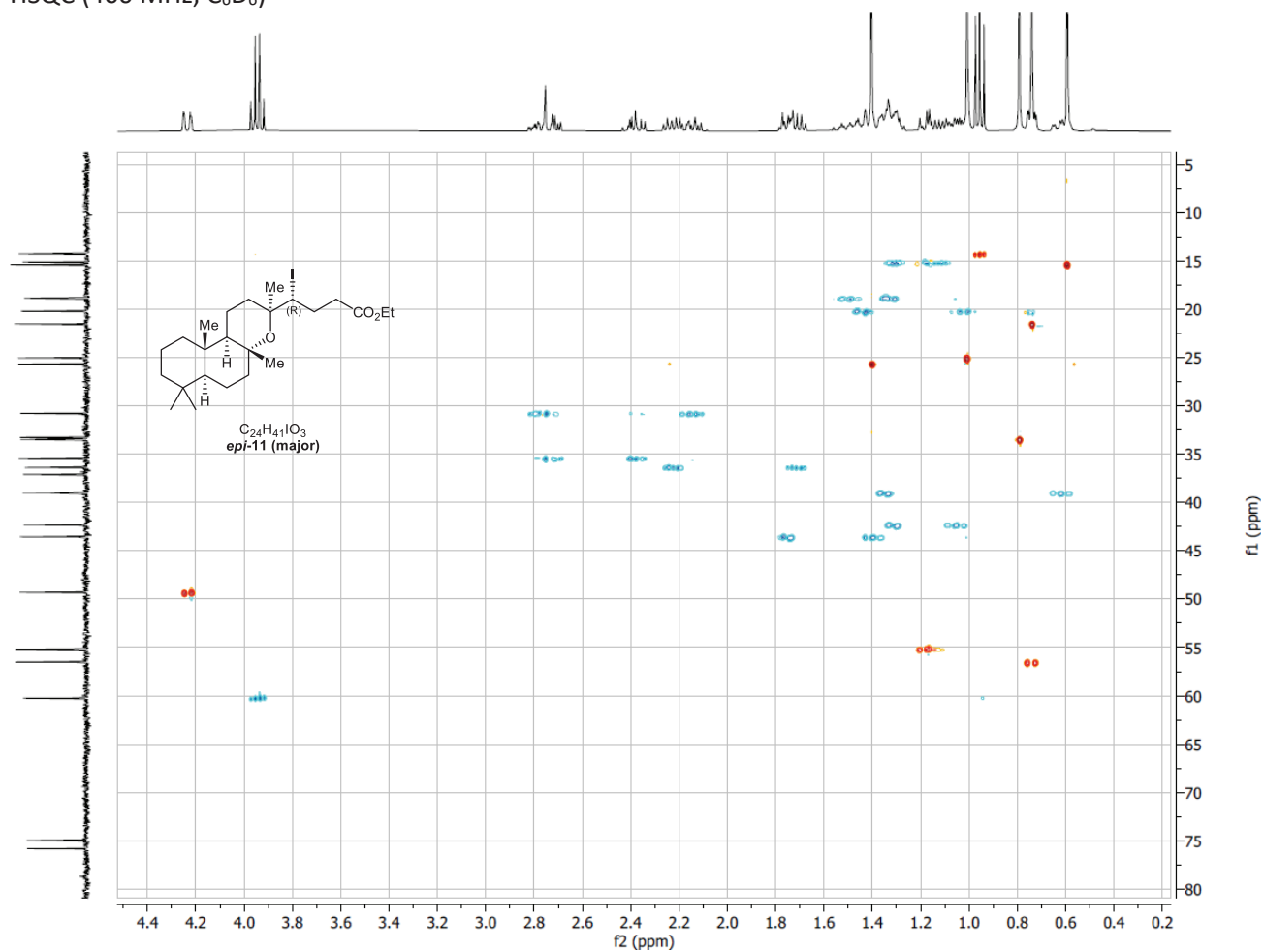
^1H NMR (300 MHz, C_6D_6)



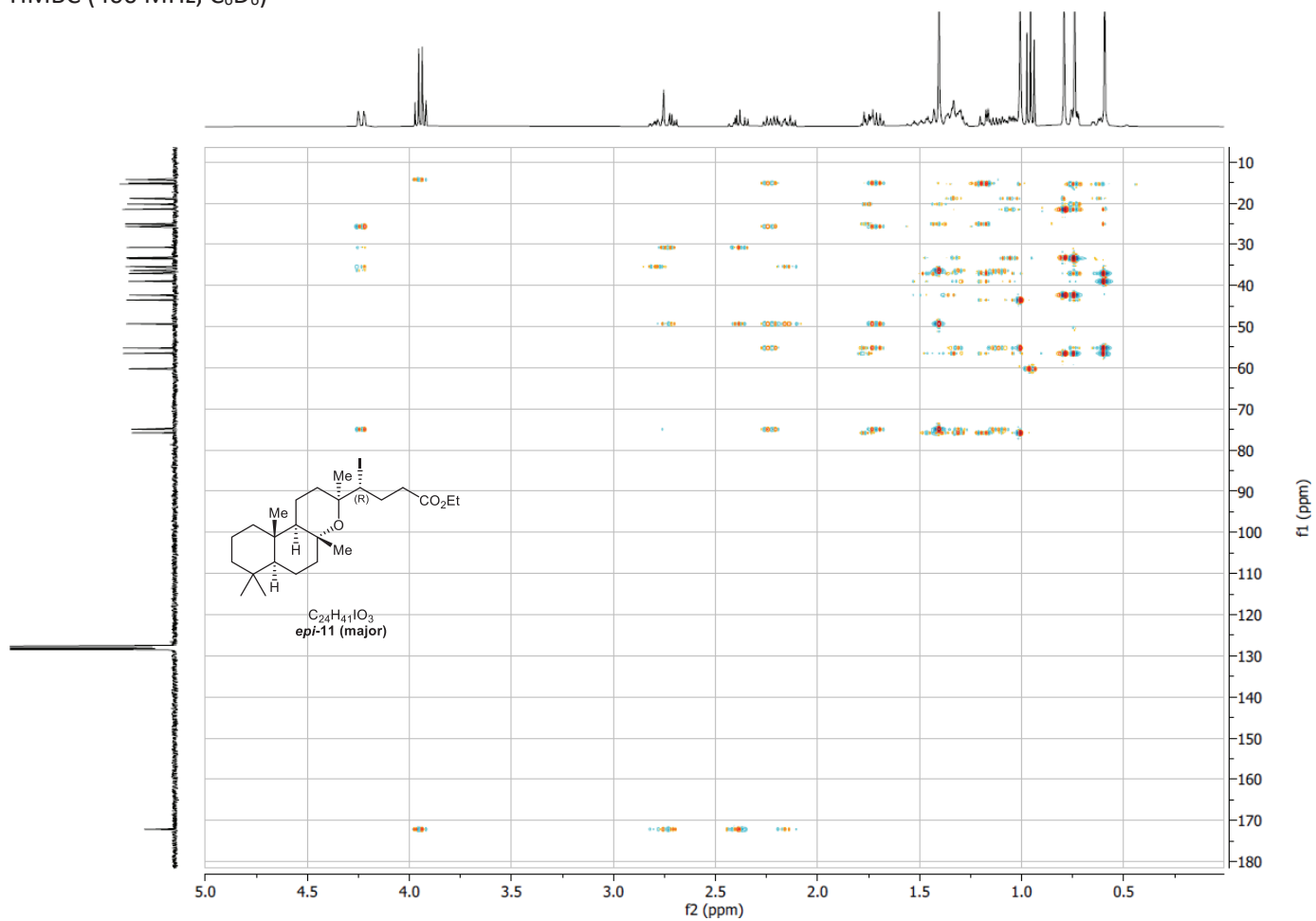
^{13}C NMR (75 MHz, C_6D_6)



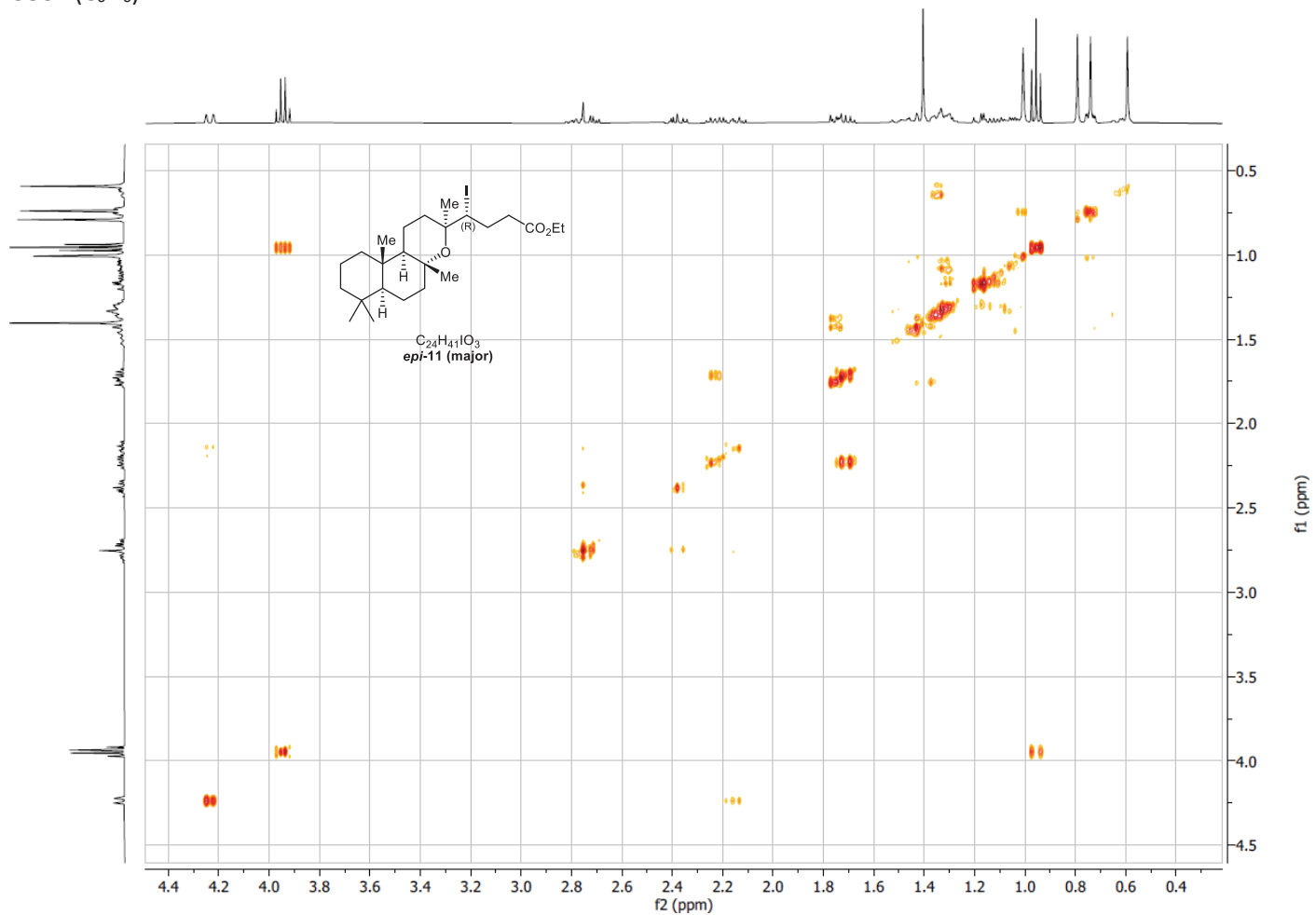
HSQC (400 MHz, C₆D₆)



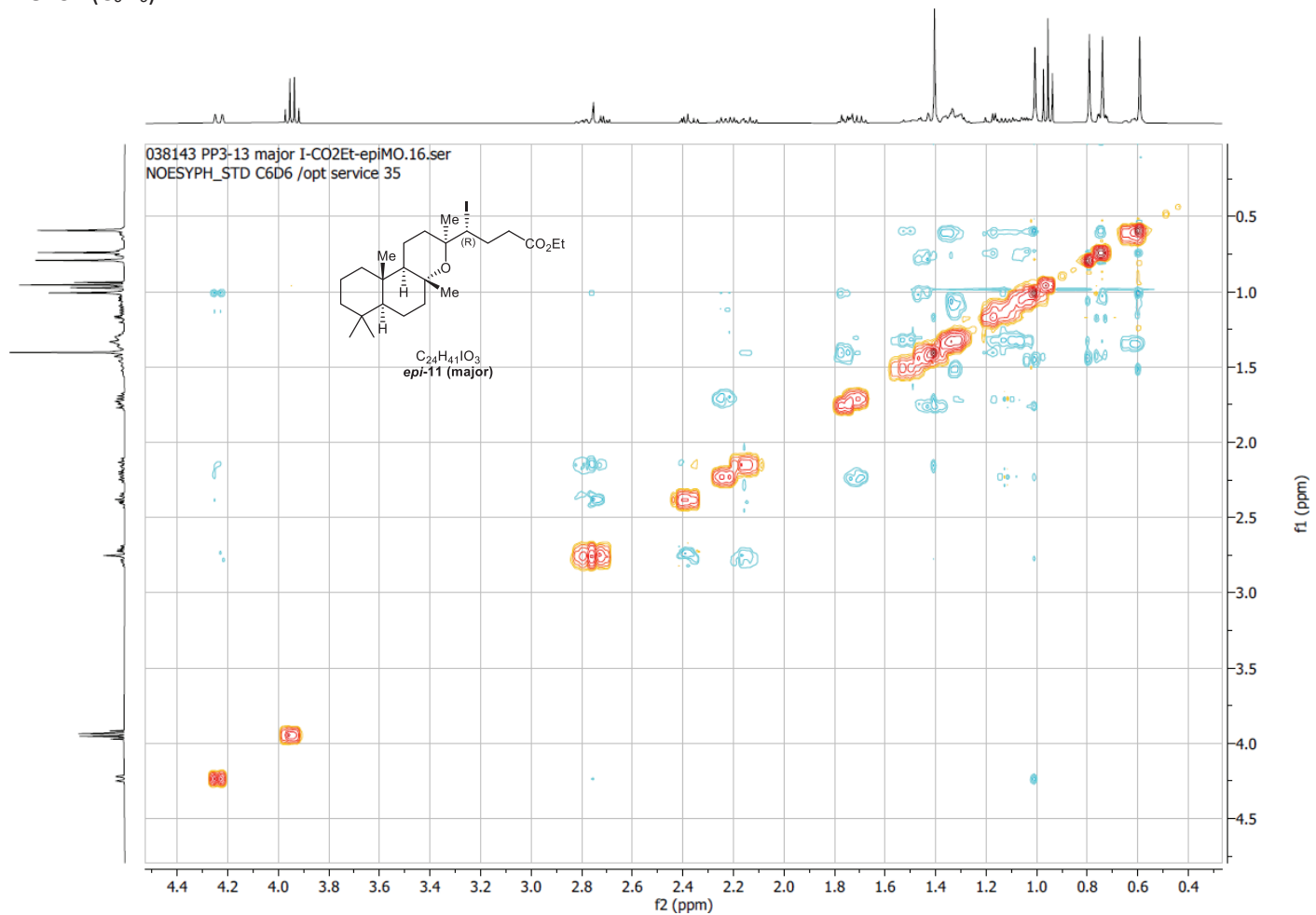
HMBC (400 MHz, C₆D₆)



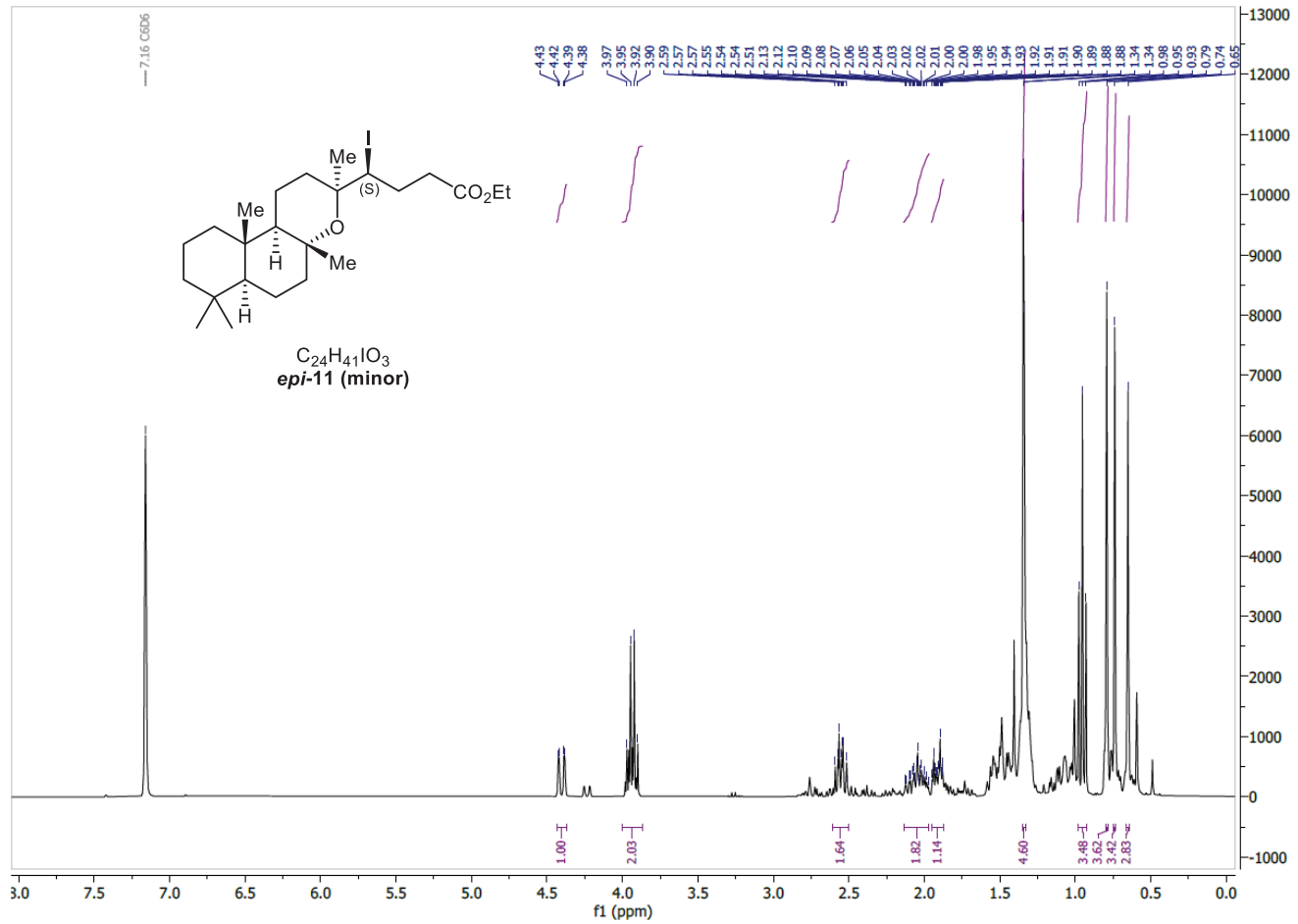
COSY (C₆D₆)



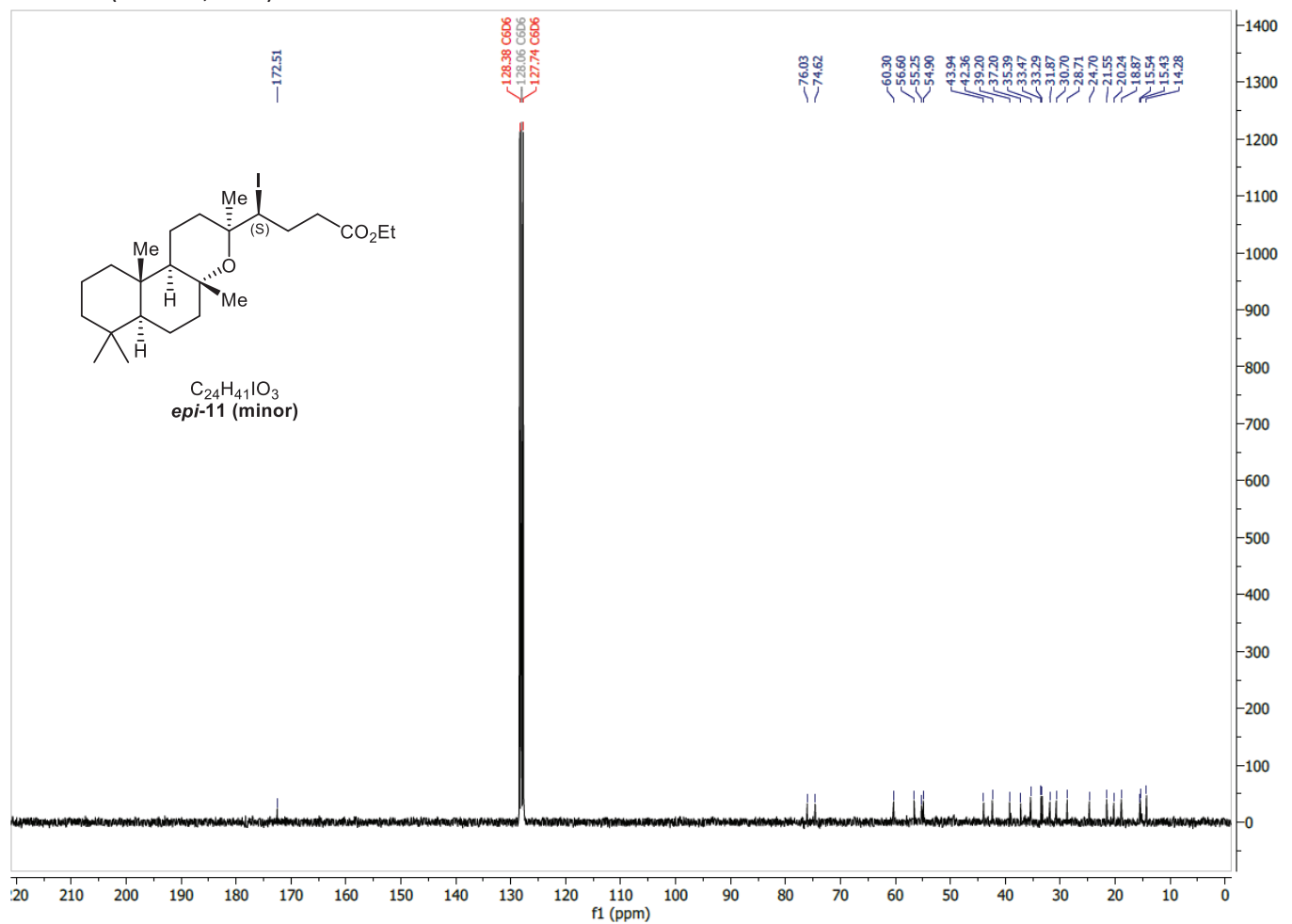
NOESY (C₆D₆)



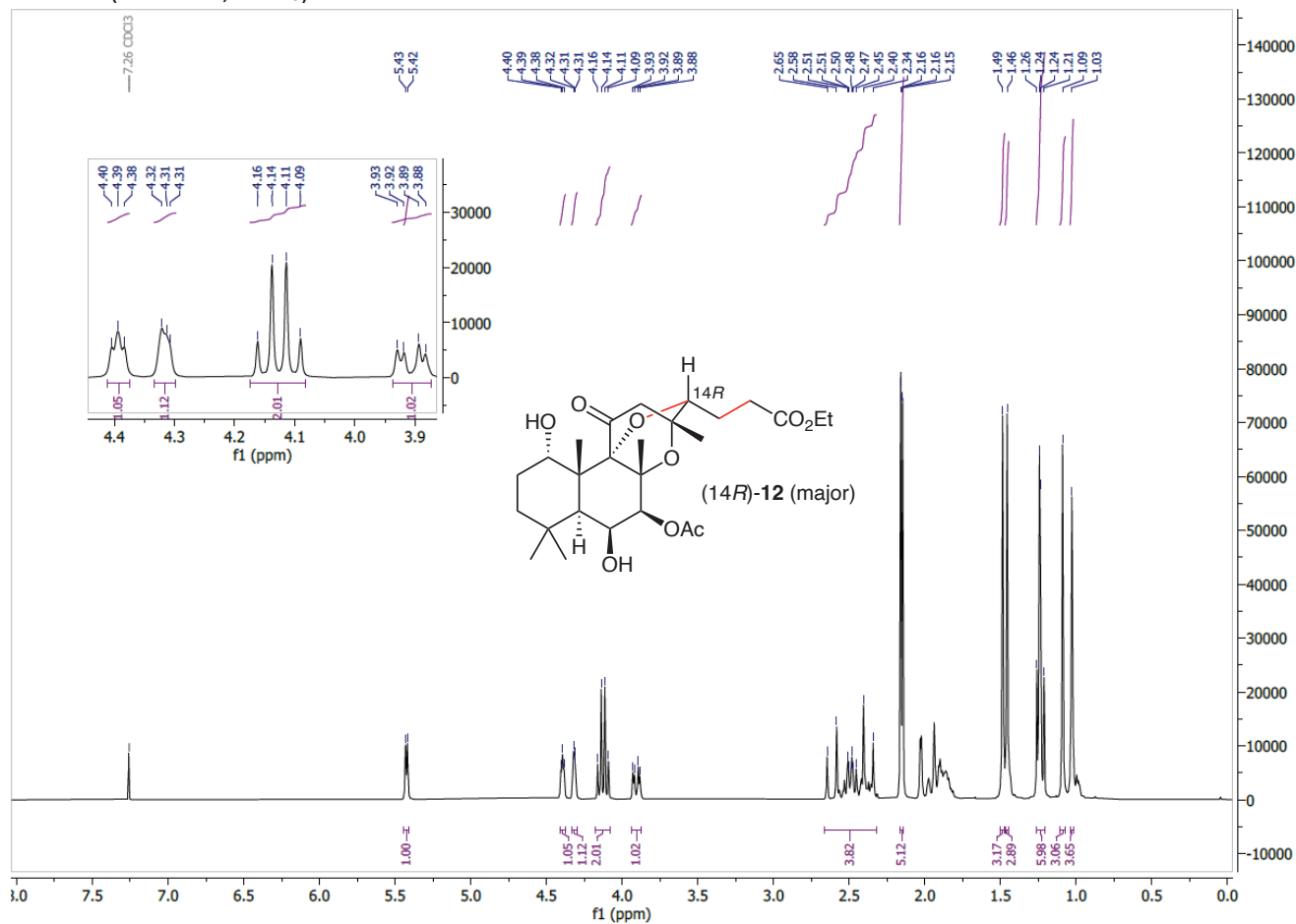
^1H NMR (300 MHz, C_6D_6)



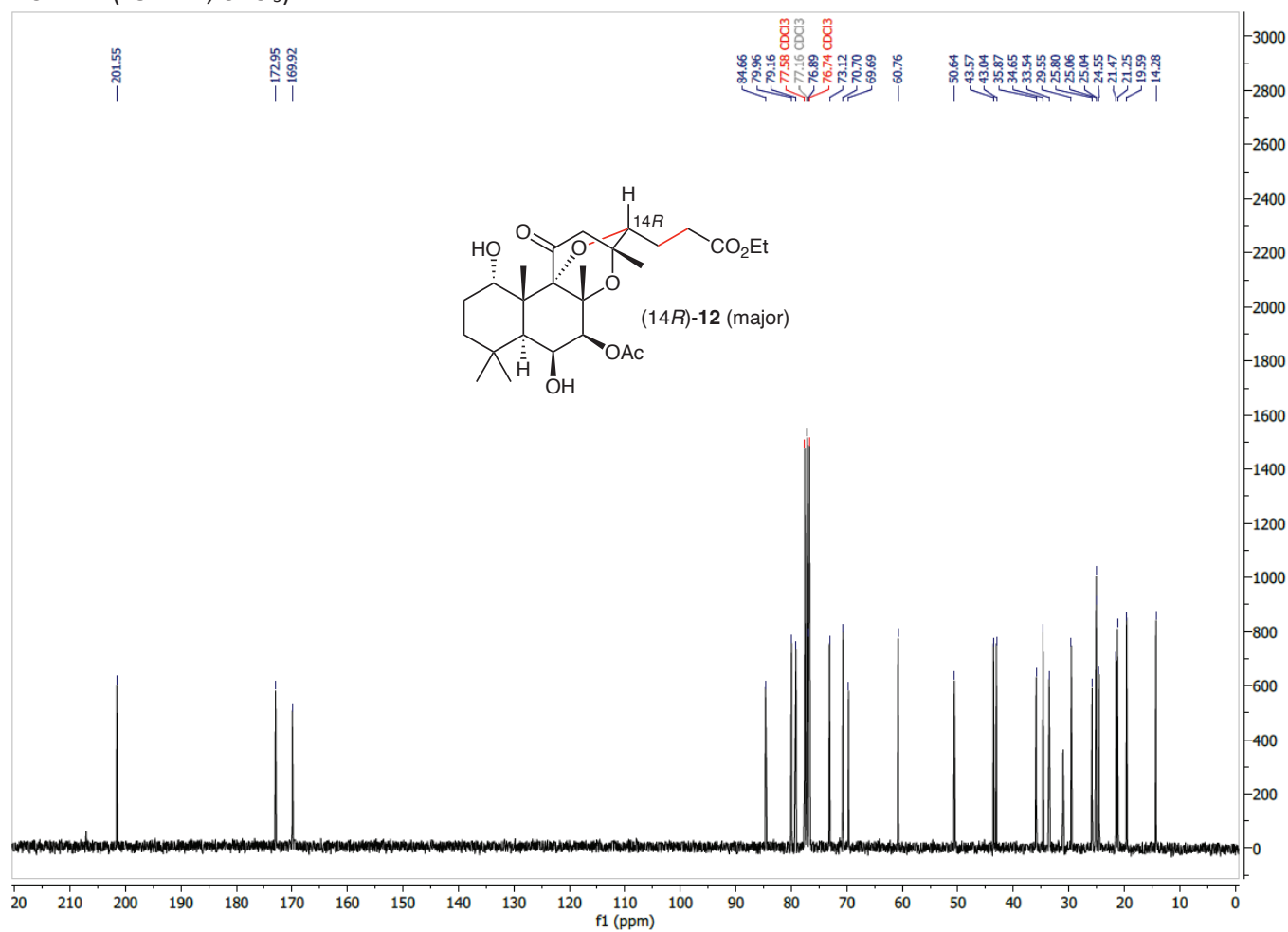
^{13}C NMR (75 MHz, C_6D_6)



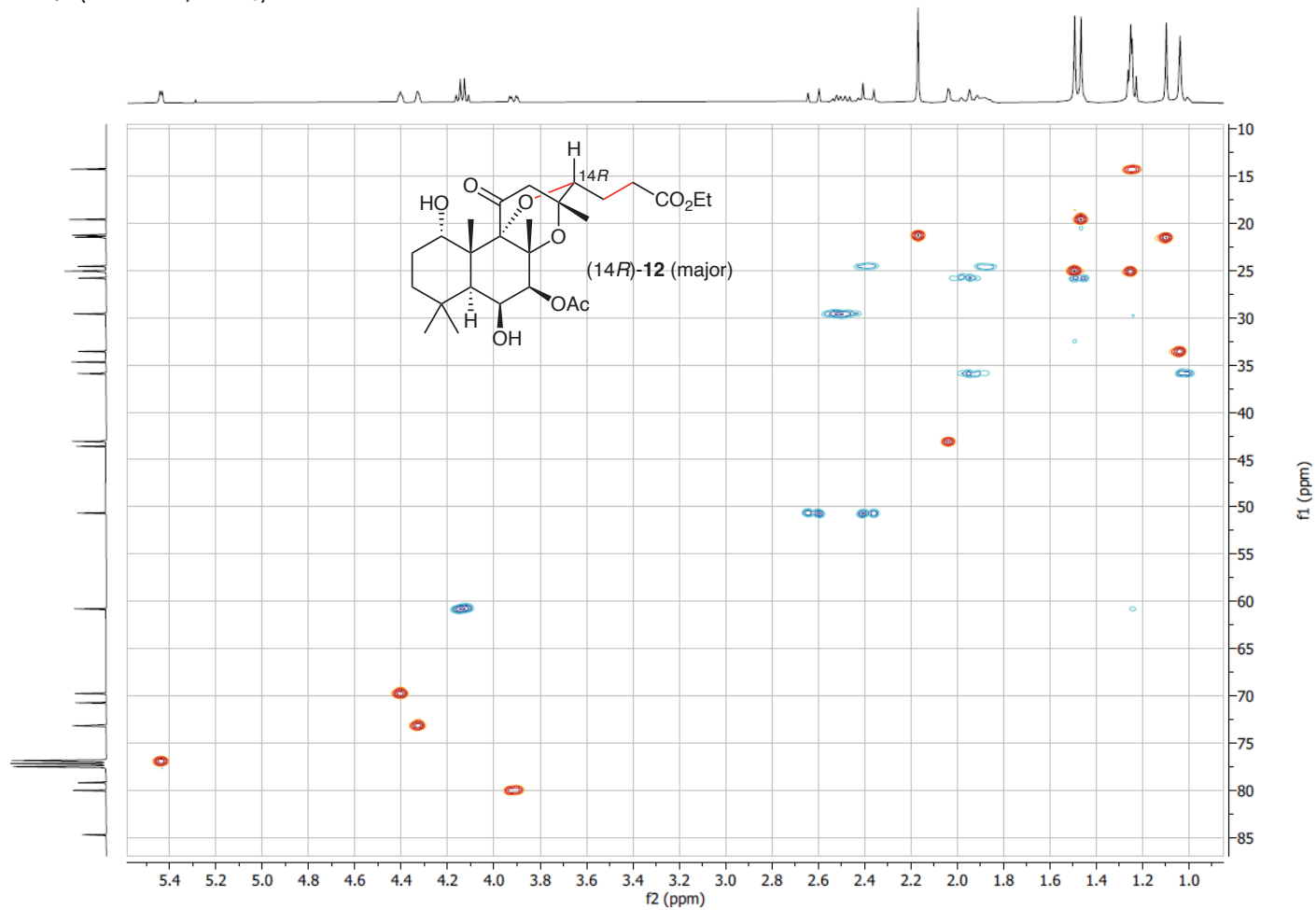
^1H NMR (300 MHz, CDCl_3)



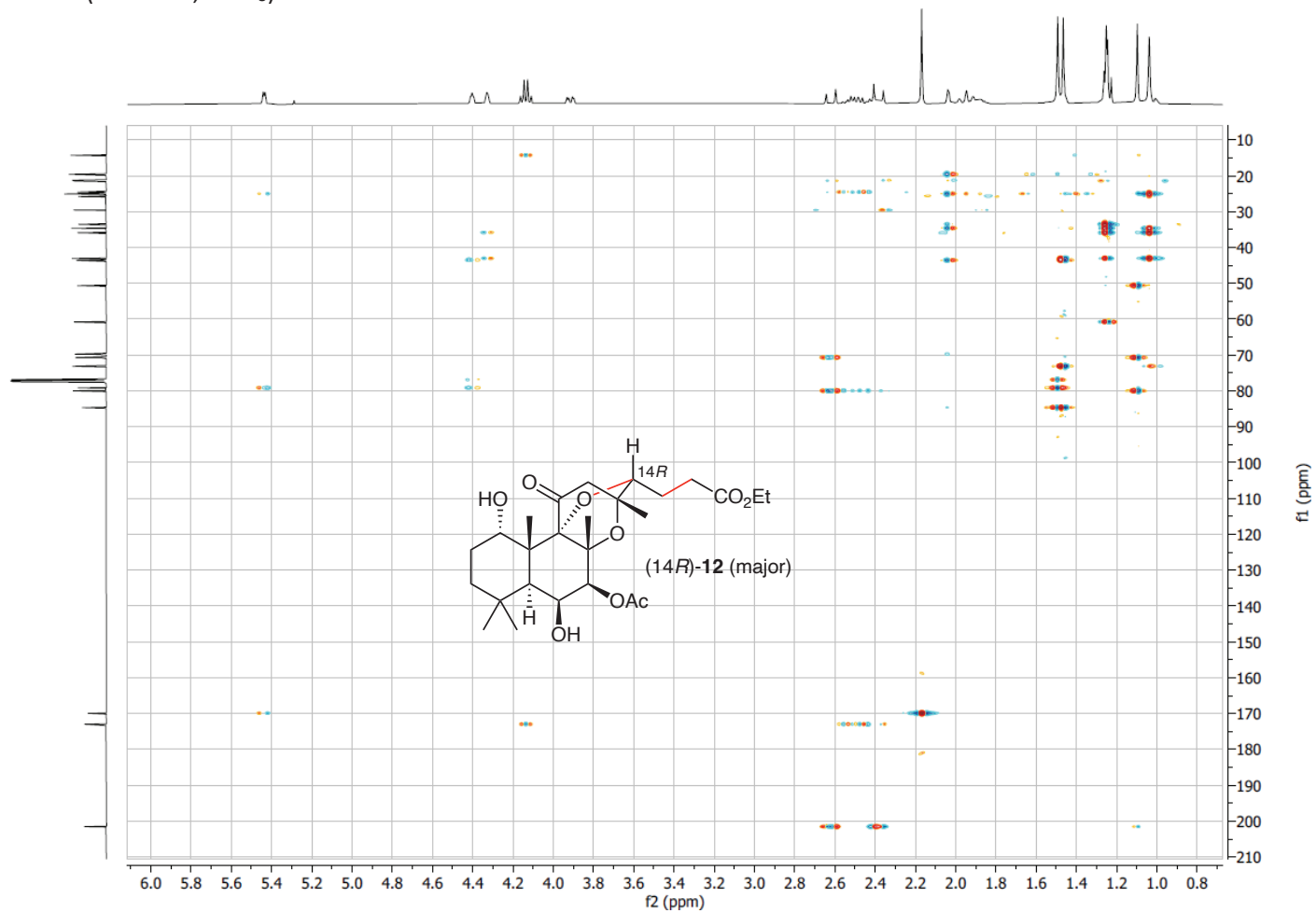
^{13}C NMR (75 MHz, CDCl_3)



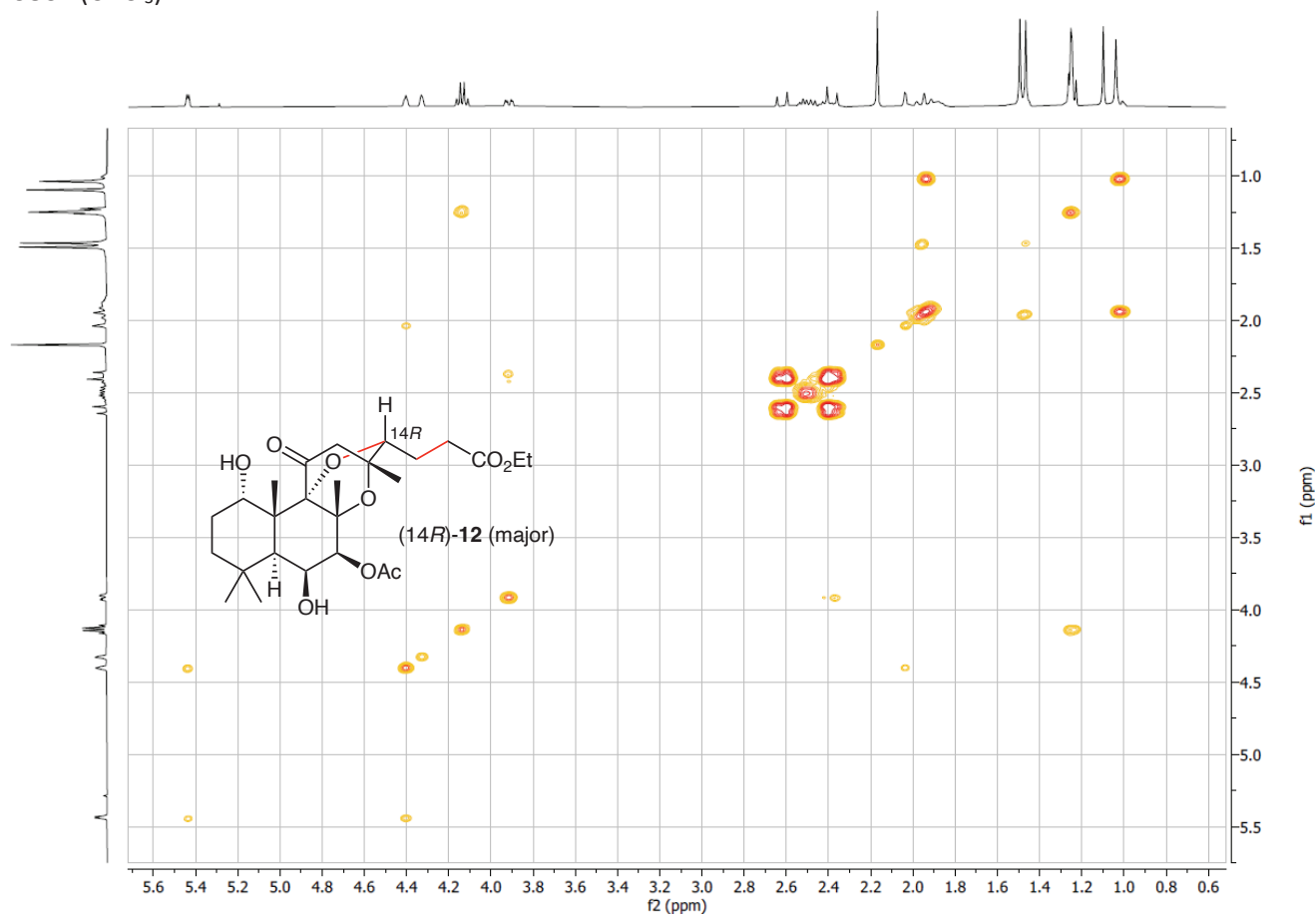
HSQC (400 MHz, CDCl₃)



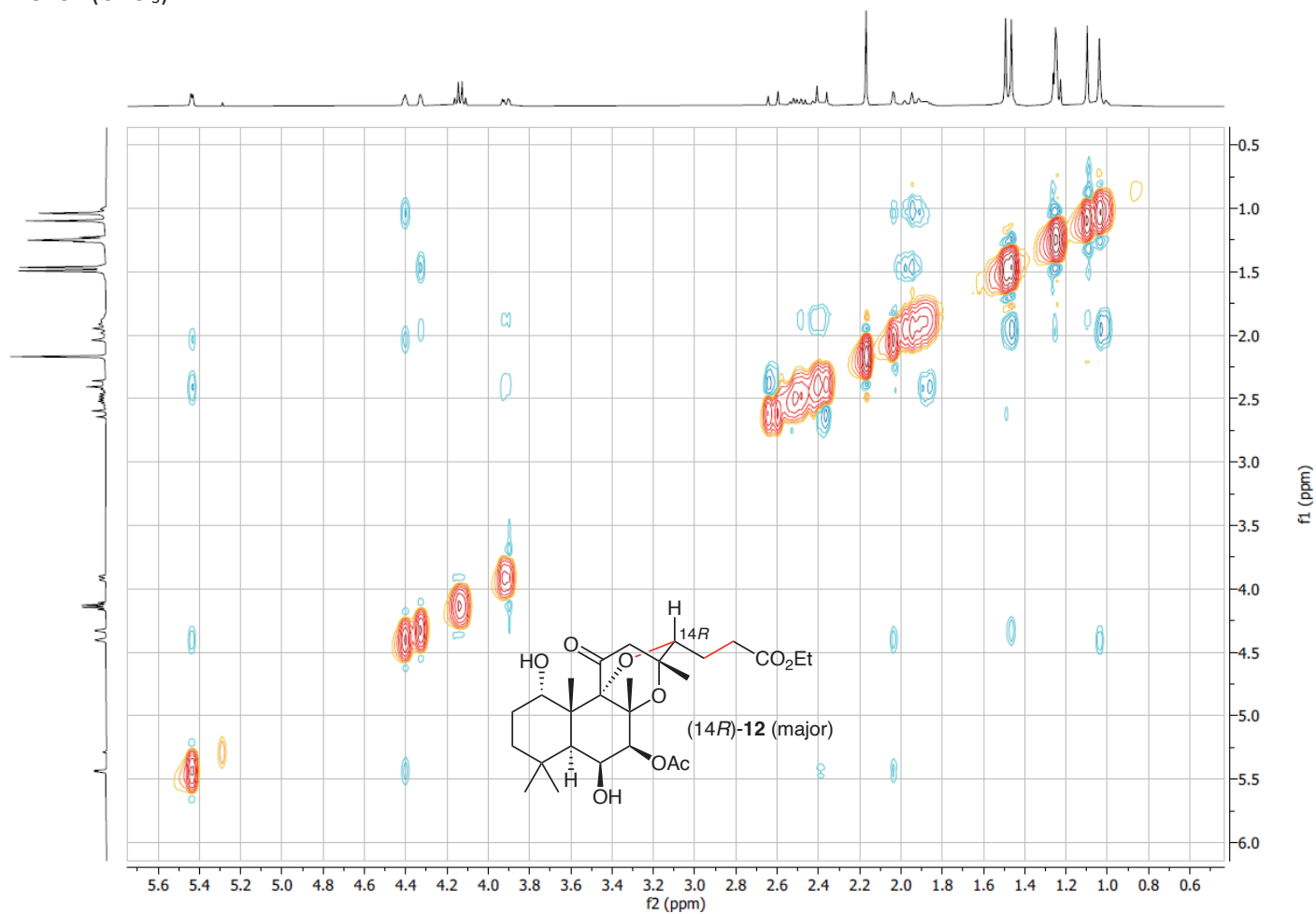
HMBC (400 MHz, CDCl₃)



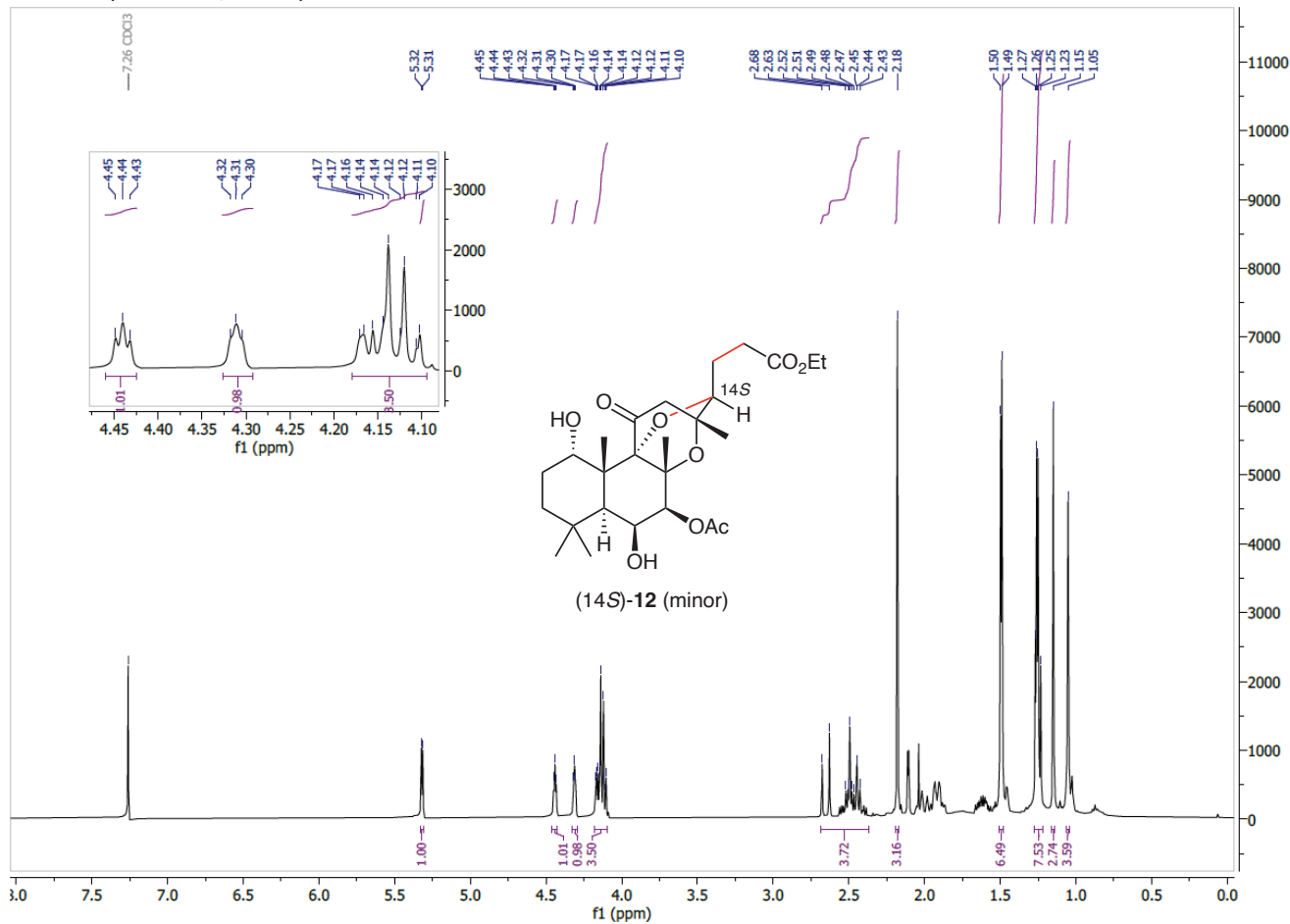
COSY (CDCl₃)



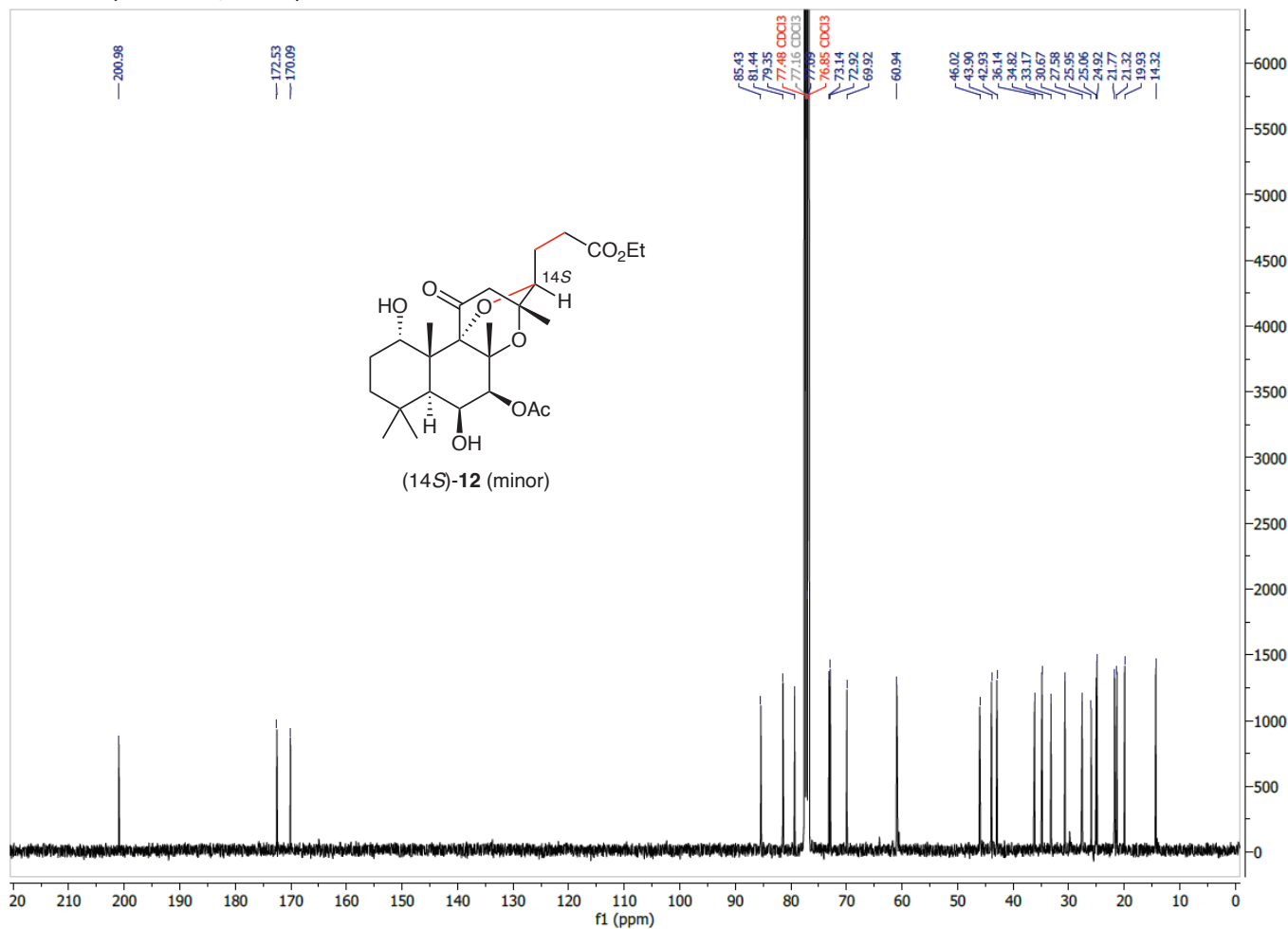
NOESY (CDCl₃)



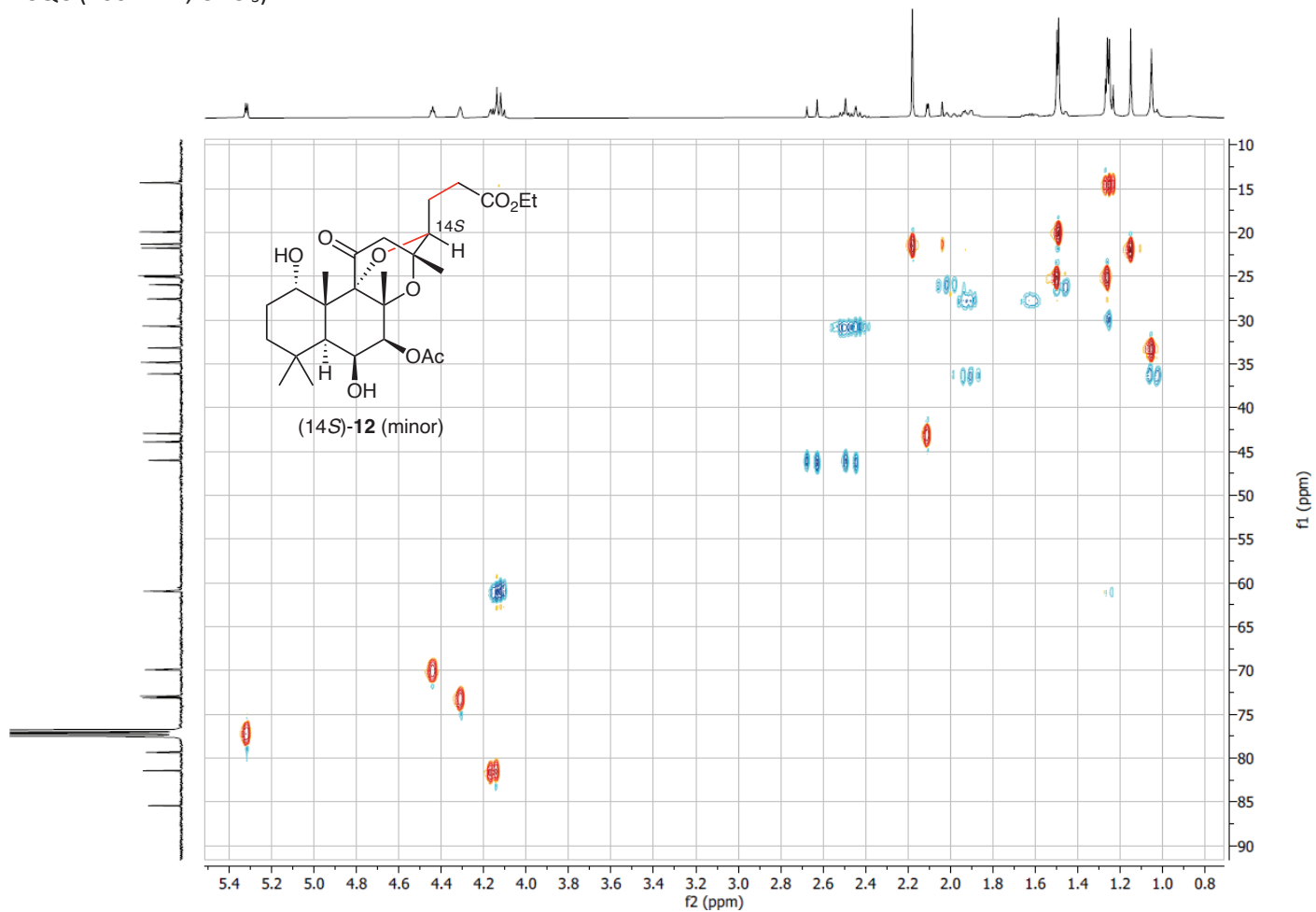
¹H NMR (400 MHz, CDCl₃)



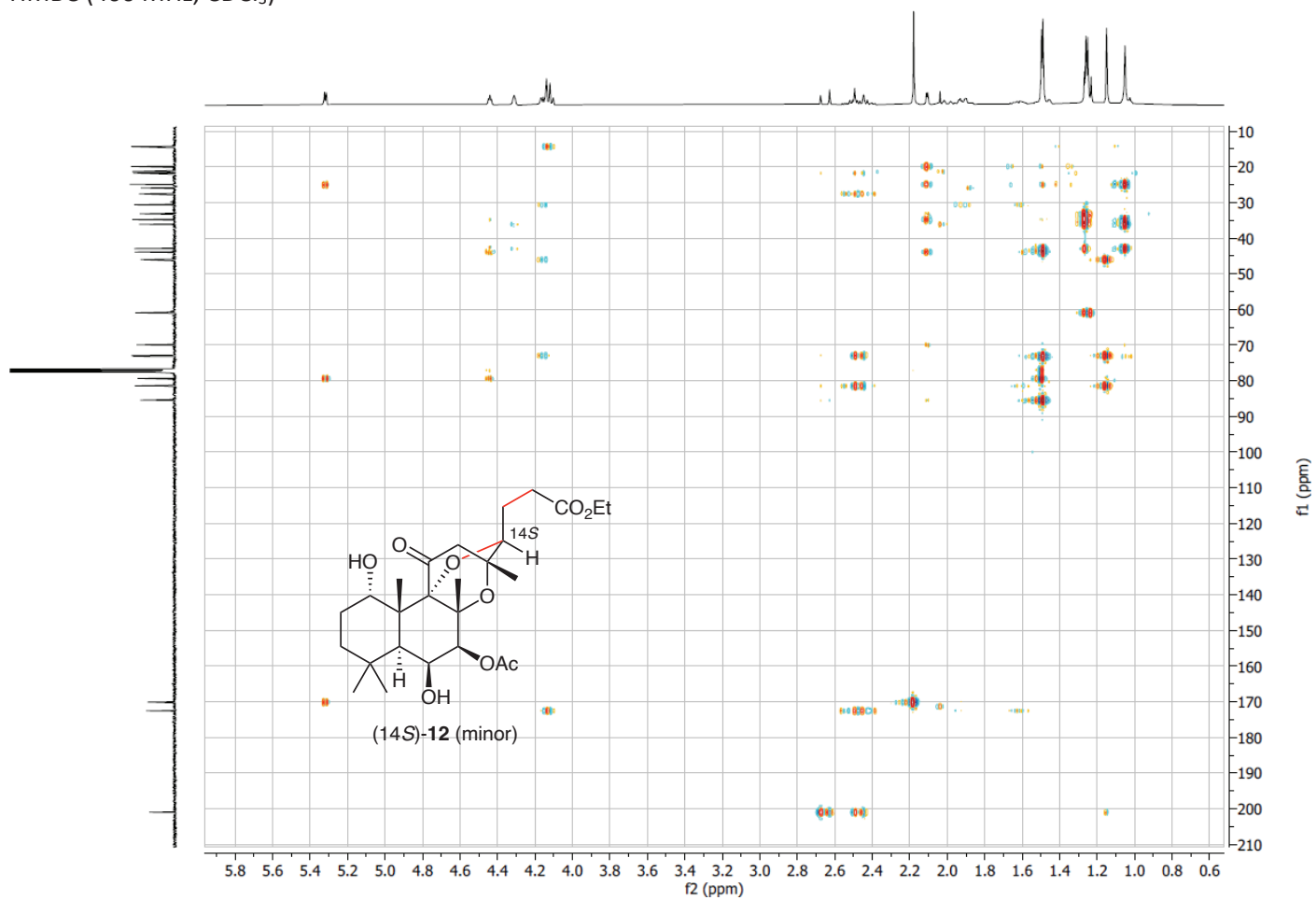
¹³C NMR (101 MHz, CDCl₃)



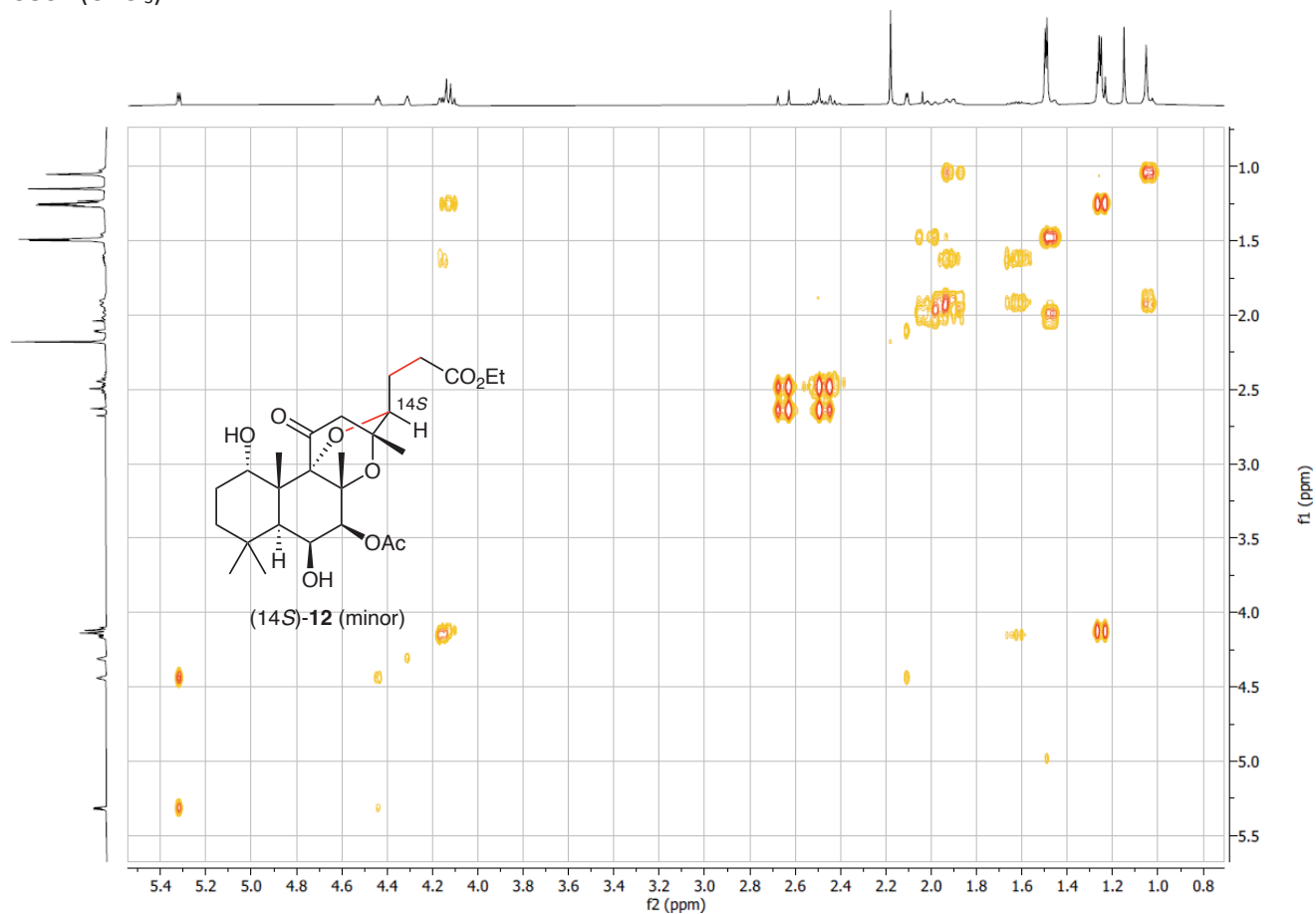
HSQC (400 MHz, CDCl₃)



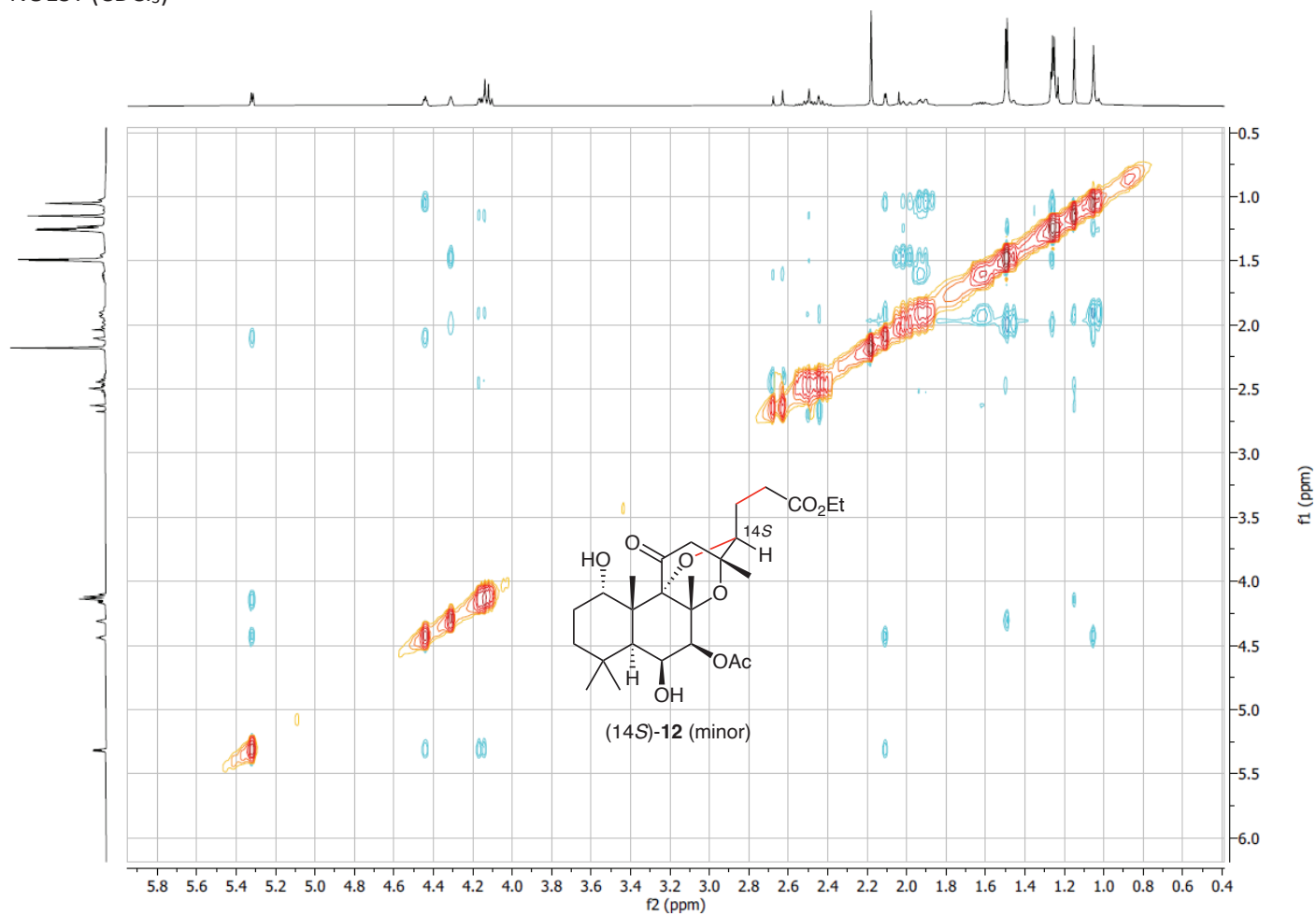
HMBC (400 MHz, CDCl₃)



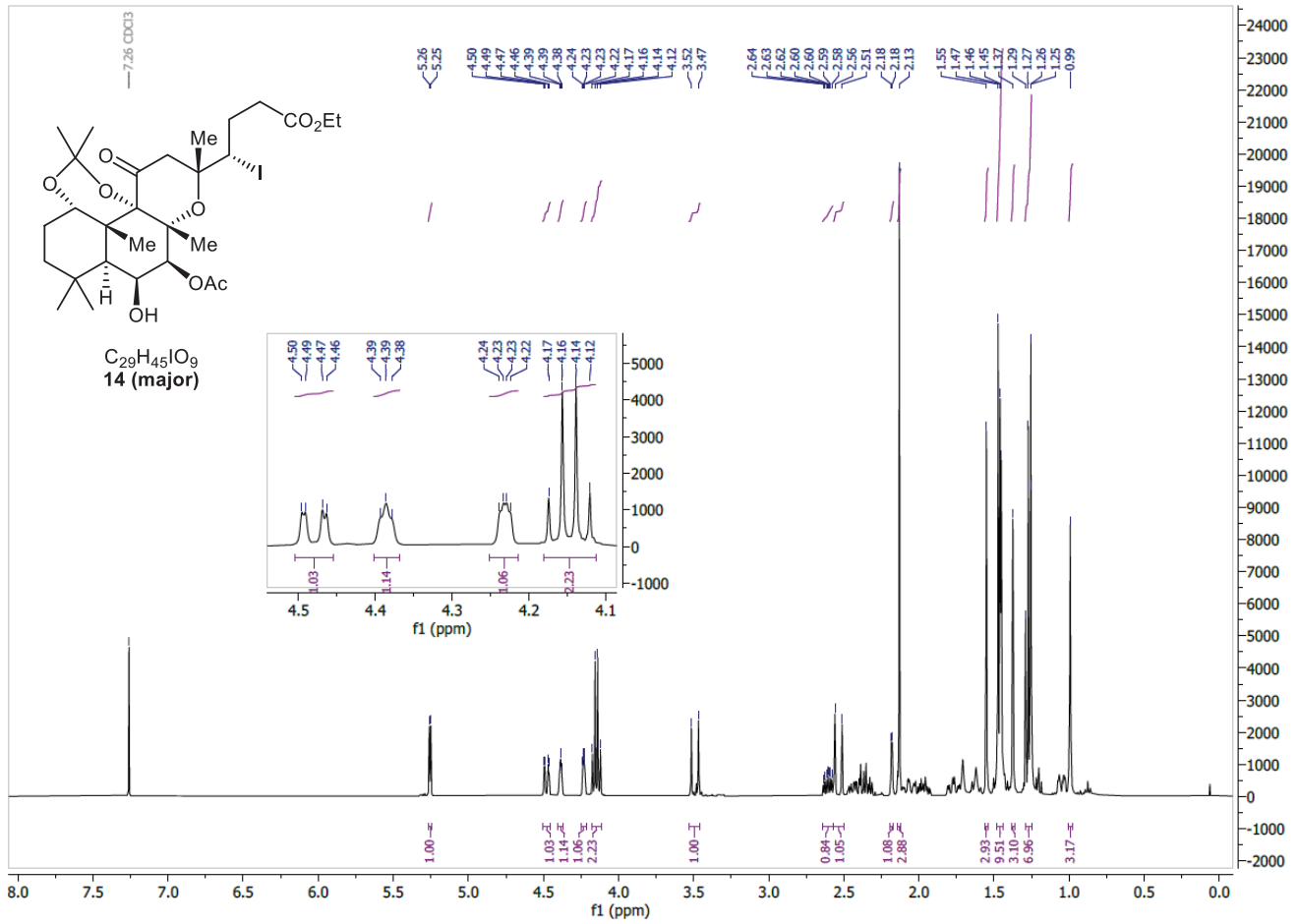
COSY (CDCl₃)



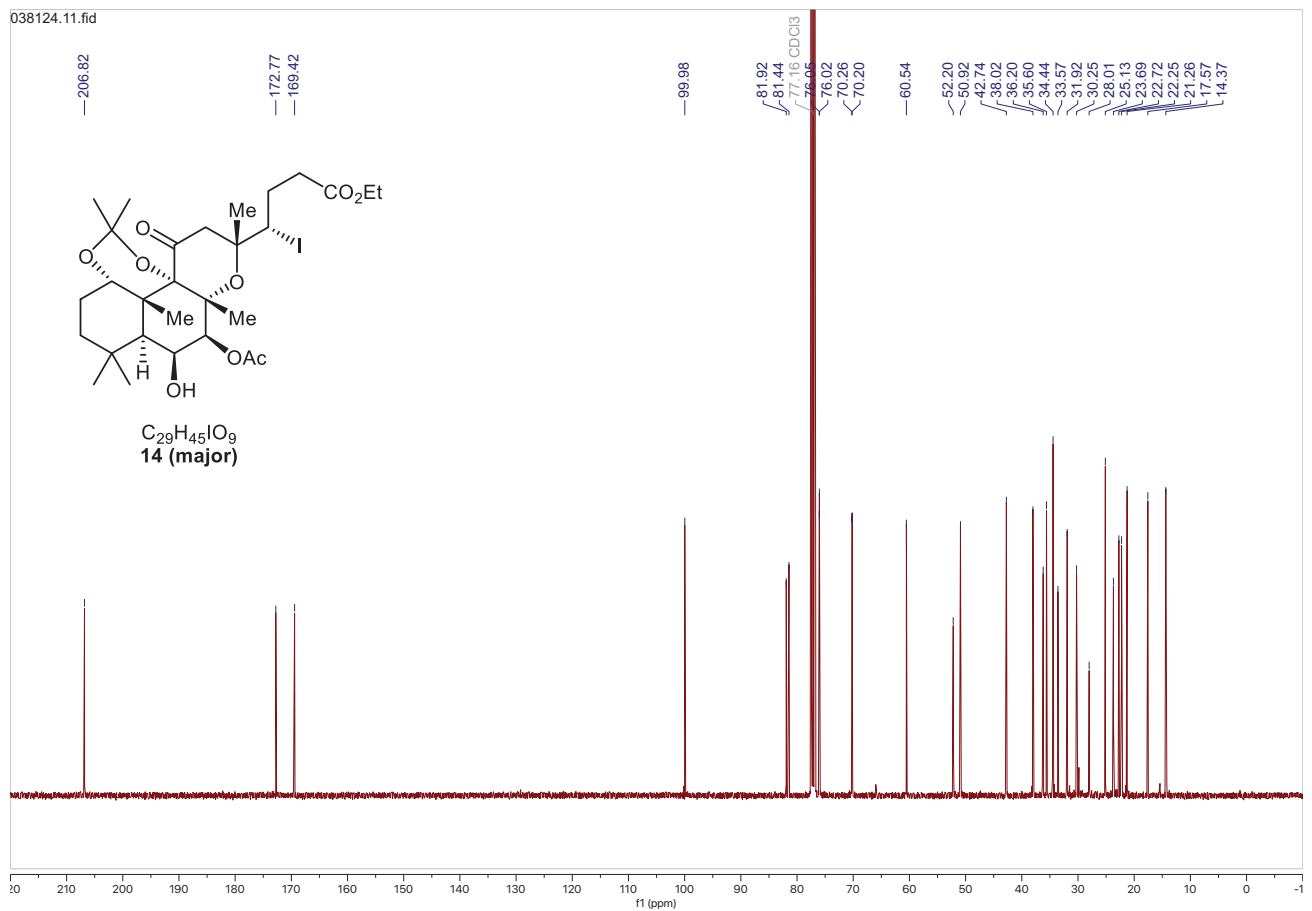
NOESY (CDCl₃)



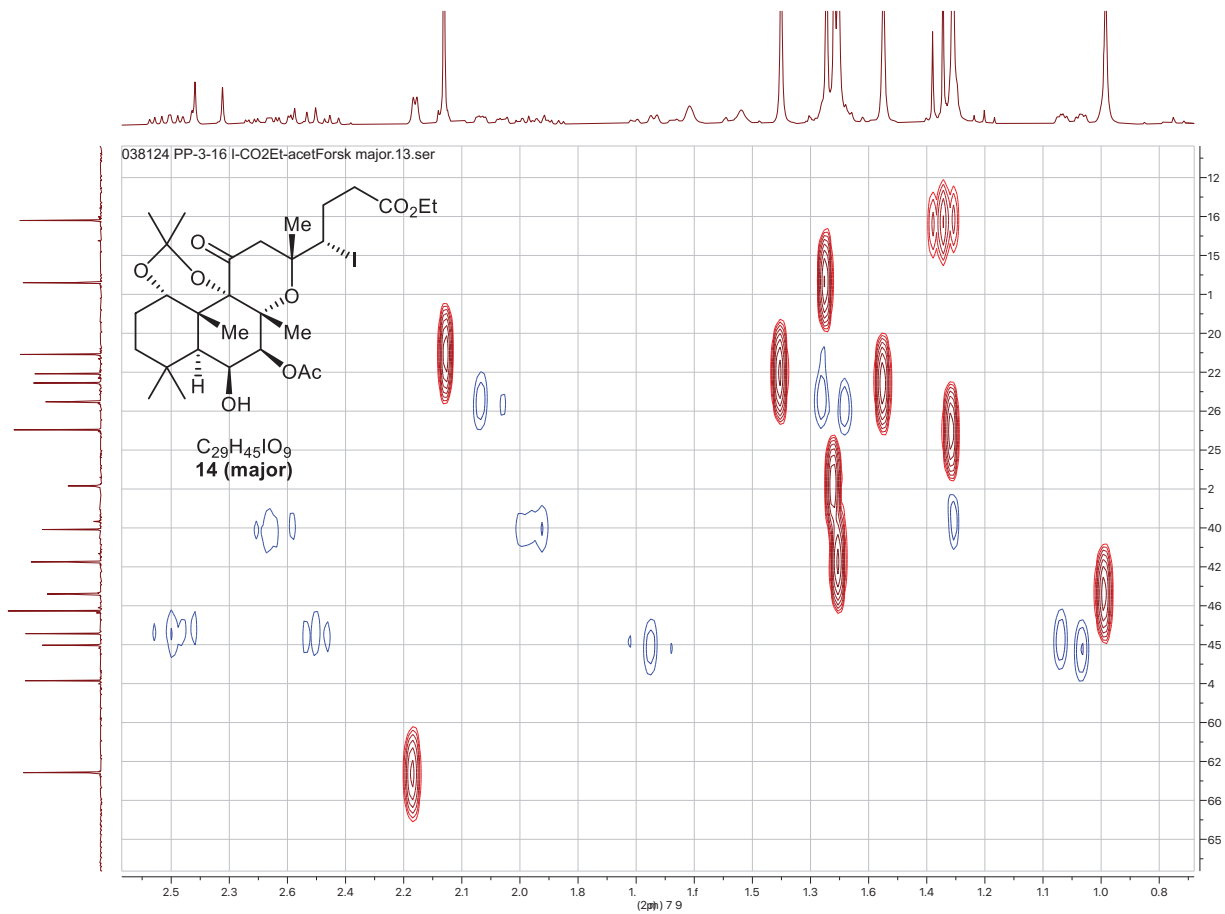
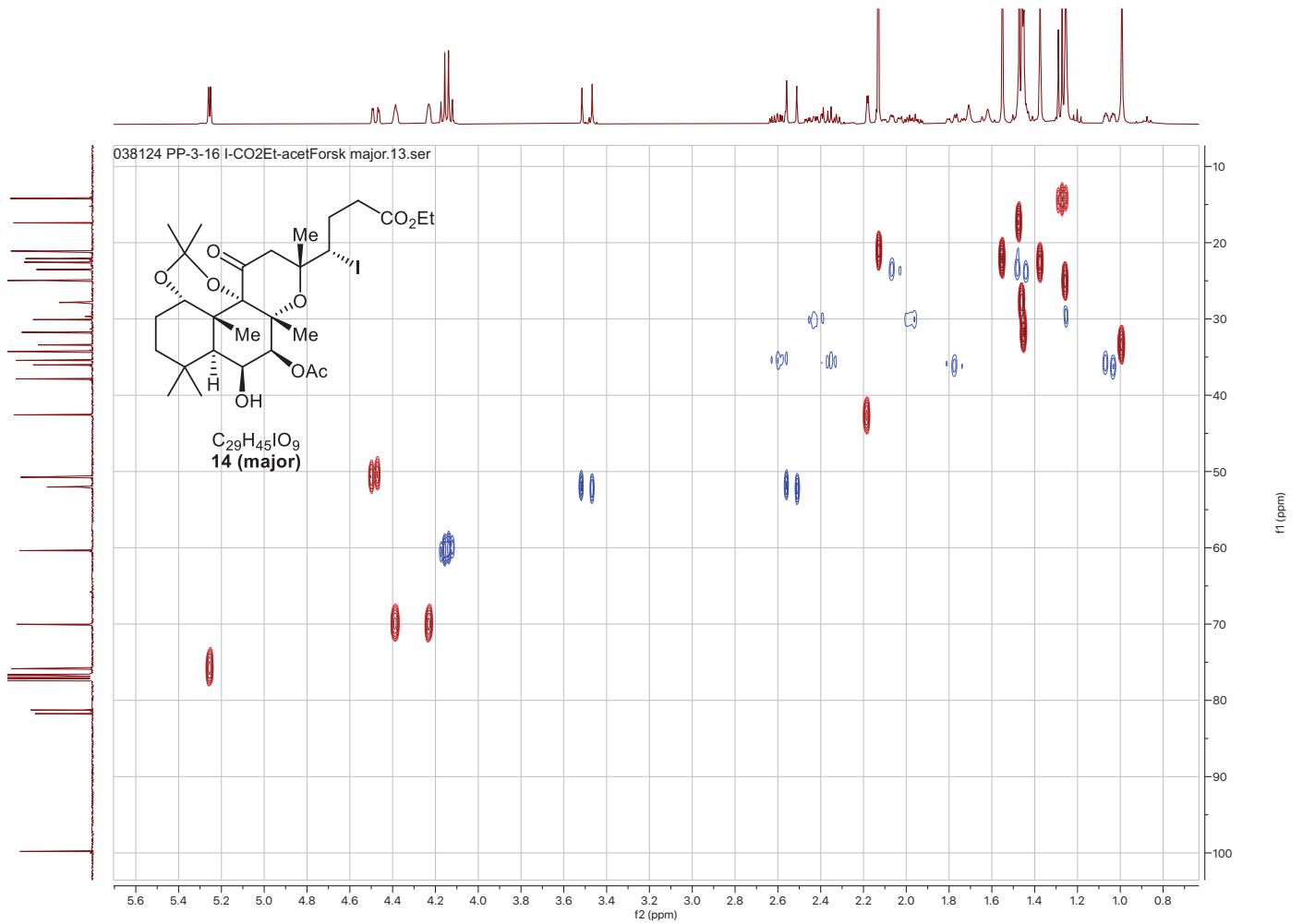
^1H NMR (400 MHz, CDCl_3)



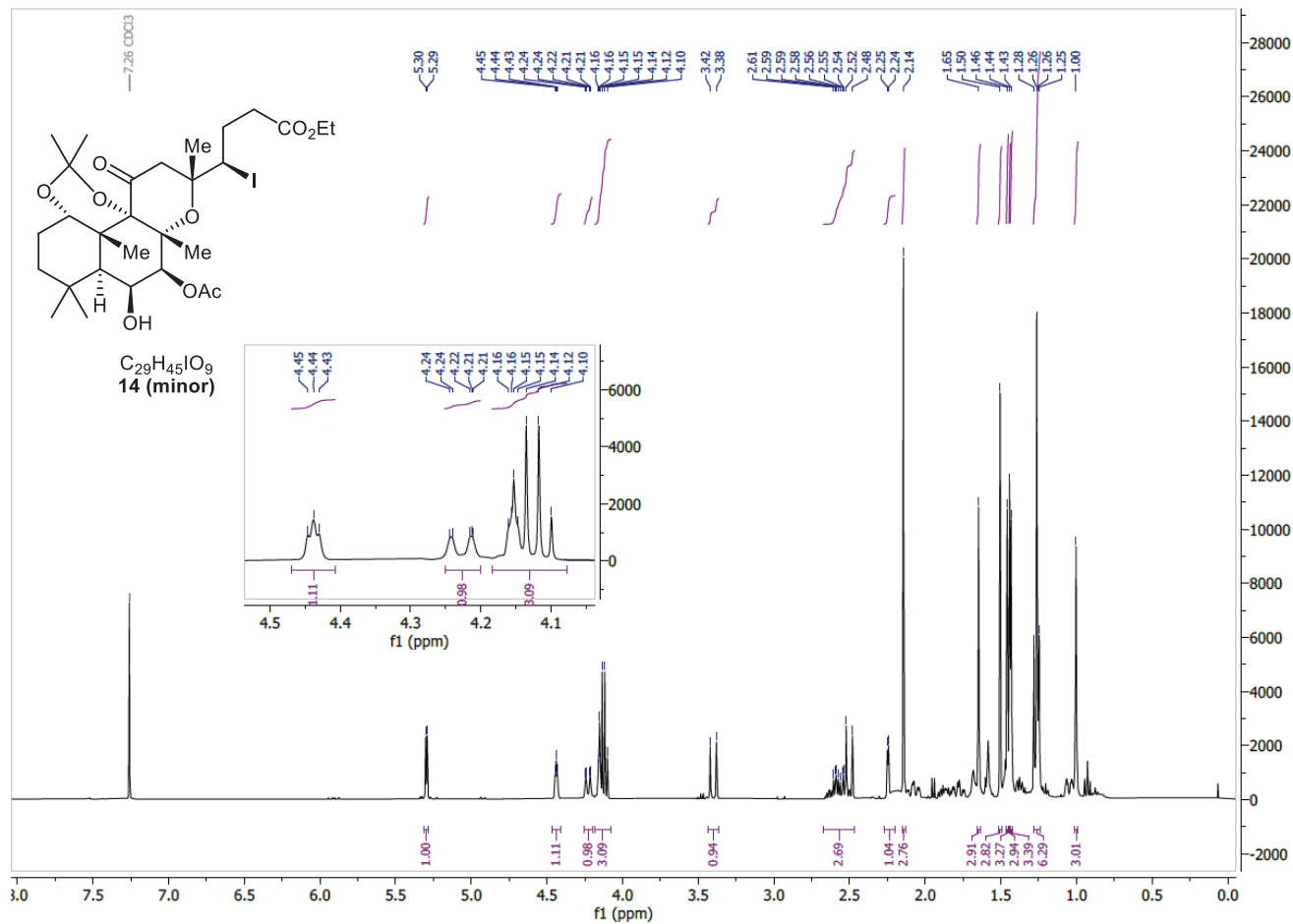
^{13}C NMR (101 MHz, CDCl_3)



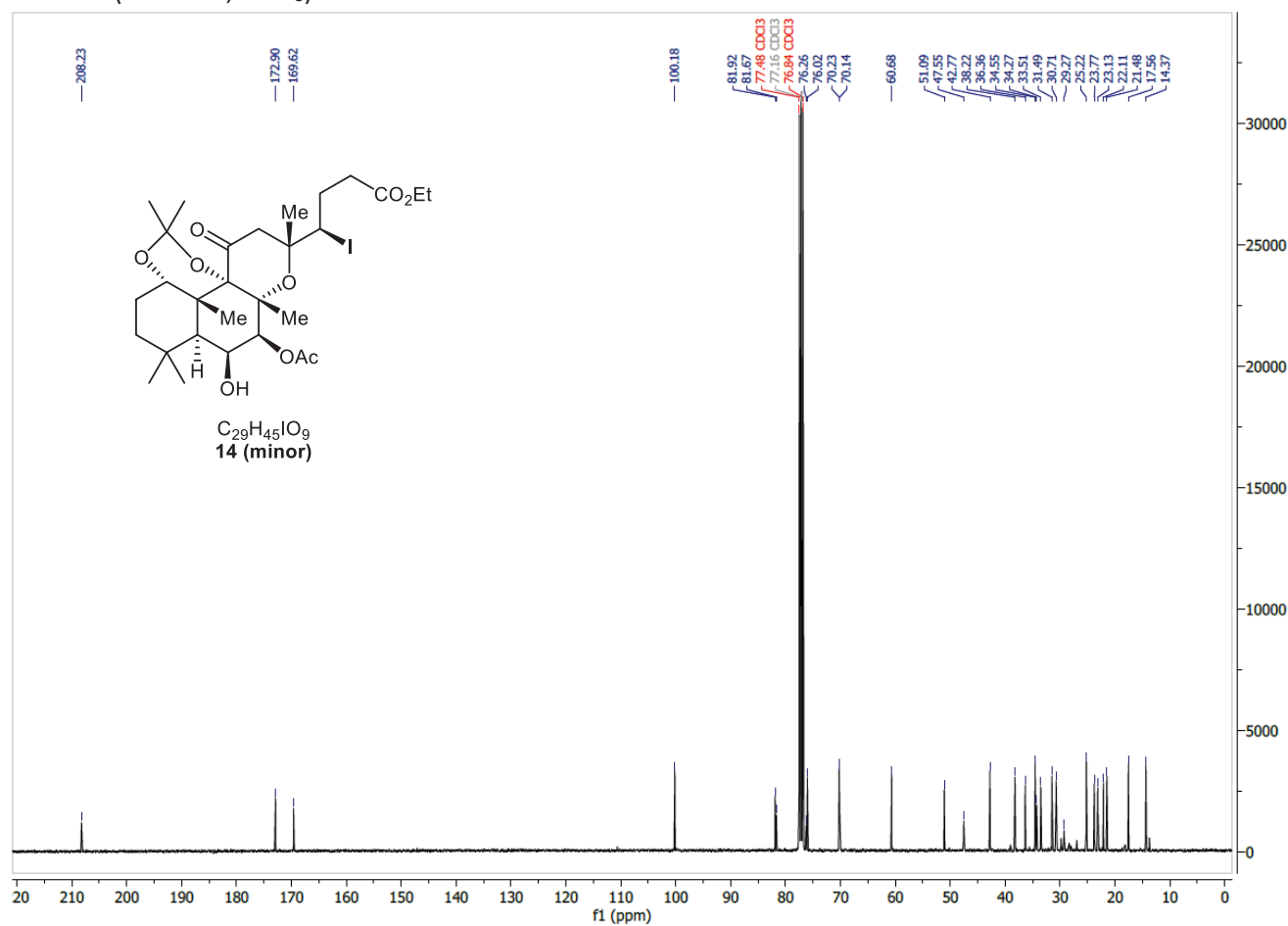
HSQC (CDCl₃):



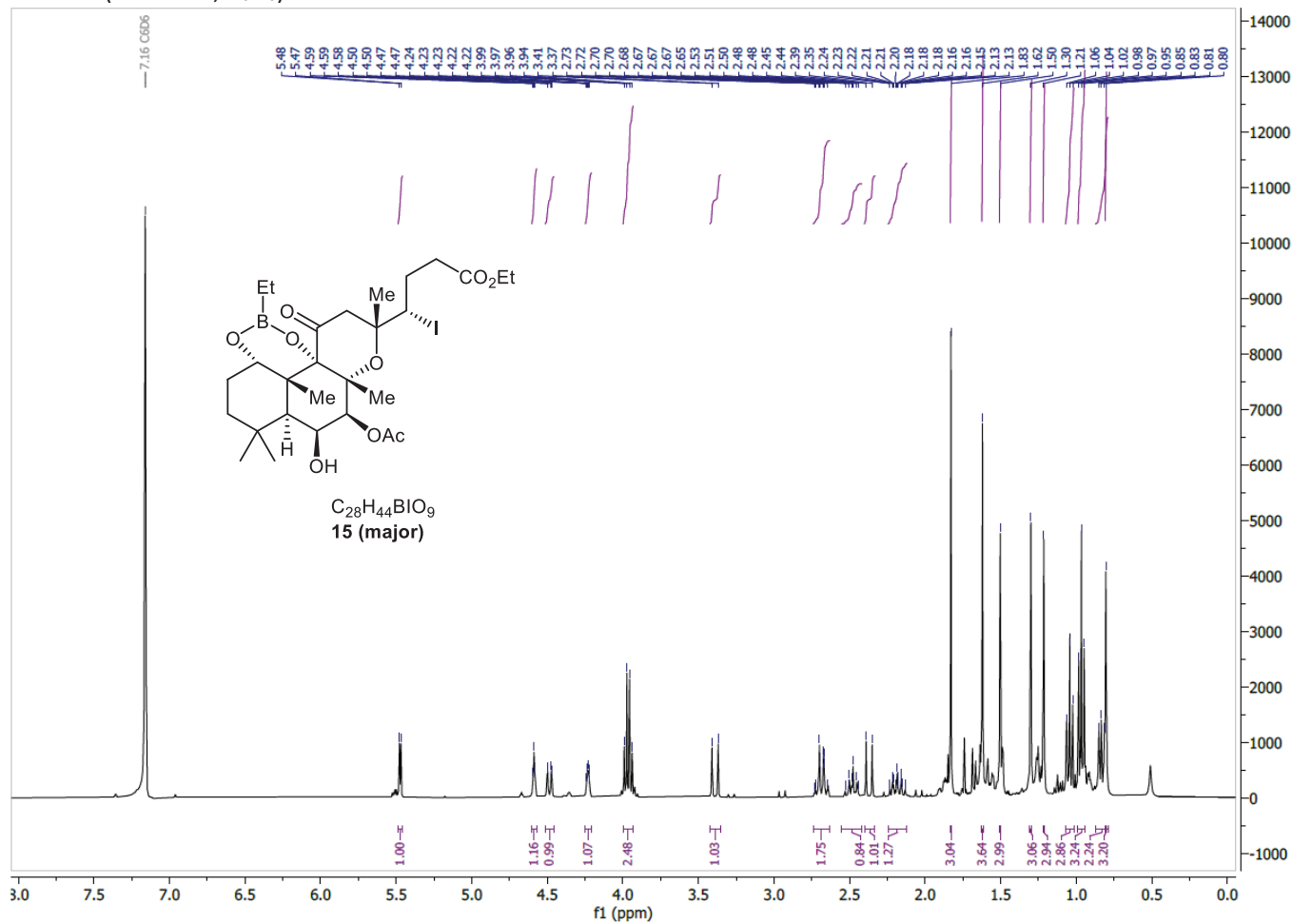
^1H NMR (400 MHz, CDCl_3)



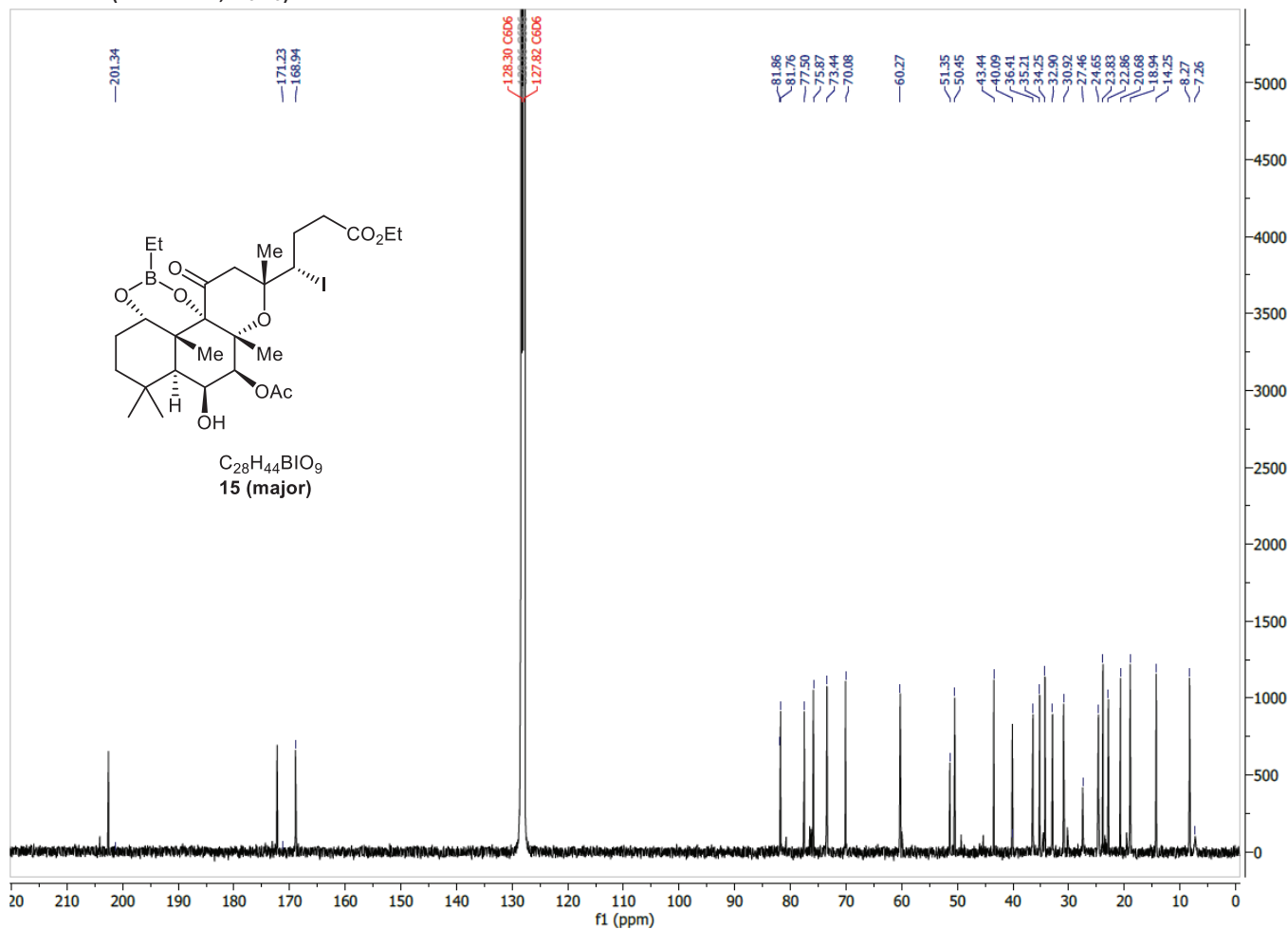
^{13}C NMR (101 MHz, CDCl_3)



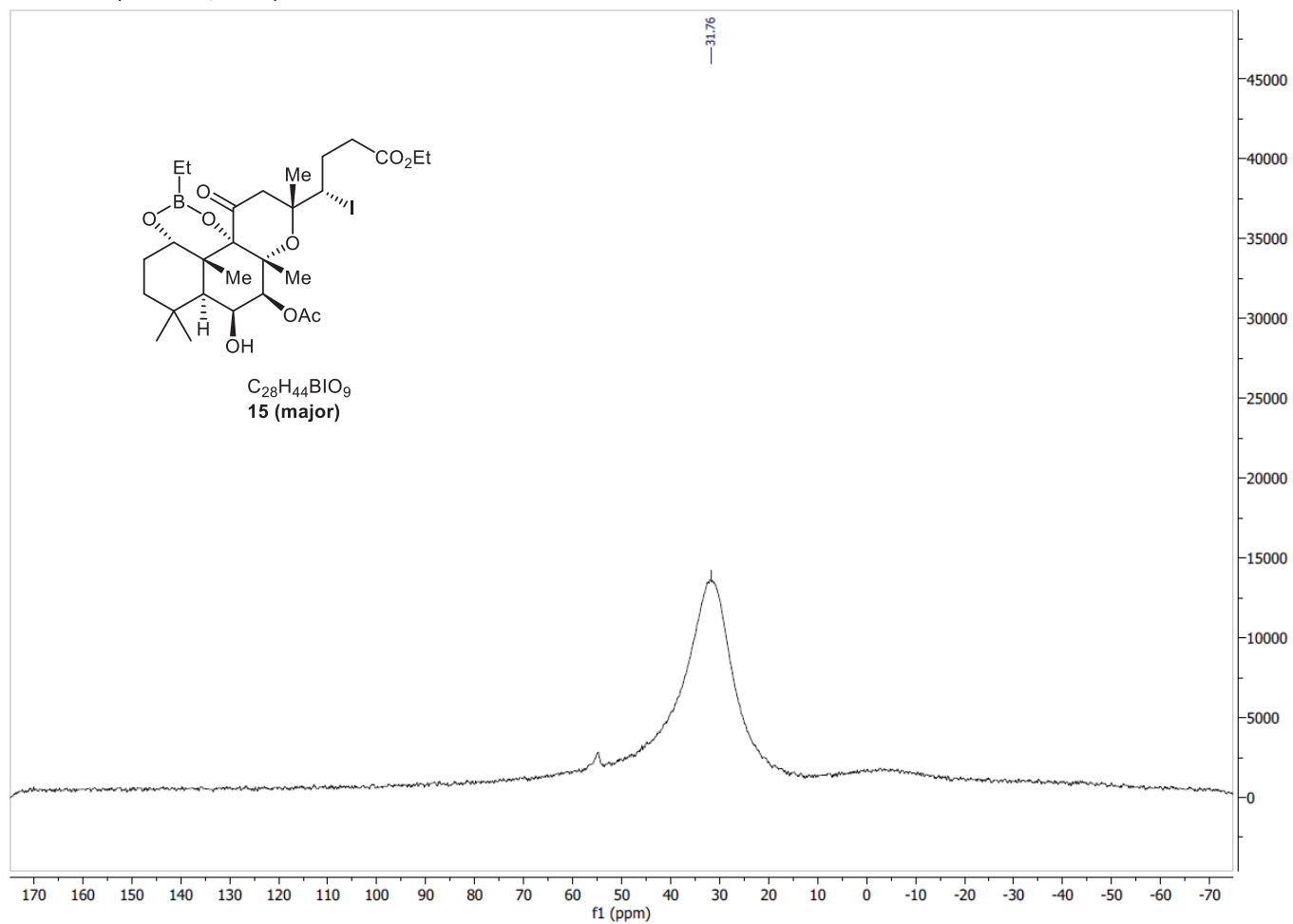
¹H NMR (400 MHz, C₆D₆)



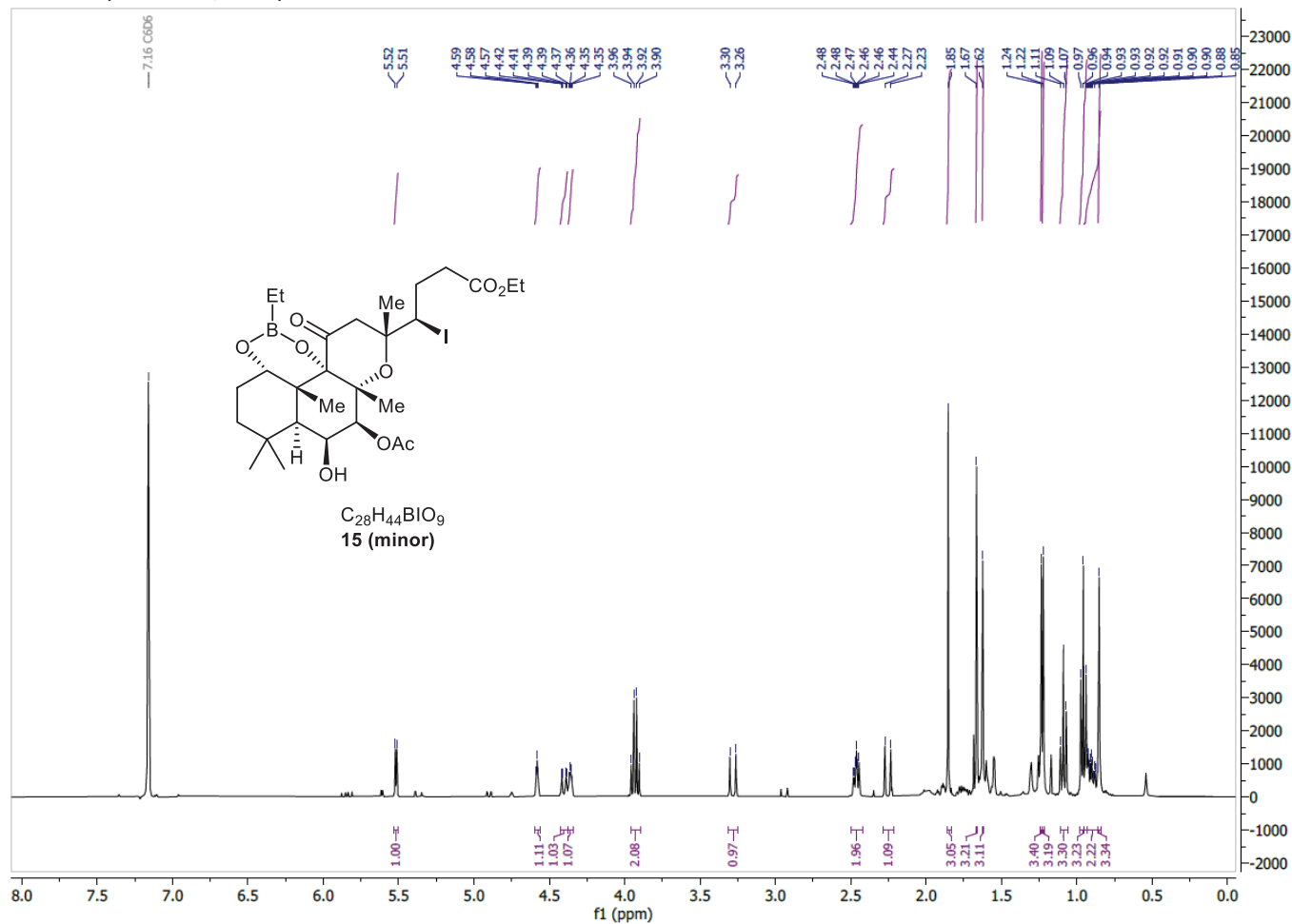
¹³C NMR (101 MHz, C₆D₆)



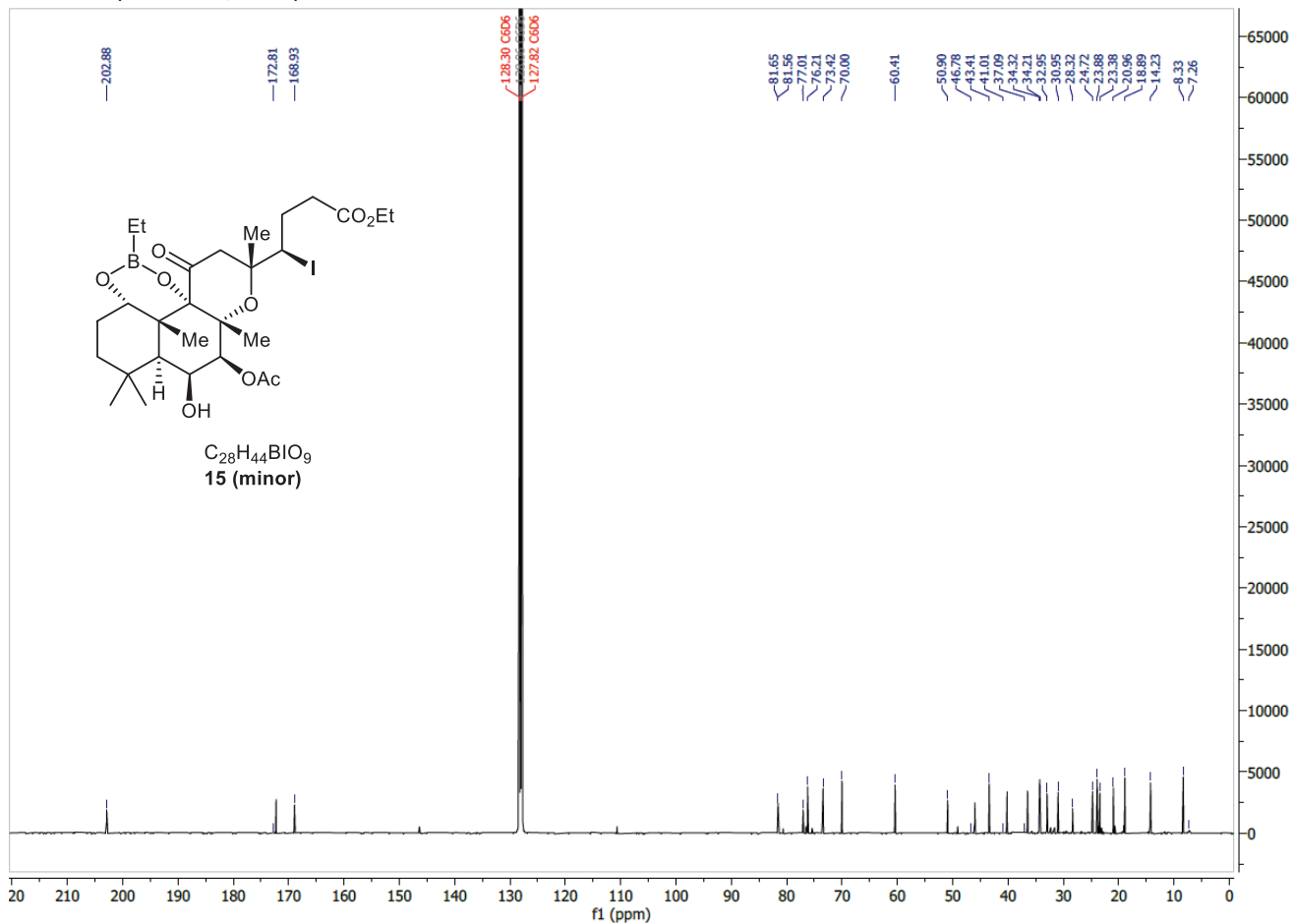
^{11}B NMR (96 MHz, C_6D_6)



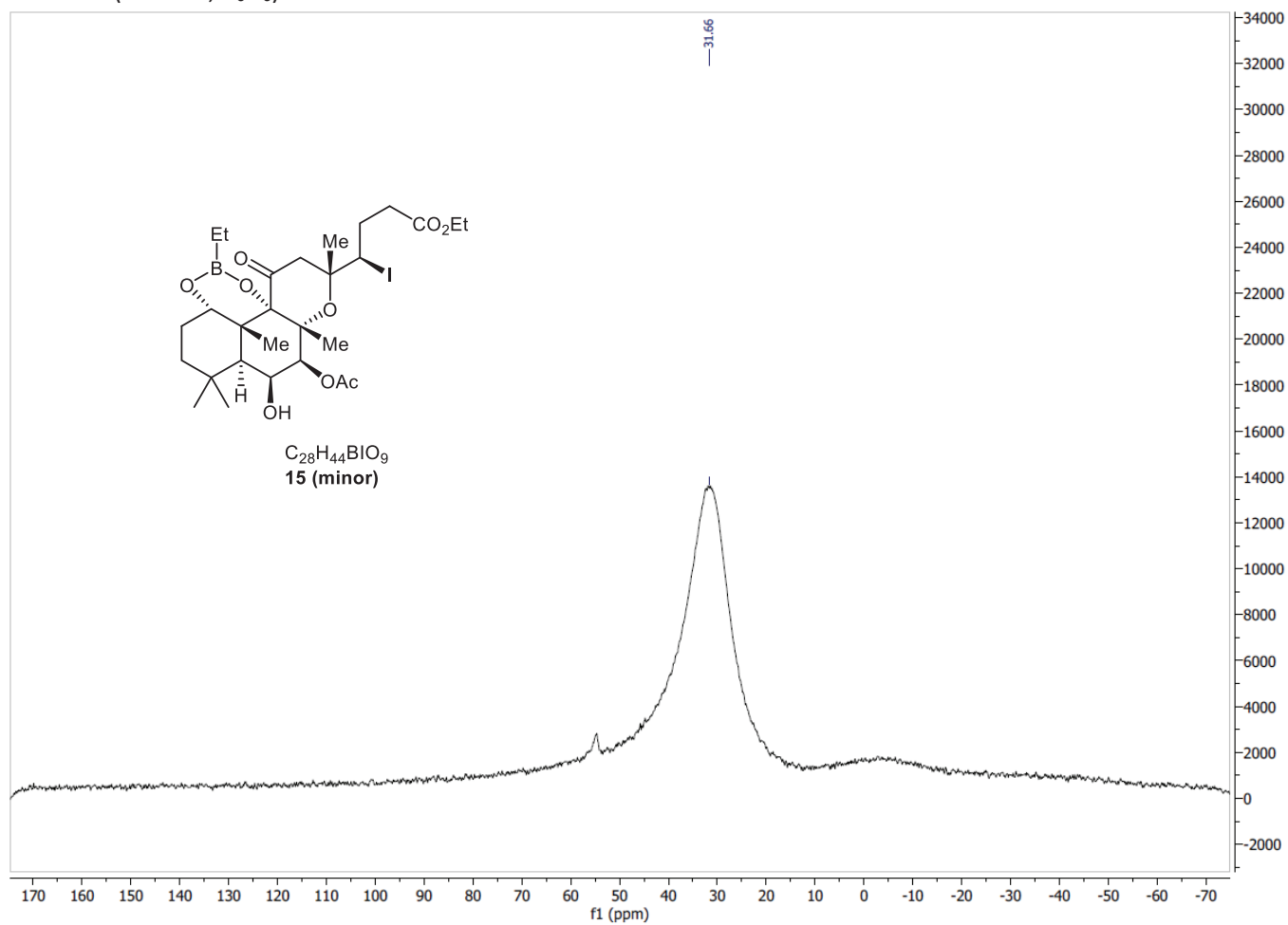
¹H NMR (400 MHz, C₆D₆)



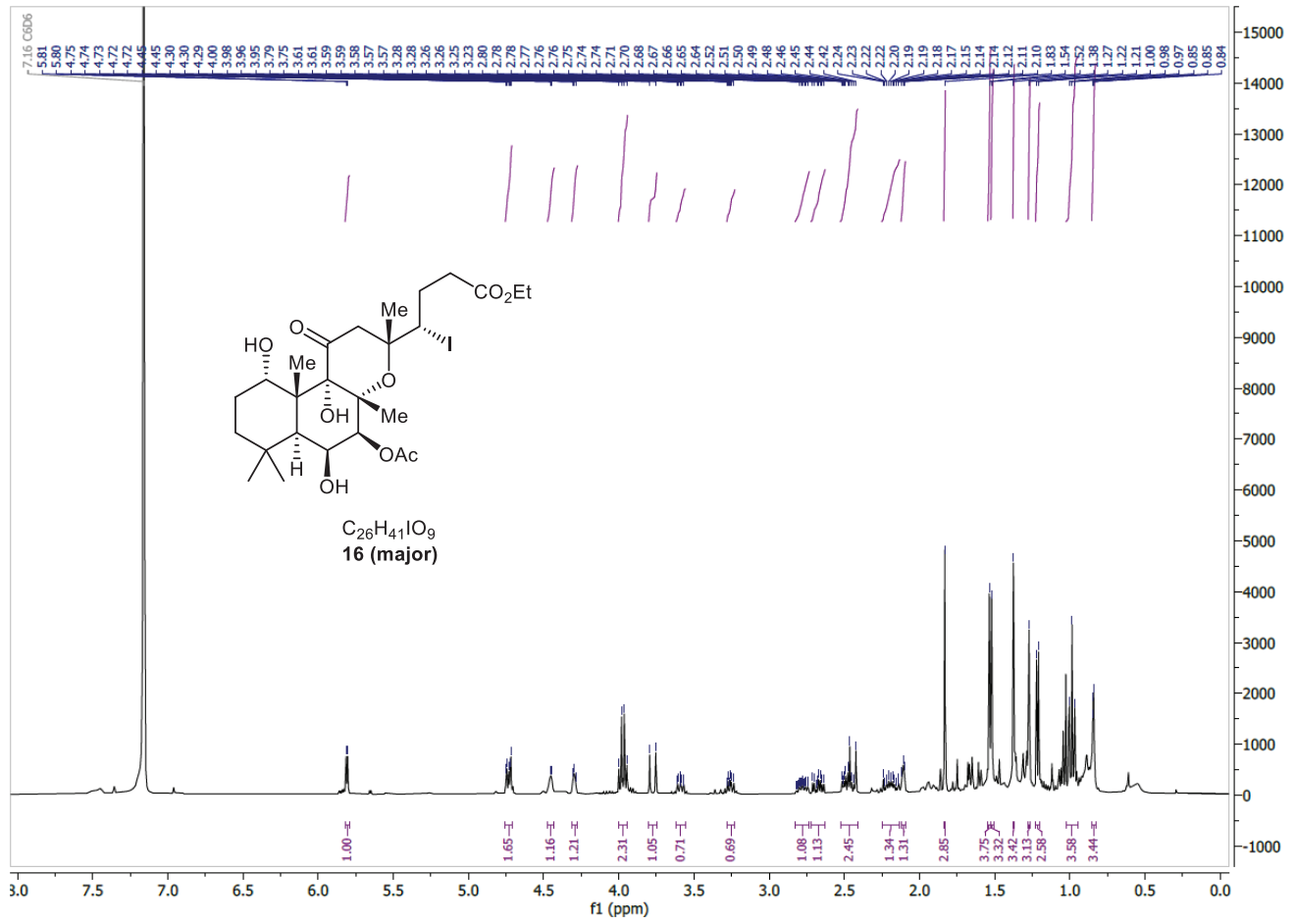
¹³C NMR (101 MHz, C₆D₆)



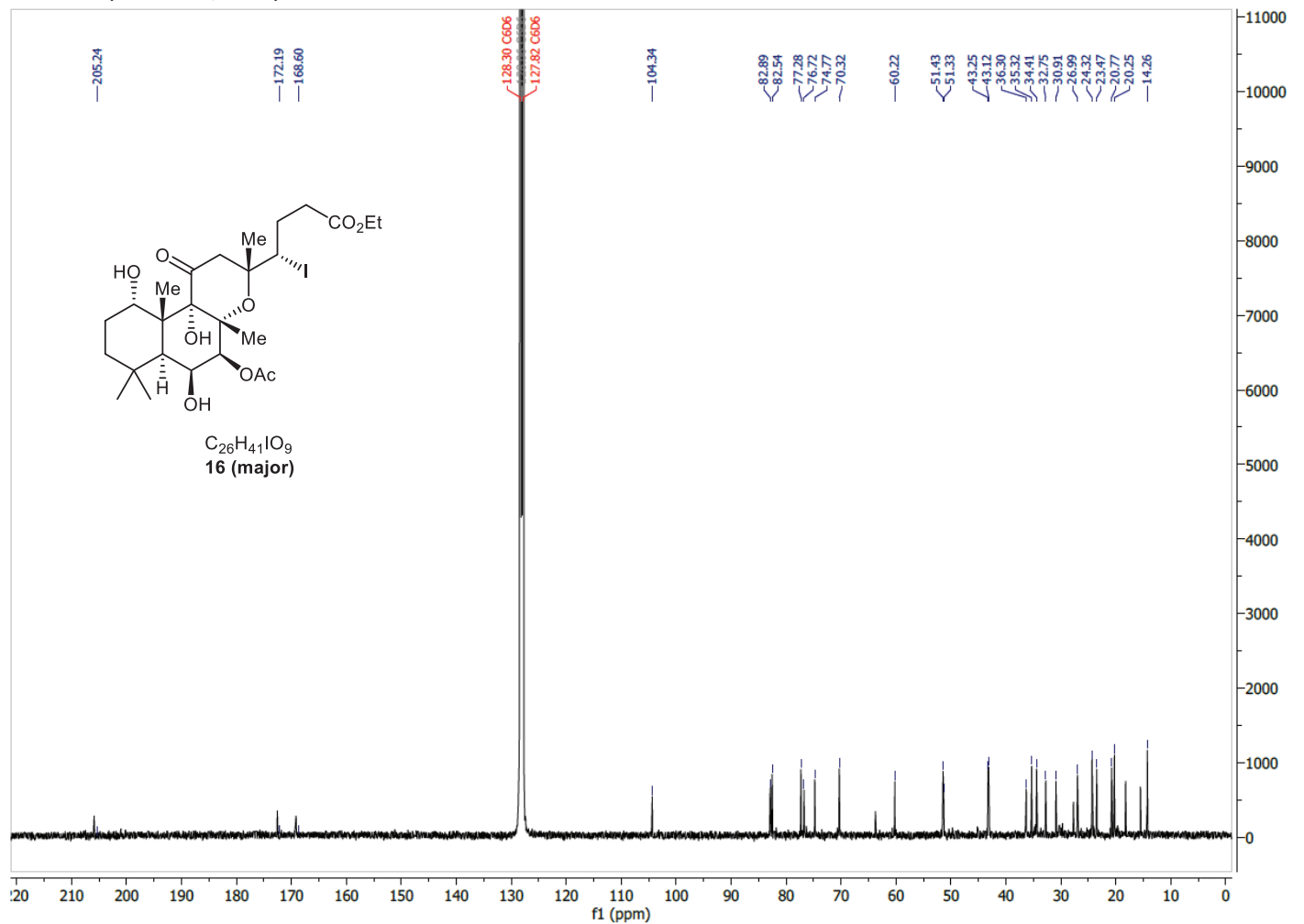
^{11}B NMR (96 MHz, C_6D_6)



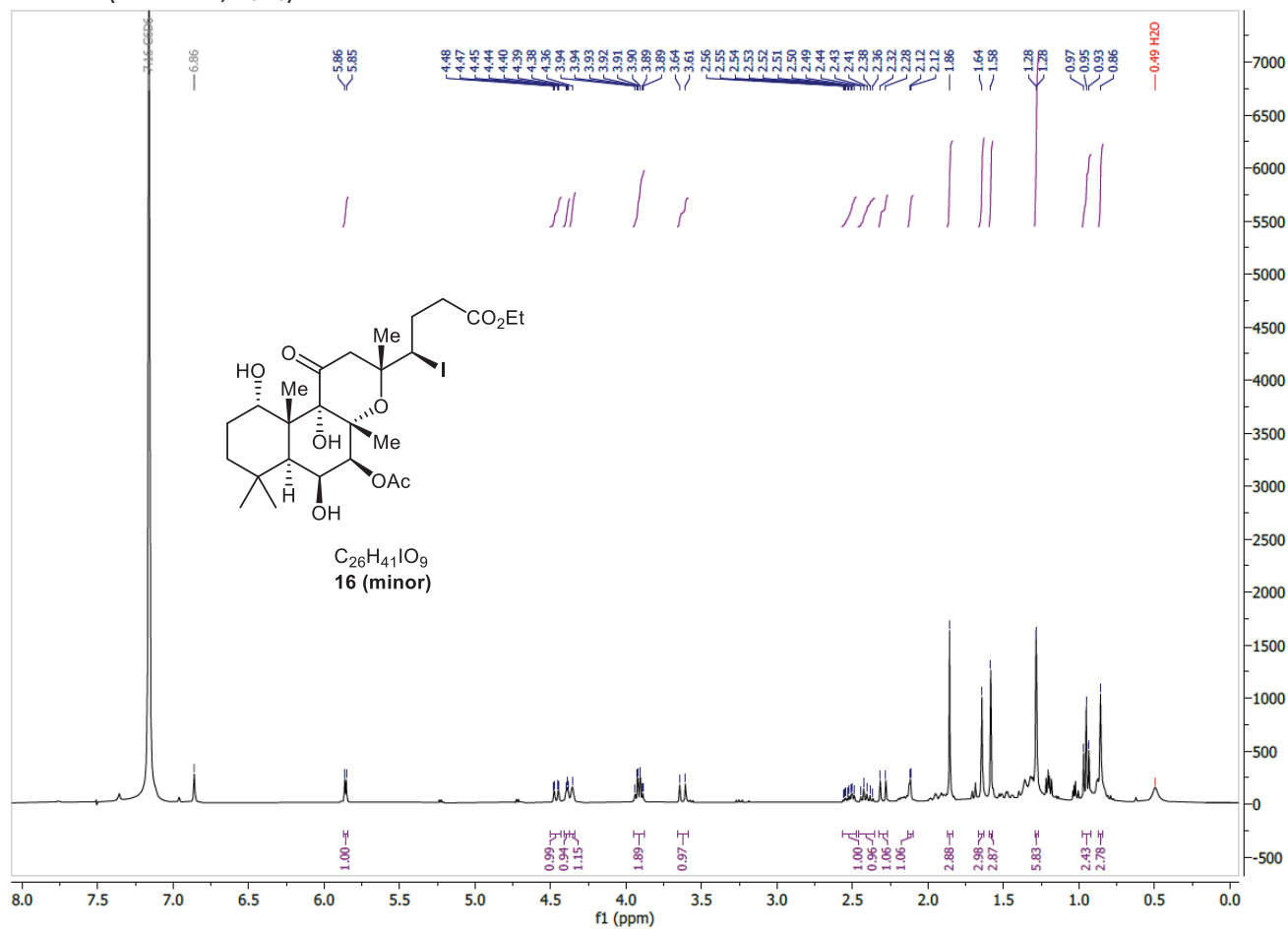
¹H NMR (400 MHz, C₆D₆)



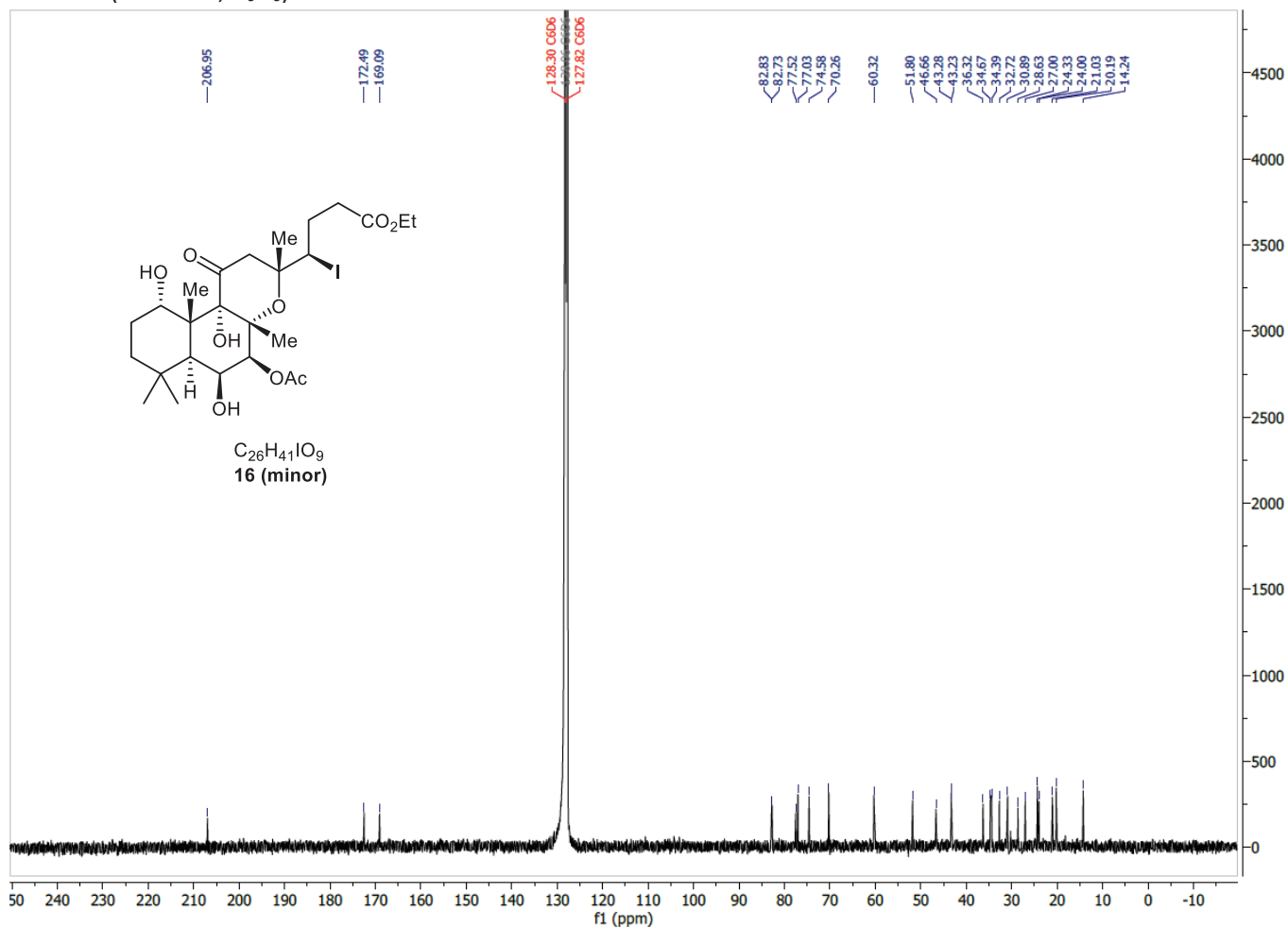
¹³C NMR (101 MHz, C₆D₆)



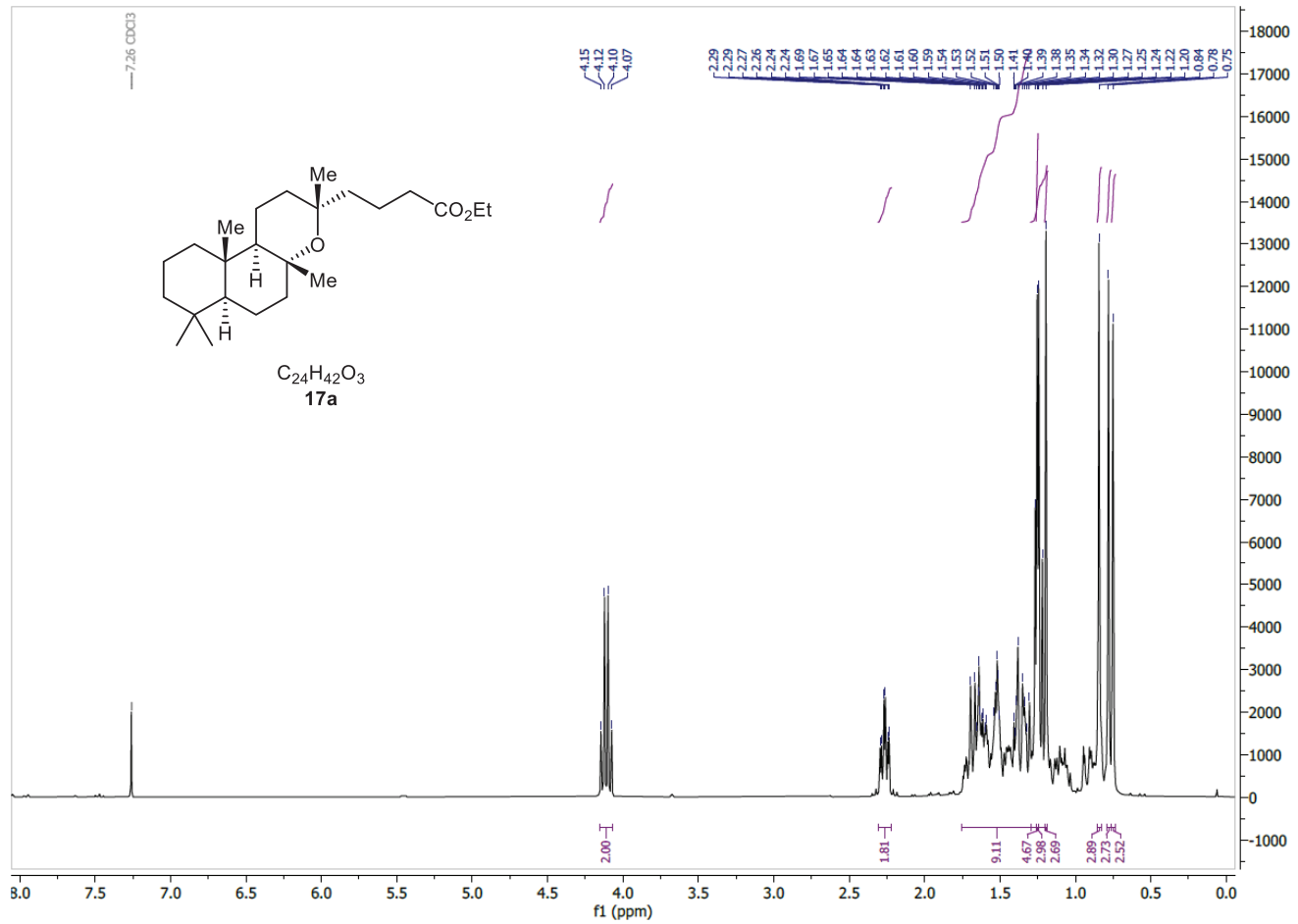
¹H NMR (400 MHz, C₆D₆)



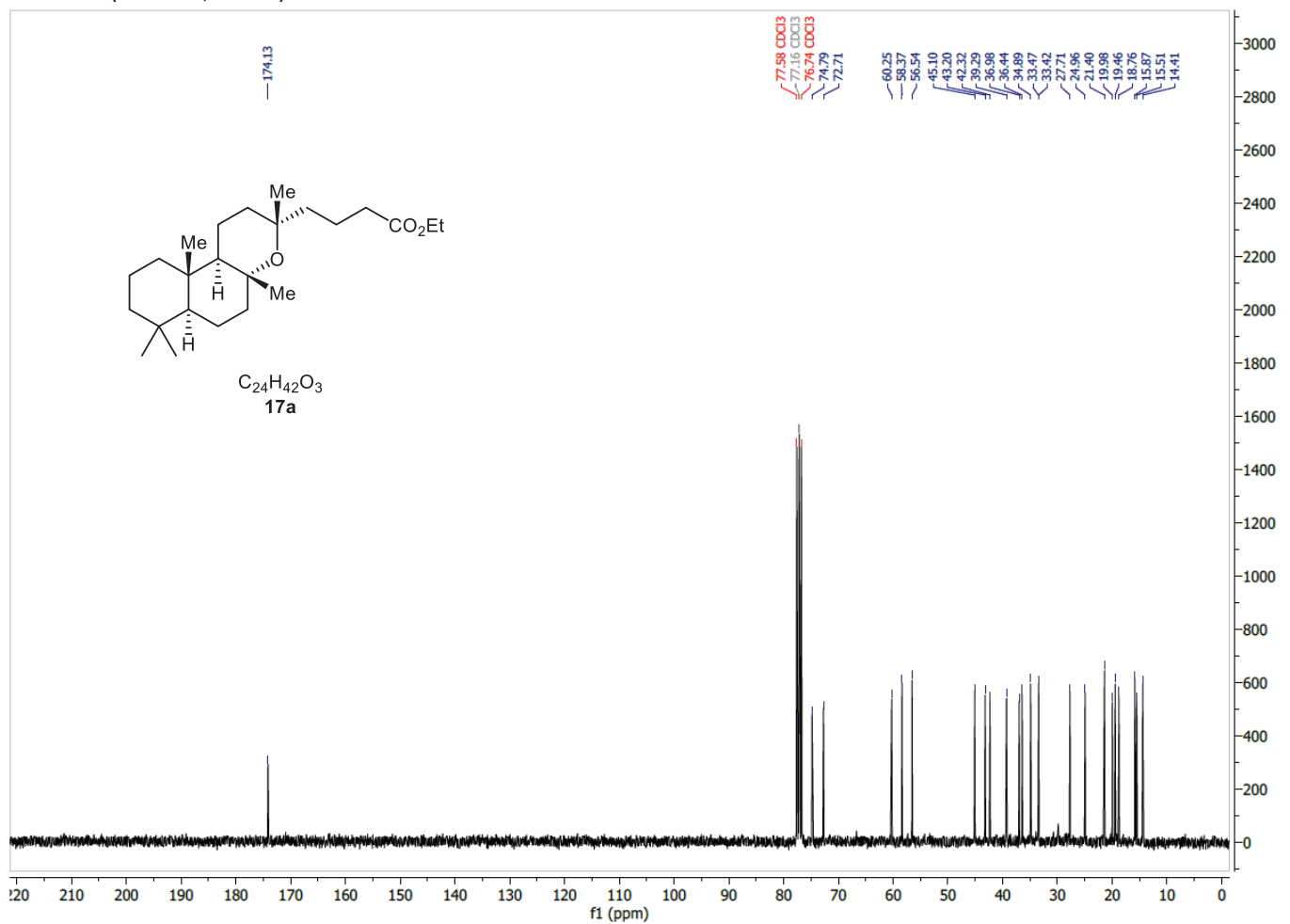
¹³C NMR (101 MHz, C₆D₆)



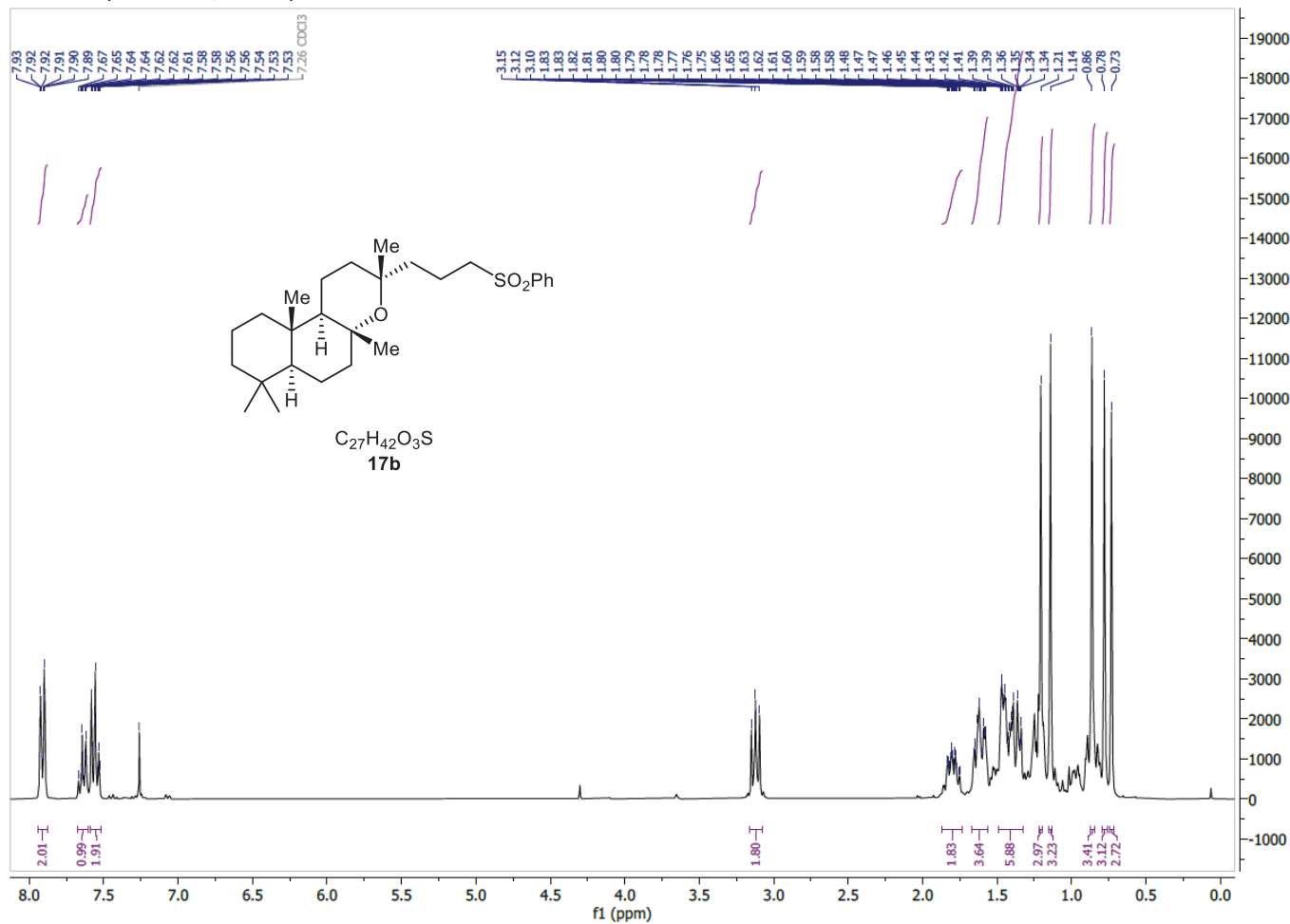
^1H NMR (300 MHz, CDCl_3)



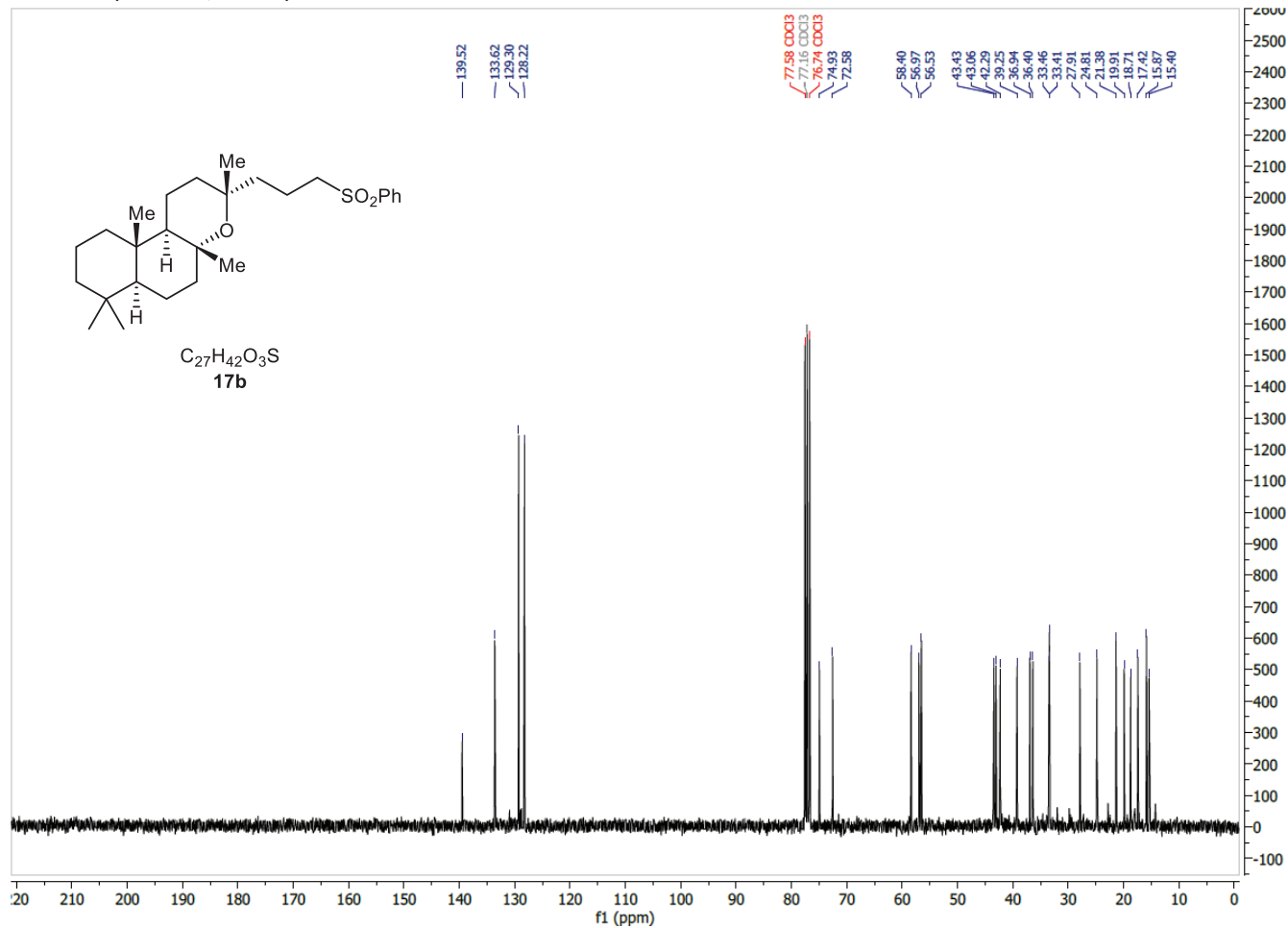
^{13}C NMR (75 MHz, CDCl_3)



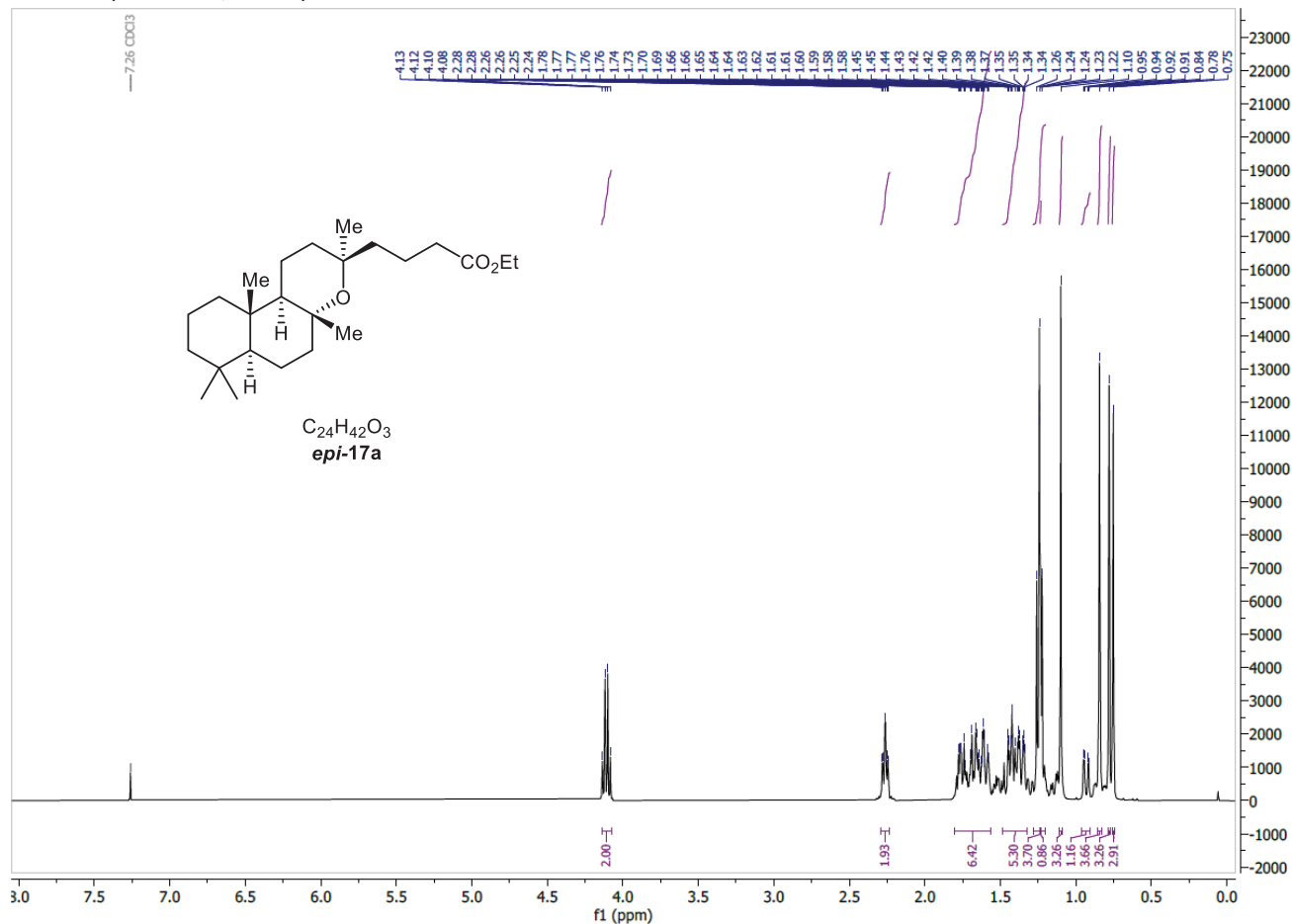
¹H NMR (300 MHz, CDCl₃)



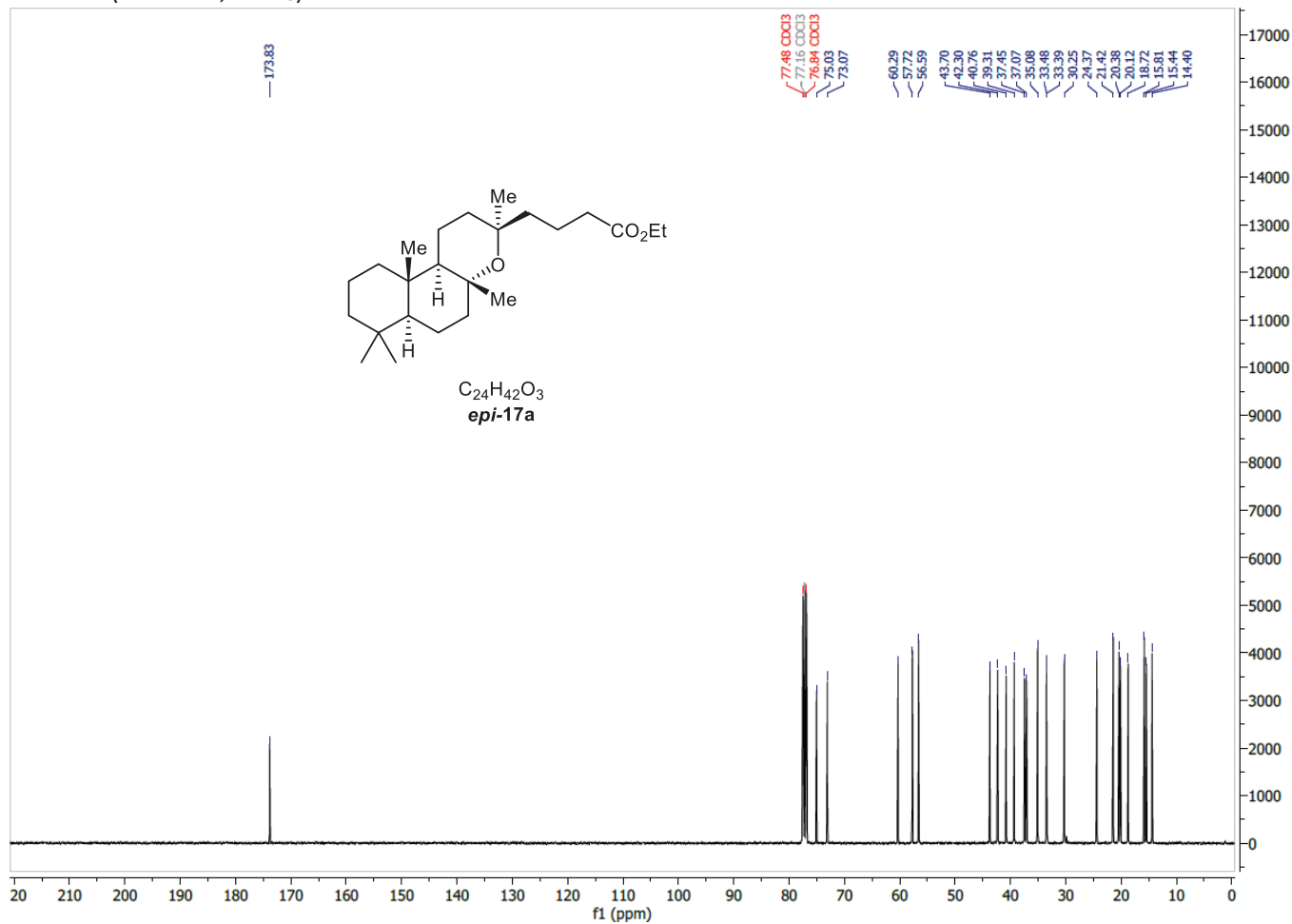
¹³C NMR (75 MHz, CDCl₃)



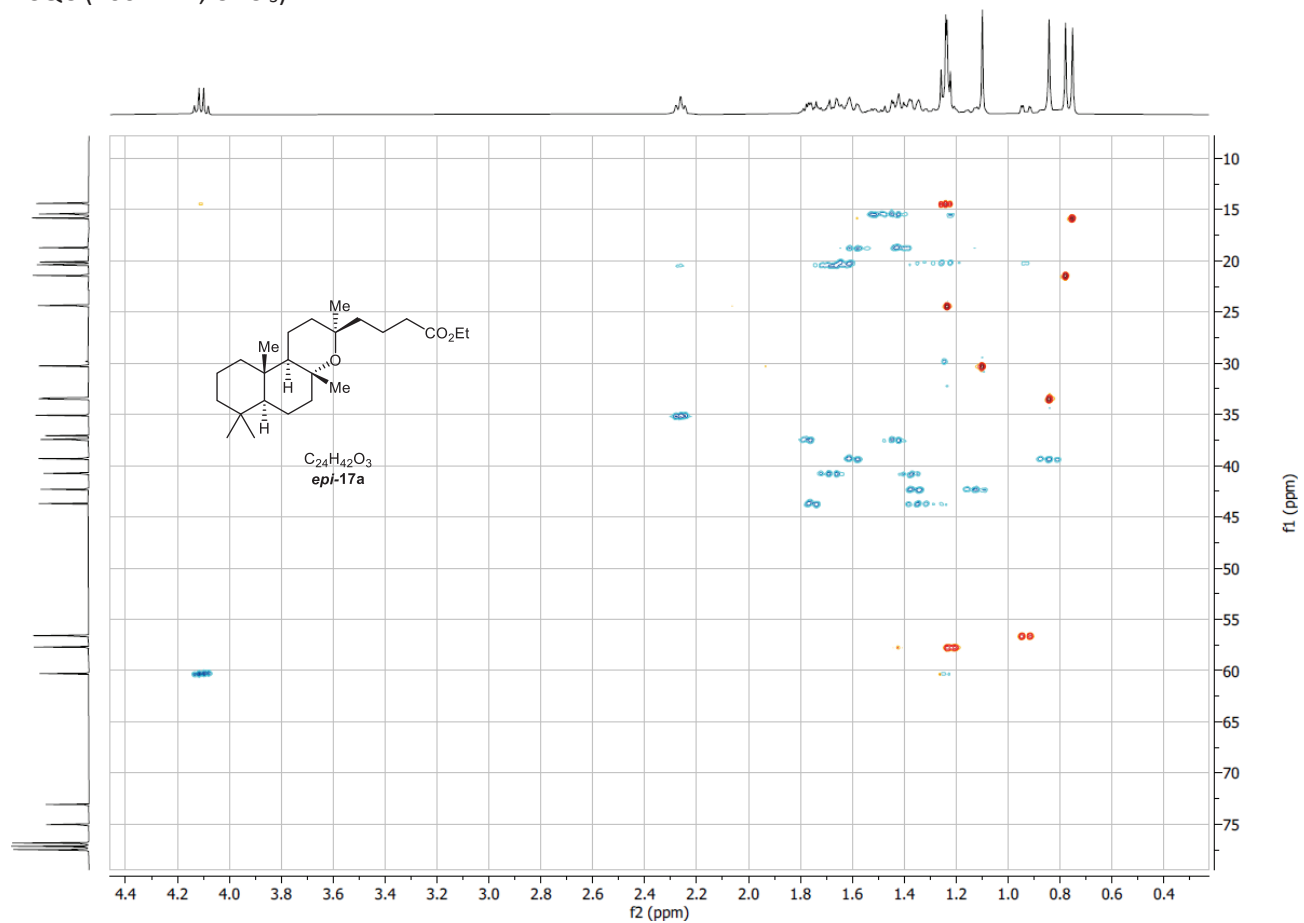
¹H NMR (400 MHz, CDCl₃)



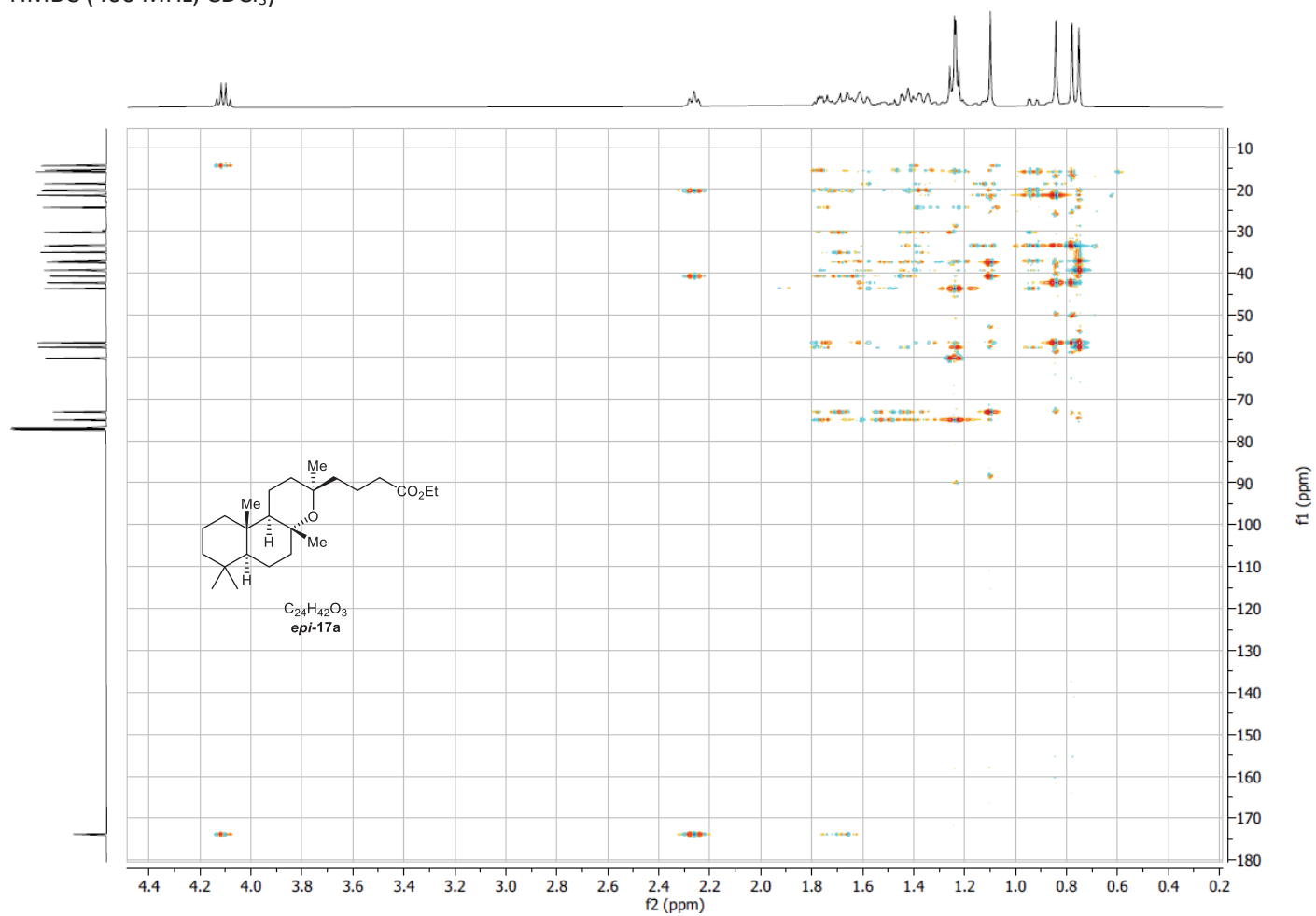
¹³C NMR (101 MHz, CDCl₃)



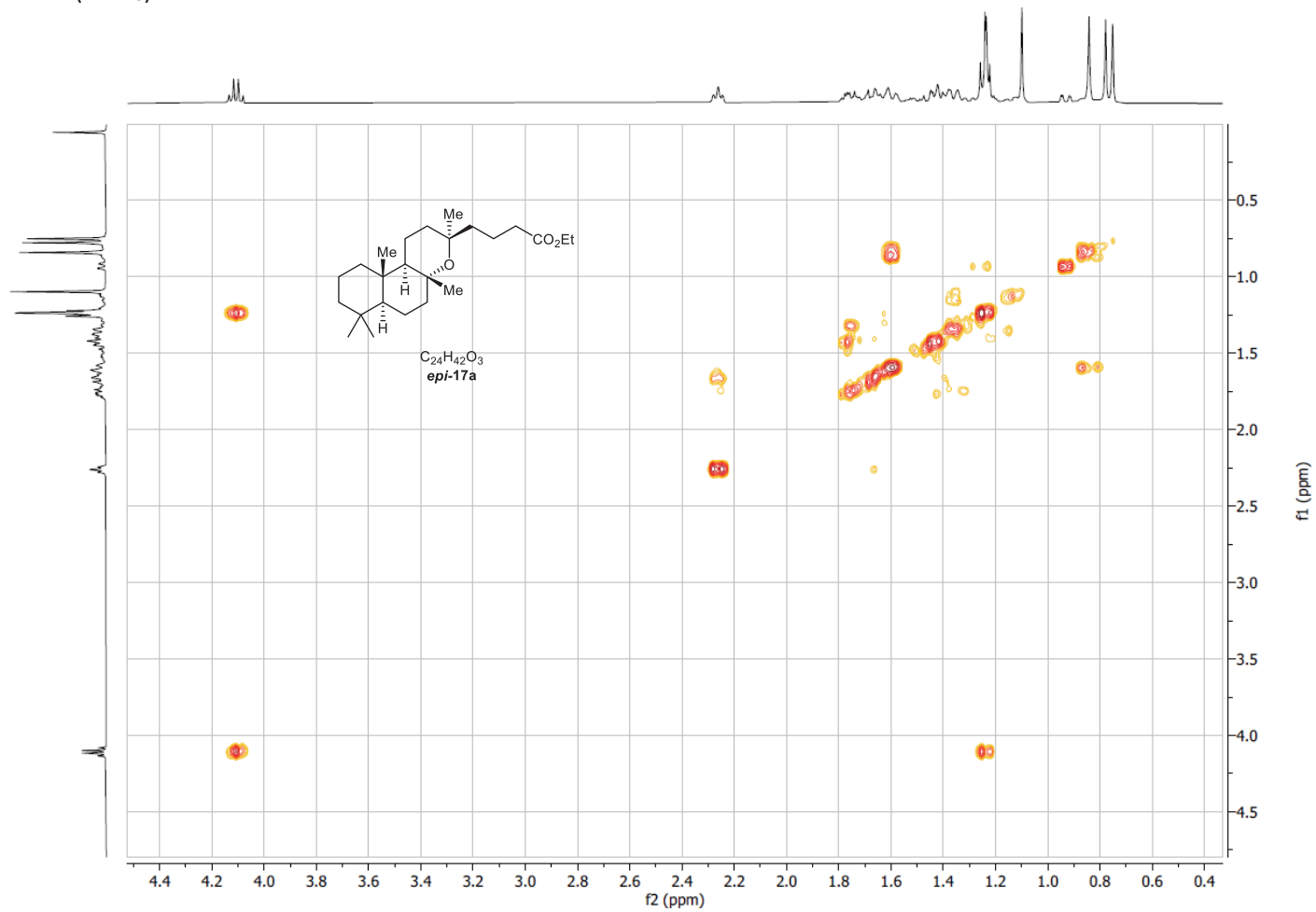
HSQC (400 MHz, CDCl₃)



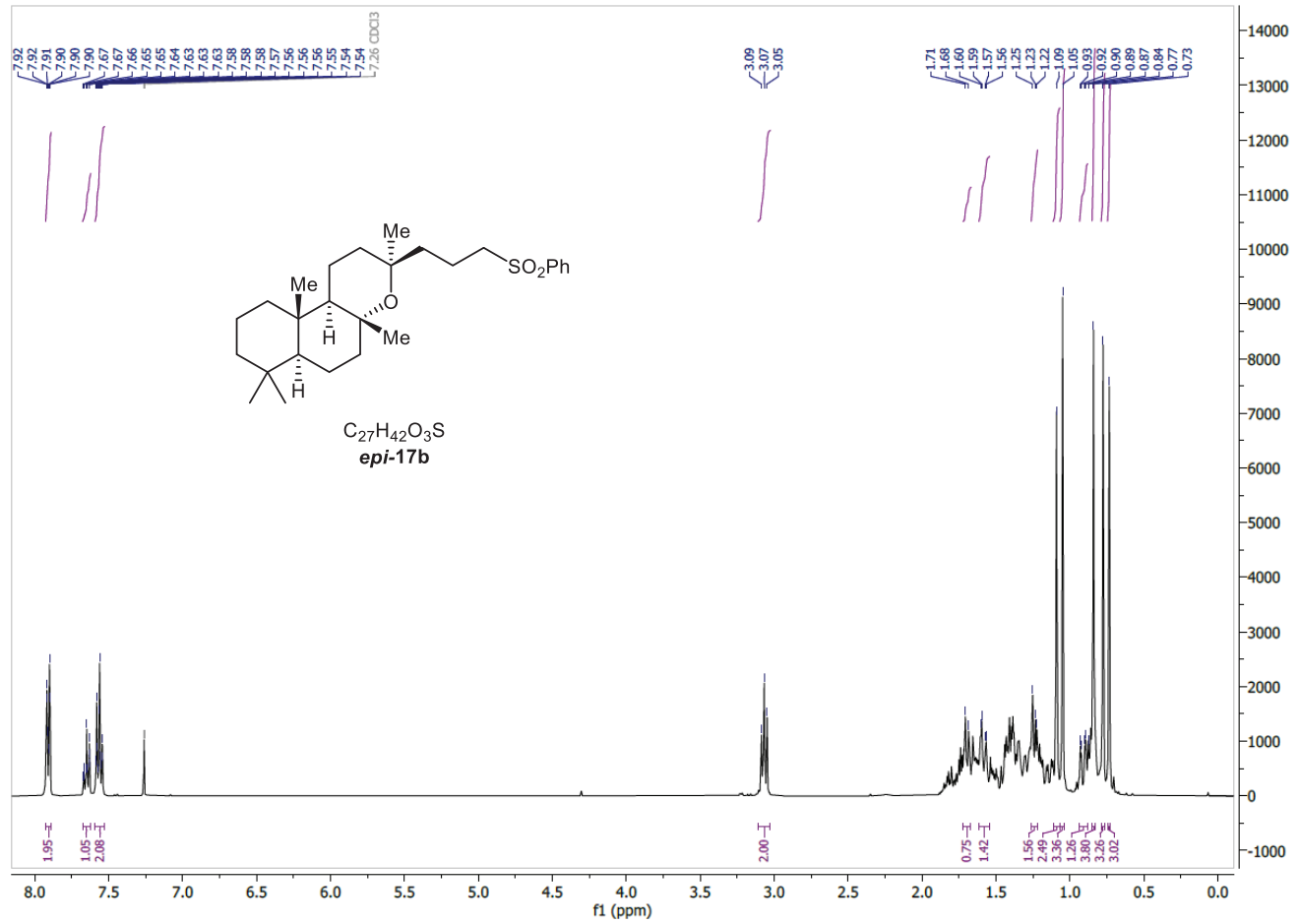
HMBC (400 MHz, CDCl₃)



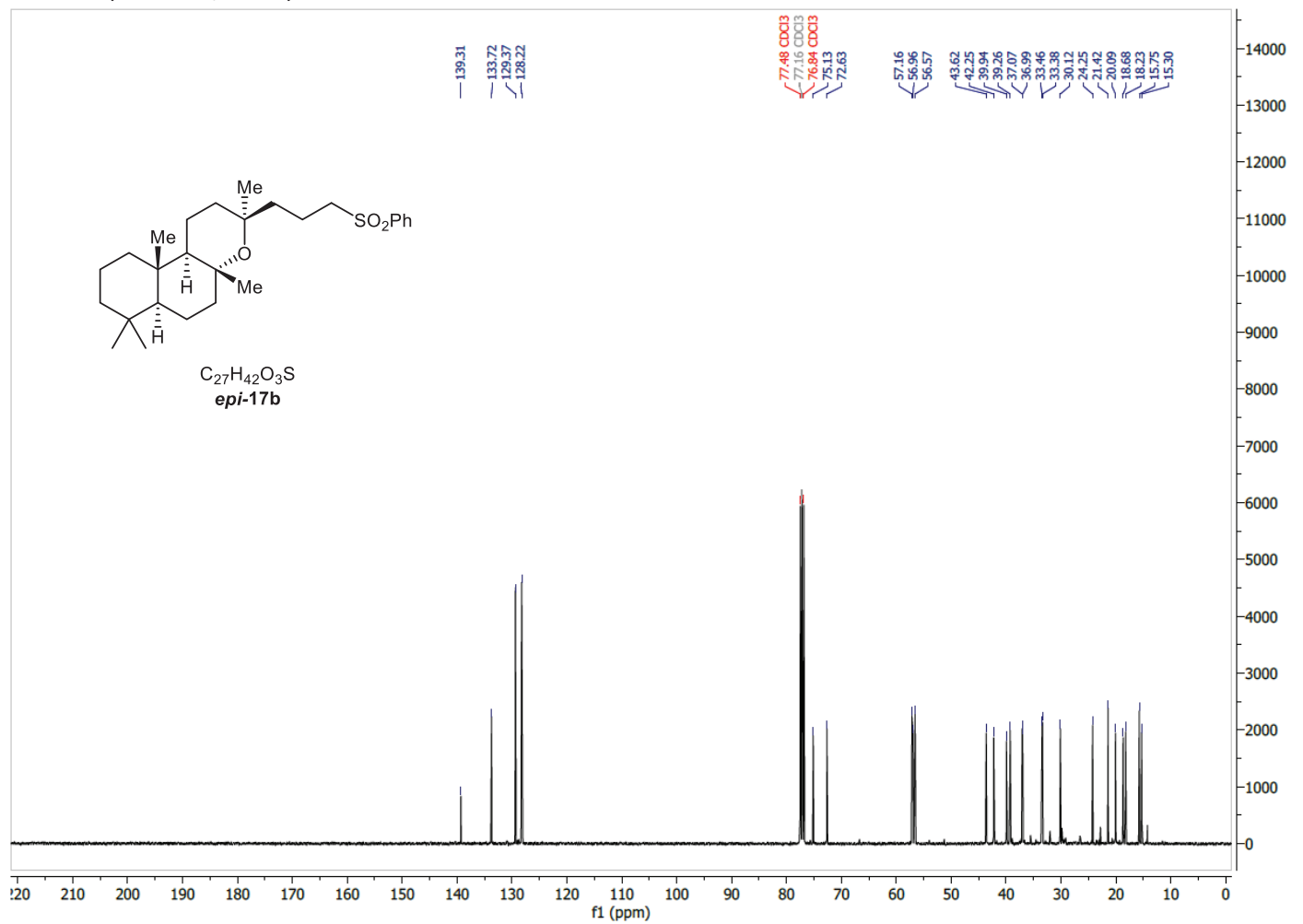
COSY (CDCl₃)



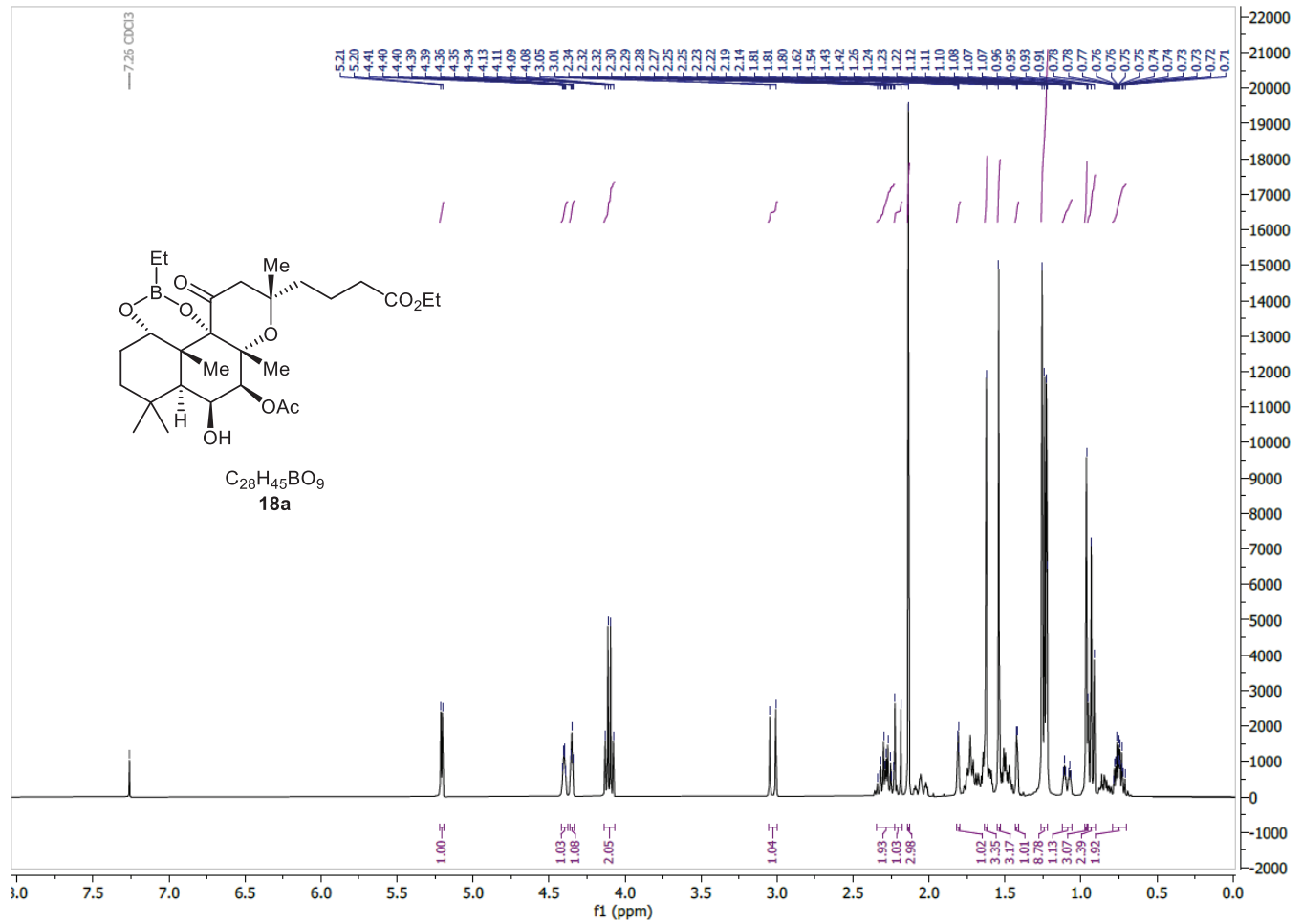
^1H NMR (400 MHz, CDCl_3)



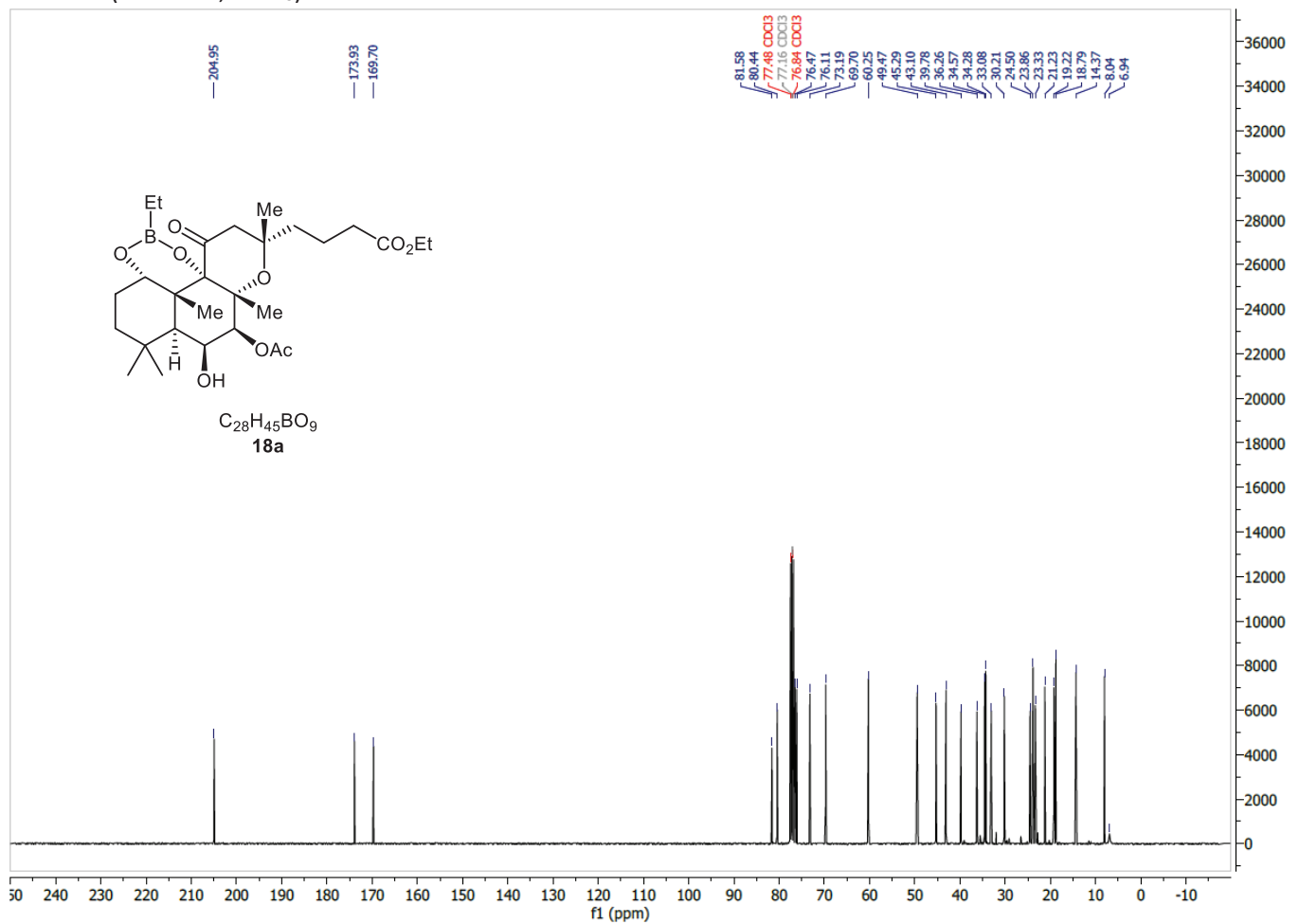
^{13}C NMR (101 MHz, CDCl_3)



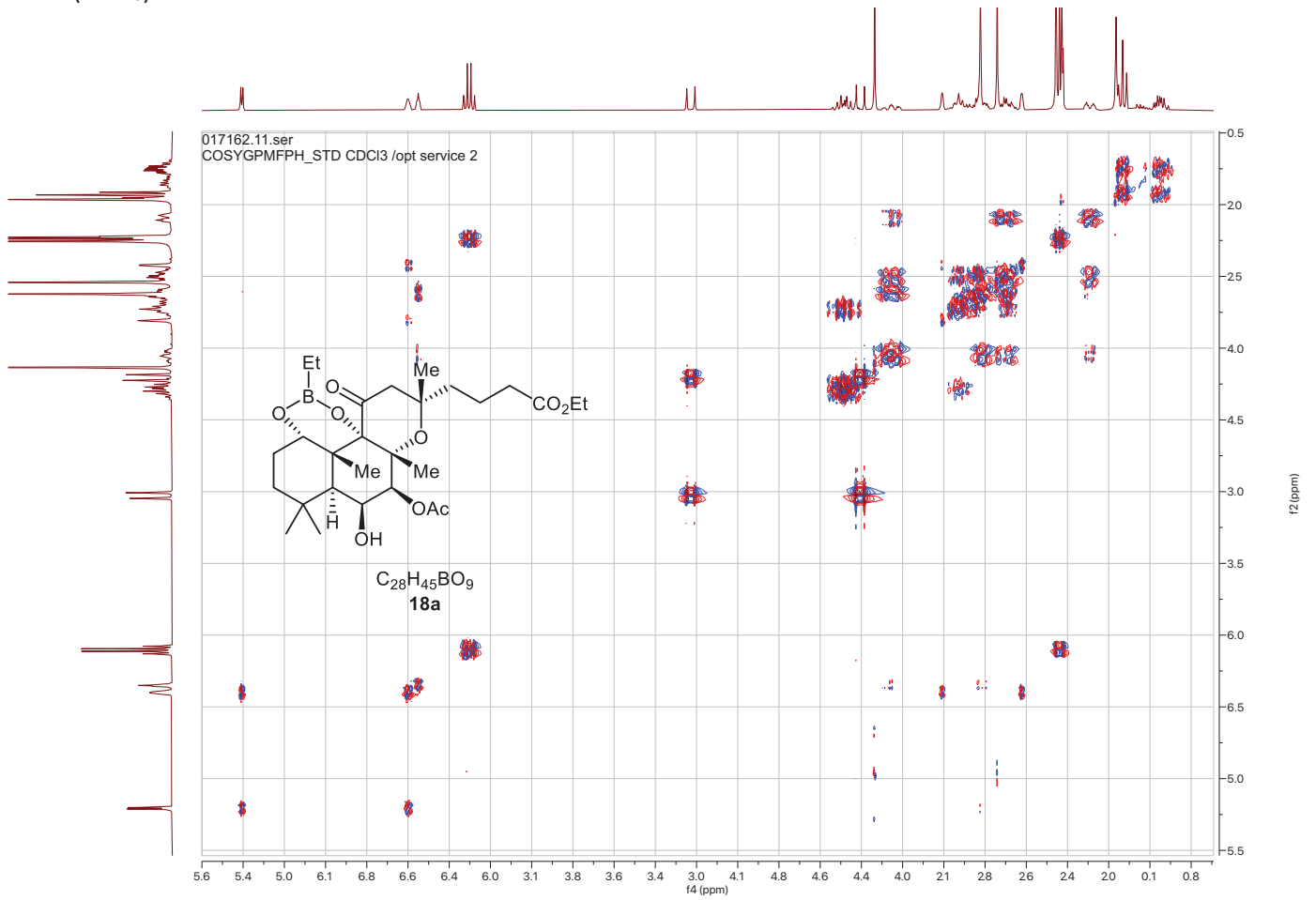
¹H NMR (400 MHz, CDCl₃)



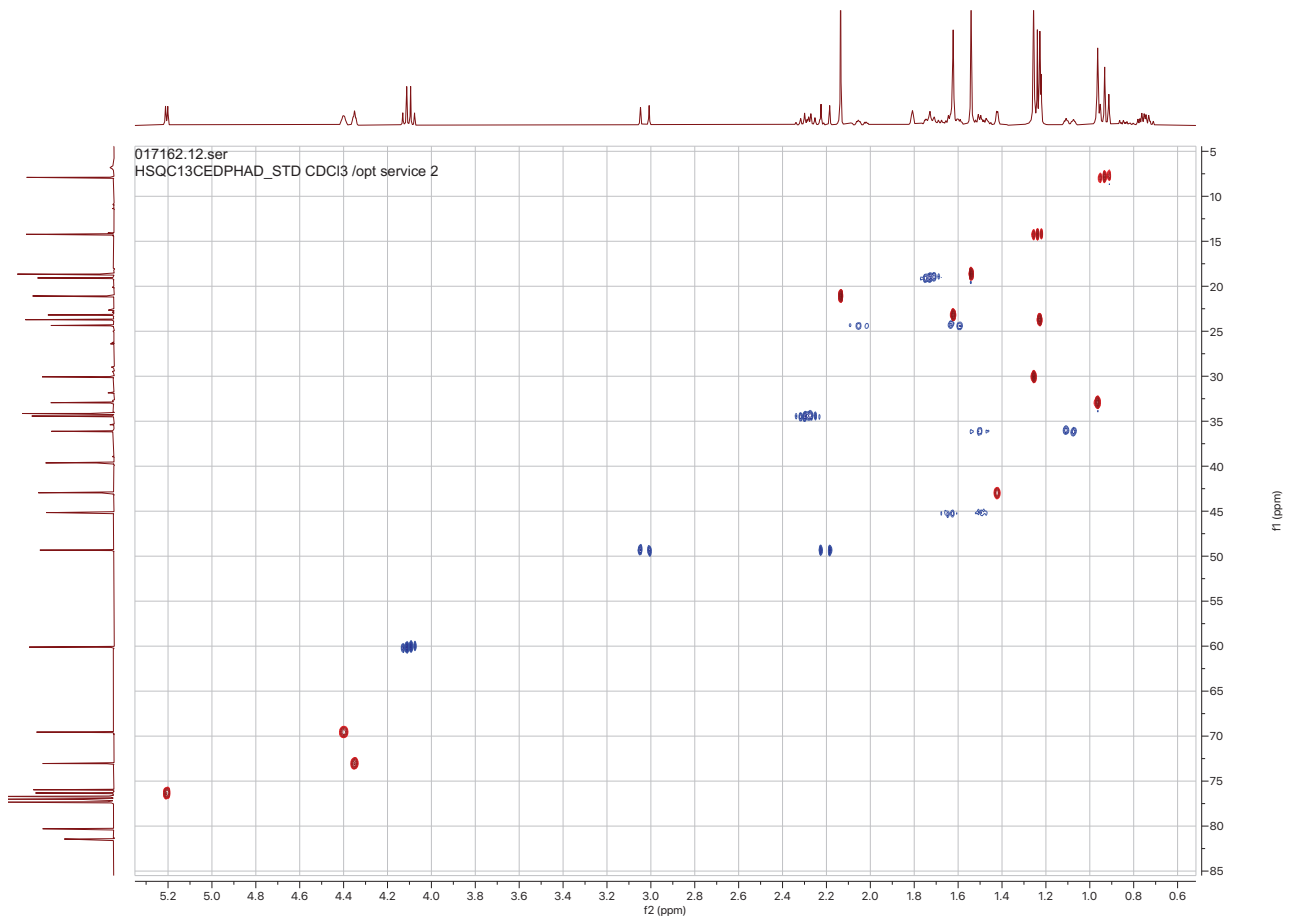
¹³C NMR (101 MHz, CDCl₃)



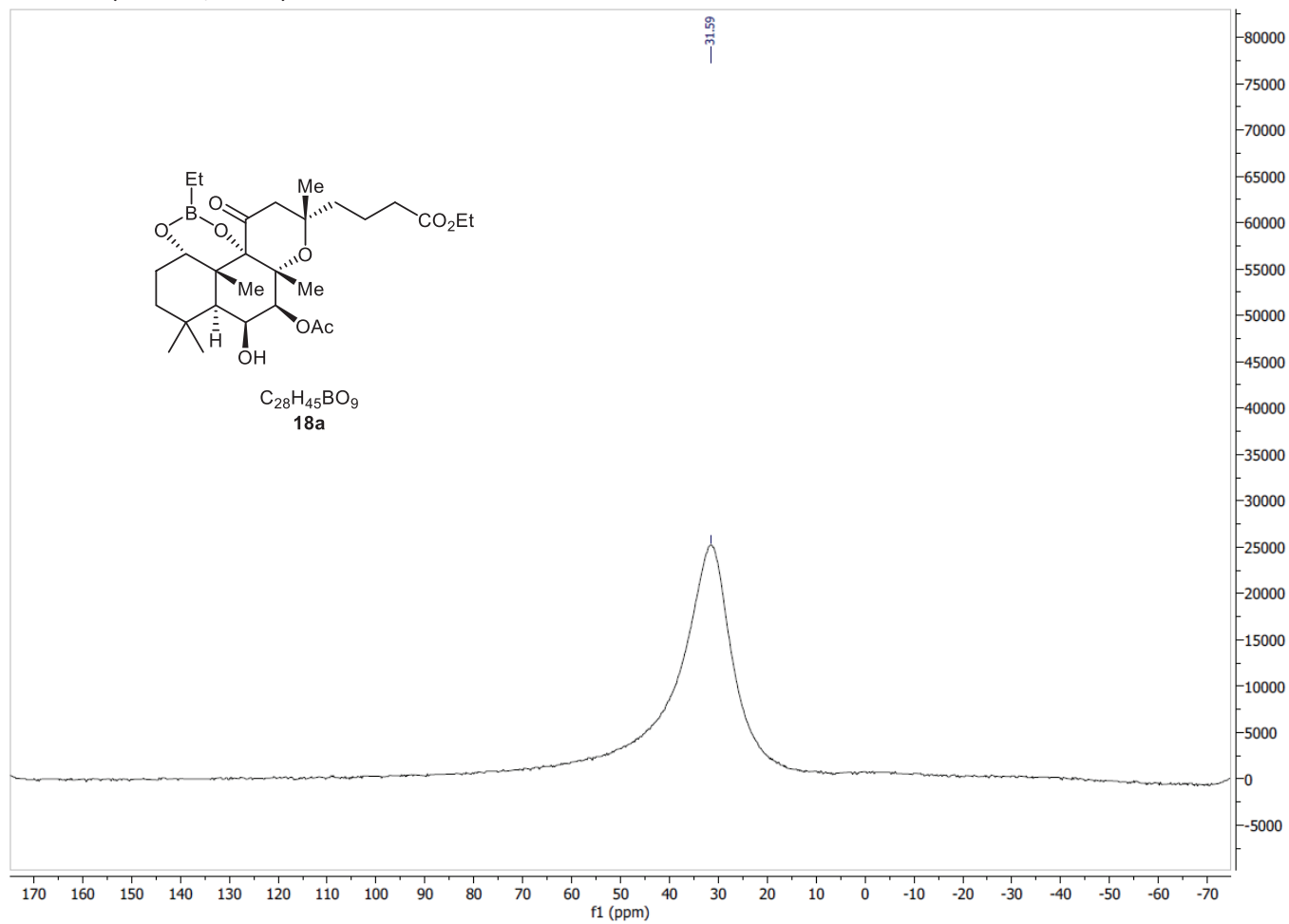
COSY (CDCl₃):



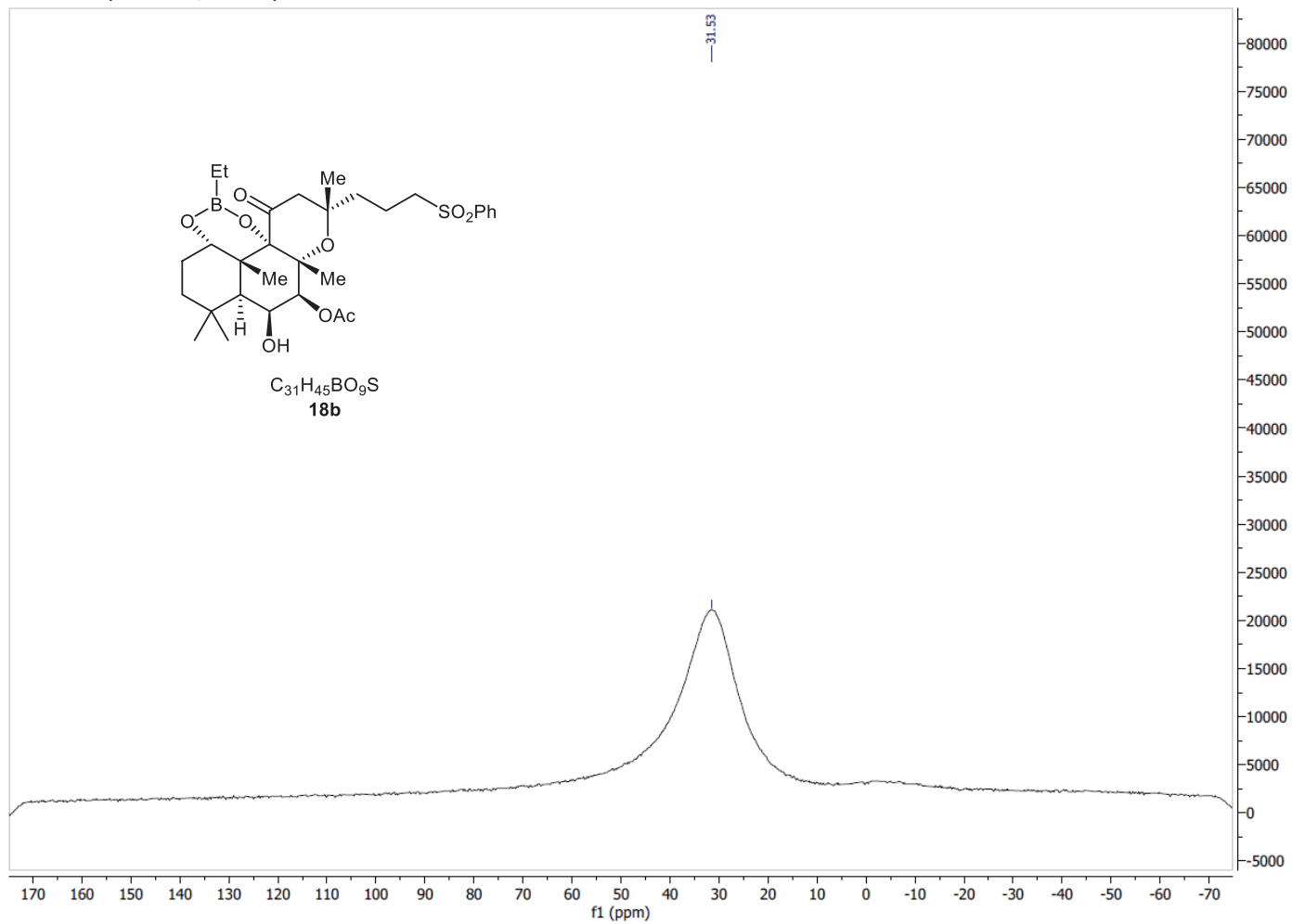
HSQC (CDCl₃):



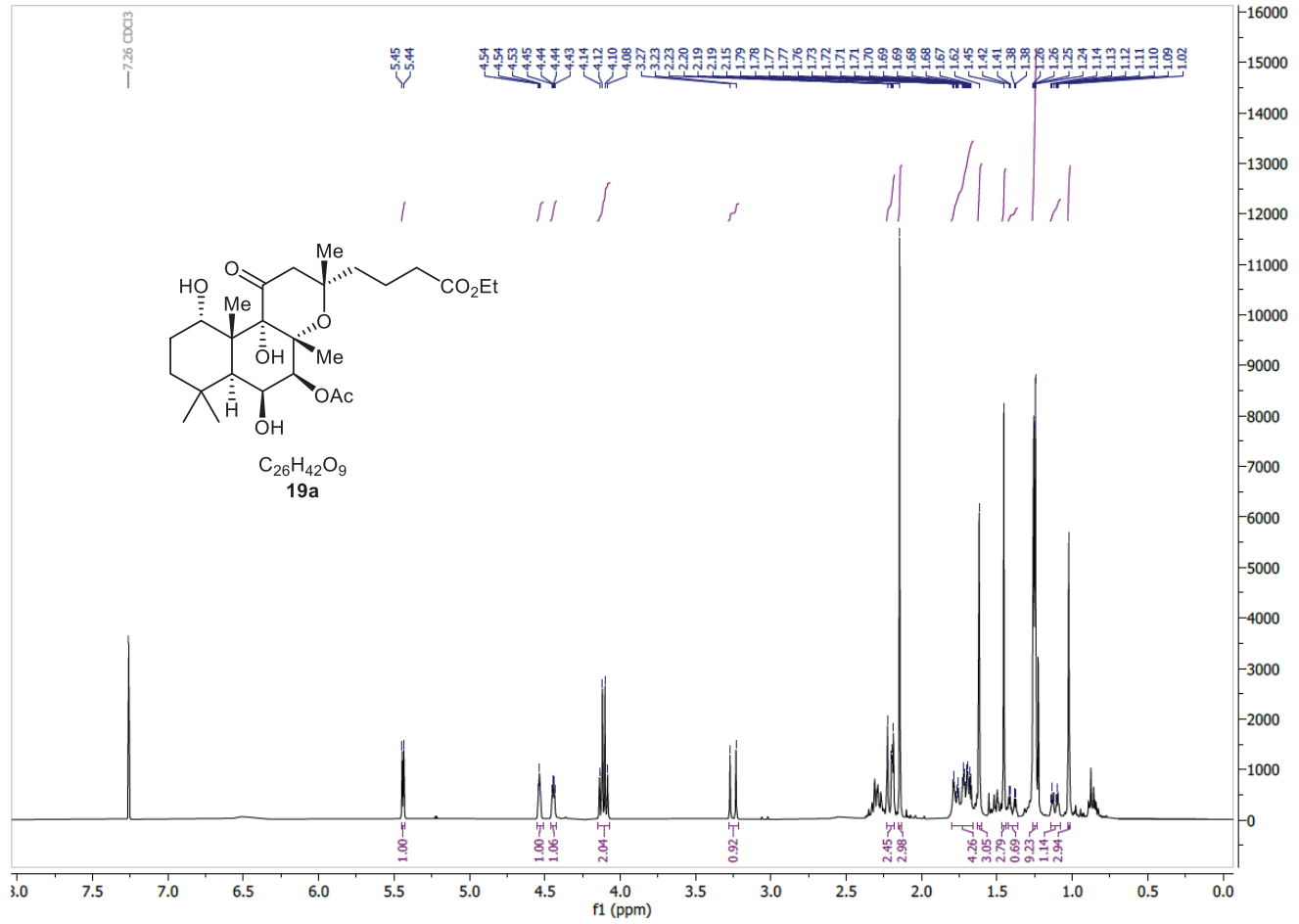
^{11}B NMR (96 MHz, CDCl_3)



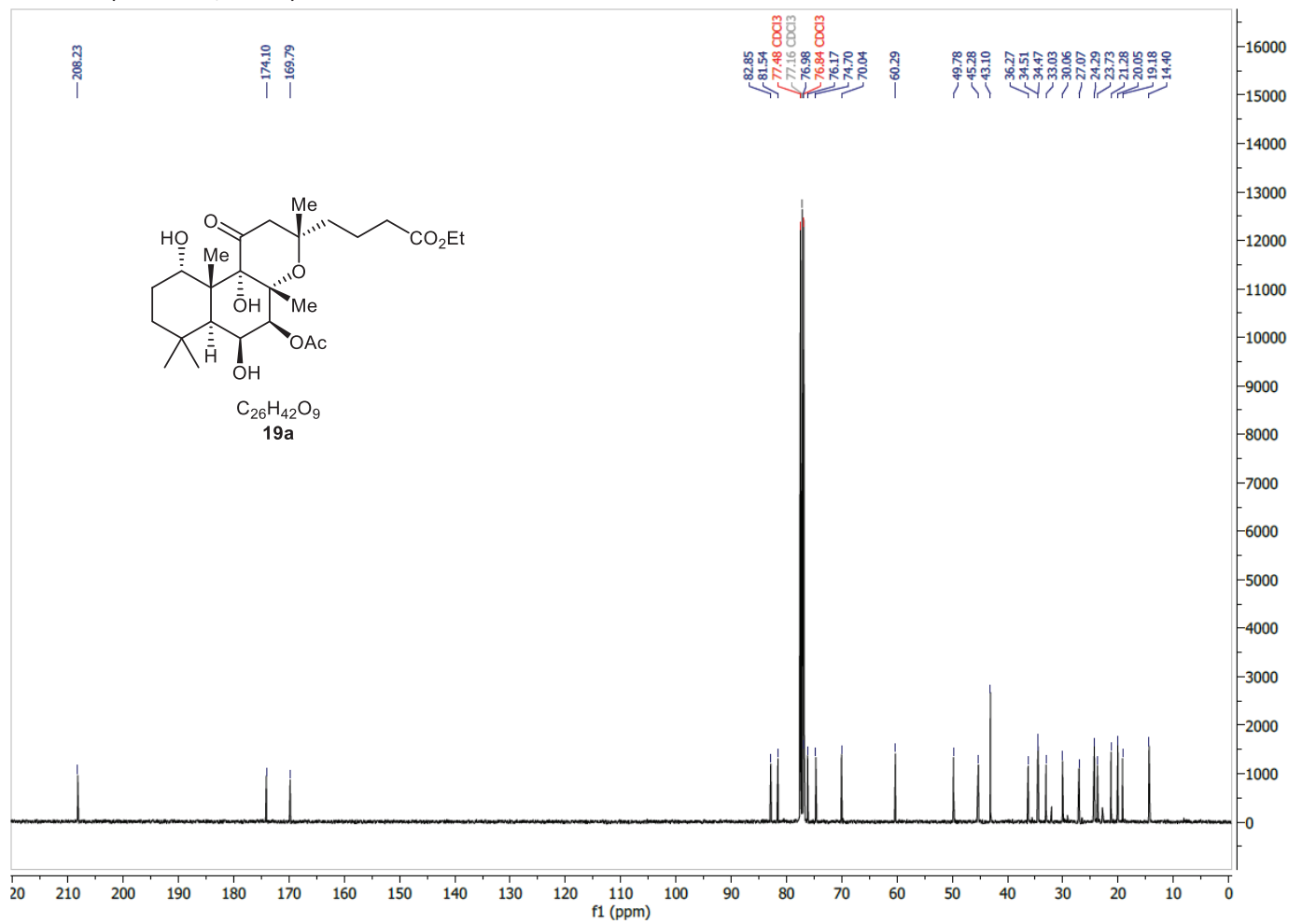
^{11}B NMR (96 MHz, CDCl_3)



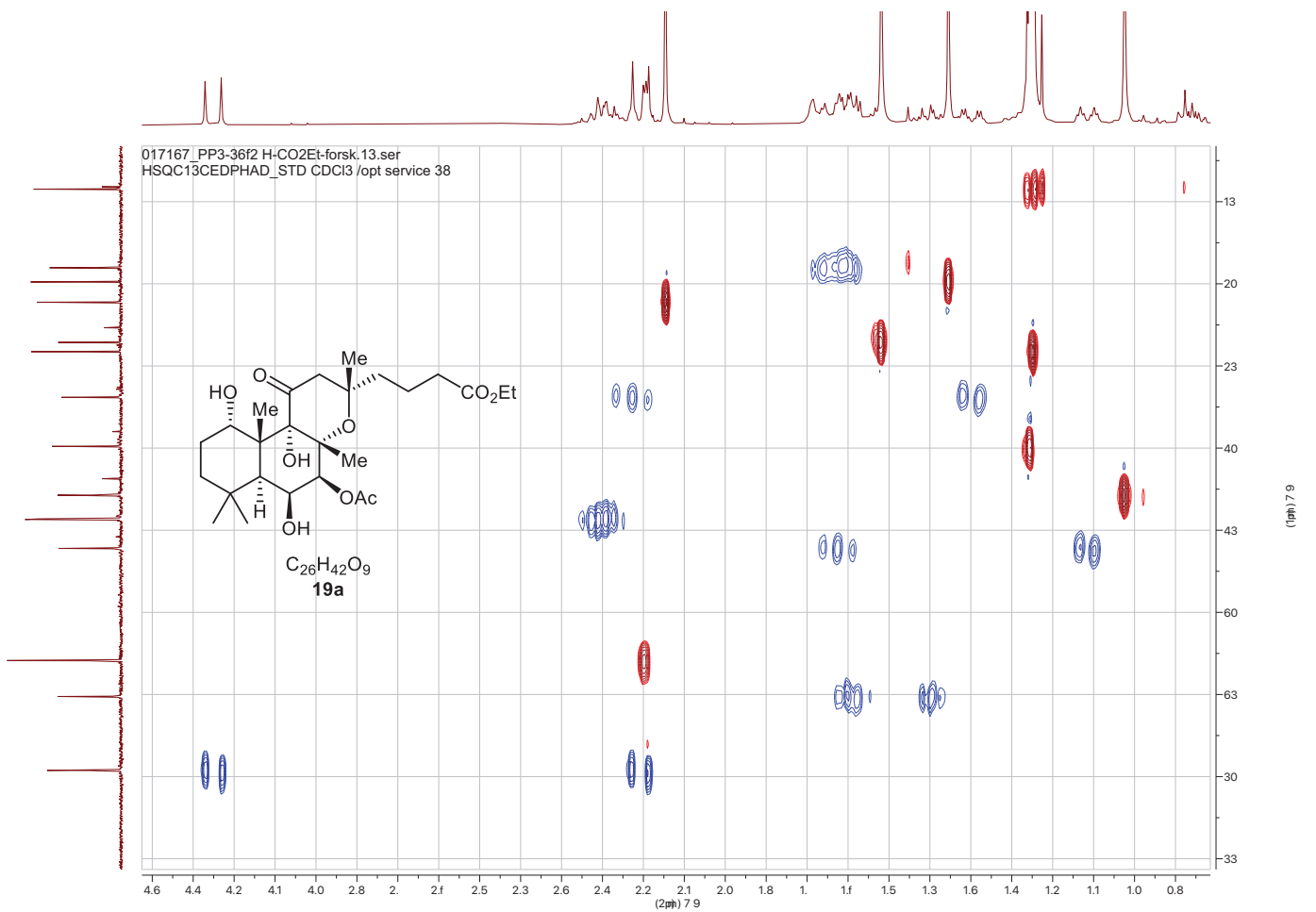
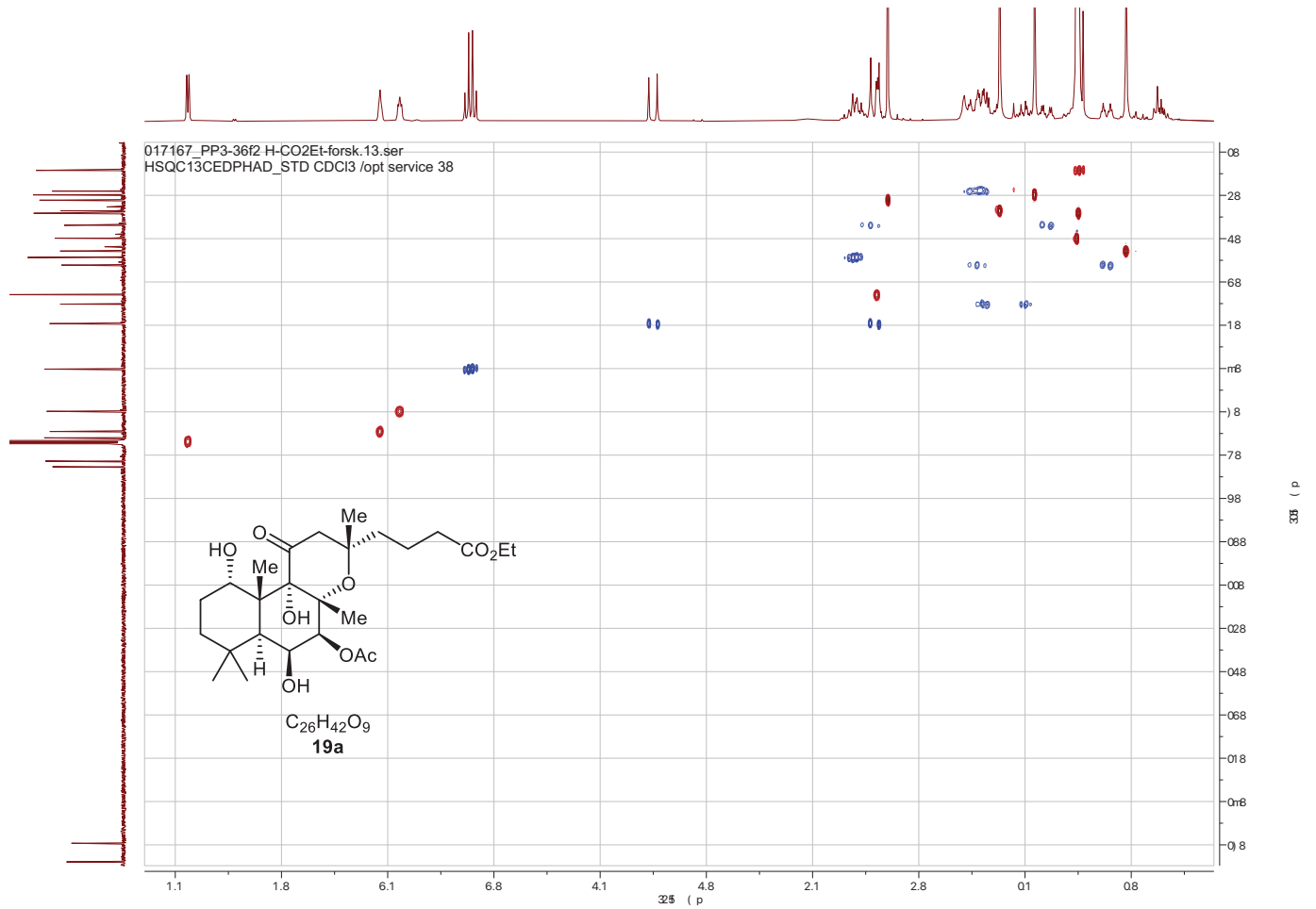
¹H NMR (400 MHz, CDCl₃)



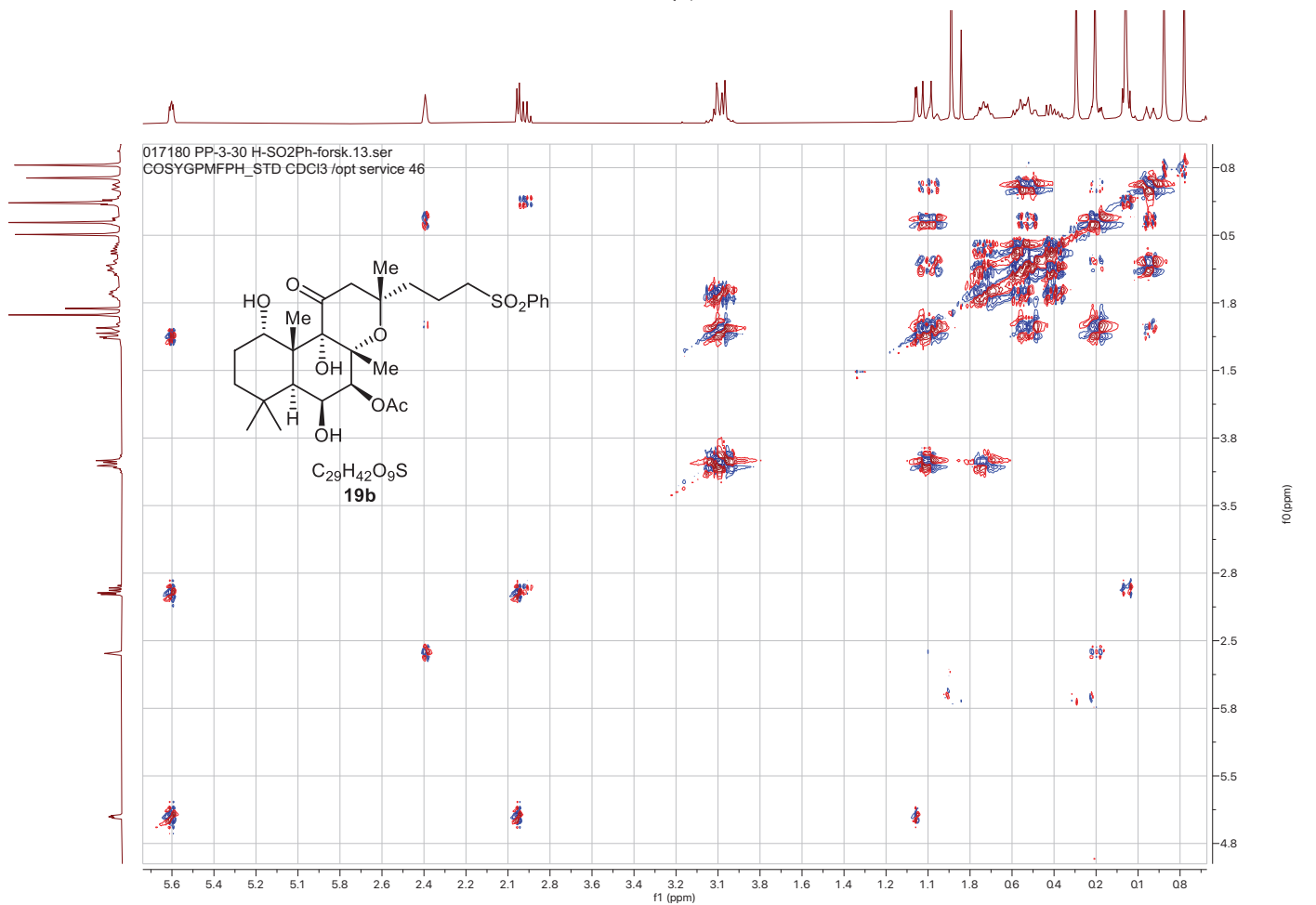
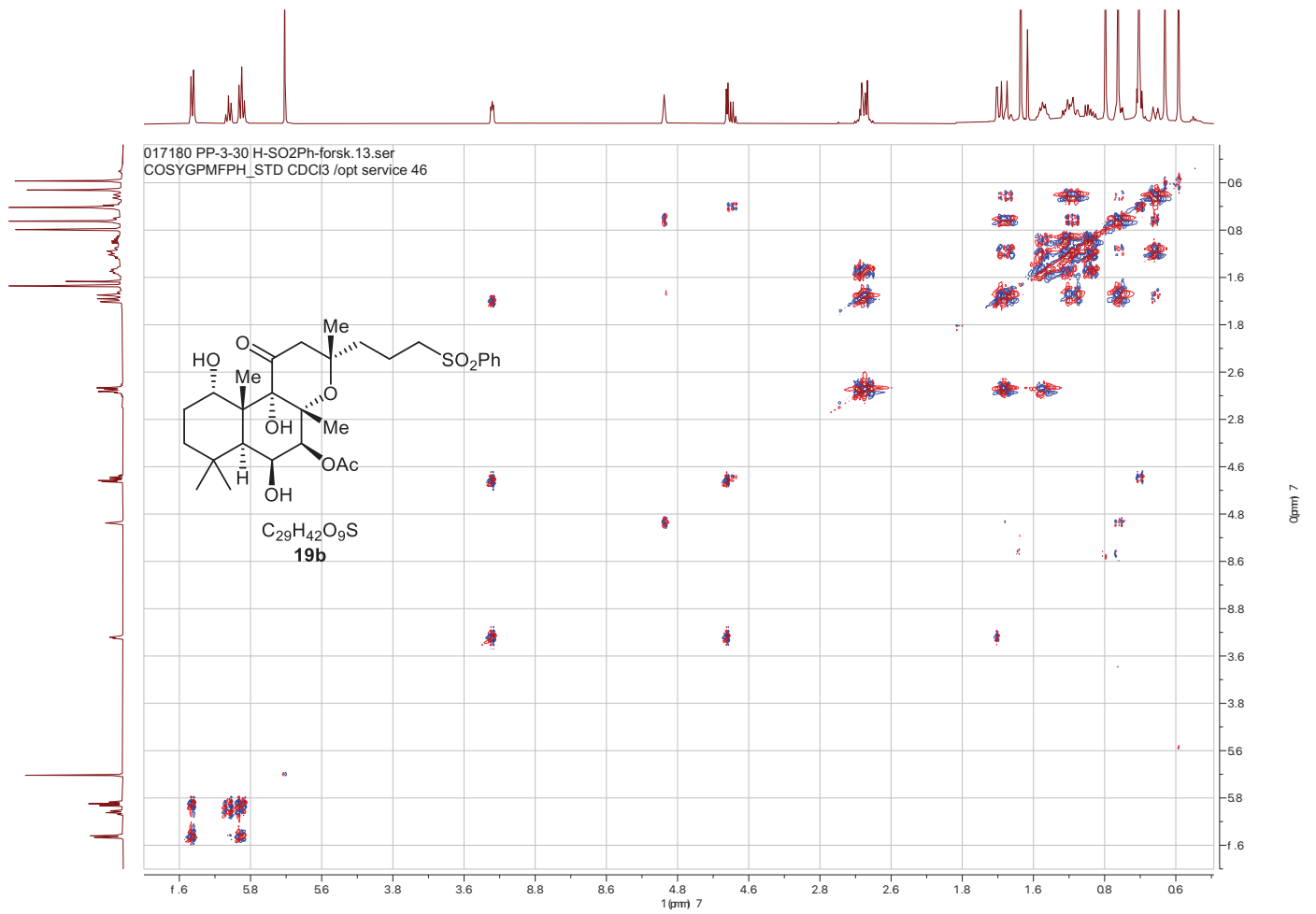
¹³C NMR (101 MHz, CDCl₃)



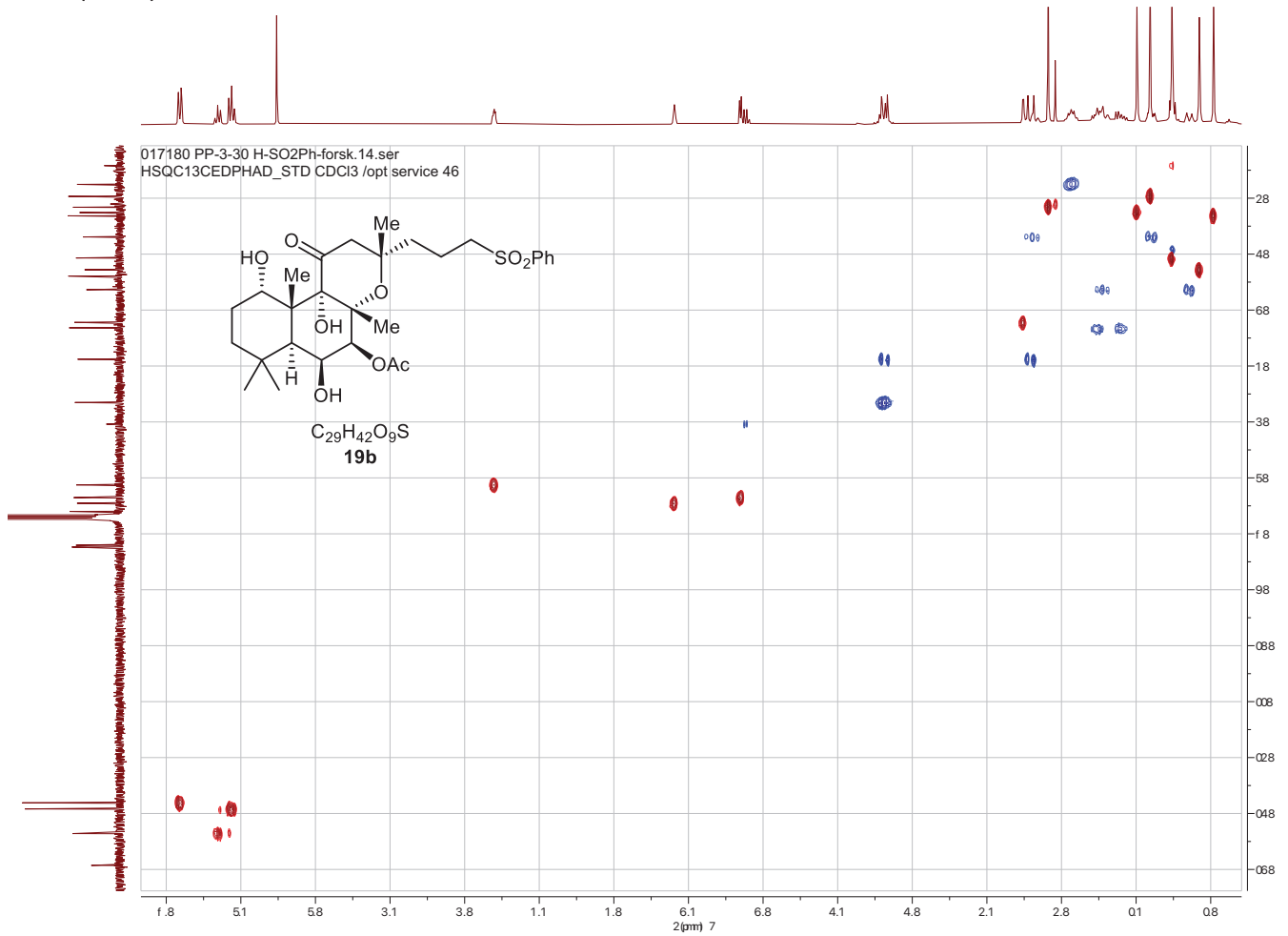
HSQC (CDCl₃):



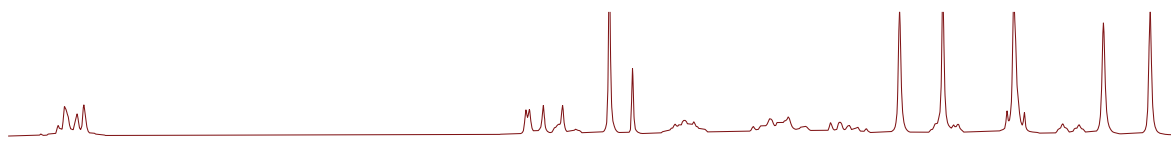
COSY (CDCl₃):



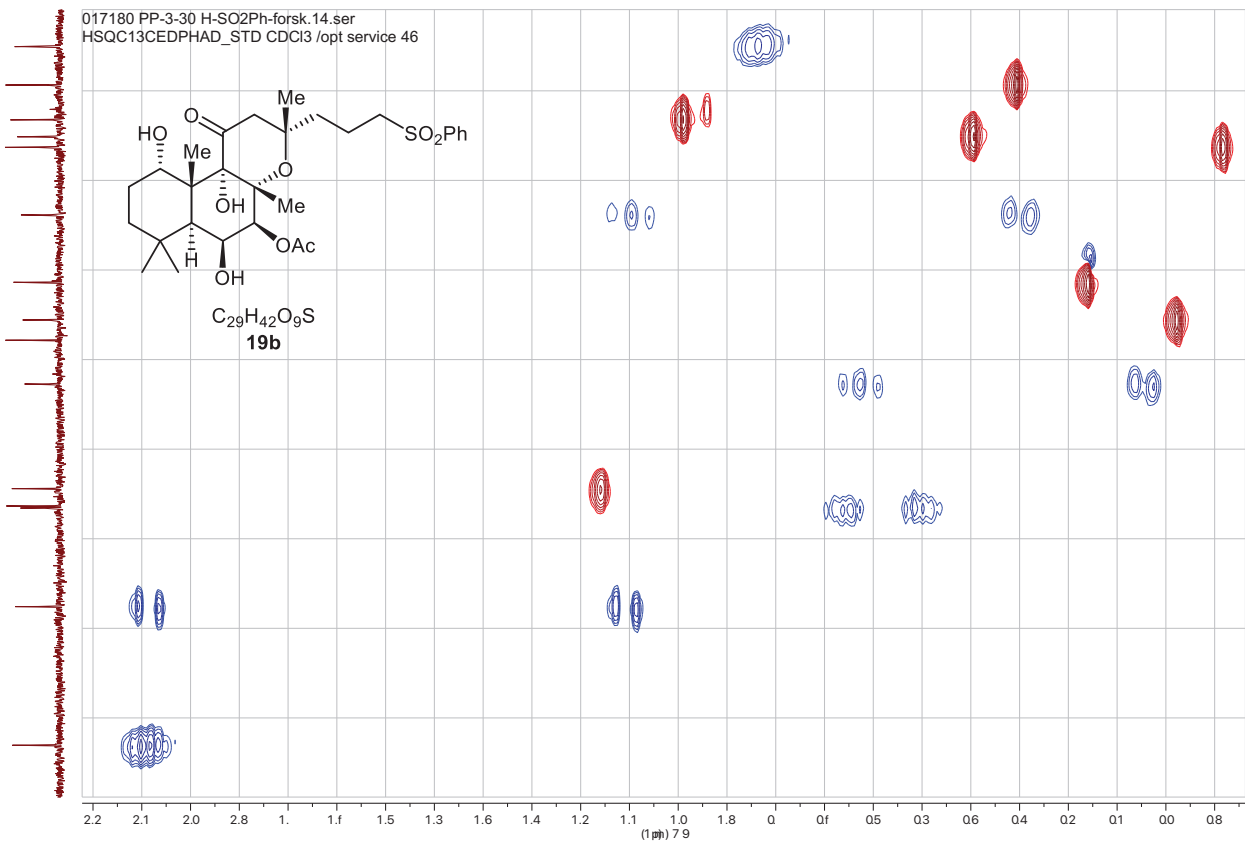
HSQC (CDCl₃):



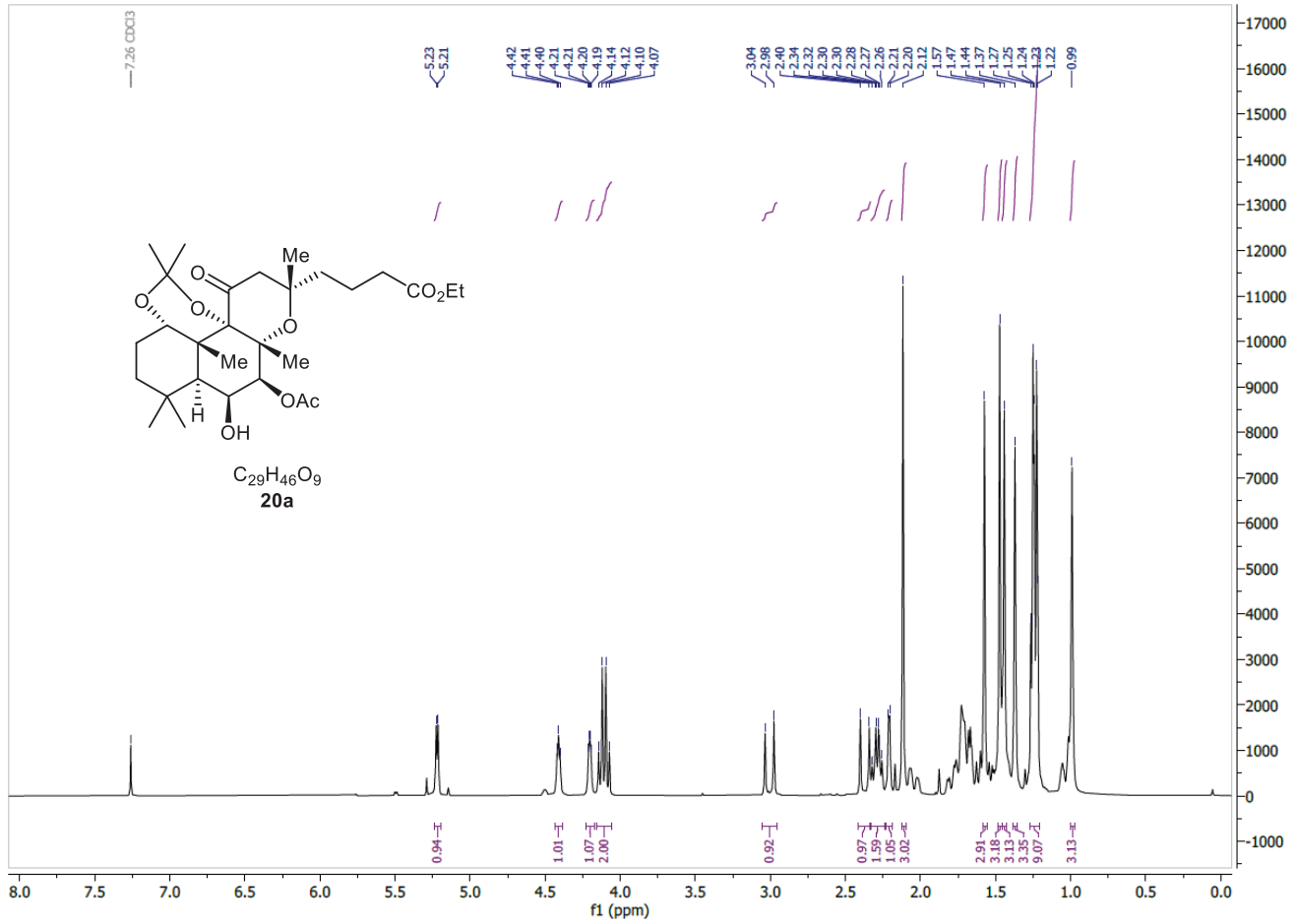
0ppm 7



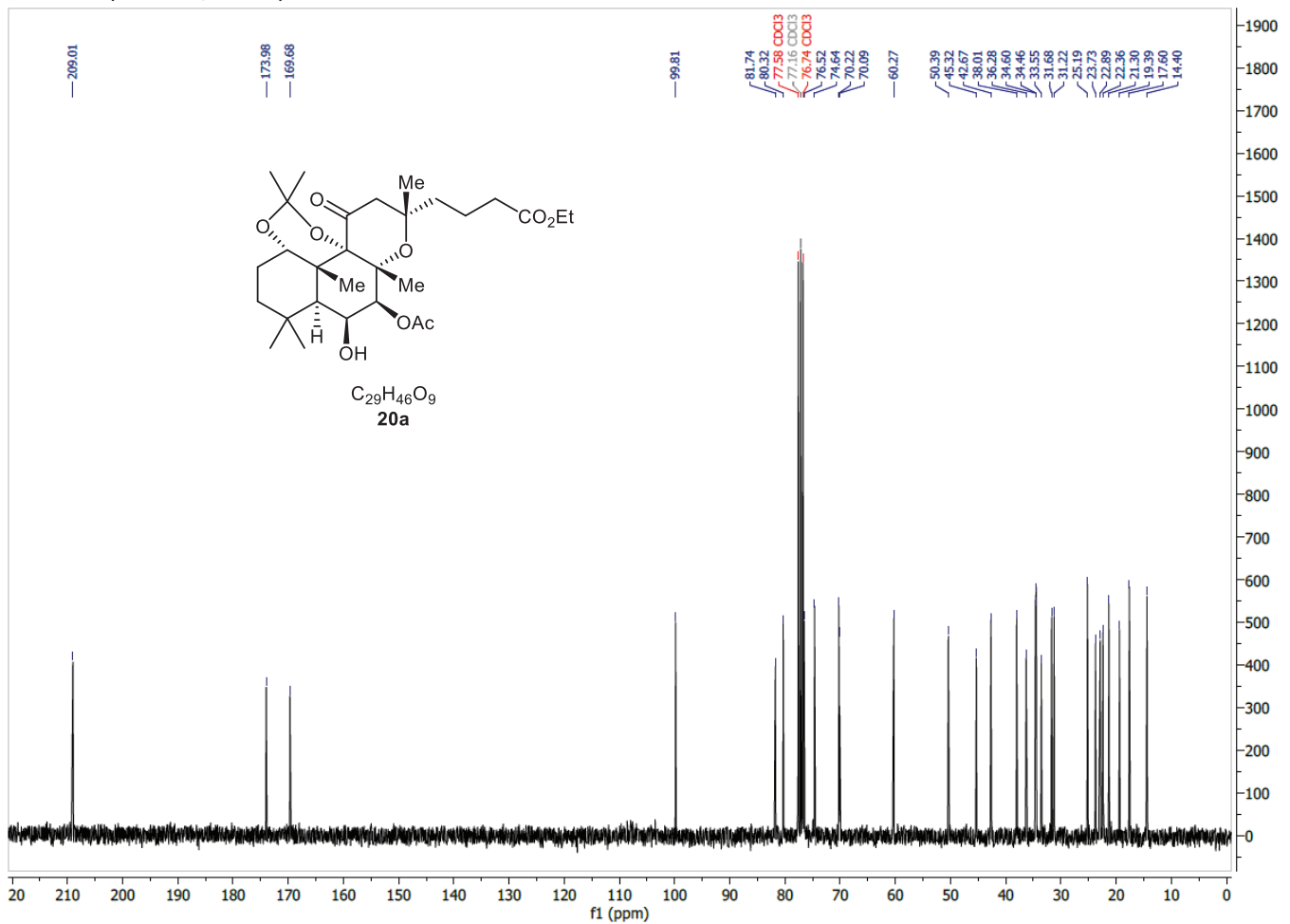
0ppm 7 9



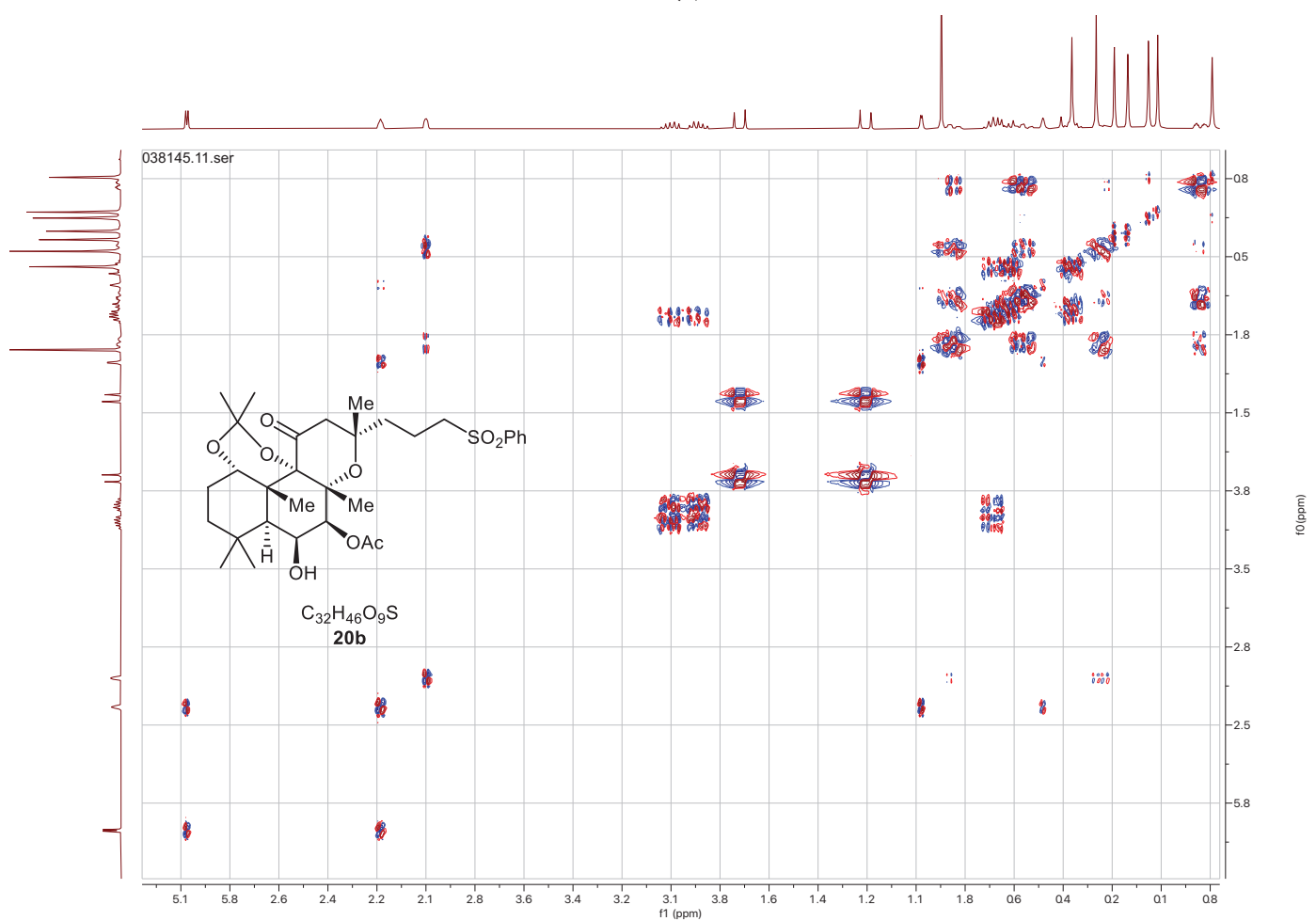
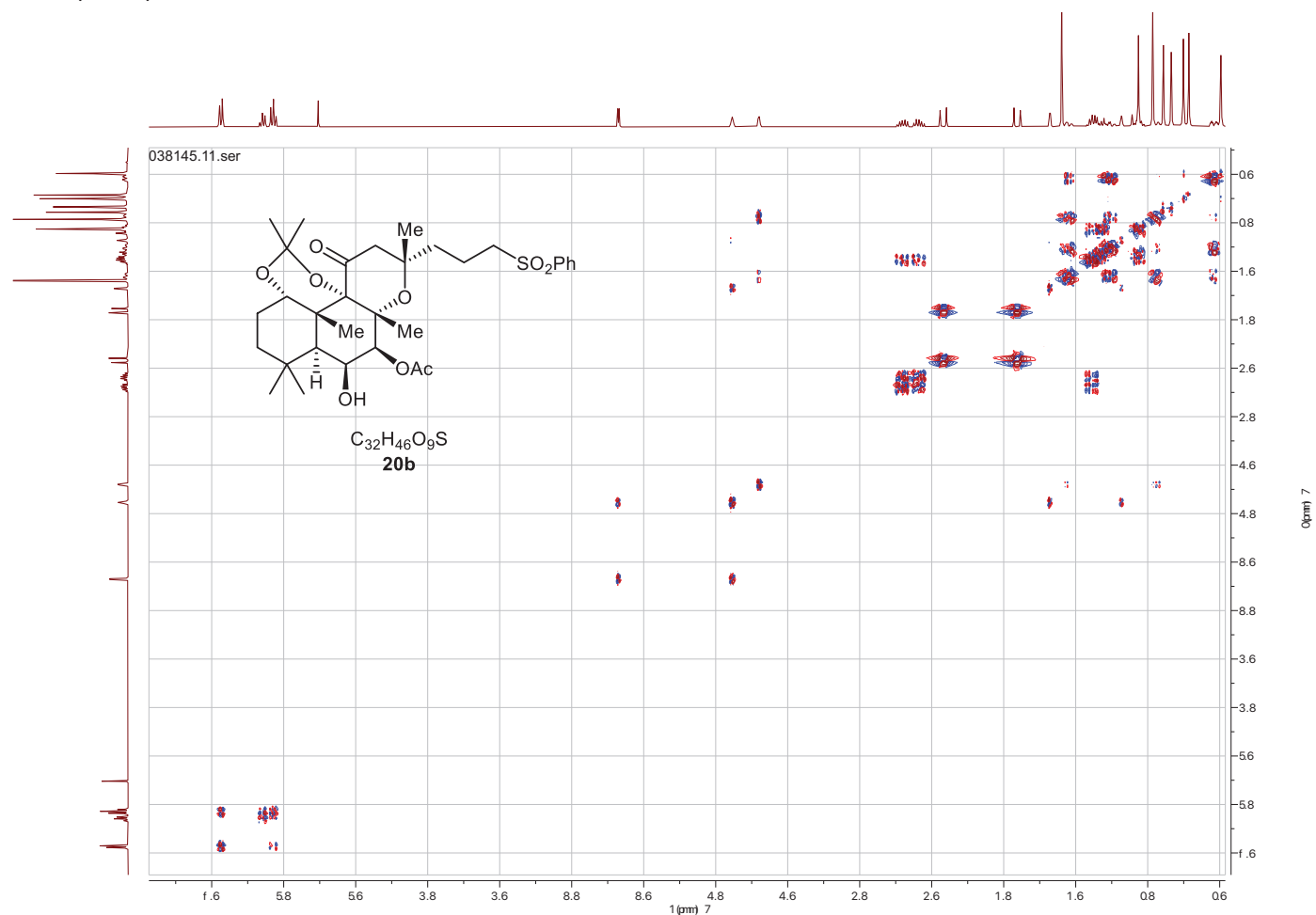
^1H NMR (300 MHz, CDCl_3)



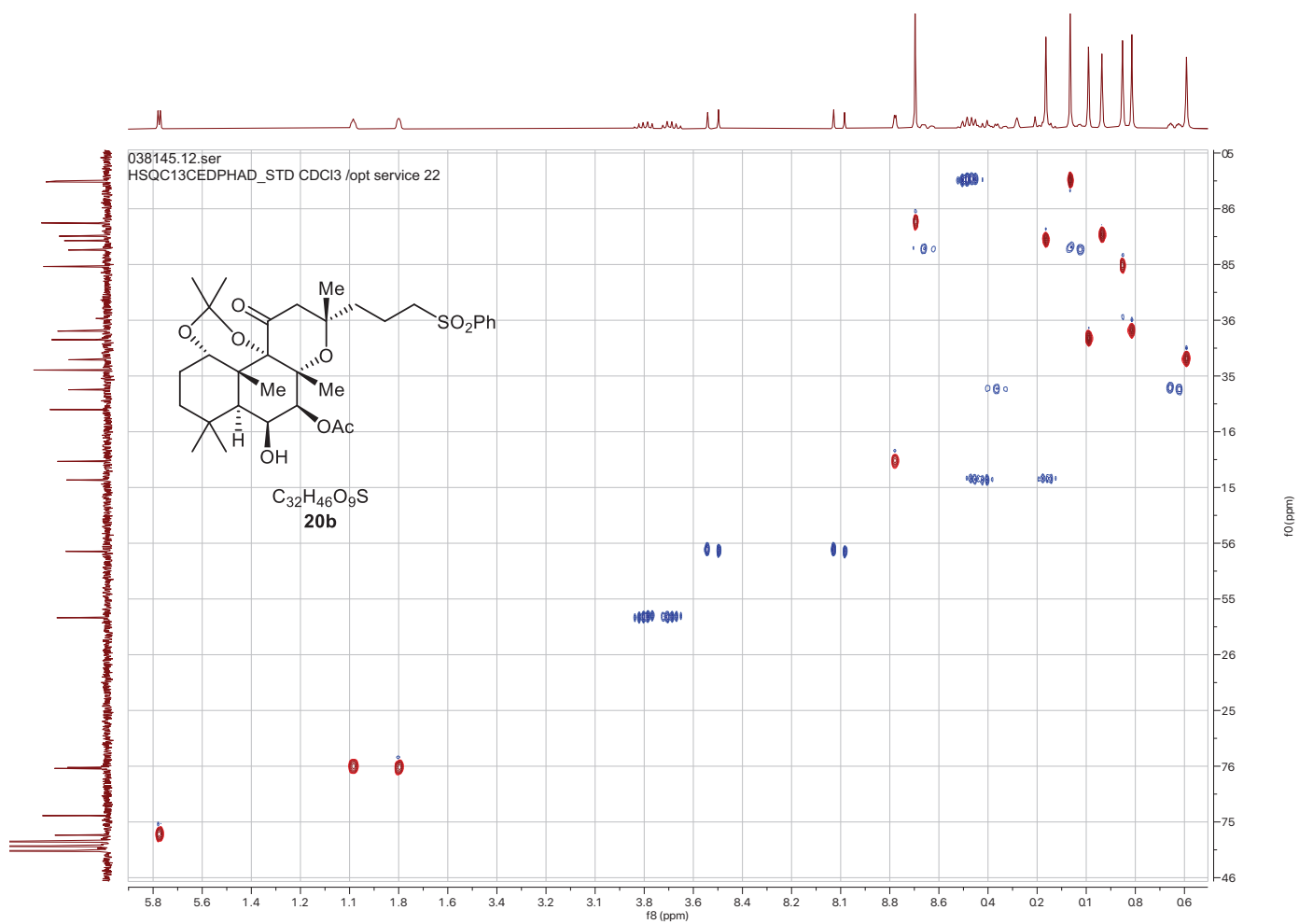
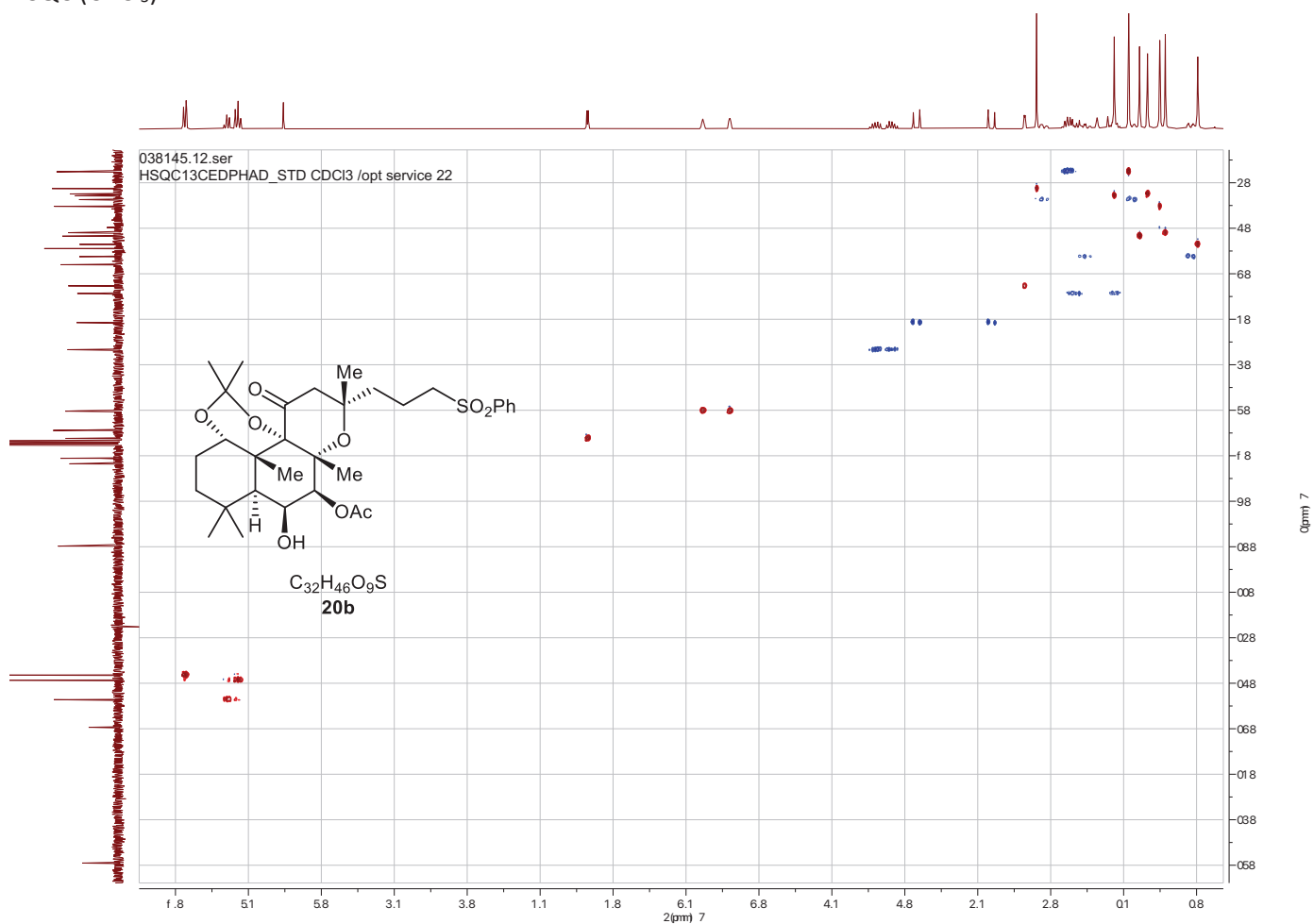
^{13}C NMR (75 MHz, CDCl_3)



COSY (CDCl₃):



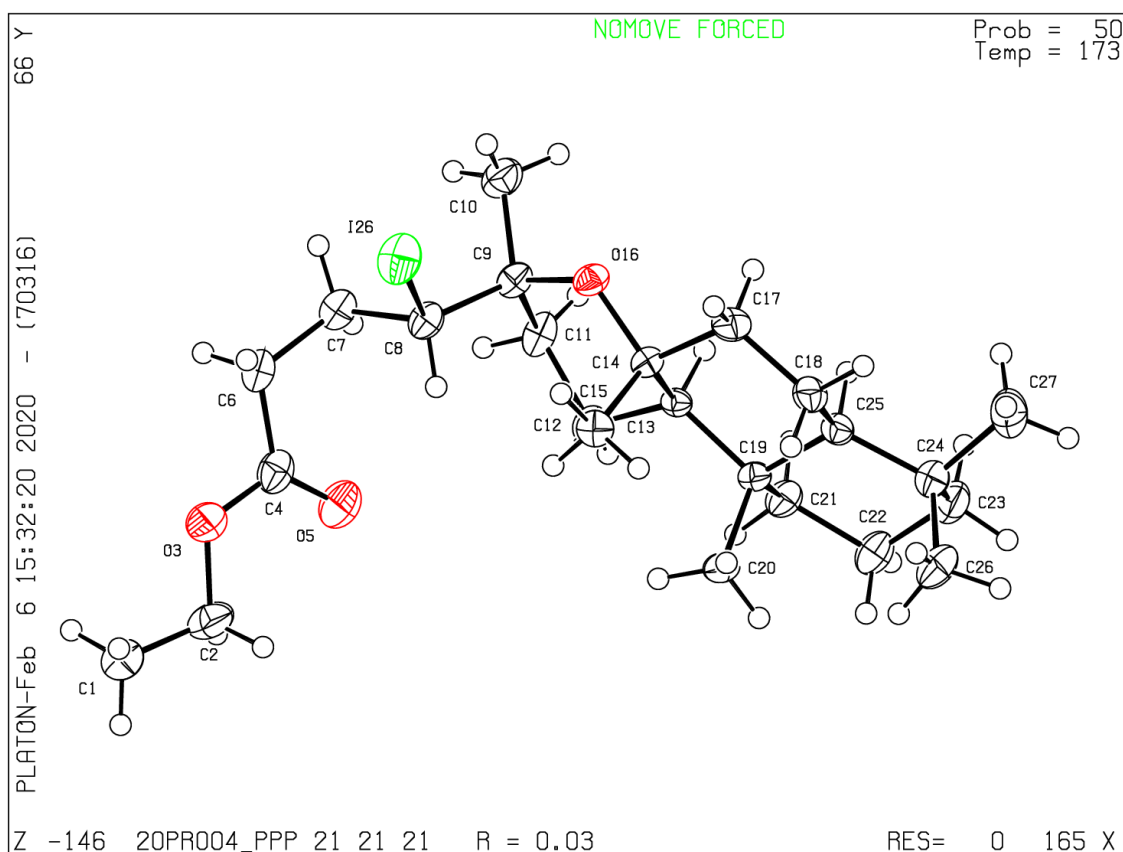
HSQC (CDCl₃):



Departement für Chemie und Biochemie
Universität Bern
Chemische Kristallographie
Freiestrasse 3, CH-3012 Bern, Switzerland

Dr. Michal Andrzejewski
Tel: +41 (0)31 631 4791
e-mail: michal.andrzejewski@dcb.unibe.ch

X-RAY CRYSTAL STRUCTURE REPORT



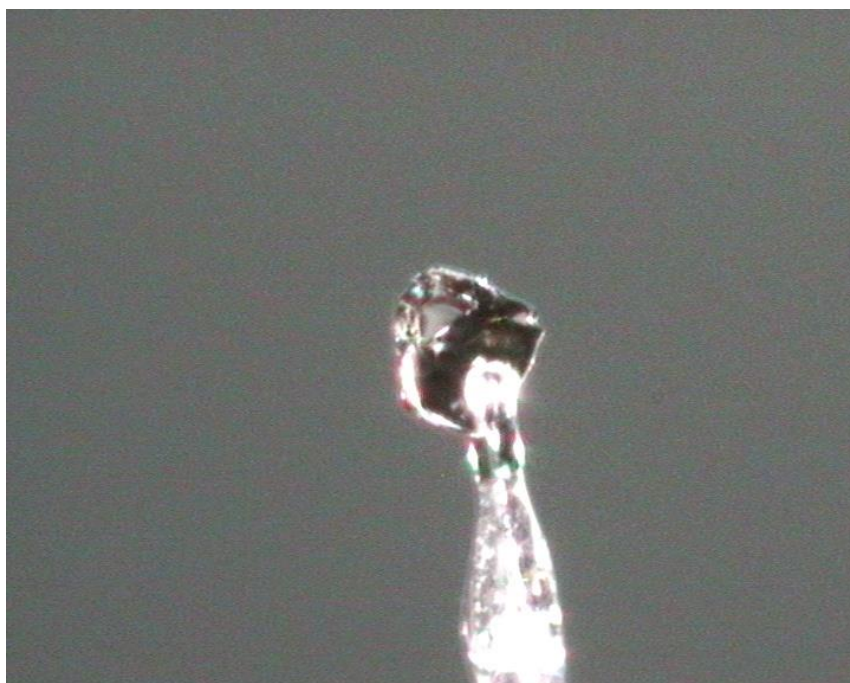
EXPERIMENTAL

Crystal-Structure Determination. A crystal of $C_{24}H_{41}IO_3$ was mounted in air at ambient conditions. All measurements were made on a *Oxford Diffraction SuperNova* area-detector diffractometer¹ using mirror optics monochromated Mo $K\alpha$ radiation ($\lambda = 0.71073 \text{ \AA}$) and Al filtered.² The unit cell constants and an orientation matrix for data collection were obtained from a least-squares refinement of the setting angles of reflections in the range $4.048^\circ < 2\theta < 56.42^\circ$. A total of 549 frames were collected using ω scans, with 3+3 seconds exposure time, a rotation angle of 1.0° per frame, a crystal-detector distance of 65.0 mm, at $T = 173(2) \text{ K}$.

Data reduction was performed using the *CrysAlisPro*¹ program. The intensities were corrected for Lorentz and polarization effects, and an absorption correction based on the multi-scan method using SCALE3 ABSPACK in *CrysAlisPro*¹ was applied. Data collection and refinement parameters are given in *Table 1*.

The structure was solved by direct methods using *SHELXT*³, which revealed the positions of all non-hydrogen atoms of the title compound. All non-hydrogen atoms were refined anisotropically, and H-atoms were assigned in geometrically calculated positions and refined using a riding model where each H-atom was assigned a fixed isotropic displacement parameter with a value equal to 1.2U_{eq} of its parent atom (1.5U_{eq} for methyl groups).

Refinement of the structure was carried out on F^2 using full-matrix least-squares procedures, which minimized the function $\Sigma w(F_o^2 - F_c^2)^2$. The weighting scheme was based on counting statistics and included a factor to downweight the intense reflections. All calculations were performed using the *SHELXL-2014/7*⁴ program in OLEX2.⁵



Single crystal of the compound mounted on a glass fiber.

REFERENCES (In case this structure is submitted for publication, please use these references in the main text of a publication)

- 1) Oxford Diffraction (2010). *CrysAlisPro* (Version 1.171.38.41). Oxford Diffraction Ltd., Yarnton, Oxfordshire, UK.
- 2) Macchi, P.; Bürgi, H.B.; Chimpri, A. S.; Hauser, J.; Gal, Z. (2011) *J. Appl. Cryst.*, **44**, 763-771
- 3) Sheldrick, G. M. (2015). *Acta Cryst.* **A71**, 3-8.
- 4) Sheldrick, G. M. (2015). *Acta Cryst.* **C71**, 3-8.
- 5) Dolomanov, O.V., Bourhis, L.J., Gildea, R.J, Howard, J.A.K. & Puschmann, H. (2009), *J. Appl. Cryst.* 42, 339-341.

Table 1. Crystal data and structure refinement for 20PR004_PP-3-13.

Identification code	20PR004_PP-3-13
Empirical formula	C ₂₄ H ₄₁ IO ₃
Formula weight	504.47
Temperature/K	173.00(10)
Crystal system	orthorhombic
Space group	<i>P</i> 2 ₁ 2 ₁ 2 ₁
<i>a</i> /Å	8.18760(10)
<i>b</i> /Å	10.85930(10)
<i>c</i> /Å	26.7400(3)
α /°	90
β /°	90
γ /°	90
Volume/Å ³	2377.50(5)
<i>Z</i>	4
ρ_{calc} /cm ³	1.409
μ /mm ⁻¹	1.368
<i>F</i> (000)	1048.0
Crystal size/mm ³	0.17 × 0.12 × 0.08
Radiation	MoK α (λ = 0.71073)
2 Θ range for data collection/°	4.048 to 56.42
Index ranges	-10 ≤ <i>h</i> ≤ 10, -14 ≤ <i>k</i> ≤ 14, -35 ≤ <i>l</i> ≤ 34
Reflections collected	20267
Independent reflections	5393 [<i>R</i> _{int} = 0.0414, <i>R</i> _{sigma} = 0.0405]
Data/restraints/parameters	5393/0/260
Goodness-of-fit on <i>F</i> ²	1.027
Final <i>R</i> indexes [<i>I</i> ≥ 2 σ (<i>I</i>)]	<i>R</i> ₁ = 0.0310, <i>wR</i> ₂ = 0.0533
Final <i>R</i> indexes [all data]	<i>R</i> ₁ = 0.0396, <i>wR</i> ₂ = 0.0567
Largest diff. peak/hole / e Å ⁻³	0.41/-0.52
Flack parameter	-0.079(12)

Table 2. Fractional Atomic Coordinates (×10⁴) and Equivalent Isotropic Displacement Parameters (Å²×10³) for 20PR004_PP-3-13. *U*_{eq} is defined as 1/3 of the trace of the orthogonalised *U*_{ij} tensor.

Atom	<i>x</i>	<i>y</i>	<i>z</i>	<i>U</i> (eq)
I26	7223.4(3)	9471.9(3)	3987.9(2)	42.43(10)
O16	4125(3)	10246(2)	3294.6(8)	25.1(6)
O3	5065(3)	5520(3)	4813.4(9)	37.5(6)
O5	3099(4)	6454(3)	4370.0(10)	49.1(8)
C14	3719(4)	9452(4)	2871.0(11)	21.6(7)
C25	1646(4)	9540(4)	1956.9(12)	24.3(7)

C13	1868(4)	9216(3)	2874.2(11)	19.2(8)
C4	4262(5)	6513(4)	4638.4(14)	33.4(10)
C8	4633(4)	9018(3)	4060.7(13)	27.2(8)
C15	4799(5)	8298(3)	2883.0(13)	27.1(8)
C11	1764(4)	9549(4)	3783.9(12)	29.0(8)
C19	1157(4)	8643(3)	2385.4(12)	21.7(7)
C24	806(5)	9354(4)	1442.5(12)	31.5(9)
C12	1381(5)	8627(4)	3370.1(12)	26.9(8)
C18	3503(5)	9710(4)	1932.4(13)	28.2(9)
C20	1718(5)	7295(3)	2311.2(13)	27.9(8)
C10	3674(5)	11231(3)	4054.0(15)	37.1(10)
C7	4281(5)	8836(4)	4617.6(13)	32.8(9)
C9	3562(5)	9985(3)	3793.3(13)	25.3(8)
C6	5013(6)	7671(4)	4838.3(14)	36.0(10)
C22	-1577(5)	8386(4)	1930.3(13)	34.4(9)
C17	4168(5)	10232(3)	2421.7(13)	27.9(9)
C23	-1048(5)	9298(4)	1532.7(14)	37.0(10)
C21	-719(5)	8641(4)	2427.2(13)	29.1(9)
C27	1136(6)	10475(4)	1105.0(14)	46.9(11)
C26	1377(6)	8201(4)	1161.5(14)	41.4(11)
C2	4403(6)	4333(4)	4680.0(16)	46.3(12)
C1	5367(7)	3397(4)	4961.8(17)	55.3(14)

Table 3. Anisotropic Displacement Parameters ($\text{\AA}^2 \times 10^3$) for 20PR004_PP-3-13. The Anisotropic displacement factor exponent takes the form: $-2\pi^2[h^2a^{*2}U_{11}+2hka^*b^*U_{12}+\dots]$.

Atom	U_{11}	U_{22}	U_{33}	U_{23}	U_{13}	U_{12}
I26	20.37(12)	60.72(17)	46.18(15)	1.75(15)	-3.87(12)	-1.49(14)
O16	23.8(14)	26.6(14)	25.1(12)	-2.9(10)	0.2(10)	-6.1(11)
O3	35.9(16)	37.1(15)	39.4(15)	-1.6(15)	-6.4(12)	-4.4(16)
O5	41(2)	56.0(19)	50.4(17)	-0.5(15)	-20.1(15)	-6.0(17)
C14	20.8(19)	22.9(16)	21.0(16)	-2.9(17)	0.4(13)	-1.3(18)
C25	29.1(19)	20.5(17)	23.5(17)	-0.2(16)	0.4(14)	2.2(18)
C13	18(2)	17.2(17)	22.1(16)	-1.3(12)	0.6(13)	2.1(14)
C4	30(2)	46(3)	24(2)	0.9(18)	2.7(18)	-5(2)
C8	19.9(19)	34.2(19)	28(2)	-2.4(15)	-2.4(16)	-1.5(15)
C15	22(2)	29(2)	30(2)	-1.2(16)	2.8(16)	2.6(17)
C11	18.7(19)	47(2)	21.4(16)	-3.5(18)	1.3(13)	3(2)
C19	20.6(19)	20.2(18)	24.2(17)	-1.9(14)	-0.4(14)	-1.3(15)
C24	40(2)	31(2)	24.2(18)	-0.5(17)	-2.2(16)	0(2)
C12	17(2)	36(2)	26.8(19)	-0.9(16)	0.7(15)	-2.5(17)

C18	35(2)	27(2)	22.5(17)	3.4(15)	5.7(16)	-3.2(17)
C20	30(2)	22.8(18)	30.4(19)	-3.4(15)	-3.8(16)	-4.1(16)
C10	38(2)	38(2)	35(2)	-10.0(19)	-6(2)	6.3(19)
C7	31(2)	39(2)	28(2)	-4.0(17)	-2.7(17)	0.8(19)
C9	21(2)	30.7(19)	24.5(18)	-5.9(14)	0.1(15)	1.9(16)
C6	41(3)	41(2)	26(2)	1.1(18)	-8.2(19)	0(2)
C22	25(2)	47(2)	32(2)	-4.7(18)	-5.1(17)	-1.1(19)
C17	24(2)	27(2)	32(2)	0.4(15)	4.5(16)	-7.5(16)
C23	38(2)	43(2)	30(2)	-4.4(19)	-10.2(17)	4(2)
C21	23(2)	34(2)	30(2)	-2.2(17)	-3.0(16)	-3.6(18)
C27	55(3)	51(3)	34(2)	10(2)	-5.7(19)	-2(3)
C26	48(3)	51(3)	25(2)	-10.8(17)	-0.6(18)	-2(2)
C2	53(3)	42(3)	43(2)	-9(2)	-10(2)	-15(3)
C1	85(4)	41(3)	39(3)	-3(2)	-14(3)	-7(3)

Table 4. Bond Lengths for 20PR004_PP-3-13.

Atom	Atom	Length/Å	Atom	Atom	Length/Å
I26	C8	2.186(4)	C8	C7	1.530(5)
O16	C14	1.462(4)	C8	C9	1.544(5)
O16	C9	1.439(4)	C11	C12	1.525(5)
O3	C4	1.346(5)	C11	C9	1.547(5)
O3	C2	1.443(5)	C19	C20	1.547(5)
O5	C4	1.194(5)	C19	C21	1.540(5)
C14	C13	1.537(4)	C24	C23	1.538(6)
C14	C15	1.535(5)	C24	C27	1.540(5)
C14	C17	1.515(5)	C24	C26	1.533(5)
C25	C19	1.556(5)	C18	C17	1.526(5)
C25	C24	1.551(5)	C10	C9	1.525(5)
C25	C18	1.533(5)	C7	C6	1.519(5)
C13	C19	1.560(4)	C22	C23	1.516(5)
C13	C12	1.525(4)	C22	C21	1.528(5)
C4	C6	1.499(6)	C2	C1	1.491(6)

Table 5. Bond Angles for 20PR004_PP-3-13.

Atom	Atom	Atom	Angle/°	Atom	Atom	Atom	Angle/°
C9	O16	C14	122.0(3)	C21	C19	C25	108.1(3)
C4	O3	C2	116.5(3)	C21	C19	C13	108.2(3)
O16	C14	C13	108.6(3)	C21	C19	C20	107.7(3)

O16	C14	C15	109.5(3)	C23	C24	C25	107.7(3)
O16	C14	C17	103.3(3)	C23	C24	C27	107.2(3)
C15	C14	C13	115.6(3)	C27	C24	C25	109.8(3)
C17	C14	C13	109.7(3)	C26	C24	C25	113.9(3)
C17	C14	C15	109.4(3)	C26	C24	C23	110.2(3)
C24	C25	C19	117.2(3)	C26	C24	C27	107.7(3)
C18	C25	C19	111.2(3)	C11	C12	C13	107.6(3)
C18	C25	C24	114.7(3)	C17	C18	C25	111.2(3)
C14	C13	C19	115.5(3)	C6	C7	C8	114.3(3)
C12	C13	C14	109.4(3)	O16	C9	C8	112.4(3)
C12	C13	C19	117.6(3)	O16	C9	C11	110.5(3)
O3	C4	C6	110.3(3)	O16	C9	C10	103.3(3)
O5	C4	O3	123.8(4)	C8	C9	C11	109.8(3)
O5	C4	C6	125.9(4)	C10	C9	C8	111.0(3)
C7	C8	I26	107.4(2)	C10	C9	C11	109.6(3)
C7	C8	C9	115.6(3)	C4	C6	C7	113.5(3)
C9	C8	I26	110.9(2)	C23	C22	C21	111.1(3)
C12	C11	C9	114.1(3)	C14	C17	C18	112.7(3)
C25	C19	C13	105.7(3)	C22	C23	C24	114.7(3)
C20	C19	C25	115.0(3)	C22	C21	C19	113.3(3)
C20	C19	C13	112.0(3)	O3	C2	C1	106.6(3)

Table 6. Torsion Angles for 20PR004_PP-3-13.

A	B	C	D	Angle/°	A	B	C	D	Angle/°
I26	C8	C7	C6	-71.0(4)	C24	C25	C19	C20	68.3(4)
I26	C8	C9	O16	48.4(3)	C24	C25	C19	C21	-52.0(4)
I26	C8	C9	C11	171.9(2)	C24	C25	C18	C17	164.3(3)
I26	C8	C9	C10	-66.7(3)	C12	C13	C19	C25	171.7(3)
O16	C14	C13	C19	166.5(2)	C12	C13	C19	C20	-62.4(4)
O16	C14	C13	C12	-58.0(4)	C12	C13	C19	C21	56.2(4)
O16	C14	C17	C18	-167.2(3)	C12	C11	C9	O16	43.5(4)
O3	C4	C6	C7	174.3(3)	C12	C11	C9	C8	-81.1(4)
O5	C4	C6	C7	-7.1(6)	C12	C11	C9	C10	156.7(3)
C14	O16	C9	C8	81.6(4)	C18	C25	C19	C13	57.7(4)
C14	O16	C9	C11	-41.5(4)	C18	C25	C19	C20	-66.4(4)
C14	O16	C9	C10	-158.7(3)	C18	C25	C19	C21	173.3(3)
C14	C13	C19	C25	-56.6(4)	C18	C25	C24	C23	-175.8(3)
C14	C13	C19	C20	69.3(4)	C18	C25	C24	C27	-59.3(5)
C14	C13	C19	C21	-172.2(3)	C18	C25	C24	C26	61.6(5)
C14	C13	C12	C11	62.9(4)	C20	C19	C21	C22	-72.2(4)

C25 C19 C21 C22 52.5(4) C7 C8 C9 O16 170.9(3)
 C25 C24 C23 C22 -51.7(4) C7 C8 C9 C11 -65.6(4)
 C25 C18 C17 C14 55.9(4) C7 C8 C9 C10 55.8(4)
 C13 C14 C17 C18 -51.6(4) C9 O16 C14 C13 49.5(4)
 C13 C19 C21 C22 166.6(3) C9 O16 C14 C15 -77.5(4)
 C4 O3 C2 C1 -173.5(4) C9 O16 C14 C17 165.9(3)
 C8 C7 C6 C4 -67.1(5) C9 C8 C7 C6 164.7(3)
 C15 C14 C13 C19 -70.0(4) C9 C11 C12 C13 -56.0(4)
 C15 C14 C13 C12 65.4(4) C17 C14 C13 C19 54.3(4)
 C15 C14 C17 C18 76.2(4) C17 C14 C13 C12 -170.3(3)
 C19 C25 C24 C23 51.1(4) C23 C22 C21 C19 -56.0(4)
 C19 C25 C24 C27 167.5(3) C21 C22 C23 C24 56.0(4)
 C19 C25 C24 C26 -71.5(4) C27 C24 C23 C22 -169.8(3)
 C19 C25 C18 C17 -59.8(4) C26 C24 C23 C22 73.2(4)
 C19 C13 C12 C11 -162.7(3) C2 O3 C4 O5 -2.9(5)
 C24 C25 C19 C13 -167.7(3) C2 O3 C4 C6 175.8(4)

Table 7. Hydrogen Atom Coordinates ($\text{\AA}\times 10^4$) and Isotropic Displacement Parameters ($\text{\AA}^2\times 10^3$) for 20PR004_PP-3-13.

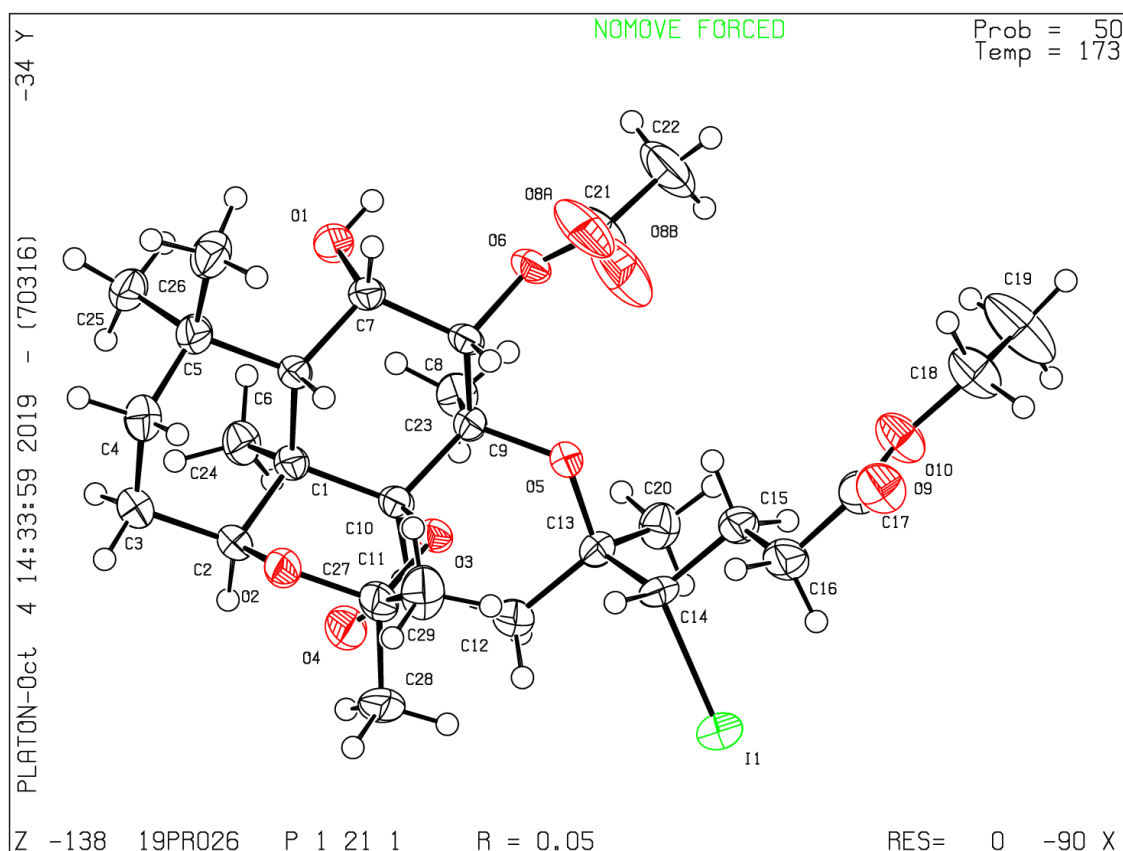
Atom	<i>x</i>	<i>y</i>	<i>z</i>	U(eq)
H25	1242	10342	2071	29
H13	1385	10041	2888	23
H8	4455	8226	3894	33
H15A	5870	8514	3000	41
H15B	4877	7958	2552	41
H15C	4326	7699	3104	41
H11A	1506	9176	4104	35
H11B	1062	10262	3743	35
H12A	225	8431	3369	32
H12B	1990	7871	3422	32
H18A	4016	8922	1865	34
H18B	3772	10264	1660	34
H20A	944	6870	2104	42
H20B	1787	6893	2630	42
H20C	2771	7285	2153	42
H10A	4790	11501	4059	56
H10B	3280	11156	4391	56
H10C	3021	11822	3877	56
H7A	4702	9540	4800	39
H7B	3107	8816	4666	39

H6A	6176	7660	4769	43
H6B	4876	7689	5199	43
H22A	-1321	7557	1820	41
H22B	-2749	8440	1977	41
H17A	5348	10288	2399	34
H17B	3744	11057	2469	34
H23A	-1424	10112	1629	44
H23B	-1582	9085	1221	44
H21A	-1046	8020	2668	35
H21B	-1076	9435	2553	35
H27A	967	11219	1292	70
H27B	404	10459	825	70
H27C	2244	10448	988	70
H26A	2548	8188	1149	62
H26B	949	8214	827	62
H26C	990	7480	1332	62
H2A	4502	4196	4323	56
H2B	3258	4285	4771	56
H1A	6486	3425	4855	83
H1B	4928	2593	4899	83
H1C	5308	3572	5313	83

Departement für Chemie und Biochemie
Universität Bern
Chemische Kristallographie
Freiestrasse 3, CH-3012 Bern, Switzerland

Dr. Michal Andrzejewski
Tel: +41 (0)31 631 4791
e-mail: michal.andrzejewski@dcb.unibe.ch

X-RAY CRYSTAL STRUCTURE REPORT



EXPERIMENTAL

Crystal-Structure Determination. A crystal of $C_{29}H_{45}IO_9$ was mounted in air at ambient conditions. All measurements were made on a *RIGAKU Synergy S* area-detector diffractometer¹ using mirror optics monochromated Cu $K\alpha$ radiation ($\lambda = 1.54184 \text{ \AA}$).² The unit cell constants and an orientation matrix for data collection were obtained from a least-squares refinement of the setting angles of reflections in the range $2.717^\circ < \theta < 71.485^\circ$. A total of 10232 frames were collected using ω scans, with 0.06 seconds exposure time, a rotation angle of 0.5° per frame, a crystal-detector distance of 65.0 mm, at $T = 173(2) \text{ K}$.

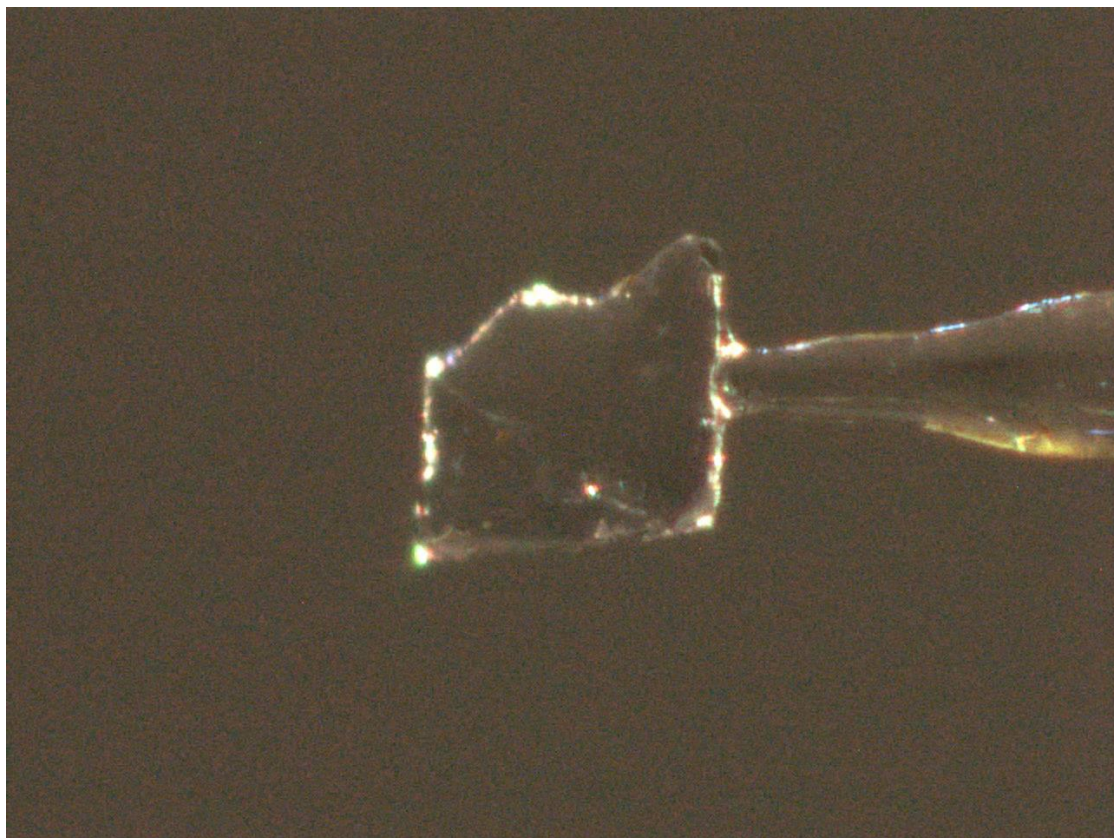
Data reduction was performed using the *CrysAlisPro*¹ program. The intensities were corrected for Lorentz and polarization effects, and an absorption correction based on the multi-scan method using SCALE3 ABSPACK in *CrysAlisPro*¹ was applied. Data collection and refinement parameters are given in *Table 1*.

The structure was solved by direct methods using *SHELXT*³, which revealed the positions of all non-hydrogen atoms of the title compound. All non-hydrogen atoms were refined anisotropically. H-atoms were assigned in geometrically calculated positions and refined using a riding model where each H-atom was assigned a fixed isotropic displacement parameter with a value equal to 1.2Ueq of its parent atom (1.5Ueq for methyl groups).

Refinement of the structure was carried out on F^2 using full-matrix least-squares procedures, which minimized the function $\sum w(F_o^2 - F_c^2)^2$. The weighting scheme was based on counting statistics and included a factor to downweight the intense reflections. All calculations were performed using the *SHELXL-2014/7*⁴ program in OLEX2.⁵

The structure contains disordered atom O8, which was been refined into two positions with 0.6 and 0.4 occupancies, respectively.

The X-ray crystal structure determination service unit of the Department of Chemistry and Biochemistry of the University of Bern is acknowledged for measuring, solving, refining and summarizing the structures of compounds XX, YY, ZZ. The Synergy diffractometer was partially funded by the Swiss National Science Foundation (SNF) within the R'Equip programme (project number 206021_177033).



A single crystal of the compound mounted on a glass fiber.

REFERENCES (In case this structure is submitted for publication, please use these references in the main text of a publication)

- 1) Oxford Diffraction (2018). *CrysAlisPro* (Version 1.171.40.37a). Oxford Diffraction Ltd., Yarnton, Oxfordshire, UK.
- 2) Macchi, P.; Bürgi, H.B.; Chimpri, A. S.; Hauser, J.; Gal, Z. (2011) *J. Appl. Cryst.*, **44**, 763-771
- 3) Sheldrick, G. M. (2015). *Acta Cryst.* **A71**, 3-8.
- 4) Sheldrick, G. M. (2015). *Acta Cryst.* **C71**, 3-8.
- 5) Dolomanov, O.V., Bourhis, L.J., Gildea, R.J, Howard, J.A.K. & Puschmann, H. (2009), *J. Appl. Cryst.* **42**, 339-341.

Table 1. Crystal data and structure refinement for 19PR026_PP-70C-03.

Identification code	19PR026_PP-70C-03
Empirical formula	C ₂₉ H ₄₅ IO ₉
Formula weight	664.55
Temperature/K	173.01(10)
Crystal system	monoclinic
Space group	<i>P</i> 2 ₁
<i>a</i> /Å	9.92220(10)
<i>b</i> /Å	9.71250(10)
<i>c</i> /Å	16.7822(2)
α /°	90
β /°	104.2690(10)
γ /°	90
Volume/Å ³	1567.40(3)
<i>Z</i>	2
ρ_{calc} /cm ³	1.408
μ /mm ⁻¹	8.431
<i>F</i> (000)	688.0
Crystal size/mm ³	0.449 × 0.289 × 0.056
Radiation	CuK α (λ = 1.54184)
2 Θ range for data collection/°	5.434 to 142.97
Index ranges	-12 ≤ <i>h</i> ≤ 11, -11 ≤ <i>k</i> ≤ 11, -20 ≤ <i>l</i> ≤ 20
Reflections collected	28965
Independent reflections	6003 [<i>R</i> _{int} = 0.0683, <i>R</i> _{sigma} = 0.0381]
Data/restraints/parameters	6003/1/371
Goodness-of-fit on <i>F</i> ²	1.146
Final <i>R</i> indexes [<i>I</i> ≥ 2 σ (<i>I</i>)]	<i>R</i> ₁ = 0.0473, <i>wR</i> ₂ = 0.1272
Final <i>R</i> indexes [all data]	<i>R</i> ₁ = 0.0480, <i>wR</i> ₂ = 0.1279
Largest diff. peak/hole / e Å ⁻³	0.68/-0.72
Flack parameter	-0.024(7)

Table 2. Fractional Atomic Coordinates (×10⁴) and Equivalent Isotropic Displacement Parameters (Å²×10³) for 19PR026_PP-70C-03. *U*_{eq} is defined as 1/3 of of the trace of the orthogonalised *U*_{ij} tensor.

Atom	<i>x</i>	<i>y</i>	<i>z</i>	<i>U</i> (eq)
I1	-1354.2(4)	1004.2(6)	7107.7(2)	46.49(17)
O1	6208(4)	5764(6)	7983(3)	34.2(12)
C23	4711(7)	2958(7)	7734(4)	33.5(14)
C14	152(7)	2592(7)	7640(4)	31.1(13)
C9	3498(6)	3965(6)	7623(4)	25.2(11)
O10	-560(6)	3187(6)	9990(3)	43.7(12)

C15	72(7)	2884(7)	8517(4)	32.3(13)
C29	-178(8)	6641(9)	6279(5)	47.5(19)
C24	5113(8)	4629(7)	6197(4)	35.2(15)
O4	2794(6)	2653(6)	5626(3)	46.3(13)
C21	3955(12)	5308(12)	9571(5)	57(2)
C11	2506(7)	2987(7)	6258(4)	32.3(13)
C10	2878(6)	4376(6)	6705(4)	25.5(12)
C12	1656(8)	2012(7)	6647(4)	36.0(14)
C4	4005(8)	8292(8)	5782(4)	40.7(16)
C28	-9(8)	4669(9)	5335(5)	47.7(19)
O9	-2166(6)	4816(6)	9557(3)	45.8(12)
C20	2183(6)	927(9)	8065(4)	36.9(13)
C2	2920(6)	5919(9)	5524(3)	31.9(12)
O5	2414(4)	3378(5)	7948(2)	28.1(9)
O3	1581(4)	5025(5)	6712(2)	26.8(8)
C7	4820(6)	6270(6)	7852(3)	27.5(13)
O6	4488(5)	4848(5)	8966(3)	34.6(10)
C27	784(7)	5689(7)	5973(4)	35.1(16)
C6	4204(6)	6643(6)	6944(4)	25.4(11)
O8B	2810(20)	5880(30)	9448(11)	85(6)
O2	1660(5)	6543(5)	5636(3)	34.1(10)
C22	4617(13)	4603(14)	10359(5)	73(3)
C16	-1321(7)	3523(9)	8567(4)	40.3(16)
C8	3846(6)	5268(7)	8133(3)	26.5(12)
C25	6429(7)	7577(8)	6514(5)	39.0(15)
C13	1628(6)	2208(6)	7558(4)	28.0(12)
C1	3823(6)	5378(7)	6354(4)	27.1(12)
C5	4949(7)	7857(7)	6609(4)	32.3(13)
C3	3620(8)	7106(8)	5173(4)	40.0(16)
C17	-1409(7)	3933(7)	9411(4)	35.5(14)
C19	289(15)	2392(14)	11364(6)	85(4)
C18	-590(9)	3460(9)	10828(5)	49.2(19)
C26	5064(9)	9082(8)	7202(5)	41.7(16)
O8A	3410(30)	6430(30)	9503(16)	65(8)

Table 3. Anisotropic Displacement Parameters ($\text{\AA}^2 \times 10^3$) for 19PR026_PP-70C-03. The Anisotropic displacement factor exponent takes the form: $-2\pi^2[h^2a^{*2}U_{11}+2hka^*b^*U_{12}+\dots]$.

Atom	U_{11}	U_{22}	U_{33}	U_{23}	U_{13}	U_{12}
I1	39.3(3)	57.8(3)	39.6(2)	-6.0(2)	4.27(17)	-19.2(2)
O1	20.9(18)	49(4)	31(2)	5(2)	3.4(16)	1.2(18)

C23	30(3)	36(3)	35(3)	4(3)	9(3)	8(3)
C14	23(3)	36(3)	31(3)	-2(2)	0(2)	-10(2)
C9	21(3)	33(3)	23(3)	1(2)	6(2)	-2(2)
O10	45(3)	55(3)	31(2)	3(2)	8(2)	20(2)
C15	24(3)	41(3)	30(3)	-1(3)	5(2)	0(3)
C29	30(4)	63(5)	50(4)	21(4)	11(3)	12(3)
C24	37(4)	42(4)	33(3)	-7(3)	19(3)	-1(3)
O4	59(3)	52(3)	34(3)	-16(2)	22(2)	-18(3)
C21	71(6)	74(6)	25(4)	-4(4)	11(4)	11(5)
C11	36(3)	36(3)	25(3)	-4(2)	7(3)	-5(3)
C10	22(3)	34(3)	20(3)	-2(2)	4(2)	0(2)
C12	41(4)	38(3)	29(3)	-5(3)	7(3)	-9(3)
C4	45(4)	43(4)	36(3)	9(3)	12(3)	-7(3)
C28	36(4)	64(5)	32(4)	10(3)	-11(3)	-14(4)
O9	38(3)	55(3)	43(3)	4(2)	9(2)	13(2)
C20	36(3)	36(3)	41(3)	5(3)	12(3)	2(3)
C2	33(3)	41(3)	20(2)	-1(3)	6(2)	-6(3)
O5	28(2)	35(2)	21.6(19)	0.7(16)	7.2(17)	-4.6(18)
O3	20.9(19)	38(2)	20.2(19)	2.7(16)	1.9(16)	0.4(17)
C7	22(3)	36(4)	24(2)	-4(2)	5(2)	-3(2)
O6	28(2)	54(3)	19(2)	1.4(19)	0.0(17)	-2(2)
C27	28(3)	48(5)	26(3)	12(3)	0(2)	3(3)
C6	24(3)	31(3)	21(3)	-2(2)	6(2)	-2(2)
O8B	95(14)	130(20)	38(7)	1(11)	30(9)	43(13)
O2	28(2)	45(2)	28(2)	8.3(18)	4.1(18)	-2.7(18)
C22	80(7)	110(9)	25(4)	9(5)	6(4)	7(6)
C16	27(3)	58(4)	34(3)	3(3)	2(3)	4(3)
C8	23(3)	37(3)	17(3)	-2(2)	2(2)	-1(2)
C25	33(4)	49(4)	39(4)	-6(3)	16(3)	-11(3)
C13	23(3)	32(3)	29(3)	1(2)	6(2)	-4(2)
C1	25(3)	34(3)	23(3)	-4(2)	8(2)	-2(2)
C5	35(3)	35(3)	30(3)	-4(3)	13(3)	-6(3)
C3	42(4)	52(4)	25(3)	4(3)	7(3)	-10(3)
C17	28(3)	43(4)	35(3)	6(3)	6(3)	5(3)
C19	113(10)	104(9)	35(4)	8(5)	9(5)	58(8)
C18	57(5)	57(5)	33(4)	-1(3)	10(3)	18(4)
C26	47(4)	35(3)	49(4)	-8(3)	23(4)	-11(3)
O8A	110(20)	63(13)	27(8)	-16(8)	20(13)	17(13)

Table 4. Bond Lengths for 19PR026_PP-70C-03.

Atom	Atom	Length/Å	Atom	Atom	Length/Å
I1	C14	2.179(6)	C12	C13	1.548(9)
O1	C7	1.428(7)	C4	C5	1.531(10)
C23	C9	1.526(8)	C4	C3	1.524(11)
C14	C15	1.520(9)	C28	C27	1.527(10)
C14	C13	1.549(9)	O9	C17	1.203(9)
C9	C10	1.565(8)	C20	C13	1.531(10)
C9	O5	1.438(7)	C2	O2	1.442(8)
C9	C8	1.519(8)	C2	C1	1.550(8)
O10	C17	1.332(8)	C2	C3	1.537(10)
O10	C18	1.439(9)	O5	C13	1.441(7)
C15	C16	1.537(9)	O3	C27	1.446(7)
C29	C27	1.507(11)	C7	C6	1.539(8)
C24	C1	1.549(9)	C7	C8	1.526(8)
O4	C11	1.209(8)	O6	C8	1.445(7)
C21	O6	1.332(10)	C27	O2	1.417(8)
C21	O8B	1.24(2)	C6	C1	1.565(8)
C21	C22	1.490(13)	C6	C5	1.567(9)
C21	O8A	1.21(3)	C16	C17	1.494(10)
C11	C10	1.543(9)	C25	C5	1.539(10)
C11	C12	1.518(9)	C5	C26	1.537(9)
C10	O3	1.435(7)	C19	C18	1.504(12)
C10	C1	1.564(8)			

Table 5. Bond Angles for 19PR026_PP-70C-03.

Atom	Atom	Atom	Angle/°	Atom	Atom	Atom	Angle/°
C15	C14	I1	109.5(4)	O3	C27	C29	103.9(5)
C15	C14	C13	113.9(5)	O3	C27	C28	113.0(6)
C13	C14	I1	111.2(4)	O2	C27	C29	106.2(6)
C23	C9	C10	113.0(5)	O2	C27	C28	111.1(6)
O5	C9	C23	109.9(5)	O2	C27	O3	110.1(5)
O5	C9	C10	109.0(4)	C7	C6	C1	114.7(5)
O5	C9	C8	101.8(5)	C7	C6	C5	115.1(5)
C8	C9	C23	113.7(5)	C1	C6	C5	115.1(5)
C8	C9	C10	108.8(5)	C27	O2	C2	116.3(5)
C17	O10	C18	116.8(6)	C17	C16	C15	115.1(6)
C14	C15	C16	113.0(5)	C9	C8	C7	115.5(5)
O6	C21	C22	110.6(9)	O6	C8	C9	107.1(5)
O8B	C21	O6	123.0(12)	O6	C8	C7	108.5(5)

O8B	C21	C22	122.8(13)	C12	C13	C14	111.4(5)
O8A	C21	O6	118.8(15)	C20	C13	C14	111.4(5)
O8A	C21	C22	126.0(15)	C20	C13	C12	110.9(6)
O4	C11	C10	125.4(6)	O5	C13	C14	100.9(5)
O4	C11	C12	119.1(6)	O5	C13	C12	113.9(5)
C12	C11	C10	115.4(5)	O5	C13	C20	107.9(5)
C11	C10	C9	104.1(5)	C24	C1	C10	111.6(5)
C11	C10	C1	117.1(5)	C24	C1	C2	109.0(5)
O3	C10	C9	103.9(4)	C24	C1	C6	113.3(5)
O3	C10	C11	106.3(5)	C10	C1	C6	108.9(5)
O3	C10	C1	110.6(5)	C2	C1	C10	106.3(5)
C1	C10	C9	113.8(5)	C2	C1	C6	107.4(5)
C11	C12	C13	119.7(5)	C4	C5	C6	107.2(5)
C3	C4	C5	113.3(6)	C4	C5	C25	109.9(6)
O2	C2	C1	110.7(4)	C4	C5	C26	107.7(6)
O2	C2	C3	102.9(6)	C25	C5	C6	116.8(6)
C3	C2	C1	112.5(5)	C26	C5	C6	108.5(5)
C9	O5	C13	120.9(4)	C26	C5	C25	106.4(6)
C10	O3	C27	119.4(4)	C4	C3	C2	111.8(6)
O1	C7	C6	111.4(5)	O10	C17	C16	111.8(6)
O1	C7	C8	113.2(5)	O9	C17	O10	123.6(7)
C8	C7	C6	109.2(5)	O9	C17	C16	124.5(6)
C21	O6	C8	118.7(6)	O10	C18	C19	108.0(7)
C29	C27	C28	112.1(7)				

Table 6. Hydrogen Atom Coordinates ($\text{\AA}\times 10^4$) and Isotropic Displacement Parameters ($\text{\AA}^2\times 10^3$) for 19PR026_PP-70C-03.

Atom	<i>x</i>	<i>y</i>	<i>z</i>	U(eq)
H1	6521	5599	8473	51
H23A	4428	2169	7389	50
H23B	4989	2670	8298	50
H23C	5479	3401	7586	50
H14	-125	3436	7321	37
H15A	820	3505	8771	39
H15B	209	2030	8826	39
H29A	-798	7080	5819	71
H29B	359	7329	6630	71
H29C	-707	6122	6582	71
H24A	5899	4786	6652	53
H24B	5309	4978	5702	53

H24C	4929	3659	6139	53
H12A	1988	1086	6591	43
H12B	703	2054	6321	43
H4A	3159	8689	5875	49
H4B	4471	9001	5542	49
H28A	-524	4046	5591	71
H28B	638	4159	5109	71
H28C	-639	5162	4903	71
H20A	2110	1052	8620	55
H20B	3140	788	8062	55
H20C	1648	139	7829	55
H2	2696	5166	5125	38
H7	4855	7116	8176	33
H6	3294	7033	6947	31
H22A	4339	3654	10327	109
H22B	4327	5041	10802	109
H22C	5610	4661	10456	109
H16A	-1491	4331	8217	48
H16B	-2057	2867	8350	48
H8	2977	5750	8130	32
H25A	6386	6943	6070	59
H25B	6982	7188	7015	59
H25C	6841	8425	6399	59
H3A	4454	6767	5035	48
H3B	2994	7440	4672	48
H19A	1205	2394	11271	128
H19B	-125	1501	11234	128
H19C	347	2599	11931	128
H18A	-1538	3416	10885	59
H18B	-226	4373	10988	59
H26A	5341	9888	6953	63
H26B	5745	8880	7703	63
H26C	4179	9241	7320	63

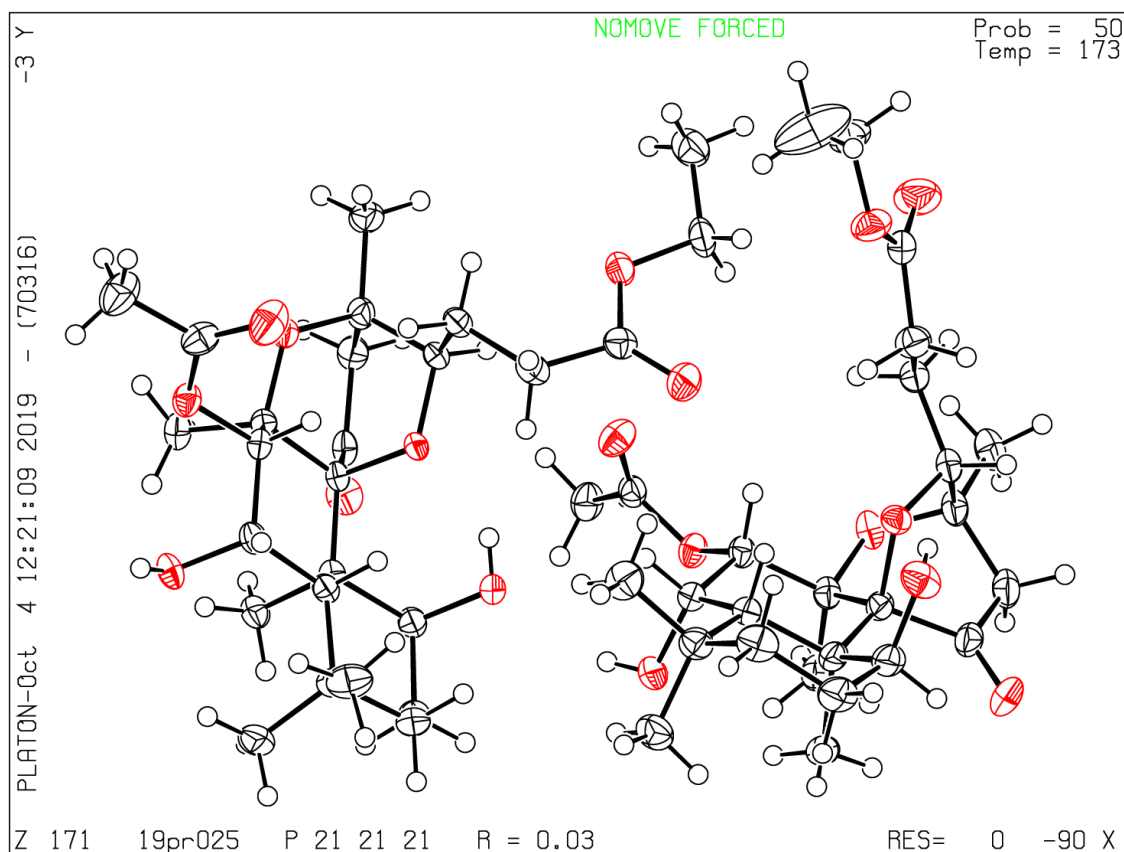
Table 7. Atomic Occupancy for 19PR026_PP-70C-03.

Atom Occupancy **Atom Occupancy** **Atom Occupancy**
O8B 0.6 O8A 0.4

Departement für Chemie und Biochemie
Universität Bern
Chemische Kristallographie
Freiestrasse 3, CH-3012 Bern, Switzerland

Dr. Michal Andrzejewski
Tel: +41 (0)31 631 4791
e-mail: michal.andrzejewski@dcb.unibe.ch

X-RAY CRYSTAL STRUCTURE REPORT



EXPERIMENTAL

Crystal-Structure Determination. A crystal of $C_{26}H_{40}O_9$ was mounted in air at ambient conditions. All measurements were made on a *RIGAKU Synergy S* area-detector diffractometer¹ using mirror optics monochromated Cu $K\alpha$ radiation ($\lambda = 1.54184 \text{ \AA}$).² The unit cell constants and an orientation matrix for data collection were obtained from a least-squares refinement of the setting angles of reflections in the range $3.532^\circ < \theta < 71.535^\circ$. A total of 5724 frames were collected using ω scans, with 0.05 and 0.17 (for high angle reflections) seconds exposure time, a rotation angle of 0.5° per frame, a crystal-detector distance of 65.0 mm, at $T = 173(2) \text{ K}$.

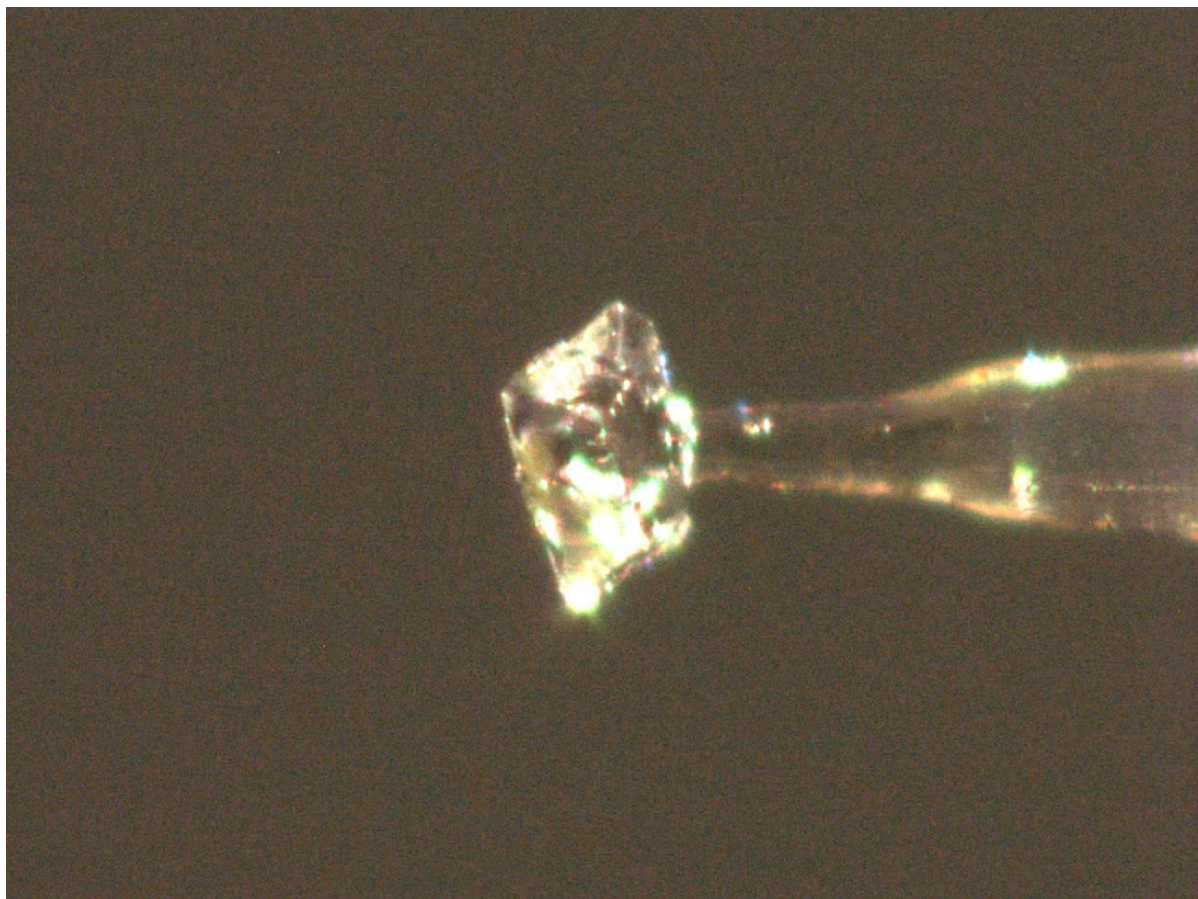
Data reduction was performed using the *CrysAlisPro*¹ program. The intensities were corrected for Lorentz and polarization effects, and an absorption correction based on the multi-scan method using SCALE3 ABSPACK in *CrysAlisPro*¹ was applied. Data collection and refinement parameters are given in *Table 1*.

The structure was solved by direct methods using *SHELXT*³, which revealed the positions of all non-hydrogen atoms of the title compound. All non-hydrogen atoms were refined anisotropically. H-atoms were assigned in geometrically calculated positions and refined using a riding model where each H-atom was assigned a fixed isotropic displacement parameter with a value equal to 1.2U_{eq} of its parent atom (1.5U_{eq} for methyl groups).

Refinement of the structure was carried out on F^2 using full-matrix least-squares procedures, which minimized the function $\sum w(F_o^2 - F_c^2)^2$. The weighting scheme was based on counting statistics and included a factor to downweight the intense reflections. All calculations were performed using the *SHELXL-2014/7*⁴ program in OLEX2.⁵

The structure contains two molecules in the independent part of the unit cell and for this reason atoms were denoted as A and B. Both C14A and C14B have R configuration.

The X-ray crystal structure determination service unit of the Department of Chemistry and Biochemistry of the University of Bern is acknowledged for measuring, solving, refining and summarizing the structures of compounds XX, YY, ZZ. The Synergy diffractometer was partially funded by the Swiss National Science Foundation (SNF) within the R'Equip programme (project number 206021_177033).



A single crystal of the compound mounted on a glass fiber.

REFERENCES (In case this structure is submitted for publication, please use these references in the main text of a publication)

- 1) Oxford Diffraction (2018). *CrysAlisPro* (Version 1.171.40.37a). Oxford Diffraction Ltd., Yarnton, Oxfordshire, UK.
- 2) Macchi, P.; Bürgi, H.B.; Chimpri, A. S.; Hauser, J.; Gal, Z. (2011) *J. Appl. Cryst.*, **44**, 763-771
- 3) Sheldrick, G. M. (2015). *Acta Cryst.* **A71**, 3-8.
- 4) Sheldrick, G. M. (2015). *Acta Cryst.* **C71**, 3-8.
- 5) Dolomanov, O.V., Bourhis, L.J., Gildea, R.J, Howard, J.A.K. & Puschmann, H. (2009), *J. Appl. Cryst.* 42, 339-341.

Table 1. Crystal data and structure refinement for 19PR025_PP-43-P2.

Identification code	19PR025_PP-43-P2
Empirical formula	C ₂₆ H ₄₀ O ₉
Formula weight	496.58
Temperature/K	173.01(10)
Crystal system	orthorhombic
Space group	<i>P</i> 2 ₁ 2 ₁ 2 ₁
<i>a</i> /Å	15.17560(10)
<i>b</i> /Å	15.22550(10)
<i>c</i> /Å	21.96660(10)
α /°	90
β /°	90
γ /°	90
Volume/Å ³	5075.52(5)
<i>Z</i>	8
$\rho_{\text{calc}}/\text{cm}^3$	1.300
μ/mm^{-1}	0.804
<i>F</i> (000)	2144.0
Crystal size/mm ³	0.15 × 0.075 × 0.05
Radiation	CuK α (λ = 1.54184)
2 Θ range for data collection/°	7.064 to 143.07
Index ranges	-17 ≤ <i>h</i> ≤ 18, -18 ≤ <i>k</i> ≤ 18, -27 ≤ <i>l</i> ≤ 24
Reflections collected	46702
Independent reflections	9641 [<i>R</i> _{int} = 0.0357, <i>R</i> _{sigma} = 0.0277]
Data/restraints/parameters	9641/0/649
Goodness-of-fit on <i>F</i> ²	1.050
Final <i>R</i> indexes [<i>I</i> ≥ 2 σ (<i>I</i>)]	<i>R</i> ₁ = 0.0313, <i>wR</i> ₂ = 0.0745
Final <i>R</i> indexes [all data]	<i>R</i> ₁ = 0.0345, <i>wR</i> ₂ = 0.0763
Largest diff. peak/hole / e Å ⁻³	0.28/-0.16
Flack parameter	-0.01(4)

Table 2. Fractional Atomic Coordinates (×10⁴) and Equivalent Isotropic Displacement Parameters (Å²×10³) for 19PR025_PP-43-P2. *U*_{eq} is defined as 1/3 of the trace of the orthogonalised *U*_{ij} tensor.

Atom	<i>x</i>	<i>y</i>	<i>z</i>	<i>U</i> (eq)
O3A	7944.5(9)	5312.8(8)	7871.0(6)	20.4(3)
O3B	3130.3(9)	5651.0(8)	6818.6(6)	23.4(3)
O4A	10147.0(9)	6770.3(8)	8461.6(6)	25.3(3)
O4B	5343.7(9)	4022.6(8)	6820.3(6)	24.8(3)
O6A	9103.1(9)	5324.3(9)	8815.5(6)	23.4(3)
O2A	10607.9(9)	6489.8(9)	7268.8(7)	26.4(3)

O9A	5549.6(10)	5718.9(10)	8898.5(6)	30.5(3)
O1A	7410.4(9)	4987.9(10)	6774.9(6)	27.8(3)
O7A	8859.8(10)	3353.1(9)	7596.9(7)	31.7(4)
O6B	3501.3(9)	3936.6(9)	6768.9(7)	27.2(3)
O2B	5891.0(9)	5272.1(10)	6005.5(6)	28.4(3)
O5B	5914.2(10)	4505.6(9)	7702.8(7)	33.3(4)
O8A	5045.5(11)	6321.9(11)	8032.0(7)	37.0(4)
O1B	2896.5(11)	7216.1(10)	6374.1(7)	35.3(4)
O9B	2845.6(11)	6881.5(10)	8933.2(6)	36.5(4)
O7B	2295.8(11)	5391.9(12)	5445.9(7)	42.0(4)
O5A	9141.2(12)	7627.0(11)	8920.5(8)	46.6(5)
O8B	2394.9(13)	5499.5(12)	9073.8(8)	50.8(5)
C8A	9467.0(13)	5395.1(12)	8204.8(9)	20.3(4)
C6A	9698.6(13)	6634.4(12)	7411.8(9)	22.1(4)
C11	9022.5(13)	5149.7(12)	7060.0(8)	20.1(4)
C21B	5872.6(13)	3957.9(13)	7306.3(9)	24.0(4)
C7B	4804.0(13)	4802.6(12)	6759.4(9)	21.9(4)
C9A	8817.7(13)	4953.0(11)	7745.9(9)	19.1(4)
C5A	9058.2(13)	6171.7(12)	6972.8(9)	20.8(4)
C14A	7597.6(13)	5210.7(13)	8489.1(8)	21.7(4)
C8B	4012.8(14)	4513.2(12)	6373.6(9)	23.3(4)
C11A	8746.8(13)	3977.2(12)	7932.9(9)	23.5(4)
C7A	9493.6(13)	6380.3(12)	8065.8(9)	20.6(4)
C46	3971.1(14)	6117.1(13)	5925.3(9)	24.0(4)
C6B	5354.3(14)	5556.7(12)	6503.8(9)	22.7(4)
C17A	5645.1(15)	6171.0(13)	8376.1(9)	26.6(5)
C1B	3370.5(15)	6950.2(14)	5840.8(10)	29.7(5)
C13A	8323.5(14)	4787.8(13)	8869.6(9)	24.0(4)
C21A	9882.4(16)	7353.2(14)	8882.1(10)	30.5(5)
C11B	2607.9(14)	5039.6(15)	5887.9(10)	29.5(5)
C9B	3451.0(13)	5341.5(13)	6227.9(9)	23.0(4)
C2A	8414.4(15)	5057.2(14)	5973.0(9)	28.4(5)
C4A	9114.5(15)	6509.4(13)	6300.5(9)	27.5(5)
C15A	7278.7(14)	6104.9(13)	8704.6(9)	25.8(4)
C23A	10381.9(14)	4981.6(13)	8244.1(10)	27.2(5)
C1A	8299.0(13)	4751.3(13)	6629.5(9)	23.4(4)
C12A	8516.3(15)	3886.9(13)	8595.8(9)	27.0(5)
C17B	2610.0(15)	6078.3(15)	8738.5(10)	30.1(5)
C13B	2584.7(14)	4163.5(13)	6831.1(10)	26.9(5)
C14B	2529.0(14)	5065.4(13)	7139.5(9)	24.1(4)
C4B	5302.2(15)	7197.0(13)	6175.1(9)	28.4(5)
C24A	9895.7(13)	4686.5(13)	6878.9(9)	25.2(4)

C22B	6394.1(15)	3129.6(13)	7279.7(11)	31.4(5)
C3A	8386.9(15)	6052.3(14)	5932.1(9)	29.8(5)
C16A	6567.8(15)	6503.6(14)	8295.4(10)	28.6(5)
C24B	4245.6(15)	5836.1(15)	5272.2(9)	30.9(5)
C15B	2738.4(14)	5103.2(13)	7809.3(9)	25.9(4)
C5B	4771.5(14)	6348.2(12)	6343.8(9)	22.0(4)
C20A	8114.5(16)	4736.2(15)	9541.5(9)	32.0(5)
C18A	4671.9(15)	5406.6(16)	9029.5(11)	34.2(5)
C2B	3905.2(17)	7755.3(14)	5660.9(10)	35.2(5)
C23B	4279.1(15)	3958.4(14)	5821.4(10)	29.5(5)
C26A	8901.1(19)	7500.1(14)	6297.3(10)	38.6(6)
C12B	2184.7(15)	4269.8(14)	6203.4(10)	31.9(5)
C16B	2647.6(16)	6033.4(14)	8056.8(9)	30.7(5)
C20B	2164.5(15)	3440.3(14)	7199.9(11)	32.7(5)
C25B	5921.7(17)	7432.4(14)	6701.4(10)	36.1(5)
C3B	4634.1(17)	7949.0(14)	6112.1(10)	35.1(5)
C25A	10005.5(16)	6389.8(16)	5980.1(10)	34.4(5)
C19A	4662.9(17)	5090.9(16)	9673.5(11)	39.8(6)
C26B	5872.6(16)	7153.8(16)	5594.6(10)	36.1(5)
C18B	2914.4(19)	7012.3(18)	9585.2(10)	44.9(6)
C22A	10624.3(18)	7595.5(17)	9291.5(12)	45.5(6)
C19B	3241(3)	7907(2)	9679.7(15)	93.7(14)

Table 3. Anisotropic Displacement Parameters ($\text{\AA}^2 \times 10^3$) for 19PR025_PP-43-P2. The Anisotropic displacement factor exponent takes the form: $-2\pi^2[h^2a^{*2}U_{11}+2hka^*b^*U_{12}+\dots]$.

Atom	U_{11}	U_{22}	U_{33}	U_{23}	U_{13}	U_{12}
O3A	14.4(7)	26.4(7)	20.4(7)	1.9(5)	1.7(5)	1.6(5)
O3B	23.1(8)	24.7(7)	22.4(7)	-2.7(6)	2.2(6)	0.8(6)
O4A	22.1(8)	25.1(7)	28.7(7)	-3.5(6)	-3.3(6)	-2.8(6)
O4B	21.8(7)	22.9(7)	29.8(7)	-1.1(6)	-4.2(6)	4.1(6)
O6A	18.9(7)	29.8(7)	21.4(7)	2.7(6)	-2.1(6)	-4.9(6)
O2A	17.6(7)	26.6(7)	35.1(8)	-0.4(6)	4.8(7)	-4.7(6)
O9A	19.9(8)	40.9(8)	30.6(8)	8.4(6)	2.0(6)	0.6(6)
O1A	17.2(7)	43.1(8)	23.1(7)	-1.5(6)	-0.8(6)	-0.8(6)
O7A	33.8(9)	21.0(7)	40.3(9)	-2.0(6)	2.3(7)	1.1(6)
O6B	18.4(7)	23.9(7)	39.1(8)	-0.1(6)	2.0(7)	0.5(6)
O2B	20.6(8)	35.4(8)	29.2(8)	-0.5(6)	2.7(6)	5.6(7)
O5B	38.1(9)	29.1(8)	32.7(8)	-3.3(7)	-10.0(7)	6.0(7)
O8A	30.9(9)	43.3(9)	36.8(9)	7.1(7)	-5.0(8)	6.4(7)
O1B	37.0(10)	31.0(8)	37.9(9)	4.1(7)	7.7(7)	12.3(7)

O9B	44.2(10)	40.2(9)	24.9(7)	-8.3(6)	-3.3(7)	2.0(8)
O7B	32.1(9)	59.7(11)	34.4(9)	-0.9(8)	-14.7(7)	1.2(8)
O5A	41.7(11)	49.2(10)	48.9(10)	-20.5(8)	-13.1(9)	18.8(9)
O8B	60.5(13)	58.2(11)	33.7(9)	10.0(8)	0.2(9)	-19.7(10)
C8A	17.6(10)	22.3(9)	21.0(9)	2.0(7)	-0.1(8)	-0.1(8)
C6A	19.4(11)	18.9(9)	27.9(10)	1.8(8)	2.0(9)	-0.1(8)
C11	17.9(10)	19.9(9)	22.4(9)	-0.5(7)	0.1(8)	-0.1(8)
C21B	19.6(11)	25.3(10)	27.1(10)	4.6(9)	0.5(9)	-1.7(8)
C7B	18.6(10)	21.4(9)	25.8(10)	-0.6(8)	-0.8(8)	4.1(8)
C9A	14.1(10)	19.8(9)	23.5(9)	0.1(7)	0.6(8)	1.5(8)
C5A	17.9(10)	21.6(9)	22.9(10)	2.4(7)	2.3(8)	0.3(8)
C14A	17.4(10)	27.9(10)	19.8(9)	1.9(8)	2.4(8)	-4.2(8)
C8B	19.0(10)	23.6(10)	27.2(10)	-2.9(8)	-0.5(9)	-0.8(8)
C11A	15.9(10)	22.2(10)	32.3(11)	2.0(9)	-2.0(9)	0.9(8)
C7A	16.3(10)	21.5(9)	23.9(10)	-0.9(7)	-2.4(8)	-0.4(8)
C46	22.2(11)	28.1(10)	21.6(10)	0.8(8)	-2.8(9)	4.0(9)
C6B	20.5(11)	26.3(10)	21.1(9)	-0.8(8)	-0.5(8)	0.1(8)
C17A	28.3(12)	25.3(10)	26.2(10)	0.3(8)	2.0(9)	6.3(9)
C1B	28.8(12)	34.3(11)	26.0(11)	3.4(9)	-1.2(9)	9.5(9)
C13A	20.6(11)	25.2(10)	26.4(10)	3.2(8)	-1.2(9)	-5.6(8)
C21A	39.0(14)	25.4(10)	27.0(11)	-3.2(8)	-4.8(10)	3.9(10)
C11B	21.2(11)	38.5(12)	28.7(11)	-10.4(9)	-4.0(9)	6.1(10)
C9B	19.9(11)	27.5(10)	21.5(10)	-5.1(8)	-1.8(8)	4.5(8)
C2A	26.1(12)	36.0(11)	23.2(10)	-3.5(9)	1.1(9)	-4.6(9)
C4A	30.8(12)	29.6(10)	22.2(10)	2.1(8)	1.0(9)	-1.3(9)
C15A	21.1(11)	32.1(11)	24.1(10)	-3.5(8)	4.3(9)	-2.0(9)
C23A	19.3(11)	26.5(10)	35.9(11)	3.0(9)	-3.4(9)	0.1(9)
C1A	20.5(11)	25.4(10)	24.4(11)	-1.0(8)	1.2(8)	-0.9(8)
C12A	25.6(11)	25.3(10)	30.2(11)	6.9(8)	-1.8(9)	-2.9(9)
C17B	21.0(11)	39.8(12)	29.4(11)	-2.1(10)	-1.3(9)	-0.9(10)
C13B	17.6(10)	28.3(10)	34.7(11)	-6.3(9)	0.2(9)	1.2(8)
C14B	16.6(10)	25.6(10)	29.9(11)	-1.5(8)	0.6(8)	0.7(8)
C4B	30.8(12)	27.3(10)	27.2(11)	4.4(8)	1.1(10)	-2.5(9)
C24A	20.8(11)	26.1(10)	28.7(11)	-2.2(8)	3.0(9)	1.6(8)
C22B	28.1(12)	28.9(11)	37.3(12)	3.9(9)	-4.2(10)	4.8(9)
C3A	30.7(12)	38.2(12)	20.5(10)	5.0(9)	0.2(9)	-0.2(10)
C16A	27.6(12)	29.3(11)	29.0(11)	2.1(9)	6.2(10)	4.2(9)
C24B	29.4(12)	41.0(12)	22.2(10)	-0.3(9)	-1.1(9)	4.1(10)
C15B	22.0(11)	28.5(10)	27.1(11)	1.0(8)	0.2(9)	-1.0(9)
C5B	21.8(11)	23.3(9)	20.7(9)	0.0(8)	0.7(8)	0.3(8)
C20A	33.1(13)	38.4(12)	24.4(11)	7.1(9)	-1.4(10)	-8.2(10)
C18A	17.5(11)	42.6(13)	42.4(13)	6.4(10)	1.7(10)	-1.8(10)

C2B	40.4(14)	33.3(11)	32.0(12)	9.5(9)	1.5(11)	10.9(11)
C23B	24.4(12)	31.4(11)	32.6(11)	-11.2(9)	-3.6(10)	3.5(9)
C26A	56.8(16)	29.3(11)	29.8(12)	9.4(9)	-0.2(12)	-2.3(11)
C12B	19.1(11)	37.3(12)	39.1(13)	-12.9(10)	-1.2(10)	-1.4(9)
C16B	34.9(13)	31.5(11)	25.9(11)	0.2(9)	-1.2(10)	-5.5(10)
C20B	23.7(12)	28.0(11)	46.4(13)	-5.3(10)	4.7(11)	-3.4(9)
C25B	40.0(14)	29.8(11)	38.4(13)	3.1(9)	-3.4(11)	-10.1(10)
C3B	44.3(15)	24.5(10)	36.6(12)	6.5(9)	3.9(11)	1.5(10)
C25A	33.8(13)	43.7(13)	25.7(11)	4.3(10)	5.6(10)	-8.8(10)
C19A	35.2(14)	44.0(13)	40.0(13)	4.1(11)	6.8(12)	-3.8(11)
C26B	34.8(14)	38.8(12)	34.7(12)	8.1(10)	6.5(11)	-3.2(11)
C18B	45.4(16)	64.0(17)	25.4(12)	-12.1(11)	-5.9(11)	18.2(13)
C22A	47.0(16)	44.9(14)	44.5(14)	-12.4(11)	-15.1(13)	2.0(12)
C19B	165(4)	65(2)	51.3(19)	-24.7(16)	-36(2)	1(2)

Table 4. Bond Lengths for 19PR025_PP-43-P2.

Atom	Atom	Length/Å	Atom	Atom	Length/Å
O3A	C9A	1.460(2)	C9A	C11A	1.545(3)
O3A	C14A	1.465(2)	C5A	C4A	1.566(3)
O3B	C9B	1.464(2)	C14A	C13A	1.525(3)
O3B	C14B	1.457(2)	C14A	C15A	1.520(3)
O4A	C7A	1.446(2)	C8B	C9B	1.555(3)
O4A	C21A	1.342(2)	C8B	C23B	1.532(3)
O4B	C21B	1.339(2)	C11A	C12A	1.504(3)
O4B	C7B	1.449(2)	C46	C1B	1.573(3)
O6A	C8A	1.455(2)	C46	C9B	1.568(3)
O6A	C13A	1.443(2)	C46	C24B	1.554(3)
O2A	C6A	1.432(2)	C46	C5B	1.563(3)
O9A	C17A	1.346(2)	C6B	C5B	1.536(3)
O9A	C18A	1.443(3)	C17A	C16A	1.500(3)
O1A	C1A	1.432(2)	C1B	C2B	1.522(3)
O7A	C11A	1.215(2)	C13A	C12A	1.526(3)
O6B	C8B	1.459(2)	C13A	C20A	1.511(3)
O6B	C13B	1.440(2)	C21A	C22A	1.487(3)
O2B	C6B	1.431(2)	C11B	C9B	1.551(3)
O5B	C21B	1.207(2)	C11B	C12B	1.505(3)
O8A	C17A	1.205(3)	C2A	C1A	1.526(3)
O1B	C1B	1.433(3)	C2A	C3A	1.518(3)
O9B	C17B	1.344(3)	C4A	C3A	1.536(3)
O9B	C18B	1.450(3)	C4A	C26A	1.543(3)

O7B	C11B	1.206(3)	C4A	C25A	1.535(3)
O5A	C21A	1.203(3)	C15A	C16A	1.530(3)
O8B	C17B	1.194(3)	C17B	C16B	1.500(3)
C8A	C9A	1.562(3)	C13B	C14B	1.533(3)
C8A	C7A	1.531(3)	C13B	C12B	1.515(3)
C8A	C23A	1.527(3)	C13B	C20B	1.508(3)
C6A	C5A	1.540(3)	C14B	C15B	1.506(3)
C6A	C7A	1.520(3)	C4B	C5B	1.567(3)
C11	C9A	1.567(3)	C4B	C25B	1.532(3)
C11	C5A	1.569(3)	C4B	C3B	1.536(3)
C11	C1A	1.571(3)	C4B	C26B	1.543(3)
C11	C24A	1.553(3)	C15B	C16B	1.523(3)
C21B	C22B	1.490(3)	C18A	C19A	1.494(3)
C7B	C8B	1.534(3)	C2B	C3B	1.514(4)
C7B	C6B	1.527(3)	C18B	C19B	1.464(4)

Table 5. Bond Angles for 19PR025_PP-43-P2.

Atom	Atom	Atom	Angle/°	Atom	Atom	Atom	Angle/°
C9A	O3A	C14A	117.45(14)	O8A	C17A	C16A	124.51(19)
C14B	O3B	C9B	116.09(14)	O1B	C1B	C46	114.97(16)
C21A	O4A	C7A	118.69(16)	O1B	C1B	C2B	104.62(17)
C21B	O4B	C7B	118.21(15)	C2B	C1B	C46	111.78(18)
C13A	O6A	C8A	115.43(14)	O6A	C13A	C14A	107.94(15)
C17A	O9A	C18A	115.96(17)	O6A	C13A	C12A	108.61(16)
C13B	O6B	C8B	115.23(15)	O6A	C13A	C20A	106.38(16)
C17B	O9B	C18B	117.29(19)	C14A	C13A	C12A	107.57(16)
O6A	C8A	C9A	108.88(15)	C20A	C13A	C14A	113.92(18)
O6A	C8A	C7A	105.45(15)	C20A	C13A	C12A	112.24(17)
O6A	C8A	C23A	105.22(15)	O4A	C21A	C22A	110.7(2)
C7A	C8A	C9A	108.07(15)	O5A	C21A	O4A	123.9(2)
C23A	C8A	C9A	115.62(16)	O5A	C21A	C22A	125.4(2)
C23A	C8A	C7A	113.03(16)	O7B	C11B	C9B	125.4(2)
O2A	C6A	C5A	113.60(16)	O7B	C11B	C12B	123.3(2)
O2A	C6A	C7A	111.44(16)	C12B	C11B	C9B	111.15(18)
C7A	C6A	C5A	110.27(16)	O3B	C9B	C8B	105.12(15)
C9A	C11	C5A	108.29(14)	O3B	C9B	C46	107.50(15)
C9A	C11	C1A	111.49(15)	O3B	C9B	C11B	104.37(15)
C5A	C11	C1A	109.49(15)	C8B	C9B	C46	114.95(16)
C24A	C11	C9A	109.19(15)	C11B	C9B	C8B	108.11(16)
C24A	C11	C5A	112.94(16)	C11B	C9B	C46	115.73(17)

C24A C11 C1A 105.47(15) C3A C2A C1A 110.94(17)
O4B C21B C22B 110.44(17) C3A C4A C5A 107.99(16)
O5B C21B O4B 123.75(18) C3A C4A C26A 106.84(19)
O5B C21B C22B 125.81(19) C26A C4A C5A 108.30(16)
O4B C7B C8B 104.96(14) C25A C4A C5A 116.19(18)
O4B C7B C6B 109.95(16) C25A C4A C3A 109.75(17)
C6B C7B C8B 116.16(17) C25A C4A C26A 107.38(19)
O3A C9A C8A 106.82(14) C14A C15A C16A 113.39(17)
O3A C9A C11 106.81(14) O1A C1A C11 115.27(15)
O3A C9A C11A 104.33(15) O1A C1A C2A 104.01(16)
C8A C9A C11 114.39(15) C2A C1A C11 111.78(16)
C11A C9A C8A 106.66(15) C11A C12A C13A 110.13(16)
C11A C9A C11 116.94(15) O9B C17B C16B 110.42(19)
C6A C5A C11 113.52(16) O8B C17B O9B 123.2(2)
C6A C5A C4A 113.96(16) O8B C17B C16B 126.3(2)
C4A C5A C11 116.28(15) O6B C13B C14B 108.06(16)
O3A C14A C13A 107.05(16) O6B C13B C12B 109.04(17)
O3A C14A C15A 107.94(15) O6B C13B C20B 106.52(16)
C15A C14A C13A 115.93(16) C12B C13B C14B 106.50(17)
O6B C8B C7B 105.10(16) C20B C13B C14B 113.16(17)
O6B C8B C9B 108.59(15) C20B C13B C12B 113.41(18)
O6B C8B C23B 106.25(15) O3B C14B C13B 107.44(16)
C7B C8B C9B 108.05(15) O3B C14B C15B 108.47(16)
C23B C8B C7B 112.90(17) C15B C14B C13B 117.00(17)
C23B C8B C9B 115.38(17) C25B C4B C5B 109.25(16)
O7A C11A C9A 125.48(18) C25B C4B C3B 107.38(18)
O7A C11A C12A 123.33(18) C25B C4B C26B 106.82(19)
C12A C11A C9A 111.19(16) C3B C4B C5B 107.27(18)
O4A C7A C8A 107.48(15) C3B C4B C26B 109.13(17)
O4A C7A C6A 108.87(15) C26B C4B C5B 116.66(18)
C6A C7A C8A 116.30(16) C2A C3A C4A 113.65(18)
C9B C46 C1B 111.45(17) C17A C16A C15A 117.07(17)
C24B C46 C1B 105.57(16) C14B C15B C16B 111.42(17)
C24B C46 C9B 108.60(16) C46 C5B C4B 116.48(16)
C24B C46 C5B 113.36(17) C6B C5B C46 113.91(16)
C5B C46 C1B 109.76(16) C6B C5B C4B 113.91(17)
C5B C46 C9B 108.13(15) O9A C18A C19A 107.65(18)
O2B C6B C7B 111.40(16) C3B C2B C1B 112.11(18)
O2B C6B C5B 112.98(15) C11B C12B C13B 109.34(17)
C7B C6B C5B 111.05(17) C17B C16B C15B 113.72(18)
O9A C17A C16A 111.96(18) C2B C3B C4B 113.33(18)
O8A C17A O9A 123.4(2) O9B C18B C19B 107.0(2)

Table 6. Torsion Angles for 19PR025_PP-43-P2.

A	B	C	D	Angle/°	A	B	C	D	Angle/°
O3A	C9A	C11A	O7A	119.8(2)	C46	C1B	C2B	C3B	-55.8(2)
O3A	C9A	C11A	C12A	-60.2(2)	C6B	C7B	C8B	O6B	-168.08(15)
O3A	C14A	C13A	O6A	54.99(19)	C6B	C7B	C8B	C9B	-52.3(2)
O3A	C14A	C13A	C12A	-62.03(19)	C6B	C7B	C8B	C23B	76.5(2)
O3A	C14A	C13A	C20A	172.89(16)	C17A	O9A	C18A	C19A	-168.64(18)
O3A	C14A	C15A	C16A	58.6(2)	C1B	C46	C9B	O3B	-59.0(2)
O3B	C14B	C15B	C16B	59.0(2)	C1B	C46	C9B	C8B	-175.61(15)
O4B	C7B	C8B	O6B	70.28(18)	C1B	C46	C9B	C11B	57.2(2)
O4B	C7B	C8B	C9B	-173.93(15)	C1B	C46	C5B	C6B	174.65(16)
O4B	C7B	C8B	C23B	-45.1(2)	C1B	C46	C5B	C4B	-49.6(2)
O4B	C7B	C6B	O2B	44.6(2)	C1B	C2B	C3B	C4B	60.4(3)
O4B	C7B	C6B	C5B	171.44(15)	C13A	O6A	C8A	C9A	7.6(2)
O6A	C8A	C9A	O3A	49.85(18)	C13A	O6A	C8A	C7A	123.33(17)
O6A	C8A	C9A	C11	167.81(14)	C13A	O6A	C8A	C23A	-116.94(16)
O6A	C8A	C9A	C11A	-61.28(19)	C13A	C14A	C15A	C16A	178.56(17)
O6A	C8A	C7A	O4A	68.05(18)	C21A	O4A	C7A	C8A	-115.36(18)
O6A	C8A	C7A	C6A	-169.68(15)	C21A	O4A	C7A	C6A	117.88(18)
O6A	C13A	C12A	C11A	-60.9(2)	C9B	O3B	C14B	C13B	14.4(2)
O2A	C6A	C5A	C11	72.5(2)	C9B	O3B	C14B	C15B	141.72(16)
O2A	C6A	C5A	C4A	-63.7(2)	C9B	C46	C1B	O1B	50.1(2)
O2A	C6A	C7A	O4A	48.5(2)	C9B	C46	C1B	C2B	169.21(17)
O2A	C6A	C7A	C8A	-73.0(2)	C9B	C46	C5B	C6B	52.9(2)
O9A	C17A	C16A	C15A	14.9(3)	C9B	C46	C5B	C4B	-171.38(16)
O7A	C11A	C12A	C13A	-173.91(19)	C9B	C11B	C12B	C13B	13.3(2)
O6B	C8B	C9B	O3B	49.52(19)	C15A	C14A	C13A	O6A	-65.5(2)
O6B	C8B	C9B	C46	167.50(15)	C15A	C14A	C13A	C12A	177.49(16)
O6B	C8B	C9B	C11B	-61.51(19)	C15A	C14A	C13A	C20A	52.4(2)
O6B	C13B	C14B	O3B	48.8(2)	C23A	C8A	C9A	O3A	167.99(15)
O6B	C13B	C14B	C15B	-73.4(2)	C23A	C8A	C9A	C11	-74.0(2)
O6B	C13B	C12B	C11B	-65.0(2)	C23A	C8A	C9A	C11A	56.9(2)
O2B	C6B	C5B	C46	73.9(2)	C23A	C8A	C7A	O4A	-46.4(2)
O2B	C6B	C5B	C4B	-63.0(2)	C23A	C8A	C7A	C6A	75.9(2)
O8A	C17A	C16A	C15A	-168.45(19)	C1A	C11	C9A	O3A	-57.23(18)
O1B	C1B	C2B	C3B	69.2(2)	C1A	C11	C9A	C8A	-175.19(15)
O9B	C17B	C16B	C15B	157.93(19)	C1A	C11	C9A	C11A	59.1(2)
O7B	C11B	C9B	O3B	112.0(2)	C1A	C11	C5A	C6A	175.50(15)
O7B	C11B	C9B	C8B	-136.4(2)	C1A	C11	C5A	C4A	-49.4(2)
O7B	C11B	C9B	C46	-5.9(3)	C1A	C2A	C3A	C4A	60.5(2)

O7B	C11B	C12B	C13B	-163.4(2)	C17B	O9B	C18B	C19B	175.8(3)
O8B	C17B	C16B	C15B	-22.9(3)	C13B	O6B	C8B	C7B	126.85(17)
C8A	O6A	C13A	C14A	-62.65(19)	C13B	O6B	C8B	C9B	11.4(2)
C8A	O6A	C13A	C12A	53.7(2)	C13B	O6B	C8B	C23B	-113.26(18)
C8A	O6A	C13A	C20A	174.71(16)	C13B	C14B	C15B	C16B	-179.37(18)
C8A	C9A	C11A	O7A	-127.4(2)	C14B	O3B	C9B	C8B	-64.96(19)
C8A	C9A	C11A	C12A	52.6(2)	C14B	O3B	C9B	C46	172.13(15)
C6A	C5A	C4A	C3A	-174.93(17)	C14B	O3B	C9B	C11B	48.7(2)
C6A	C5A	C4A	C26A	-59.6(2)	C14B	C13B	C12B	C11B	51.4(2)
C6A	C5A	C4A	C25A	61.3(2)	C14B	C15B	C16B	C17B	164.64(19)
C11	C9A	C11A	O7A	2.1(3)	C24A	C11	C9A	O3A	-173.37(14)
C11	C9A	C11A	C12A	-177.92(17)	C24A	C11	C9A	C8A	68.66(19)
C11	C5A	C4A	C3A	50.1(2)	C24A	C11	C9A	C11A	-57.0(2)
C11	C5A	C4A	C26A	165.48(19)	C24A	C11	C5A	C6A	-67.3(2)
C11	C5A	C4A	C25A	-73.6(2)	C24A	C11	C5A	C4A	67.8(2)
C21B	O4B	C7B	C8B	-154.15(16)	C24A	C11	C1A	O1A	171.13(16)
C21B	O4B	C7B	C6B	80.2(2)	C24A	C11	C1A	C2A	-70.4(2)
C7B	O4B	C21B	O5B	1.4(3)	C3A	C2A	C1A	O1A	67.3(2)
C7B	O4B	C21B	C22B	-178.16(17)	C3A	C2A	C1A	C11	-57.7(2)
C7B	C8B	C9B	O3B	-63.98(19)	C24B	C46	C1B	O1B	167.86(19)
C7B	C8B	C9B	C46	54.0(2)	C24B	C46	C1B	C2B	-73.1(2)
C7B	C8B	C9B	C11B	-175.01(16)	C24B	C46	C9B	O3B	-174.85(16)
C7B	C6B	C5B	C46	-52.1(2)	C24B	C46	C9B	C8B	68.5(2)
C7B	C6B	C5B	C4B	170.97(16)	C24B	C46	C9B	C11B	-58.7(2)
C9A	O3A	C14A	C13A	4.4(2)	C24B	C46	C5B	C6B	-67.6(2)
C9A	O3A	C14A	C15A	129.89(16)	C24B	C46	C5B	C4B	68.1(2)
C9A	C8A	C7A	O4A	-175.64(14)	C5B	C46	C1B	O1B	-69.6(2)
C9A	C8A	C7A	C6A	-53.4(2)	C5B	C46	C1B	C2B	49.4(2)
C9A	C11	C5A	C6A	53.7(2)	C5B	C46	C9B	O3B	61.75(18)
C9A	C11	C5A	C4A	-171.12(16)	C5B	C46	C9B	C8B	-54.9(2)
C9A	C11	C1A	O1A	52.7(2)	C5B	C46	C9B	C11B	177.89(16)
C9A	C11	C1A	C2A	171.22(16)	C5B	C4B	C3B	C2B	-55.3(2)
C9A	C11A	C12A	C13A	6.1(2)	C20A	C13A	C12A	C11A	-178.27(18)
C5A	C6A	C7A	O4A	175.61(15)	C18A	O9A	C17A	O8A	0.6(3)
C5A	C6A	C7A	C8A	54.1(2)	C18A	O9A	C17A	C16A	177.27(18)
C5A	C11	C9A	O3A	63.29(19)	C23B	C8B	C9B	O3B	168.61(16)
C5A	C11	C9A	C8A	-54.7(2)	C23B	C8B	C9B	C46	-73.4(2)
C5A	C11	C9A	C11A	179.62(16)	C23B	C8B	C9B	C11B	57.6(2)
C5A	C11	C1A	O1A	-67.1(2)	C26A	C4A	C3A	C2A	-170.81(18)
C5A	C11	C1A	C2A	51.4(2)	C12B	C11B	C9B	O3B	-64.51(19)
C5A	C4A	C3A	C2A	-54.5(2)	C12B	C11B	C9B	C8B	47.0(2)
C14A	O3A	C9A	C8A	-57.28(19)	C12B	C11B	C9B	C46	177.59(16)

C14A O3A C9A C11	179.90(14)	C12B C13B C14B O3B	-68.2(2)
C14A O3A C9A C11A	55.45(19)	C12B C13B C14B C15B	169.61(18)
C14A C13A C12A C11A	55.7(2)	C20B C13B C14B O3B	166.54(17)
C14A C15A C16A C17A	79.5(2)	C20B C13B C14B C15B	44.3(3)
C8B O6B C13B C14B	-63.9(2)	C20B C13B C12B C11B	176.51(17)
C8B O6B C13B C12B	51.5(2)	C25B C4B C5B C46	167.74(18)
C8B O6B C13B C20B	174.26(16)	C25B C4B C5B C6B	-56.5(2)
C8B C7B C6B O2B	-74.4(2)	C25B C4B C3B C2B	-172.65(18)
C8B C7B C6B C5B	52.5(2)	C3B C4B C5B C46	51.6(2)
C7A O4A C21A O5A	-6.2(3)	C3B C4B C5B C6B	-172.63(17)
C7A O4A C21A C22A	173.02(18)	C25A C4A C3A C2A	73.1(2)
C7A C8A C9A O3A	-64.21(18)	C26B C4B C5B C46	-71.0(2)
C7A C8A C9A C11	53.7(2)	C26B C4B C5B C6B	64.7(2)
C7A C8A C9A C11A	-175.34(15)	C26B C4B C3B C2B	71.9(2)
C7A C6A C5A C11	-53.4(2)	C18B O9B C17B O8B	5.8(3)
C7A C6A C5A C4A	170.43(16)	C18B O9B C17B C16B	-175.02(19)

Table 7. Hydrogen Atom Coordinates ($\text{\AA}\times 10^4$) and Isotropic Displacement Parameters ($\text{\AA}^2\times 10^3$) for 19PR025_PP-43-P2.

Atom	x	y	z	U(eq)
H2A	10887	6944	7327	40
H1A	7363	5054	7144	42
H2B	6352	5064	6137	43
H1B	2797	6785	6587	53
H6A	9591	7267	7375	26
H7B	4591	4971	7164	26
H5A	8476	6370	7109	25
H14A	7093	4810	8475	26
H7A	8918	6630	8172	25
H6B	5755	5746	6828	27
H1BA	2944	6828	5517	36
H2AA	8974	4847	5817	34
H2AB	7949	4810	5723	34
H15A	7777	6503	8721	31
H15B	7046	6048	9114	31
H23A	10668	5174	8610	41
H23B	10725	5158	7898	41
H23C	10328	4353	8249	41
H1AA	8348	4110	6640	28
H12A	9003	3615	8812	32

H12B	8003	3512	8639	32
H14B	1929	5290	7083	29
H24A	10385	5063	6973	38
H24B	9891	4564	6450	38
H24C	9951	4146	7101	38
H22D	6001	2637	7260	47
H22E	6754	3083	7637	47
H22F	6763	3136	6925	47
H3AA	7818	6255	6077	36
H3AB	8441	6224	5508	36
H16A	6563	7133	8362	34
H16B	6738	6405	7875	34
H24D	3786	5487	5094	46
H24E	4779	5498	5291	46
H24F	4341	6350	5027	46
H15C	3336	4897	7875	31
H15D	2342	4716	8029	31
H5B	4494	6500	6733	26
H20A	8563	4402	9745	48
H20B	7554	4456	9597	48
H20C	8095	5318	9709	48
H18A	4518	4931	8756	41
H18B	4248	5877	8977	41
H2BA	4161	7661	5262	42
H2BB	3517	8260	5635	42
H23D	4440	3379	5954	44
H23E	4772	4228	5621	44
H23F	3792	3920	5544	44
H26A	8369	7603	6523	58
H26B	8824	7696	5885	58
H26C	9377	7818	6482	58
H12C	2279	3740	5967	38
H12D	1555	4366	6238	38
H16C	3143	6380	7916	37
H16D	2116	6294	7892	37
H20D	2128	2917	6958	49
H20E	1583	3617	7321	49
H20F	2515	3327	7555	49
H25D	5598	7429	7077	54
H25E	6165	8006	6634	54
H25F	6390	7009	6722	54
H3BA	4374	8065	6507	42

H3BB	4942	8476	5984	42
H25A	10454	6697	6203	52
H25B	9970	6621	5574	52
H25C	10149	5776	5963	52
H19A	5110	4651	9727	60
H19B	4096	4844	9765	60
H19C	4777	5575	9942	60
H26D	6291	6683	5631	54
H26E	6181	7699	5543	54
H26F	5501	7052	5248	54
H18C	3319	6589	9761	54
H18D	2343	6940	9776	54
H22A	10755	7112	9557	68
H22B	10462	8098	9530	68
H22C	11135	7733	9052	68
H19D	2836	8319	9503	141
H19E	3807	7969	9490	141
H19F	3293	8020	10108	141

7.3 NMR and X-ray Chapter 6

C–H Functionalization of Manoyl Oxide Derivatives via Selective 1,5-HAT

Manoyl oxide derivatives:

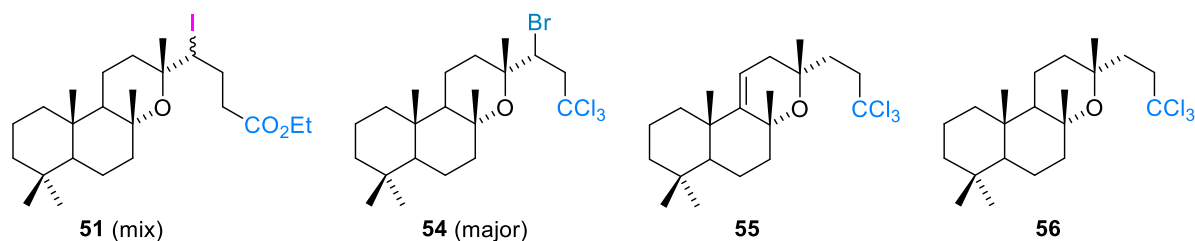


Table 1. NMR data for compounds **51**, **54**, **55** and **56** (assigned basing on ^1H , ^{13}C , DEPT, HSQC, HMBC, COSY-45, NOESY NMR experiments).

N ^o C	51		54 (major epimer)		55		56	
	δ ^1H ; m/J, Hz	δ ^{13}C ; m	δ ^1H ; m/J, Hz	δ ^{13}C ; m	δ ^1H ; m/J, Hz	δ ^{13}C ; m	δ ^1H ; m/J, Hz	δ ^{13}C ; m
1	1.60; m 0.83; m	39.13; t	1.61; m 0.86; m	39.15; t	1.74; m 1.35; m	38.75; t	1.61; m 0.87; m	39.23; t
2	1.59; m 1.42; m	18.59; t	1.60; m 1.43; m	18.56; t	1.66; m 1.53; m	19.09; t	1.61; m 1.43; m	18.63; t
3	1.37; m 1.13; m	42.17; t	1.37; m 1.14; m	42.16; t	1.37; m 1.11; m	41.96; t	1.37; m 1.14; m	42.21; t
4	-	33.27; s	-	33.27; s	-	33.73; s	-	37.32; s
5	0.92; m	56.45; d	0.89; dd/12.1; 2.5	56.55; d	0.92; dd/12.2; 2.2	54.00; d	0.95; dd/12.1; 2.7	56.50; d
6	1.63; m 1.24; m	19.88; t	1.62; m 1.25; m	19.84; t	1.66; m 1.40; m	20.11; t	1.65; m 1.31; m	19.85; t
7	1.72; d 1.40; m	42.69; t	1.73; m 1.37; m	42.76; t	1.85; m 1.55; m	43.00; t	1.72; m 1.32; m	43.03; t
8	-	76.01; s	-	76.45; s	-	74.55; s	-	74.90; s
9	1.16; m	57.42; d	1.18; m	57.23; d	-	153.00; s	1.10; m	58.13; d
10	-	36.84; s	-	36.94; s	-	39.67; s	-	36.90; s
11	1.56; m 1.45; m	15.54; t	1.59; m 1.47; m	15.28; t	5.51; dd/6.2; 3.6	112.60; d	1.59; m 1.54; m	15.36; t
12	1.86; m 1.54; m	37.84; t	2.00; m 1.54; m	36.72; t	2.11; m 2.05; m	35.74; t	1.62; m 1.52; m	36.69; t
13	-	73.93; s	-	74.40; s	-	71.11; s	-	71.71; s
14	3.95; dd/11.3; 2	54.13; d	3.99; dd/7.8; 0.8	58.82; d	1.98; m 1.79; m	37.70; t	1.85; m 1.77; m	41.78; t
15	2.29; m 1.90; m	30.10; t	3.73; dd/15.8; 1.2 3.06; q/7.9	57.36; t	2.78; m 2.72; m	50.50; t	2.88; m 2.73; m	50.18; t
16	1.37; s	23.05; q	1.32; s	22.26; q	1.24; s	28.76; q	1.26; s	28.00; q
17	1.24; s	24.55; q	1.25; s	24.71; q	1.40; s	30.78; q	1.27; s	24.70; q
18	0.84; s	33.29; q	0.84; s	33.32; q	0.84; s	33.38; q	0.86; s	33.32; q
19	0.78; s	21.27; q	0.78; s	21.27; q	0.83; s	21.61; q	0.79; s	21.28; q
20	0.74; s	15.65; q	0.76; s	15.55; q	1.07; s	22.31; q	0.76; s	15.72; q
21	2.66; m 2.38; m	35.40; t	-	98.61; s	-	101.05; s	-	101.11; s
22	-	172.89; s						
CH ₂ (OEt)	4.12; q/7	60.35; t						
CH ₃ (OEt)	1.25; t/7	14.24; q						

Epi-Manoyl oxide derivatives:

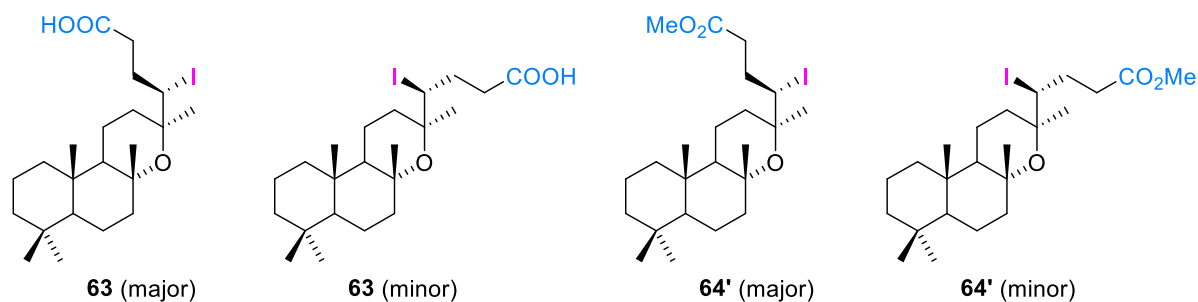


Table 2. NMR data for compounds **63** and **64** (assigned basing on ^1H , ^{13}C , DEPT, HSQC, HMBC, COSY-45, NOESY NMR experiments).

N ^o C	63 (major)		63 (minor)		64' (major)		64' (minor)	
	δ ^1H ; m/J, Hz	δ ^{13}C ; m	δ ^1H ; m/J, Hz	δ ^{13}C ; m	δ ^1H ; m/J, Hz	δ ^{13}C ; m	δ ^1H ; m/J, Hz	δ ^{13}C ; m
1	1.56; m 0.85; m	38.92; t	1.56; m 0.88; m	39.04; t	1.55; m 0.84; m	38.89; t	1.56; m 0.85; m	39.03; t
2	1.59; m 1.42; m	18.46; t	1.59; m 1.49; m	18.48; t	1.55; m 1.32; m	18.43; t	1.57; m 1.42; m	18.47; t
3	1.37; m 1.15; m	42.08; t	1.37; m 1.15; m	42.07; t	1.36; m 1.14; m	42.04; t	1.37; m 1.15; m	42.06; t
4	-	33.18; s	-	33.19; s	-	33.14; s	-	33.18; s
5	0.93; d/12	56.52; d	0.94; dd/12.4; 2.4	56.49; d	0.92; dd/12.1; 2.2	56.45; d	0.93; dd/12.2; 2.4	56.46; d
6	1.63; m 1.24; m	20.00; t	1.64; m 1.24; m	20.00; t	1.62; m 1.21; m	19.15; t	1.63; m 1.23; m	19.96; t
7	1.76; m 1.33; m	43.28; t	1.82; m 1.40; m	43.50; t	1.75; m 1.32; m	43.42; t	1.81; m 1.38; m	43.47; t
8	-	75.89; s	-	76.27; s	-	75.80; s	-	75.18; s
9	1.34; m	55.01; d	1.43 m	55.08; d	1.30; m	55.20; d	1.41 m	55.34; d
10	-	36.93; s	-	36.93; s	-	36.93; s	-	37.03; s
11	1.56; m 1.34; m	14.85; t	1.57; m 1.43; m	15.14; t	1.55; m 1.32; m	14.80; t	1.55; m 1.41; m	15.19; t
12	2.25; m 1.76; m	36.00; t	2.17; m 1.76; m	36.26; t	2.26; m 1.73; m	36.12; t	2.15; m 1.74; m	30.42; t
13	-	74.74; s	-	74.54; s	-	74.72; s	-	74.49; s
14	4.18; d/ 11.1	48.31; d	4.27; dd/11.5; 1.8	53.56; d	4.17; dd/11.3; 1.5	48.31; d	4.28; dd/11.5; 1.8	54.12; d
15	2.56; m 2.01; m	30.22; t	2.17; m 1.76; m	31.26; t	2.53; m 2.32; m	30.22; t	2.12; m 1.91; m	31.49; t
16	1.34; s	25.28; q	1.32; s	28.73; q	1.32; s	25.43; q	1.30; s	28.75; q
17	1.17; s	24.94; q	1.36; s	24.34; q	1.16; s	24.85; q	1.34; s	24.20; q
18	0.85; s	33.29; q	0.85; s	33.33; q	0.84; s	33.29; q	0.85; s	33.32; q
19	0.76; s	21.32; q	0.76; s	21.32; q	0.76; s	21.28; q	0.78; s	21.22; q
20	0.76; s	15.24; q	0.76; s	15.24; q	0.74; s	15.27; q	0.77; s	15.36; q
21	2.75; 2.39	34.79; t	2.76; m 2.54; m	34.90; t	2.68; 2.38	34.97; t	2.68; m 2.50; m	34.07; t
22	-	178.01; s	-	177.5; s	-	173.16; s	-	173.37; s
OMe					3.65; s	51.58; q	3.69; s	51.66; q

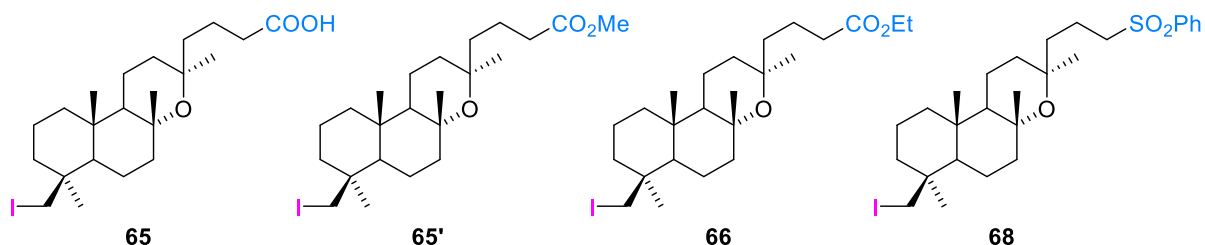


Table 3. NMR data for compounds **65**, **65'**, **66** and **68** (assigned basing on ^1H , ^{13}C , DEPT, HSQC, HMBC, COSY-45, NOESY NMR experiments).

N ^o C	65		65'		66		68	
	δ ^1H ; m/J, Hz	δ ^{13}C ; m	δ ^1H ; m/J, Hz	δ ^{13}C ; m	δ ^1H ; m/J, Hz	δ ^{13}C ; m	δ ^1H ; m/J, Hz	δ ^{13}C ; m
1	1.05; m 0.85; m	39.1; t	1.03; m 0.85; m	39.10; t	1.04; m 0.89; m	39.14; t	1.63; m 0.85; m	39.07; t
2	1.43; m	17.88; t	1.45; m 1.41; m	17.82; t	1.43; m	17.86; t	1.72; m 1.42; m	17.80; t
3	1.85; m 1.65; m	39.1; t	1.85; m 1.65; m	39.10; t	1.86; m 1.66; m	39.09; t	1.85; m 1.02; m	39.02; t
4	-	36.68; s	-	36.64; s	-	36.67; s	-	36.63; s
5	1.42; m	55.51; d	1.42; m	55.43; d	1.43; m	55.47; d	1.23; m	57.21; d
6	1.29; m	19.95; t	1.64; m 1.29; m	19.93; t	1.69; m 1.29; m	19.97; t	1.68; m 1.24; m	19.92; t
7	1.77; m 1.33; m	43.55; t	1.77; m 1.33; m	43.48; t	1.78; m 1.34; m	43.52; t	1.69; m 1.29; m	43.41; t
8	-	74.70; s	-	74.56; s	-	74.58; s	-	74.65; s
9	1.24; m	57.46; d	1.23; m	57.71; d	1.25; m	57.75; d	1.41; m	56.75; d
10	-	36.95; s	-	36.90; s	-	36.94; s	-	36.90; s
11	1.49; m 1.44; m	15.38; t	1.50; m 1.44; m	15.35; t	1.47; m	15.39; t	1.51; m 1.20; m	15.24; t
12	1.76; m 1.44; m	37.03; t	1.76; m 1.44; m	37.31; t	1.79; m 1.45; m	37.31; t	1.71; m 1.43; m	36.90; t
13	-	73.10; s	-	73.02; s	-	73.09; s	-	72.63; s
14	1.67; m 1.37; m	40.56; t	1.67; m 1.37; m	40.43; t	1.68; m 1.38; m	40.48; t	1.69; m 1.38; m	39.64; d
15	1.69; m	20.02; t	1.71; m 1.66; m	20.13; t	1.29; m 1.68; m	20.20; t	1.81; m 1.73; m	18.02; t
16	1.11; s	29.96; q	1.09; s	30.06; q	1.10; s	30.09; q	1.05; s	29.63; q
17	1.23; s	24.21; q	1.22; s	24.05; q	1.23; s	24.11; q	1.08; s	23.96; q
18	1.02; s	32.48; q	1.01; s	33.43; q	1.02; s	32.46; q	1.00; s	32.43; q
19	3.59; d/9.8 3.15; dd/9.8; 1.8	19.32; t	3.58; d/9.8 3.15 dd/9.8; 1.8	19.46; t	3.59; d/9.8; 3.16 dd/9.8; 1.8	19.48; t	3.57; d/9.8; 3.14 dd/9.9; 1.6	19.33; q
20	0.78; s	16.44; q	0.77; s	16.42; q	0.77; s	16.46; q	0.75; s	16.38; q
21	2.34; m	34.57; t	2.30; m 2.26; m	34.57; t	2.27; td/7; 1.2	34.90; t	3.06; t/7.4	56.76; t
22	-	176.55; s	-	174.09; s	-	173.69; s	-	-
OMe	-	-	3.65; s	51.44; q	-	-	-	-
CH ₂ (OEt)	-	-	-	-	4.12; q/7.2	60.21; t	-	-
CH ₃ (OEt)	-	-	-	-	1.25; t/7.2	14.27; q	-	-
Ph 1'	-	-	-	-	-	-	-	139.13; s
2'	-	-	-	-	-	-	7.91; m	129.24; d
3'	-	-	-	-	-	-	7.57; m	128.06; d
4'	-	-	-	-	-	-	7.64; m	133.60; d
5'	-	-	-	-	-	-	7.57; m	128.06; d
6'	-	-	-	-	-	-	7.91; m	129.24; d

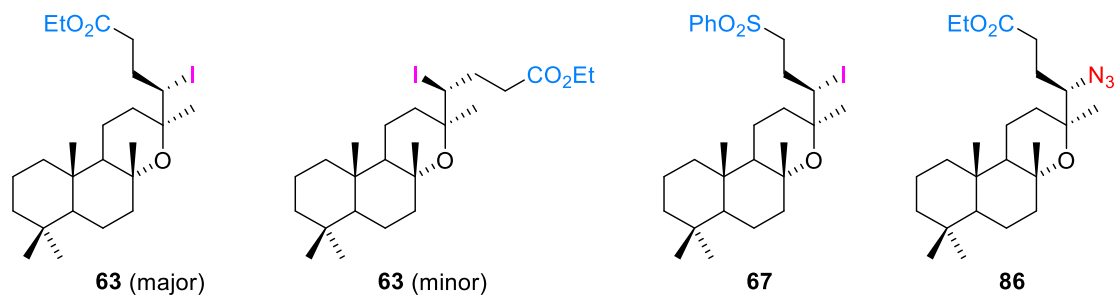


Table 4. NMR data for compounds **63**, **67** and **86** (assigned basing on ^1H , ^{13}C , DEPT, HSQC, HMBC, COSY-45, NOESY NMR experiments).

N° C	63 (major epimer)		63 (minor epimer)		67		86	
	δ ^1H ; m/J, Hz	δ ^{13}C ; m	δ ^1H ; m	δ ^{13}C ; m	δ ^1H ; m	δ ^{13}C ; m	δ ^1H ; m	δ ^{13}C ; m
1	1.56; m 0.85; m	38.98; t	1.57; m 0.85; m	39.09; t	1.52; m 0.83; m	38.98; t	1.56; m 0.87; m	39.03; t
2	1.58; m 1.42; m	18.47; t	1.59; m 1.42; m	18.48 t	1.55; m 1.40; m	18.47; t	1.59; m; 1.41; m	18.48; t
3	1.37; m 1.13; m	42.12; t	1.39; m 1.15; m	42.12; t	1.36; m 1.11; m	42.10; t	1.38; m 1.14; m	42.11; t
4	-	33.18; s	-	33.19; s	-	33.19; s	-	33.19; s
5	0.93; dd/12; 2	56.57; d	0.94; dd/12; 2.3	56.56; d	0.89; dd/12.2; 2.4	56.57; d	0.93; m	56.62; d
6	1.63; m 1.21; m	20.00; t	1.65; m 1.23; m	19.99; t	1.62; m 1.17; m	19.98; t	1.63; m 1.23; m	20.09; t
7	1.76; m 1.34; m	43.35; t	1.83; m 1.38; m	43.58; t	1.65; m 1.29; m	43.24; t	1.78; d/12 1.34; m	43.80; t
8	-	75.80; s	-	76.11; s	-	74.62; s	-	75.62; s
9	1.32; m	55.03; d	1.42 m	55.12; d	1.28; m	54.97; d	1.46; m	53.93; d
10	-	37.03; s	-	37.09; s	-	37.02; s	-	36.93; s
11	1.56; m 1.36; m	14.87; t	1.57; m 1.43; m	15.21; t	1.53; m 1.29; m	15.83; t	1.63; m 1.47; m	14.35; t
12	2.26; m 1.75; m	35.98; t	2.17; m 1.76; m	30.32; t	1.70; m 2.20; m	35.75; t	2.03; m 1.48; m	29.68; t
13	-	74.73; s	-	74.46; s	-	76.01; s	-	75.91; s
14	4.19; dd/11.2; 1.6	48.76; d	4.29; dd/12; 2	54.21; d	4.11; dd/11.5; 1.9	45.33; t	3.28; d/ 11	70.56; d
15	2.58; m 1.98; m	30.25; t	2.11; m 1.91; m	31.48; t	2.70; m 2.03; m	28.50; t	2.11; m 1.57; m	24.80; t
16	1.34; s	25.36; q	1.31; s	28.76; q	1.26; s	25.25; q	1.13; s	25.43; q
17	1.17; s	24.98; q	1.34; s	24.34; q	1.01; s	24.80; q	1.23; s	24.96; q
18	0.85; s	33.31; q	0.86; s	33.31; q	0.85; s	32.32; q	0.85; s	33.33; q
19	0.79; s	21.30; q	0.79; s	21.32; q	0.77; s	21.32; t	0.79; s	21.28; q
20	0.76; s	15.21; q	0.78; s	15.29; q	0.73; s	15.23; q	0.74; s	15.27; q
21	2.67; 2.30	35.31; t	2.69; m 2.48; m	35.38; t	3.48; m 3.07; m	57.22; t	2.65; m 2.39; m	32.27; t
22	-	172.73; s	-	172.86; s	-	-	-	173.04; s
CH ₂ (OEt)	4.13; q/7	60.34; t	4.14; q/7	60.41; q	-	-	4.13; q/7	60.62; t
CH ₃ (OEt)	1.26; t/7	14.21; q	1.27; t/7	14.21; q	-	-	1.26; t/7	14.23; q
Ph 1'	-	-	-	-	-	139.19; s	-	-
2'	-	-	-	-	7.93; m	129.30; d	-	-
3'	-	-	-	-	7.58; m	128,16; d	-	-
4'	-	-	-	-	7.67; m	133.69; d	-	-
5'	-	-	-	-	7.58; m	128,16; d	-	-
6'	-	-	-	-	7.93; m	129.30; d	-	-

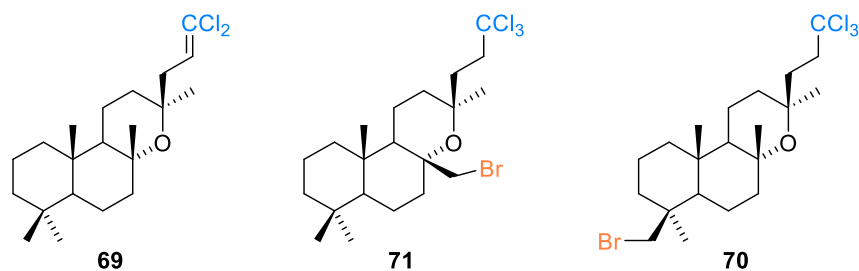
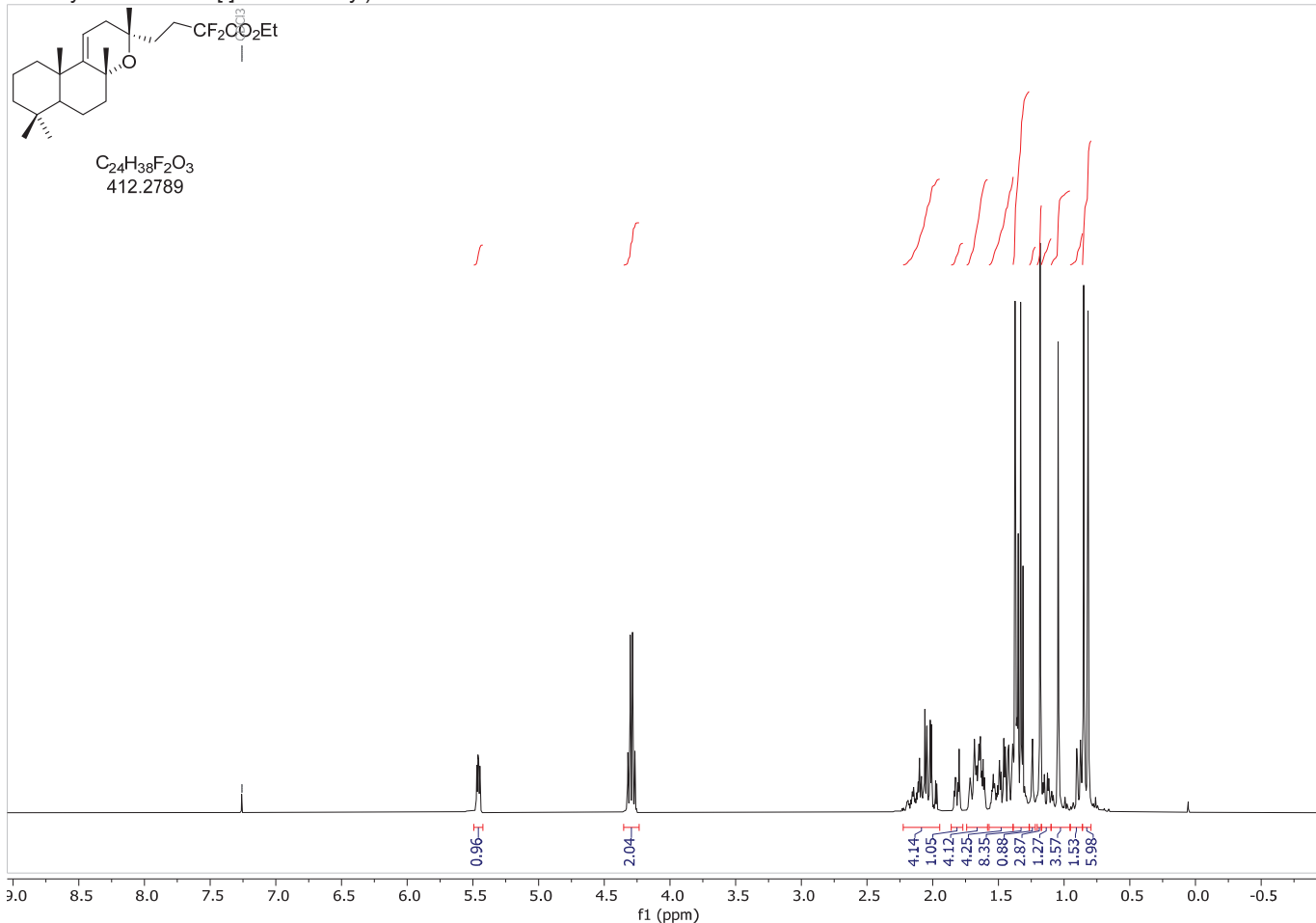


Table 5. NMR data for compounds **69**, **71** and **70** (assigned basing on ^1H , ^{13}C , DEPT, HSQC, HMBC, COSY-45, NOESY NMR experiments).

N° C	69		71		70	
	δ ^1H ; m/J, Hz	δ ^{13}C ; m	δ ^1H ; m/J, Hz	δ ^{13}C ; m	δ ^1H ; m/J, Hz	δ ^{13}C ; m
1	1.62; m 0.87; m	39.23; t	1.58; m 0.89; m	39.05; t	1.67; m 0.90; m	39.18; t
2	1.60; m 1.45; m	18.61; t	1.60; m 1.46; m	18.51; t	1.48; m	17.91; t
3	1.37; m 1.15; m	42.20; t	1.39; m 1.15; m	41.90; t	1.97; m 1.02; m	37.00; t
4	-	33.34; s	-	33.19; s	-	37.73; s
5	0.94; dd/12.0; 2.5	56.52; d	0.99; dd/12.4; 1.9	56.91; d	1.34; m	57.25; d
6	1.64; m 1.26; m	20.00; t	1.65; m 1.15; m	19.50; t	1.74; m 1.33; m	19.91; t
7	1.77; m 1.38; m	43.44; t	2.33; m 1.16; m	39.56; t	1.80; m 1.34; m	43.63; t
8	-	75.38; s	-	74.58; s	-	74.94; s
9	1.21; m	57.49; d	1.84 m	53.63; d	1.25; m	57.68; d
10	-	36.93; s	-	37.22; s	-	36.90; s
11	1.55; m 1.48; m	15.42; t	1.71; m 1.47; m	14.47; t	1.58; m	15.43; t
12	1.76; m 1.48; m	37.30; t	1.83; m 1.67; m	33.00; t	1.82; m 1.54; m	38.02; t
13	-	72.67; s	-	72.55; s	-	72.07; s
14	2.56; dd/15.6; 6.2 2.28; dd/15.6; 7.9	41.24; t	2.21; m 1.90; m	40.31; t	2.26; m 1.70; m	37.81; t
15	6.02; dd/7.7; 6.00	127.62;d	3.04; m 2.74; m	50.34; t	2.88; m 2.73; m	50.78; t
16	1.12; s	30.65; q	1.24; s	28.43; q	1.15; s	30.47; q
17	1.29; s	24.28; q	3.76; d/11.2 3.56; dd/11.2; 2.0	40.71; t	1.30; s	24.22; q
18	0.89; s	33.32; q	0.86; s	33.20; q	1.04; s	29.64; q
19	0.76; s	21.29; q	0.74; s	21.23; q	3.75; d/10 3.31; dd/10.0; 1.6	41.55; t
20	0.77; s	15.69; q	0.81; s	15.80; q	0.79; s	16.51; q
21	-	120.40; s	-	100.84; s	-	100.78; s

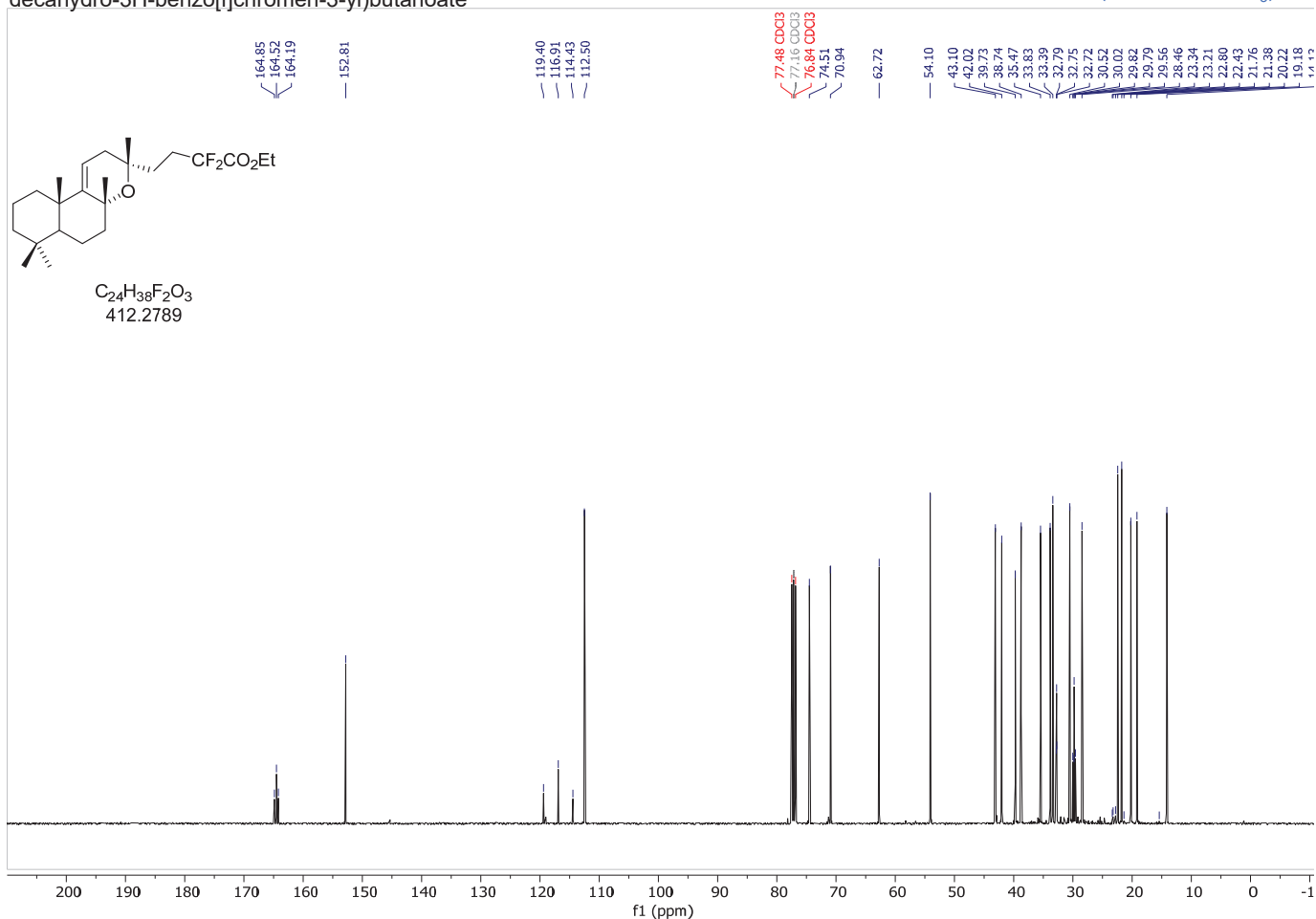
ethyl 2,2-difluoro-4-((3S,4aR,10aS)-3,4a,7,7,10a-pentamethyl-2,4a,5,6,6a,7,8,9,10,10a-decahydro-3H-benzof[*f*]chromen-3-yl)butanoate

¹H-NMR (400 MHz, CDCl₃)



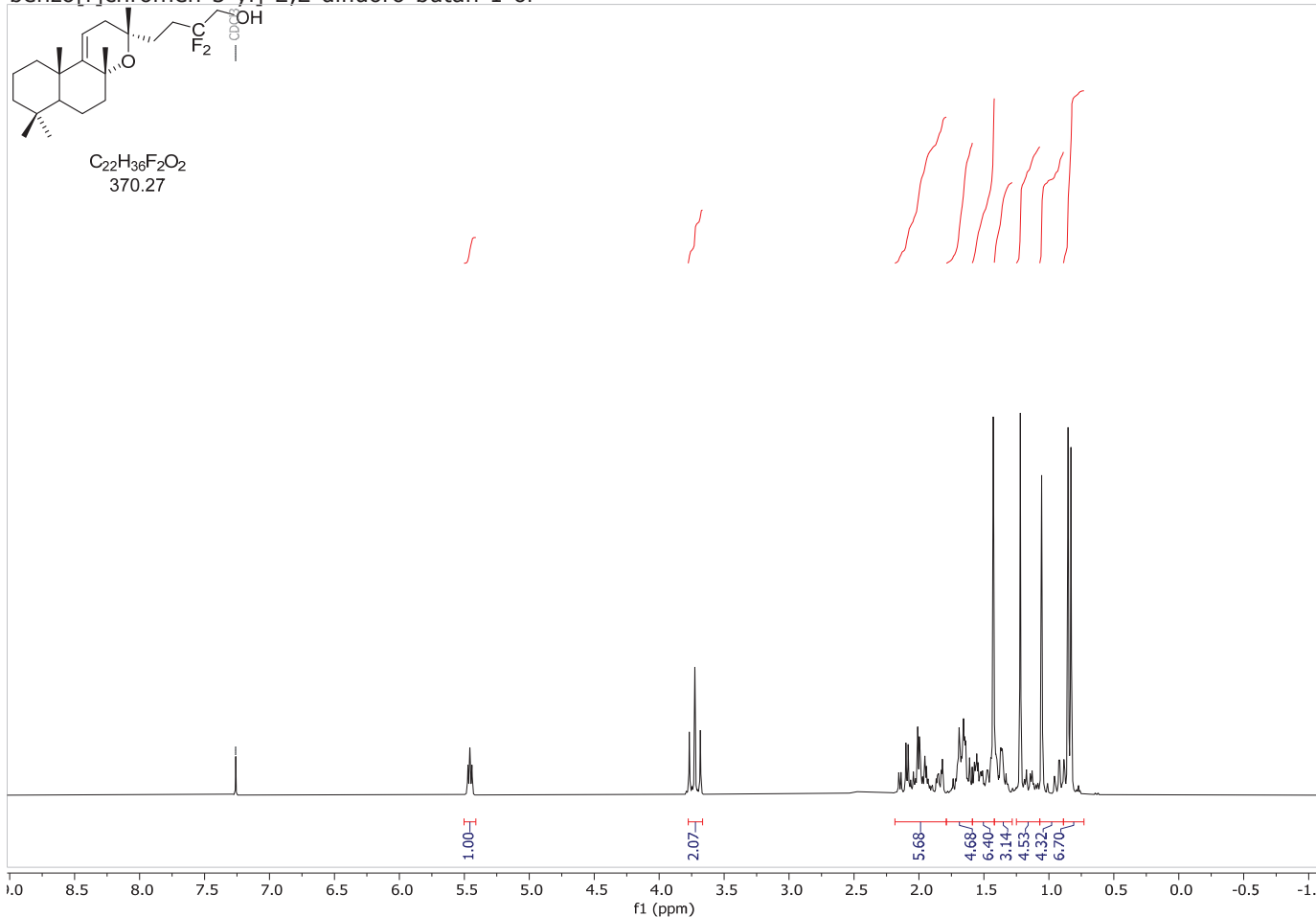
ethyl 2,2-difluoro-4-((3S,4aR,10aS)-3,4a,7,7,10a-pentamethyl-2,4a,5,6,6a,7,8,9,10,10a-decahydro-3H-benzof[*f*]chromen-3-yl)butanoate

¹³C-NMR (100 MHz, CDCl₃)



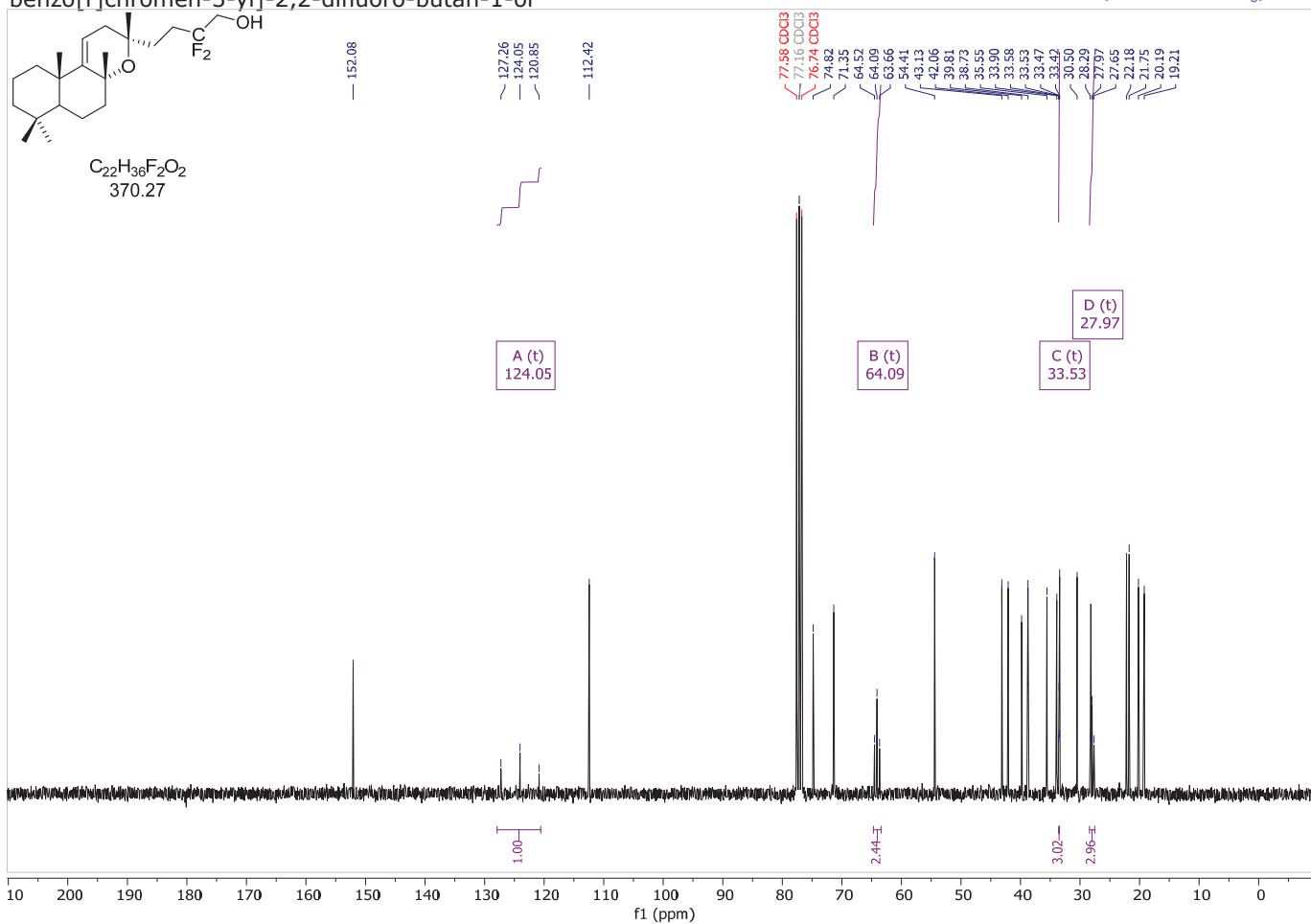
4-[(3S,4aR,10aS)-3,4a,7,7,10a-pentamethyl-5,6,6a,8,9,10-hexahydro-2H-benzo[f]chromen-3-yl]-2,2-difluoro-butan-1-ol

¹H-NMR (300 MHz, CDCl₃)



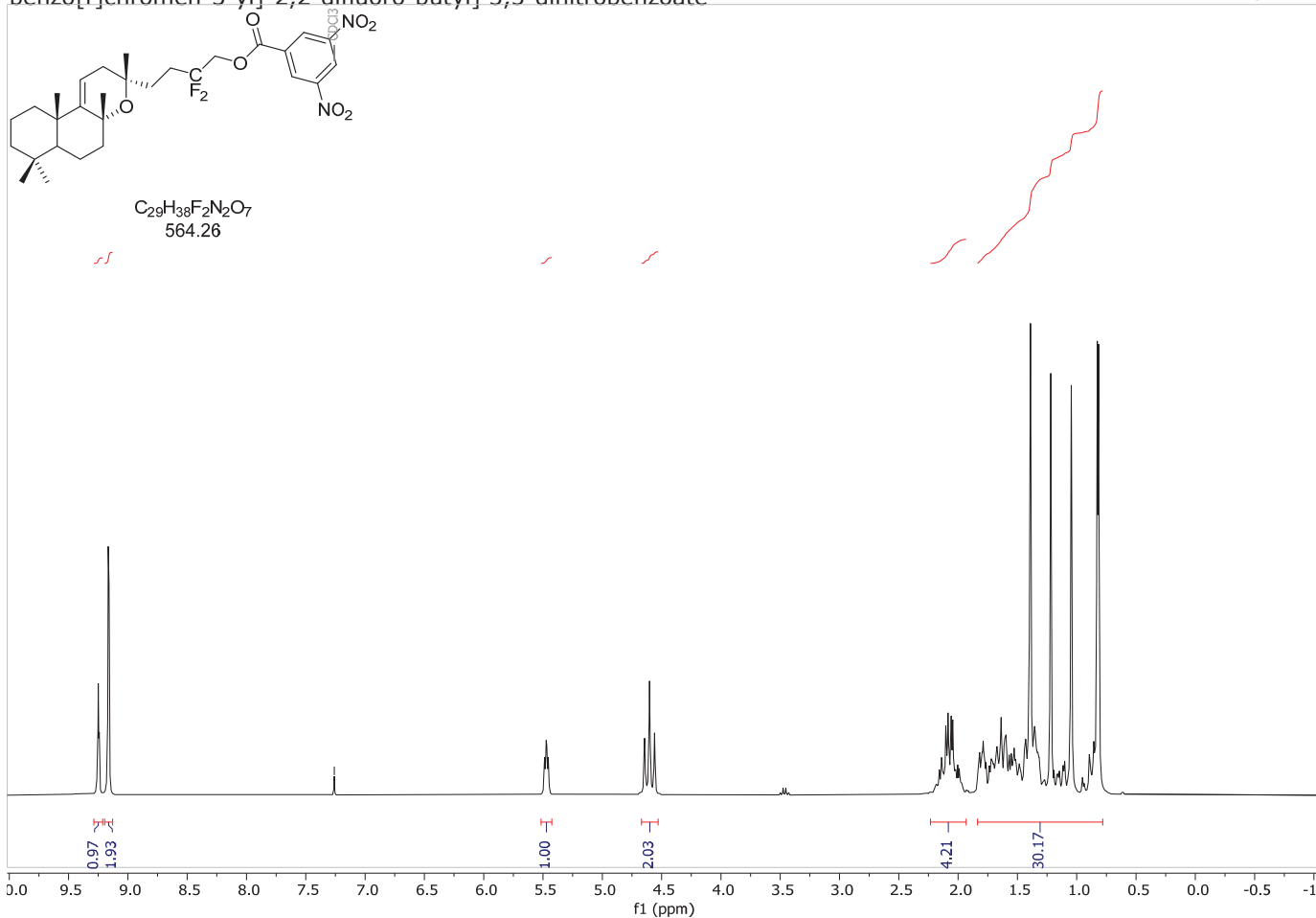
4-[(3S,4aR,10aS)-3,4a,7,7,10a-pentamethyl-5,6,6a,8,9,10-hexahydro-2H-benzo[f]chromen-3-yl]-2,2-difluoro-butan-1-ol

¹³C-NMR (75 MHz, CDCl₃)



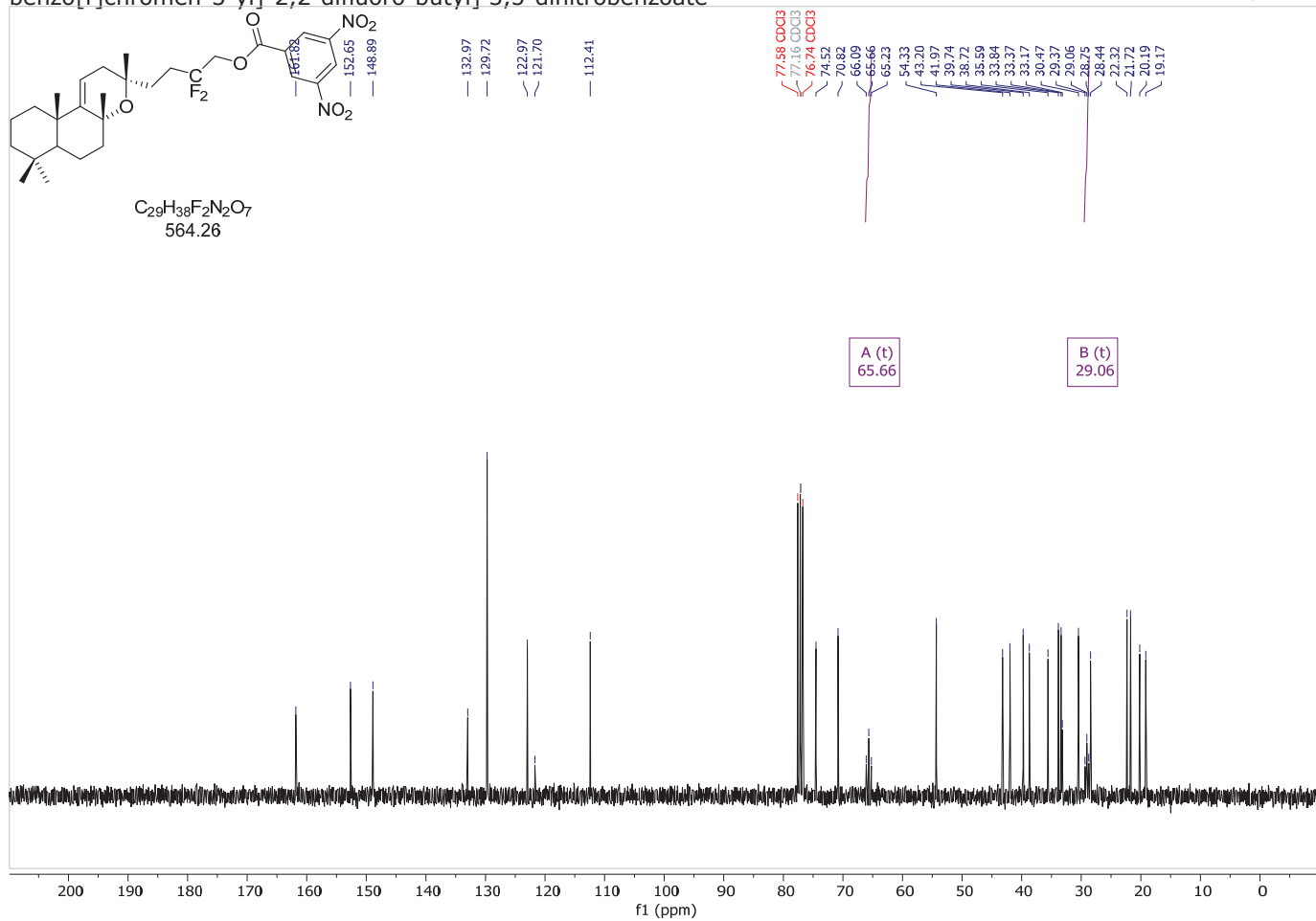
[4-[(3S,4aR,10aS)-3,4a,7,7,10a-pentamethyl-5,6,6a,8,9,10-hexahydro-2H-benzo[f]chromen-3-yl]-2,2-difluoro-butyl] 3,5-dinitrobenzoate

¹H-NMR (300 MHz, CDCl₃)



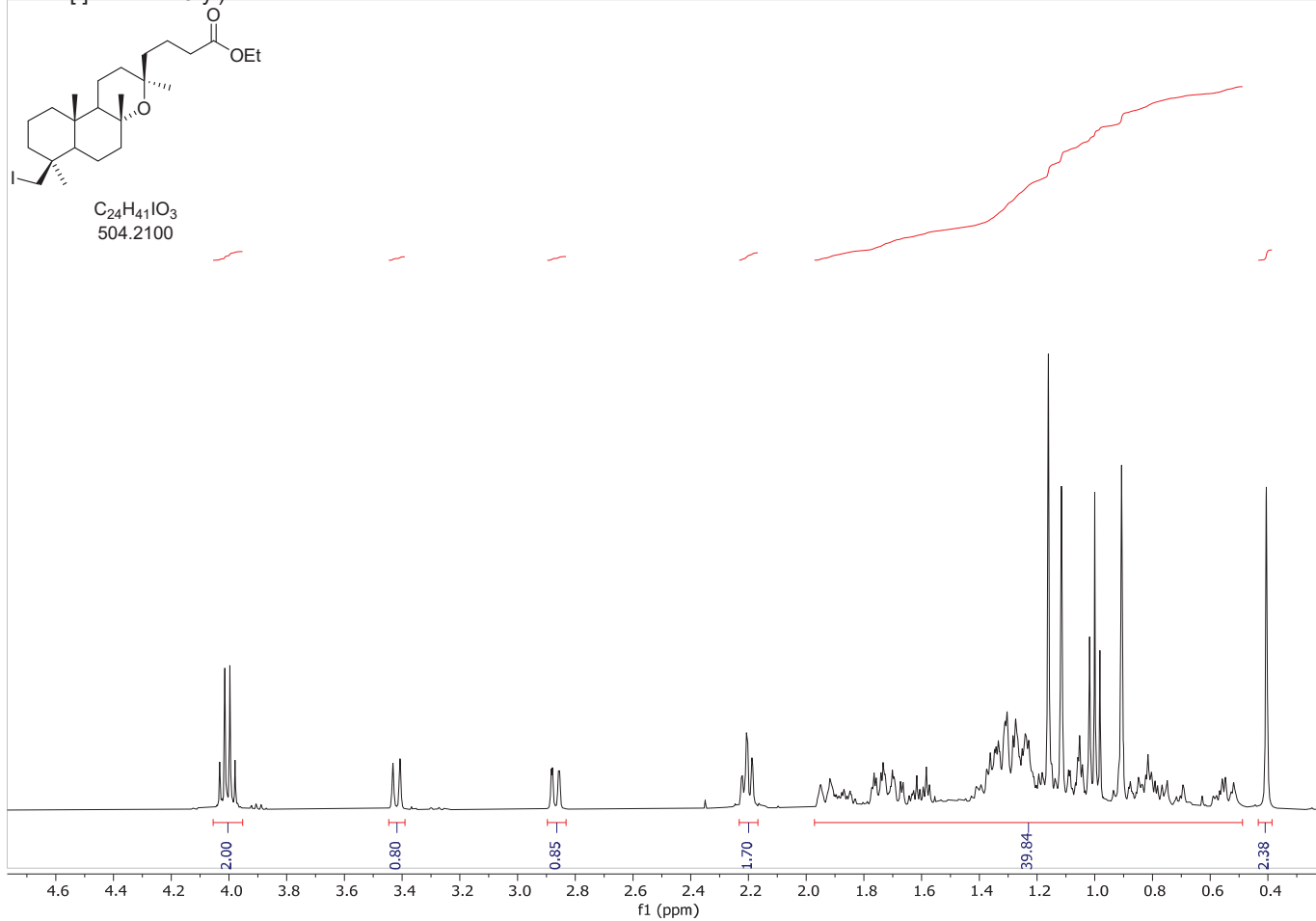
[4-[(3S,4aR,10aS)-3,4a,7,7,10a-pentamethyl-5,6,6a,8,9,10-hexahydro-2H-benzo[f]chromen-3-yl]-2,2-difluoro-butyl] 3,5-dinitrobenzoate

¹³C-NMR (75 MHz, CDCl₃)



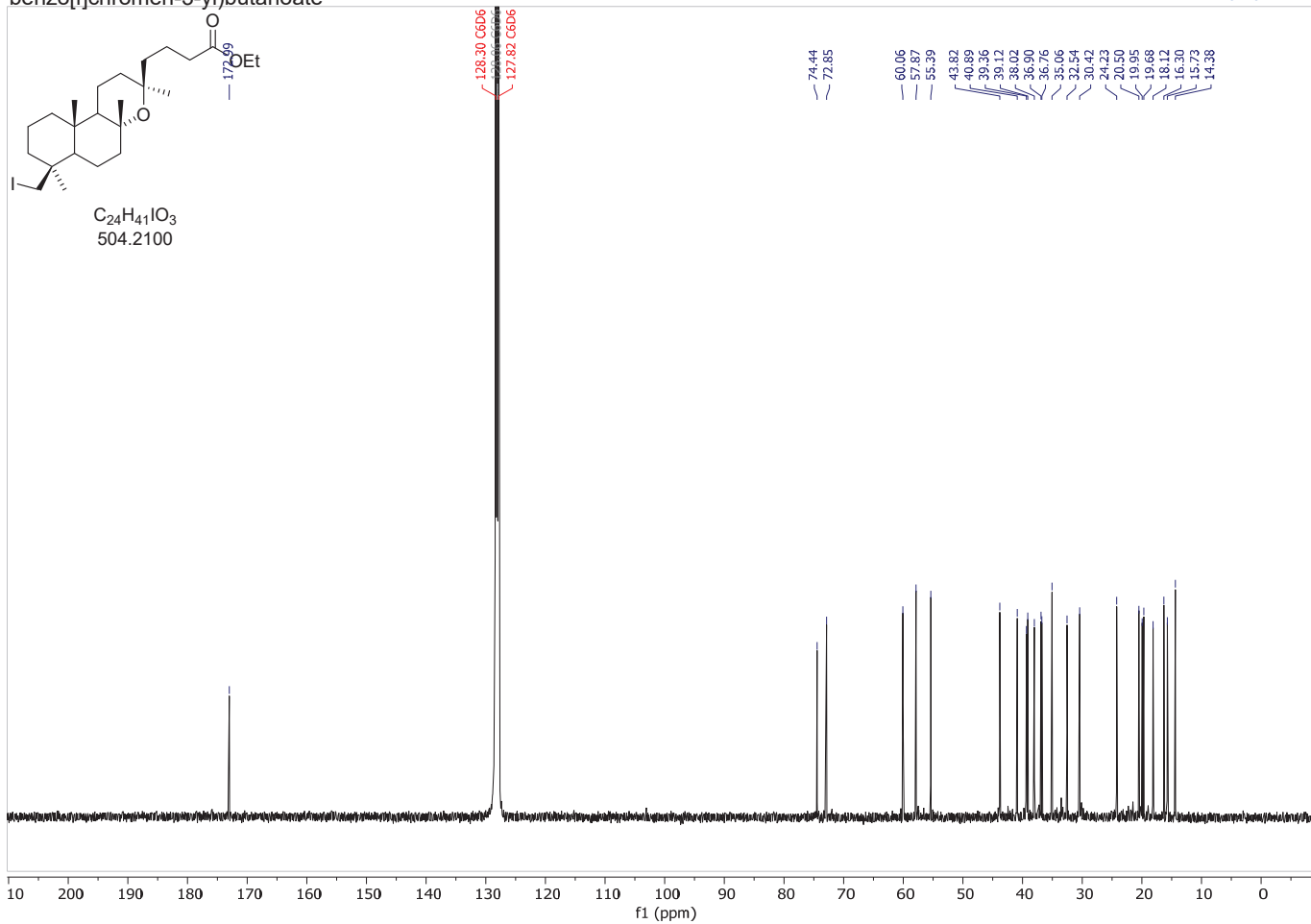
ethyl 4-((3R,4aR,7S,10aS)-7-(iodomethyl)-3,4a,7,10a-tetramethyldodecahydro-1H-benzo[f]chromen-3-yl)butanoate

$^1\text{H-NMR}$ (400 MHz, C_6D_6)

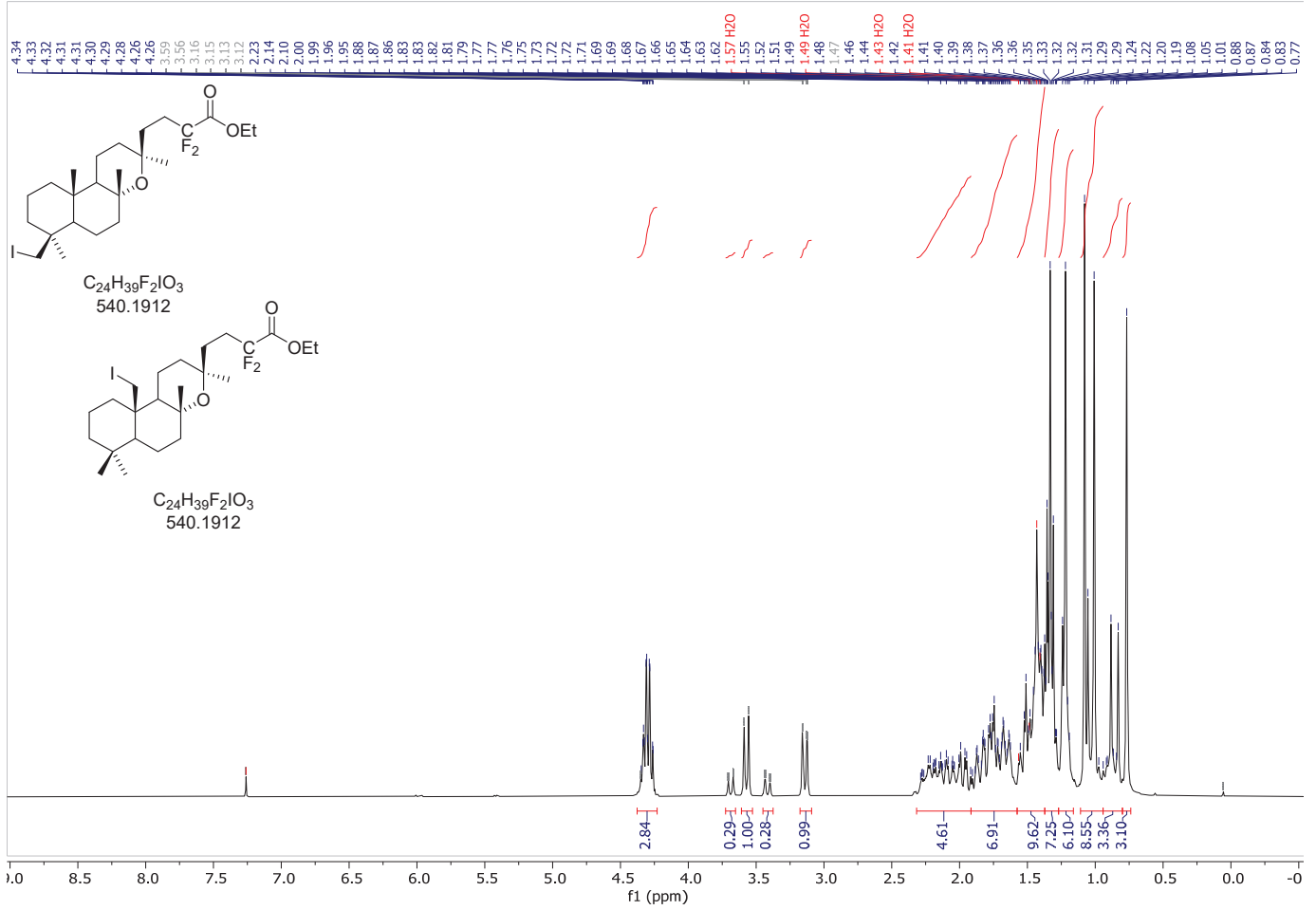


ethyl 4-((3R,4aR,7S,10aS)-7-(iodomethyl)-3,4a,7,10a-tetramethyldodecahydro-1H-benzo[f]chromen-3-yl)butanoate

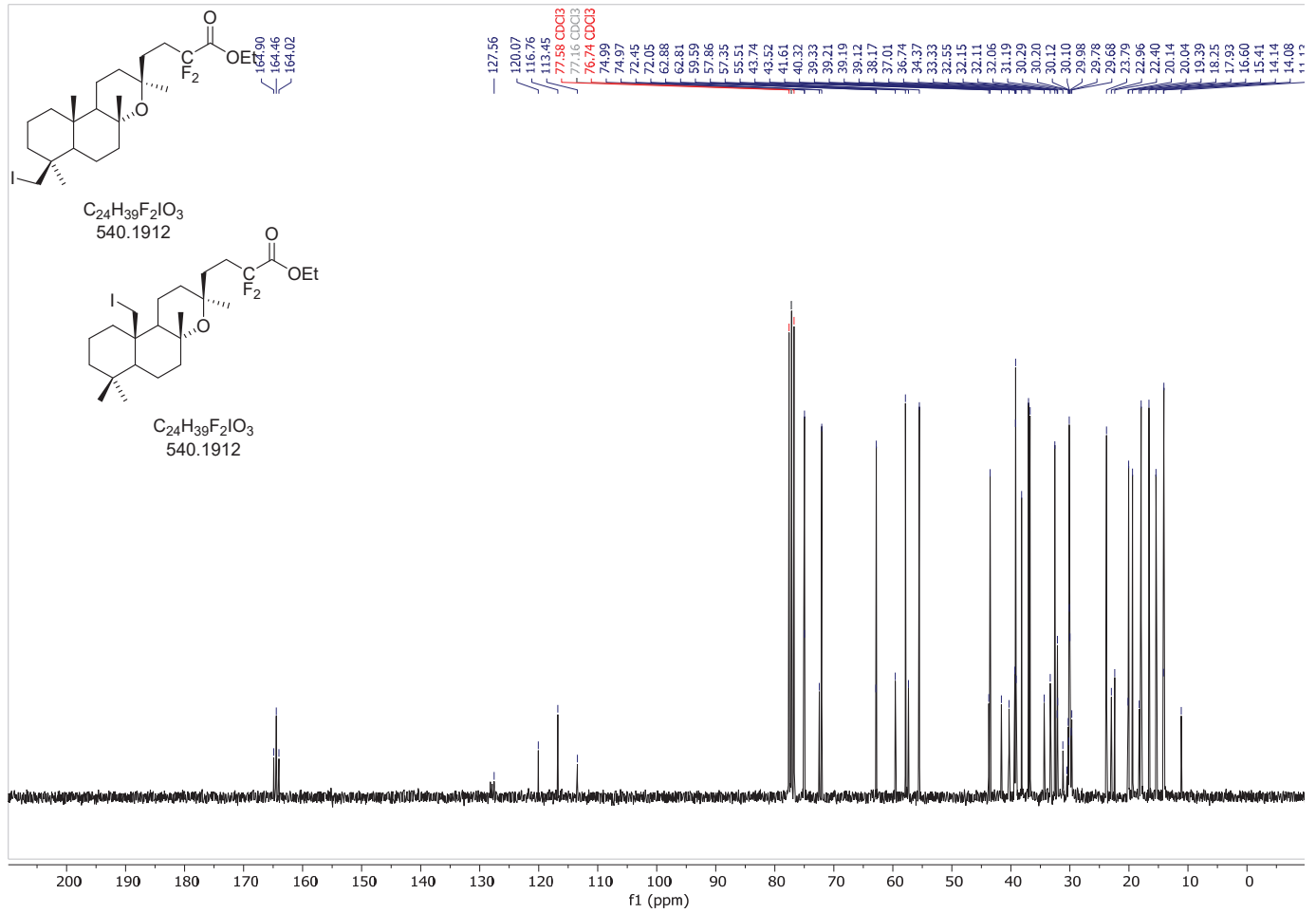
$^{13}\text{C-NMR}$ (100 MHz, C_6D_6)



¹H-NMR (400 MHz, CDCl₃)

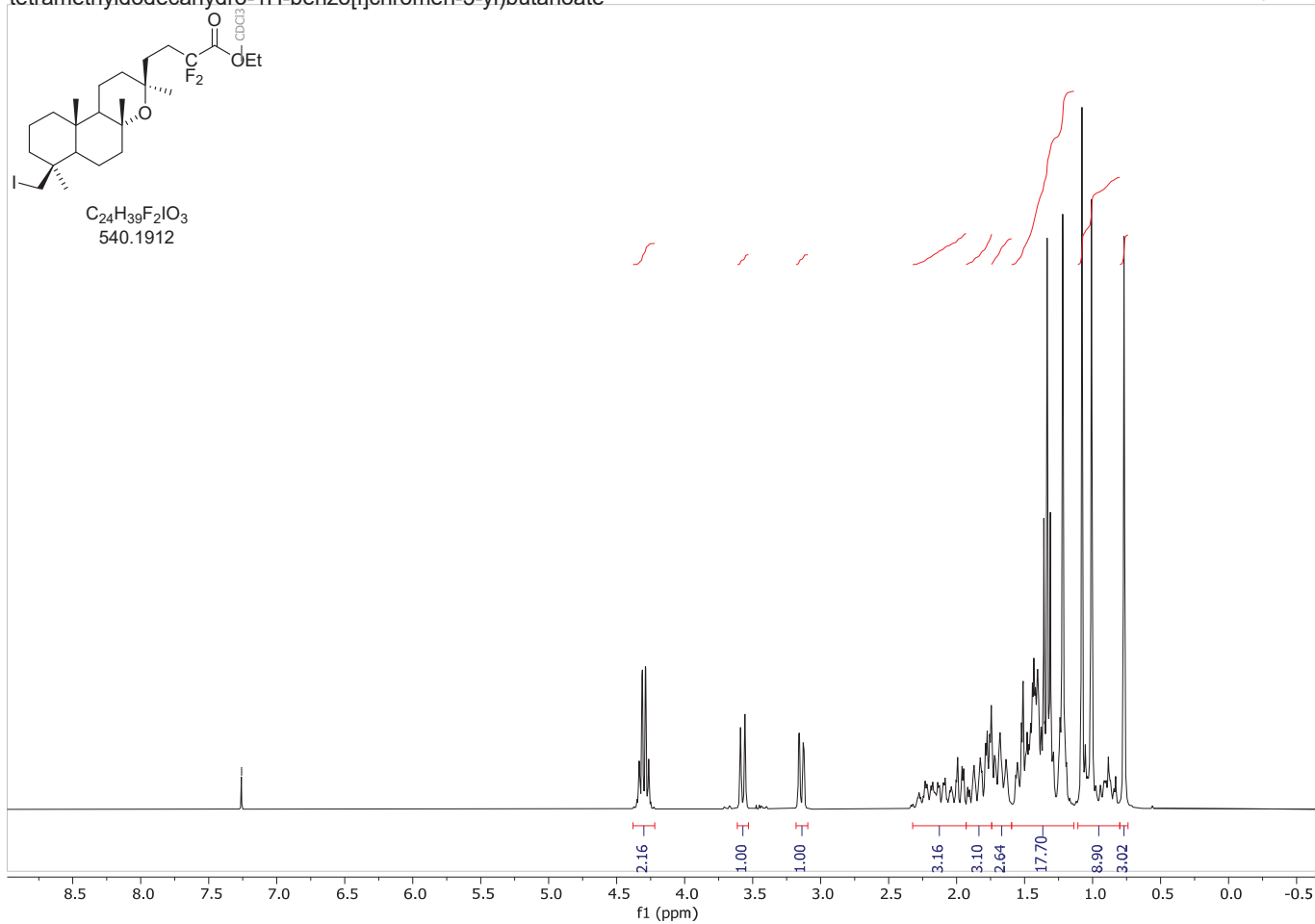


¹³C-NMR (100 MHz, CDCl₃)



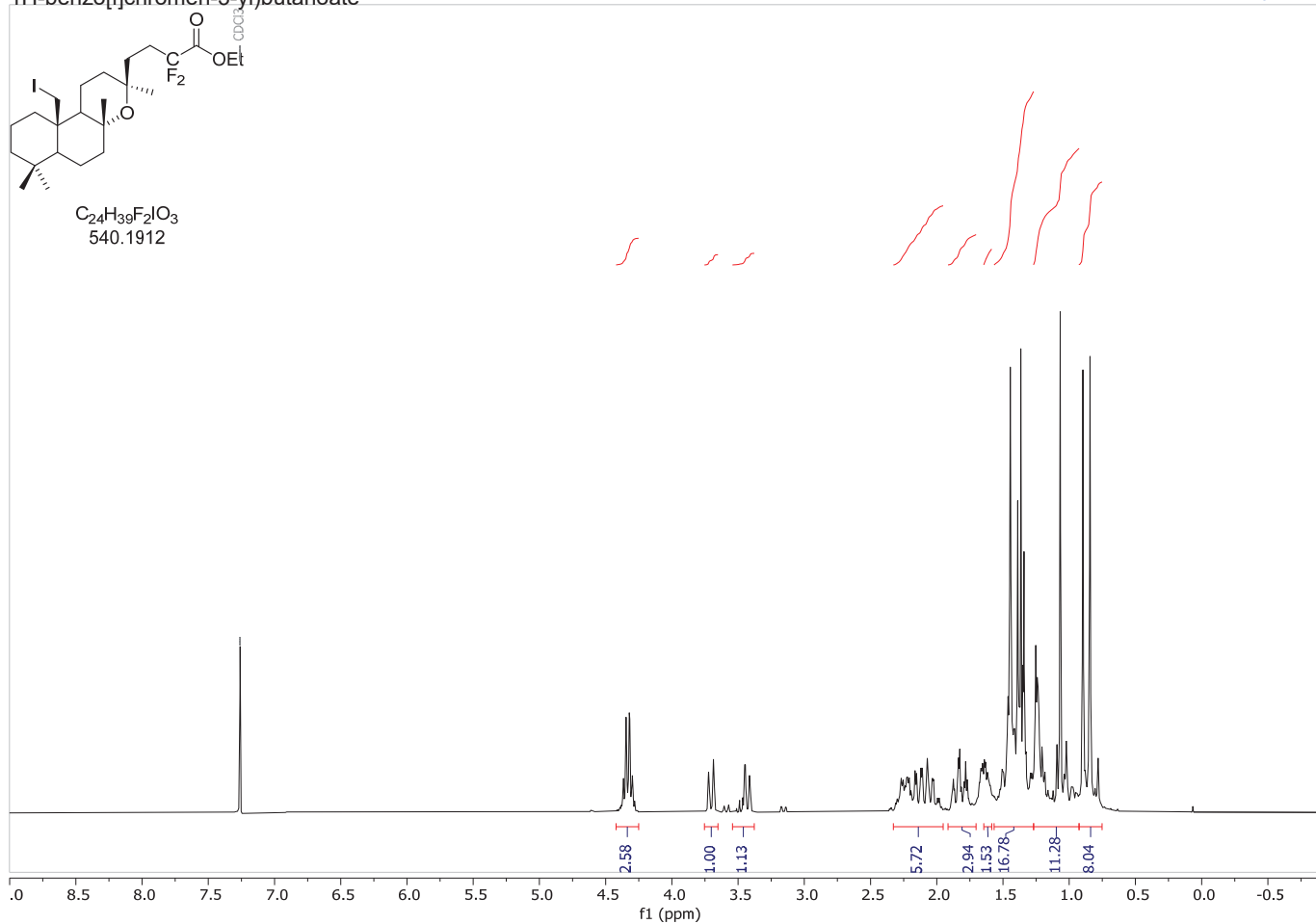
ethyl 2,2-difluoro-4-((3S,4aR,7S,10aS)-7-(iodomethyl)-3,4a,7,10a-tetramethyldodecahydro-1H-benzo[f]chromen-3-yl)butanoate

$^1\text{H-NMR}$ (300 MHz, CDCl_3)



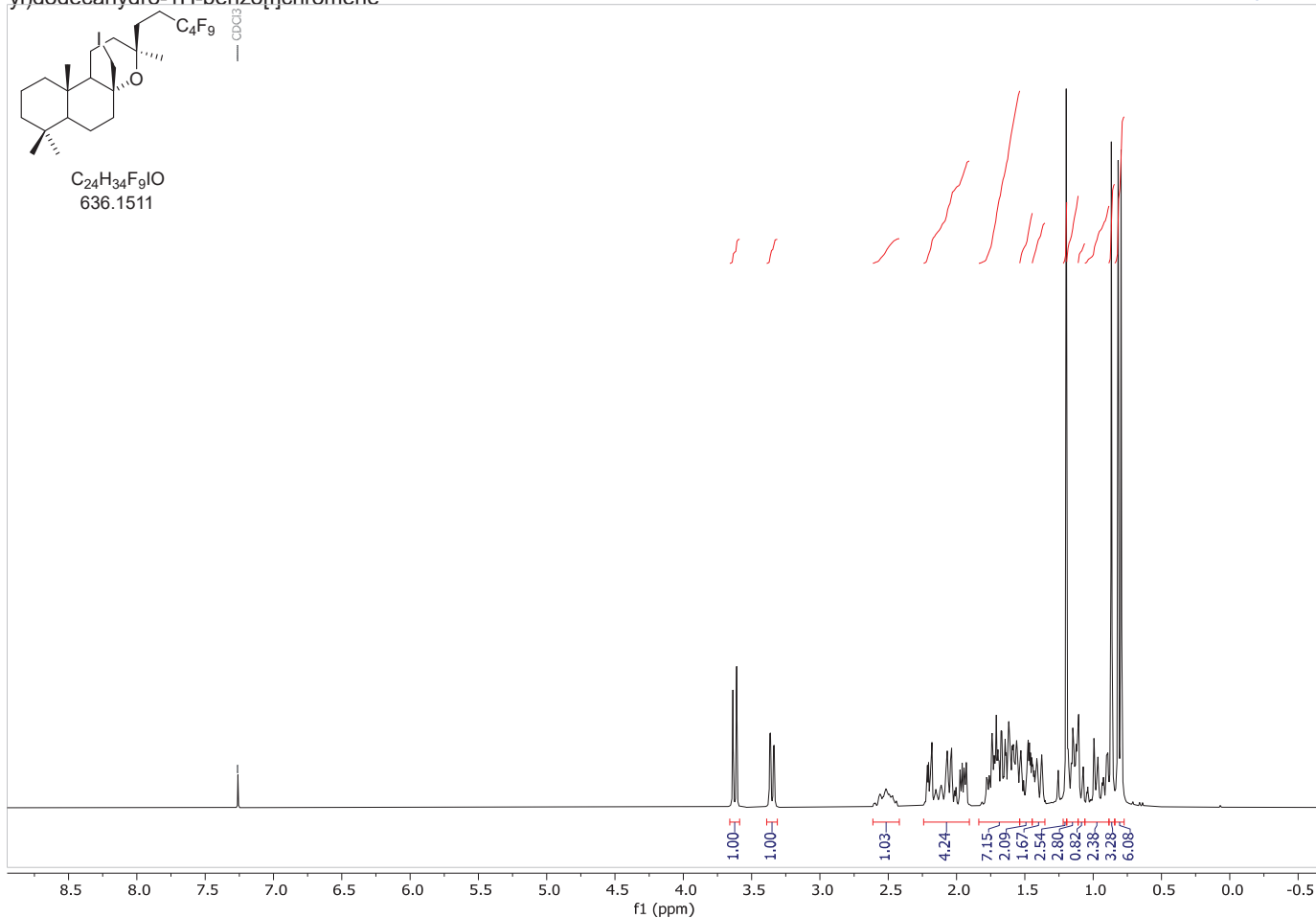
ethyl 2,2-difluoro-4-((3S,4aR,10aR)-10a-(iodomethyl)-3,4a,7,7-tetramethyldodecahydro-1H-benzo[f]chromen-3-yl)butanoate

$^1\text{H-NMR}$ (300 MHz, CDCl_3)



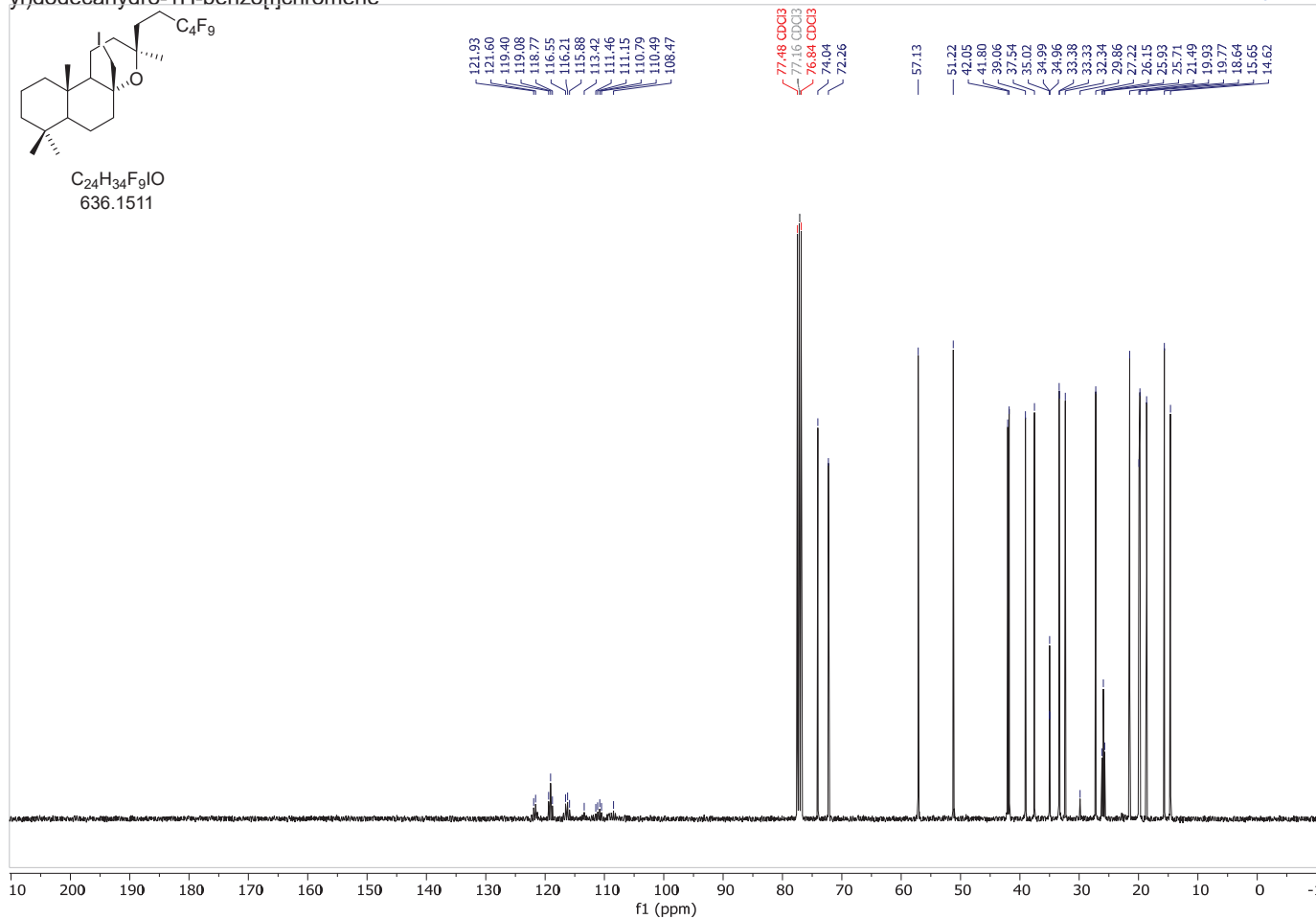
(3S,4aR,10aS)-4a-(iodomethyl)-3,7,7,10a-tetramethyl-3-(-nonafluoro-6I12-hexa-3,5-diy-1-yl)dodecahydro-1H-benzo[f]chromene

¹H-NMR (400 MHz, CDCl₃)



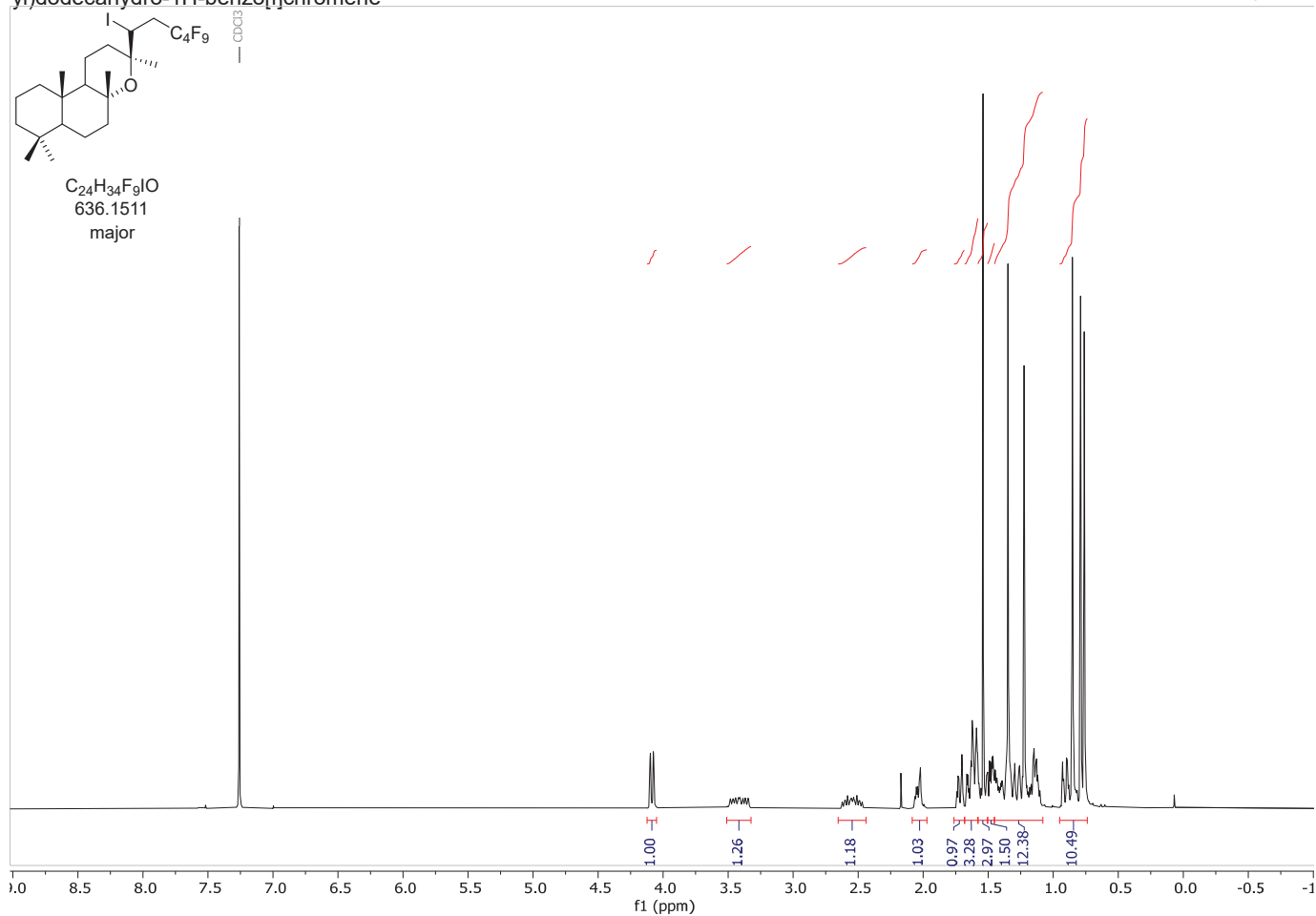
(3S,4aR,10aS)-4a-(iodomethyl)-3,7,7,10a-tetramethyl-3-(-nonafluoro-6I12-hexa-3,5-diy-1-yl)dodecahydro-1H-benzo[f]chromene

¹³C-NMR (100 MHz, CDCl₃)



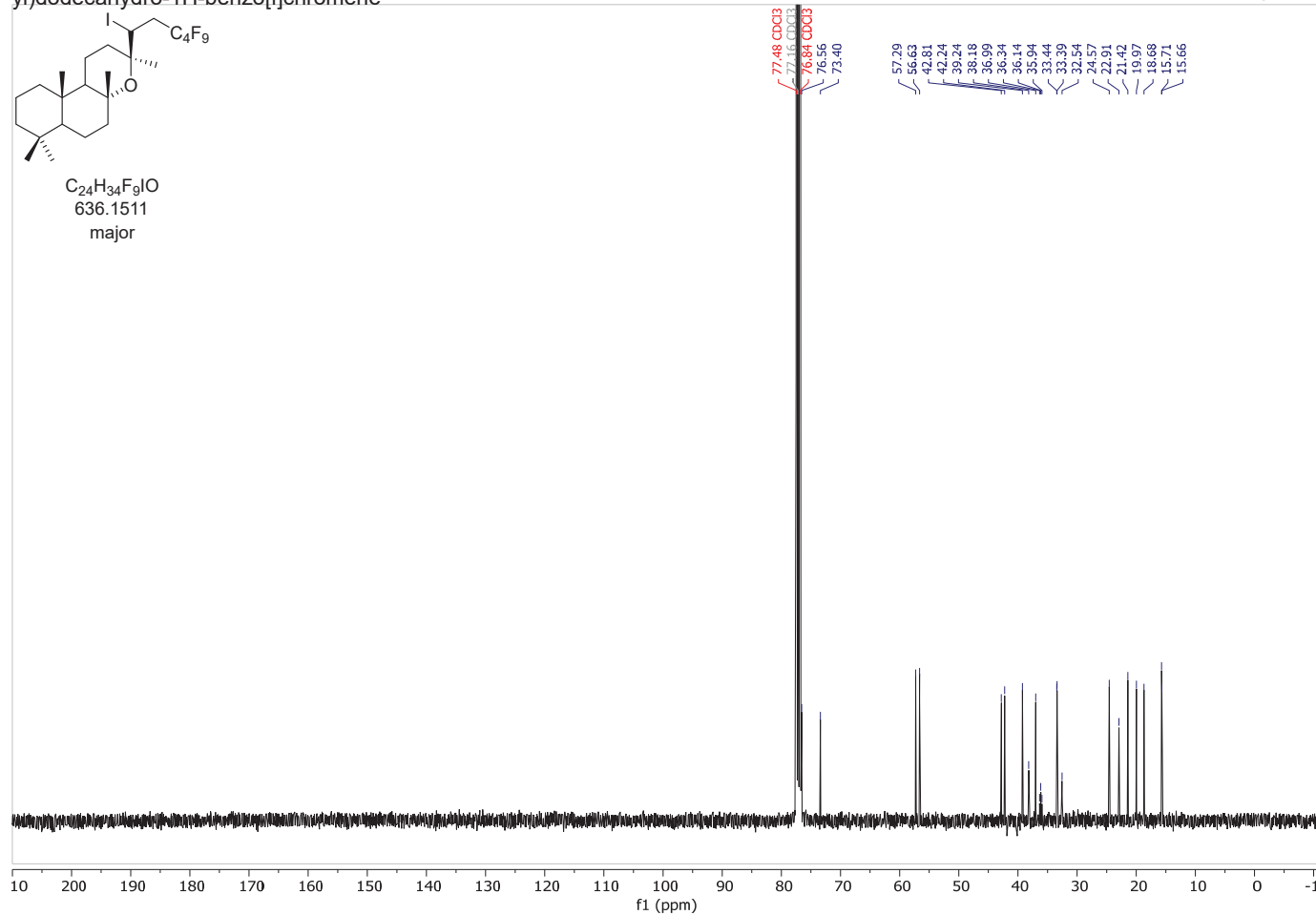
(3S,4aR,10aS)-3,4a,7,7,10a-pentamethyl-3-((R)-nonafluoro-1-iodo-6-iodo-12-hexa-3,5-diyne-1-yl)dodecahydro-1H-benzo[f]chromene

¹H-NMR (400 MHz, CDCl₃)



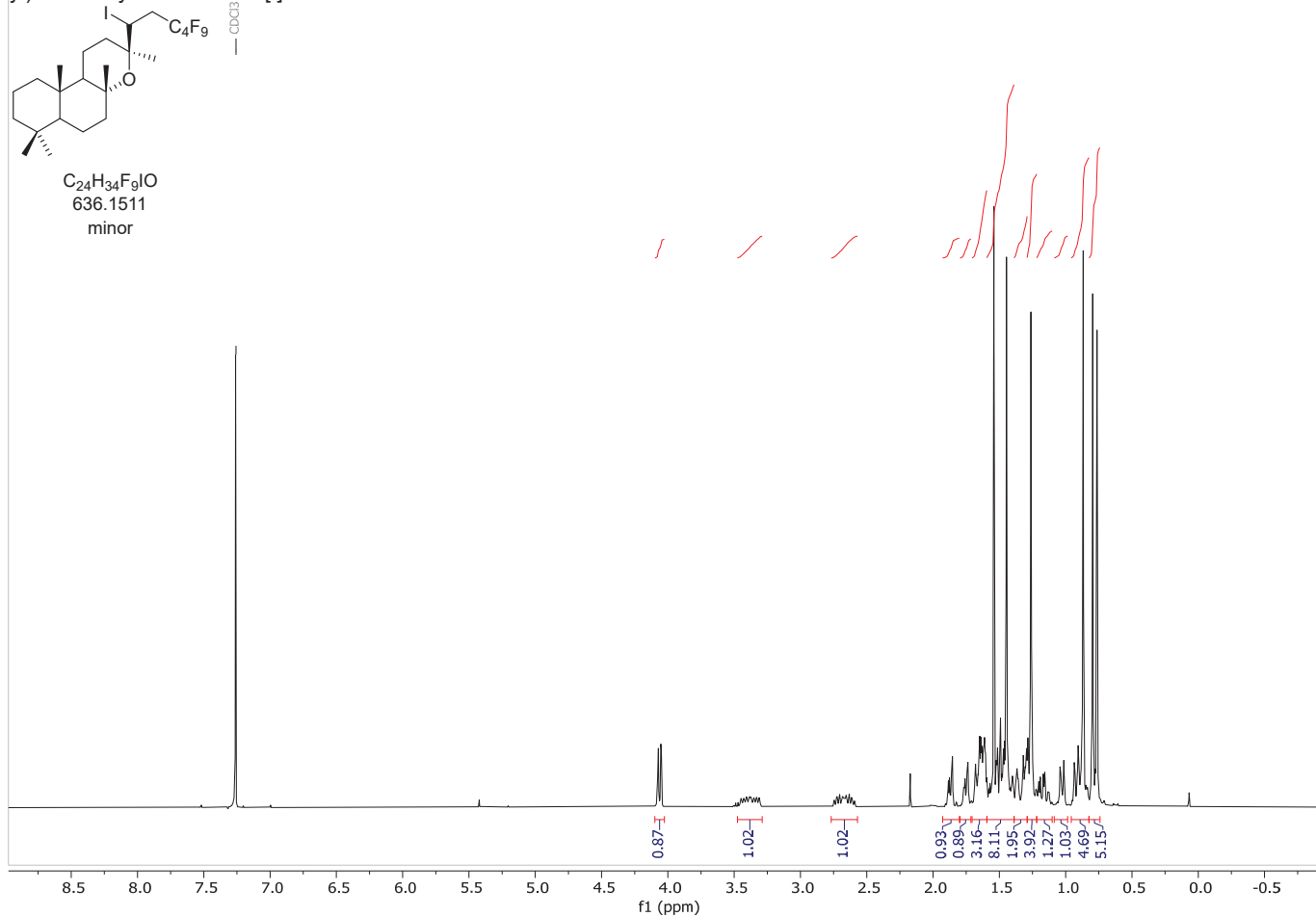
(3S,4aR,10aS)-3,4a,7,7,10a-pentamethyl-3-((R)-nonafluoro-1-iodo-6-iodo-12-hexa-3,5-diyne-1-yl)dodecahydro-1H-benzo[f]chromene

¹³C-NMR (100 MHz, CDCl₃)



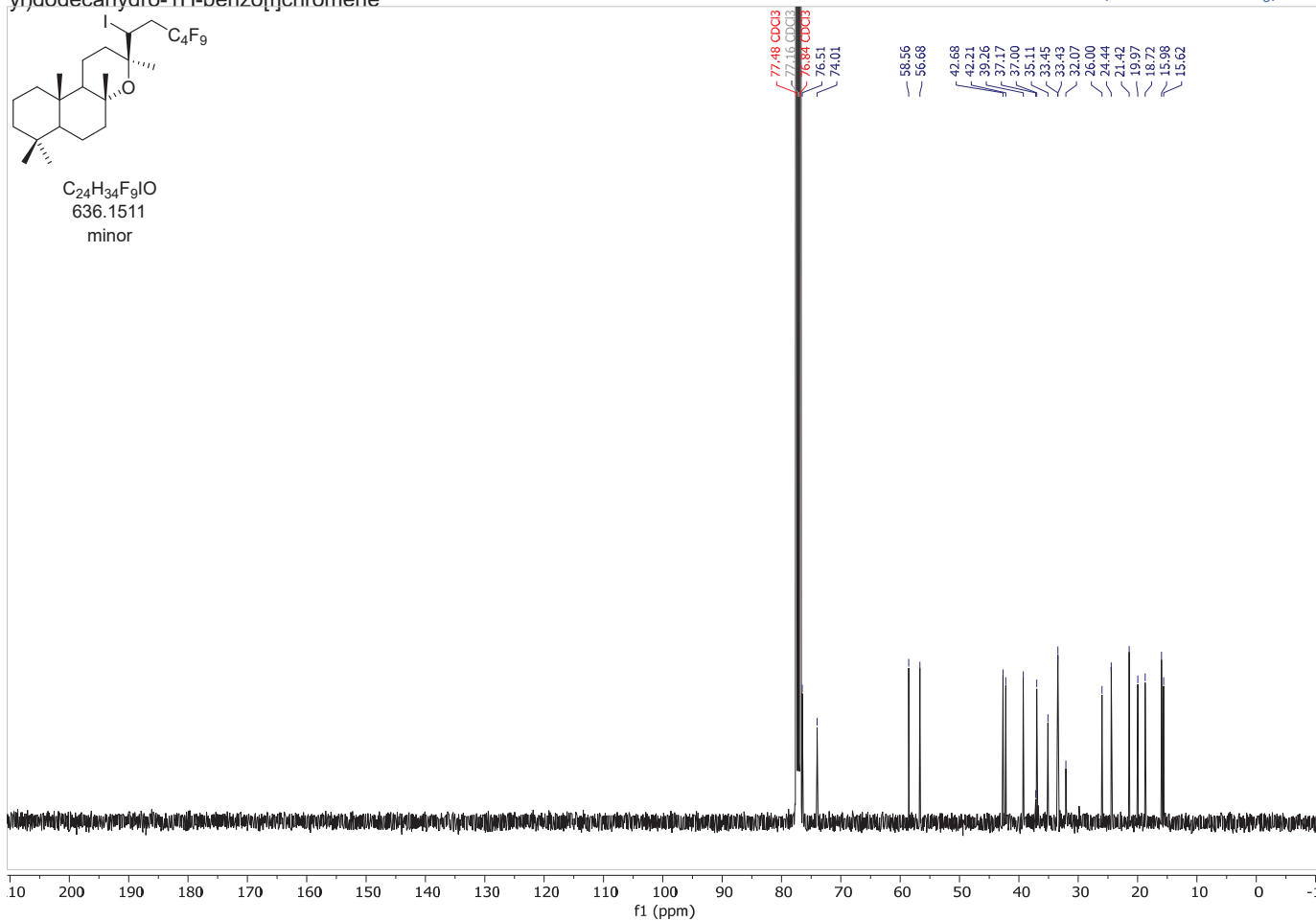
(3S,4aR,10aS)-4a-(iodomethyl)-3,7,7,10a-tetramethyl-3-(-nonafluoro-6I12-hexa-3,5-diy-1-yl)dodecahydro-1H-benzo[f]chromene

¹H-NMR (400 MHz, CDCl₃)



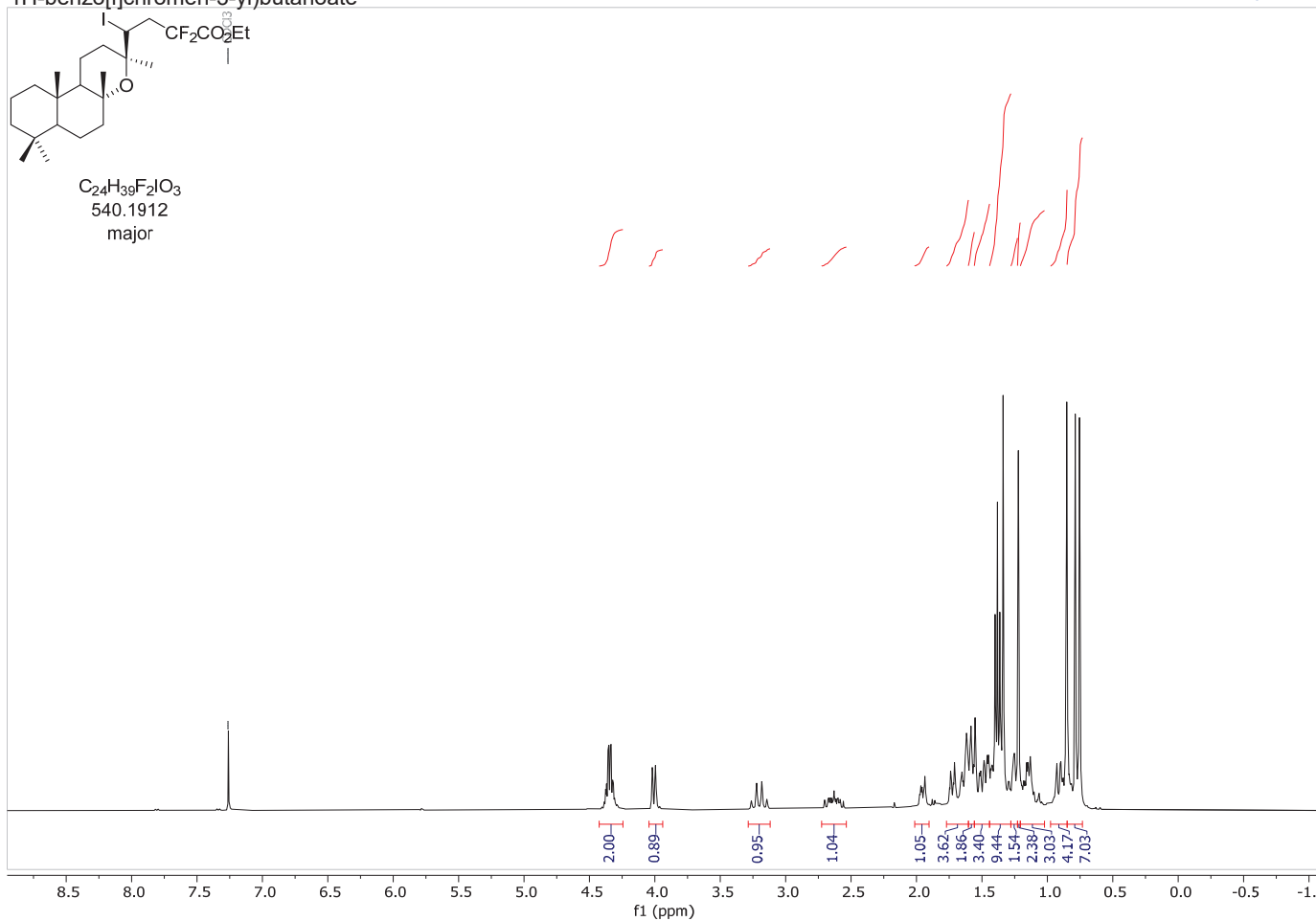
(3S,4aR,10aS)-4a-(iodomethyl)-3,7,7,10a-tetramethyl-3-(-nonafluoro-6I12-hexa-3,5-diy-1-yl)dodecahydro-1H-benzo[f]chromene

¹³C-NMR (100 MHz, CDCl₃)



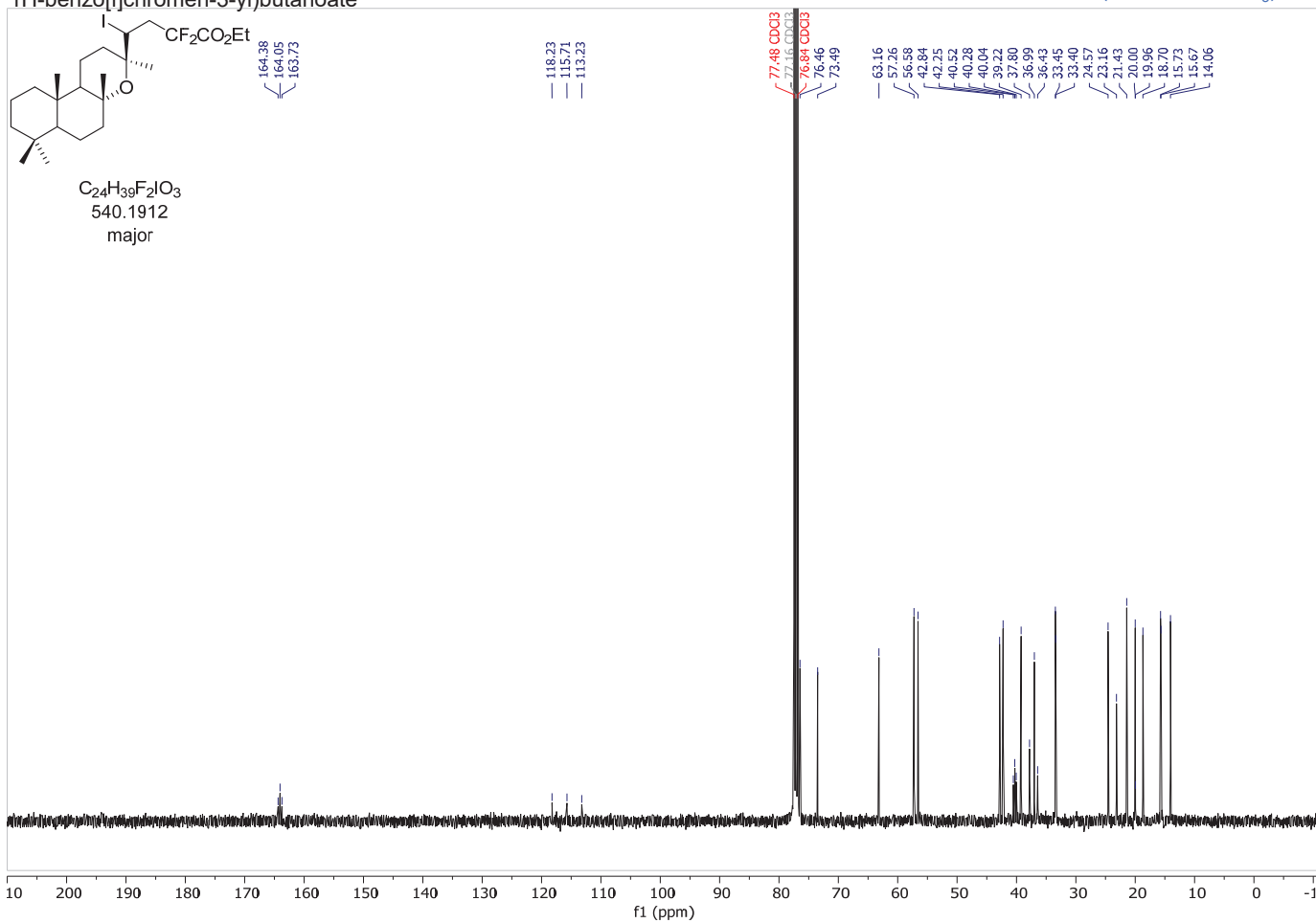
ethyl (4R)-2,2-difluoro-4-iodo-4-((3S,4aR,10aS)-3,4a,7,7,10a-pentamethyldodecahydro-1H-benzo[f]chromen-3-yl)butanoate

¹H-NMR (400 MHz, CDCl₃)



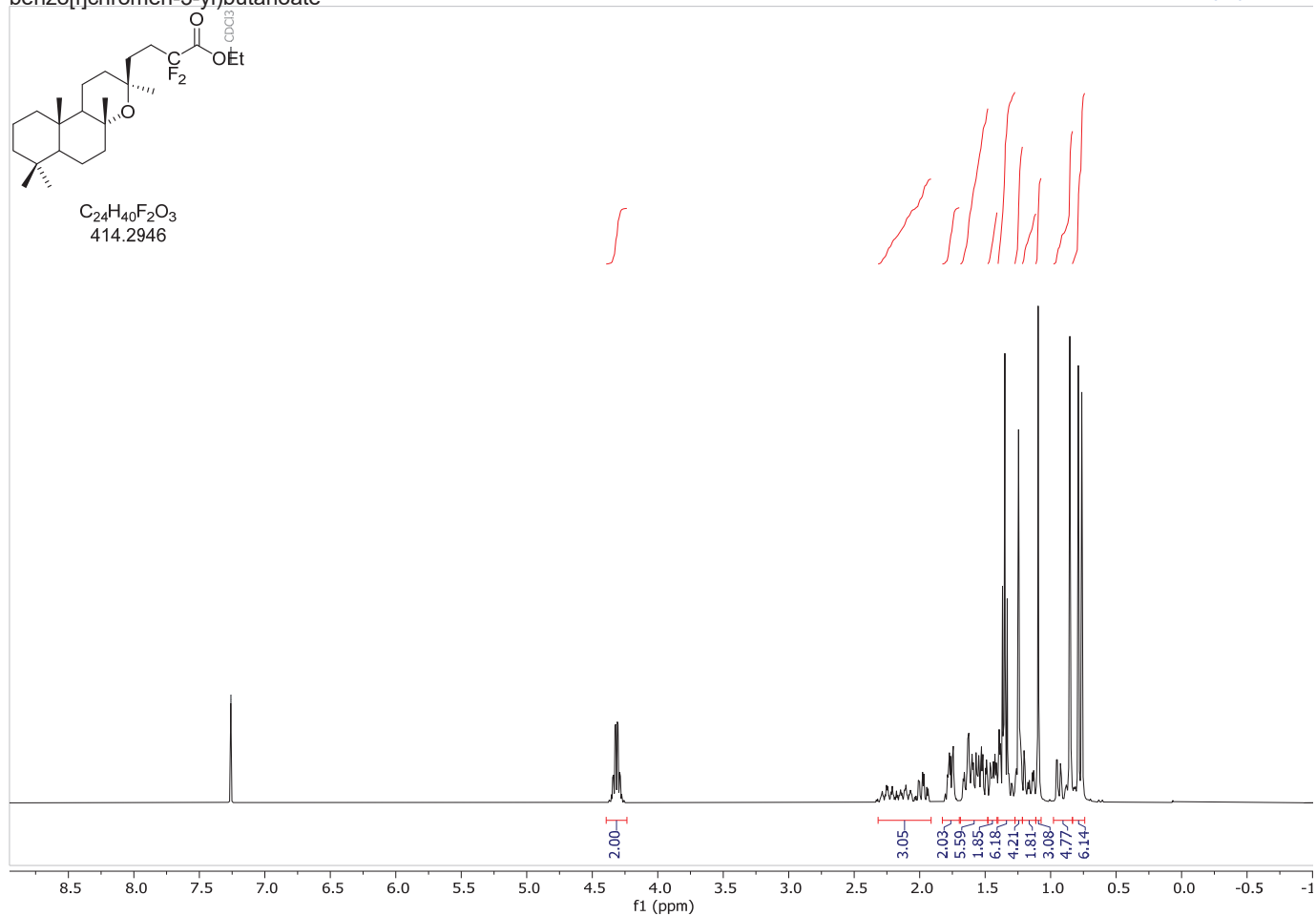
ethyl (4R)-2,2-difluoro-4-iodo-4-((3S,4aR,10aS)-3,4a,7,7,10a-pentamethyldodecahydro-1H-benzo[f]chromen-3-yl)butanoate

¹³C-NMR (100 MHz, CDCl₃)



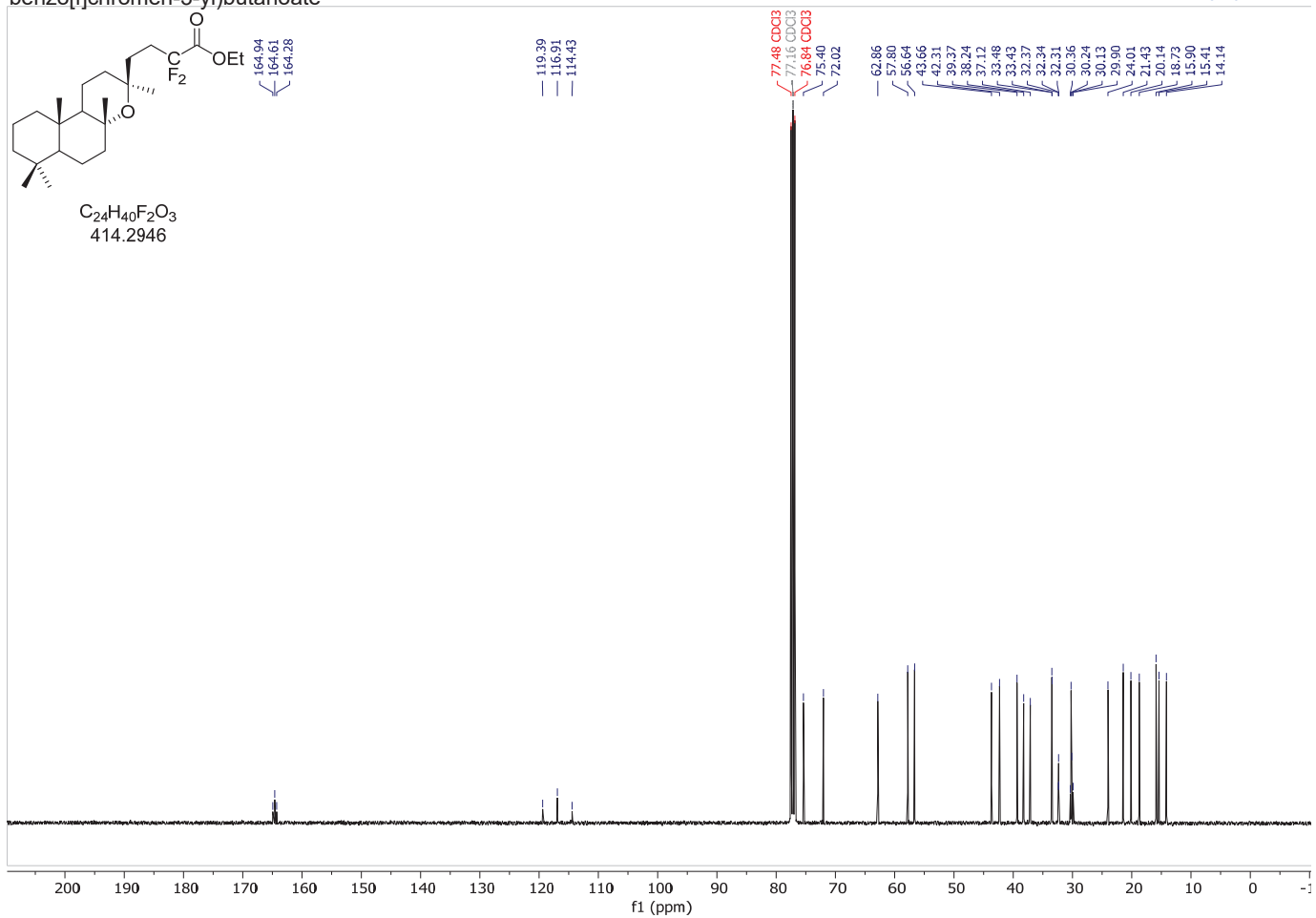
ethyl 2,2-difluoro-4-((3S,4aR,10aS)-3,4a,7,7,10a-pentamethyldodecahydro-1H-benzo[f]chromen-3-yl)butanoate

¹H-NMR (300 MHz, C₆D₆)



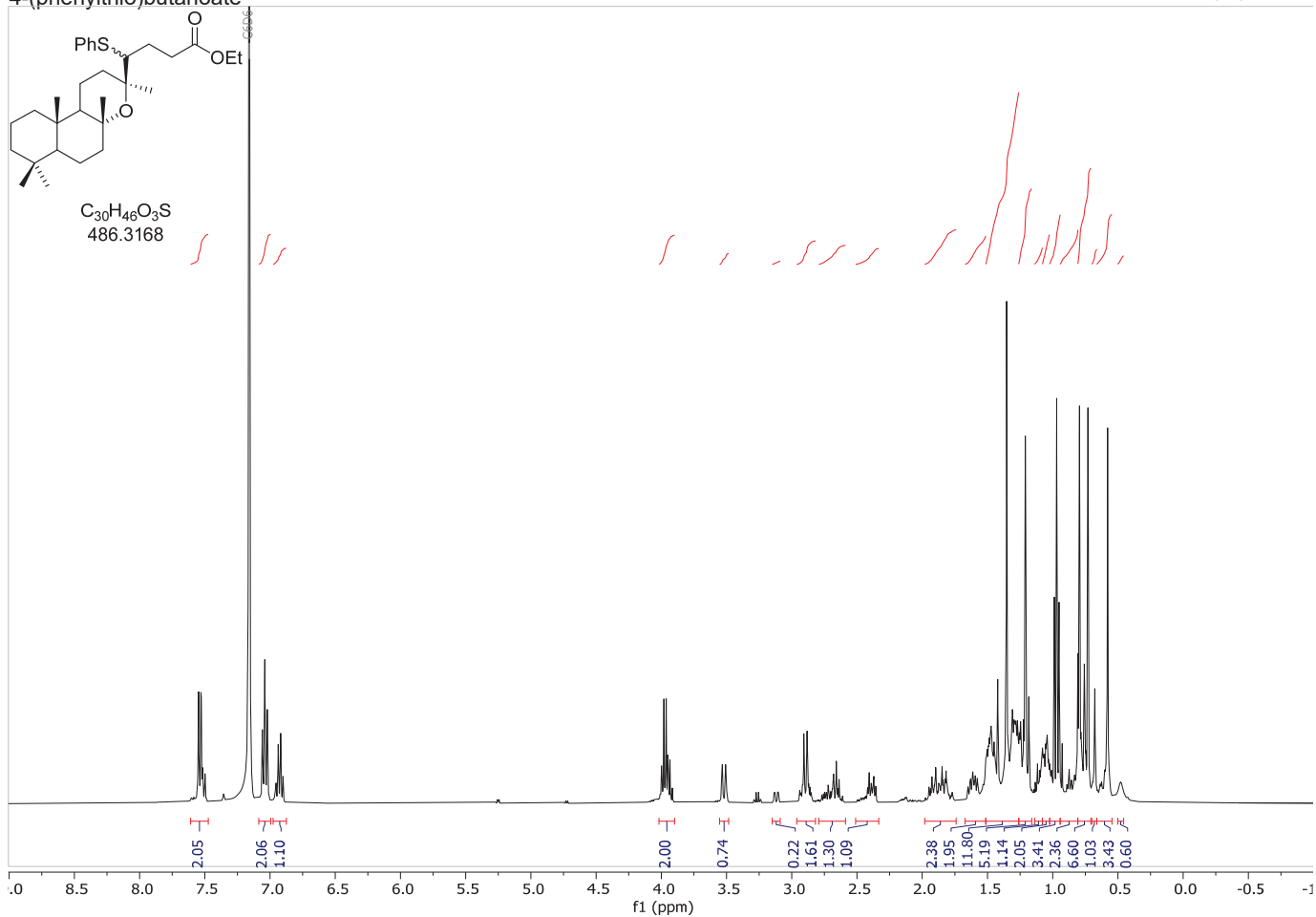
ethyl 2,2-difluoro-4-((3S,4aR,10aS)-3,4a,7,7,10a-pentamethyldodecahydro-1H-benzo[f]chromen-3-yl)butanoate

¹³C-NMR (75 MHz, C₆D₆)



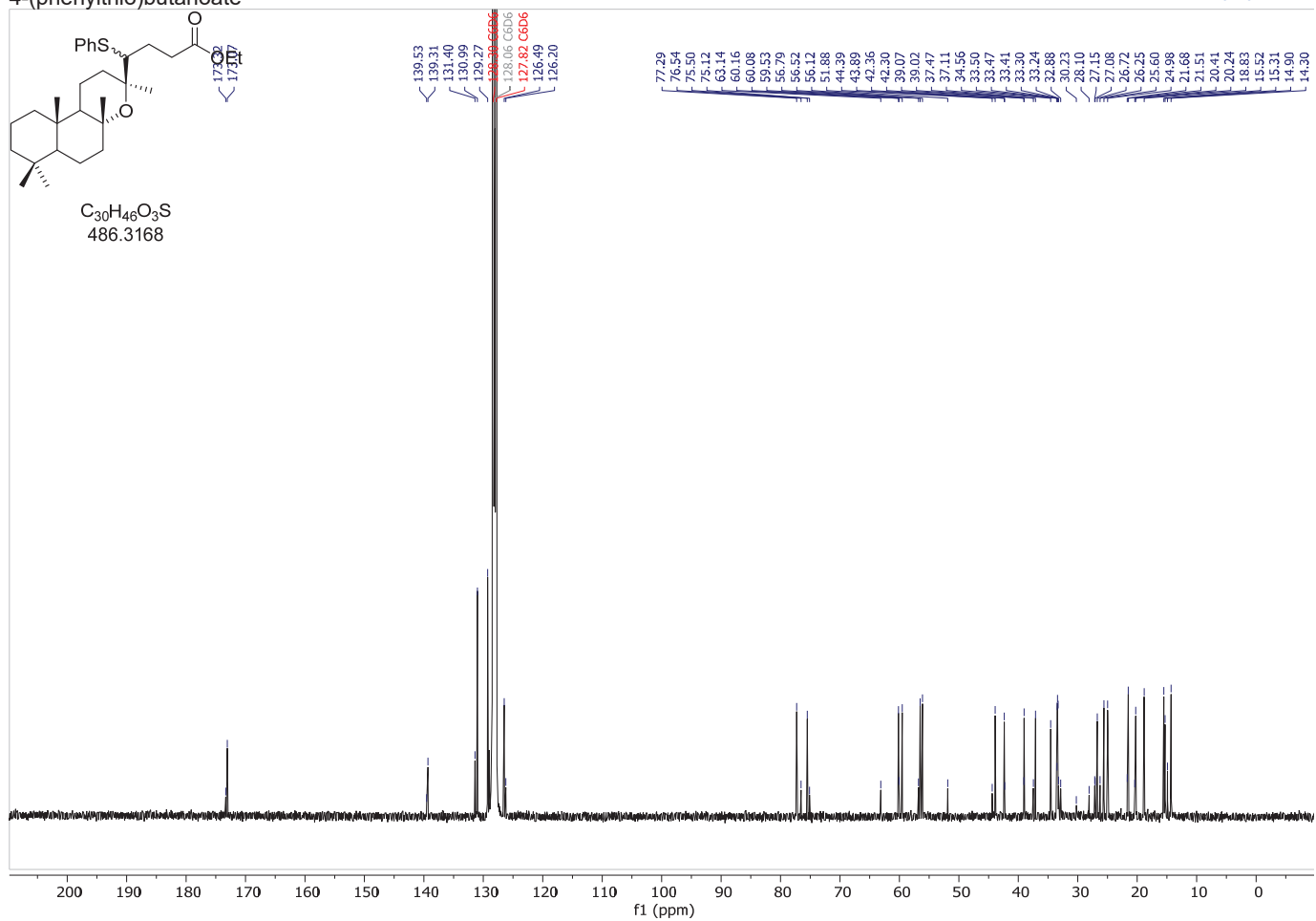
ethyl 4-((3S,4aR,10aS)-3,4a,7,7,10a-pentamethyldodecahydro-1H-benzo[f]chromen-3-yl)-4-(phenylthio)butanoate

¹H-NMR (300 MHz, C₆D₆)



ethyl 4-((3S,4aR,10aS)-3,4a,7,7,10a-pentamethyldodecahydro-1H-benzo[f]chromen-3-yl)-4-(phenylthio)butanoate

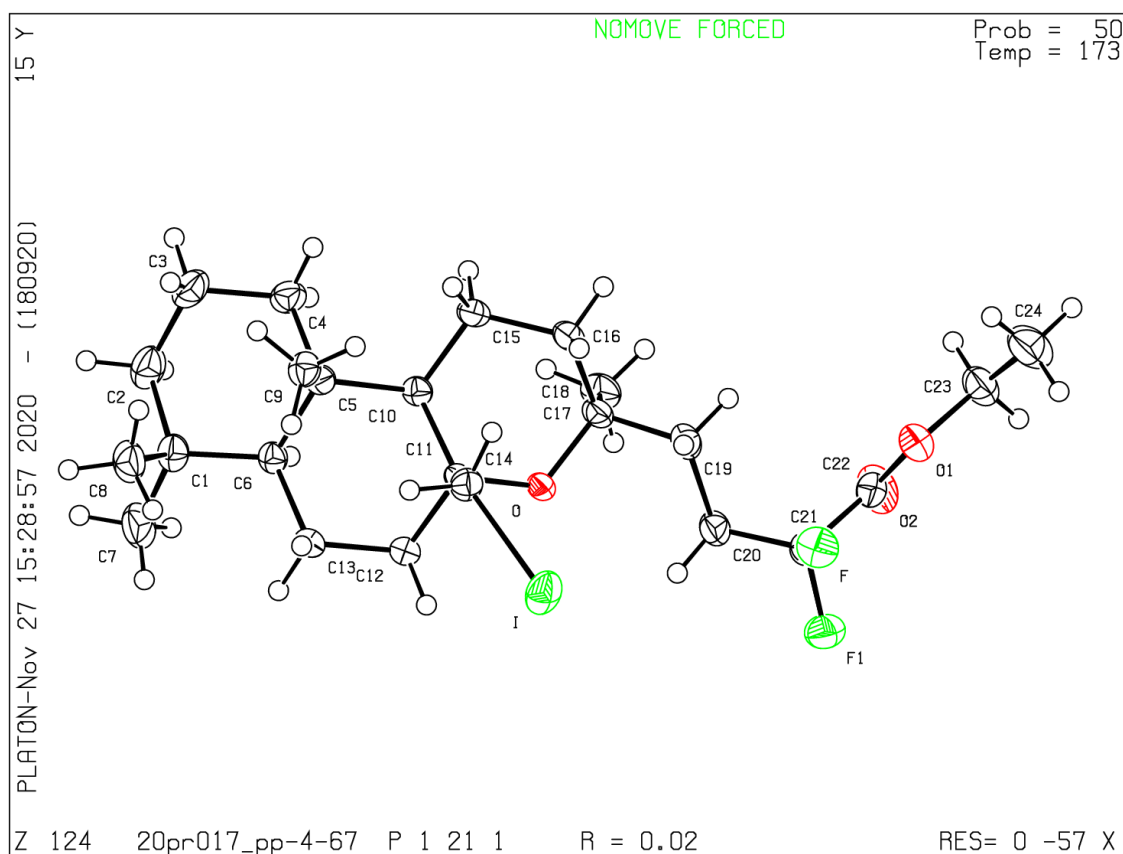
¹³C-NMR (100 MHz, C₆D₆)



Departement für Chemie und Biochemie
Universität Bern
Chemische Kristallographie
Freiestrasse 3, CH-3012 Bern, Switzerland

Dr. Lorraine Andrade Malaspina
Tel: +41 (0)31 631 4273
e-mail: lorraine.malaspina@dcb.unibe.ch

X-RAY CRYSTAL STRUCTURE REPORT



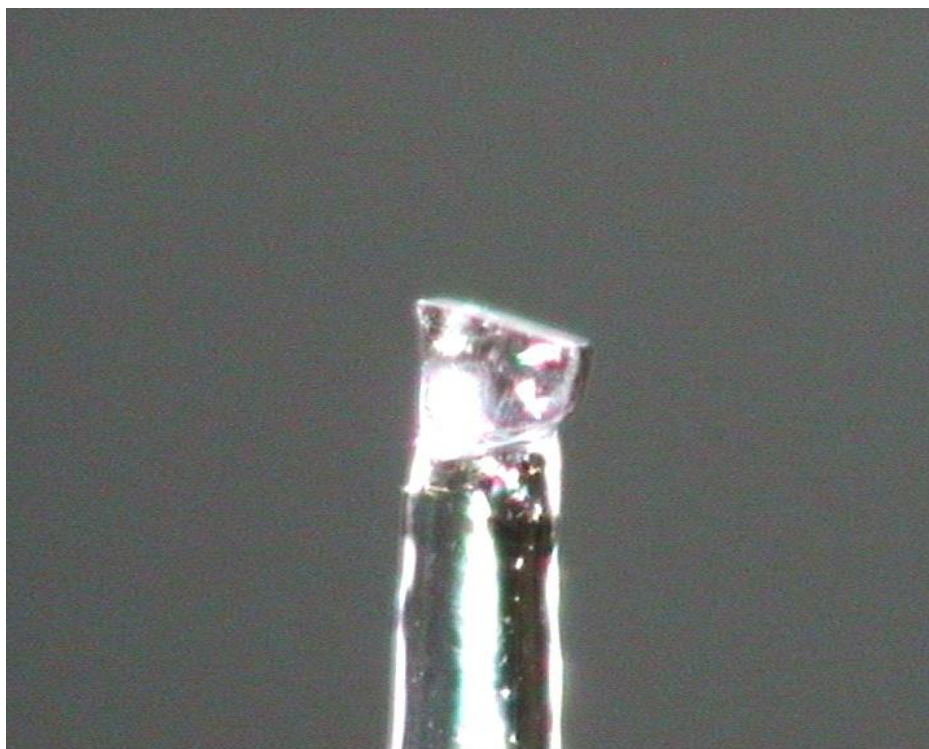
EXPERIMENTAL

Crystal-Structure Determination. A crystal of $C_{24}H_{39}F_2IO_3$ immersed in parabar oil was mounted at ambient conditions and transferred into the stream of nitrogen (173 K). All measurements were made on a *Oxford Diffraction SuperNova* area-detector diffractometer¹ using mirror optics monochromated Mo $K\alpha$ radiation ($\lambda = 0.71073 \text{ \AA}$) and Al filtered.² The unit cell constants and an orientation matrix for data collection were obtained from a least-squares refinement of the setting angles of reflections in the range $2.083^\circ < \theta < 28.526^\circ$. A total of 2838 frames were collected using ω scans, with 0.5+2.5 seconds exposure time, a rotation angle of 0.5° per frame, a crystal-detector distance of 65.20 mm, at $T = 173(2) \text{ K}$.

Data reduction was performed using the *CrysAlisPro*¹ program. The intensities were corrected for Lorentz and polarization effects, and an absorption correction based on the multi-scan method using SCALE3 ABSPACK in *CrysAlisPro*¹ was applied. Data collection and refinement parameters are given in *Table 1*.

The structure was solved by intrinsic phasing using *SHELXT*³, which revealed the positions of all non-hydrogen atoms of the title compound. All atoms were refined anisotropically and H-atoms were assigned in geometrically calculated positions and refined using a riding model where each H-atom was assigned a fixed isotropic displacement parameter with a value equal to 1.2U_{eq} of its parent atom (1.5U_{eq} for methyl groups).

Refinement of the structure was carried out on F^2 using full-matrix least-squares procedures, which minimized the function $\sum w(F_o^2 - F_c^2)^2$. The weighting scheme was based on counting statistics and included a factor to downweight the intense reflections. All calculations were performed using the *SHELXL-2014/7*⁴ program in OLEX2.⁵



Single crystal of the compound mounted on a glass fiber.

REFERENCES (In case this structure is submitted for publication, please use these references in the main text of a publication)

- 1) Oxford Diffraction (2010). *CrysAlisPro* (Version 1.171.38.41). Oxford Diffraction Ltd., Yarnton, Oxfordshire, UK.
- 2) Macchi, P.; Bürgi, H.B.; Chimpri, A. S.; Hauser, J.; Gal, Z. (2011) *J. Appl. Cryst.* **44**, 763-771
- 3) Sheldrick, G. M. (2015). *Acta Cryst.* **A71**, 3-8.
- 4) Sheldrick, G. M. (2015). *Acta Cryst.* **C71**, 3-8.
- 5) Dolomanov, O.V., Bourhis, L.J., Gildea, R.J, Howard, J.A.K. & Puschmann, H. (2009), *J. Appl. Cryst.* 42, 339-341.

The X-ray crystal structure determination service unit of the Department of Chemistry and Biochemistry of the University of Bern is acknowledged for measuring, solving, refining and summarizing the structures of compounds XX, YY, ZZ.

Table 1 Crystal data and structure refinement for 20PR017_PP-4-67.

Identification code	20PR017_PP-4-67
Empirical formula	C ₂₄ H ₃₉ F ₂ IO ₃
Formula weight	540.45
Temperature/K	173.00(10)
Crystal system	monoclinic
Space group	P2 ₁
a/Å	7.83365(6)
b/Å	19.40843(12)
c/Å	8.18321(6)
α/°	90
β/°	95.2623(7)
γ/°	90
Volume/Å ³	1238.922(15)
Z	2
ρ _{calc} /cm ³	1.449
μ/mm ⁻¹	1.312
F(000)	556.0
Crystal size/mm ³	0.24 × 0.215 × 0.193
Radiation	Mo Kα (λ = 0.71073)
2θ range for data collection/°	4.198 to 54.206
Index ranges	-10 ≤ h ≤ 10, -24 ≤ k ≤ 24, -10 ≤ l ≤ 10
Reflections collected	27338
Independent reflections	5456 [R _{int} = 0.0290, R _{sigma} = 0.0207]
Data/restraints/parameters	5456/1/276
Goodness-of-fit on F ²	1.028
Final R indexes [I ≥ 2σ (I)]	R ₁ = 0.0233, wR ₂ = 0.0562
Final R indexes [all data]	R ₁ = 0.0239, wR ₂ = 0.0567
Largest diff. peak/hole / e Å ⁻³	0.42/-0.52
Flack parameter	-0.055(13)

Table 2 Fractional Atomic Coordinates (×10⁴) and Equivalent Isotropic Displacement Parameters (Å²×10³) for 20PR017_PP-4-67. U_{eq} is defined as 1/3 of of the trace of the orthogonalised U_{ij} tensor.

Atom	x	y	z	U(eq)
I	2129.8 (3)	3402.3 (2)	7326.1 (3)	41.40 (8)
F1	-1773 (3)	3492.5 (16)	1662 (2)	39.2 (5)
C22	-4548 (4)	3438 (3)	2488 (3)	27.8 (6)
C20	-2005 (5)	2891 (2)	4117 (5)	32.0 (8)
F	-2261 (3)	4102.7 (12)	3800 (3)	37.6 (5)
C21	-2629 (4)	3490 (2)	3063 (4)	28.7 (7)
O1	-5452 (3)	3950.3 (13)	3022 (3)	32.4 (5)

Table 2 Fractional Atomic Coordinates ($\times 10^4$) and Equivalent Isotropic Displacement Parameters ($\text{\AA}^2 \times 10^3$) for 20PR017_PP-4-67. U_{eq} is defined as 1/3 of of the trace of the orthogonalised U_{ij} tensor.

Atom	x	y	z	U(eq)
C6	2186 (4)	811.6 (15)	10163 (4)	22.8 (6)
C9	1341 (5)	1771.2 (17)	12158 (4)	27.9 (7)
C5	715 (4)	1218.6 (16)	10879 (4)	22.6 (6)
C17	-2321 (4)	2253.1 (18)	6805 (4)	25.8 (6)
C11	581 (4)	1996.7 (15)	8239 (4)	21.2 (6)
C19	-2735 (4)	2904.5 (18)	5781 (4)	30.1 (7)
C16	-2797 (4)	2390.6 (18)	8540 (4)	28.5 (7)
C14	1191 (4)	2680.6 (16)	9039 (4)	27.1 (6)
C8	4463 (5)	714 (2)	12682 (5)	38.0 (8)
C15	-2088 (4)	1858.1 (18)	9810 (4)	27.8 (7)
C10	-394 (4)	1533.0 (15)	9385 (4)	21.6 (6)
C1	3279 (5)	334.1 (18)	11373 (4)	30.8 (7)
C3	622 (5)	239 (2)	12973 (5)	38.4 (8)
C13	3226 (4)	1283.0 (17)	9119 (4)	26.0 (6)
C18	-3258 (5)	1624 (2)	6056 (5)	35.3 (8)
C7	4420 (6)	-124 (2)	10397 (5)	44.4 (9)
C23	-7286 (5)	3941 (2)	2507 (5)	38.7 (9)
O	-499 (3)	2129.3 (12)	6755 (3)	24.1 (4)
C4	-411 (5)	695.1 (19)	11723 (4)	30.8 (7)
C24	-8016 (6)	4597 (2)	3076 (7)	52.8 (11)
O2	-5097 (4)	2966.3 (14)	1654 (4)	43.1 (6)
C12	2092 (4)	1591.1 (17)	7684 (4)	25.3 (6)
C2	2045 (5)	-141 (2)	12197 (5)	39.1 (9)

Table 3 Anisotropic Displacement Parameters ($\text{\AA}^2 \times 10^3$) for 20PR017_PP-4-67. The Anisotropic displacement factor exponent takes the form: - $2\pi^2[h^2a^{*2}U_{11}+2hka^*b^*U_{12}+\dots]$.

Atom	U_{11}	U_{22}	U_{33}	U_{23}	U_{13}	U_{12}
I	40.48 (13)	35.43 (12)	46.56 (13)	14.32 (12)	-5.38 (9)	-12.96 (12)
F1	38.2 (10)	47.8 (16)	32.9 (9)	1.2 (11)	9.1 (8)	-0.4 (12)
C22	29.8 (14)	28.8 (15)	24.4 (12)	2.3 (18)	-0.4 (10)	1.4 (18)
C20	30.8 (18)	38.1 (19)	27.1 (17)	0.7 (15)	2.9 (14)	12.1 (15)
F	36.7 (12)	36.7 (12)	38.7 (12)	-8.4 (10)	-0.5 (10)	-7.1 (10)
C21	28.2 (14)	30 (2)	27.6 (13)	1.2 (15)	1.0 (11)	0.2 (14)
O1	27.4 (12)	32.6 (12)	36.6 (13)	-1.9 (10)	-0.4 (10)	2.0 (10)
C6	21.3 (14)	22.6 (14)	24.0 (15)	0.0 (12)	-1.1 (12)	-1.4 (11)
C9	31.2 (18)	28.9 (16)	23.2 (15)	-2.0 (12)	-0.3 (13)	0.9 (13)
C5	21.3 (14)	23.9 (14)	22.4 (14)	-0.9 (11)	0.9 (11)	-2.6 (12)
C17	16.8 (14)	35.2 (17)	25.2 (16)	-0.7 (13)	1.0 (12)	1.5 (12)
C11	16.0 (14)	25.4 (14)	22.1 (14)	1.5 (11)	1.3 (11)	-0.3 (11)

Table 3 Anisotropic Displacement Parameters ($\text{\AA}^2 \times 10^3$) for 20PR017_PP-4-67. The Anisotropic displacement factor exponent takes the form: - $2\pi^2[h^2a^{*2}U_{11}+2hka^*b^*U_{12}+\dots]$.

Atom	U_{11}	U_{22}	U_{33}	U_{23}	U_{13}	U_{12}
C19	27.1 (17)	36.3 (17)	26.1 (16)	-2.8 (13)	-0.6 (13)	9.2 (14)
C16	19.9 (15)	38.2 (18)	27.8 (17)	0.3 (13)	3.7 (12)	5.3 (13)
C14	25.7 (15)	25.9 (15)	29.6 (16)	3.1 (12)	1.7 (13)	-3.3 (12)
C8	31.1 (19)	44 (2)	37 (2)	5.2 (16)	-8.5 (15)	1.2 (16)
C15	20.2 (15)	39.1 (18)	24.8 (16)	1.1 (13)	5.1 (12)	1.5 (13)
C10	19.4 (14)	23.5 (14)	21.6 (14)	-2.1 (11)	0.1 (11)	-2.9 (11)
C1	32.0 (18)	27.4 (16)	32.3 (17)	3.9 (13)	-1.1 (14)	1.7 (14)
C3	42 (2)	39 (2)	34.4 (19)	12.4 (16)	2.4 (16)	-7.6 (16)
C13	19.6 (15)	30.1 (15)	28.6 (16)	2.5 (12)	4.4 (12)	2.0 (12)
C18	26.5 (17)	44 (2)	34.4 (19)	-6.7 (15)	-0.2 (14)	-6.2 (15)
C7	46 (2)	37 (2)	49 (2)	4.3 (17)	1.4 (18)	17.5 (18)
C23	25.3 (18)	41 (2)	49 (2)	2.1 (16)	-0.1 (16)	3.1 (15)
O	17.0 (10)	34.4 (12)	20.9 (10)	1.9 (9)	1.5 (8)	3.3 (9)
C4	27.6 (17)	35.1 (17)	29.8 (17)	3.3 (13)	3.5 (13)	-6.3 (14)
C24	38 (2)	47 (2)	75 (3)	1 (2)	12 (2)	9.2 (19)
O2	39.0 (15)	37.7 (14)	50.1 (16)	-13.9 (12)	-9.4 (12)	0.7 (12)
C12	21.1 (15)	29.0 (16)	26.2 (15)	2.7 (12)	4.9 (12)	1.9 (12)
C2	44 (2)	30.9 (19)	41 (2)	10.4 (15)	-2.2 (17)	-4.4 (15)

Table 4 Bond Lengths for 20PR017_PP-4-67.

Atom Atom	Length/ \AA	Atom Atom	Length/ \AA
I C14	2.158 (3)	C17 C16	1.524 (5)
F1 C21	1.381 (4)	C17 C18	1.523 (5)
C22 C21	1.536 (4)	C17 O	1.452 (4)
C22 O1	1.318 (5)	C11 C14	1.537 (4)
C22 O2	1.199 (5)	C11 C10	1.551 (4)
C20 C21	1.502 (5)	C11 O	1.438 (4)
C20 C19	1.525 (5)	C11 C12	1.524 (4)
F C21	1.353 (5)	C16 C15	1.533 (5)
O1 C23	1.459 (4)	C8 C1	1.539 (5)
C6 C5	1.555 (4)	C15 C10	1.538 (4)
C6 C1	1.554 (4)	C1 C7	1.536 (5)
C6 C13	1.536 (4)	C1 C2	1.536 (5)
C9 C5	1.546 (4)	C3 C4	1.527 (5)
C5 C10	1.558 (4)	C3 C2	1.524 (6)
C5 C4	1.549 (4)	C13 C12	1.528 (4)
C17 C19	1.535 (5)	C23 C24	1.488 (6)

Table 5 Bond Angles for 20PR017_PP-4-67.

Atom	Atom	Atom	Angle/°	Atom	Atom	Atom	Angle/°
O1	C22	C21	113.0(4)	C14	C11	C10	113.2(2)
O2	C22	C21	120.9(4)	O	C11	C14	109.9(2)
O2	C22	O1	126.1(3)	O	C11	C10	109.3(2)
C21	C20	C19	111.8(3)	O	C11	C12	104.7(2)
F1	C21	C22	106.4(2)	C12	C11	C14	110.7(3)
F1	C21	C20	108.8(3)	C12	C11	C10	108.6(2)
C20	C21	C22	112.5(3)	C20	C19	C17	113.3(3)
F	C21	F1	105.5(3)	C17	C16	C15	114.1(3)
F	C21	C22	110.8(3)	C11	C14	I	113.3(2)
F	C21	C20	112.3(3)	C16	C15	C10	113.0(3)
C22	O1	C23	116.1(3)	C11	C10	C5	115.6(2)
C1	C6	C5	116.5(3)	C15	C10	C5	114.5(2)
C13	C6	C5	110.9(2)	C15	C10	C11	112.4(2)
C13	C6	C1	114.9(3)	C8	C1	C6	114.8(3)
C6	C5	C10	106.4(2)	C7	C1	C6	109.1(3)
C9	C5	C6	114.0(3)	C7	C1	C8	107.3(3)
C9	C5	C10	112.3(3)	C7	C1	C2	107.4(3)
C9	C5	C4	108.2(3)	C2	C1	C6	107.8(3)
C4	C5	C6	107.9(3)	C2	C1	C8	110.2(3)
C4	C5	C10	107.9(2)	C2	C3	C4	111.4(3)
C16	C17	C19	107.9(3)	C12	C13	C6	111.1(3)
C18	C17	C19	111.8(3)	O1	C23	C24	107.1(3)
C18	C17	C16	111.4(3)	C11	O	C17	120.7(2)
O	C17	C19	106.3(3)	C3	C4	C5	113.0(3)
O	C17	C16	112.3(2)	C11	C12	C13	112.7(3)
O	C17	C18	107.1(3)	C3	C2	C1	113.9(3)

Table 6 Hydrogen Bonds for 20PR017_PP-4-67.

D	H	A	d(D-H)/Å	d(H-A)/Å	d(D-A)/Å	D-H-A/°
C12	H12A	I	0.97	2.98	3.528(3)	116.7

Table 7 Torsion Angles for 20PR017_PP-4-67.

A	B	C	D	Angle/°	A	B	C	D	Angle/°
C22	O1	C23	C24	-173.6(3)	C10	C11	O	C17	39.2(4)
C21	C22	O1	C23	179.2(3)	C10	C11	C12	C13	-52.6(3)
C21	C20	C19	C17	172.4(3)	C1	C6	C5	C9	66.9(3)
O1	C22	C21	F1	-122.9(3)	C1	C6	C5	C10	-168.8(3)
O1	C22	C21	C20	118.0(4)	C1	C6	C5	C4	-53.3(4)
O1	C22	C21	F	-8.7(4)	C1	C6	C13	C12	165.3(3)
C6	C5	C10	C11	-56.5(3)	C13	C6	C5	C9	-67.0(3)

Table 7 Torsion Angles for 20PR017_PP-4-67.

A	B	C	D	Angle/°	A	B	C	D	Angle/°
C6	C5	C10	C15	170.5 (3)	C13	C6	C5	C10	57.3 (3)
C6	C5	C4	C3	53.1 (4)	C13	C6	C5	C4	172.8 (3)
C6	C1	C2	C3	-52.6 (4)	C13	C6	C1	C8	61.7 (4)
C6	C13	C12	C11	57.5 (4)	C13	C6	C1	C7	-58.7 (4)
C9	C5	C10	C11	68.9 (3)	C13	C6	C1	C2	-175.1 (3)
C9	C5	C10	C15	-64.1 (3)	C18	C17	C19	C20	-68.4 (4)
C9	C5	C4	C3	-70.7 (4)	C18	C17	C16	C15	70.3 (4)
C5	C6	C1	C8	-70.4 (4)	C18	C17	O	C11	-109.2 (3)
C5	C6	C1	C7	169.2 (3)	C7	C1	C2	C3	-170.0 (3)
C5	C6	C1	C2	52.8 (4)	O	C17	C19	C20	48.1 (4)
C5	C6	C13	C12	-60.0 (3)	O	C17	C16	C15	-49.9 (4)
C17	C16	C15	C10	29.5 (4)	O	C11	C14	I	-46.9 (3)
C19	C20	C21	F1	173.1 (3)	O	C11	C10	C5	168.0 (2)
C19	C20	C21	C22	-69.3 (4)	O	C11	C10	C15	-58.0 (3)
C19	C20	C21	F	56.7 (4)	O	C11	C12	C13	-169.3 (3)
C19	C17	C16	C15	-166.6 (3)	C4	C5	C10	C11	-172.0 (3)
C19	C17	O	C11	131.2 (3)	C4	C5	C10	C15	55.0 (3)
C16	C17	C19	C20	168.8 (3)	C4	C3	C2	C1	56.2 (4)
C16	C17	O	C11	13.5 (4)	O2	C22	C21	F1	57.8 (5)
C16	C15	C10	C5	157.7 (3)	O2	C22	C21	C20	-61.3 (4)
C16	C15	C10	C11	23.2 (4)	O2	C22	C21	F	172.0 (3)
C14	C11	C10	C5	-69.1 (3)	O2	C22	O1	C23	-1.4 (5)
C14	C11	C10	C15	64.9 (3)	C12	C11	C14	I	68.3 (3)
C14	C11	O	C17	-85.7 (3)	C12	C11	C10	C5	54.3 (3)
C14	C11	C12	C13	72.3 (3)	C12	C11	C10	C15	-171.7 (3)
C8	C1	C2	C3	73.4 (4)	C12	C11	O	C17	155.4 (3)
C10	C5	C4	C3	167.6 (3)	C2	C3	C4	C5	-56.1 (4)
C10	C11	C14	I	-169.4 (2)					

Table 8 Hydrogen Atom Coordinates ($\text{\AA} \times 10^4$) and Isotropic Displacement Parameters ($\text{\AA}^2 \times 10^3$) for 20PR017_PP-4-67.

Atom	x	y	z	U(eq)
H20A	-763.46	2902.76	4280.48	38
H20B	-2337.86	2464.28	3557.75	38
H6	1594.94	494.61	9368.87	27
H9A	1383.09	1576.98	13239.49	42
H9B	564.19	2154.79	12080.12	42
H9C	2465.01	1925.06	11947.12	42
H19A	-3969.67	2957.87	5611.21	36
H19B	-2278.54	3302.02	6393.18	36
H16A	-4036.54	2399.52	8524.5	34
H16B	-2373.72	2842.53	8882.25	34

Table 8 Hydrogen Atom Coordinates ($\text{\AA}\times 10^4$) and Isotropic Displacement Parameters ($\text{\AA}^2\times 10^3$) for 20PR017_PP-4-67.

Atom	<i>x</i>	<i>y</i>	<i>z</i>	U(eq)
H14A	2096.02	2586.25	9899.98	33
H14B	245.86	2889.99	9545.13	33
H8A	5088.57	1065.24	12166.05	57
H8B	5253.27	391.87	13226.79	57
H8C	3786.02	921.08	13469.91	57
H15A	-2931.84	1496.56	9887.37	33
H15B	-1906.14	2078.84	10874.71	33
H10	-750.91	1133.66	8704.75	26
H3A	1119.57	522.18	13870.71	46
H3B	-136.9	-92.6	13418.04	46
H13A	3736.89	1651.72	9798.25	31
H13B	4144.92	1020.48	8699.71	31
H18A	-4465.85	1716.93	5907.92	53
H18B	-3051.26	1236.53	6776.05	53
H18C	-2846.49	1522.74	5013.28	53
H7A	3748.01	-315.14	9465.31	67
H7B	4889.12	-491.02	11086.27	67
H7C	5336.21	146.38	10028.74	67
H23A	-7826.2	3550.22	2990.48	46
H23B	-7476.31	3904.51	1322.23	46
H4A	-1267.53	944.41	12271.03	37
H4B	-1007.43	404.92	10890.41	37
H24A	-7502.4	4978.47	2557.32	79
H24B	-7782.73	4634.37	4245.16	79
H24C	-9232.21	4601.21	2793.26	79
H12A	2778.93	1893.39	7064.81	30
H12B	1659.99	1222.45	6959.47	30
H2A	1530.07	-460.88	11383.56	47
H2B	2697.09	-409.1	13038.41	47

Declaration of consent

on the basis of Article 18 of the PromR Phil.-nat. 19

Name/First Name: Hofstetter/Elena

Registration Number: 18-120-436

Study program: Chemistry and Molecular Sciences

Bachelor

Master

Dissertation

Title of the thesis: Enantioselective Hydroalkylation and Natural Product Modification Mediated by Radical Reactions

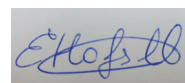
Supervisor: Renaud/Philippe

I declare herewith that this thesis is my own work and that I have not used any sources other than those stated. I have indicated the adoption of quotations as well as thoughts taken from other authors as such in the thesis. I am aware that the Senate pursuant to Article 36 paragraph 1 litera r of the University Act of September 5th, 1996 and Article 69 of the University Statute of June 7th, 2011 is authorized to revoke the doctoral degree awarded on the basis of this thesis.

For the purposes of evaluation and verification of compliance with the declaration of originality and the regulations governing plagiarism, I hereby grant the University of Bern the right to process my personal data and to perform the acts of use this requires, in particular, to reproduce the written thesis and to store it permanently in a database, and to use said database, or to make said database available, to enable comparison with theses submitted by others.

12.08.2022

Place/Date



Signature

